이학박사 학위논문

Pyrene Derivatives as Donors and Acceptors

전자 증여체와 수용체로 쓰이는 파이렌 유도체 연구

2015 년 8 월

서울대학교 대학원

화학부

Dennis Chercka

Table of Content

Index of Abbreviations

2D WAXS	two-dimensional wide-angle X-ray scattering
AcOH	acetic acid
^{13}C-APT	attached proton test – (NMR)
B3LYP	Becke, three-parameter, Lee-Yang-Parr (DFT hybrid functional)
BuLi	butyl lithium
br	broad signal (NMR)
COSY	correlation spectroscopy
CT	Charge- transfer
CV	cyclic voltammetry
d	doublet (NMR)
d	days
D	Debye
DCM	dichloromethane
dd	doublet of doublets (NMR)
DDQ	2,3-dichlor-5,6-dicyano-1,4-benzoquinone
DFT	density functional theory
DMF	N,N-dimethylformamide
DMSO	dimethyl sulfoxide
DPPF	bis(diphenylphosphino)ferrocene
ε	extinction coefficient
EA	elemental Analysis
EL	electro luminescence
ESI MS	electrospray ionization mass spectrometry
ESR	electron spin resonance
EtOAc	ethyl acetate
Et$_2$O	diethylether
EtOH	ethanol
F$_4$-TCNQ	7,7,8,8-tetracyano-2,3,5,6-tetrafluoroquinodimethane
Fc	ferrocene
FD MS	field desorption mass spectrometry
FWHM	full width at half maximum
GPC	gel permeation chromatography
h	hours
HAXPES	hard X-ray photoelectron spectroscopy
H,H COSY	two-dimensional correlated proton NMR spectroscopy
NEXAFS	near edge X-ray absorption fine structure
HMP	2,4,5,7,9,10-hexamethoxypyrene
Me	methyl
HOMO	highest occupied molecular orbital
HR MS	high resolution mass spectrometry
HSQC	heteronuclear single quantum coherence
IR	infrared spectroscopy
IRTG	international research training group
ISC	inter system crossing
ITO	indium tin oxide
LUMO	lowest unoccupied molecular orbital

m	multiplet (NMR)
MALDI-TOF	matrix-assisted laser desorption/ionization time-of-flight
MeOH	methanol
min	minutes
MS	mass spectrometry
MW	microwave
NBS	N-bromosuccinimide
N/I	neutral /ionic
NMP	N-methylpyrrolidone
NMR	nuclear magnetic resonance
NOE	nuclear Overhauser effect
NOESY	nuclear Overhauser enhancement spectroscopy
OFET	organic field-effect transistor
OLED	organic light emitting diode
OMe	methoxy
OMP	1,3,4,5,6,8,9,10-octamethoxypyrene
OPV	organic photovoltaics
PAH	polycyclic aromatic hydrocarbon
PDI	perylene diimide
PES	photoelectron spectroscopy
PL	photoluminescence
Ph	phenyl
ppm	parts per million
q	quartet (NMR)
RISC	reverse inter system crossing
RT	room temperature
s	singlet (NMR)
sec	seconds
SFB/TR 49	*Sonderforschungsbereich Transregio 49*
STS	scanning tunneling spectroscopy
t	triplet (NMR)
TBAF	tetra-iso-butyl ammonium fluoride
TBS	*tert*-butyl-dimethylsilyl
^{t}Bu	*tert*-butyl
TCNQ	7,7,8,8-tetracyanoquinodimethane
TEA	triethylamine
THF	tetrahydrofuran
TINIT	temperature induced neutral/ionic transitions
TIPS	triisopropylsilyl
TLC	thin layer chromatography
TMEDA	N,N,N",N"-tetramethylene-diamine
TMS	trimethylsilyl
TMP	4,5,9,10-tetramethoxypyrene
UHV	ultrahigh vacuum
UPS	ultraviolet photoelectron spectroscopy
UV/Vis	ultraviolet-visible absorption spectroscopy
XANES	X-ray absorption near edge structure
XPS	X-ray photoelectron spectroscopy

I.   Introduction

I.1   Pyrene
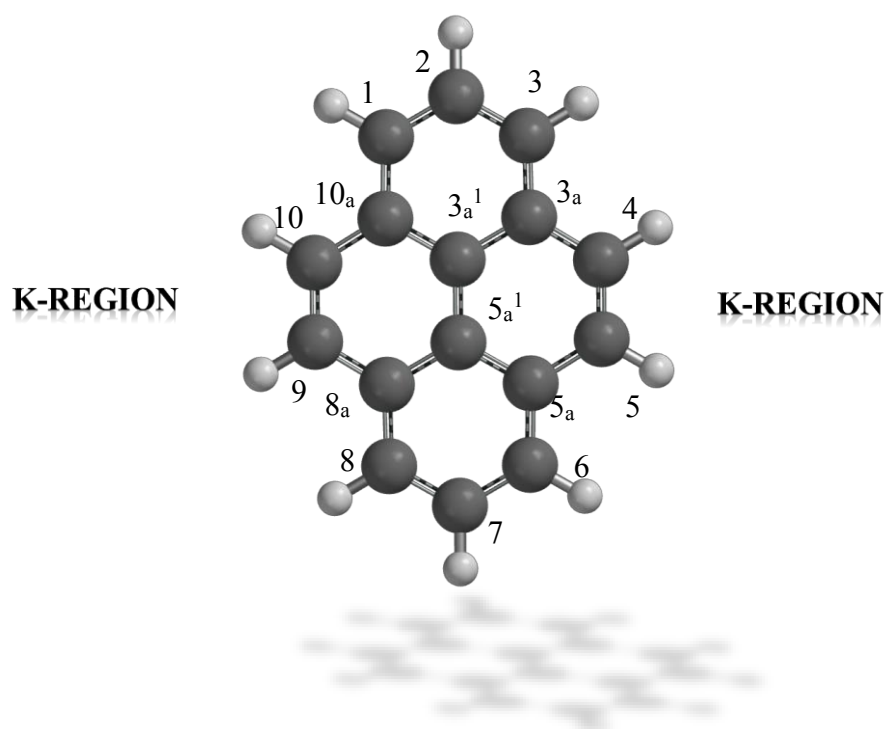
I-1: Ball and stick model of pyrene (DFT calculation). The atom numbering and the designation of the K-regions (C_4, C_5 / C_9, C_{10}) are given according to IUPAC recommendations.[1]

Pyrene is a polycyclic hydrocarbon consisting of four fused aromatic rings. Its sum formula is $C_{16}H_{10}$. LAURENT was the first to isolate the hydrocarbon from coal tar. The name "pyrene" derives from the ancient Greek word πυρ (pyr) meaning fire, as LAURENT believed pyrene to be formed when organic substances react with fire.[2] About one hundred and twenty years later, advances in industrial chemistry turned pyrene into a readily available, inexpensive building block for dye industry.[3] Coke-oven coal tar is an

abundant source of polycyclic aromatic hydrocarbons (approx. $20*10^6$ t/a) which is relatively rich in pyrene (2 - 2.1 %). Nowadays, pyrene is prepared on a multi-ton scale and utilized in its own right, especially due to its outstanding photophysical properties (e.g. as optical brightener *Fluolite XMF*™[4], reactive dye *C.I. Direct Blue 109*[5] or fluorescent dye *Pyranine*[6]).

The carbon atoms in pyrene are labeled according to the IUPAC recommendation of 1998 as shown in figure I-1.[1] Pyrene can be considered as biphenyl bridged with two ethenyl units in positions 2,2' and 6,6'. The commonly used expression *K-region* collectively describes these ethenyl bridges, i.e. the positions 4,5,9 and 10 of pyrene. Recently, the expression n*on-K-region* was used by ZOU *et al.* to collectively identify the biphenyl positions (1,2,3,6,7 and 8) of pyrene.[7]

I.1.1   Properties
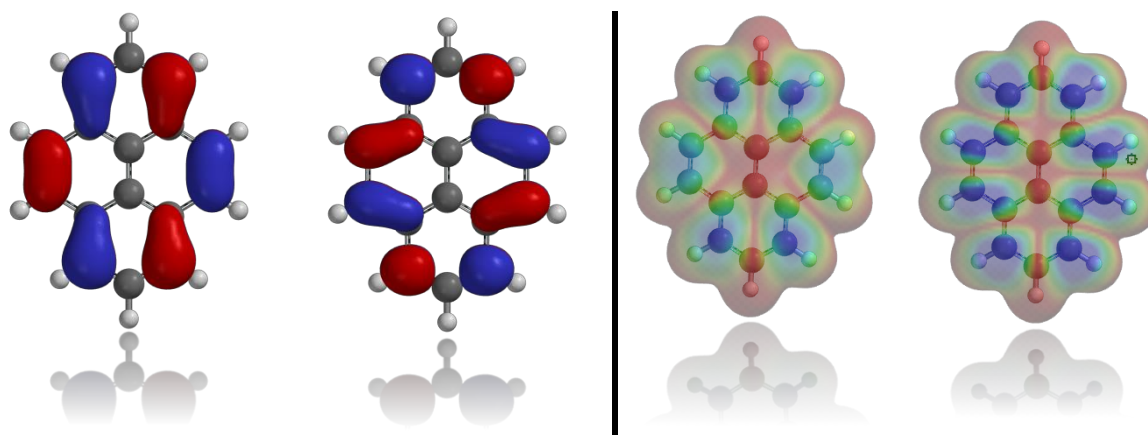
I-2: Frontier orbitals of pyrene (HOMO left, LUMO center left) and the corresponding orbital densities (HOMO center right, LUMO right) as calculated by DFT (B3LY, 6-311G*).

Pyrene is an archetypical polycyclic aromatic hydrocarbon. Its flat geometry offers full delocalization of the π-electron cloud extending above and below the carbon backbone as shown in figure I-2. The nodal plane along the molecular long axis (C2, $C3_a{}^1$, $C5_a{}^1$, C7) has significant effects on the reactivity, which will be discussed in chapter *I.1.2*. The photophysical properties of pyrene have been studied extensively. In the UV-vis absorption spectrum (figure I-3) four transitions can be resolved.[8, 9] A full assignment of the transitions is given by YOSHINAGA *et al.*[10] The S_0->S_1 transition is very weak ($\lambda = 372$ nm, $\varepsilon = 510$ L*mol^{-1}*cm^{-1}) whereas the higher S_0->S_{2-4} transitions are intense ($\lambda = 334$ nm, $\varepsilon_{S0->S2} = 5.5*10^5$ L*mol^{-1}*cm^{-1}, $\lambda = 272$ nm, $\varepsilon_{S0->S3} = 5.4*10^5$ L*mol^{-1}*cm^{-1} and $\lambda = 243$ nm, $\varepsilon_{S0->S4} = 8.8*10^5$ L*mol^{-1}*cm^{-1}).[11] Furthermore, it was shown by dichroism studies that the S_0->S_1 and S_0->S_3 transitions are polarized along the molecule's short axis, while S_0->S_2 and S_0->S_4 are polarized along the molecule's long axis.[12, 13]
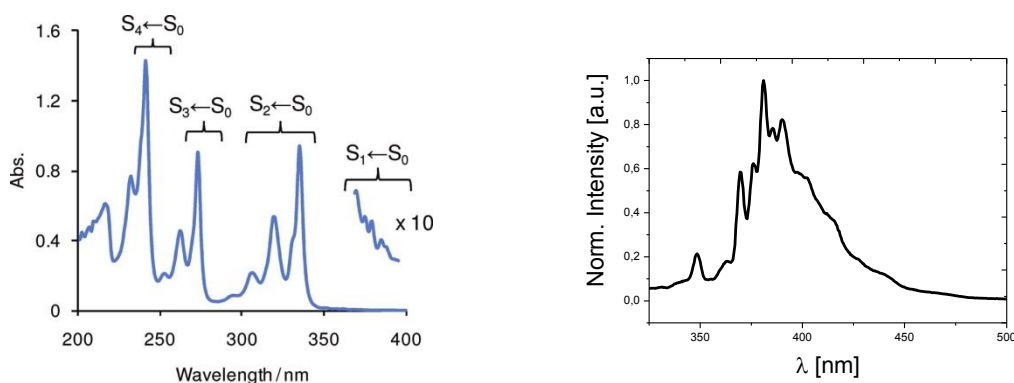
I-3: Left: UV-vis absorption spectrum of pyrene in cyclohexane. The respective transitions are labeled [figure adapted from CRAWFORD et al.[11]]. Right: Fluorescence spectrum of pyrene in cyclohexane.[14]

Its deep blue, intense fluorescence ($\lambda_{max,cyclohexane}$ = 380 nm, $\phi_{PL,EtOH}$ = 0.65) is one property that pyrene is well known for.[15] Furthermore, the fluorescence life time of $\tau \approx 300$ ns is remarkably long.[16] The fluorescence fine structure is very sensitive to the solvent environment. It was shown by DONG that this can be exploited to define an experimental scale of solvent polarities (Py-scale).[17]
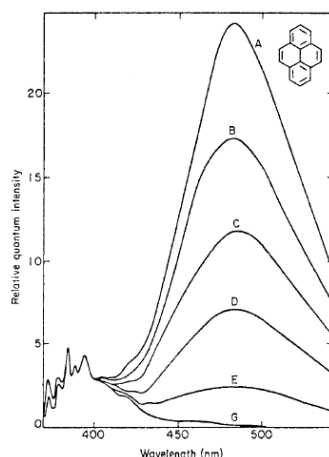
*I-4: Fluorescence spectra of pyrene at different concentrations in cyclohexane (concentration (in mol/l): A = 10^{-2}, B = 7.75*10^{-3}, C = 5.5*10^{-3}, D = 3.25*10^{-3}, E = 10^{-3}, F = 10^{-4}) [figure adapted from BIRKS[18]].*

Even more interesting were the findings by FÖRSTER and KASPER[19]. They describe the formation of excited dimers (*excimers*) in pyrene solutions of higher concentration (>1*10^{-4} mol/l). In figure I-4 the development of the unstructured, very intense excimer fluorescence band with increasing concentration (from F to A) is clearly visible.

An excimer is formed between an electronically excited- and a ground state molecule. As both species approach each other at close distances (3.37 Å) a bound state can be formed.[20]

$$^1M^* + \ ^1M \ \rightleftarrows \ ^1(MM)^*$$
(I-1)

Eq. (I-1): M* denotes an electronically excited molecule, M a molecule in the ground state and (MM)* the excimer.

This process is diffusion controlled so that the long lived excited state in pyrene is essential for this mechanism.

Fluorescence quenching by excimer formation has been frequently used as a distance probe in biochemical studies[21-23] or to investigate phase transitions in bilamellar vesicles.[24] Recently, pyrene-based molecular beacon DNA probes have been developed by CONLON *et al*.[25]

Besides excimer formation, *p-type* delayed fluorescence[1] constitutes a second, bimolecular luminescence process in pyrene solutions.[15, 26] The long lived pyrene triplet states ($\tau_3 = 5*10^{-3}$ s at c $= 3*10^{-3}$ mol/l) can form a vibrationally excited dimer which, in turn, splits into an excited and a ground state molecule. The excited moiety finally relaxes to the ground state under emission of a (*delayed*) fluorescence photon.[20, 27]

$$T + T \rightarrow S_2^{**} \rightarrow S^* + S + h\nu \qquad\qquad (\text{I-2})$$
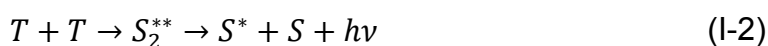
Eq. (I-2): T denotes triplet state, S_2^{**} a vibrationally excited dimer, S^* an excited singlet state, S a ground state pyrene molecule and $h\nu$ a photon.

Not only does pyrene hold great promise as a fluorescence probe, its high thermal and photochemical stability, deep blue fluorescence and planar geometry make it an ideal candidate for applications in the area of organic electronics.[28] The use as emitter in organic light emitting diodes is hampered, however, by the complex photo-physics of pyrene. This is especially true for the bathochromic shift of the electroluminescence due to excimer formation.[29]

I.1.2   Reactivity of pyrene

This work's main topic is the development of new, selective functionalization procedures for pyrene. In this section, the reactivity of pyrene and some of its derivatives will briefly be discussed.

As mentioned in the introduction to this chapter, pyrene behaves like an archetypical hydrocarbon, especially when its reactivity towards electrophiles is considered. Already in the early days of pyrene chemistry it became clear that many reactions that will transform benzene will also affect pyrene.[30] Yet, the regioselectivity of these reactions is more complex.

In order to understand the reactivity of pyrene it is useful to consider two different formalisms (figure I-5): *CLAR's sextet rule* [31] and the *frontier orbital theory*.[32, 33]

---

[1] This type of delayed fluorescence was first observed in pyrene solutions and designated accordingly *p-type*.
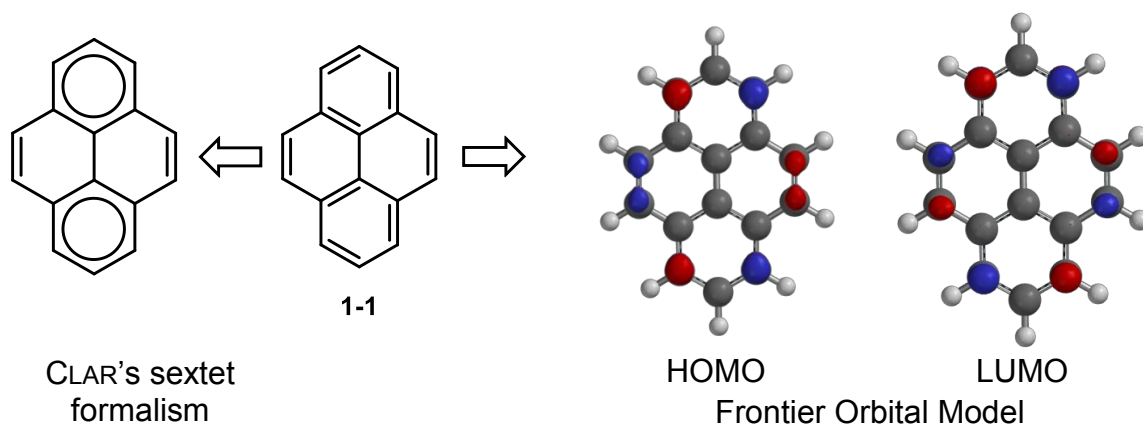
I-5: Models of pyrene according to the CLAR's sextet formalism (left) and frontier orbital model (red and blue) (right).

Using CLAR's sextet rule pyrene can be represented with two full aromatic rings and two double bonds (the K-region of pyrene) i.e. as biphenyl annulated by two double bonds.[31] The frontier orbital theory indicates high electron densities in positions 1,3,6 and 8 as well as moderate densities in position 4,5,9 and 10. Significant is the nodal plane bisecting pyrene and passing through positions 2 and 7 (fig. I-5, right).

I.1.2.1 Selective functionalization of pyrene

As a polycyclic hydrocarbon pyrene can be functionalized by electrophiles, oxidants, reducing agents and transition metal mediated C-H activation to give a few examples. Depending on the agent acting on pyrene, different positions of the hydrocarbon can be addressed.

CASAS-SOLVAS, HOWGEGO and DAVIS recently published an excellent overview of current methods to prepare functionalized pyrenes.[34] Pyrene-based materials for organic electronics were comprehensively reviewed by FIGUEIRA-DUARTE and MÜLLEN in 2011.[28]

I.1.2.1.1 Functionalization in positions 1,3,6 and 8

Pyrene's reactivity towards electrophiles can easily be understood if frontier orbital theory is employed and its HOMO distribution is considered. As shown in figure I-5 (right), the highest electron densities are predicted for positions 1,3,6 and 8. In figure I-6 the stepwise 1,3,6,8-functionalization using bromine as a common electrophile is presented.
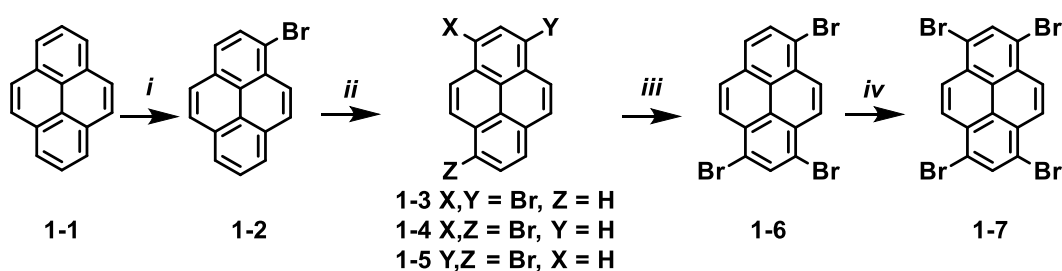

I-6: Bromination of pyrene. The degree of bromination is dependent on the equivalents of bromine added (i = 1 eq, ii = 2 eq, iii = 3 eq and iv = 4 and more eq).

The addition of elemental bromine was described as early as 1871 by GRÄBE in his ground-breaking work on pyrene. He was able to identify **1-3** and **1-4** as a mixture of isomers as well as **1-6**.[35] **1-5** is formed in small amounts ($\approx 5\,\%$) and was only later isolated.[36] VOLLMANN *et al*. later reported that, depending on the reaction conditions, either one-, two-, three- or fourfold functionalization is possible.[37] As bromine substituents deactivate pyrene due to their electron withdrawing effect, it is necessary to employ more drastic conditions to prepare higher functionalized pyrene derivatives. This holds generally true for electrophiles.

Good availability of **1-2** and **1-7** make these compounds widely used building blocks for pyrene based materials. **1-2** is commonly used when pyrene is introduced as a pennant group e.g. in conjugated polymers[28], π-binding anchor groups for graphene/carbon nanotube functionalization[38, 39], organometallic complexes[40, 41] or in biochemistry.[42, 43] In contrast, **1-7** is often used as a central building block for dendrimers[44-47] and materials for organic electronics [48] due to its D_{2h} symmetry.

1,6- and 1,8-functionalized pyrenes can be prepared according to scheme I-6 by partial bromination. The isomers can be separated by a lengthy recrystallization procedure.[49] For the synthesis of functionalized materials it was often advantageous to isolate the desired isomer by chromatographic methods at a later stage of the synthetic route.[50, 51]
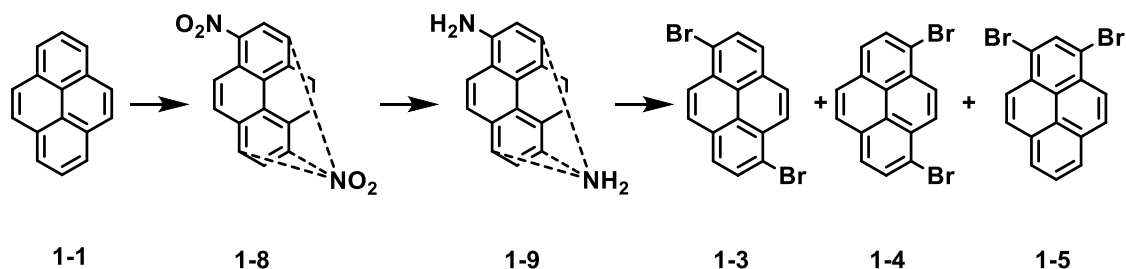
I-7: Nitration-reduction-bromination protocol.

A three step protocol of nitration, reduction, chromatographic isomer resolution and SANDMEYER reaction gives an alternative access to **1-3**, **1-4** and **1-5**. The isomers of **1-9** can be isolated in an 2:2:1 ratio by column chromatography.[52]

Electrophilic substitutions on pyrene exceeding fourfold functionalization in a single reaction step are rarely reported. Instances are for example FRIEDEL-CRAFTS alkylation reactions with secondary alkyl halides [53] or perhalogenation reactions (*vide infra*).

I.1.2.1.2   Functionalization in positions 4,5,9 and 10
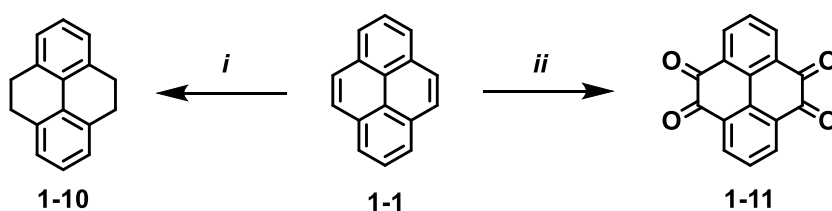
I-8: Selective functionalization in positions 4,5,9 and 10. i: Pd/C, H₂, 100 bar. ii: RuCl₃, NaIO₄, MeCN, CH₂Cl₂ 4 h.

In order to understand the selective functionalization of the K-region of pyrene, i.e. positions 4,5,9 and 10, CLAR's sextet rule is very helpful. According to this formalism (recalling figure I-5), the K-region has an alkene-like character. Thus, reagents like palladium on charcoal[54] or osmium tetroxide, which are known to act on alkene double bonds, also selectively transform pyrene.

The reduction to **1-10** by hydrogen and palladium on carbon was extensively used as access to 2,7-dibromopyrene (figure I-11).[55]

OBERENDER and DIXON state that oxidation of pyrene can be specific to the K-region if the oxidation has a cyclic transition state.[56] This was initially reported for OsO₄ and soon expanded to RuO₄.[56-58] Both reagents provided 4,5,9,10-tetrahydropyrene-4,5,9,10-tetraol as the main outcome and **1-11** as a mere side product. HU *et al.* revisited this reaction in 2004 and found that the addition of acetonitrile stabilizes the transition state sufficiently to prepare **1-11** in gram scale quantities.[59] HU's report is central for this work and will be discussed in further detail in chapter *II*. More recently, KASSAEE reported the synthesis of **1-11** in 92 % yield by benzyltrimethylammonium fluorochromate.[60] This seems surprising as chromate reagents are generally known to oxidize pyrene in 1,6 or 1,8 position.[37] It was not possible to verify this claim due to the unavailability of the reagent.
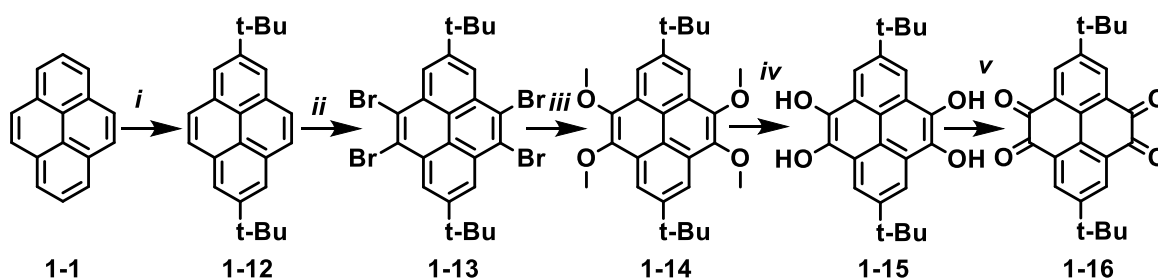
I-9: YAMATO's 2,7-bistertbutylpyrene-4,5,9,10-tetraone synthesis. i: ᵗBuCl, AlCl₃, CH₂Cl₂. ii: 6 eq. Br₂, FeCl₃. iii. NaOMe, CuI, DMF. iv: BBr₃, CH₂Cl₂. v: SiO₂, air.

The synthesis of **1-16** by YAMATO *et al.* can give further insights into selective pyrene functionalization.[61] In order to block the otherwise active positions 1,3,6 and 8 from nucleophilic attacks, *tert*-butyl groups are introduced (*vide infra*) to afford **1-12**. This, in

turn, enables a regioselective bromination in the K-region to give **1-13**.[2] While it is problematic to convert 4,5,9,10-tetrahydropyrene-4,5,9,10-tetraol to **1-11**, pyrene-4,5,9,10-tetraol **1-15** can be prepared by air oxidation on SiO_2. This procedure was further improved by WASSERFALLEN *et al.* by using salcomine as oxygen transfer agent.[62] They found that **1-16** can be useful in the preparation of extended PAHs. **1-13** is also a versatile building block for pyrene-fused pyrazaacenes, as recently reviewed by MAETO-ALONSO.[63]

I.1.2.1.3   Functionalization in positions 2 and 7

Once more, it should be stressed that the nodal plane in pyrene makes the synthesis of 2,7-functionalized pyrene derivatives difficult (FOM-theory). To address these positions, three basic concepts have emerged: Exploitation of the favorable steric of positions 2 and 7, the total synthesis of a pyrene and elimination of the nodal plane. For each of these concepts representative examples will be discussed below.

For sterically demanding substituents, positions 2 and 7 are thermodynamically favored. FRIEDEL-CRAFTS alkylation with *tert*-butyl chloride and aluminum chloride gives 2,7-di-*tert*-butylpyrene (**1-12**) in good regioselectivity as the thermodynamic product (see fig. I-9).[64] The same reaction gives a broad mixture of isomers if isopropyl chloride is used instead.[53]
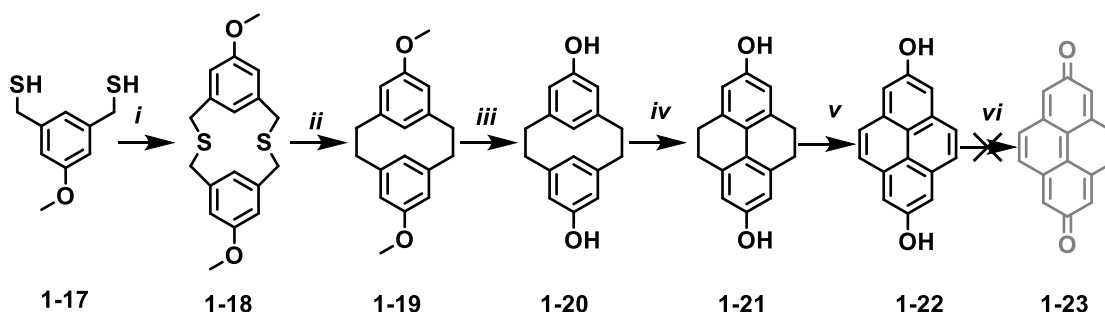
I-10: Attempted pyrene-2,7-dione total synthesis according to BOLDT and BRUHKE.[65] *i: m-MeOPh(CH₂Br), KOH. ii: hν, (CH₃O)₃P. iii: BBr₃. iv: AgCO₃/celite. v: Pd/C. vi: Pb(OAc)₄.*

For a long time, only multi-step synthesis provided access to the 2-7 substitution pattern (other than **1-12**).[66] Often thiocyclophanes (e.g. **1-18**) have been prepared that yielded the desired pyrene derivative after sulfur extrusion (**1-19**) and a subsequent $3_a{}^1$-$5_a{}^1$ bond formation (**1-20**) followed by a final oxidation step to the aromatic pyrene derivative (**2-21**).[67] BOLDT and BRUHKE presented a total synthesis of 2,7-dihydroxypyrene (**2-21**) based on this concept.[65] Their attempt to form the quinoidal **1-22** failed.

---

[2] **1-10** can only be prepared if iron powder and an excess of bromine (6 eq.) are added to the reaction mixture. If 2.2 eq. of bromine are added functionalization in positions 1, 6 and 1, 8 is observed.
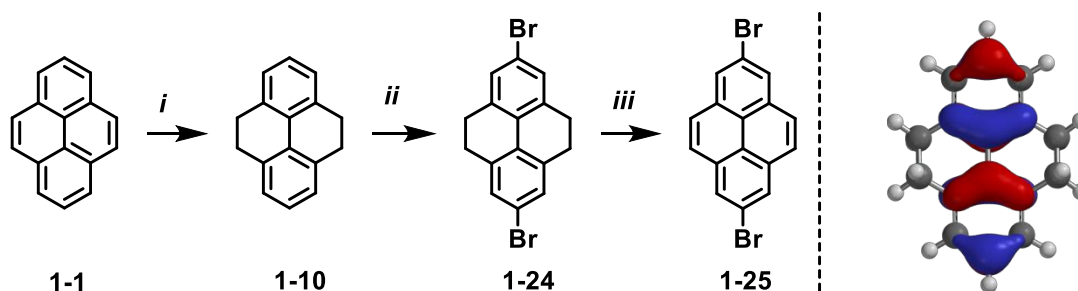
I-11: Left: 2,7-dibromopyrene (1-25) synthesis according to LEE and HARVEY.[55] i: H₂, Pd/C. ii: Br₂ / CHCl₃.
iii: Br₂, CS₂. Right: HOMO of 1-10 (DFT-B3LYP 6-31G*).

In their three step route to 2,7-dibormopyrene (**1-25**), LEE and HARVEY use the concept of the *elimination of the nodal plane*.[55] **1-10** behaves in principle like a 2,2',6,6'-tetraalkyl-1,1'-biphenyl. DFT calculations (HOMO of **1-10** shown in figure I-11) predict high frontier orbital densities in the positions attacked by the electrophile. The rearomatization can be carried out by bromine in carbon disulfide in an "*unusual method of dehydrogenation*" as the authors describe it.[55] **1-25** has been a useful building block for synthetic [68-71] and polymer chemistry.[72, 73]
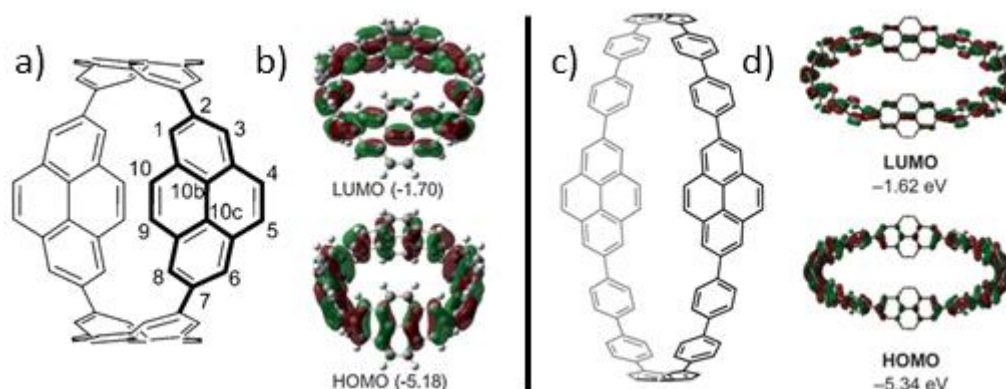
*I-12: Two cycloparaphenylenes based on 1-23. A: Structure of [4]CPY. B: Frontier orbital distribution in [4]CPY. C: Cycloparaphenylene-2,7-pyrenylene. D: Frontier orbital distribution (figure A and B adapted from IWAMOTO et al.[74] figure C and D adapted from OMACHI et al. [75]).*

A fascinating application of **1-24** was recently reported.[74] The YAMAGO group prepared a [4]cyclo-2,7-pyrenylene ([4]CPY) via a tetranuclear platinum complex with four **1-24** units. Rather surprisingly, the electronic properties of [4]CPY were very similar to those of [8]cycloparaphenylene. DFT calculations show that in [4]CPY conjugation extends over the 2,7-positions of pyrene, the nodal plane is removed. This was explained by a large quinoidal character of the pyrene moieties in [4]CPY.[74] The ITAMI group reported an cycloparaphenylene-2,7-pyrenylene that was prepared by stepwise transition metal mediated macrocyclization of **1-24** followed by a rearomatization to the final product.[76] In contrast to [4]CPY it behaved similar to a combination of hexaparaphenylene and pyrene due to weak conjugation over the nodal plane in pyrene.[75]

The 2,7-bromination of pyrene-4,5,9,10-tetraone (**1-11**) also utilizes the elimination of the nodal plane concept. This reaction is essential for this work. It gives access to 2,4,5,7,9,10-hexa-functionalized pyrene derivatives which will be discussed further in chapter *II*.[77]


1-1   **1-26**   **1-27**
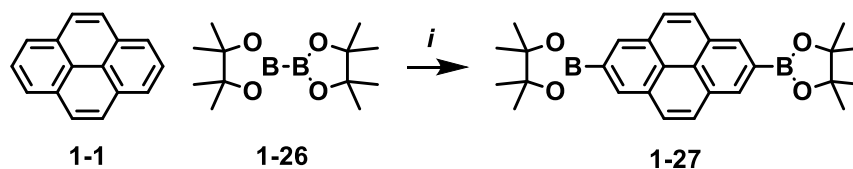
I-13: Iridium catalyzed borylation of pyrene. i:[Ir(μ-OMe)(COD)]₂, tBuBipyr, Hex. 60 °C, 24 h.

The advent of transition metal C-H activation in organic chemistry also had a significant impact on direct pyrene functionalization. COVENTRY *et al*. adapted an iridium/bipyridyl catalyst system for borylation of arenes, initially presented by ISHIYAMA *et al.[78]*, for the 2,7 borylation of pyrene.*[79]* Pyrene boronate esters (**1-27**) can thus be prepared in excellent yields. SUZUKI-MIYAURA reactions with **1-27** have been used to prepare numerous small molecules[7, 80] and polymers.[81-83] CRAWFORD *et al*. reported a series of pyrene derivatives prepared by boronate ester exchange.[84] **1-27** can further be brominated in 1,3,6 and 8 position yielding the only 1,2,3,6,7,8-functionalized pyrene derivative so far described in literature.[85] The borylation can be extended to introduce an additional boronate ester in the 4 position of **1-27**.[86]

This reaction was central in the synthesis of *Py series* OLED emitters as discussed in chapter *V*.

I.1.2.1.4   Desymmetrization of pyrene

Recently, the desymmetrization of pyrene has attracted some academic interest. In order to afford the desired functionalization pattern careful planning of the synthetic procedure is essential. Reactive positions can be chemically (de)activated either by stepwise substitution or steric blocking.

1-28   **1-29**   **1-30 R = Alyl**
   **1-31 R = Triflat**
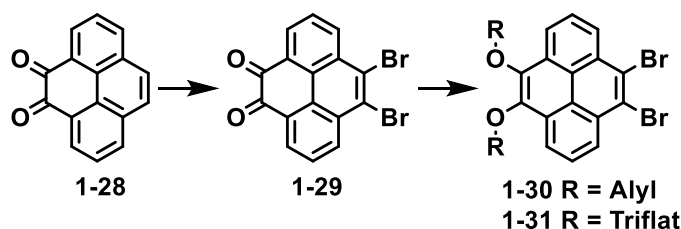
I-14: Pyrene-4,5-dione bromination according to ZÖPHEL. [87]

Starting from the pyrene-4,5-dione (**1-28**) it is possible to address the 9,10 (**1-29**) or the 1,8 (**1-33**) positions of pyrene. In **1-28** the 9 and 10 positions are activated towards

electrophilic attacks[3] and can selectively be brominated by NBS in sulfuric acid to afford **1-29**. ZÖPHEL successfully used this to prepare push-pull dyes[87] and phthalocyanines [88] based on **1-30**. Furthermore, **1-31** can be used for transition metal catalyzed cross coupling reactions to prepare 4,5,9,10-functionalized pyrene derivatives without the need for *tert*-butyl blocking units in positions 2 and 7 (see figure I-9).[89, 90]
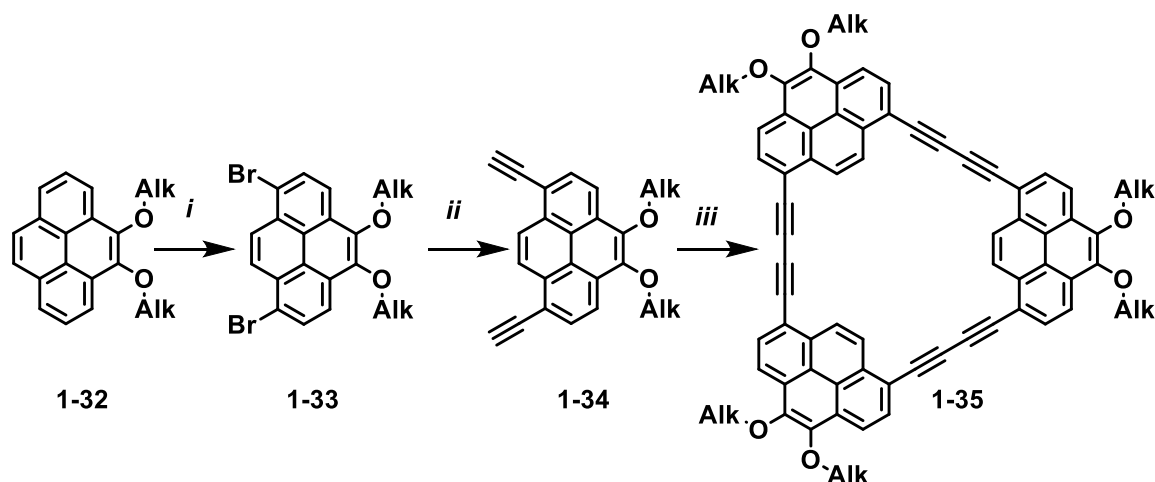
I-15: Synthesis of 1,8-pyrenylene-ethynylene macrocycles according to VENKATARAMANA *et al.*

VENKATARAMANA *et al.* showed that in **1-32** the 1 and 8 position is activated and can be brominated selectively to afford **1-33**. This was exploited to prepare a series of 1,8-pyrenylene-ethynylene macrocycles (**1-35**) by GLASER-type coupling reaction.[91]
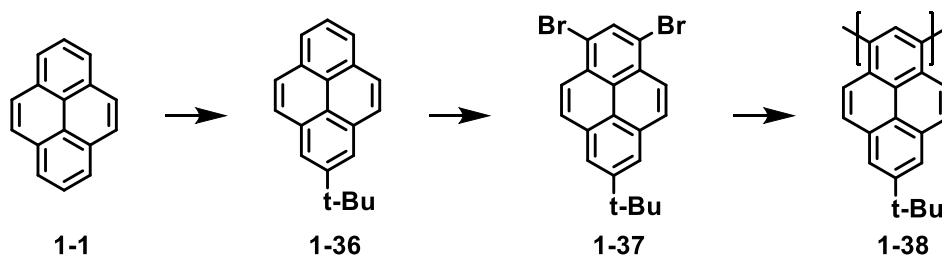
*I-16: Steric blocking strategy used to prepare 1,3-polypyrenes (**1-38**).*

Desymmetrization of pyrene is also possible by steric blockage of active positions. The *tert*-butyl group in **1-36** hinders the electrophilic attack to positions 1 and 3 to afford **1-37** selectively.[29] **1-37** proved very useful in the preparation of 1,3-poly-pyrenes for OLED applications (**1-38**). Recently, **1-37** was also used as a building block for efficient small molecule OLED emitters.[92] It can be functionalized further in the K-region by oxidation to the corresponding pyrene-4,5,9,10-tetraone[93] or selective 4,9-bromination.[94] In combination with 1,3,6,8-tetrabromopyrene dendrimers[95] and hyperbranched poly-pyrenes were prepared.[96] The BODWELL group used a similar blocking strategy to prepare 1,1,8,8-tetramethyl[8](2,11)teropyrenophane.[97]

---

[3] While the diketo-substitution in **1-30** generally deactivates the molecule, the 9 and 10 positions have a high frontier orbital contribution. Therefore, selective electrophilic substitution is possible.
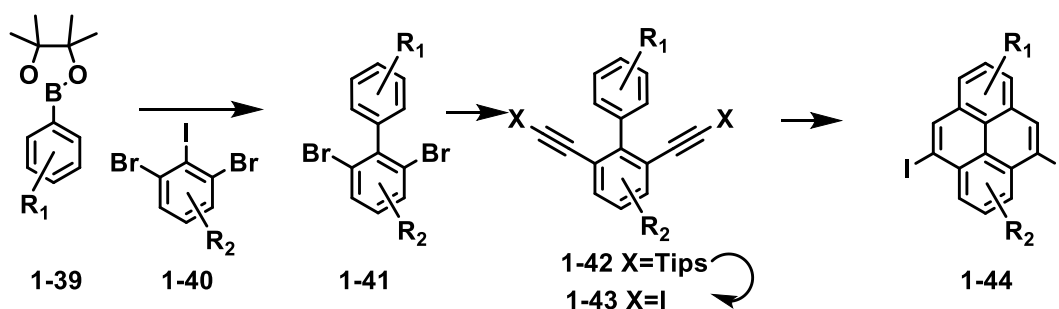
I-17: Pyrene total synthesis according to WALKER *et al.*[98]

Finally, a pyrene total synthesis as for example reported by WALKER *et al.* can provide access to non-symmetric pyrene derivatives.[98] LORBACH *et al.* used a similar strategy to prepare a series of 4,10-functionalized pyrenes with the goal to improve the reactivity of pyrenes in SCHOLL type reactions.[99]

A new non-symmetric pyrene derivative will be discussed in chapter *VI*.

I.1.2.2 Perfunctionalization of pyrene
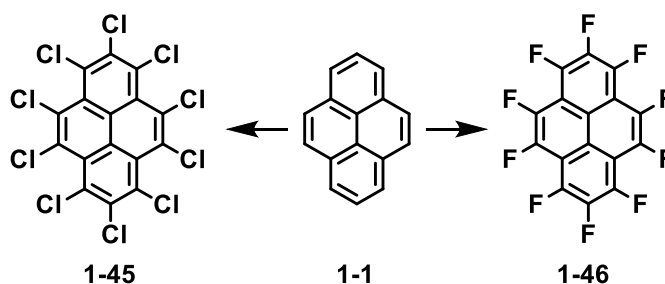
I-18: Literature reported pyrene perfunctionalization reactions.

Perhalogenation reactions are a synthetic approach to 1,2,3,4,5,6,7,8,9,10-functionalized pyrenes. Perchloropyrene (**1-45**) can be prepared from pyrene in a wet-chemical process that has also been used to perchlorinate the periphery of larger PAHs.[100, 101] In contrast, synthesis of perfluoropyrene (**1-46**) requires a specifically designed fluorination reactor set-up.[102] Alternatively, **1-46** was prepared by a halogen exchange (HALEX) process from **1-45** in the KF melt.[103]

I.2   Organic semiconducting materials

I.2.1   Historic overview

Electrical conductivity in anthracene crystals was initially reported by KOENIGSBERGER and SCHILLING in 1910.[104] For semiconductor application organic materials were first considered with the observation of electroluminescence of single crystalline materials in the mid-1950s to the mid-1960s. High driving voltage and the limited availability of organic single crystals restricted the practical use of these findings.[105, 106] In the following decade the research focus shifted to the field of conducting polymers. By doping polyacetylene the first organic materials with metallic conductivity were presented.[107-109] The 1980s saw the advent of organic thin-film technology.[110] Thus, (cost-)efficient fabrication of organic light emitting diodes (OLEDs), organic field effect transistors (OFETs)[111, 112] and organic photovoltaic cells (OPVs) became possible.[113, 114] Inorganic nanoparticles were intensively studied in the 1990s and are of high interest to this day e.g. in dye sensitized solar cells (DSSCs).[115-118] Recently, developments split into two main directions. *Conjugated polymers* are a current topic of academic polymer research.[119-121] They can be processed from solution which enables low cost processing e.g. by ink-jet or roll-to-roll printing.[122] So far, printed electronics have enjoyed only limited industrial success due to low reproducibility.[123] *Small molecules* based organic electronics is a current topic of organic chemistry.[124] Higher reproducibility due to easier materials purification led this academic field to quick industrial success. Industrial scale production of hand-held (monochromatic) device displays started in 1997, early in the new millennium the first full color displays were mass produced. In 2013 OLED based television sets have become available.[125] The discovery of isolated graphene sheets by GEIM and NOVOSELOV in 2005[126] (Nobel Prize in 2010), a material's outstanding physical properties, gave a new direction to the academic field of organic electronics.[127-129]

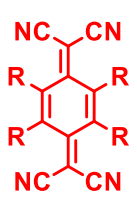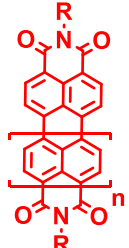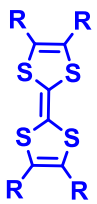## I.2.2   Electron deficient / electron rich organic materials
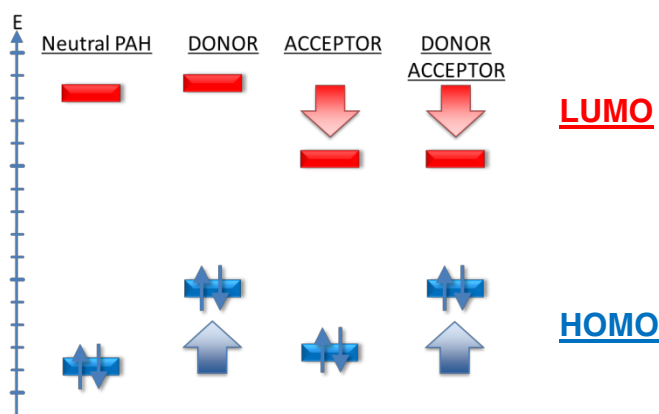
I-19: Schematic energy level diagram of organic materials (blue: HOMO, red: LUMO).

Generally speaking, donors provide energetically high lying occupied molecular orbitals (HOMO). Thus, oxidation of these compounds is easy as they are prone to donate electrons. Acceptors on the other hand provide energetically low lying unoccupied molecular orbitals (LUMO). Accordingly, these molecules are readily reduced as they are prone to accept electrons. Figure I-19 gives a schematic donor-acceptor compound. The energetic proximity of the high lying (donor) HOMO and the low lying (acceptor) LUMO results in a reduced energy gap. In case of a donor-acceptor complex the band-gap of the new material is significantly reduced compared to the pure components (*vide infra*).[130]

I.2.2.1   Classical donors and acceptors in organic electronics

For the past twenty years interest in electron acceptors mostly stems from the field of organic electronics.[131-133] Some typical donors / acceptors and their use in the field of organic electronics are collected in table I-1. For the sake of brevity only a few representative examples are given.

Table I-1: Typical acceptors (drawn in red) and donors (in blue) and their use in organic electronics.

	TCNQs	Rylenes	Fullerenes	Tetrathia-fulvalenes	Triphenylamines
OLED - Charge transport					+++
OLED - Dopant	+++	+			
OPV - Bulk heterojunction	+	+	+++	+	+
OFET - Active layer	++		+	+	+

With the advent of organic electronics these new donors and acceptors attract considerable scientific and industrial interest. Weak donors (e.g. functionalized triphenylamines) are frequently used as hole-transport materials (HTL) and weak acceptors (e.g. oxadiazoles or pyridines) as electron-transport material (ETL).[134-136] The need of dopants for charge transport layers in OLEDs is a significant driving force in the search for new strong donors and acceptors.[133, 137] They are also utilized as injection layers in work-function tuning of metal electrodes.[138] Small molecule acceptors (e.g. fullerenes, rylenediimides[139] or (sub)phthalocyanines[140]) are indispensable for bulk-heterojunction solar cells.[114, 141] Depending on the choice of the active material (donor or acceptor), field effect doping can generate (varying amounts) of p- or n-type charge carrier in OFETs (p-type or n-type).

Typical examples for p-type OFET materials are thia- and seleno-fulvalene derivatives.[142] Rylene dyes[143] and TCNQ derivatives are used in n-type OFETs.[144, 145]

I.2.2.2   TCNQ type acceptors

For organic electronic applications tetracyanoquinodimethane (TCNQ) or one of its derivatives are frequently utilized, as indicated in table I-1. The quinoid structure of this class of materials makes them exceptionally well suited for uptake of one or even two electrons from their (electron rich) environment in single electron transfer (SET) steps. While oxidizing its redox partner, the TCNQ derivative is reduced; in the first step to a stable radical anion TCNQ$^{-\bullet}$and in the second to the dianionic structure TCNQ^{2-} (see figure I-20).
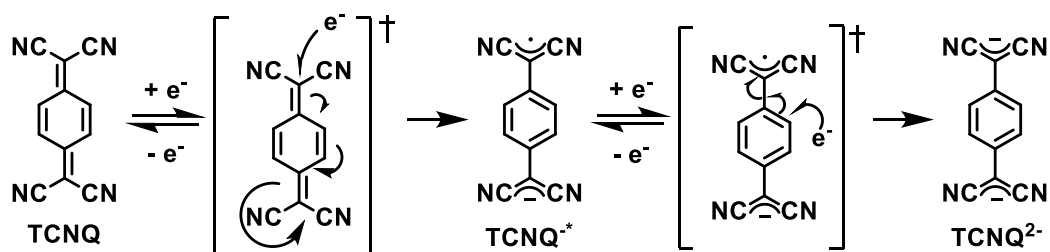
I-20: Two step single electron reduction of TCNQ to TCNQ^{2-} (adapted from [146]).

The radical anion TCNQ$^{-\bullet}$ is stabilized by the high electron affinity of dicyanomethylene as well as the re-formation of an aromatic system and its stabilization energy. Rearomatization as a means to stabilize the reduced species after electron uptake is generally applicable to quinoidal organic molecules. As a consequence of their chemical usefulness, a large variety of quinoidal dicyanomethylene derivatives has been prepared (some examples are shown figure I-21).[147-151]
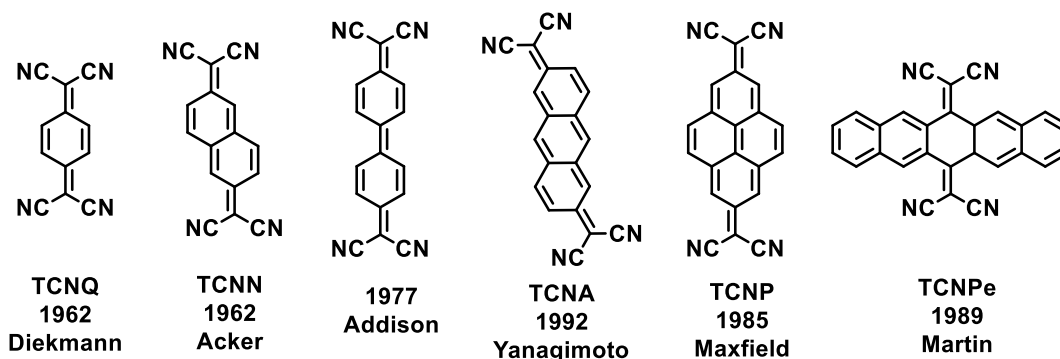
I-21: TCNQ derivatives with extended π-systems.

As shown in figure I-21 it was attempted to enlarge the parent aromatic system in TCNQ derivatives. It was expected that, by enlarging the π-system of the acceptor, its π-π-interactions in charge-transfer complexes would improve and that new organic metals could be developed.[152, 153]

I.2.3   Charge-transfer complexes
(donor-acceptor complexes)

According to the *IUPAC Compendium of Chemical Terminology, 2nd ed*. a charge-transfer complex[4] (CT-complex) is:

> *"An electron-donor–electron-acceptor complex, characterized by electronic transition(s) to an excited state in which there is a partial transfer of electronic charge from the donor to the acceptor moiety."*[155]

This definition summarizes several important facts about charge-transfer complexes. In order to make a CT-complex an electron rich donor and an electron deficient acceptor moiety are needed (figure I-19).

If the donor and the acceptor are covalently bound, charge-transfer is likely to occur within that molecule; this is called *intra*molecular charge-transfer (ICT).[156] This type of transition is for example often observed in organometallic complexes between the metallic center and a ligand (MLCT).[157] One prime example is the *Z907* dye[5] frequently used in DSSCs.[158, 159] While the ICT has experienced an outstanding amount of attention in the field of organic electronics, this work is not concerned with this type of CT-interactions.

Instead, the focus lies on the *inter*molecular charge-transfer phenomena. CT-complexes are formed between a (small molecule) donor and an acceptor. Upon contact, an electron is partially or fully transferred from the donor to the acceptor. They form a (weakly) bound D/A dimer. Charge-transfer complexes are characterized by a broad, featureless band in the absorption spectra. The shape of the band is a consequence of the spatial arrangement of donor and acceptor which can undergo strong fluctuations in solution.[160]

In the solid state two donor-acceptor arrangements are generally distinguished: alternating stacks[6] and segregated stacks (figure I-22). Probably the best known examples of donor-acceptor complexes are TTF-TCNQ[7] and $(TMSTF)_2$-PF_6[8].[161] In its crystalline state TTF-TCNQ adopts a segregated stack arrangement. This packing confers a high electrical conductivity on the crystals. This material is commonly referred to as the first *organic metal*.[132] The conductivity is highly anisotropic, along the packing axis it is as high as $\sigma_\parallel = 400 \pm 100$ $(\Omega\ cm)^{-1}$ (at RT). Perpendicular to this axis the conductivity is by orders of magnitude lower.[162] Along the packing axis the electrons are located in the acceptor stack,

---

[4] In the chemical vernacular the termini donor–acceptor complex and CT-complex are used interchangeably. Yet, the term donor–acceptor complex is also used to refer to LEWIS acid/base adducts or in biochemistry for hydrogen bond molecular complexes .[154]
[5] (cis-di(thiocyanato)bis(2,2-bipyridyl-4,4'-dicarboxylate) ruthenium(II))
[6] Also known as mixed stack.
[7] Tetrathiofulvalene / tetracyanoquinodimethane.
[8] Tetramethyl-tetraselenafulvalene - phosphorus hexafluoride

whereas (electron-)holes are located within the donor stack. Thus, both charge carriers can move freely along this axis resulting in high conductivity. Perpendicular to the packing axis, charge carriers are not free to move, but must hop from stack to stack.[162] This discovery sparked massive academic interest in the field and a large number of fulvalenes and quinodimethanes was studied.[152, 153] In 1980 this led to the discovery of the first organic superconductor $TMTSF_2-PF_6$. The field of organic conductors and organic superconductors was recently reviewed by ISHIGURO, YAMAJI and SAITO.[163]

Segregated stack	Alternating (mixed) stack
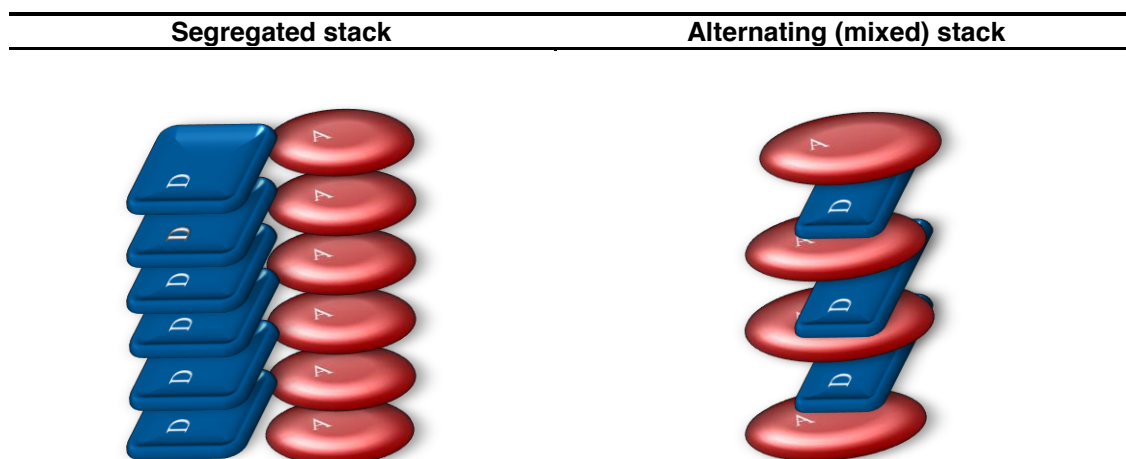
I-22: Typical donor-acceptor arrangements in the solid state. Blue squares symbolize donors, red ovals symbolize acceptors.

The alternating stack arrangement is more often found for CT-complexes in the solid state.[164] MAYERLE *et al*. devised a frontier orbital argument to predict whether segregated or mixed stack arrangement is probable.[165] They state that opposite orbital symmetries of the donor and the acceptor will diminish the donor-acceptor interaction in an eclipsed arrangement. Thus, if no other donor-acceptor overlap is possible, a segregated stack arrangement will be adopted. Furthermore, they state that for neutral solids (i.e. non-ionic CT-complexes) the charge-transfer stabilization in a segregated stack is very low, thus a mixed stack arrangement is likely to be adopted. In this arrangement charge carriers are strongly localized and not free to move along the stacking axis. Movement along this axis would rather lead to a recombination of opposite charges.

Yet, under certain circumstances CT-complexes in the alternating stack arrangement can give a mixed valent state.[166] Upon an external stimulus (pressure and/or temperature) the complex undergoes a neutral/ionic transition (NI), i.e. changes from an uncharged (A^0,D^0) to a charged radical state (A^-,D^+ $s = \frac{1}{2}$) or *vice versa*.[167] It is noteworthy that the NI is a collective CT-process of the whole crystal. This transition is accompanied by a significant change in electronic conductivity.[168] The TTF – *p*-chloranil system was the first reported example possessing an NI transition.[166] As this transition can be triggered by external stimuli it is highly interesting as a nano-scale switch.

The so called TORRANCE plot (figure I-23) gives a guideline for which CT-complexes the mixed valent state can occur.

$$I_P - E_A = \alpha C = M$$
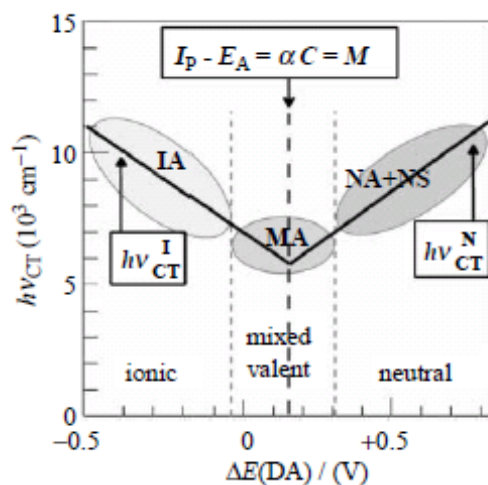
I-23: TORRANCE plot [figure adapted from SAITO and MURATA[168]].

TORRANCE *et al*. found that for CT-complexes with a HOMO$_{Donor}$/LUMO$_{Acceptor}$ energy gap $\Delta E_{(DA)} = 0 - 0.5$ V and a CT-band maximum between $\lambda \approx 1200$ nm and $\lambda \approx 1800$ nm (near-IR region) a mixed valent state may occur.[169]

In the framework of the *Sonderforschungsbereich-Transregio 49* (SFB/TR 49) new charge-transfer complexes containing a pyrene donor were investigated. The neutral/ionic transition was one property studied. This work will be discussed in chapter *IV*.

I.3   Organic light emitting diodes (OLEDs)

Organic light emitting diodes (OLEDs) have been the driving element in the development of organic electronics. In their wake OPV and OFET technology developed.[136] Research now reached a point at which large scale industrial production of OLEDs for display application has become possible. Current OLED display technology was reviewed by KWON *et al*. in 2013.[170] OLEDs are further investigated for lighting applications.[134, 171] While technology samples do exist since 2008, this technology is evolving at a slower pace.[172]

I.3.1   The operational principle
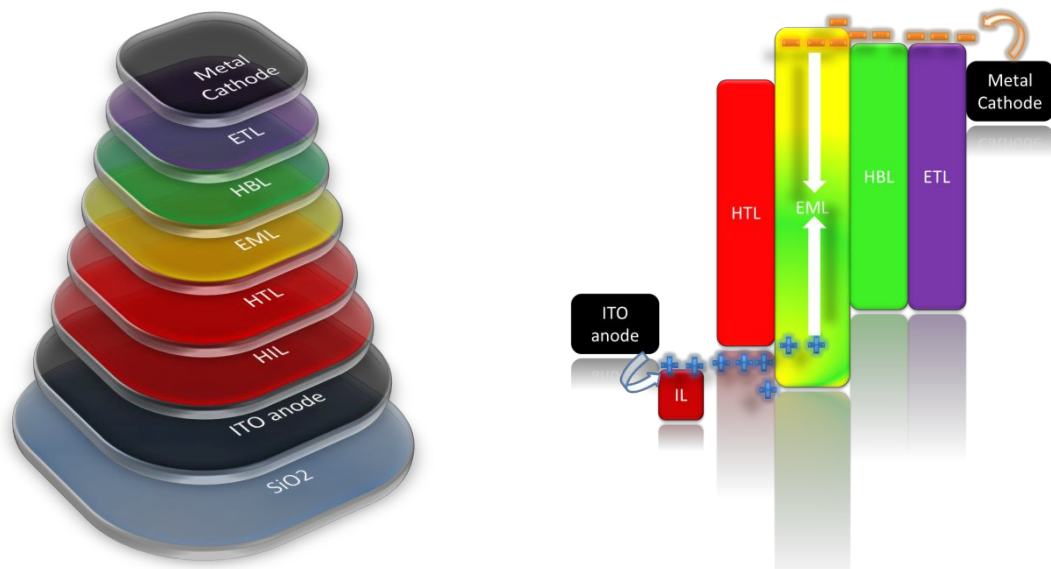
I-24: Left: Schematic OLED device architecture (not drawn to scale). Right: Working principle. Black: Electrodes. IL (deep red): Hole injection layer. HTL (red): Hole transport layer. EML (yellow): Emissive layer. HBL (green): Hole blocking layer. ETL (purple): Electron transport layer.

The components and the working principle of an OLED are illustrated in figure I-24. In a typical device a thin layer of indium-tin-oxide (ITO) is deposited as transparent electrode on a glass substrate. On top of ITO a hole-injection-layer (HIL) and a hole-transport-layer (HTL) are deposited. The emissive layer (EML) is then followed by a hole blocking layer (HBL) and the electron transport layer (ETL). All is covered with a reflective metal cathode. The HBL (often combined with an electron BL) is aimed at confining the generated exciton in the EML.

When a current is applied to the OLED, electrons (holes) are injected at the cathode (anode to the HIL) and carried by the ELT (HTL) to the emissive layer. In the EML hole and electron recombine to form an excited state (exciton) that can decay to the ground state under the emission of a photon (figure I-24 right). During this process it is three times more likely to generate a triplet (T_1) over a singlet exciton (S_1).[173, 174] In OLEDs with

traditional fluorescent emitters this poses a severe limitation. Only 25 % of the electrical excitation energy can be harvested for fluorescence. The energy "*trapped*" in triplet states slowly dissipates in the form of heat. This limitation is typically circumvented by the use of phosphorescent emitter materials. Commonly, platinum group metal complexes with very strong spin-orbit coupling are used. These materials provide very high phosphorescence quantum yield. Fast ISC minimizes losses due to fluorescence deactivation. Therefore, 100 % of the electrical energy can be used for light generation. The stability of blue phosphorescent emitters is still insufficient for technological applications. Hence, blue fluorescent materials are used in commercial products.[170] Recently, fluorescence mechanisms (e.g. thermally activated delayed fluorescence TADF and triplet-triplet annihilation TTA) that allow the harvesting of triplet states have attracted significant academic interest.

I.3.2 Efficiency of OLEDs

The external quantum efficiency η_{EQE} is the ratio of emitted photons to the number of injected charge carriers (either hole or electron).

Therefore, η_{EQE} can be expressed in terms of the PL quantum yield ϕ_{PL}:[175]

$$\eta_{EQE} = \gamma \times \chi \times \phi_{PL} \times \xi \qquad\qquad (I-3)$$

Eq (I-3): γ denotes the charge balance factor, χ the exciton spin factor, ϕ_{PL} the PL quantum yield, ξ the out-coupling efficiency.

The charge balance γ describes the probability that an injected charge carrier finds a carrier with opposite polarity and forms an exciton. In a balanced device $\gamma = 1$. If the device uses a fluorescent emitter exciton spin factor $\chi = 0.25$, in the case of a phosphorescent emitter $\chi \approx 1$. The out-coupling efficiency ξ gives the number of photons that are able to leave the device instead of being trapped in either the glass or organic mode.

In an OLED device as illustrated in figure I-25 light is reflected on the ITO/glass and glass/air interface, leading to a glass mode (1) and an organic (total reflection) mode (2). ξ is usually considered to be ≈ 20 % following the works of GREENHAM *et al.*[176]
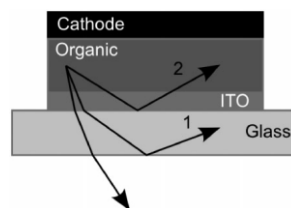
I-25: Internal reflection on the air/glass and glass/organic interfaces [figure adapted from MEERHEIM et al.].[177]

In a hypothetical electronically balanced ($\gamma = 1$) OLED using a fluorescent emitter ($\chi = 0.25$) with $\phi_{PL} = 1$ and an out-coupling efficiency $\xi = 0.2$:

$$\eta_{EQE} = 1 \times 0.25 \times 1 \times 0.2 = 0.05 \qquad \text{(I-4)}$$

The maximum EQE for such a device is $\eta_{EQE} = 5\ \%$.

The luminous efficacy η_p gives a relationship between the energy of the injected charge carriers and the energy of the emitted photons. It is usually reported in photometric quantities, i.e. measured by the sensitivity of the human eye.

$$\eta_p = \eta_{EQE} \times \frac{\overline{h\nu}}{eV} \qquad \text{(I-5)}$$

Eq. (I-5): h*ν gives the average energy of an emitted photon, e*V the energy of an injected charge carrier.

Modern high performance OLEDs reach $\eta_p > 100$ lm/W, similar to fluorescent light bulbs.[178]

I.3.3   Thermally activated delayed fluorescence (TADF)

Thermally activated delayed fluorescence (TADF) is a unimolecular fluorescence mechanism. Excitation energy is transferred from the triplet to the singlet manifold by thermal activation and is then dissipated as fluorescence.[179] This mechanism requires a small singlet-triplet energy difference ΔE_{ST}, long lifetime of the triplet state and a modicum of thermal energy. Strong TADF is for example observed in the fullerenes C_{60} and especially C_{70}.[180] In their landmark publication ADACHI *et al.* (2011) demonstrated that TADF can be exploited in organic light emitting diodes.[181]
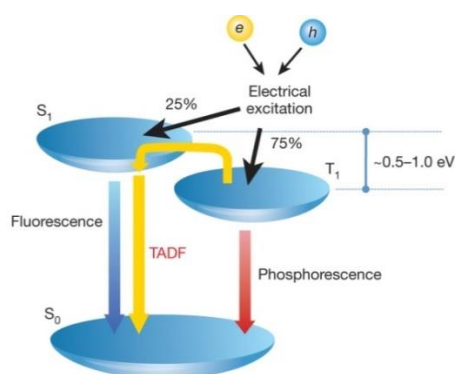
I-26: Schematic representation of TADF mechanism (yellow pathway) [figure adapted from UOYAMA et al.[182]].

In a first step the OLED's electrically populated S_1-state relaxes under fluorescence to the ground state S_0. Subsequently, $S_1 \leftarrow T_1$ reversed inter system crossing (RISC) repopulates the S_1-state which, in turn, relaxes under fluorescence to the ground state. The second process is considerably slower than regular fluorescence (thus *delayed* fluorescence). The

RISC has to occur from a high vibrational state within the triplet multiplicity, which is reached by thermal activation. Therefore, the designation thermally activated delayed fluorescence. The RISC is a forbidden process according to the spin selection rule and as such not likely to happen. In consequence transfer rates are usually quite slow so radiationless deactivation (ISC followed by vibronic relaxation) is a competing mechanism.

First Generation Emitter   **Second Generation Emitter**
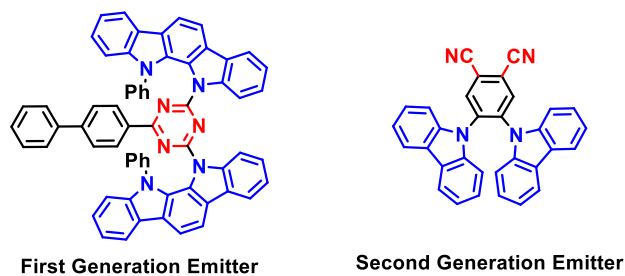
I-27: Two TADF chromophores for OLEDs reported by ADACHI group. The donor moiety is colored blue, the acceptor red.

In their first publication ADACHI *et al.* reported 30 % RISC and 70 % radiationless deactivation from the excited triplet state. The external fluorescence quantum yield is given with η_{EQE} = 5.3 %.[181] In just under two years of research the group was able to prepare working OLED devices based on TADF with an external quantum yield of η_{EQE} = 19.3 ± 1.5%.[182] Assuming an outcoupling efficiency of ξ = 20 to 30 % the internal electroluminescence quantum yield reaches 64.3–96.5 %.[183, 184]

In their 2011 publication it was suggested that the energy difference between S_1 and T_1 should be ΔE_{ST} < 0.5 eV in the chromophore to enable efficient TADF. To achieve this goal, the use of donor-acceptor chromophores was encouraged. In a later publication they reported a ΔE_{ST} < 0.1 eV in combination with a high radiative decay rate (>10^6 s^{-1}). This made it possible to suppress non-radiative deactivation processes.

In their molecular design they used a rigid, conformationally locked molecule (to suppress non-radiative deactivation) with a push-pull arrangement (orbital partitioning to reduce ΔE_{ST}). In the first generation chromophore 1,3,5-triazine was used as acceptor and N-phenyl-indolocarbazole as donor (figure I-27). The phenyl substituent on the donors ensures twisted molecule geometry for efficient orbital partitioning. In the recent design dicyanobenzene was used as acceptor. It was argued that this further suppresses the non-radiative decay. Additionally, it induces a change from S_1 to T_1 geometry which, in turn, ensures high fluorescence quantum yields.[182] Significant academic interest has recently arisen in this topic.[185, 186]

An alternative process of harvesting the energy of triplet states generated during electric excitation in OLEDs is triplet-triplet annihilation (TTA). In this bimolecular process two triplet states interact to give an S_1 and S_0 state.[187] The high energy S_1 state can decay to

the ground state by fluorescence. This mechanism has also been exploited in highly efficient fluorescent OLEDs.[188, 189] LUO and AZIZ investigated a series of host:guest emitter OLEDs. They found that TTA can play an important role in the OLED and contributes significantly to the EQE.[190] MONKMAN recently reviewed this research field.[191]

In chapter *V* the design, synthesis and characterization of low ΔE_{ST} chromophores for TADF OLED emitters is discussed.

I.4   Objects and motivation

In this work, synthetic approaches to highly functionalized pyrene derivatives will be explored. On the basis of K-region oxidation the selective functionalization of the 2 and 7- or 1,3,6 and 8 positions was investigated. The extension of the K-region has been comprehensively studied before.[63] Yet, only few works investigate the functionalization of the pyrene scaffold.[77, 89, 192]
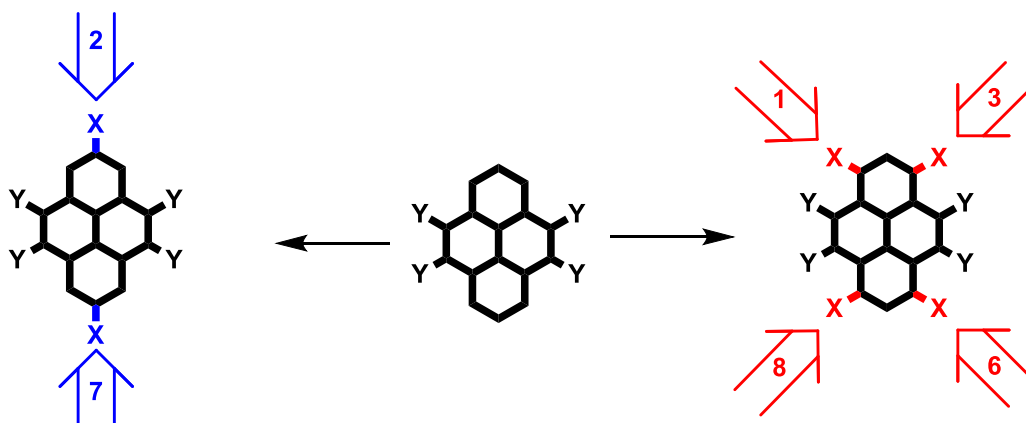
I-28: Schematic illustration of pyrene functionalization patterns investigated in this work.

The functionalization of positions 2 and 7 aimed at the synthesis of new pyrene based acceptors. Quinoid structures are excellent for accepting electrons. Thus, it was planned to prepare exceptionally strong acceptors by introducing a quinoidal structure to pyrene-4,5,9,10-tetraone. According to quantum chemical calculations these materials are among the strongest acceptors reported. While 2,7-functionalized pyrene acceptors have been reported in literature (figure II-3) the functionalization of pyrene-4,5,9,10-tetraone (an electron deficient molecule in its own right) will give a significantly stronger acceptor. K-region functionalized pyrenes can also serve as useful building blocks for extended PAHs as shown by WASSERFALLEN[193] and later ZÖPHEL.[89] Yet, the versatility of 2,4,5,7,9,10-functionalized pyrenes to prepare extended PAHs was so far overlooked.

In addition to the 2,7-functionalization a 1,3,6,8-functionalization of K-region substituted pyrene was investigated. A few examples of 1,3,4,5,6,8,9,10-functionalized pyrene derivatives are known in the literature (as discussed in section *III-1*). The route of ZÖPHEL *et al.* has some flexibility in the non-K-region substitution (1,3,6,8), yet it is limited to phenyl substituents in the K-region. The synthetic approach according to ALONSO-MATEO *et al.* on the other hand, shows great flexibility in the terms of K-region substitution but is limited to alkyl chains in the non-K-region positions. In this work a fully flexible functionalization route was sought after. It was panned to get an access to non-quinoidal strong acceptors as well as new electron donors. The sheer number of substituents on the pyrene scaffold enables tuning of the frontier orbital energies. New donors prepared by this

approach give the opportunity to prepare new charge-transfer complexes with tailored band gaps and electron transfer.

From a materials chemistry viewpoint three main topics are addressed in this work:

- The synthesis of strong acceptors based on the pyrene scaffold by quinoidization or functional group modification.

- Preparation of electron rich pyrene derivatives for complexation with acceptors in charge-transfer salts.

- Provision of new OLED emitter materials harvesting triplet states via TADF.

As discussed in chapter *I.2.2* organic acceptor molecules find broad application in organic electronics.[133, 194-196] Being a relatively electron deficient molecule from the outset ($E_{HOMO} \approx -3.9$ eV), pyrene-4,5,9,10-tetraone (**1-8**) is an excellent starting point for the synthesis of stronger acceptors. The works of KAWANO[77] and MATEO-ALONSO[63] show that functional group modifications are well suited to adjust the energetic position of the LUMO. Based on the work of KAWANO as well as the diploma thesis of this author[197] **1-8** was chosen as a starting point for the synthesis of strong acceptors.

Charge-transfer phenomena are central to any organic electronic application. Charge-transfer salts can be used as models to study these processes. Yet, they also have interesting physical properties in their own right. Certain charge-transfer complexes have conductivities approaching that of metals while others are MOTT-type insulators[9] that can be switched to a conductive state by external impetus (chapter *I.2.3*). In the context of the *Sonderforschungsbereich Transregio 49* (SFB/TR49) new charge-transfer complexes were investigated.

As OLEDs enter the consumer market for display applications, basic research is still very much needed. The works of ADACHI prove that novel OLED working principles can still be developed.[181] TADF holds great promise to significantly increase the efficacy of OLEDs without the need of transition metal complexes. As especially blue electroluminescence is still problematic, the attention of this work was directed towards the synthesis of new blue TADF emitter materials. As part of the *International Research Training Group 1404 (IRTG 1404)* not only the chromophore design and synthesis was conducted in this project. In collaboration with the group of Prof. J. J. KIM of Seoul National University, Korea also the characterization and OLED device fabrication were investigated. In the course of this investigation two molecular designs have been tested.

---

[9] A material that should be conductive according to the standard band model of conductors, but behaves like an insulator due to strong local electron correlations.[198]
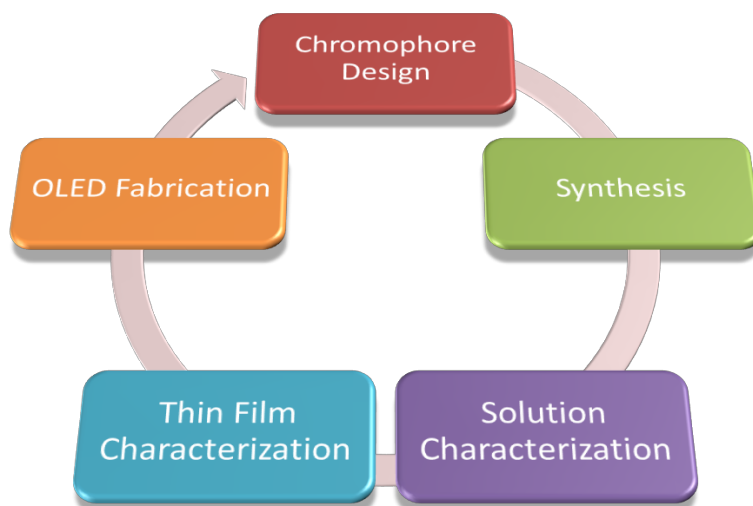
I-29: Chromophore optimization process.

The combination of chromophore design, synthesis and solid state characterization in this study allows the selection of the more promising emitter structure over the other. From this, 2,7-pyrene derivatives (*Py series*) emerged as the superior materials. To minimize the singlet-triplet energy gap ($\Delta E_{S1 \to T1}$), the triplet state is destabilized by orbital partitioning. For this, the nodal plane in pyrene is utilized in combination with an *m*-phenylene bridge. This project is discussed in chapter *V*.

II.   Functionalization of pyrene in positions 2 and 7

The targeted functionalization of pyrene is, to this date, a challenging topic for current research. In chapter *I.1.2.1* selected synthetic approaches to new substitution patterns have been presented. The route of KAWANO *et al*. allows the introduction of six functional groups in only two synthetic steps starting from pyrene.[77]

II-1: Two step route for sixfold functionalization of pyrene. i: RuCl₃, NaIO₄, MeCN, CH₂Cl₂ 4 h. ii. NBS (2-3a) or NIS (2-4) H₂SO₄, RT, 16 h.

What makes this strategy even more remarkable is the fact that the positions addressed in this route are the less (4,5,9 and 10) and least reactive (2 and 7) positions of pyrene.

As indicated in section *I.1.2.1*, pyrene-4,5,9,10-tetraone (**2-2**) does not behave like pyrene, but rather like a biphenyl system with electron withdrawing substituents. Thus, positions 2 and 7 become viable for electrophilic attacks. As **2-2** is rather electron deficient a strong electrophile is needed to attack the substrate. RAJESH *et al*. reported the use of superacids (e.g. conc. sulfuric acid, trifluoromethanesulfonic acid) to enhance the reactivity of

N-bromosuccinimide. The electrophilicity of the reagent is improved due to protonation of the succinimide.[199, 200] Furthermore, protonation of the substrate **2-2** will increase the solubility, thus assisting in the reaction. Hence, bromination or iodination (by using N-iodosuccinimide) of **2-2** is possible as reported by KAWANO *et al.*[201]

2-5 has been an essential building block for the diploma thesis of CHERCKA.[197] Based on this it was possible to prepare 2,4,5,7,9,10-hexamethoxypyrene (**2-6**) by ULLMANN-type reaction and diphenylamine derivatives (**2-7**) by BUCHWALD-HARTWIG amination.[77]
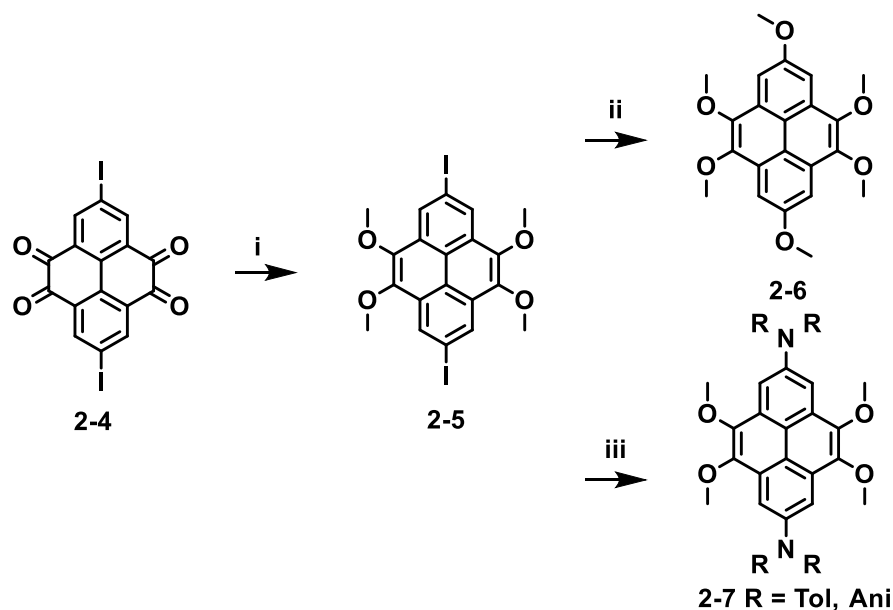
II-2: Representative synthesis based on **2-5**. *i: NIS, H₂SO₄, 40° C 4 h 30 %. ii: NaOMe, CuI, DMF, 75°C, 55 %. iii: R₂NH, XPhos, Pd₂DBA₃ NaOtBu, Tol, 100 °C, 16 h, 70-85 %.*

In continuation of this work, the synthesis of 2,4,5,7,9,10-functionalized pyrene-based acceptors and donors for organic electronics was explored.

In section *II.1* approaches towards quinoidal pyrene derivatives will be discussed. Electron rich molecules based on **2-5** will be discussed in chapter *II.2*.

II.1   Electron deficient materials

II.1.1   Target structure and theoretical calculations

The quinoidal pyrene derivatives **2-8** and **2-9** were designed as strong acceptors. 2,4,5,7,9,10-hexaketopyrene (2-9) is an extension of the pyrene-2,7-dione (**1-22**) investigated by BOLDT.[65] In contrast, target structure **2-9** is the 4,5,9,10-tetraketoderivative of tetracyanoquionopyrene (TCNP).
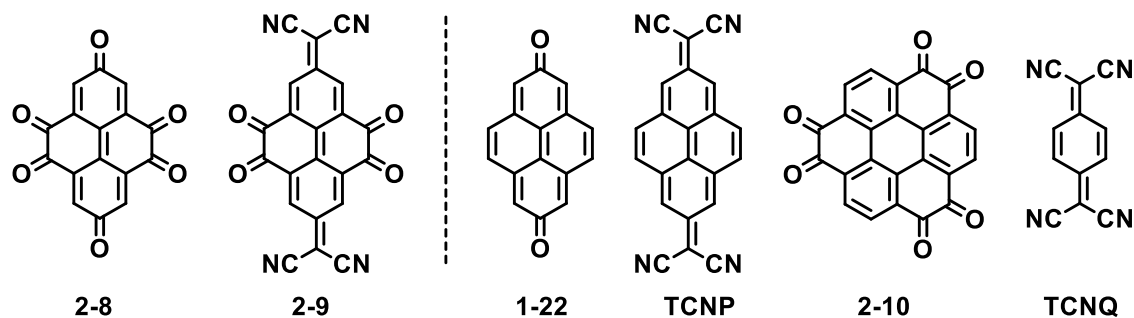
II-3: Target structures (left) and acceptors used for comparison (right).

Theoretical calculations of the frontier orbital energies (DFT, B3LYP, 6-311G*) provide a basis to compare the tetraketone target structures (**2-8** and **2-9**) to **1-22**, **TCNP**, **2-10** and TCNQ.

*Table II-1: Calculated frontier orbital energies of acceptors (DFT, B3LYP, 6-311G*).*

Compound	$E_{(HOMO)}$ (eV)	$E_{(LUMO)}$ (eV)
2-8	-7.51	-4.94
2-9	-7.03	-5.54
1-22	-6.34	-4.04
TCNP	-6.26	-4.93
2-10	-7.39	-4.29
TCNQ	-7.33	-4.82

According to these calculations (table II-1), **2-8** and **2-9** are outstanding acceptors. The LUMO energy of **2-8** is lowered by 0.9 eV compared to that of the pyrene-2,7-dione (**1-22**). A similar effect of the K-region oxidation is observed between **2-9** and **TCNP** (ΔE_{LUMO} = 0.61 eV). Referenced to **2-9** / TCNQ the LUMO is 0.65 eV /0.12 eV (**2-8**) and even 1.25 eV /0.6 eV (**2-9**) lower in energy . The higher LUMO energy of **2-9** in comparison to **2-8** can be attributed mostly to the quinoidal structure of the molecule. In **2-9** three of the six aromatic rings are still intact, a fully quinoidal backbone is not formed. In **2-9** the stronger EWG (dicyanomethylene) further stabilizes the LUMO. Both molecules are attractive synthetic goals. The availability of **2-6** made the synthesis of **2-8** the initial target.

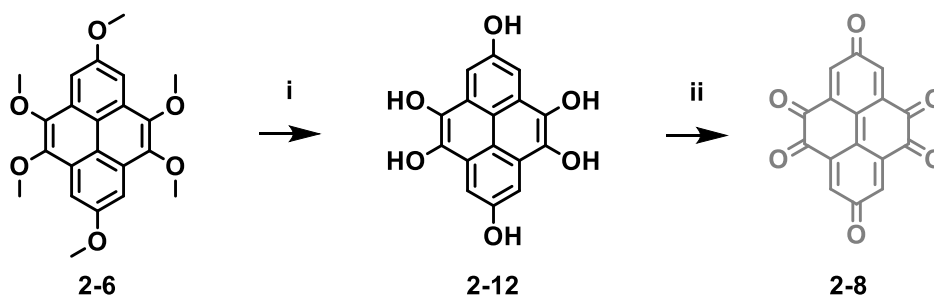## II.1.2 Deprotection of 2,4,5,9,10-hexamethoxypyrene (2-6)

RIEGER *et al*. presented an elegant coronen-1,2,5,6,9,10-hexaone (**2-10**) synthesis.[202] **2-10** was prepared in a multi-step route. The pivotal step was a *one-pot* deprotection/oxidation sequence to provide **2-11**. Methyl-ethers were initially cleaved by boron tribromide. The intermediate boronic esters were then hydrolyzed and oxidized *in-situ*. It was not possible to find a common organic solvent to prepare CT-complexes of **2-11** (D) and **2-10** (A). To

circumvent this problem a gas-phase deposition technique to prepare CT-thin films on metal surfaces was developed in collaboration with SCHÖNHENSE.[203]

2-11   **2-10**
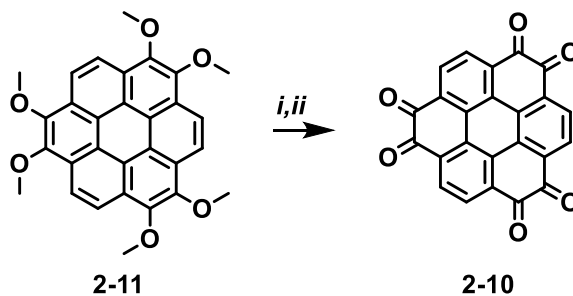
*II-4: Pivotal steps of RIEGER's coronen-1,2,5,6,9,10-hexaone (**2-10**) synthesis. i: BBr₃, CH₂Cl₂. ii: HNO₃.*

In analogy to RIEGER's coronen-1,2,5,6,9,10-hexaone synthesis the preparation of pyrene-2,4,5,7,9,10-hexaone (**2-8**) starting from 2,4,5,7,9,10-hexamethoxypyrene (**2-6**) was intended.

2-6   **2-12**   **2-8**

*II-5: Planned two step synthesis of pyrene-2,4,5,7,9,10-hexanone (**2-8**). i: Demethylation of 2,4,5,7,9,10-hexamethoxypyrene. ii: In-situ oxidation to the quinoidal target structure **2-8**.*

II.1.2.1   Attempted synthesis of pyrene-2,4,5,7,9,10-hexaone (2-8)

In table II-2 synthetic approaches to **2-8** and their outcomes are listed. With most reagents tested no conversion was observed, i.e. they were unable to cleave the methoxy ethers of **2-6**. In this chapter these reagents will not be discussed further. An extensive discussion of ether deprotection regents and mechanisms will be given in chapter *III*.

As displayed in table II-2 (entries 7 – 10) deprotection of methyl-groups is possible with hydrobromic acid in acetic acid and boron tribromide in a chlorinated solvent. When *in-situ* oxidation of **2-12** was attempted (table II-2, entries 7 and 8) it resulted in a red, insoluble solid. It was not possible to identify the desired product **2-8** within this material. NMR was not applicable due to low solubility. Mass spectrometry (FD / MALDI-TOF) showed a broad distribution of signals, mostly at m/z ratios which exceeded expectations. Powder IR bands associated with aromatic carbonyl functions ($\upsilon = 1690$ cm^{-1}) were observed; the $\upsilon = 1550$ cm^{-1} band associated with quinones was not observed.[204] This implies that decomposition and/or oligomerization reactions occurred in the reaction mixture.

Table II-2: Synthetic approaches to 2-8.

Number	Reagent	Outcome
1	TMSI[205]	No deprotection observed
2	RuCl₃ / NaIO₄ [206]	No deprotection observed
3	Ceric ammonium nitrate (CAN)[207]	No deprotection observed
5	AlBr₃[208]	No deprotection observed
5	BCl₃	No deprotection observed
6	BBr₃/Et₂S[209]	No deprotection observed
7	HBr/AcOH[210]	Complex mixture of products -> **2-8** not identified
8	BBr3/HNO₃[202]	Complex mixture of products -> **2-8** not identified
9	1 M BBr₃ in CH₂Cl₂ (commercial reagent)	Deprotection to **2-12** observed; unreliable
10	1 M BBr₃ in CH₂Cl₂, (freshly prepared)	Deprotection to **2-12**
11	2.5 eq Br₂ / CH₂Cl₂	Selective twofold demethylation; core bromination

RIEGER *et al*. utilized *in-situ* oxidation to avoid two problems: Instability of the diol-species and undesired stability of boronic ester species. A combination of both factors prevented the isolation of **2-9**. Initially, these issues were assumed to hamper the synthesis of **2-8** as well. When the *in-situ* oxidation protocol failed repeatedly an isolation of **2-12** was studied.

II.1.2.2 Isolation and partial oxidation of 2-12
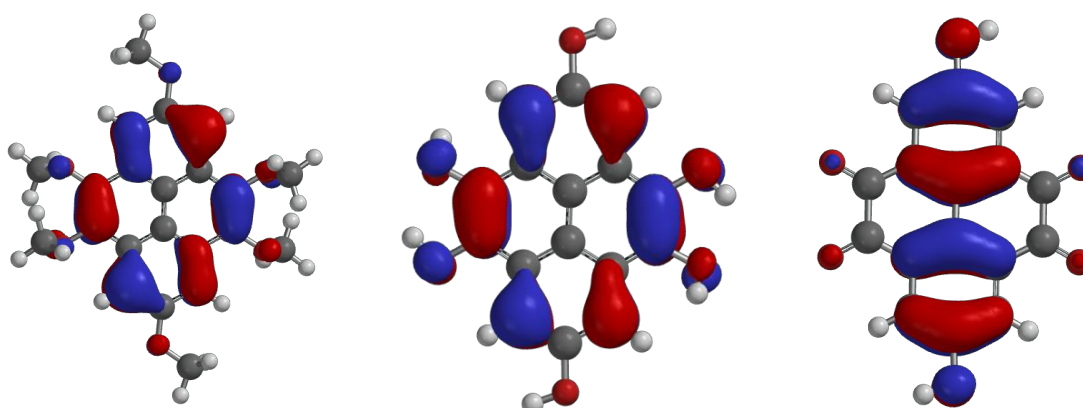
II-6: Calculated HOMO distribution in 2-6 (left), 2-12 (center) and 2-13 (right).

As stated in table II-2 (entries 9 and 10), it is possible to deprotect **2-6** when using boron tribromide. It was found that the quality of commercially available boron tribromide solution varied significantly, rendering this reaction unreliable. The best results were obtained when a 1 mol/l boron tribromide solution in DCM was prepared in the laboratory.

The reaction was stirred for 24 h and quenched by the addition of water. If the dried organic phase was isolated after phase separation, the pyrene-2,4,5,7,9,10-hexaol **2-12**

could be obtained and identified in MALDI-TOF spectrometry. Impurities resulting from BBr$_3$-substrate complexes, as reported by RIEGER, could not be removed (m/z > 320, figure II-7 inset). The compound did not tolerate chromatographic purification.
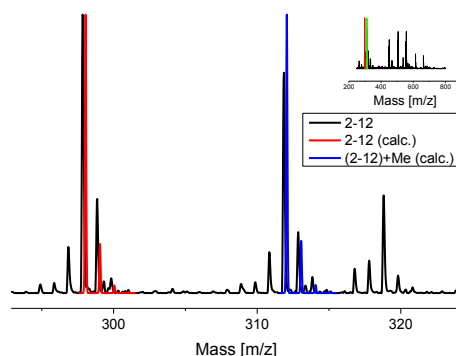
*II-7: MALDI-TOF spectrum of **2-12** (black), calculated isotopic pattern of **2-12** (red) and the calculated isotopic pattern of a fivefold deprotected side product (blue, [**2-12**+Me]). The inset shows the full spectrum (top-right). BBr$_3$-substrate complexes remain in the sample.*

In figure II-7 the dominant signal is found at m/z = 297.84 and very closely matched by the calculated isotopic pattern for **2-12** (shown in red). A second, strong signal is observed at m/z = 311.85 that fits the isotopic pattern of the monomethoxy pyrene pentaol side-product (in blue).The apparent stability of **2-12** was surprising; immediate oxidation in contact with air was expected for such an electron-rich polycyclic aromatic compound. Especially oxidation in the pyrene K-region to **2-13** was predicted.[61, 211]
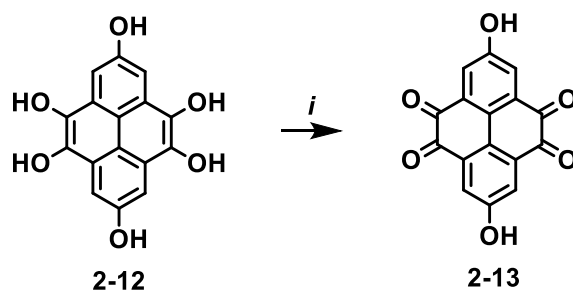

*II-8: Oxidation of **2-12** to **2-13**. i: Air, THF, RT, 48 h.*

In fact, K-region oxidation can be achieved simply by dissolving **2-12** in THF and stirring it in air for 48 h (see fig. II-8). An oxidant or oxygen transfer catalyst was not added to promote the conversion. This allows a better reaction control as well as easier purification. During oxidation a deep orange/red color arises.

The resulting MALDI-TOF spectrum is shown in figure II-9:
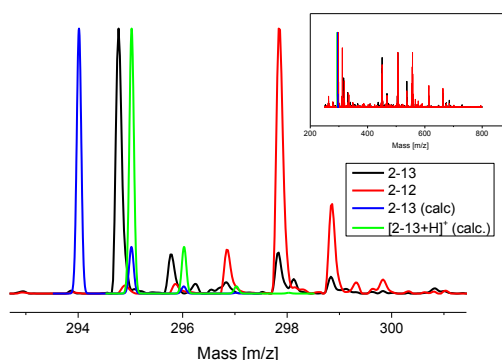
*II-9: MALDI-TOF spectra of **2-13** (black), **2-12** (red), calculated isotopic pattern of **2-13** (blue) and the calculated isotopic pattern of [**2-13**+H]$^+$ (green). The inset shows the full spectra.*

In this figure the spectrum of the oxidation product is shown in black, a strong signal at m/z = 294.78 is observed. Simulated isotopic patterns of **2-13** (in blue, m/z = 295.02) and [**2-13**+H]$^+$ (in violet, m/z = 295.02) are superimposed. The observed signal corresponds closely to the latter, suggesting the addition of a proton to the electron deficient α-diketone during ionization.[212] Abstracting an odd number of protons (i.e. three) in the oxidation step does not lead to chemically viable structures (figure II-10). **2-13** appears to be the chemically most favored isomer, due to its two resonance stabilized benzene rings. Furthermore, pyrene-4,5,9,10-tetraone is a stable compound; the K-region oxidation is quite easy. **2-14** is a quinoid system with an enediol, a unit usually prone to oxidation. **2-15** can be seen as a biphenylquinone with an unsymmetrical oxidation in the former pyrene K-region.
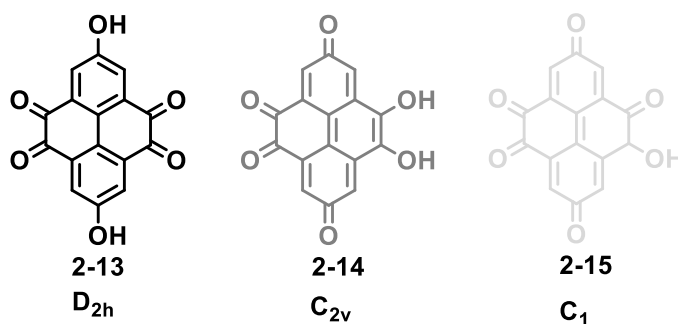

*II-10: Chemically plausible products of the abstraction of four hydrogens from **2-22**.*

The structure of the oxidation product is studied by NMR spectroscopy. Prior to these experiments, the material was purified by GPC chromatography[10], using THF as eluent due to its low solubility in less polar solvents. A simple symmetry discussion[11] will provide predictions for the ^{1}H-NMR spectrum of each isomer. **2-13** has D$_{2h}$ symmetry, hence two ^{1}H-NMR signals are expected. In contrast to this, for **2-14** (C$_{2v}$) three and for **2-15** (C$_1$) five

---

[10] *Biorad Biobeads X8.*

[11] Phenolic protons are omitted in this discussion of isomer symmetry in the ^{1}H-NMR spectrum. On the NMR timescale (at room temperature) free rotation of phenolic protons is not resolved and signals coalesce into one peak.[213]

signals are expected in the proton NMR spectrum. Furthermore, a significant change in chemical shift is to be expected for **2-14** and **2-15**. Protons of quinoidal C-H groups are typically observed at $\delta = 5.9 - 6.8$ ppm.[204]
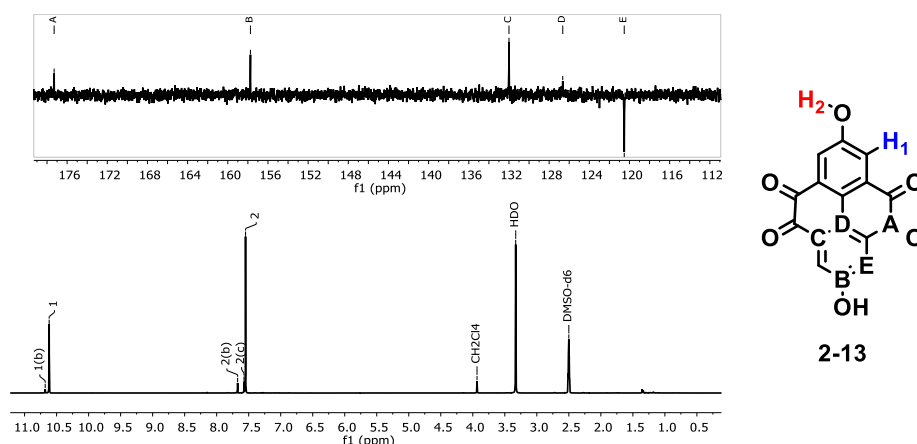

*II-11: ^{1}H-NMR (bottom) and ^{13}C-APT-NMR- (inset, top) spectra of **2-13** recorded in DMSO at 298 K.*

In the ^{1}H-NMR spectrum only two signals are observed. Integration gives a ratio of one to two. Following the symmetry discussion, structures **2-14** and **2-15** can be ruled out from this finding alone. Signal *1* ($\delta = 10.6$ ppm, s) is assigned to two phenolic protons in DMSO in compound **2-13**. Signal *2* ($\delta = 7.5$ ppm, s) is resulting from four aromatic protons (positions 1,3,6 and 8 in **2-13**). Further evidence for **2-13** can be gained from ^{13}C-NMR spectroscopy. In the ^{13}C-attached proton test (^{13}C-APT) spectrum (shown in the inset of figure II-11) secondary and quaternary carbons generate positive peaks (with respect to the base line) while primary and tertiary carbon peaks are negative. Whereas signal *A* ($\delta = 176$ ppm, positive) is assigned to carbonyl carbons, signal *B* ($\delta = 168$ ppm, positive) is assigned to a phenolic carbon. Signals related to the residual pyrene core are *C* ($\delta = 132$ ppm, positive), *D* ($\delta = 127$ ppm, positive, weak) and *E* ($\delta = 121$ ppm, negative). Signal *C* is attributed to carbon 3a, 5a, 8a, and 10a, signal *D* to carbon 3a^1 and 5a^1, signal *E* to carbon 1,3,6 and 8 of **2-13**.[12]

II.1.2.3   Attempted synthesis of 2-8 on the basis of 2-13

With the structure of **2-13** established, oxidation to **2-8** was attempted.
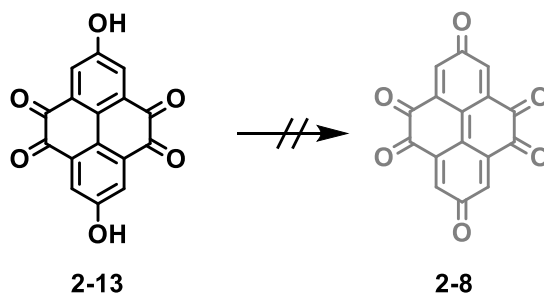
*II-12: Attempted oxidation of **2-13***

---

[12] For this assignment the numbering scheme for pyrene is also used for the pyrene-4,5,9,10-tetraone **2-13**.

If the model of pyrene-4,5,9,10-tetraones as a biphenyl with ketone substituents is evoked, this oxidation step can be seen as the conversion of 4,4'-biphenol to dibenzoquione. This reaction has first been described in 1905 using PbO_2 in benzene.[214] Yields were significantly enhanced by BROWN and TODD by changing the oxidant to $Pb(OAc)_4$ in acetic acid.[215] More recently, hypervalent iodine reagents ($PhIO$[216], $PhI(OAc)_2$[217] and $PhI(TFA)_2$[218]) have been used for this transformation. In 2011 TEPPER and HABERHAUER prepared a 3,3'-diketo-bipehnyl-4,4'-diol.[219] Screening several conditions they found that $PhI(OAc)_2$ in MeOH converts the electron deficient diol to the corresponding quinone. Other reagents like $Cu(OAc)_2$, H_2O_2 or DDQ failed in this reaction altogether.

For the oxidation of **2-13** all reagents that were successfully used in literature have been tested. None of the used conditions verifiably promoted the formation of **2-8**. Hypervalent iodine reagents failed to give any conversion. Lead(IV)acetate in acetic acid gave a complex mixture of products from which the identification of **2-8** was not possible.

It should be kept in mind that, according to DFT calculations (table II-1), **2-8** is an extremely strong acceptor. With four keto-groups (in 2, 2', 6 and 6') the biphenyl is already very electron deficient. It is not clear whether the strength of the used oxidants was insufficient or the desired product is intrinsically not a stable organic compound. The smaller yet stronger acceptor F_4-TCNQ ($E_{LUMO} \approx -5.3$ eV) is a commercially available compound.[220] However, during the synthesis it is not necessary to de-aromatize (the remaining) two aromatic rings. It is probable that this step destabilizes the product so that **2-8** could not be isolated.

II.1.3 Attempted quinoidization of pyrene

As the deprotection / oxidation strategy according to RIEGER did not provide the desired pyrene-2,4,5,7,9,10-hexaone (**2-8**), attempts were made to quinoidize pyrene as the first step. It was hoped that electron donating substituents in the K-region would facilitate the oxidation and stabilize the resulting quinoidal structure by +M mesomeric effects. If the isolation of a quinoidal pyrene derivative would be possible, deprotection and further oxidation could be studied subsequently.

To this point, only very few groups have reported work on quinoidal pyrenes. Most work has been done in the 1980s in the context of the search for new, extended acceptors of organic metals. BOLDT *et al.* tried to prepare pyrene-2,7-diol but failed to oxidize it to the quinoid form.[221] MAXFILED, BLOCH and COWAN report in the synthesis of TCPQ that limited solubility was hampering the isolation of the material from the parallel formed polymeric matrix.[222, 223] The analogous trans-10b,10c-dimehtyl-10b10c-dihydropyrene

was described in 1997.[224] Very recently RAVAT *et al.* prepared pyrene based biradicals with partial quinoidal ground states.[225]

In order to test the hypothesis that K-region substitution can stabilize a quinoidal pyrene derivatives suitable precursors had to be found. It was decided to prepare 2,7-diol (**2-18**), 2,7-dimalononitrile (**2-19**) and 2,7-di(*p*-hexylphenylamine) (**2-20**).

## II.1.3.1   4,5,9,10-Tetramethoxypyrene-2,7-diol (2-18)

2-16   **2-5**   **2-17**   **2-18**
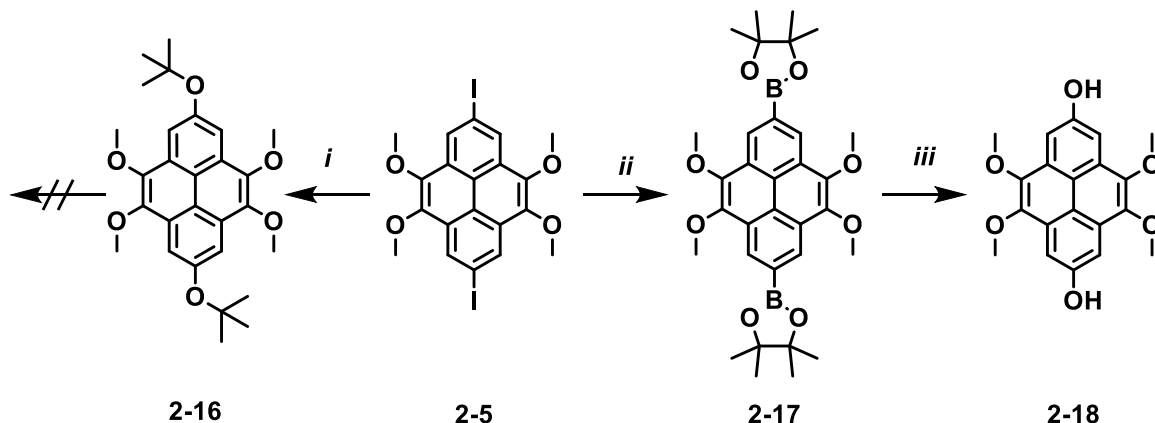
II-13: Synthesis routes towards 4,5,9,10-tetramethoxypyrene-2,7-diol (2-18). i:NaOtBu, QPhos, PdDBA$_2$, Tol, 100 °C, 16 h, 53 %. ii: B$_2$Pin$_2$, PdDPPF, Dioxane, 80 °C, 16 h, 72 %, H$_2$O$_2$, NaOH, acetone, H$_2$O, 45 °C, 3 h.

The synthesis of 4,5,9,10-tetramethoxypyrene-2,7-diol (**2-18**) was problematic. Compared to 1,3,6,8-tetraboromopyrene, the nodal plane of **2-5** significantly lowers the reactivity of the halogen substituents in transition catalyzed cross-coupling reactions.[226] Palladium catalyzed hydroxylation reactions failed on this substrate.[227] Instead it was possible to introduce a *tert*-butyl ether residue.[228] Yet, a selective deprotection under mild conditions to **2-18** was not achieved.[229]

Boronic acid hydrolysis is a well-established alternative route for introducing hydroxyl groups to aromatic systems. Direct introduction of boronic acids using tetrahydroxydiboron under palladium catalysis failed.[230] Using MIYAURA borylation reaction in dioxane **2-17** was prepared.[231] Surprisingly, **2-17** withstood hydrolysis by sodium periodate.[232] It was finally possible to prepare **2-18** by oxidative boronic ester hydrolysis using finely ground sodium hydroxide and hydrogen peroxide in a water/acetone mixture.[84] The crude product was filtered through a silica plug. As can be seen from the NMR spectra shown below, it was not possible to fully purify the compound.

In the ^{1}H-NMR spectrum signals *1* (δ = 10.1 ppm, s,-O*H*), *2* (δ = 7.7 ppm, s, -C$_{pyrene}$-*H*) and *3* (δ = 4.2 ppm, s -O-C*H*$_3$) can be assigned to compound **2-18**. Two weak singlets at δ = 6.9 ppm and δ = 6.6 ppm are resulting from approximately 10 % oligomerization products in the sample. In the ^{13}C-NMR spectrum signal *A* (δ = 156.6 ppm) is assigned to

the carbon connected to the hydroxyl residue. Signals *B* (δ = 144.1 ppm), *C* (δ = 128.0 ppm), *D* (δ = 114.8 ppm) and *E* (δ = 105.9 ppm) are generated by the pyrene framework. The methoxy-C- signal (*F*) is observed at δ = 60.1 ppm.
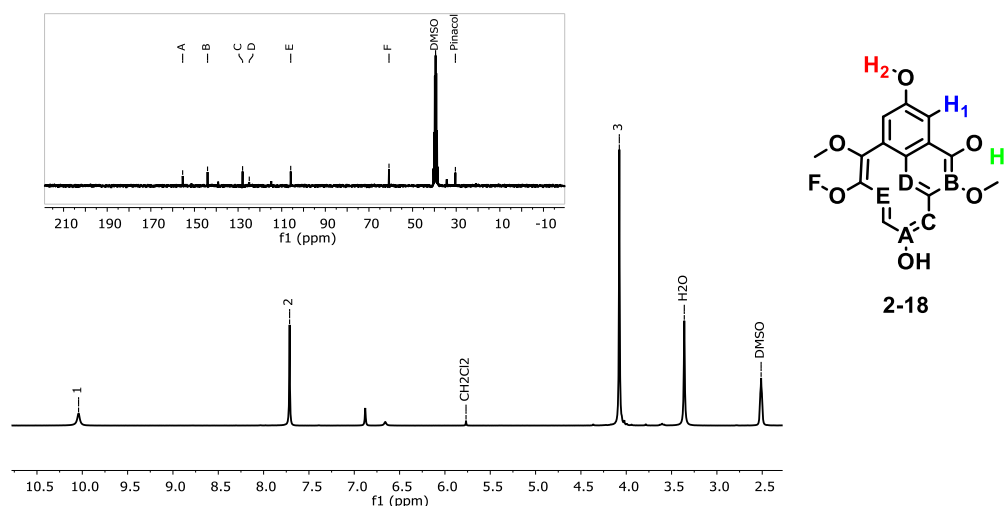
II-14: ¹H-NMR and ¹³C-NMR (inset) spectra of 2-18 in DMSO at 298 K.

While it was possible to isolate **2-18**, the addition of even a mild oxidant (H₂O₂) resulted in the formation of oligomers. It was not possible to identify the desired oxidation product.

### II.1.3.2 Tetracyano dimethane and diamine derivatives of 2-5
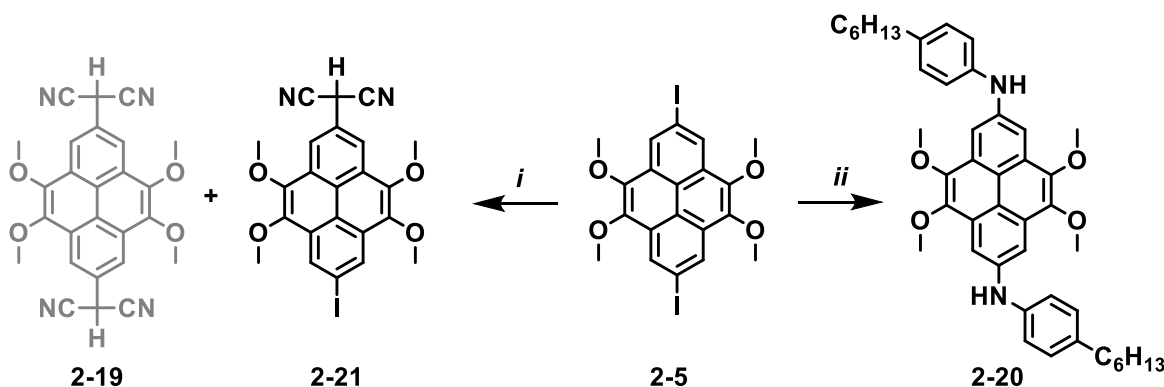
II-15: Synthesis of tetracyano-dimethane and bis(phenylamine) derivatives of 2-6. i: (NC)₂CH₂, NaH, PdCl₂(PPh₃)₂, Dioxane, 100 °C, 72 h. ii: p-Hexylphenyl amine, NaOtBu, DPEPhos, Pd(OAc)₂, Tol, 80 °C, 16 h.

As mentioned in the introduction to this section, the synthesis of TCNP is disputable. It is still not clear whether it was merely impossible to isolate due to low solubility or whether the compound is not stable as a monomer and immediately oligomerizes. In order to investigate this issue on a more soluble substrate and to provide a precursor for a planned synthesis of **2-9**, it was attempted to prepare **2-19**. Based on the work of TSUBATA *et al*. a palladium catalyzed cross coupling reaction of the *in-situ* generated dicyanomethanide was employed.[233] **2-5**'s low reactivity required more forceful conditions (100 °C, dioxane

instead of 50 °C in THF) and extended reaction duration. Under these conditions full conversion of **2-5** was observed but a substantial amount of mono-substituted intermediate **2-21** was retained in the mixture. **2-19** was identified by FD-MS from the crude mixture. Isolation of the product by column chromatography was not possible as decomposition occurred on silica as well as alumina. Solubility was insufficient for CPG. Purification by recrystallization did not afford the product. In contrast, it was possible to isolate **2-21** from the reaction mixture by column chromatography.

Considering the behavior towards chromatography adsorbents it can be speculated that oxidation of **2-19** takes place. Unfortunately, the oxidation product was not identified under the conditions used.

II.1.3.2.1   Leucoemeraldine base of 2-20
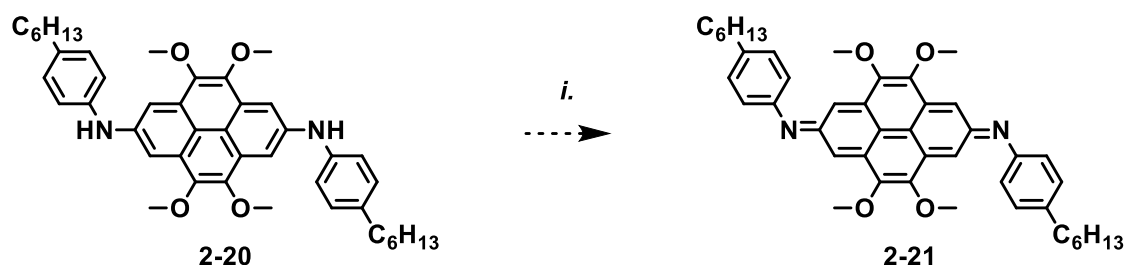
*II-16: Attempted formation of emeraldine base **2-21**. i.: DDQ, CD₂Cl₂, RT, 4 h.*

Just as quinodimethanes, anilines have had a significant impact on molecular electronics. This holds true for the polymeric and to a lesser extent also for the small molecule approach.[234, 235] The transition from the leucoemeraldine base (with amine-like nitrogen) to the emeraldine base (with imine-like nitrogen) state occurs easily in poly-anilines (e.g. by electronic or chemical oxidation).[234] This ease of oxidation makes leucoemeraldine bases an attractive starting point for the desired quinoidization of pyrene.

BUCHWALD-HARTWIG cross coupling reaction of **2-5** and *p*-hexylaniline using DPEPhos provided access to the amine **2-20**.[236, 237] *P*-Hexylaniline was chosen to provide good solubility but also some steric protection for the critical nitrogen atoms. **2-20** can be purified by column chromatography on silica.

The product forms yellow, needle-like crystals with a triclinic system and a P^1 space group. Short contacts are observed between –O-Me units and the pyrene framework of the next layer (d = 3.45 Å). CH-π-edge to face interactions are present between a phenyl ring and the pyrene framework (d = 3.33 Å) in the next layer. The amine bonds show no significant bond length alteration (1.396 Å Pyr-N vs. 1.409 Å N-Ph). There is no indication for emeraldine base formation. Imine bond length is typically 1.279 Å for the carbon - nitrogen double bond.[238]
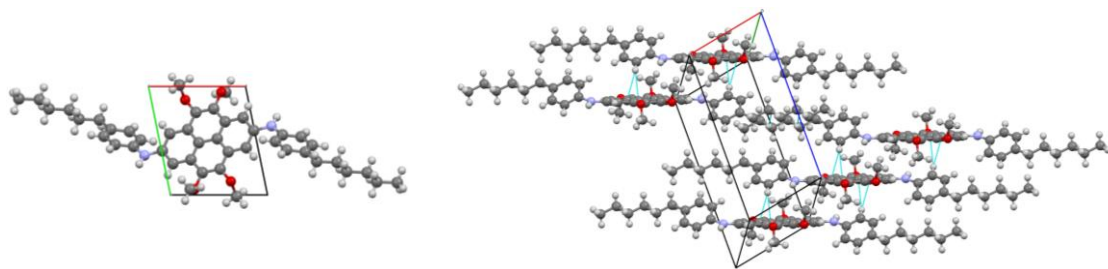
*II-17: Crystal structure of **2-20**. Left: Molecule structure along C-axis / top view. Right: Stacking motive. Phenyl-pyrene CH-π interactions between molecules are observed (short contacts in sky blue).*

As a consequence of the failed attempts to identify the desired quinoidization products (**2-20** to **2-21**) due to low stability, it was attempted to study emeraldine base (**2-21**) formation by ^{1}H-NMR in an on-line experiment. Spectra were recorded in five minutes intervals after DDQ addition. DDQ was employed as oxidant as it does not carry protons that could interfere with ^{1}H-NMR spectroscopy and is not paramagnetic (as many inorganic oxidants).
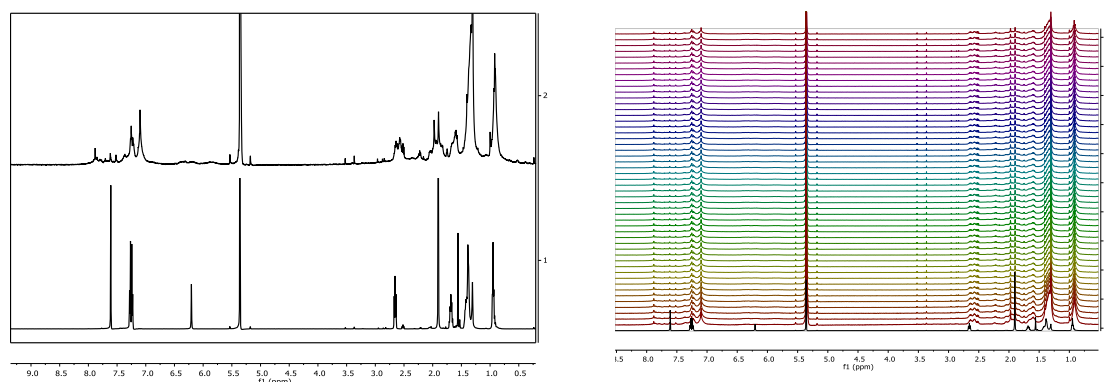
*II-18: Results ^{1}H-NMR online oxidation experiments. Left: Spectra recorded prior- (bottom) and post-DDQ addition (top). Right: ^{1}H-NMR reaction monitoring, temporal evolution (1 giving the spectrum of **2-20**).*

A color change was observed immediately after addition of the oxidant. The reaction was monitored by ^{1}H-NMR spectroscopy. When spectra 1 and 51 are compared (figure II-18, left) it is apparent that a large number of additional signals result from oxidation. Especially in the aromatic region a severe signal broadening is evident. This can be interpreted as the formation of open-shell species which remained unidentified. The temporal evolution of the NMR spectra (right of figure II-18) indicates that the reaction mixture did not change in the period of 4 h. Apparently, the reaction was completed before the first spectrum was recorded.

It is interesting to note that the singlet associated with the amine ($\delta = 6.4$ ppm, in **2-20**) is not observed after DDQ was added. The same is true for the pyrene scaffold singlet ($\delta = 7.7$ ppm). The disappearance of the amine signal suggests proton abstraction has taken place. It cannot be delineated whether the emeraldine base (**2-21**) or a dianionic salt is formed as the pyrene scaffold protons are not observed.

II.1.4   Alternative protection groups

Initially, reductive methylation was employed to afford a methyl ether protected pyrene. KOCIENSKI points out the following about this group in his textbook "Protecting Groups":

> *"For sheer ruggedness and simplicity there are few protection groups that can top a methyl ether. Of course there is a price to pay: the conditions required for deprotection are rather harsh and so comparatively few functional groups are compatible."[239]*

Therefore, different protective groups were introduced to **2-4.** Figure II-19 summarizes the attempted and successful protection methods.
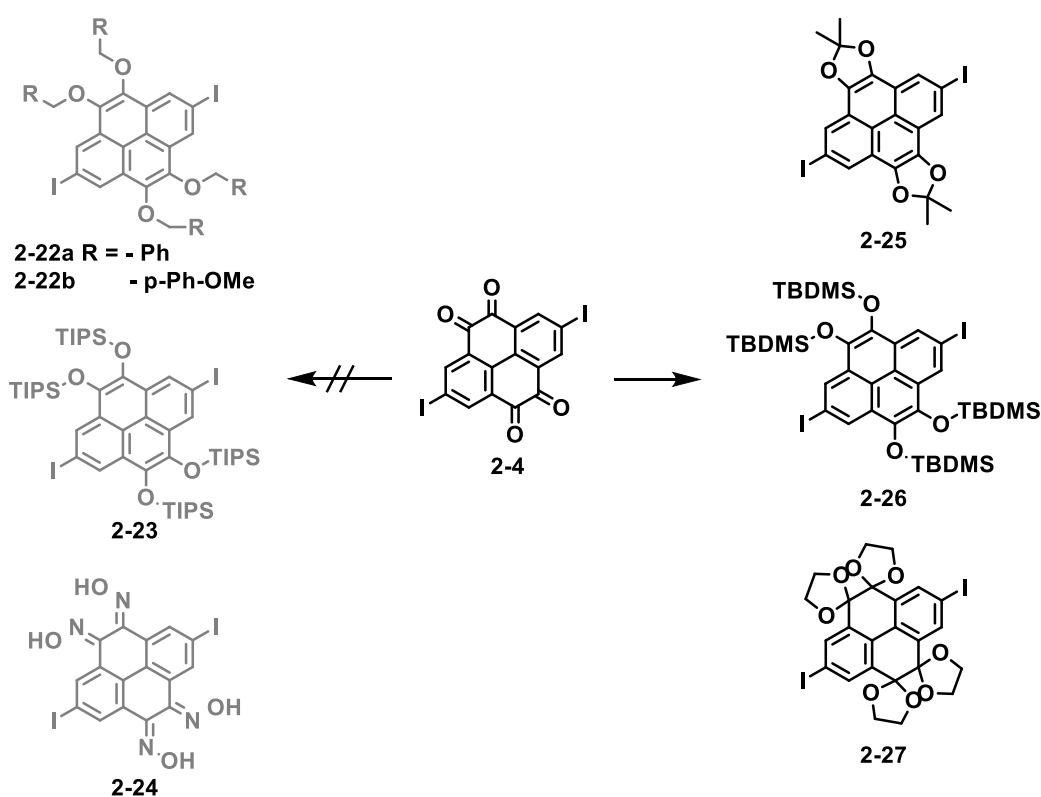
II-19: Attempted (gray) and successful (black) introductions of alternative protective groups in **2-4.**

With the exception of **2-24** and **2-27** protection is preceded by reducing (*in-situ*) the α-diketone to the α-diol. Thus, the pyrene core is rearomatized. This will have severe repercussions for the deprotection after functionalization. As can be deduced from the large amount of protecting groups studied, it was not possible to find a singular solution for all synthetic problems.

II.1.4.1   2,2-Dimethly-1,3-dioxolane

2,2-Dimethly-1,3-dioxolan (DDO) as a protecting group for α-diketones can easily be introduced by 2-nitropropane in basic conditions as described by ITOH *et al.*[240] It should

be noted that no additional reducing agent is needed in this reaction. So far the mechanism is only insufficiently understood. ZÖPHEL successfully utilized this group in his work on 4,5 vs. 9,10-desymmetrized donor-acceptor pyrene derivatives.[87] He was able to demonstrate that DDO is a superior donor compared to two methoxy groups in the same position. Deprotection to the corresponding α-diketones is not reported.

II.1.4.1.1   Synthetic application

2-25 was prepared from **2-4** in moderate yields (typically around 40 %) as a yellow, poorly soluble solid. DDO's increased rigidity and planarity accounts for the low solubility of **2-28**.
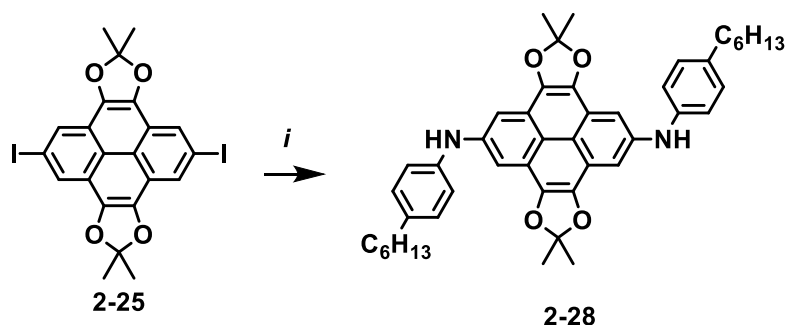
*II-20: Synthesis of **2-28**. i: p-(C₆H₁₃)PhNH₂, QPhos, NaOᵗBu, Tol, 105 °C, 24 h.*

This excluded **2-25** from generally replacing **2-5** as precursor for pyrene acceptor synthesis, e.g. ROSENMUND-VON BRAUN cyanation resulted in a virtually insoluble solid. It was possible to prepare **2-28**, a derivative of **2-20,** using similar reaction conditions (figure II-20). **2-28** can be prepared due to the solubility provided by amine substituents.

II.1.4.1.2   Characterization
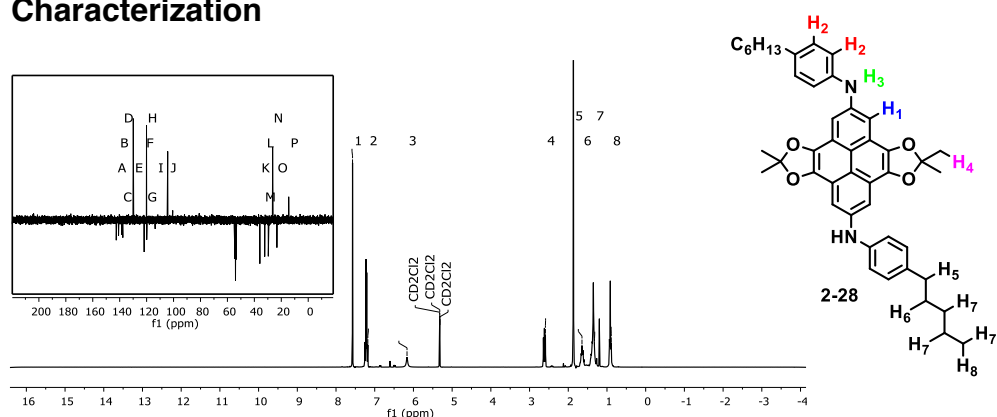
*II-21: ¹H-NMR spectrum and ¹³C-APT-NMR spectrum (inset, top left) of **2-28** recorded in CD₂Cl₂ at 298 K.*

The ¹H-NMR spectrum can be segmented into five signal groups (*1 - 8*). Signal *1* corresponds to four residual protons on the pyrene core, *2* to eight protons on a para-substituted phenyl ring, *3* to two aniline protons, *4* to two methyl groups on DDO and *5* to *8* to two hexyl chains on phenyl rings.

II.1.4.1.3   Crystal structure

In order to fully understand the low solubility of **2-25** it is helpful to compare the crystal structures of **2-20** (figure II-17, left) and **2-28** (figure II-20). For **2-28** the planar 1,3-dioxolane structure significantly expands the pyrene core along the short axis compared to **2-20** (9.11 Å vs. 4,91 Å). In addition to this, the methoxy units in **2-20** possess extra motion degrees of freedom.
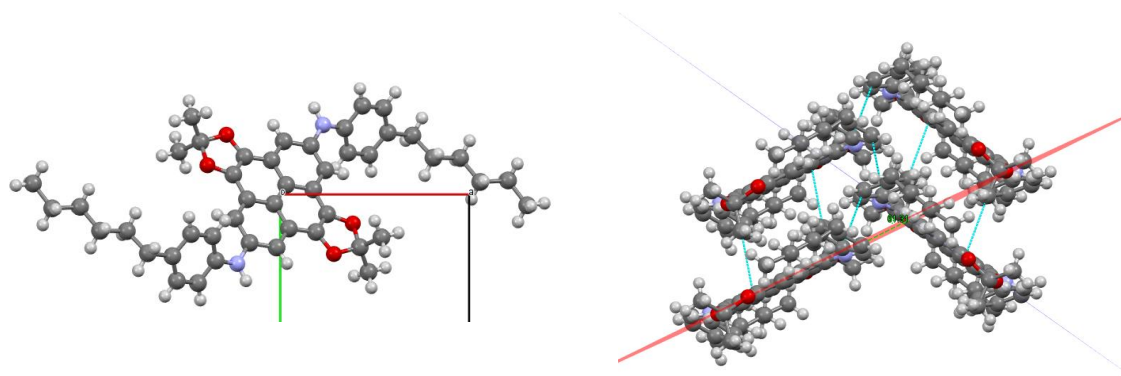
*II-22: Crystal structure of **2-28**. Left: Single molecule. Right: Packing. Short contacts are shown in blue.*

2-28 forms monoclinic crystals with a $P2_1$ space group. The unit cell has a volume of $V = 1862$ Å^3 and contains more than twice the volume found for **2-20** ($V = 904$ Å^3). The dihedral angle between the pyrene scaffold and the phenyl residue is widened from 19° (in **2-20**) to 26°. The amine bond lengths do not change, i.e. no indication for the formation of the emeraldine base structure is found. **2-28**'s packing motive (figure II-22) is more complex showing a herringbone pattern (fig. II-22, bottom left). As in the case of methoxy- or TBS-protected 2,7-functionalized pyrenes, π–π interactions between pyrene scaffolds is practically not observed.

II.1.4.1.4   Quinoidization attempt
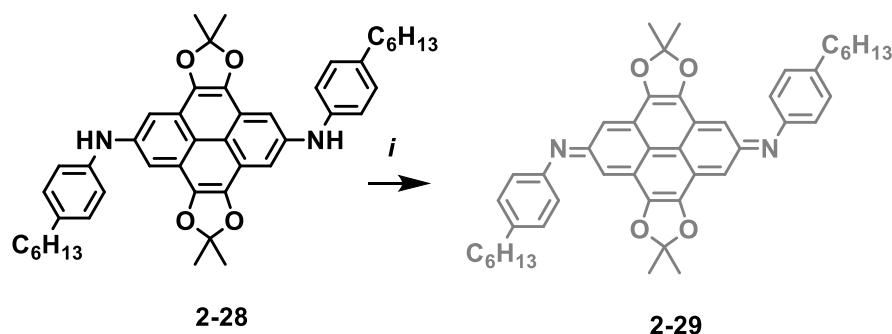
*II-23: Quinoidization attempt of **2-28**. i: DDQ, CD$_2$Cl$_2$, RT, 4 h.*

As in the case of **2-20** the quinoidization to the emeraldine base was studied in an on-line ^{1}H-NMR experiment using DDQ as oxidant. In figure II-24 on the left, NMR spectra of **2-28** prior to and after oxidation are compared. On the right the temporal evolution of the oxidation over four hours is studied.
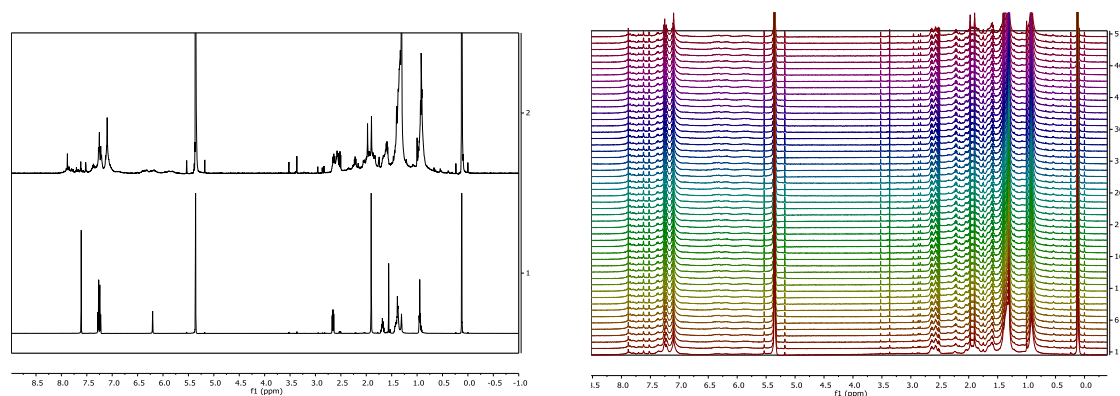
II-24: Results ^{1}H-NMR oxidation study. Left: ^{1}H-NMR spectra prior to (bottom) and after oxidation (top) in CD$_2$Cl$_2$ at 298 K. Right: Temporal evolution of oxidation reaction (2 min interval).

The post-oxidation ^{1}H-NMR spectrum shows a multitude of signals, in the aromatic as well as in the aliphatic region. This is in clear contradiction to the formation of **2-29** as sole product. As in the case of the oxidation of **2-20** the amine and pyrene proton signals cannot be identified after the addition of the oxidant.

Furthermore, the sample has a weak para-magnetic behavior (studied by EPR, not shown). This suggests a radical species in the mixture. If the radical was centered on the pyrene core, this would explain the suppressed pyrene signal in ^{1}H-NMR. In addition, this would mean that single electron oxidation took place to a certain degree. DDQ is known to act as a single electron transfer (SET) agent.[241]

In conclusion, it has to be stated that the modified stereo-electronic effects (better blocking, higher electron density) did not sufficiently stabilize **2-29** for isolation as a pure compound.

II.1.4.2 Silyl protection groups

Silyl ethers are frequently utilized as protecting groups for alcohols.[242] Ease of introduction combined with selective deprotection accounts for their popularity. A broad variety of silyl groups is reported which allows tailoring the chemical stability of the resulting ethers according to synthetic needs. While trimethylsilyl (TMS) ethers are very easily cleaved, bulky silyl ethers (e.g. *t*-butyldiphenylsilyl, TIPS) will tolerate harsher conditions.[243] Still, even very bulky silyl ethers will be selectively cleaved by fluoride reagents like tetrabutylammonium fluoride (TBAF).[244] In the case of protecting pyrene-4,5,9,10-tetraones the good solubility of bulky silyl ethers is a valuable side effect.

For the protection of **2-3**, the *tert*-butyldimethylsilyl (TBS) group was found as a compromise between stability and synthetic yield. Trimethylsilyl (TMS) did not tolerate SUZUKI-MIYAURA cross coupling reaction conditions, whereas triisopropylsilyl (TIPS) or *tert*-butyldiphenylsilyl could not be introduced into the α-diol due to their steric bulk. The crystal structure of **2-26**, as grown by slow evaporation of dichloromethane, is shown in figure II-25.
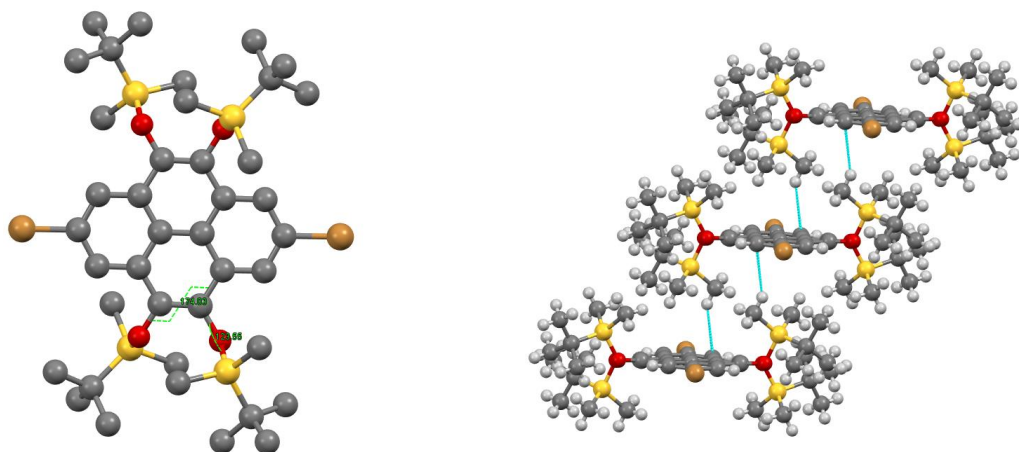
*II-25: Packing of **2-26** top view (left), packing motive (right). Short contacts are shown in blue.*

2-26 forms a triclinic crystal system with a P^1 space group. The unit cell contains a volume of $V = 1141$ Å^3. As in **2-28**, π–π interactions between two pyrene units are suppressed by the bulky protective groups. The large TBS substituent leads to a significant widening of the pyrene – ether bond by 10° (123.6°) compared to **2-6** (113.6°). It is quite obvious that protecting groups with even higher steric demand (e.g. TIPS) cannot be introduced in the available space.

II.1.4.2.1   Synthetic application

While **2-26** did not tolerate harsh basic conditions (e.g. MIYAURA borylation or ULLMANN methoxylation) it did provide sufficient stability for SUZUKI cross coupling reactions.

Recently, ZHANG *et al.* reported a phenanthrenequinone macrocyclic trimer which can be used as heterogeneous organocatalyst for oxidative dehydrogenation of ethylbenzene.[245] α-diketones are the active site in the reaction. Pyrene-4,5,9,10-tetraone (**2-2**) was tested for this application but it was partly soluble in the reaction mixture. Thus, it was necessary to prepare a less soluble derivative. **2-34** was designed with this aim in mind. Its rigid backbone and rod-like shape will provide strong intermolecular interactions thus offering low solubility.

Initially, it was attempted to prepare the target compound starting from **2-5** using a SUZUKI-MIYAURA coupling reaction to prepare **2-30** followed by a deprotection/oxidation sequence. As **2-30** was already insoluble in halogenated solvents (e.g. tetrachloroethane at 120°C), the planned deprotection with BBr₃ was not possible. In contrast, **2-31** is well soluble and can be deprotected by TBAF to **2-32**. Oxygen was used for reoxidation of **2-32** to **2-34**. Characterization of the target compound was hampered by low solubility. At the time of writing, the catalytic activity of the material was still under investigation.
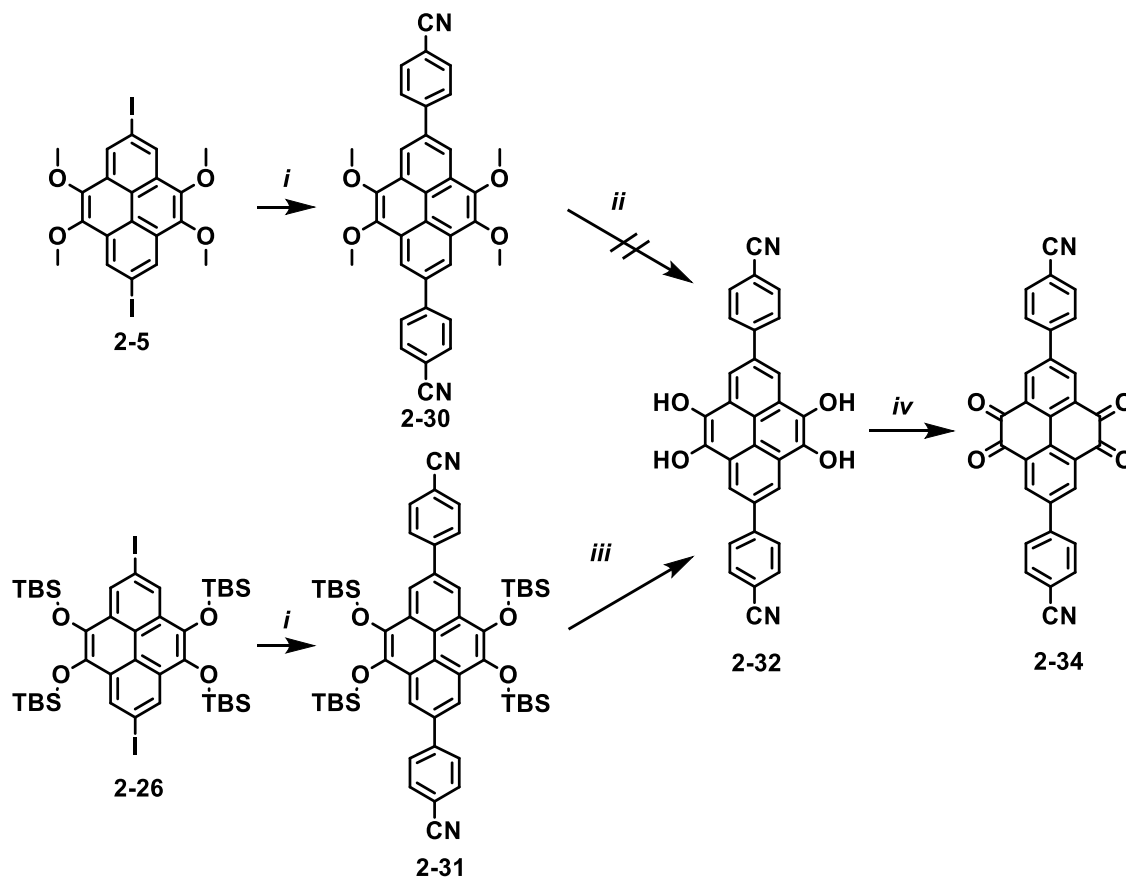
*II-26: Synthesis of **2-34**: i: p-NCPhB(OH)₂, Pd(PPh₃)₄, Na₂CO₃, H₂O, Tol, 100 °C 16 h. ii: BBr₃, C₂H₂Cl₄, 120 °C, 24 h. iii: TBAF, CH₂Cl₂, RT, 3 h, 73 %. iv: O₂, THF, 16 h, 20 %.*

II.2   Electron-rich materials

II.2.1   Laterally expanded pyrene derivatives
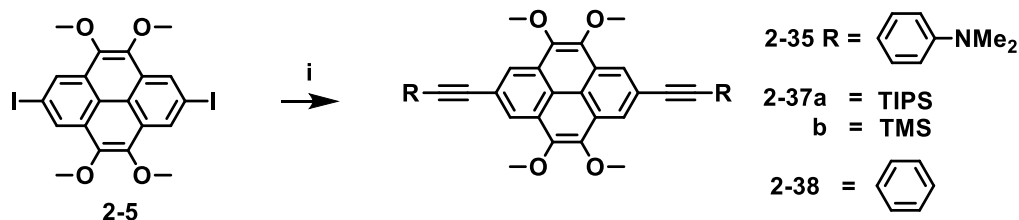
II-27: General synthesis of laterally expanded pyrene derivatives: R-CCH, Pd(PPh₃)₂Cl₂, PPh₃, NEt₃, Tol, 90 °C, 16 h, 85 %.

SONOGASHIRA-HAGIHARA-type cross-coupling reactions are very useful in the formation of $C(sp^2) - C(sp)$ bonds, i.e. the synthesis of tolanes.[246, 247] **2-35**, **2-37a**, **2-37b** and **2-38** were prepared by reaction of the appropriate ethynyl precursor with **2-5**. The palladium-catalyzed reaction provided the target compound in high yields (around 85%). All materials were purified by column chromatography although the solubility of **2-38** was problematic.

II.2.1.1   [2+2] Cycloaddition of TCNE to expanded pyrene derivatives
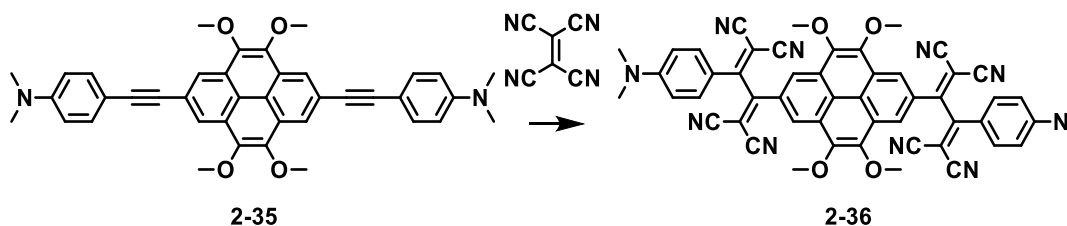
*II-28: Addition of TCNE to **2-35**. TCNE, DCM, 3 h, RT, 80 %.*

By introducing 4-ethynyl-N,N-dimethylaniline instead of diphenylamines as in **2-7** the electron density is distributed on the long-axis of the molecule. This should provide higher polarizability thus improving the absorptivity of **2-35**. Furthermore, for charge-transfer complexes, the size mismatch with small electron acceptors like TCNQ should alter packing in the solid state.[248] The addition of tetracyanoethylene (TCNE) provides an efficient approach to *intra*molecular charge-transfer complexes. The addition of TCNE to 4-ethynyl-N,N-dimethylaniline-derivatives has been described by MICHINOBU *et al*. as a new type of "click-reaction". Consequently, the reaction proceeds selectively under mild conditions in high yields.[249, 250] Recently, this reaction was also used as a post-functionalization method for polymers.[251] The reaction proceeds via a [2+2] cycloaddition of TCNE to the triple-bond to afford a 1,1,4,4-tetracyanobuta-1,3-diene, opening under cyclo-revision to the final product. Due to *inter*molecular charge-transfer

these compounds are intensely colored materials often exhibiting non-linear optical properties.[250, 252]

The addition of TCNE to **2-35** proceeded in high yields when the components were mixed in water-free dichloromethane under the exclusion of air for 3h. After column chromatography the product was isolated in 80% yield.

II.2.1.1.1   Characterization

The product was identified by MALDI-TOF mass spectrometry at $m/z = 864.37$ ($m_{calc.} = 864.26$) and nuclear magnetic resonance spectroscopy.
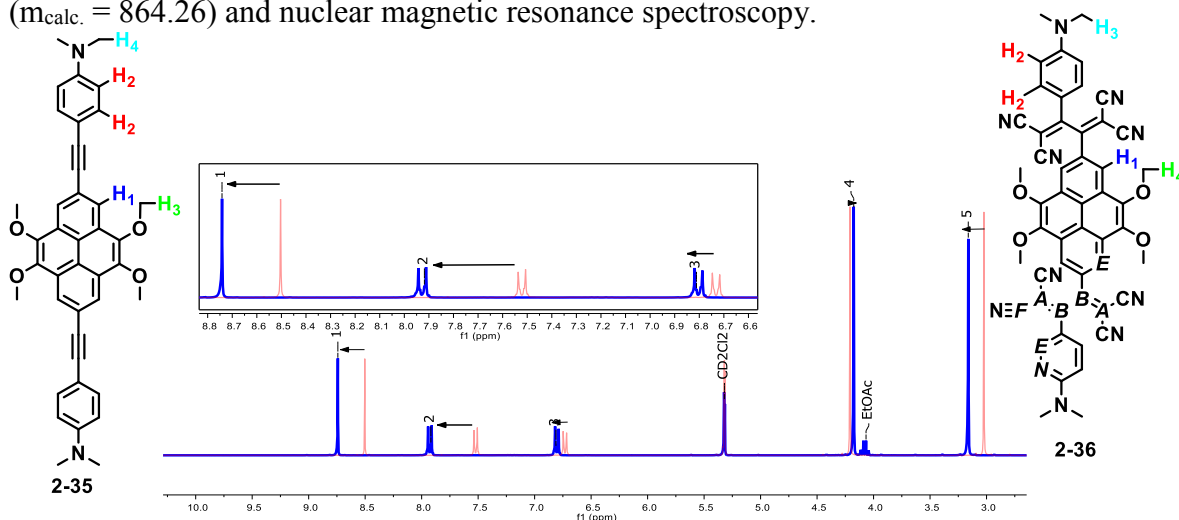

*II-29: ^{1}H-NMR spectra (300 MHz) of **2-36** (blue) and **2-35** (red) in CD$_2$Cl2 at 292 K. Upon addition of TCNE the signals in the aromatic region are shifted to lower fields (see also inset).*

Figure 2-7 shows the proton NMR spectra of **2-35** (red) and **2-36** (blue). For **2-35**, signal *1* ($\delta = 8.5$ ppm, s) is assigned to the protons located at the pyrene-core. Signal *2* (d = 7.51 ppm, dd) stems from the phenyl-protons in positions 3 and 5, while signal *3* is identified as phenyl-protons in 2 and 6 respectively. The methoxy-units on pyrene are assigned to signal *4* ($\delta = 4.2$ ppm, s) and signal *5* ($\delta = 3.0$ ppm, s) to methyl-amine residues on the aniline termini. TCNE addition did not give rise to new signal groups for **2-36**, so the basic assignment does not change. Nevertheless, there is a significant down-field shift observable for signals *1* ($\Delta\delta = 0.25$ ppm), *2* ($\Delta\delta = 0.45$ ppm) and *5* ($\Delta\delta = 0.2$ ppm). Signal *3* experiences only slight down-field alteration by $\Delta\delta = 0.07$ ppm while *4* is shifted up-field by $\Delta\delta = 0.05$ ppm. Protons in closer proximity to the introduced acceptor group experience a stronger change in their electronic environment and thus show a more pronounced shift in the NMR-spectrum.
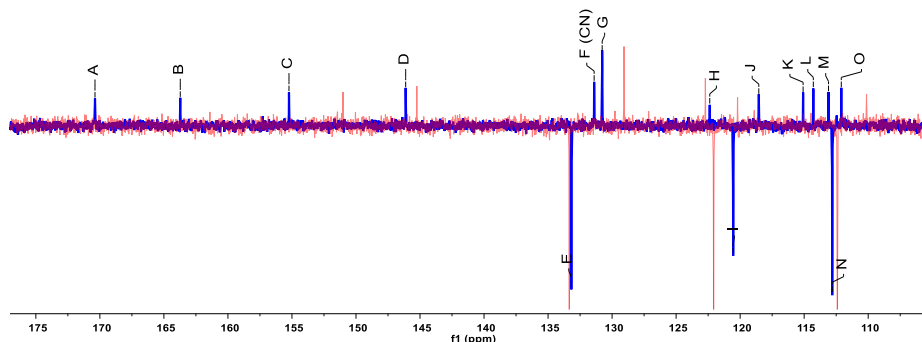
*II-30: ^{13}C-NMR spectra (75 MHz) of **2-35** (red) and **2-36** (blue) in CD$_2$Cl$_2$ at 292 K.*

In contrast to the proton spectra, the ^{13}C-NMR spectrum of **2-36** shows several new signals compared to **2-35**. Characteristic for **2-36** are peaks *A* (δ = 169 ppm), *B* (δ = 164 ppm) and *F* (δ = 132 ppm). *A* and *B* stem from the quino-dimethane residues, while signal *F* is characteristic for the nitrile carbons. It is noteworthy that the two signals at around δ = 90 ppm found for **2-35** that are associated with the ethynyl carbons are not present for **2-36**. Thus further proof of the conversion of the ethynyl function is given.
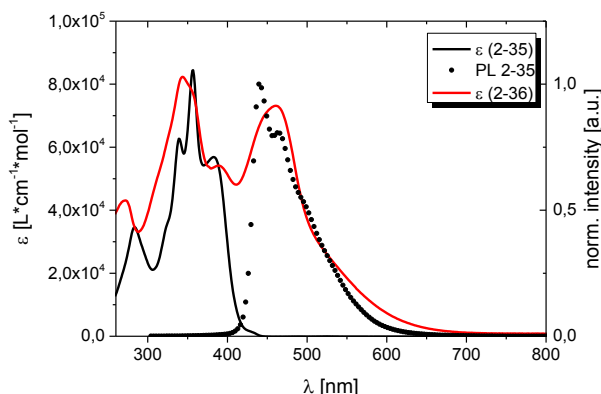

*II-31: UV-vis absorption spectra of **2-35** (black line), **2-36** (red line) and fluorescence spectrum of **2-35** (black dots). All spectra were recorded in CH$_2$Cl$_2$.*

UV-vis absorption spectra of compound **2-35** and **2-36** are shown in figure II-31. The black curve gives the results for **2-35**. Four distinct absorption maxima can be identified (λ = 383 nm, 356 nm, 339 nm and 284 nm), with the maximum absorption at 356 nm providing a very high molar absorption coefficient of $\varepsilon \approx 8.4*10^5$ L*cm^{-1}*mol^{-1}. Spectral features are sharp signals. The fluorescence spectrum has its maximum at λ = 442 nm, an additional band at λ = 474 nm and a tail to λ > 600 nm. From the spectra the optical band gap is determined as the *0-0* transition to ΔE_{Opt} = 417 nm or 2.97 eV.

The absorption spectrum of **2-36** (shown in red) is significantly broadened. Again four absorption peaks can be identified (λ = 461 nm, ε = 7.3*10^5 L*cm^{-1}*mol^{-1}; λ = 390 nm, ε = 5.3*10^5 L*cm^{-1}*mol^{-1}; λ = 344 nm, ε = 8.2*10^5 L*cm^{-1}*mol^{-1}; λ = 272 nm, ε = 4.2*10^5 L*cm^{-1}*mol^{-1}). The absorption maxima are featureless and rather broad. The

effect of the acceptor moieties is manifested not only in the bathochromically shifted absorption maximum but also in the long absorption tail. Fluorescence was quenched. The band gap is determined from the onset of the absorption to $\Delta E_{Opt} = 693$ nm or 1.79 eV.

2-37a = TIPS
**b = TMS**

2-39

2-40
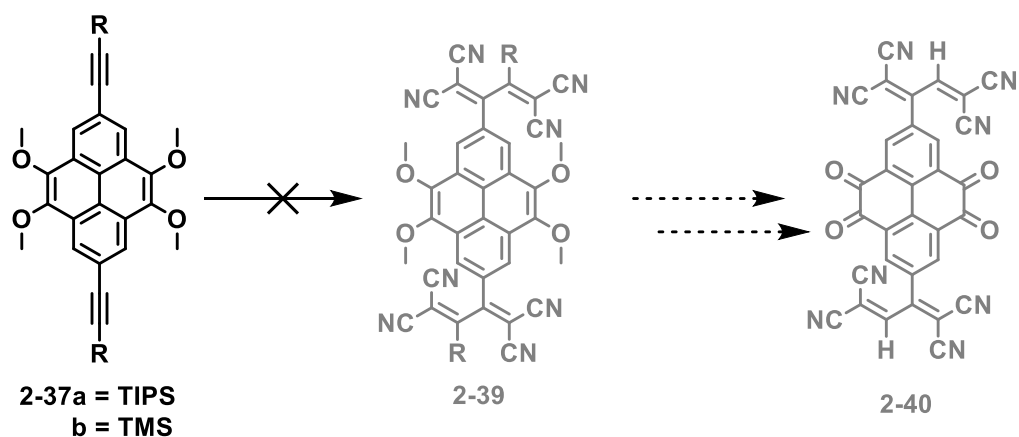
*II-32: Intended synthesis of **2-12**. Silyl protected ethylene functions did not promote the addition of TCNE.*

It was planned to extend the TCNE addition chemistry to silyl-protected ethylene derivatives (**2-37a** and **2-37b**) in order to prepare an acceptor type molecule as illustrated in figure II-32. It was anticipated that the electron-rich character of the pyrene-core would provide sufficient electron density to promote the [2+2]-cycloaddition of TCNE. **2-39** would subsequently be deprotected (silyl- and ether-protecting groups) to provide **2-40**.

2-37a and **2-37b** were prepared according to the procedure stated in chapter *2.1.1*. The addition of TCNE to **2-37a** did not succeed even at elevated temperatures (up to 130 °C) and extended reaction duration (up to 4d). As a consequence of the failure of **2-37a** to react in the desired manner, it was assumed that the steric bulk of the TIPS residue might hinder the reaction. Thus, **2-37b** was prepared and employed. The compound was subjected to the same procedure but decomposed at temperatures exceeding 90 °C. At the tolerated temperature range the addition of TCNE did not take place. These results mirror reports that anisoyl residues on tolanes do not promote [2+2]-cycloaddition.[253]

II.2.1.2   Laterally extended 4,5,9,10-tetramethoxypyrene

**2-41**   **2-42**   **2-43**   **2-44**
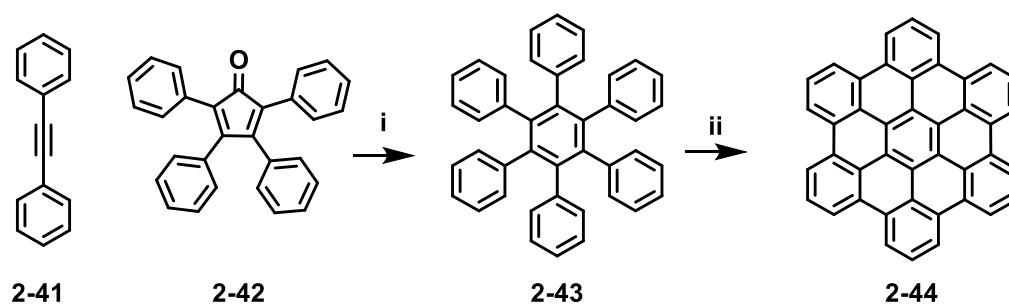
*II-33: Synthesis of hexa-benzocoronene (HBC, **2-44**) by DIELS-ALDER cycloaddition reaction. i: PhOPh, 240 °C, 10 h. ii: FeCl3, MeNO3, DCM, RT.*

The MÜLLEN group has a long-standing interest in extended discotic molecules.[254, 255] These materials are often related to hexa-benzocoronene (HBC, **2-44**), which can be considered the archetypical structure.[254, 256] Usually, these materials are prepared from a well soluble hexaphenylbenzene (HPB, **2-43**) precursor. One well established method to prepare HPB-type molecules is by DIELS-ALDER-[4+2] cycloaddition of an appropriate cyclopentadienone (**2-41**) to a tolane (**2-42**) as shown in figure II-33.[257] The HPB thus formed is converted to HBC by oxidative intra-molecular ring closure or so-called cyclodehydrogenation. This type of oxidative aryl-aryl bond formation by LEWIS acids is frequently named SCHOLL reaction in literature.[258] The mechanism of this reaction is not yet fully understood; two pathways are discussed in literature: a radical and an arenium ion mechanism. It has been argued that room temperature reactions are more likely to proceed via the radical mechanism, while reactions taking place only at elevated temperature will probably involve the arenium ion mechanism.[259] KING *et al*. have shown that SCHOLL-type reactions can be controlled by judicial introduction of electron donating substituents (EDGs) (e.g. methoxy).[260]

Recently, LORBACH *et al*. have studied cyclodehydrogenation reactions on pyrene.[99] They report that positions 1,3,6 and 8 are highly reactive in SCHOLL type reactions in contrast to pyrene's K-region which only reacts under harsh conditions. Using this insight it was possible to selectively prepare π-extended pyrene derivatives under mild conditions without any alkyl chain degradation.

Considering the results of LORBACH and KING the synthetic route shown in figure II-34 was developed in order to prepare a discotic molecule based on pyrene derivative **2-5**. In **2-18** phenyl rings are arranged in a way to allow cyclodehydrogenation to take place on the positions 1,3,6 and 8 of the pyrene core. Electron density is further increased in these positions (as compared to pyrene) by virtue of the four methoxy groups in the K-region. Oxidative ring closure should thus be easy.[260]

The initial step of the synthesis was a SONOGASHIRA-HAGIHARA cross-coupling reaction between **2-5** and ethynylbenzene to yield **2-38**. As mentioned in the introduction to this section, yields are very good (83 %) but solubility is rather poor. **2-38** was purified by repeated recrystallization from hot toluene. A microwave-assisted twofold DIELS-ALDER [4+2] cyclo-addition reaction of tetraphenyl-cyclopentadienone (**2-42**) to **2-45** at elevated temperatures was the second step. **2-45** is well soluble and can be purified by column chromatography.
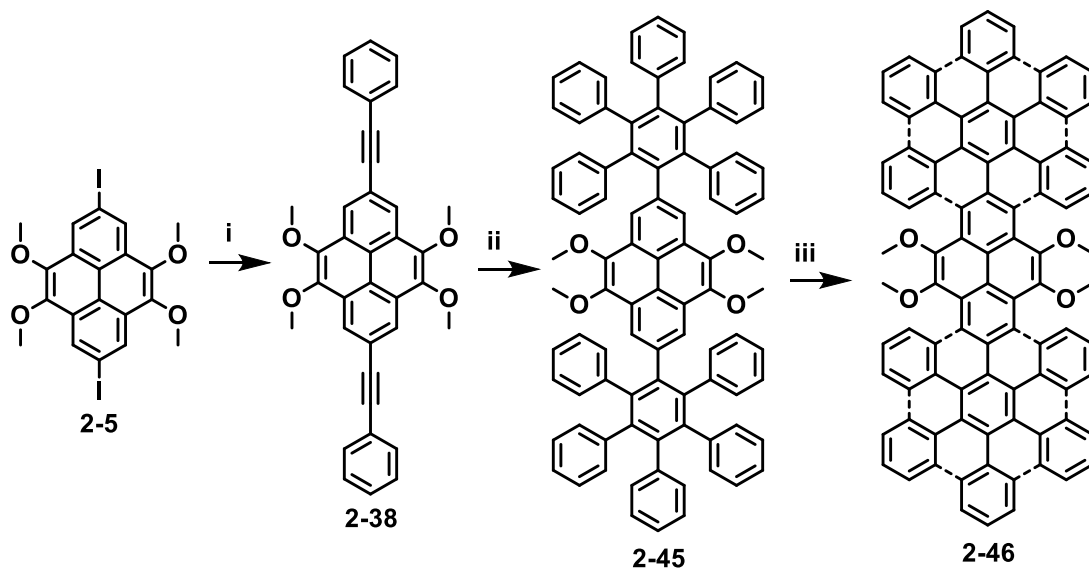
*II-34: Synthesis of **2-19**. i: PhCCH, Pd(PPh₃)₂Cl₂, PPh₃, NEt₃, Tol, 90 °C, 16 h, 83 %. ii: **2-14**, PhOPh, 240 °C, 16 h 300 W (MW). iii: FeCl₃, MeNO₃, DCM, 35 °C, 7 d.*

Cyclodehydrogenation of **2-45** was studied using ferrous chloride in dichloromethane as LEWIS-acid in analogy to LORBACH *et al*. For the reaction up to 72 equivalents of oxidant (i.e. 3 eq FeCl₃ per removable proton) and reaction times of 7 days were employed. At relatively low oxidant loadings (up to 48 eq.) and/or short reaction times (>2 d) a selective loss of $\Delta m/z = 8$ is observed in MALDI-TOF mass spectrometry (figure II-35). This is equivalent to the formation of four carbon-carbon bonds. In figure II-35 a simulated isotopic pattern is added (shown in red) to illustrate the close match of the experimental findings.
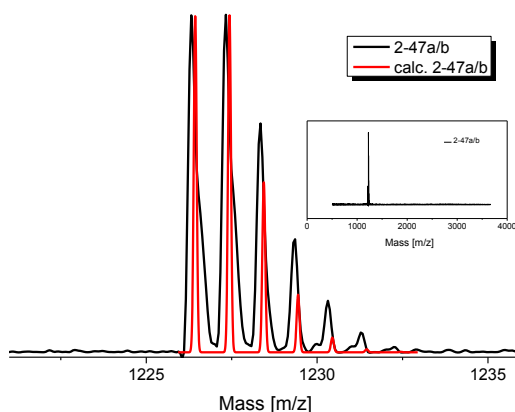
*II-35: MALDI-TOF spectrum of **2-47a/b** (black) and simulated isotopic pattern of **2-47a/b** (red). The full spectrum is given in the inset.*

Assuming bonds were not formed in a purely statistical fashion, two possibilities are most probable: **2-47a** and **2-47b** (shown in figure II-36). While **2-47b** is more favorable from an electronic perspective with high electron densities located on the pyrene core, **2-47a** has less steric repulsion to overcome in its formation. Both isomers are modeled by DFT using the B3LYP functional (figure II-36 bottom row). For **2-47a** theory predicts in effect a benzopyrene-tetramethoxypyrene-benzopyrene trimer in which the free phenyl rings are

twisted at 45° angle towards the benzopyrene as well as 4,5,9,10-tetramethoxypyrene moiety. In order for additional ring closure to take place H-H and H-O repulsions must be overcome. Frontier orbital densities are located on the 4,5,9,10-tetramethoxypyrene residue. In contrast, for **2-47b** a severely twisted tetrabenzo[*a,h,l,s*]teropyrene-like structure is predicted.[261] The aromatic system is warped by 36° out of planarity due to H-O repulsion that cannot be alleviated. Peripheral phenyl rings can adopt a propeller-like arrangement, often found in HPBs.[262] The frontier orbitals are distributed along the molecular main axis. A comparison of calculated total energies gives -2410109.1 Kcal/mol for **2-47a** and -2410047.04 Kcal/mol for **2-47b**. Thus, **2-47a** is estimated to be 62 Kcal/mol more stable giving an indication that this is the more feasible structure.[13] Furthermore, HPBs, in their propeller like conformation, can successfully be cyclodehydrogenated. Thus, it seems unlikely for the reaction to stop after formation of four bonds in the case of structure **2-47b**. In summary, **2-47a** is likely to be formed as product when low oxidant loading is used.
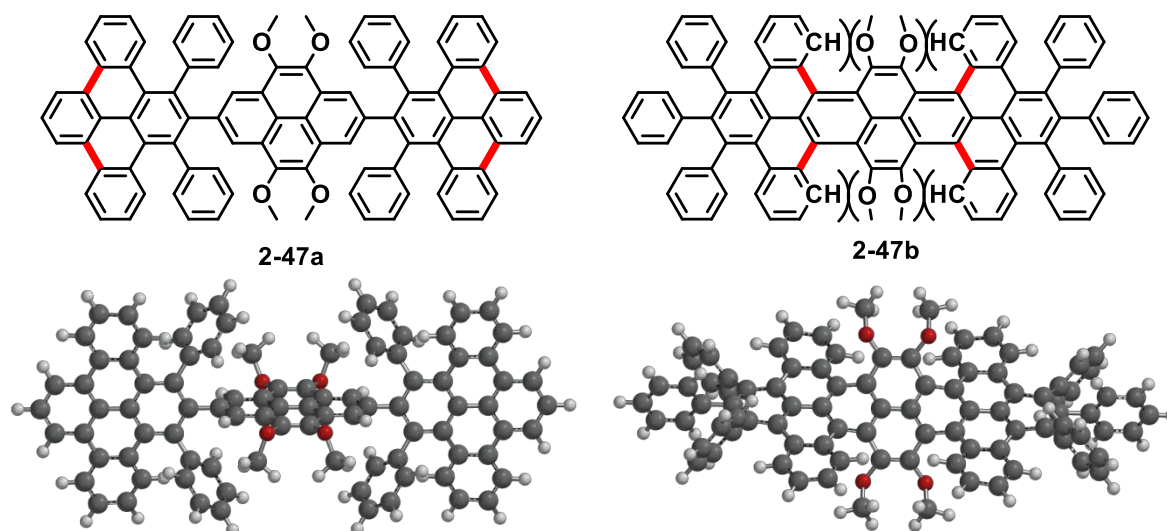
*II-36: Most probable isomers of incomplete cyclodehydrogenation of **2-45** as two dimesional representations (top row) and calculated stuctures (DFT, B3LYP,6-31*; bottom row). O-H repusion distorts **2-47b** aromatic system (36° out of plane) while **2-47a** has three distinct planar (benzo)pyrene-type subunits.*

At higher oxidant loading and long reaction times a small fraction of material was isolated that had lost Δm/z = 20 (according to MALDI-TOF). This is equivalent to the formation of 10 bonds and is consistent with the desired product **2-46**. Furthermore, the isotopic pattern matches the calculated one shown in red closely (see figure II-37). It is noteworthy that in none of the reactions studied ether cleavage (i.e. demethylation) was observed.

---

[13] KRUSE, GOERIGK and GRIMME recently discouraged the use of the B3LYP functional for thermochemistry, yet the accuracy is deemed sufficient for this simple discussion.[263]
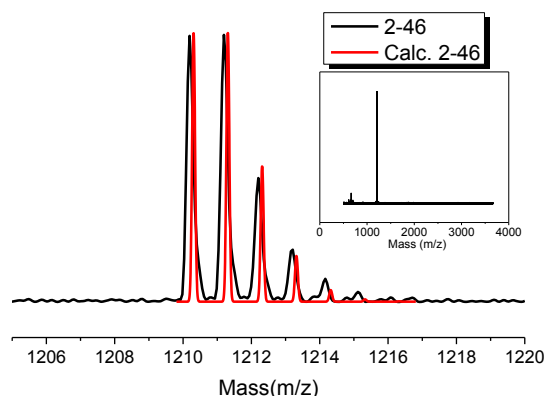
*II-37: MALDI-TOF spectrum of **2-46** (black) and simulated isotopic pattern of **2-46** (red). An offset by 0.1 m/z is observed. The full spectrum is shown in the inset.*

A DFT calculated structure of **2-46** is shown in figure II-38. As in the case of **2-47b** the methoxy-residues are experiencing severe CH-O repulsion from the HBC subunits. In consequence the central naphthalene unit is twisted out of the molecular plane by 36° in this calculation. Furthermore, the HBC subunits are distorted as a way to reduce repulsion.
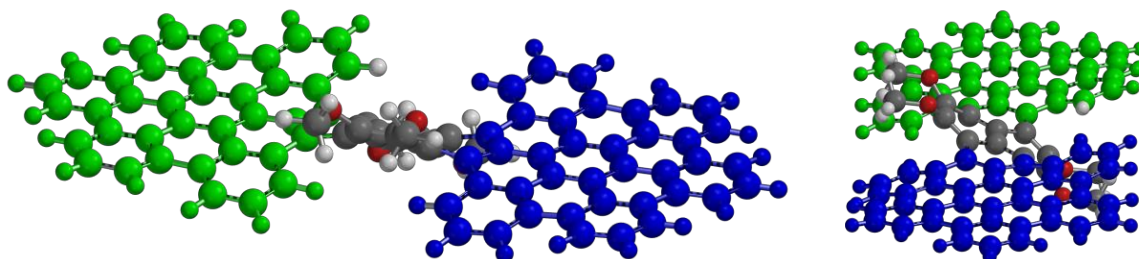
*II-38: Calculated structure of **2-46** (DFT, B3LP, 6-31*). The methoxy-residues are twisted by 36° out of plane due to steric repulsion (colors are added for clarity).*

II.3   Summary

In this chapter the synthesis of electron rich as well as electron deficient pyrene derivatives based on the 2,7-diiodopyrene-4,5,9,10-tetraone (**2-4**) was explored. In previous works 4,5,9,10-tetraalkoxypyrene was used as electron rich building block for copolymers.[201] In this work only small molecules were prepared instead.

It could be shown that **2-5** is well suited for extension using a number of ethynylenes. K-region substitution alleviates solubility issues often encountered for unsubstituted pyrenes. **2-35** can be converted by [2+2]-cycloaddition reaction with TCNE to give a push-pull type dye. Less electron rich derivatives (**2-37**, **2-38**) did not react. **2-38** was also employed as building block for discotic (*dumbbell*) molecules. The steric demand of the methoxy units in the K-region severely hinders planarization and negates the effect

expected by increasing the electron density of the system. Full cyclodehydrogenation was only possible under harsh conditions.

The attempted synthesis of quinoidal pyrene-4,5,9,10-tetraones was not successful. This was due to a combination of low solubility, low stability and harsh deprotection conditions necessary. It was possible to identify the 2,7-dihydroxypyrene-4,5,9,10-tetraone (**2-13**), yet the oxidation to the quinonoid **2-14** failed. The use of electron-rich precursors (**2-18** -OH; **2-20** -NH(Ph)) did not result in stable quinoidal structures. Increasing the steric demand of the protective group (**2-28**) did not sufficiently stabilize the molecule to allow its isolation. The synthesis of quinoidal pyrene-4,5,9,10-tetraones based on a protection/deprotection route was not achieved and will pose an exciting synthetic challenge for future studies.

The variation of the protective groups did allow the synthesis of **2-33**. While **2-30** was virtually insoluble in solvents needed for LEWIS-acid mediated ether cleavage, **2-31** was well soluble in standard solvents due to its TBS groups. Thus, deprotection using TBAF was successful and the target compound was attained.
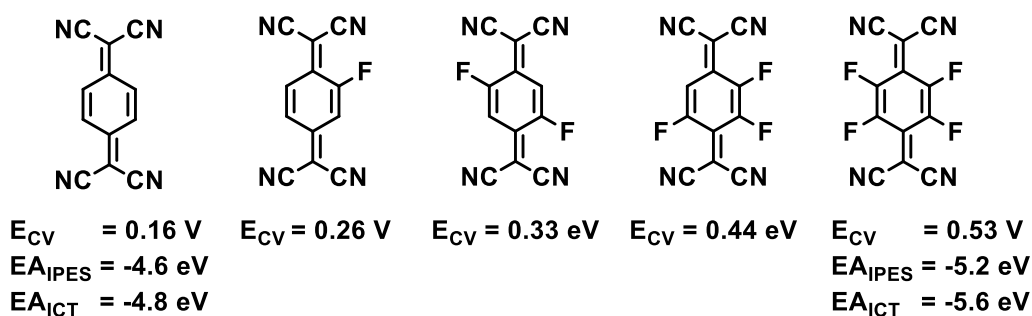
III.   Functionalization of pyrene in positions 1,3,6 and 8

In chapter *II* the sixfold (2,4,5,9,10)-functionalization of pyrene was discussed. While this work provided new, strong electron donors and charge-transfer complexes (as will be discussed in chapter *IV*), the synthesis of acceptors and quinoidal pyrene derivatives was less successful. While they had very promising calculated properties, the synthesis attempts were not fruitful. 2,7-Dicyanopyrene-4,5,9,10-tetraone remains the strongest isolated acceptor in this class.[77]

In an attempt to prepare stronger donors or acceptors, introducing additional functional groups is a viable strategy. One example for this conceptually trivial approach is the series TCNQ to F$_4$-TCNQ.[264] The electron affinity increases from $EA_{TCNQ} = -4.6$ eV to $EA_{F4\text{-}TCNQ} = -5.2$ eV (inverse photoemission spectroscopy, IPES data) just by the addition of electron withdrawing groups.[138, 265, 266]

|				
E_{CV} = 0.16 V	E_{CV} = 0.26 V	E_{CV} = 0.33 eV	E_{CV} = 0.44 eV	E_{CV} = 0.53 V
EA_{IPES} = -4.6 eV				EA_{IPES} = -5.2 eV
EA_{ICT} = -4.8 eV				EA_{ICT} = -5.6 eV

III-1: Reduction potentials[267] and electron affinities (IPES[268]) in the series TCNQ – F$_4$-TCNQ.

The 1,3,6,8-functionalization of pyrene-4,5,9,10-tetraone was studied with this concept in mind. In analogy to 2,7-dicyano-pyrene-4,5,9,10-tetraone the work presented in this section focused on 1,3,6,8-tetracyano-pyrene-4,5,9,10-tetraone.

III.1 The 1,3,6,8-functionalization of 4,5,9,10-substituted pyrenes

As mentioned in the introductory chapter, perhalogenation of pyrene has been known for a long time.[37, 269] In contrast, only recently examples of eightfold functionalized pyrene derivatives have been described in literature.[89, 270] ZÖPHEL et al. used **3-1** as a building block for extended PAHs. It allows only limited variation of the K-region functionalization.
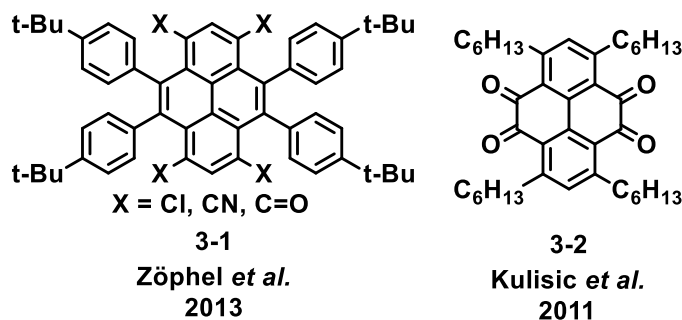

III-2: Examples of eightfold substituted pyrene derivatives found in literature.

As this section will focus on the synthesis of pyrene-4,5,9,10-tetraone derivatives, the route of KULISIC et al. to tetraketone **3-2** merits a brief discussion.[271]
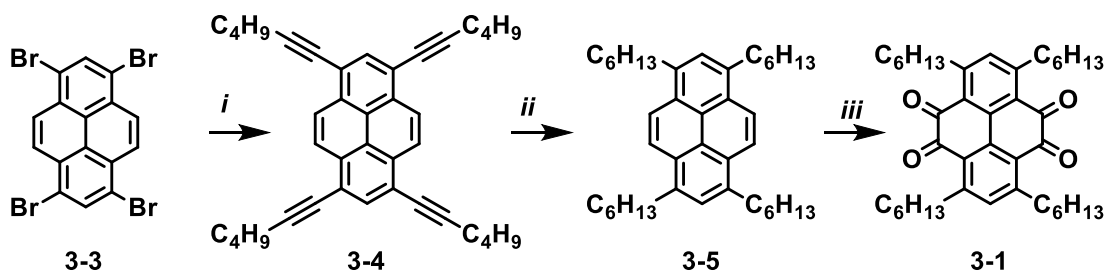
III-3: Synthesis of **3-1** according to KULISIC et al.[271] i: hex-1-yne PdCl₂(PPh₃)₂, PPh₃, Et₃N, Tol. ii: H₂, Pd/C. iii: RuCl₃, NaIO₄, MeCN, H₂O, CH₂Cl₂.

Starting point for this synthesis is the readily available 1,3,6,8-tetraboromopyrene (**3-3**). SONOGASHIRA-HAGIHARA reaction gives **3-4** in good yields, which can easily be reduced by palladium on charcoal to afford **3-5**. To prepare the tetraketone **3-2** KULISIC et al. employ the same ruthenium(VIII)oxide oxidant system that was used in the synthesis of pyrene-4,5,9,10-tetraone (**3-7**).[59] This route provides great flexibility in K-region functionalization. A series of soluble azaacenes was prepared by the MATEO-ALONSO group based on **3-2**.[63] The alkyl chains provide good solubility and can be varied in length depending on the application.
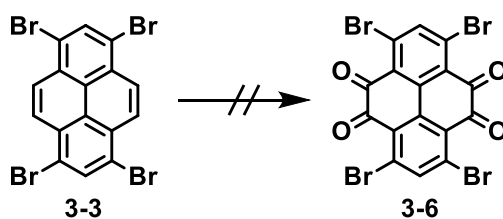
*III-4: Limitation of KULISIC et al.'s method: Insoluble substrates do not undergo oxidation to **3-6**.*

While this route is very useful for subsequent K-region functionalization, the possibility for functionalization in non-K-region positions is very limited. The oxidation conditions are very harsh and tolerate only few functional groups. Furthermore, the oxidation step is limited to the solvent system employed.[59] If the substrate is insoluble oxidation fails, as tested on 1,3,6,8-tetrabromopyrene (**3-3**) by the author of this study.

III.1.1   A flexible 1,3,6,8-functionalization strategy for pyrene-4,5,9,10-tetraones

In order to overcome the limitation of KULISIC *et al.*'s method and to provide a more general route to eightfold functionalized pyrenes (positions 1,3,4,5,6,8,9 and 10) a different synthetic approach is needed.

Pyrene-4,5,9,10-tetraone (**3-7**)		4,5,9,10-tetramethoxypyrene (**3-8**)	

HOMO	LUMO	HOMO	LUMO
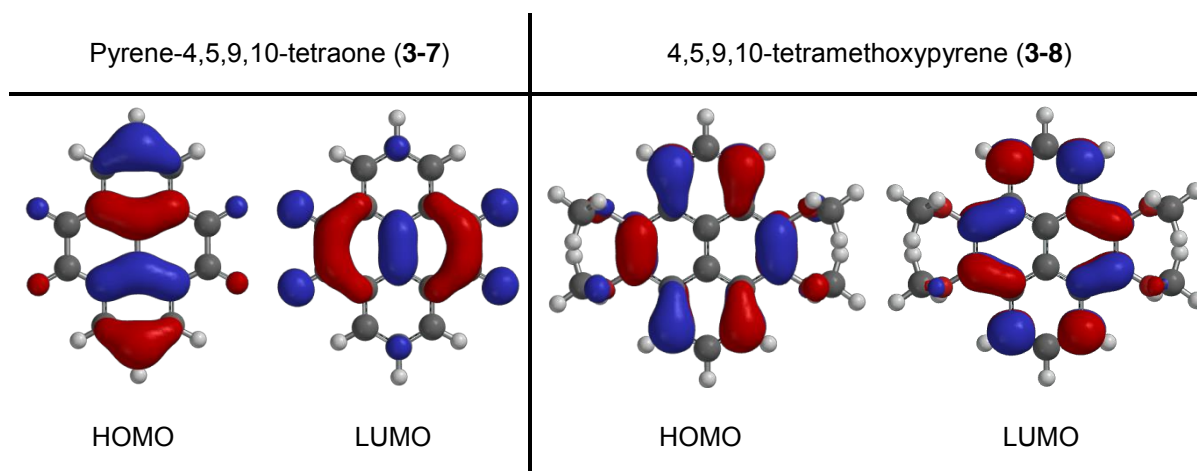
*III-5: Frontier orbital distribution of pyrene-4,5,9,10-tetraone (**3-7**) (left) and 4,5,9,10-tetramethoxypyrene (**3-8**) (right).*

The calculated frontier orbital distributions of pyrene-4,5,9,10-tetraone (**3-7**) and 4,5,9,10-tetramethoxypyrene (**3-8**) are compared in figure III-5. Electron density distribution in **3-7** favors functionalization in positions 2 and 7. In contrast, for **3-8** the frontier orbitals are distributed similaly to unfunctionalized pyrene (figure 1-2) with high electron density in positions 1,3,6 and 8. Thus, electrophilic aromatic substitution in these positions will be possible. The four alkoxy groups enhance solubility as well as electron density (+*I* effect) of **3-8** when compared to pyrene.
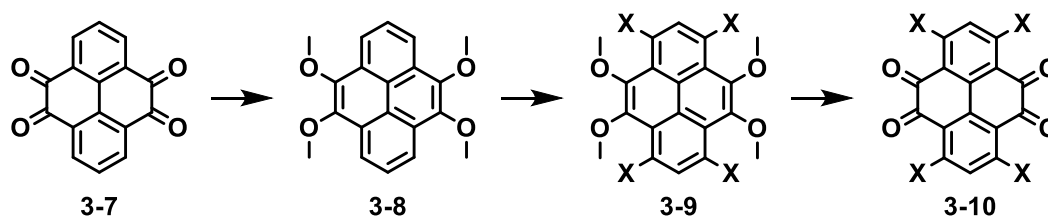
III-6: New general approach to fourfold substituted pyrene-4,5,9,10-tetraones (3-10).

From this outline, a new synthesis route (illustrated in figure III-6) for eightfold functionalized pyrenes was developed. Pyrene is oxidized by the well-established ruthenium chloride / sodium periodate system to give **3-7**.[59] Protection by reductive alkylation yields 4,5,9,10-tetramethoxypyrene (**3-8**). Fourfold electrophilic aromatic substitution in positions 1,3,6 and 8 gives **3-9**. This protected pyrene-4,5,9,10-tetraone is suitable for functional group modifications as discussed in chapter *II*. The target compound **3-10** is prepared by a deprotection/oxidation step similar to the synthesis of 2,7-dicyano-pyrene-4,5,9,10-tetraone.

III.1.2   Bromination of 4,5,9,10-tetramethoxypyrene

III.1.2.1   Failed attempts / unreliable methods

It was expected that the bromination of **3-8** would be a straightforward reaction. 1,3,6,8-Tetrabrompyrene was already reported by VOLLMANN *et al.* in 1937.[37] As outlined above, **3-8** is a well soluble, electron rich aromatic hydrocarbon and as such well suited for electrophilic substitution reactions (e.g. bromination). Methoxy-substituents activate aromatic systems sufficiently to enable e.g. fourfold bromination of 1,2-diemethoxybenzene.[272] The synthesis of 1,8-dibromo-9,10-dialkoxypyrene by VENKATARAMANA *et al.* also supports this strategy. [91]
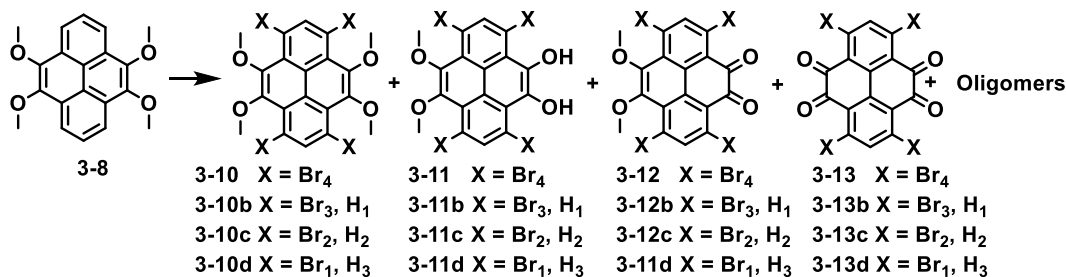
III-7: Isomers observed as outcome of bromination attempts.

While twofold bromination of **3-8** worked as expected, the fourfold bromination was problematic. Most reaction conditions conceived for fourfold bromination (listed in table III-1) gave a broad mixture of products. Mainly two- and threefold bromination was observed, co-occurring was a partial or total cleavage of the methoxy ethers. Depending on the conditions utilized, the ratio of two- and threefold bromination varied.

*Table III-1: Attempted fourfold bromination of **3-8***.

Reaction	Conditions	Reaction	Conditions
A	4, 6, 10, 20, 50 eq. Br_2 CH_2Cl_2	H	2, 4, 10, 50 eq. Br_2, $Zn(OAc)_2$, AcOH
B	4, 10, 20 eq. Br_2 $FeCl_3$ CH_2Cl_2	I	2, 4, 10, 50 eq. Br_2, $Zn(OAc)_2$, DMF
C	2, 4, 10 eq. Br_2 $FeCl_3$ AcOH	J	Pyr*Br_3 CH_2Cl_2
D	10 eq. Br_2 $AlCl_3$ CH_2Cl_2	K	Pyr*Br_3 DMF
E	2, 5, 10, 20 eq. Br_2 K_2CO_3 CH_2Cl_2	L	NBS, CH_2Cl_2[273]
F	5, 10 eq. Br_2 K_2CO_3 $CHCl_3$	M	NBS, H_2SO_4[77]
G	2, 5, 10, 50 eq. Br_2 Na_2CO_3 $CHCl_3$	N	NBS, DMF[274]

It is noteworthy that deprotection products were overwhelmingly two- and fourfold de-methylated, while odd numbered demethylation products were hardly identifiable.

In order to understand the outcome it is helpful to recall the fact that during electrophilic aromatic substitution of bromine an equivalent of hydrobromic acid is generated as a side product. This acid can mediate methyl ether cleavage.[14]
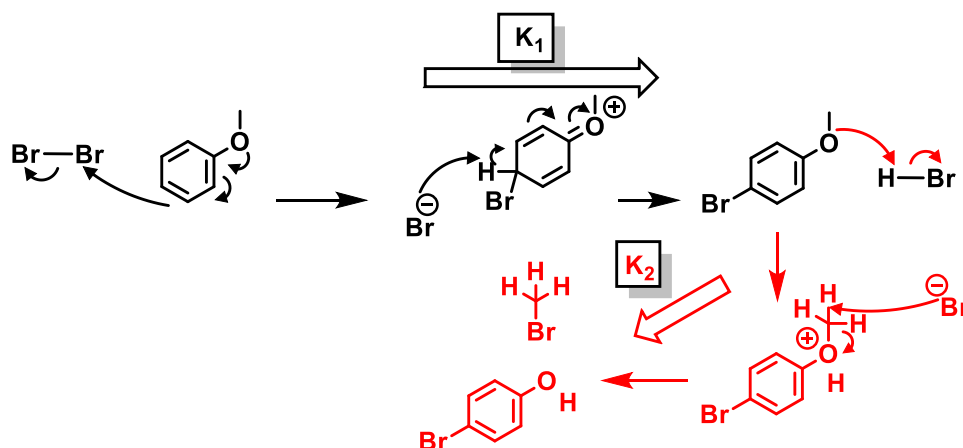

III-8: Mechanism of S_EAr (black) and acid mediated ether cleavage (red).

Figure III-8 gives the S_EAr mechanism in black and the acid mediated ether cleavage in red, using anisole as an example. In S_EAr Br_2 is polarized by anisole, a bromonium ion is added to anisole, Br^- is liberated. The aromatic system is reestablished by the release of a proton from the oxonium ion; hydrobromic acid is generated. This can, in turn, protonate the methoxy-oxygen. The nucleophile Br^- attacks the methyl group in an S_N2 fashion, phenol being the leaving group. Bromomethane is generated. The reactions can be described by two rate constants K_1 and K_2.

---

[14] Hydrobromic acid (40 %) in acetic acid is traditionally used to cleave methyl-ether protection groups.[275]

In the case of **3-8** demethylation generates an o-methoxyphenol structure in the K-region. It has been shown that these *o*-alkoxy phenols are easily cleaved under acidic conditions to give the corresponding diketone.[276] It is not clear whether the diketones **3-12b** and **3-12c** are the exclusive reaction products or **3-11b** and **3-11c** are formed as well. A sample purified by column chromatography was studied in a high resolution NMR CH correlation experiment.

The existence of **3-12b** and **3-12c** would help to explain why the bromination attempts mostly provided two- and threefold bromination. The α-diketone significantly reduces the electron density in the aromatic scaffold compared to **3-11b** and **3-11c**. If the reaction is considered in FMO-theory, DFT calculations indicate a reduced electron density[15] in one or both of the yet to be brominated positions. In consequence, S_EAr is not favored in these positions. In all likelihood, the reaction stops and fourfold bromination is not achieved.
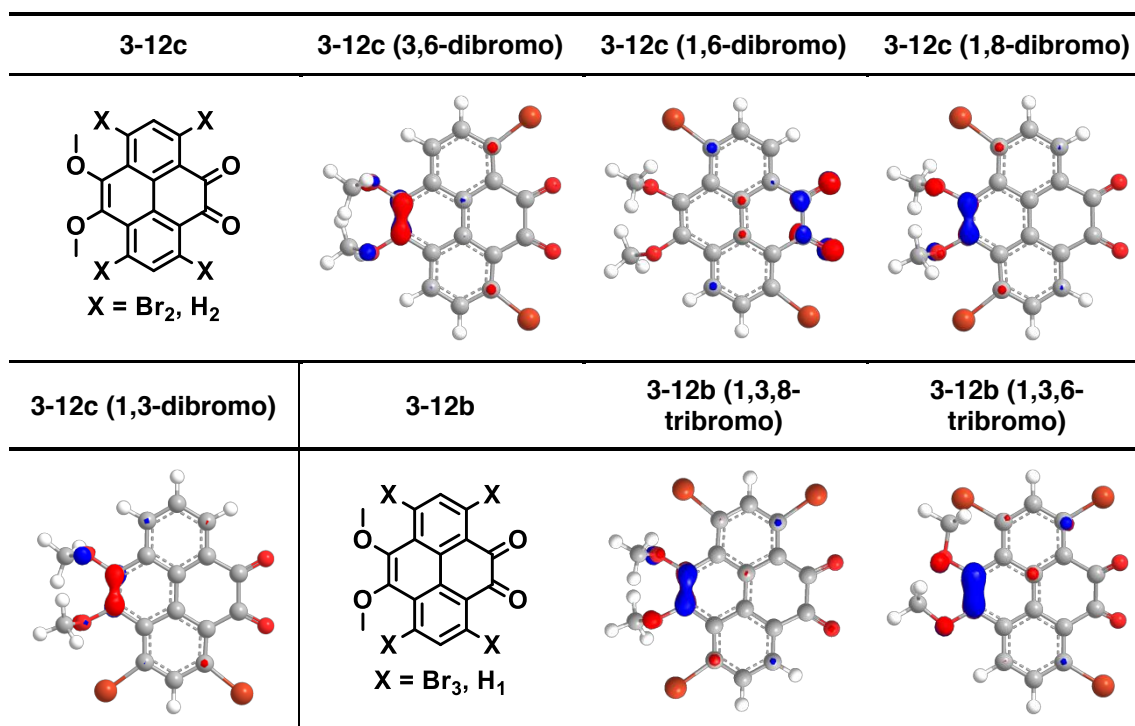
*III-9: Calculated HOMO distributions for possible isomers of **3-12b** and **3-12c**.*

In order to prepare **3-10** successfully, it was necessary to identify conditions in which the bromination is faster than the deprotection, or $K_1 > K_2$ (figure III-8). As can be seen in table III-1, the use of LEWIS acids like $FeBr_3$ of $AlCl_3$ did not afford the desired product as they probably promoted methyl ether cleave.[243] More surprisingly, the addition of bases (Na_2CO_3, K_2CO_3, $Zn(OAc)_2$, pyridine, lutidine) did not give the desired product either. It can be speculated that the bases form complexes with Br_2.[199, 277] This might reduce K_1 sufficiently for demethylation to take place.[61]

---

[15] Figure III-9 shows orbital coefficients, i.e. the probability of electron distribution.
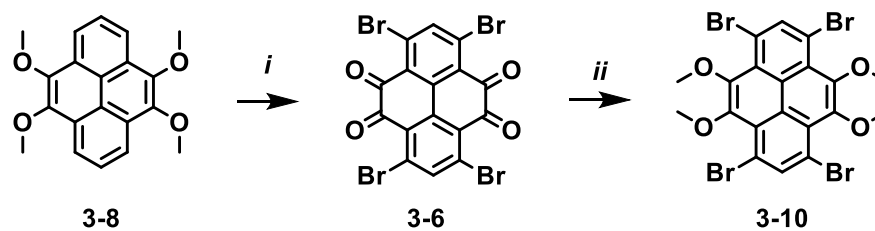
III-10: Modified VOLLMER method: i: 50 eq. Br$_2$, PhNO$_2$, 160 °C, 24 h, 5 – 7 %. ii: Na$_2$S$_2$O$_3$, MeSO$_4$, NaOH, THF, H$_2$O, 16 h, 30 %.

It is possible to prepare **3-10** in a modified VOLLMANN bromination method, adding 50 equivalents of bromine to a solution of **3-8** in hot nitrobenzene.[37] Under these harsh conditions **3-6** was obtained in low yields as an orange solid. Reductive re-methylation provided very small amounts of **3-10** yet in a reproducible manner. In this case the high reaction temperature enables rapid bromination ($K_1 > K_2$).

III.1.2.2 Successful route

The VOLLMER protocol allowed the synthesis of **3-10** in analytical quantities over two steps. To be able to use **3-10** as a building block for organic materials a more efficient route was necessary.
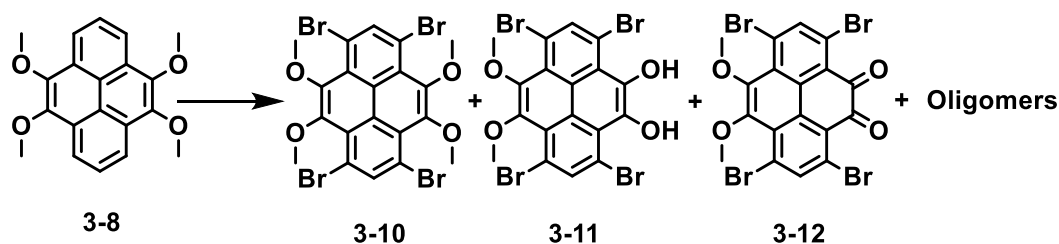
III-11: Successful synthesis route for 3-10. i: Br$_2$, CCl$_4$, 60 °C.

It was found that eight equivalents of freshly distilled bromine added to a solution of **3-8** in water free tetrachloromethane at 60 °C gives **3-10** in 40 % yield. Side products (e.g. **3-11**, **3-12**) can be removed by column chromatography and reductively methylated to further improve the yield. The elevated reaction temperature allows rapid bromination while the water free condition makes CCl$_4$ a poor solvent for hydrogen bromide, so it can rapidly leave the reaction mixture.

III.1.3   Characterization of 1,3,6,8-tetrabromo-4,5,9,10-tetramethoxypyrene (3-10)
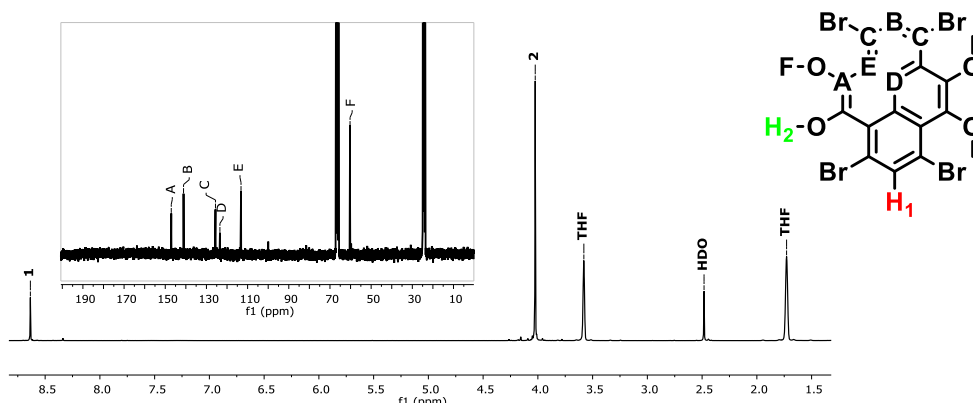
*III-12: ^{1}H- and ^{13}C-NMR spectra of **3-10** in D8-THF at 295 K. Panel: ^{1}H-NMR. Inset: ^{13}C-NMR.*

The solubility of **3-10** in deuterated THF was sufficient to record the NMR spectra at room temperature. In the ^{1}H-NMR spectrum two signals (both singlet) are observed, integrating to 1:6. This is in agreement with the postulated structure, as only two aromatic (signal *1*, $\delta = 8.64\ ppm$) and 12 ether protons (signal *2*, $\delta = 4.02\ ppm$) are present. The spectrum also supports C_{2h} symmetry. In the ^{13}C-NMR six signals (*A - F*) are observed. The low signal count is indicative for a symmetrical molecule. The signals are assigned to **3-7**, as shown in the inset.
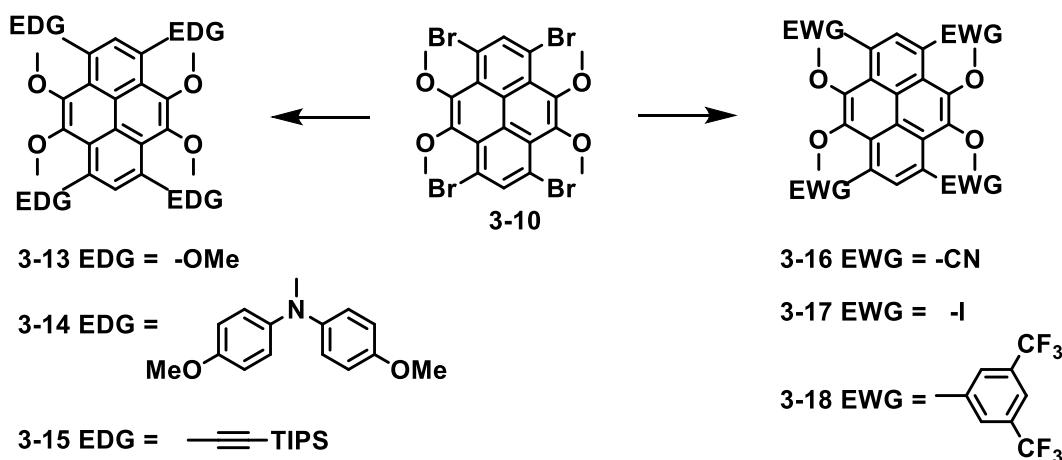
III.1.3.1   Crystal structure
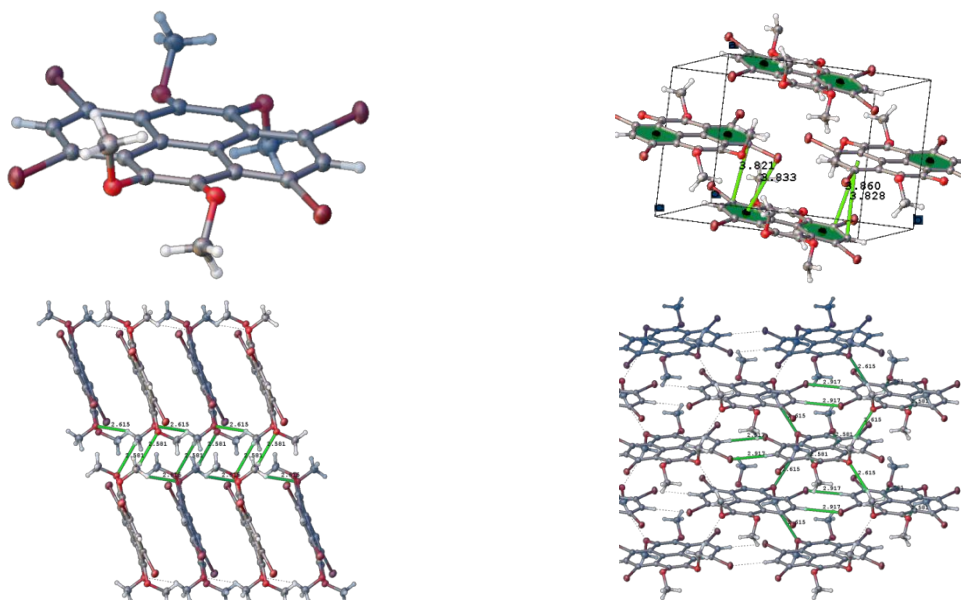
*III-13: Crystal structure analysis of **3-10**.*

A crystal suitable for X-ray diffraction crystallographic analysis was grown by slow evaporation of THF. **3-10** forms monoclinic crystals with a P2$_1$/a space group. The unit cell contains 4 molecules and has a volume of V = 965 Å^3. The bulky bromine substituents

force the methyl ether groups to twist 67° from the molecular framework (90° in **3-8**). Intermolecular short contacts are identified between the methoxy-units as well as between bromine and methoxy. The π–π distance is determined to $d_{\pi-\pi}$ = 3.8 Å.

3-13 EDG = -OMe

3-14 EDG = [structure with MeO and OMe groups]

3-15 EDG = ──═─TIPS

3-16 EWG = -CN

3-17 EWG = -I

**3-18 EWG =** [structure with CF$_3$ groups]

*III-14: Materials prepared based on 3-**10**.*

With the structure of **3-10** established, a series of new eightfold functionalized pyrene derivatives was prepared. It was possible to introduce electron donating (EDG) as well as electron withdrawing groups (EWG) (figure III-14). The resulting materials will be discussed in chapter *III.2* and *III.3*.

III.1.4   Alternative protective groups

III.1.4.1   Dioxolane

As will be discussed in more detail in section *III.3*, the removal of the methoxy ether protective group was problematic for electron deficient materials. In chapter *II*, the use of alternative protective groups was studied. The relatively harsh reaction conditions established for fourfold bromination of **3-8** made the usage of many protective groups impossible. Most phenol protection groups will be cleaved by elemental bromine and/or HBr at elevated temperatures.[278]
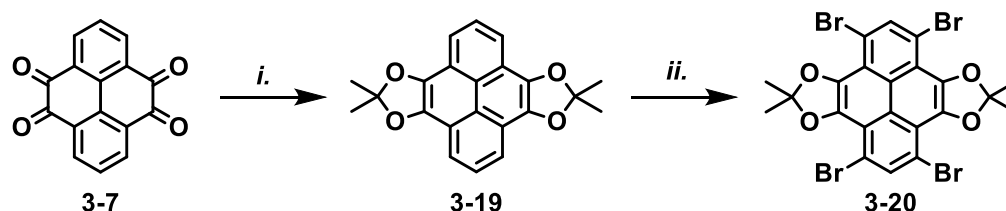
III-15: Alternative protection / bromination of dioxolane.

It was found that the dioxolane protective group, also utilized in chapter *II*, tolerated the bromination conditions for **3-10**. **3-20** was prepared starting from **3-19** in 30 % yield.

A single crystal suitable for X-ray diffraction crystallography was grown by vapor diffusion of hexane into a DMF solution of **3-20**. The material forms monoclinic crystals with a P$_1$ low symmetry space group. Its unit cell contains three molecules and has a volume of V = 2083 Å^3, approximately twice the size of **3-10**. In the crystal two molecules form a pair while the third forms an interlayer. The shortest π−π distance is d$_{π−π}$ = 3.68 Å and found in-between the paired molecules). Molecules are arranged in slipped stack columns.
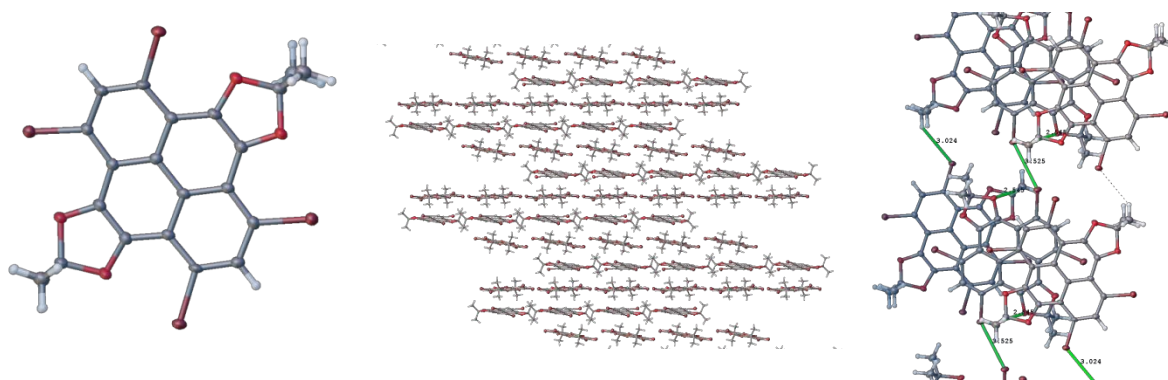
*III-16: Crystal structure of **3-20**. Left: Molecule viewed along the c-axis Middle: Packing viewed along the b-axis. Right: Stacking along the c-axis.*

As in the case of **2-38**, the low solubility of **3-20** in common organic solvents prevented its use as a general substitute for **3-10**.

III.1.4.2   Attempted protection of 1,3,6,8-tetrabromopyrene-4,5,9,10-tetraone (3-6) with glycol

MORE *et al*. reported the ketalization of 2,7-dibromo-4,5,9,10-tetraketopyrene with glycol as well as subsequent efficient deprotection to the functionalized tetraketone.[192] The advantage of the di-ketal protection of ketones is that no reduction/oxidation step is needed for the protection/deprotection. Furthermore, the deprotection is usually facile even under mild (acidic) conditions.

As no reduction is taking place, the ketal protected pyrene-4,5,9,10-tetraone would behave just like **3-7** in S$_E$Ar reactions during bromination, thus being functionalized in positions 2 and 7.[16] Therefore, **3-6** prepared according to the modified VOLLMER method, (figure III-10) was chosen as starting material.

---

[16] This is in the rather unlikely case that the protective groups would tolerate the bromination conditions.
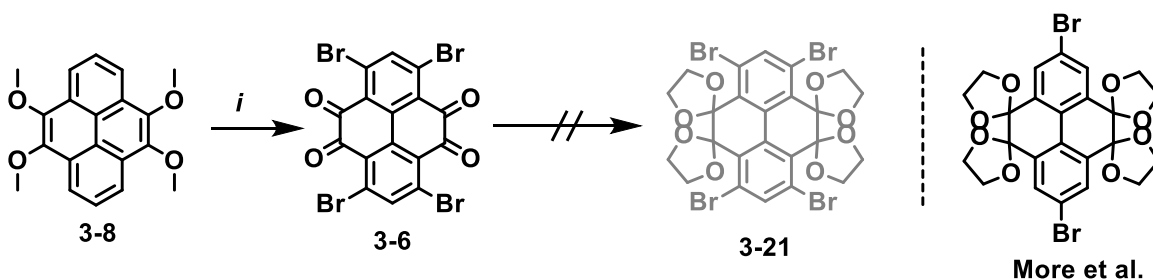
III-17: Attempted protection of 3-6. i: Br₂, PhNO₂, 160 °C, 24 h. ii: NMP, PTSA, MW 250° C 16 h.

It was not possible to prepare **3-21** under the tested reaction conditions.[192, 279, 280]The ketalization of α-diketones is very sensitive to steric influences.[280, 281] In figure III-18 space filling representations of **3-10** (derived from crystallographic data) and **3-21** (calculated by DFT) are juxtaposed.
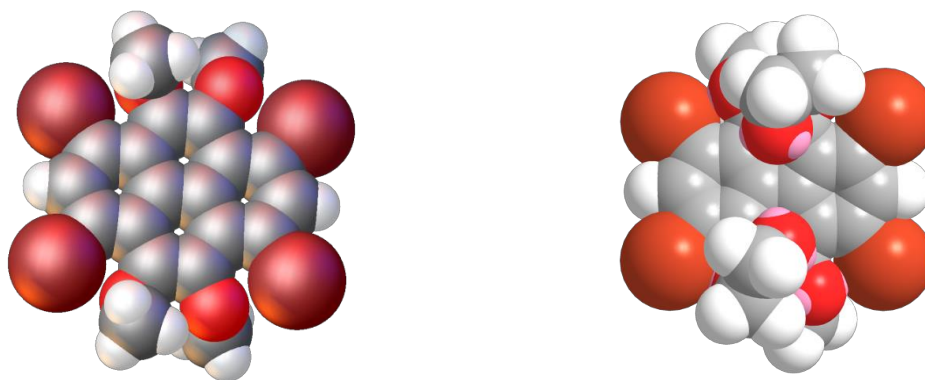
III-18: Left: Space-filling illustration of 3-10 (derived from crystallographic data). Right: Molecular modelling of 3-21.

The O – Br (center to center) distance in **3-10** is 2.87 Å. When this is compared to the sum of the van-der-Waals radii of bromine $(R_{v-d-W,Br} = 1.20\,\text{Å})$ and oxygen $(R_{v-d-W,O} = 0.66\,\text{Å})$ $\sum R_{O,Br} = 1.86\,\text{Å}$ it follows that very little room is available for sterically demanding moieties. The space filling view of **3-21** makes the steric demand of the ketals clearly visible. Thus, it is safe to assume that the ketalization reactions mainly failed due to steric factors.

III.2   Electron rich materials

As indicated in the introduction to this chapter the synthesis of new strong acceptors was at the center of interest. New electron rich materials were studied as building blocks for new donor-acceptor complexes as will be discussed in chapter *IV*.

Introducing functional groups in positions 1,3,6 and 8 of pyrene will have a stronger influence on the frontier energy compared to 2,7-functionalization. Two reasons are responsible for this: the larger number of substituents being introduced to the pyrene scaffold and the substituents not being in the nodal plane of pyrene. By extending the conjugation the $\Delta E_{HOMO \rightarrow LUMO}$ energy gap will also be affected.

III.2.1   1,3,4,5,6,8,9,10-Octamethoxypyrene (3-13)

III.2.1.1   Synthesis
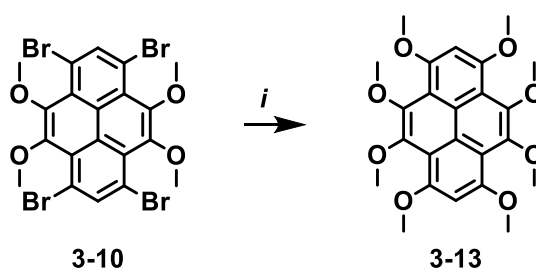
*III-19: Synthesis of **3-13**. i: NaOMe, CuI, DMF, 120 °C 16 h, 60 %.*

1,3,4,5,6,8,9,10-Octamethoxypyrene (**3-13**) is prepared from **3-10** by a copper iodide mediated ULLMANN-methoxylation reaction (figure III-19). Catalytic amounts of CuI, as used in the synthesis of 2,4,5,7,9,10-hexamethoxypyrene (**2-6**), failed to promote the desired conversion.[77] Stoichiometric quantities of copper iodide had to be used to promote the conversion of the less reactive bromo groups.[61, 282] The formation of heptamethoxypyrene side-products was reduced by decreasing the reaction temperature to 120 °C.

III.2.1.2   Characterization

The NMR spectra of a pristine sample of **3-13** are given in figure III-20 (left). Additionally, ^{1}H-NMR spectra of an aged sample of **3-13** prior to and after the addition of a reducing agent (hydrazine) are shown in figure III-20 in the right panel.
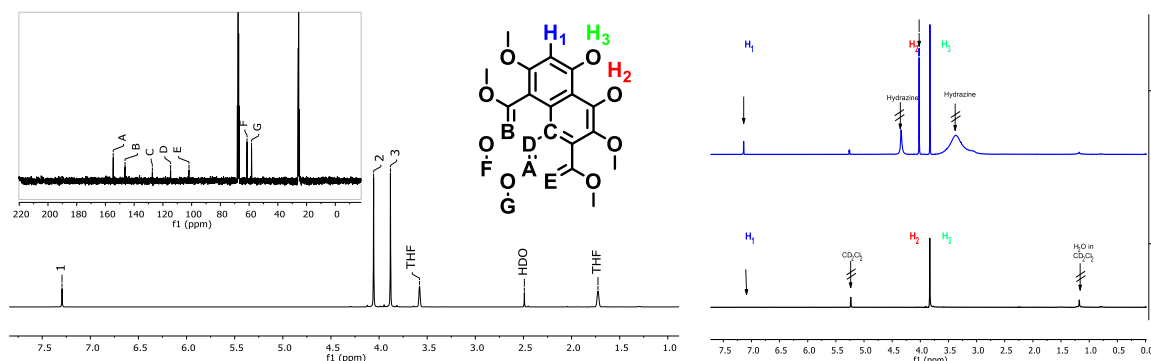
*III-20: Left: NMR spectra of **3-13** recorded in D8-THF at T = 298 K. Panel: ^{1}H-NMR spectrum (300 MHz). Inset: ^{13}C-NMR (75 MHz). Right: ^{1}H-NMR spectra of an aged sample **3-13** (in air) prior to (bottom) and after addition of hydrazine (top). Spectra recorded in CD$_2$Cl$_2$ at T = 298 K (250 MHz).*

As expected, the ^{1}H-NMR spectrum of the pristine sample shows three singlets ($\delta_1 = 7.29$ ppm, $\delta_2 = 4.06$ ppm, $\delta_3 = 3.88$ ppm) in a 1:6:6 integration ratio. This is in good agreement with two aromatic protons and two sets of methoxy units (K-region versus non-K-region). The assignment of the ^{13}C-NMR spectrum is given in the overlaying structure representation. Again K-region and non-K-region methoxy-signals have a significantly different chemical shift.

In the case of the aged sample (two months exposed to laboratory atmosphere) only one signal ($\delta = 3.82$ ppm) for **3-13** is observed. Only after reduction, the proton signals of the pyrene core ($\delta = 7.29$ ppm) and the second set of methoxy units ($\delta = 4.08$ ppm) can be resolved. This suggests the formation of a radical species by air oxidation.

This hypothesis was tested by recording an electron spin resonance (ESR) spectrum (figure III-21).
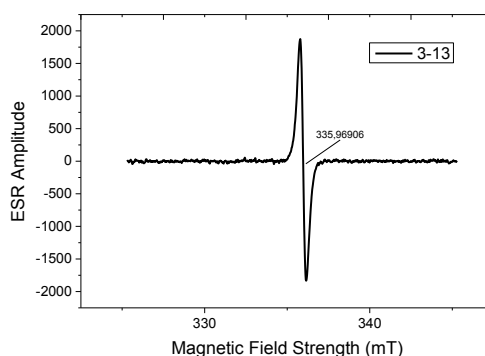

*III-21: Solid state ESR-spectrum of an aged sample of **3-13**.*

Indeed, it was found that the sample is weakly ESR active, giving a one line spectrum. Hyper-fine coupling is not resolved. This suggests a low interaction of the unpaired electron with the protons in 2 position and the methyl protons from the methoxy residues.[283] The signal was eliminated upon hydrazine addition.

A combination of the ^{1}H-NMR and the ESR spectroscopy results for the aged sample of **3-13**, suggests the formation of a radical cation. Therefore it can be concluded that **3-13** is not long-time stabile under laboratory atmosphere. The selective quenching of one methoxy signal suggests chemical inequality between K-region and non-K-region methoxy groups. The chemical shift difference between both sets of methoxy substituents suggests non-identical electronic environments. Although free rotation is allowed in solution, the crystal structure (figure III-23) indicates how they may arise. Methyl-protons in the K region are predominantly above and below the molecular plane and experience stronger shielding from the π-electron system of the pyrene scaffold than the complementary set.

III.2.1.3   Crystal structure

A crystal suitable for X-ray diffraction crystallography was grown by slow evaporation of dichloromethane.
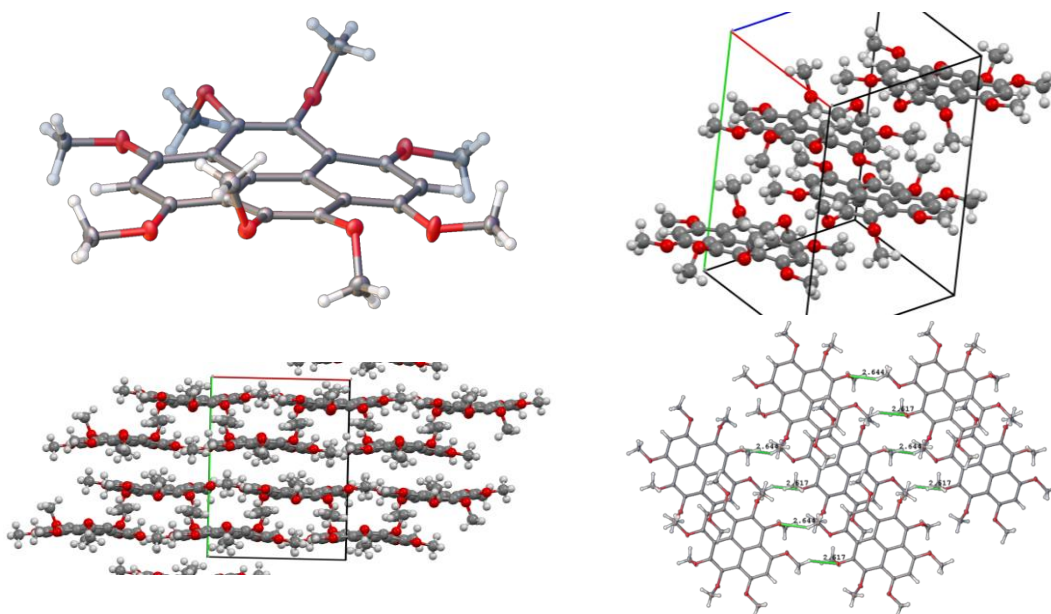
*III-22: Crystal structure **3-13**. Top-left: Representative molecule view. Top-right: Molecule along b-axis. Bottom left: Packing viewed along a-axis. Bottom right: Packing viewed along the b-axis.*

3-13 forms monoclinic crystals with a P2$_1$/n space group. Its unit cell contains four molecules and has a volume of V = 2061 Å^3. In solid state the pyrene scaffold of **3-13** is bent by 0.45 Å out of planarity (fig. III-22, top left). Methoxy-units on carbon 1,3,6 and 8 are oriented parallel to the pyrene scaffold while the moieties on carbon 4,5,9 and 10 are oriented almost perpendicularly (89.5°). For the former moieties the orientation maximizes interaction of oxygen lone-pairs with the pyrene π-system. For the latter, steric constraints force the substituents out of the molecular plane. The packing (figure III-22, top right, bottom left) confirms a layered structure. Alternating from strata to strata the molecules buckle up- or downwards. Short C–C- contacts of d$_{\pi-\pi}$ = 3.7 to 3.8 Å are found.

III.2.1.3.1 Optoelectronic properties

Cyclic voltammetry (CV) was used to establish the frontier orbital energies of **3-13**. The experiment was performed under argon atmosphere with a 1 mM solution of **3-13** in anhydrous THF using tetrabutylammonium hexafluorophosphate (*n*-Bu$_4$NPF$_6$) as conductive salt. The cyclic voltammograms of **3-13** are shown in figure III-23 before (black) and after the addition of ferrocene (Fc) (red) as an internal standard.[284]

The use of ferrocene as a solvent independent internal standard for CV experiments, the so-called "*ferrocene assumption*",[285] has been criticized in scientific literature.[286] It was found that Fc/Fc$^+$ does not behave fully independent of the solvent and electrolyte employed.[286] Is has been argued that decamethyl-ferrocene (CP$^*_2$Fe) is the superior standard.[287] Withstanding this, in accordance with the IUPAC recommendation Fc was used as internal standard in this work.[288] The variety of solvents (dichloromethane and THF) and electrolyte (Bu$_4$NPF$_6$) used for the experiments is small. According to HUPP the error is most pronounced for the reduction in non-polar solvents while the errors mostly cancel out for the oxidation in polar solvents.[285] Furthermore, the use of Fc as standard is widely spread. Thus, for the sake of comparison with the literature, this standard was deemed the most useful option despite its flaws.
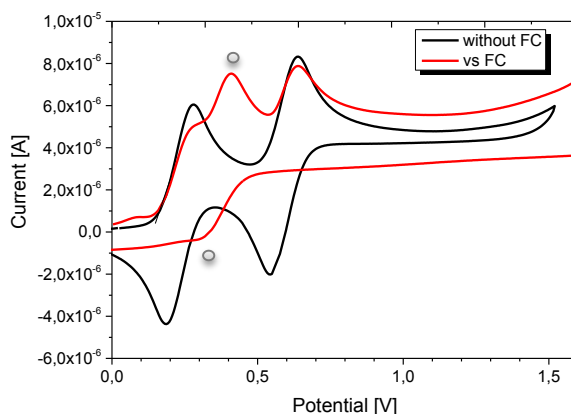
*III-23: Cyclic voltammograms of **3-13** recorded in THF using Bu$_4$NPF$_6$ as electrolyte (V = 100 mV s^{-1}). The oxidation signal of **3-13** is recorded with ferrocene (Fc) as internal standard (shown in red) and without it (shown in black).*

As a consequence of the low electron affinity only the oxidation signal of **3-13** was resolved. Prior to the addition of Fc two reversible signals at $U_{onset,1} = 0.15$ V and $U_{onset,1} = 0.52$ V are identified. When Fc was added, the oxidation was irreversible. The curve has two distinct oxidation waves ($U_{max,1} = 0.41$ V and $U_{max,2} = 0.64$ V). The first wave has a shoulder with $U_{sh,1} = 0.27$ V. $U_{sh,1}$ and $U_{max,2}$ align with the maxima of **3-13** oxidation signals prior to Fc addition.

From the black curve it can be concluded that, during the CV experiment, **3-13** can release two electrons reversibly. The red curve suggests an irreversible electron transfer between

Fc and **3-13** taking place during the CV experiment. The HOMO energy of **3-13** was determined from the onset of the oxidation wave in reference to ferrocene.[288]

$$E_{HOMO} = -[(E_{ox,onset} - E_{ox,onset,Fc}) + 4.8] = -[(0.15 - 0.22) + 4.8] = -4.73\ eV \qquad \text{(III-1)}$$

Eq. (III-1): E_{HOMO} gives the experimental HOMO energy in eV, $E_{ox,onset}$ the onset of the analyte oxidation in V, $E_{ox,onset,FC}$ the onset of the ferrocene oxidation signal in V.

The UV-vis absorption and photoluminescence spectra of **3-13** are shown in III-24.
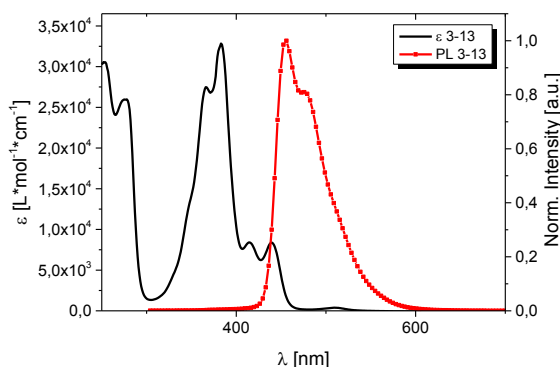
*III-24: UV-vis absorption (black) and photoluminescence (red) spectra of **3-13** ($5*10^{-5}$ mol/l in CH_2Cl_2).*

In the absorption spectrum three distinct bands are observed ($\lambda_{max,abs1} = 276$ nm, $\varepsilon_{max,abs1} = 3*10^5$ L*mol^{-1}*cm^{-1}, $\lambda_{max,abs2} = 382$ nm, $\varepsilon_{max,abs2} = 3*10^5$ L*mol^{-1}*cm^{-1}, $\lambda_{max,abs3} = 438$ nm, $\varepsilon_{max,abs3} = 8*10^4$ L*mol^{-1}*cm^{-1}). All bands show vibrational splitting. The onset of the absorption is determined to $\lambda_{onset} = 456$ nm. The optical bandgap is determined from the S_1->S_0 (0-0) transition to $\Delta E_{opt} = 2.76$ eV.[17] The PL spectrum has its maximum at $\lambda_{max,PL} = 457$ nm and a distinct shoulder at $\lambda_{PL} = 480$ nm. A long fluorescence tail is also observed. The physical properties of **3-13** will be compared to methoxypyrene congeners in section *III.2.1.4*.

III.2.1.4   Comparison to other methoxypyrenes

For this comparison the following methoxypyrenes are considered.
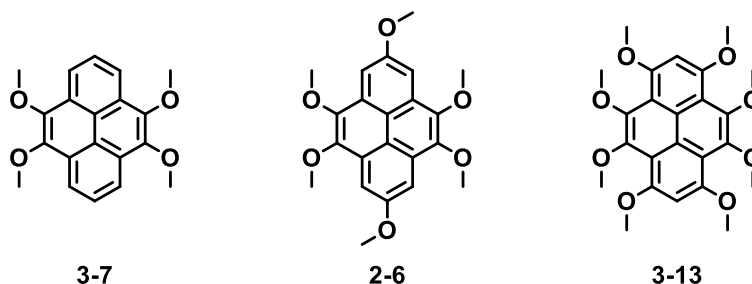
III-25: Structures of methoxy pyrenes used for comparison.

---

[17] Commonly used is the intersection of PL and absorption spectrum.[145]

The synthesis and properties of **3-7** were reported by ZÖPHEL *et al.*[87] while **2-6** was reported by KAWANO *et al.*[77] ^{1}H-NMR spectra of the three materials are compared in the following figure. It can be seen that signal *A* as well as signal *B* (and *C* if present) are shifted to lower field strength as the derivative's electron density is increased. It holds generally true that EDGs tend to shift aromatic protons (signal *A*) to higher fields strength.[289]
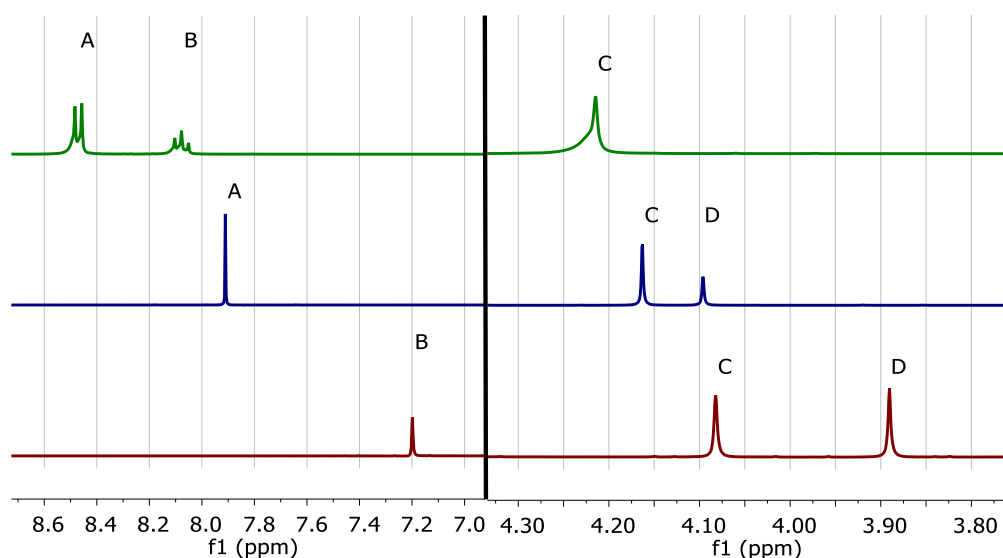
III-26: [1]*H-NMR spectra of* ***3-7*** *(in green),* ***2-6*** *(in blue) and* ***3-13*** *(red) compared. Left: The aromatic region (8.6 – 7.0 ppm). Right: The methoxy region (4.3 – 3.8 ppm).*

Going from **3-7** to **2-6** signal *A* is shifted by $\Delta\delta_A = 0.56$ ppm whereas signal *B* is shifted by $\Delta\delta_B = 0.88$ ppm (**3-7** to **3-13**). The alteration in the methyl signal position is less pronounced. Signal *C* is moved by $\Delta\delta_C = 0.05$ ppm and $\Delta\delta_C = 0.13$ ppm respectively. Due to the larger electronic difference between positions 2 and 7 (**2-6**) and 1,3,6 and 8 (**3-13**) in pyrene signal *D* is changed by $\Delta\delta_D = 0.21$ ppm. The discussed NMR data are compiled in table III-2:

Table III-2: NMR signals and ESR activity of ***3-7****,* ***2-6*** *and* ***3-13*** *compared.*

	Signal *A* (ppm)	Signal *B* (ppm)	Signal *C* (ppm)	Signal *D* (ppm)	ESR activity
3-7 (TMP)	8.47	8.08	4.21		Not observed
2-6 (HMP)	7.91	N/A	4.16	4.10	Not observed
3-13 (OMP)	N/A	7.14	4.02	3.82	Aged sample
[a] samples measured in CH_2Cl_2					

The absorption and photoluminescence spectra of the three materials are collected in figure III-27. The corresponding optoelectronic properties are compiled in table III-3.
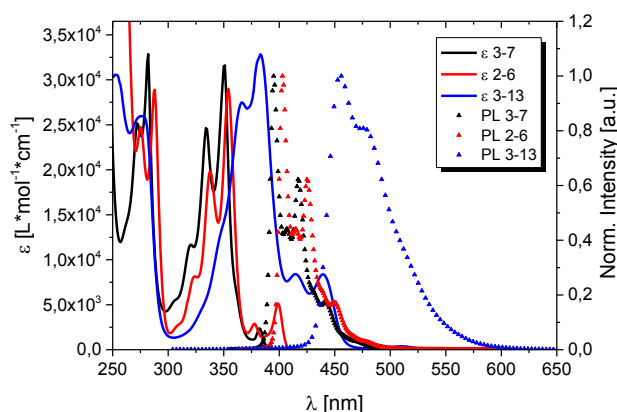
*III-27: UV-vis absorption and PL spectra of **3-7** (black), **2-6** (red) and **3-13** (blue) recorded in CH₂Cl₂.*

While the difference of the optical spectra between **3-7** and **2-6** is limited ($\Delta\lambda_{Abs} \approx 4$ nm; $\Delta\lambda_{PL} \approx 8$ nm), **3-13** has a significant bathochromic shift by $\Delta\lambda_{Abs} \approx 38$ nm and $\Delta\lambda_{PL} \approx 52$ nm. In all absorption spectra the vibrational fine structure is resolved. Besides the maximum at $\lambda = 455$ nm, the fluorescence spectrum of **3-13** shows only a shoulder at $\lambda = 480$ nm and a broad tail up to 575 nm. **2-6** in contrast displays three sharp features ($\lambda_{max} = 455$ nm, $\lambda_{max,2} = 425$ nm and $\lambda_{max,3} = 455$ nm) and virtually no tail. The full width at half maximum (FWHM) for **3-7** and **2-6** is as low as 9 or 10 nm respectively in contrast to 61 nm observed in **3-13**.

*Table III-3: Optoelectronic properties of **3-7**, **2-6** and **3-13**.*

Entry	Color (solid state)	λ_abs,max (nm)	ΔE_opt (eV)	λ_PL,max (nm)	FWHM_PL (nm)	E_HOMO,CV (eV)[a]	E_LUMO,CV (eV)[a]	E_HOMO,DFT (eV)[b]	E_LUMO,DFT (eV)[b]
3-7 (TMP)	colorless	382, 351, 285, 245	3.16	385	9	5.44	2.28	5.37	1.71
2-6 (HMP)	colorless	399, 354, 285, 260	3.02	403, 425	10	5.01	1.99	5.03	1.34
3-13 (OMP)	yellow	437, 382, 276	2.67	455, 480	61	4.73	2.06		

[a]Cyclic voltammetry, Fc used as internal standard. [b] determined by $E_{LUMO\,Exp} + \Delta E_{Op} = E_{HOMO,Exp}$; [c]DFT - B3LYP, 6-31*.

As predicted by theoretical calculations, the HOMO is destabilized within the series (TMP > HMP > OMP). The computational and experimental values are generally in good agreement. LUMO energy is usually predicted less accurately by DFT calculations employing the B3LYP functional. While **3-7** and **2-6** are stable under laboratory atmosphere for long periods of time (>1 a), **3-13** is slowly oxidized (within months). The behavior of these materials in donor-acceptor complexes will be discussed in chapter *IV*.

To compare the materials in the solid state, X-ray diffraction results can be used.
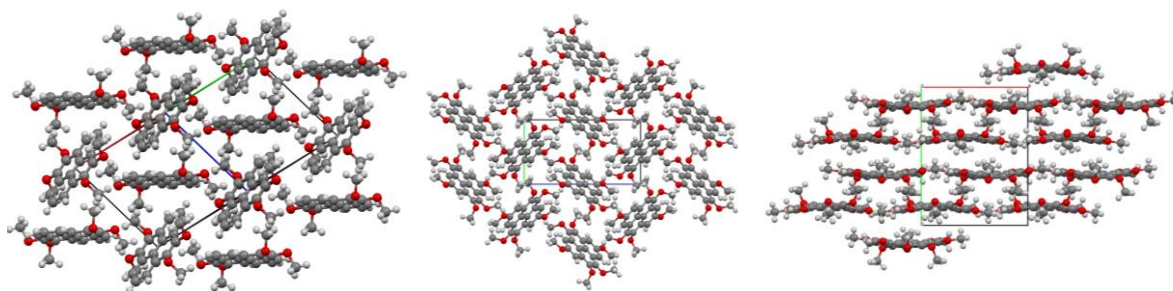
*III-28: Packing motives of **3-7** (left), **2-6** (middle) and **3-13** (right).*

In the crystalline state **3-7** and **2-6** are planar molecules. In contrast, the pyrene scaffold in **3-13** is slightly buckled (figure III-28). Whereas **3-7** and **2-6** grow in a herringbone type packing, **3-13** is organized in a sheet-like packing. The herringbone motive provides good intermolecular π–π interactions and is thus generally found in high-mobility single crystal OFET materials.[144] Field effect transistors were fabricated by drop casting, field effect mobility was not observed for any material. In all materials methoxy-units in the K-region are twisted out of the molecule's plane disrupting intermolecular π–π interactions. In contrast, non-K-region methoxy units (as found in **3-13** and **2-6**) are in parallel to the molecule's pyrene scaffold (e.g. figure III-22 top left).

III.2.2 1,3,6,8-[Bis(*p*-anisoyl)amine]-4,5,9,10-tetramethoxypyrene (3-14)

III.2.2.1 Synthesis
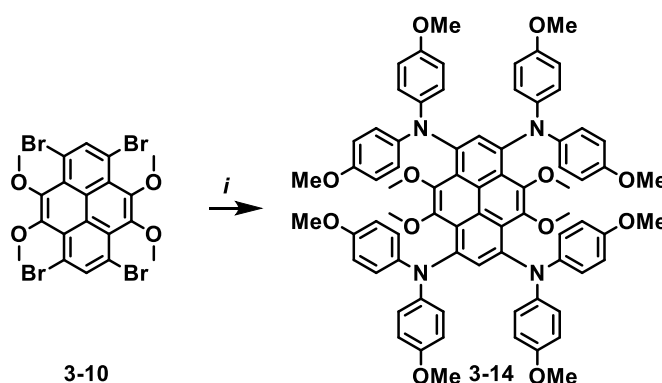
*III-29: Synthesis of **3-14**. i: (p-MeOPh)₂NH, Pd₂DBA₃, QPhos, Tol, 105 °C, 16 h, 85 %.*

In order to increase the electron density of pyrenes even further in comparison to **3-13** bis(*p*-anisoyl)amine was chosen as substituent. Very electron rich donors allow the use of weaker acceptors in the search for new CT-complexes with neutral-ionic transitions.[166, 169] Amines are generally better EDGs than ethers, bis(*p*-anisoyl)amine is a very electron rich amine yet still relatively insensitive to air oxidation. The formation of quinoidal (leuco)

bases is less favored than in the even more electron rich bis(*p*-dimethylaminephenyl)amine which is unstable in air.[290]

3-14 was prepared by BUCHWALD-HARTWIG amination reaction of **3-10** with bis(*p*-anisoyl)amine. For this palladium catalyzed cross-coupling reaction the Qphos ligand system gave the desired product in high yields. The product tolerated purification by column chromatography on silica gel.

III.2.2.2   Characterization

3-14 is soluble in common organic solvents and can be characterized by field-desorption mass spectrometry and NMR spectroscopy. The molecular ion $[M]^+$ was identified at m/z = 1231.1 in good agreement with the calculated mass of M = 1230.5 g/mol. The NMR spectra were recorded at 300 MHz resolution in deuterated dichloromethane.
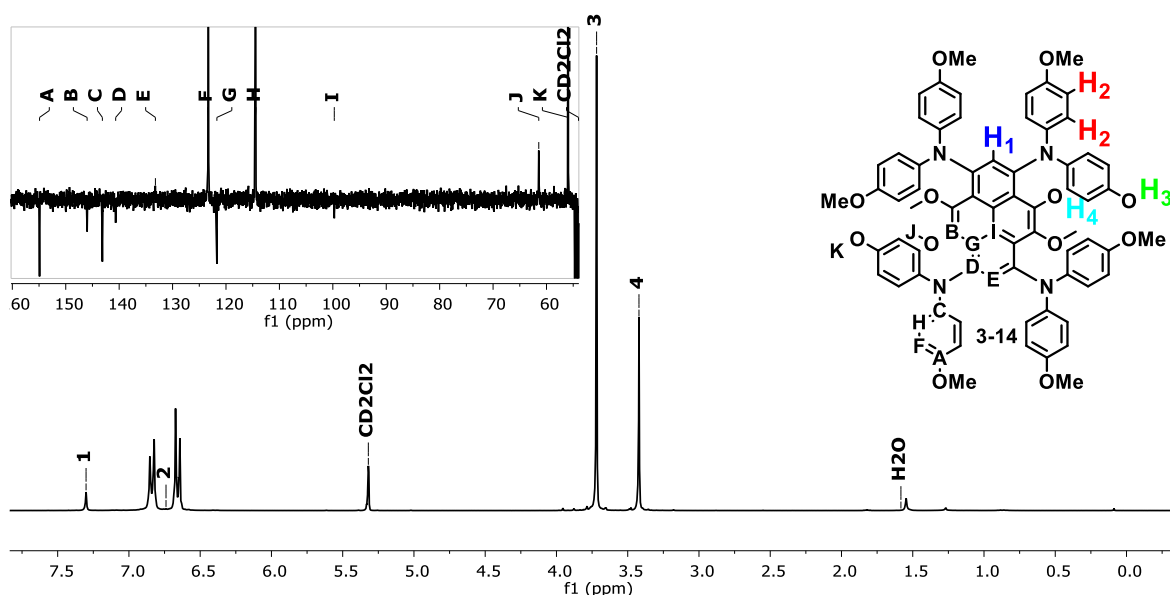
*III-30: NMR spectra of **3-14** in CD$_2$Cl$_2$ (recorded at 298 K). Panel: ^{1}H-NMR. Inset: ^{13}C-APT-NMR.*

The ^{1}H-NMR spectrum consists of four signals. Signal *1* (δ = 7.3 ppm, s) is associated with the pyrene core protons. The *p*-phenyl protons are combined in signal *2* (δ = 6.74 ppm, dd) characterized by a pronounced roof effect. Signal *3* and *4* are generated by two chemically unequal methoxy groups. Signal *3* (δ = 3.72 ppm, s) is assigned to the anisoyl residues whereas the pyrene-bound methoxy units can be consigned to the remaining signal (δ = 3.42 ppm, s). As Signal *3* has twice the area under the curve as signal *4* this assignment is safe. The ^{13}C-APT-NMR spectrum reveals 11 signals (*A* - *K*). Signals *A, C, F, H* and *K* are assigned to the anisoyl moieties due to their intensity and phase in the ^{13}C-APT experiment. It is surprising that signal *E* is quite weak as it is a tertiary carbon. Signals *J* and *K* are assigned to the methoxy carbons due to their chemical shift.

III.2.2.2.1 Crystal structure

It was possible to grow a single crystal of **3-14** suitable for X-ray diffraction crystallography in order to study the structure in the solid state.
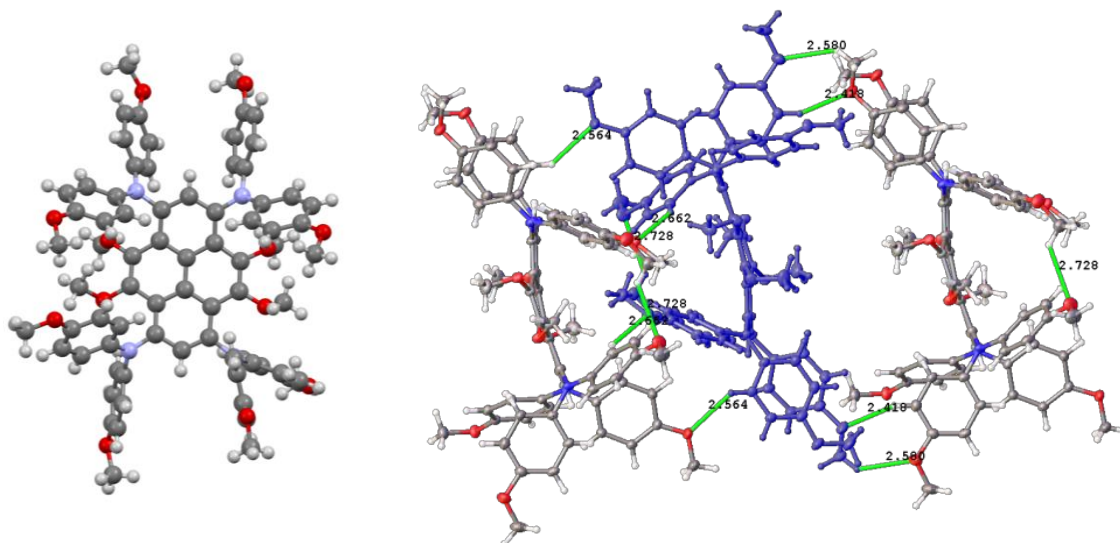
*III-31: X-ray diffraction structure of **3-14**. Left: Top view of a single molecule. Right: Cutout of the packing motive. For clarity one molecule is displayed in blue.*

**3-14** forms triclinic crystals and grows in a P1 space group. Its unit cell contains 14 molecules and has a volume of V = 3111 Å³. The symmetry of **3-14** is very low, as is to be expected from a molecule with numerous degrees of freedom. The packing is complex and dominated by hydrogen bonding. Several inter- and intramolecular O···H-C short contacts are identified between the anisoyl residues (figure III-31, right). Furthermore, C-H-π-interactions between the anisoyl residues are identified with shortest distances of 3.3 Å. The pyrene-scaffold is not involved.

III.2.2.3 1,3,6,8-Tetra[bis(*p*-anisoyl)amine]pyrene (3-25)

Independent of the synthesis of **3-14** it was attempted to prepare **3-26**. Computational chemistry calculations performed by WONNEBERGER at *BASF SE Ludwigshafen, Germany* identified **3-26** as a promising candidate for a hole-transport material in OPVs, by virtue of its predicted LUMO energy. Additionally, the material is required to be transparent in the visible region of the light spectrum to allow efficient light harvesting. Already **3-25** showed a strong absorption in the UV/Vis spectrum (*vide infra*). Therefore, **3-26** was eliminated as a viable candidate, as probably will have an even stronger absorption in the visible range. In consequence, the project was aborted.
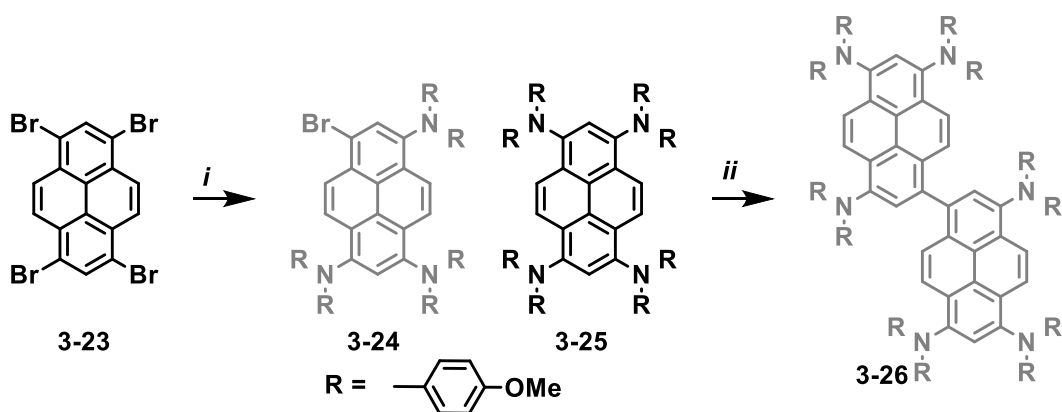
*III-32: Planned synthesis of **3-26**. i: (p-MeOPh)₂NH, Pd₂DBA₃, QPhos, Tol, 105 °C, 16 h, 76 % (**3-25**).*

The synthesis of **3-26** was planned in two steps. BUCHWALD-HARTWIG amination was expected to give **3-24**, which was to be dimerized by a YAMAMOTO type reaction to the target compound. Contrary to expectation, the first step gave almost exclusively **3-25** and the starting material (**3-23**) although only three equivalents of the amine were added. The low solubility of **3-23** was identified as the key problem, since the starting material was merely suspended in the reaction mixture. Consequently, the stoichiometric ratios were not operational. Attempts were made to run the reaction at higher dilution, with less active catalyst systems (e.g. Xphos or PEt₃) and slow addition of the amine. These attempts were marred by a broad distribution of products from which **3-24** was isolated only in low amounts. Before optimal conditions were identified, the project was stopped.

Recently, JEON *et al*. reported the use of **3-25** as hole transport material in a solid state DSSC.[291] They highlight the good energy matching between gold and **3-25**. Compared to spiro-MeOTAD traditionally used in DSSCs the charge carrier mobilities are low.[292]

3-25 provides an ideal reference point for identifying the effects of K-region functionalization on very electron rich pyrene derivatives. Henceforth, it will be used in this manner.

In the ¹H-NMR spectrum of **3-25** the protons in 2 and 7 position of pyrene are giving a signal at $\delta = 7.46$ ppm. This little deshielding compared to **3-14** ($\delta = 7.30$ ppm) can be attributed to reduced electron density on the pyrene core.

The crystal structure of **3-25** was not reported by JEON *et al*. [291] Therefore, a crystal suitable for X-ray diffraction crystallography was grown by slow evaporation of a solution of **3-25** in dichloromethane.
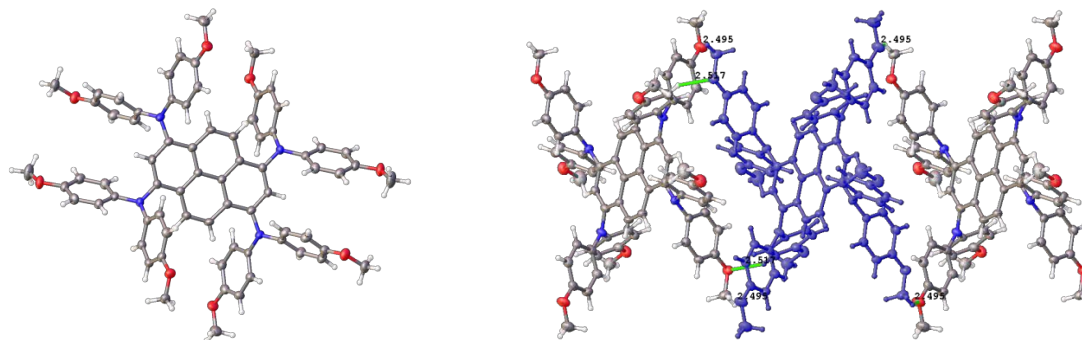
*III-33: Solid state structure of **3-25** derived by X-ray diffraction crystallography. Left: Molecule in top view. Right: Cut-out of the packing motive.*

The material forms triclinic crystals and grows in a P_1 space group. Its unit cell contains six molecules and has a volume of $V = 1413$ Å^3. Compared to **3-14** the unit cell contains less than half the volume and 42% of the molecules. In **3-25** CH-O short contacts dominate the packing motive. The molecule is higher in symmetry compared to **3-14**. The amino substituents are twisted by 47° and 54° out of the pyrene plane, whereas in **3-14** each amine substituent is arranged differently (43.5°, 47.8°, 54.1°, 68.5°). The ability of **3-14** to form additional hydrogen bonds from the pyrene K-region accounts for this difference.

III.2.2.4   Optoelectronic properties
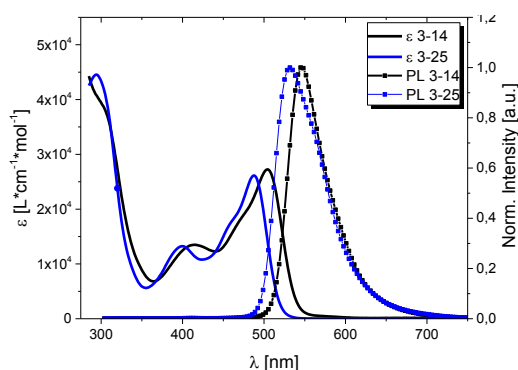
*III-34: UV-vis absorption (solid) and photoluminescence spectra (symbol) of **3-14** (in black) and **3-25** (in blue) recorded in CH$_2$Cl$_2$ (5*10^{*-5} mol/l).*

The absorption spectra of **3-14** and **3-25** show similar features. The absorption maxima of the latter are hypsochromically shifted (by $\lambda \approx 10$ nm to 15 nm). The extinction coefficient of **3-14** is slightly increased. For the first absorption band ($\lambda_{max1,\textbf{3-14}} = 504$ nm) a molar extinction coefficient of $\varepsilon_{max1,\textbf{3-14}} = 2.7*10^{*5}$ L*cm^{-1}*mol^{-1} is found, compared to $\varepsilon_{max1,\textbf{3-25}} = 2.6*10^{*5}$ L*cm^{-1}*mol^{-1} ($\lambda_{max1,\textbf{3-25}} = 488$ nm) for **3-25**. The optical band-gap of **3-14** ($\Delta E_{Opt,\textbf{3-14}} = 2.36$ eV) is about 0.1 eV smaller than for **3-25** ($\Delta E_{Opt,\textbf{3-25}} = 2.45$ eV). The photoluminescence spectra have a single maximum and a long tail (approx. 75 nm). Additional features are not resolved. The PL maximum of **3-14** is found at $\lambda_{maxPL,\textbf{3-14}} = 545$ nm. For **3-25** a hypsochromic shift by 13 nm ($\lambda_{maxPL,\textbf{3-25}} = 532$ nm) is

detected. The PL spectrum of **3-25** is broader, with a full width at half maximum (FWHM) of 69 nm compared the only $FWHM_{PL,\textbf{3-14}}$ = 58 nm of **3-14**.

From this it can be concluded that the additional methoxy-moieties in the K-region reduce the optical band-gap by 0.1 eV, red-shift the PL maximum by $\Delta\lambda_{PL}$ = 13 nm and improve the spectral purity at the same time.
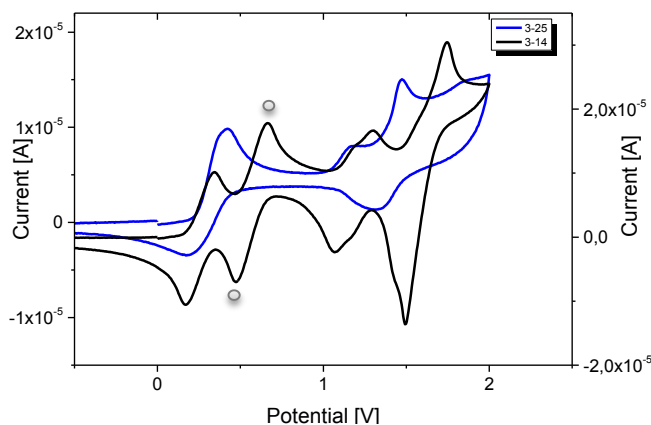
*III-35: Cyclic voltammograms of **3-14** (black) and **3-25** (blue) recorded in THF using Bu₄NPF₆ as electrolyte (V = 100 mV s⁻¹). **3-14** was referenced versus ferrocene (Fc) as internal standard (black symbol).*

The voltammogram of **3-14** has three reversible waves (U_{onset} = 0.18 V, 1.11 V and 1.54 V) that can be identified. As the second wave has a clearly discernable shoulder at U = 1.03 V it can be deduced that **3-14** can be oxidized electrochemically four times in the CV experiment. Most probably, the oxidation occurs at the nitrogen centers. Spectroelectrochemistry could be used to verify this assumption.[293] Triphenylamines are well known to form stable cations, hence their usefulness as hole transport materials.[145]

$$E_{HOMO} = -\left[\left(E_{ox,onset} - E_{onset,Fc}\right) + 4.8\right]eV = -[(0.18 - 0.41) + 4.8] = -4.57\ eV \quad \text{(III-2)}$$

Eq. (III-2): E_{HOMO} gives the experimental HOMO energy in eV, $E_{ox,onset}$ the onset of the analyte oxidation in V, $E_{ox,onset,FC}$ the onset of the ferrocene oxidation signal in V.

From this **3-14** emerges as a very electron rich material. Oxidation in air seems probable. Indeed, discoloration on the surface of aged solid samples was observed, yet this process is slow. Steric congestion around the nitrogen centers most probably stabilizes the molecule. For **3-25** to reversible oxidation waves are resolved (U_{onset} = 0.29 V and 1.37 V) which translates to $E_{HOMO,\textbf{3-25}}$ = -4.68 eV using equation (III-2). The reduction peaks of **3-14** or **3-25** were not resolved in CV experiments due to their low electron affinity. Consequently, the energy of the LUMO was derived in conjunction with the optical band-gap ΔE_{opt}. For **3-14** $E_{LUMO,\textbf{3-14}}$ = -2.21 eV and $E_{LUMO,\textbf{3-25}}$ = -2.21 eV.

JEON *et al.* report the HOMO energy of **3-25** in their publication as low as $E_{HOMO,LIT}$ -5.11 eV.[291] This discrepancy is due to a different evaluation of Fc referenced CV spectra. Using equation (III-2) to assess the data reported in the literature, a good agreement with the results given in figure III-35 is reached.

Optoelectronic properties of both materials are compared in table III-4. As in the case of **3-13**, computational data has been able to predict the experimental results reasonably well. K-region methoxy units can affect the electron density even in already electron rich compounds ($DE_{HOMO} \approx 0.1$ eV). Thus, K-region substitution can be exploited for the fine-tuning of HOMO energies in pyrene based donors and possible charge carrier transport materials.

*Table III-4: Optoelectronic properties of **3-14** and **3-25**.*

Entry	Color (solid state)	$\lambda_{abs,max}$ (nm)	ΔE_{opt} (eV)	$\lambda_{PL,max}$ (nm)	$FWHM_{PL}$ (nm)	$E_{HOMO,CV}$ (eV)[a]	$E_{LUMO,CV}$ (eV)[a]	$E_{HOMO,DFT}$ (eV)[b]	$E_{LUMO,DFT}$ (eV)[b]
3-14	Red	504, 414, 304	2.36	545	58	-4.57	2.21	-4.12	-1.52
3-25	Orange	488, 398, 294	2.45	532	69	-4.68	2.21	-4.27	-1.52

[a]Cyclic voltammetry, Fc used as internal standard. [b] determined by $E_{LUMO\,Exp} + \Delta E_{Op} = E_{HOMO,Exp}$; [c]B3LYP,6-31*

The observation that amine substituents render **3-14** a stronger electron donor compared to **3-13** is little surprising. The extent, about 0.2 eV, was smaller than initially expected.

III.2.3   1,3,6,8-(Trisisopropylethynyl)-4,5,9,10-tetramethoxypyrene (3-15)

It was planned to use **3-15** as a building block for polyphenylene dendrimers. As mentioned in the introduction, 1,3,6,8-tetraethynyl pyrene derivatives have been studied extensively as core units for dendrimer synthesis.[47] Using **3-15** instead gives access to a donor-acceptor dendrimer with donor shell and eventually a pyrene-4,5,9,10-tetraone acceptor core. This provides a good opportunity to study intramolecular energy and charge transport processes. In this work only the core building block will be presented.
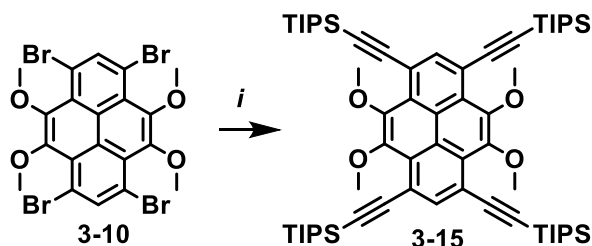
III-36: i: TIPS-CC-H, PdCl$_2$(PPh$_3$)$_2$, PPh$_3$, NEt$_3$, Tol, 80 °C, 12 h, 83 %.

3-15 is readily soluble in common organic solvents and can be purified by column chromatography with silica gel. It grows into centimeter-sized single crystals from a concentrated dichloromethane solution.

III-37: Solid state structure derived from X-ray diffraction data. Left: Top view. Right: Packing motive.

3-15 forms triclinic crystals and grows in a P$_1$ space group. Its unit cell contains five molecules and has a volume of V = 1562 Å^3. π–π Distances exceed 6 Å between two pyrene scaffold units. Short packing contacts are only observed within the TIPS periphery.
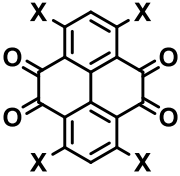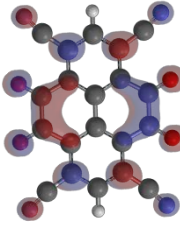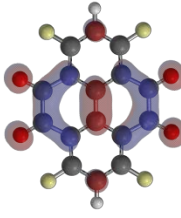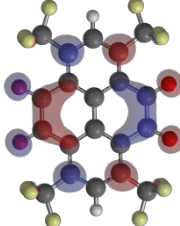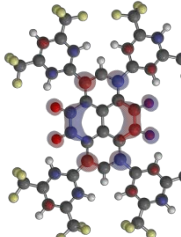
III.2.3.1   OFET properties

Large single crystals of **3-15** were readily available. Attempts were made to contact one of these for a single crystal OFET device even before X-ray diffraction crystallography data were available. In the experiments no field effect was observed. The failure is easily explained considering the lack of π–π interactions observed in the crystal structure (figure III-37). For charge carrier mobility these interactions are essential.[111]

III.3 Electron deficient materials

A series of 1,3,6,8-substituted pyrene-4,5,9,10-tetraketones was planned. The calculated frontier orbital energies are collected in table III-5.

Table III-5: Calculated frontier orbital energies of planned pyrene-4,5,9,10-tetraketones.

3-29 X = -CN 3-30 -F 3-31 -CF$_3$ 3-32 -Ph(CF$_3$)$_2$	3-29	3-30	3-31	3-32
LUMO (eV)[a]	-5.36	-4.38	-4.92	-4.68
HOMO (eV)[a]	-8.45	-7.60	-8.22	-7.87
[a] DFT – B3LYP 6-31G*				

As can be seen in the table above, variation of the electron withdrawing group has a significant impact on the calculated frontier orbital energies. By far the lowest LUMO energy is predicted for **3-29** ($E_{LUMO,\textbf{3-29}}$ = -5.36 eV). This is close to the quinoidal acceptor **2-24** (-5.54 eV) and even -5.65 eV calculated for F$_4$-TCNQ. For **3-31** a LUMO energy ($E_{LUMO,\textbf{3-31}}$ = -4.92 eV) comparable to TCNQ ($E_{LUMO,TCNQ,DFT}$ = -4.81 eV) is predicted. Slightly more inferior as acceptor to TCNQ is **3-32**. The most surprising result is the high energy LUMO ($E_{LUMO,\textbf{3-30}}$ = -4.38 eV) predicted for fluorine substituted **3-30**. Often fluorine is thought to have a stronger electron withdrawing effect than a CF$_3$-unit. Contrary to this, CF$_3$ substitution has a stronger impact on the lowering of pk$_a$ values of substituted phenols than fluorine.[294] Nevertheless, it is probable that the effect of fluorine substitution is underestimated in these calculations.[295]

It is noteworthy that, in the case of **3-29** and **3-32**, the calculated LUMO extends onto the EDGs while this is not the case for **3-30** and **3-31** (top row, table III-5). For all optimized geometries a flat pyrene scaffold is anticipated.

III.3.1 Failed synthesis 1,3,6,8-tetracyanopyrene-4,5,9,10-tetraone (3-29)

1,3,6,8-Tetracyanopyrene-4,5,9,10-tetraone (**3-29**) was identified as a very strong electron acceptor. Instead of using the unstable quinoidal derivative of pyrene to lower the LUMO (as attempted in chapter *II*) in this approach the number of electron withdrawing substituents was to be increased.
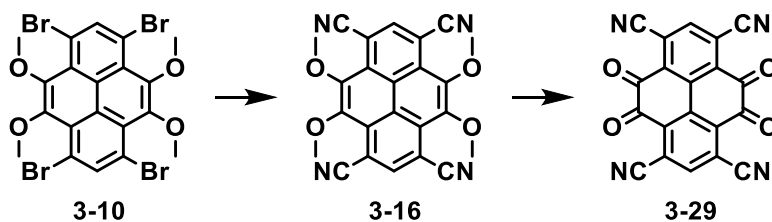
III-38: Planned synthesis of 3-29.

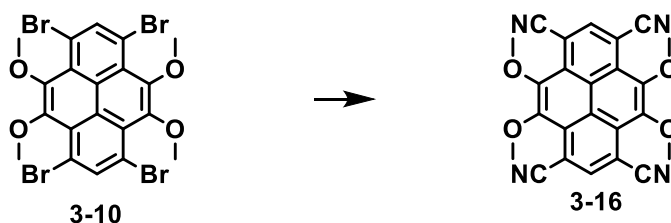Starting from **3-10** it was planned to prepare 1,3,6,8-tetracyano-4,5,9,10-tetramethoxypyrene (**3-16**) which was to be deprotected to yield the target compound **3-29** in a subsequent step. In general, the synthetic route is similar to the synthesis of 2,7-tetracyanopyrene-4,5,9,10-tetraone.[77]

III.3.1.1   1,3,6,8-Tetracyano-4,5,9,10-tetramethoxypyrene (3-16)

III-39: Synthesis of 1,3,6,8-tetracyano-4,5,9,10-tetramethoxypyrene.

The cyanation of aryl bromides is considered to be a standard reaction in organic chemistry.[296, 297] On a laboratory scale ROSENMUND-VON BRAUN reaction of i.e. copper(I)cyanide in a high boiling polar solvent is well established and often provides the desired product.[298] This holds true for the cyanation of 2,7-diiodo-4,5,9,10-tetramethoxypyrene (**2-5**) and even 1,3,6,8-tetrachloro-4,5,9,10-tetraphenylpyrene as reported by ZÖPHEL et al.[77, 89]

The synthesis of the tetracyano derivative of **3-10** was unexpectedly problematic. It was not possible to isolate the target compound from ROSENMUND-VON BRAUN reaction mixtures. Electron rich substrates are generally considered to be deactivated towards cyanation reactions.[299] The reactivity of Aryl-X in cyanation reactions is inversely proportional to the bond dissociation energy (reactivity: I > Br > Cl).[300] This may account for the higher reactivity of **2-5** in ROSENMUND-VON BRAUN reactions. Furthermore, the electron density in the 2 and 7 positions is much lower (ergo less deactivated) than in 1,3,6,8 positions. As **3-16** has exceptionally low solubility in common organic solvents the possibility that small amounts of **3-16** were formed but discarded with the copper sludge cannot be ruled out.

In recent years palladium catalyzed cyanation reactions have gained in popularity. Catalysis allows the transformation of otherwise inert aryl chlorides. Often, milder reaction conditions (lower reaction temperature, less transition metal) and less toxic CN sources ($Zn(CN)_2$, $Na_4Fe(CN)_6$) can be used.[299] Table III-6 lists reactions screened to prepare **3-16**.

*Table III-6: Reaction screening cyanation of **3-10**.*

Entry	Conditions	Outcome
1	CuCN, high boiling solvent (tested: DMF, DMAc, NMP)[301]	Broad mixture of products, **3-16** not identified
2	$Zn(CN)_2$, $Pd(PPh_3)_4$, DMF	No conversion
3	$Zn(CN)_2$, $Pd_2(DBA)_3$, XANTPHOS, TMEDA, DMF[302]	Broad mixture of products, **3-16** not identified
4	$Zn(CN)_2$, $Pd_2(DBA)_3$, DPPF, NMP,H_2O[303]	Broad mixture of products, **3-16** not identified
5	$K_4[Fe(CN)_6] \cdot H_2O$,CM-Phos, CuI, Na_2CO_3, $MeCN/H_2O$	No conversion
6	$K_4[Fe(CN)_6]$, $Pd(OAc)_2$, DPPF, NMP[304]	Broad mixture of products, **3-16** not identified
7	$Zn(CN)_2$, $Pd_2(DBA)_3$, S-Phos, DMF[305]	Broad mixture of products, **3-16** not identified
8	NaCN, CuI, KI, $MeNCH_2CH_2NMe$, Tol[306]	Partial iodination, partial cyanation, **3-16** was not isolated. Low reproducibility
9	$Pd(PPh_3)_4$ $Zn(CN)_2$, DMF, microwave heating	**3-16** identified in reaction mixture, irreproducible
10	$Zn(CN)_2$, $Pd(OAc)_2$, DPPF, DMF[307]	Reproducible isolation of **3-16** in low yields.

Reaction conditions 1 to 7 gave either no conversion or a broad mixture of reaction products in which **3-16** was not identified. It would appear that **3-10** can undergo some, not fully understood, degradation processes leading to a broad mixture of undesired products. In reaction 8, a domino cyanation reaction takes place. The bromine -> iodine exchange is supposedly followed by iodine -> cyano exchange. Unfortunately, for **3-10** a mixture of partially iodinated and cyanated products was found. The concept of an aromatic FINKELSTEIN reaction, i.e. bromine -> iodine exchange, will be used in the synthesis of **3-17**.[308] The microwave assisted palladium catalyzed cyanation (entry 9 in table III-6) gave the tetra-nitrile **3-16** only in low yields with poor reproducibility. Finally, it was possible to reliably prepare the target compound by palladium catalyzed cyanation using DPPF as ligand and zinc (II) cyanide as palladium source.[307] Due to its low solubility the compound could not be purified by column chromatography but was isolated by repeated recrystallization from THF in very low yields (< 5 %). The low availability hampered the deprotection attempts.

III.3.1.2   Deprotection of 1,3,6,8-tetracyano-4,5,9,10-tetramethoxypyrene (3-16)

Essential for the preparation of the strong acceptor **3-29** is the demethylation of **3-16** to afford the corresponding alcohol which, in turn, is oxidized to the final product. As discussed for the demethylation of 2,4,5,7,9,10-hexamethoxypyrene (**2-6**), the cleavage of methyl ethers on pyrenes can be problematic. In their standard text book "Greene's Protective Groups in Organic Synthesis" the authors list 17 methods for the cleavage of methoxy ethers.[278] Protocols applicable to aromatic ethers have been tested on **3-16** and all failed.
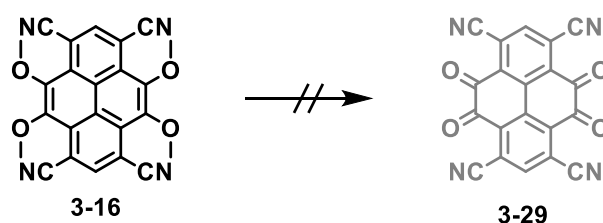
*III-40: Failed synthesis of 1,3,6,8-tetracyanopyrene-4,5,9,10-tetraone (**3-29**).*

Most approaches have in common that the point of attack is the free electron pair of the oxygen. With the exception of trimethylsilyl iodide (TMSI), ceric ammonium nitrate (CAN) and hydrobromic acid strong LEWIS acids were employed.
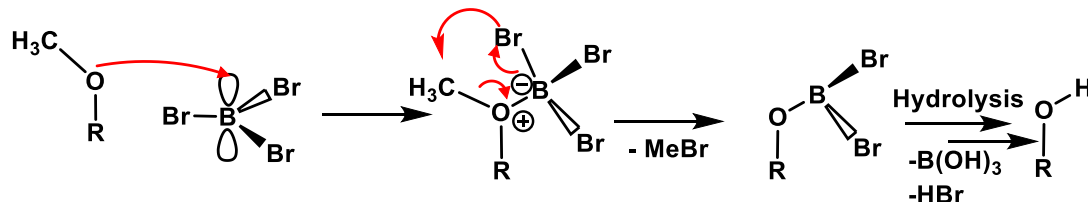
III-41: Mechanism commonly assumed for BBr₃ mediated methyl ether cleavage.

In figure III-41 the mechanism for LEWIS acid (BBr₃) mediated methyl ether cleavage is illustrated.[309] Boron tribromide is commonly used for demethylation reactions (e.g. deprotection of **2-6**). In the first step, the LEWIS acid engages the oxygen lone pair to form a zwitterionic complex. In a concerted backside S_N1-type attack bromine removes the methyl group so that methylbromide is liberated. The remaining neutral borate complex is later hydrolyzed to give the free alcohol. Recently, SOUSA and SILVA found in an extended theoretical study that only primary ethers (R = n-alky) proceed via this unimolecular mechanism.[310] For phenyl ethers a bimolecular mechanism is proposed:
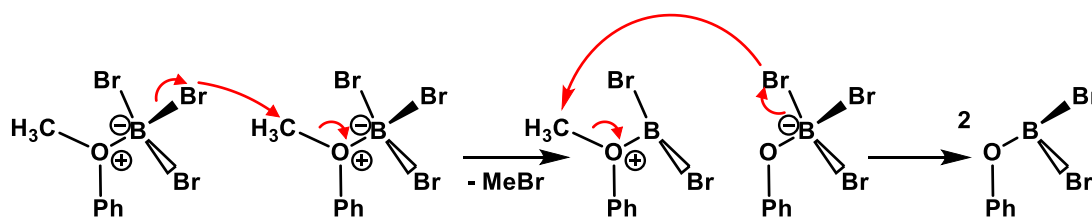
III-42: Bimolecular mechanism of phenyl ether cleavage proposed by SOUSA and SILVA. [310]

According to this work two zwitterionic complexes release methylbromide in a S_N2 type substitution reaction. The formed ionic species can repeat a bimolecular reaction to give the stable borate. Whereas the transition state energy in the unimolecular mechanism is calculated to be as high as 38.8 kcal/mol, it is merely 13.3 kcal/mol for the bimolecular mechanism.

Already MᴄOMIE *et al*. suggested for α-diols the formation of a cyclic borate as intermediate.[311] Hydrolysis of this borate can be difficult as it can be surprisingly stable.[202] It is frequently reported that the electron density of aromatic methyl ethers has a significant effect on the deprotection rate. Electron rich compounds in general are rapidly converted, while electron deficient substrates react sluggishly.[278, 311]

All mechanistic considerations have in common that the initial step is described as attack of the LEWIS acid on the oxygen lone pair. An electron deficient aromatic scaffold will also reduce the electron density on the ether oxygen and reduces its LEWIS basicity. In consequence, the LEWIS acid attack on the oxygen center is hindered. In the case of **3-29** two additional factors help to understand why deprotection failed: i) Nitriles also form coordinative bonds to boron tribromide (via nitrogen lone pairs) and ii) the low solubility of the substrate in halogenated solvents. Low solubility also hampered the deprotection of **2-42** as discussed in chapter *II*. By coordination to the nitrile, the electron density of **3-29** is even further reduced and a bulky BBr_3 moiety can hinder the approach to the methoxy units.

Hydrobromic acid in acetic acid has been used to cleave methyl ethers for a long time.[312] In the case of **3-29** hydrolysis of the nitriles to the corresponding carbonic acid readily occurred and preceded ether cleavage. A complex product mixture resulted. Reconversion of the carboxylic acids to the nitrile failed.[313]

In TMSI the formation of a strong Si-O bond is the main driving force, promoting a trans-etherification to form the easily cleavable TMS ether. In literature this procedure is described as very successful for aliphatic ethers, while being retarded for aromatic ethers. High conversions are nevertheless reported.[205] The surprising lack of conversion can be explained for the pyrene K-region by steric congestion. The transition state proposed by JUNG *et al*. states that TMSI adds to oxygen forming an oxonium ion with iodide as anion. It can be assumed that this addition is hindered by the second K-region oxygen.[205] In case of the oxidative cleavage by CAN the attenuation of electron density in **3-16** is most probably responsible for the failed reaction.

III.3.1.3   Dioxolane protected 1,3,6,8-tetracyanopyrene-4,5,9,10-tetraone (3-33)
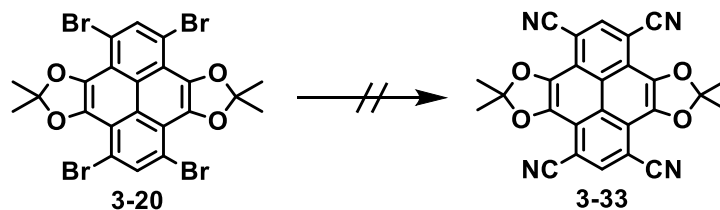
*III-43: Attempted synthesis of **3-33**.*

As a consequence of the failed deprotection of **3-16**, the dioxolane protecting group was to be used. Unfortunately, the cyanation of **3-20** was not possible using the established method for **3-16**. **3-33** was not isolated.

III.3.2   1,3,6,8-Tetra(trifluormethyl)pyrene-4,5,9,10-tetraone (3-31)

As a consequence of the failed attempts to prepare 1,3,6,8-tetracyanopyrene-4,5,9,10-tetraone (**3-29**) the synthesis of alternative molecules was considered. **3-31** emerged from the theoretical calculations as the second strongest acceptor (table III-5). In contrast to a nitrile substituent, trifluoromethyl is non-coordinating towards main-group LEWIS acids, chemically inert (tolerates acidic and oxidative conditions) and generally improves the solubility in common (halogenated) organic solvents.[314] Accordingly, trifluoromethyl is a promising replacement for the nitrile unit in the preparation of acceptor substituted pyrene-4,5,9,10-tetraones.

III.3.2.1   Synthesis
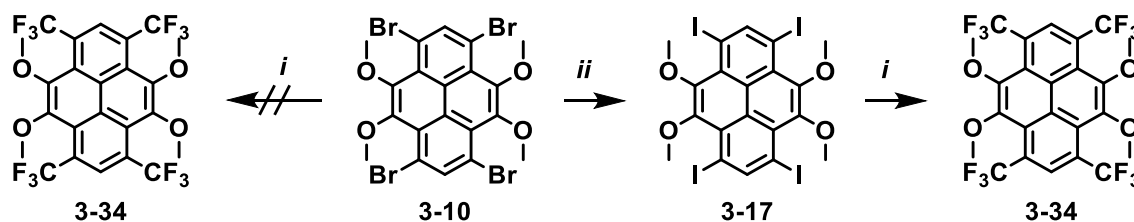
*III-44: Synthesis of **3-34**. i: Trifluoromehtylator®, DMF, 16 h, 50 °C. ii: NaI, CuI, N,N'-dimethyl-1,2-cyclohexanediamine, dioxane, 110 °C, 48 h, 63 %.*

Until recently, introducing a trifluoromethyl unit required stoichiometric amounts of copper and high-boiling solvents. Based on the work of OISHI *et al.*[315], MORIMOTO *et al.* reported an isolatable, air-stable copper-trifluoromethyl-complex that can introduce trifluoromethyl units in aryl-iodides.[316] The complex has been commercialized under the trade name *Trifluoromehtylator®*.

Both procedures failed to convert **3-10**. It is reported that only electron deficient aryl bromides are reactive under these conditions. In order to investigate the activity of aryl iodides, **2-5b** was converted to **3-36** (figure III-45) using the conditions described by OISHI *et al.*[315] As expected, **3-36** is well soluble in halogenated solvents. The deprotection/reoxidation procedure described by RIEGER *et al.* (BBr₃ followed by *aq.* HNO₃)[202] provided access to 2,7-bis(trifluoromethyl)pyrene-4,5,9,10-tetraone (**3-37**) in moderate yields.
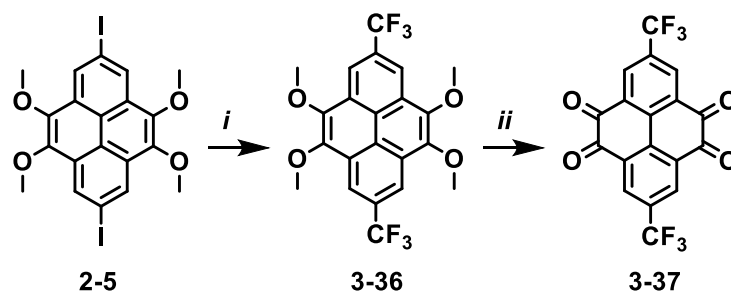
III-45: Synthesis of 3-37. i: F₃C-SiEt₃, CuI, phen, KF, NMP, DMF, 16 h, 120 °C, 72 %. ii: BBr₃, CH₂Cl₂, 48 h, RT; 65 % HNO₃, 6 h, 12 %.

In order to extend this reaction onto **3-10** a copper catalyzed halogen exchange reaction was utilized. Named "aromatic FINKELSTEIN reaction" by KLAPARS and BUCHWALD this reaction allows an efficient halogen (Br->I) exchange.[308] The traditionally used method via n-butyl lithium was not applicable due to **3-10**'s low solubility.[317, 318] **3-17** was obtained in 63% yield.
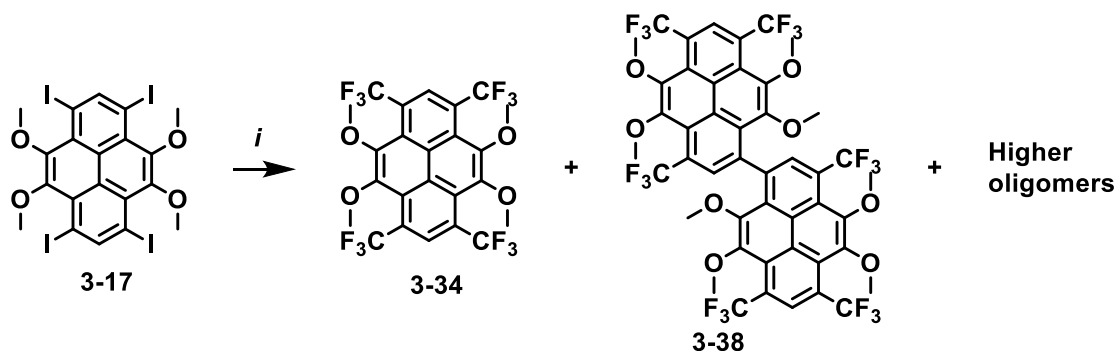
III-46: Trifluoromethylation of 3-17 by OISHI method. i: F₃C-SiEt₃, CuI, phen, KF, NMP, DMF, 16 h, 120 °C.

Using the OISHI trifluoromethylation method not only **3-34** was obtained but also several ULLMANN-type aryl-aryl coupling products. **3-38** was isolated. The MORIMOTO method gave **3-34** as clean product, oligomers were not observed.

III.3.2.2 Characterization

The structure of all materials was confirmed by ¹H-, ¹³C- and ¹⁹F-NMR, FD-MS and elemental analysis. In the case of **3-34**, **3-36** and **3-38** single crystal X-ray diffraction crystallography give an independent proof.

The NMR spectra of **3-36** are collected in figure III-47:
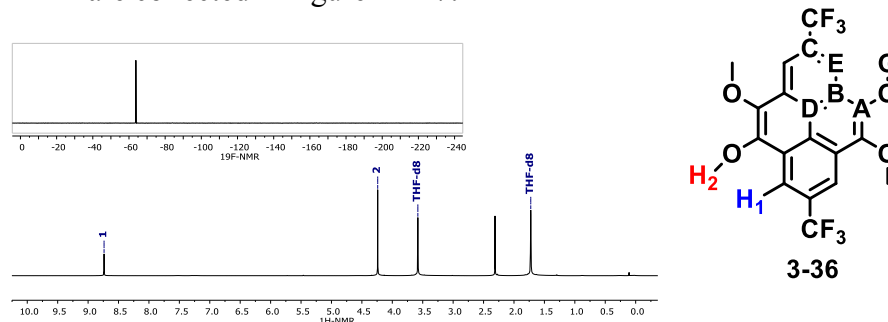
*III-47: NMR spectra of **3-36** in d8-THF at 298 K. Panel: ^{1}H-NMR (700 MHz). Inset: ^{19}F-NMR (471 MHz).*

The ^{1}H-NMR spectrum shows two singlet signals, as expected for 2,7-substituted-4,5,9,10-tetramethoxypyrenes. Compared to other derivatives, the pyrene-scaffold protons (signal *1*, $\delta = 8.74$ ppm) experienced a significant shift towards lower field strength. As discussed above, the signal position is (weakly) correlated to the electron density in the pyrene core. For comparison, the pyrene-scaffold signal of 2,7-dicyano-4,5,9,10-tetramethoxypyrene is reported at $\delta = 8.75$ ppm.[77]
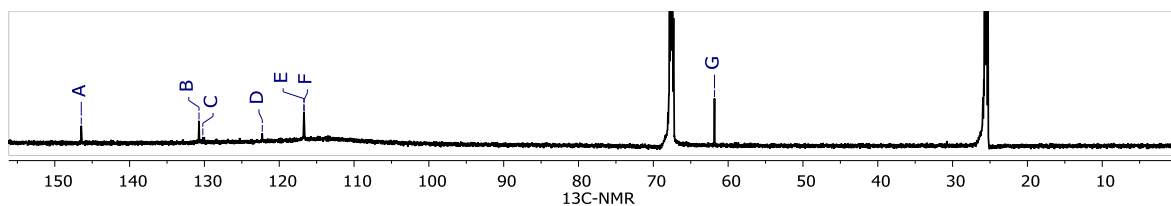
*III-48: ^{13}C-NMR (176 MHz) spectrum of **3-36** in d8-THF at 298 K.*

In the standard ^{13}C-experiments signals of fluorinated carbons are difficult to resolve. Large ^{13}C-^{19}F coupling leads to spectral broadening not suppressed by proton decoupling. Signal *C* ($\delta = 131$ ppm), assigned to the carbon ortho to the CF$_3$ substituent (positons 2 and 7 of pyrene), is split into a doublet with a coupling constant of J = 25 Hz. Also signal *E* (1,3,6,8 position of pyrene) is split into a doublet J = 2.5 Hz. In the ^{19}F-NMR spectrum (top panel) only one singlet at $\delta = -63$ ppm is recorded for the trifluoromethyl units.

NMR spectra recorded for **3-34** are combined in figure III-49.
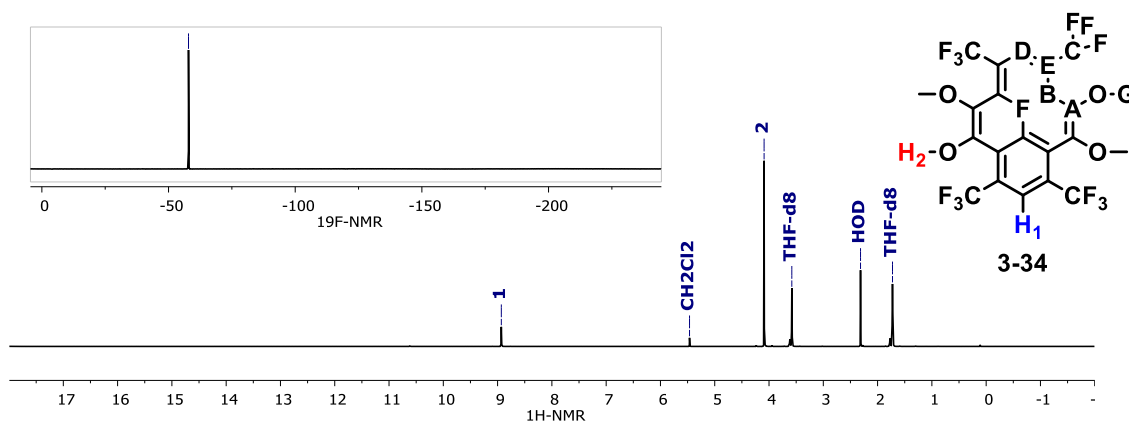
*III-49: NMR spectra of **3-34** in d8-THF at 323 K. Panel: ^{1}H-NMR (500 MHz). Inset: ^{19}F-NMR (471 MHz).*

In the ^{1}H-NMR the anticipated two signal pattern is observed. Signal *1* (*δ = 8.93 ppm)* is shifted slightly to lower field strength (*δ$_{3-10}$ = 8.64 ppm*) while the methyl-ether signal (signal *2*, *δ = 4.08 ppm*) remains practically unaffected (*δ$_{3-10}$ = 4.02 ppm*) when compared to **3-10**.
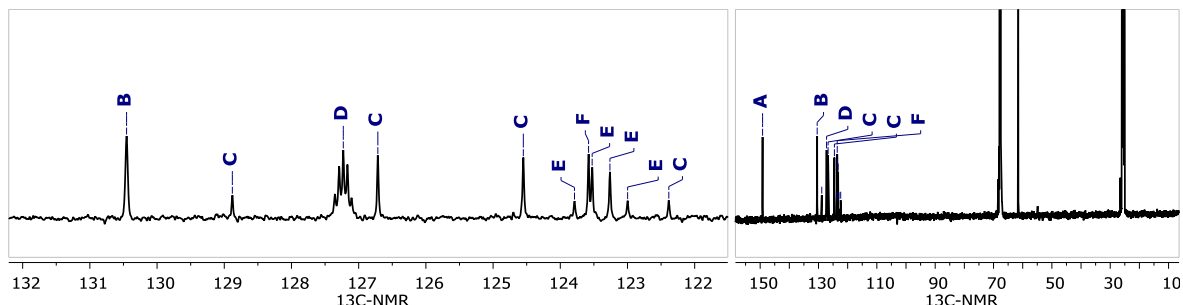
III-50: ^{13}C-NMR (126 MHz) spectra of 3-34 in d8-THF at 323 K. left: Expanded spectrum between δ = 132 and 122 ppm. Right: overview spectrum

In contrast, the ^{13}C-NMR spectrum is more complex due to signal splitting caused by ^{13}C-^{19}F coupling. Signals *A* (*δ = 149.2 ppm*) and *G* (*δ = 63.7 ppm*) can easily be assigned to the phenyl/methyl ether functions in the pyrene *K*-region. The CF$_3$-group signal (*C*, *δ = 125.6 ppm, q*) is characterized by its enormous scalar coupling of J = 272 Hz. The adjacent pyrene-carbon signal (*E*, *δ = 125.6 ppm, q*) still experience significant ^{13}C-^{19}F coupling, causing a splitting of J = 33 Hz. In the pyrene 2 and 7-position the carbon signal (*D*, *δ = 127.2 ppm*) is split into a heptet with a J coupling of J = 7.8 Hz. For signals *B* (*δ = 130.5 ppm*) and *F* (*δ = 123.6 ppm*) J coupling is not observed. In the ^{19}F-NMR spectrum a singlet at *δ = -57.9 ppm* is recorded.

III.3.2.2.1   Crystal structure

In figure III-51 the conformation and packing of **3-36** in a single crystal, as determined by X-ray diffraction crystallography, are presented.
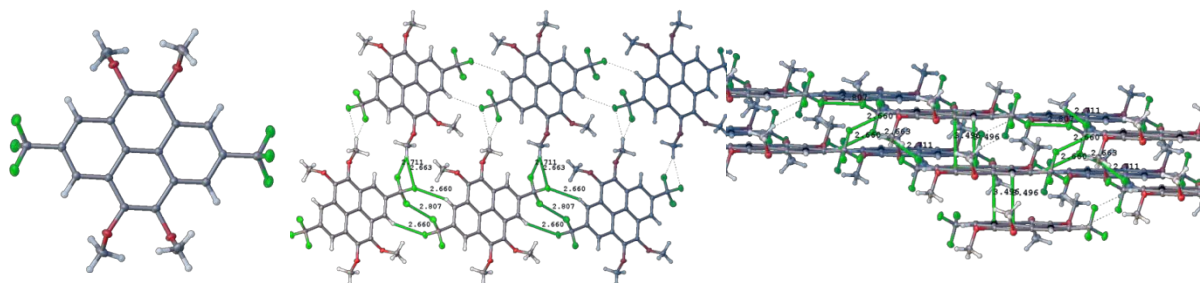
III-51: Single crystal X-ray diffraction crystallography results for 3-36. Left: Molecule in top view. Middle: Crystal packing viewed along a-axis. Right: Crystal packing viewed along b-axis. Short contacts are illustrated in green (distances in Å).

In the solid state conformation the pyrene scaffold is not distorted but flat. The α-methoxy units adopt a *trans* arrangement, as usually observed for these molecules. A sheet like packing arrangement is found with a π−π short distance of 3.50 Å between two sheets.

Within one sheet short contacts are observed among CF$_3$ substituents (2.80 Å) but also amid a CF$_3$ unit and protons of the pyrene backbone (2.68 Å). Similar interactions are also observed between two sheets.

In the case of the tetra-substituted derivative **3-34** the steric demand of the trifluoromethyl unit has a significant effect on the molecule in its solid state conformation. As can be seen in the top right panel of figure III-52 the pyrene scaffold is twisted by 7.5° (when viewed along its c-axis) to accommodate the substituents. When viewed along the a-axis (top left panel) it can be seen that the methyl residues are pointing towards each other so that steric repulsion from the CF$_3$ group is avoided.
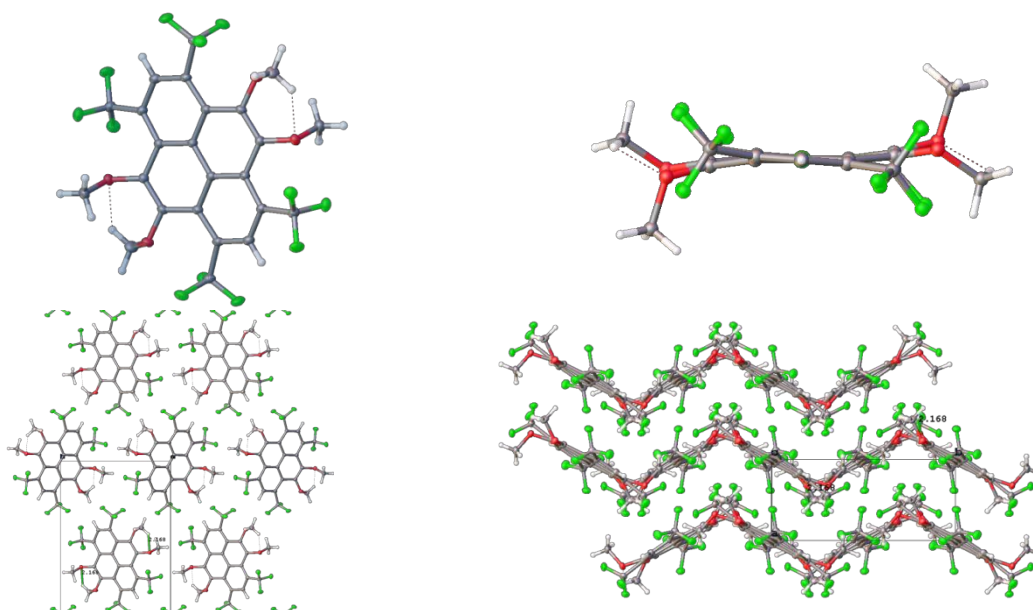
*III-52: Single crystal X-ray diffraction crystallography results for **3-34**. Top left: Molecule viewed along a-axis. Top right: Molecule viewed along c-axis. Bottom left: Crystal packing viewed along a-axis. Bottom right: Packing viewed along c-axis.*

A face-on packing is adopted along the a-axis. Short π−π contacts are determined to 4.3 Å. A carbon − fluorine distance of 3.1 Å is found within a stack. Viewed along its c-axis a puckered arrangement is revealed.
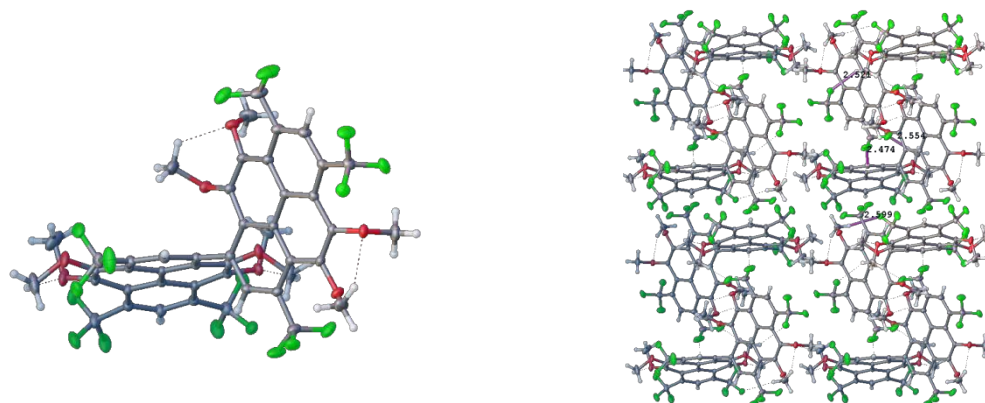
*III-53: Single crystal structure of **3-38**. Bending of the pyrene scaffold is significant. Left: Single molecule structure. Right: Packing along a-axis.*

For the 1,1' C-C coupled side product of the OISHI method (**3-38**), the packing is complex. This complexity mostly arises from the significant bending of the pyrene scaffolds. Thus, multiple CH – F (2.4 Å), F – F (2.8 Å) and F – π (3.3 Å) short contacts are possible. CH - F interactions appear to have a directing effect on the crystal growth. The dihedral angle along the 1,1'-bond is 76.5°.

III.3.2.2.2   Optoelectronic properties

Absorption and photoluminescence spectra of **3-34** and **3-36** have been recorded in dichloromethane. The results are given in figure III-54.
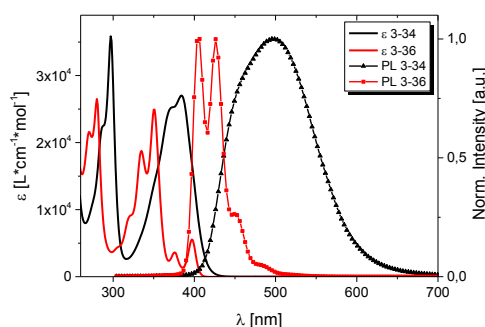
*III-54: UV-vis- (solid line) and PL- (symbols) spectra of **3-34** (black) and **3-36** (red) in CH$_2$Cl$_2$.*

In the absorption spectra multiple transitions can be identified for both molecules. For **3-34** the spectral features are generally red shifted and vibrational fine splitting is less resolved. The spectrum of **3-36** is similar to that of unsubstituted pyrene.[11] Three distinct bands arising from excited states (S$_1$ to S$_3$) are observed. At $\lambda = 392$ nm the (S$_0$ -> S$_1$) transition ($\varepsilon = 5.5*10^3$ L*mol^{-1}*cm^{-1}) with vibrational fine splitting is observed. Compared to pyrene this band is bathochromically shifted by 20 nm and its molar absorption coefficient is increased by the factor 10 ($\varepsilon_{pyrene,S0 -> S1} = 5.1*10^2$ L*mol^{-1}*cm^{-1}). The (S$_0$ -> S$_2$) and (S$_0$ -> S$_3$) transitions ($\lambda_{S0 -> S2} = 351$ nm, $\lambda_{S0 -> S3} = 280$ nm) are similar in intensity ($\varepsilon_{S0 -> S2} = 2.5*10^5$ L*mol^{-1}*cm^{-1}, $\varepsilon_{S0 -> S3} = 2.7*10^5$ L*mol^{-1}*cm^{-1}) and show vibrational fine splitting. In pyrene both bands are observed at similar wavelength ($\lambda_{S0 -> S2} = 334$ nm, $\lambda_{S0 -> S3} = 272$ nm) yet the intensity is higher by a factor of two.

For **3-34** only two distinct spectral features are observed. The (S$_0$ -> S$_1$) and (S$_0$ -> S$_2$) transitions are not resolved, an intense ($\varepsilon = 2.7*10^5$ L*mol^{-1}*cm^{-1}), broad absorption at $\lambda = 385$ nm is detected instead. As in **3-36**, the (S$_0$ -> S$_3$) transition is sharp and shows fine splitting. It is red shifted by 17 nm ($\lambda = 297$ nm) and is higher in intensity ($\varepsilon = 3.6*10^5$ L*mol^{-1}*cm^{-1}). It is noteworthy that both molecules show no significant internal charge-transfer band withstanding the mixed donor and acceptor type substitution. Both materials retain the wide bandgap character of pyrene as a consequence of their high symmetry. Both materials exhibit no permanent dipole moment (according to DFT-calculations) which could give rise to charge-transfer bands.[319] The optical band

gaps are determined for **3-34** to $\Delta E_{Op,\textbf{3-34}} = 3.00$ eV and for **3-36** to a slightly wider $\Delta E_{Op,\textbf{3-36}} = 3.12$ eV. **3-36** behaves similar to other 2,4,5,7,9,10-substituted pyrene derivatives in terms of its photoluminescence. As in **2-6** two strong emission maxima ($\lambda_{max1} = 404$ nm and $\lambda_{max2} = 427$ nm) and a weak shoulder ($\lambda = 450$ nm) are present. The FWHM is only 39 nm. In the case of **2-6** the second emission maximum is significantly weaker. In contrast to this, **3-34** exhibits a very broad (FWHM = 118 nm) photoluminescence devoid of features. The PL maximum is located at $\lambda_{PL,max} = 496$ nm. The fluorescence tail reaches beyond $\lambda = 650$ nm. As excimer formation is unlikely in a molecule that sterically encumbered, this PL behavior can be attributed to an ICT interaction. The PL spectrum of **3-13** for comparison is narrower (FWHM = 50 nm), structured and hypsochromically shifted ($\lambda_{max} = 455$ nm). The data are compiled in table III-7:

*Table III-7: Optical properties of **3-34** and **3-36** compared to **3-13** and **2-6**.*

	$\lambda_{abs,max}$ (nm)[a]	ΔE_{Op} (eV)[b]	$\lambda_{max\ PL}$ (nm)[a]	FWHM$_{PL}$ (nm)
3-34	385, 297	3.00	496	118
3-36	392, 351, 280	3.12	404, 427	39
3-13	437, 382 276	2.86	455	50
2-6	399, 354, 287	3.13	403, 426	30
	[a] measured in CH_2Cl_2, [b] onset of absorption band			

III.3.2.3   OFET properties

Although pyrene derivatives generally give poor results when used as OFET materials, reasonable charge carrier mobilities are achievable as shown by ZÖPHEL *et al.*[90] Independent of that work, short fluorinated side chains often beneficially influence the packing behavior of organic materials and improve their properties in OFETs.[320, 321] With this in mind the suitability of **3-34** as OFET material was investigated in collaboration with MARSZALEK.

Thin films were prepared from dichloromethane solution by dropcasting onto a SiO_2 dielectric. After fabrication, films were annealed for 1 h at 100 °C.

The films prepared in this manner were characterized by grazing incidence wide angle X-ray scattering (GIWAXS).[322] The results are given in figure III-55.
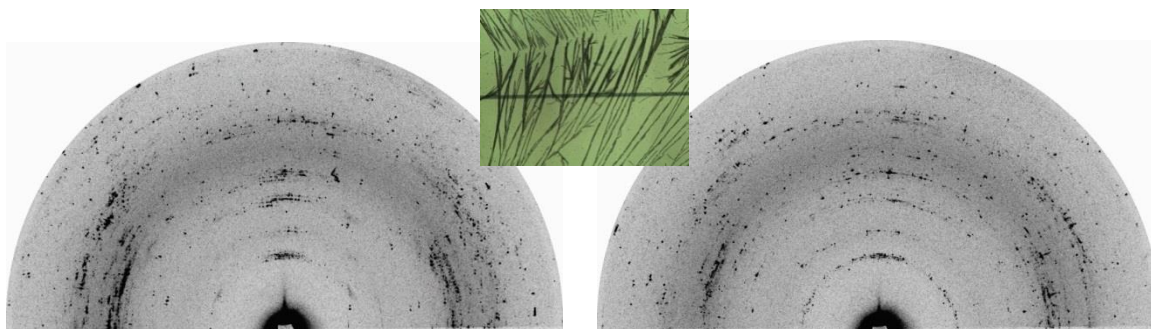
*III-55: GIWAXS results of **3-34** thin films. Superimposed is the polarized optical micrograph of the film.*

In the GIWAXS experiments a large number of reflections are observed. This confirms high crystallinity and uniformity of the prepared thin films. From the strong signal in the experiments an edge-on arrangement of the molecules on the silicon/silicon dioxide substrate was determined.[323] Furthermore, $\pi-\pi$ stacking interactions on the off-equatorial plane are identified. The $\pi-\pi$-packing distance is identified with 3.7 Å. Generally, the GIWAXS results are in good agreement with the single crystal X-ray diffraction data. Substrate-molecules interactions do not affect the molecular arrangement in thin polycrystalline film.

Polarized optical microscopy confirmed the growth of **3-34** crystallites instead of an continuous film in the OFET-device channel. Nevertheless, field effect behavior was not observed in **3-34**. It is probable that the steric demand of the substituents weakens the $\pi-\pi$ interactions between the molecules. This, in turn, diminishes the possible charge carrier mobility.

III.3.2.4   Deprotection of 3-34 and 3-36

As mentioned in III.3.2.1 the deprotection/reoxidation procedure of **3-36** to yield **3-37** was successful. In figure III-56 ^{1}H-NMR spectra prior (top panel) and posterior (bottom panel) to this reaction are presented.
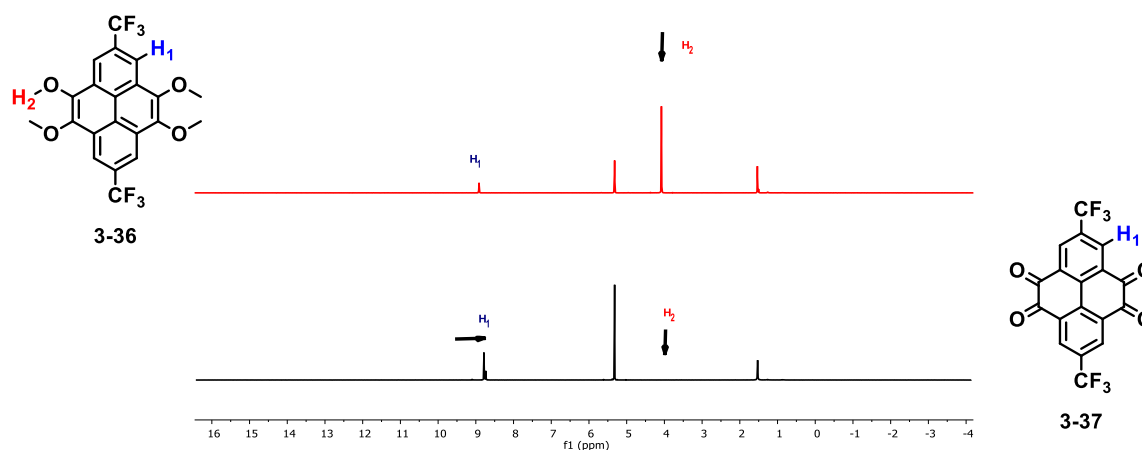
*III-56: ^{1}H-NMR spectra of **3-36** (top, red) and **3-37** (bottom, black) recorded in CD_2Cl_2 at 298 K in comparison.*

The spectrum reveals that the methoxy-signal at $\delta = 4.05$ ppm is absent in **3-37** (highlighted by an arrow). Noteworthy is also the shift of the aromatic proton signal towards higher field strength by 0.12 ppm ($\delta = 8.91$ ppm to $\delta = 8.79$ ppm). In this work the chemical shift of the pyrene-scaffold proton is often used as indictor for electron density of the respective pyrene derivative. **3-37** may not be considered as a pyrene but rather as a biphenyl system. The observed shift for the scaffold protons is in good agreement with data reported for 2,7-dicyano-4,5,9,10-tetraketopyrene ($\delta = 8.80$ ppm).[77] Field desorption mass spectrometry gives further evidence for the successful conversion. It was possible to (qualitatively) monitor the progress of the deprotection reaction. The reaction was stopped when mass signals associated with methylated species were no longer detected. Furthermore, a loss of $\Delta m/z = 4$ is registered after oxidative workup.

In contrast to this, it has not been possible to convert **3-34** to the corresponding 4,5,9,10-tetraketone **3-31**. Monitoring the deprotection reaction it was found that the ether cleavage proceeded much more sluggishly than in the case of **3-36**. A full conversion was not observed even at prolonged reaction times (14 d) and elevated temperatures (120 °C, $C_2H_2Cl_4$). Oligomerization and decomposition reactions led to a complex product mixture from which the target compound **3-31** could not be isolated.

Figure III-57 gives the UV-vis absorption spectrum (left) and cyclic voltammogram (right) of **3-37**.
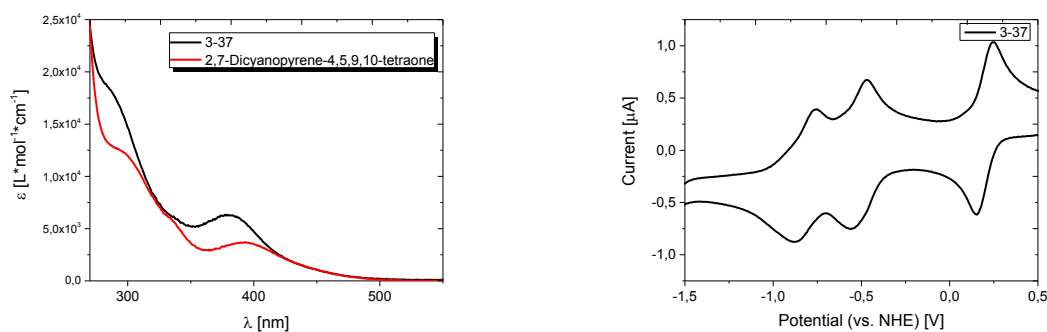
*III-57: UV-vis absorption spectrum (left) and cyclic voltammogram (right) of **3-37** recorded in THF.*

The absorption spectrum of **3-37** shows features typically observed in pyrene-4,5,9,10-tetraones.[77] Strong, sharp absorption bands as observed in pyrenes are absent. A broad absorption maximum is detected at $\lambda = 381$ nm ($\varepsilon = 6.4*10^3$ L*mol^{-1}*cm^{-1}). At shorter wavelength ($\lambda = 289$ nm) a stronger band is found. As a consequence of the long absorption tail, the determination of the optical bandgap is rather uncertain. It is established to be $\Delta E_{Opt} = 2.46$ eV. Similarities to the absorption spectrum of 2,7-dicyanopyrene-4,5,9,10-tetraone (recorded in DMF, shown in red) are striking. From the cyclic voltammetry data the reduction onset is determined to $U_{Red} = -0.36$ V (vs. NHE).

From this the LUMO energy is identified as $E_{LUMO} = -4.3$ eV. Compared to 2,7-dicyanopyrene-4,5,9,10-tetraone ($E_{LUMO} = -4.4$ eV), **3-37** is a slightly weaker acceptor. For both acceptors the oxidation wave could not be resolved. The HOMO energy was therefore determined in conjunction with the optical bandgap ΔE_{op}. The results are collected in table III-8.

*Table III-8: Optoelectronic properties of **3-37**.*

$\lambda_{max,abs}$ (nm)	ΔE_{Op} (eV)	$E_{LUMO,Exp}$ (eV)[a]	$E_{HOMO,Exp}$ (eV)[b]	$E_{LUMO,DFT}$ (eV)[c]	$E_{HOMO,DFT}$ (eV)[c]
381, 289	2.46	-4.3	-6.8	-4.06	-7.51

[a] Cyclic voltammetry, Fc used as internal standard. [b] determined by $E_{LUMO\ Exp} + \Delta E_{Op} = E_{HOMO,Exp}$; [c]B3LYP,6-311*

III.3.3   1,3,6,8-Tetra(3,5-bis(trifluormethyl)phenyl)pyrene-4,5,9,10-tetraone (3-32)

III.3.3.1   Synthesis
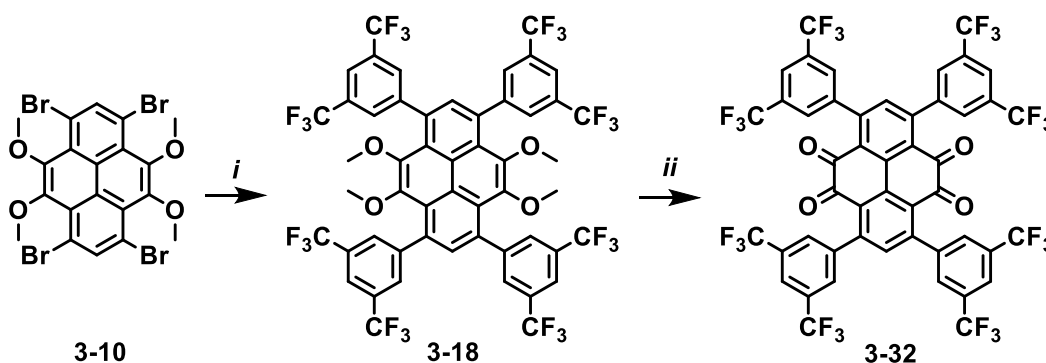
*III-58: Synthesis of **3-32**. i: Pd(PPh₃)₄, Na₂CO₃, Tol, H₂O, 100 °C, 16 h, 83 %. ii: BBr₃, CH₂Cl₂, 6 d.*

The synthesis of **3-32** was possible in a two-step protocol starting from **3-10**. In the first step **3-18** was prepared by SUZUKI-MIYAURA-type transition metal catalyzed cross coupling reaction of (3,5-bis(trifluoromethyl)phenyl)boronic acid with **3-10**. The product was purified by column chromatography which yielded **3-18** as a yellow solid (83%). The target compound **3-32** was prepared by boron tribromide mediated deprotection followed by nitric acid hydrolysis/oxidation. The product was recrystallized from THF followed by column chromatography on SiO₂.

III.3.3.2   Characterization
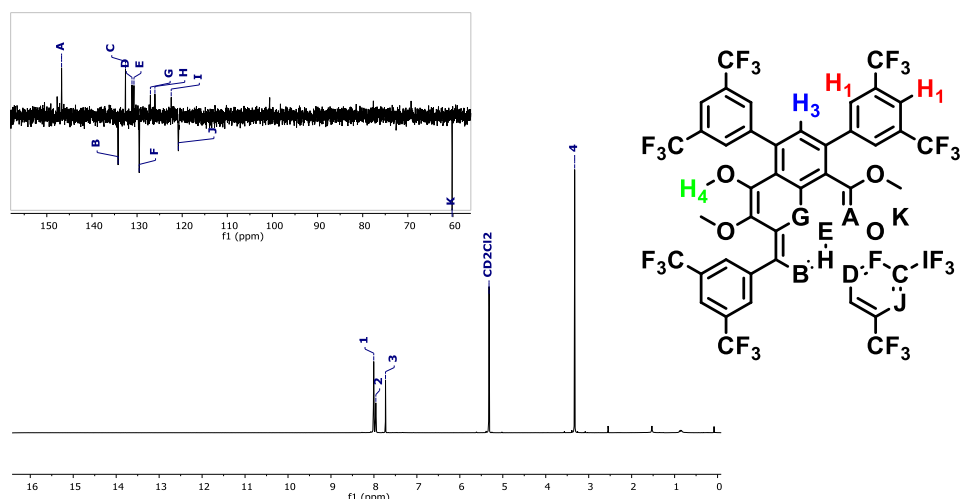
*III-59: ¹H- and ¹³C-APT NMR spectra of **3-18** recorded in CD₂Cl₂ at 298 K.*

In the ¹H-NMR spectrum four singlets are observed for **3-18**. The integration gives a ratio of 4:2:1 for signals *1* through *3*. Accordingly, the signals *1* ($\delta = 8.01$ ppm) and *2* ($\delta = 7.96$ ppm) are assigned to the phenyl substituents and signal *3* ($\delta = 7.73$ ppm) to the residual proton on the pyrene scaffold. Signal *4* ($\delta = 3.33$ ppm) stems from the methoxy units. In the ¹³C-APT spectrum 11 signals are identified. Being primary carbons, signals *B* ($\delta = 134.2$ ppm, s), *F* ($\delta = 129.5$ ppm, br, m) and *I* ($\delta = 120.8$ ppm, J = 3.8 Hz hept) can be assigned to the pyrene 2,7 positions (*B*), phenyl 2,6 (*F*) and phenyl 4 position (*J*) respectively. The heptet J splitting of *J* is especially characteristic (see chapter *III.3.2.2*). Signals *A* ($\delta = 146.7$ ppm) and *K* ($\delta = 60.2$ ppm) are assigned to K-region methoxy groups. Surprisingly, neither signals *C* nor *I* show strong J coupling.
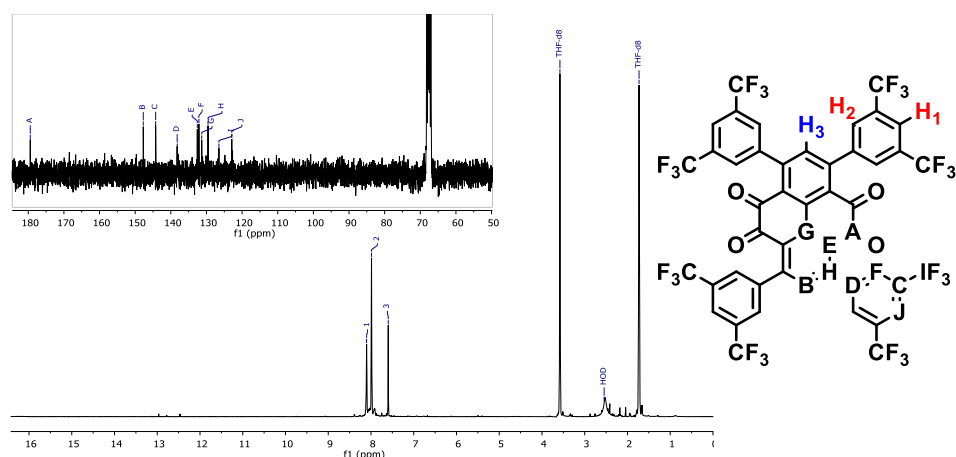
*III-60: ¹H- and ¹³C-NMR spectra of **3-32** recorded in THF-d8 at 298 K*

For **3-32** three singlets (*1 – 3*) are observed in the ¹H-NMR spectrum. The integration ratios are 2:4:1. Again signals *1* ($\delta = 8.10$ ppm) and *2* ($\delta = 7.99$ ppm) are assigned to the phenyl substituents whereas signal *3* ($\delta = 7.60$ ppm) is generated by the pyrene scaffold. Most significantly, the signal generated by the methoxy-groups (signal *4* in **3-18**) is absent.

Comparison of the NMR shifts of **3-18** and **3-32** is hampered by the fact that different deuterated solvents had to be used in the experiments to dissolve the analytes. Nevertheless, two points should be noted. The signal generated by the 4-phenyl protons are shifted down-field in **3-32** (by 0.14 ppm) and signal *3* is shifted up-field by 0.13 ppm. An up-field shift of the pyrene scaffold protons is also observed in 2,7-substituted pyrene-4,5,9,10-tetraones and is associated with an enhanced biphenyl character (see chapter *III.3.2.2*). In the ^{13}C-NMR signal *A* (δ = 178.3 ppm) is shifted down-field by 31.6 ppm into a region common for carbonyl carbons. Signal *K* (associated with the methyl ether carbon) is not observed in **3-32**.

III.3.3.3   Optoelectronic properties:

The UV-vis spectrum and the cyclic voltammogram of **3-32** are reproduced in figure III-61
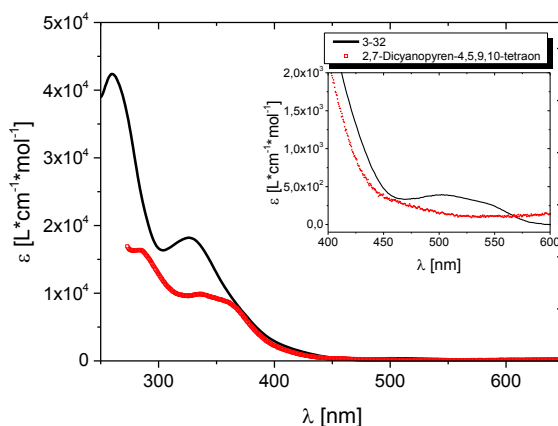
*III-61: Left: UV-vis spectra of **3-32** (black) in THF and 2,7-dicyanopyrene-4,5,9,10-tetraone (red) in DMF. Inset: Expansion of the spectrum between 400 and 600 nm.*

The absorption spectrum of **3-32** shows three broad featureless bands. A very weak and broad absorption band is observed at λ_{max} = 505 nm (ε_{max} = 5*10^2 L*mol^{-1}*cm^{-1}). A stronger absorption is recorded at λ_{max} = 325 nm (ε_{max} = 1.8*10^4 L*mol^{-1}*cm^{-1}) and the absorption maximum is reached at 260 nm with a modest extinction coefficient[18] of ε_{max} = 4.2*10^5 L*mol^{-1}*cm^{-1}. The absorption onset is located at 585 nm, this translates to an optical bandgap of ΔE_{Op} = 2.1 eV. Compared to 2,7-dicyanopyrene-4,5,9,10-tetraone the spectrum shows sharper absorption bands as well as a significantly higher extinction coefficient. The low frequency band is also missing in the 2,7-substituted reference. The strong absorption at the high energy end can be attributed to the phenyl substituents. A fluorescence spectrum is not reproduced as fluorescence of **3-32** is fully quenched. For pyrene-4,5,9,10-tetraones this is typical.

---

[18] When compared to other pyrene derivatives.
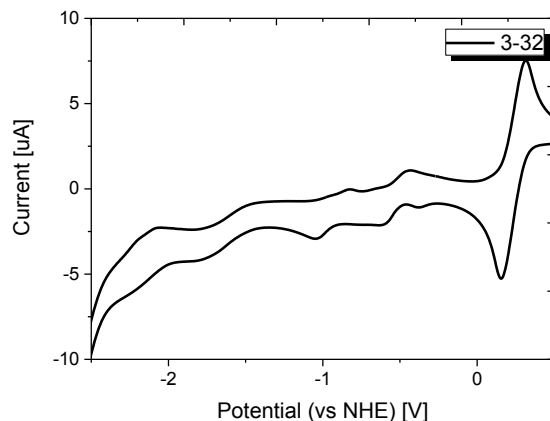
*III-62: Cyclic voltammogram of **3-32** in THF referenced versus NHE with Fc used as internal standard.*

In the cyclic voltammogram (figure III-62) one irreversible and two reversible reduction signals are observed. At U_{Red} = -0.4 V (vs. NHE) the first reduction signal is observed which gives a LUMO energy of E_{LUMO} = -4.2 eV. As an oxidation signal was not resolved, the HOMO energy is determined in conjunction with the optical bandgap to E_{HOMO} = -6.3 eV.

*Table III-9: Optoelectronic properties of **3-32**.*

$\lambda_{max,abs}$ (nm)	ΔE_{Op} (eV)	$E_{LUMO,Exp}$ (eV)[a]	$E_{HOMO,Exp}$ (eV)[b]	$E_{LUMO,DFT}$ (eV)[c]	$E_{HOMO,DFT}$ (eV)[c]
505, 325, 260	2.1	-4.2	-6.3	-4.68	-7.87

[a] Cyclic voltammetry, Fc used as internal standard. [b] determined by $E_{LUMO,Exp}$ + ΔE_{Op} = $E_{HOMO,Exp}$; [c]B3LYP,6-311*

The data collected in table III-9 gives an opportunity to compare the experimental and calculated frontier energy levels. ΔE_{Op} was determined to 2.1 eV. Theoretical calculations predicted it as large as 3.2 eV, thus overestimating the bandgap by 1.1 eV. Also the acceptor strength was overvalued, the experiment (CV) places the LUMO at -4.2 eV, about 0.5 eV higher than predicted. This discrepancy probably results from the limited theoretical treatment of the molecule. While DFT calculations using the B3LYP functional are able to provide quite reliable HOMO energy results very quickly, the performed calculations were limited to the gas phase. Furthermore, the results of this method for LUMO energies are less consistent. A LUMO energy of -4.2 eV still puts **3-32** is in the region of 2,7-dicyanopyrene-4,5,9,10-tetraketone (-4.4 eV). This is, to this day, the strongest pyrene-4,5,9,10-tetraone based acceptor reported.

III.4   Summary and outlook

In this chapter a new method to prepare eightfold functionalized pyrene derivatives was presented. This method allows the synthesis of diverse 1,3,6,8-functionalized-4,5,9,10-tetralkoxypyrenes in four synthetic steps. While the bromination occurs in electronically favored positions in **3-8** side-reactions (deprotection) marred the conversion. Suitable reaction conditions were identified eventually. It has been shown that the bromine substituents in **3-10** allow a variety of transition metal catalyzed functional group modifications. Thus, it becomes possible to introduce electron donating as well as electron withdrawing substituents onto the pyrene core. In contrast to the 2,7-functionalization discussed in chapter *II* this allows the introduction of a larger number of substituents in positions that ensure a good conjugation with the pyrene scaffold. Therefore, this new substitution pattern allows the synthesis of stronger donors based on pyrene.

III.4.1   Donors

A series of very electron rich pyrene derivatives was prepared. Variation of the donor substituent allowed tuning of the HOMO energy from $E_{HOMO} = -5.4$ eV in 4,5,9,10-tetramethoxypyrene **(3-8)** to $E_{HOMO} = -4,7$ eV in 1,3,4,5,6,8,9,10-octamethoxypyrene (**3-13**) and even $E_{HOMO} = -4.5$ eV in **3-14**. While **3-13** is slowly oxidized in air to form a radical species, **3-14** is stable in a laboratory environment probably due to improved steric shielding. Both molecules were studied as donors for CT-complexes. Details on this will be presented in the following chapter. It was also possible to convert **3-10** in Sonogashira-type cross coupling reaction to give **3-15**. It could give rise to a new class of ICT type polyphenylene dendrimers. Many phenylene dendrimers use either electronically neutral (e.g. tetraphenylmethane, pyrene) or electron deficient (e.g. PDI) units for their core. An electron rich core like 4,5,9,10-tetramethoxypyrene may give ICT interactions to an electron deficient dendron (in figure III-63 pyridine is chosen as a sample EWG substituent). The arising ICT band can be monitored by absorption and/or emission spectroscopy. Upon protonation (or metal coordination) the electronic environment of the dendrimer shell will be modified. This, in turn, will alter the ICT interaction (in this example, enhancing it). This alteration can be probed spectroscopically, thus these materials can be used as indicators. If oxidatively cleavable ether (e.g. *p*-methoxybenzyl) is introduced to the pyrene core, a dendrimer with electron rich dendrons may be used as an on-off probe for oxidants. Oxidation of the protected pyrene to the corresponding tetraketone would trigger ICT which could then be observed spectroscopically.
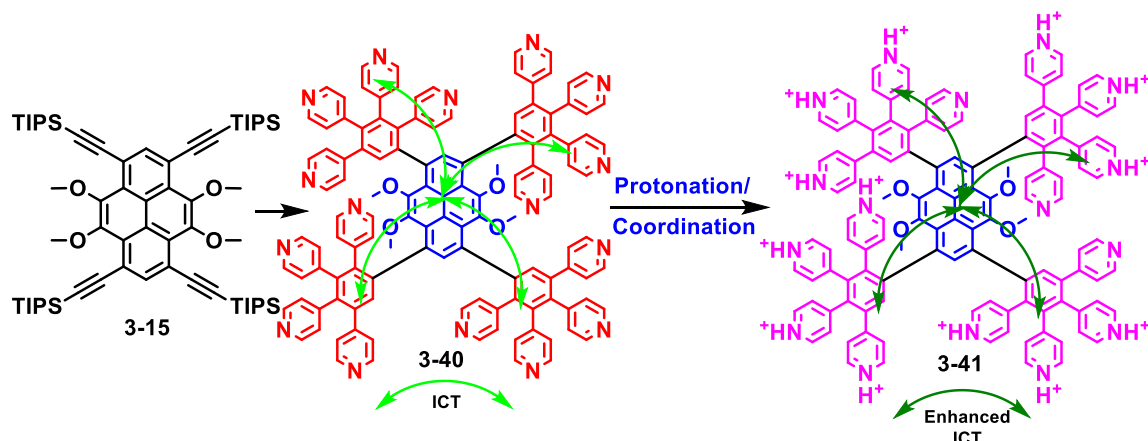
*III-63: Proposed ICT type dendrimers based on **3-15**.*

Considering the works of JEON *et al*. a long wave-length absorption could lessen the usefulness of **3-25** in DSSCs as electron transport material, although it does not render it useless.[292] The higher-energy HOMO of **3-14** may further reduce the contact resistance, thus enabling a more efficient device.

After developing suitable conditions for fourfold bromination of 4,5,9,10-tetramethoxypyrene (**3-8**) it was attempted to extend this method to 2,4,5,7,9,10-hexamethoxypyrene (**2-6**). This would give access to the first selectively per-functionalized pyrene derivative **3-42** (disregarding per-halogenated pyrenes). Unfortunately, this substrate did not tolerate the harsh bromination conditions; oxidative oligomerization was the consequence instead. It was not possible to identify the target compound in the reaction mixture. When milder reaction conditions were employed (0° C, 4 eq. Br2) the reaction yielded twofold bromination accompanied with two-/fourfold demethylation. Obviously, the enhanced electron density in **2-6** increases the tendency for demethylation.
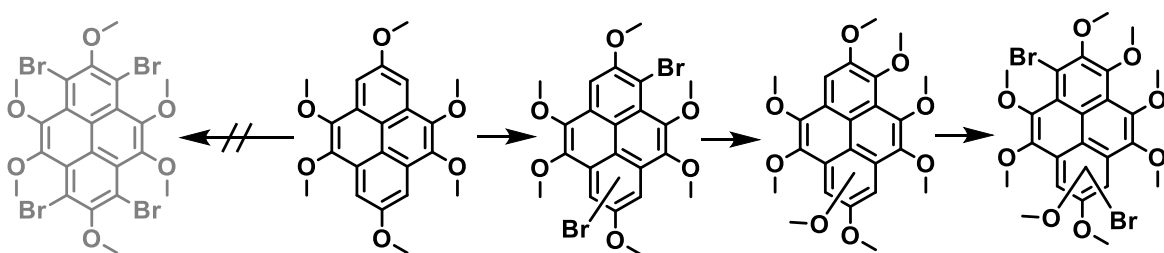
III-64: Synthetic approaches to a per-methoxy functionalized pyrene derivative.

It was possible to re-introduce the methyl-protecting groups and perform an ULLMANN-type methoxylation to give **3-44** as a mixture of isomers in small amounts. A bromination was attempted; **3-45** was identified in FD-MS next to a series of demethylated by-products and thus could not be isolated. The author is convinced that it will be possible to prepare a decamethoxy-pyrene if work on this topic is continued. Apart from being an

interesting synthetic challenge it would allow further tailoring of the frontier-orbital energies of pyrene derivatives. This may give rise to new charge-transfer complexes exhibiting a neutral-ionic transition (*vide infra*).

III.4.2 Acceptors

It was possible to extend the synthesis of pyrene-4,5,9,10-tetraone based acceptors to 1,3,6,8-substituted derivatives. Whereas 1,3,6,8-tetrabromopyrene-4,5,9,10-tetraone is an insoluble pigment, **3-32** is a fully characterized, well soluble pyrene based acceptor. While being a weaker acceptor than predicted by DFT calculations, its LUMO energy is close to 2,7-dicyanopyren-4,5,9,10-tetraone and therefore a reasonably strong acceptor. The inadvertent synthesis of **3-38** with its highly twisted solid state conformation suggests one way of expanding the chemistry of pyrene-4,5,9,10-tetraones. By 1,1'-connection of two protected pyrene-4,5,9,10-tetraones a class of three dimensional acceptors would become available. Increasing the dimensionality of acceptors is considered essential in the search for fullerene replacement materials for OPV applications.[324-326]
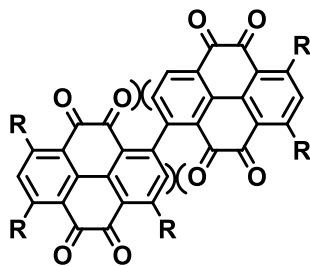
III-65: Non-planar pyrene-4,5,9,10-tetraone based acceptor.

While this may be a way to prepare new acceptors of intermediate strength, the author is rather pessimistic about the prospect of preparing very strong acceptors based on the method discussed here. It has been shown that strong EWGs (CN, CF$_3$) hinder Lewis acid mediated ether cleavage. Even if some degree of deprotection was achieved, the reoxidation to the desired 4,5,9,10-tetraketone proved difficult. The EWGs seem to stabilize the corresponding diol form significantly.

IV.   Charge-transfer complexes

IV.1   Donor – acceptor interactions

Novel Donors

4-1   4-2   4-3   4-4   R = *p*-PhOMe   4-5

Known Acceptors

TCNQ   F4-TCNQ   Bromanil   4-9   TCNE   4-11
4-6   4-7   4-8   4-10

IV-1: Materials used in this study. Novel donors are represented in blue, known acceptors in red.
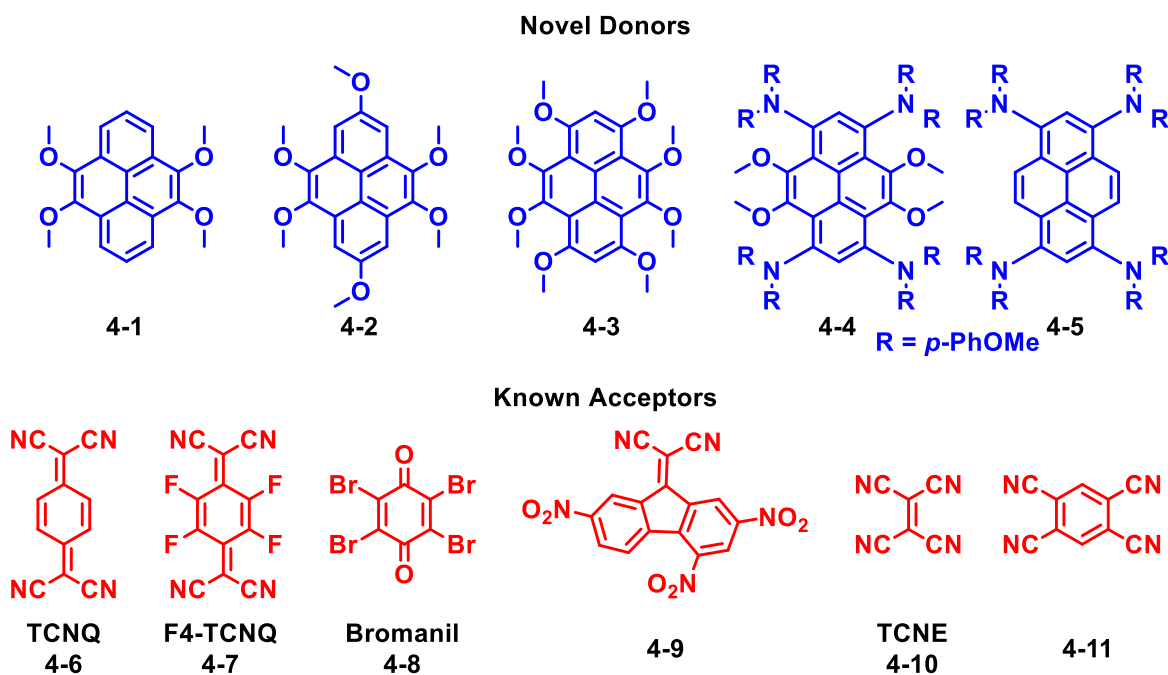
Chapters *II* and *III* described the synthesis of new electron rich materials (henceforth referred to as *donors*). This chapter will discuss charge-transfer complexes (CT-complexes, see also chapter *I.4*) comprising these compounds. Donors shown in figure IV-1 were studied in charge-transfer complexes with commercially available acceptors.

Due to their crystallinity, interesting HOMO energy and their high chemical stability CT-complexes of 4,5,9,10-tetramethoxypyrene (**4-1**, TMP) and 2,4,5,7,9,10-hexamethoxypyrene (**4-2**, HMP) have been used in extensive studies within the SFB/TR 49 context (see chapter *IV.3*).

CT-complexes containing donors **4-3, 4-4** or **4-5** did not grow in single crystals suitable for X-ray diffraction crystallography. The materials tend to form fibrils instead which are often observed in sterically demanding donors.[220] The lack of macroscopic crystals prevented the use of these compounds in SFB/TR 49 studies.

IV.2   New CT-complexes

IV.2.1   Absorption spectroscopy

The feature CT-complexes are probably best known for is the so-called charge-transfer band. This absorption band is absent in samples of the pure donor or acceptor. Only upon complexation this transition, usually situated in the visible or near IR (NIR) region of the electromagnetic spectrum, is observed.[327] As described in the introduction, this band arises from the interaction of the high energy HOMO of the donor with the low energy LUMO of the acceptor (see figure IV-15). Optical absorption spectroscopy is a useful tool to investigate charge-transfer phenomena.[328]
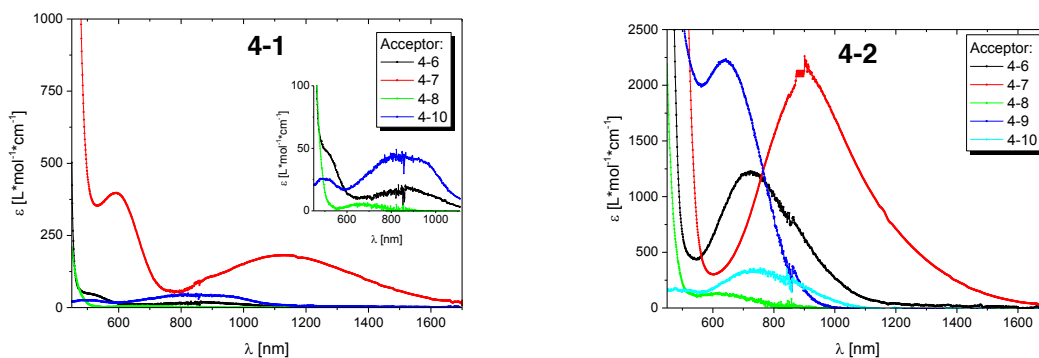
*IV-2: UV-vis spectra of charge-transfer complexes comprising of **4-1** (right) and **4-2** (left) in combination with a series of acceptors (samples measured in a CH$_2$Cl$_2$ solution, c = 1*10^{-3} mol/l).*

In order to evaluate the formation of CT-complexes with 4,5,9,10-tetramethoxypyrene derivatives **4-1** and **4-2** were combined with a series of acceptors. The resulting UV-vis absorption spectra are collected in figure IV-2. It is obvious that the nature of the donor and the acceptor influences possible CT-transitions.[329] The absorption maxima as well as the extinction coefficients are collected in table IV-1. F$_4$-TCNQ (**4-7**) for both donors (**4-1** and **4-2**) gives a very intense, broad absorption band. Compared to the other acceptors the band is bathochromically shifted by $\lambda \approx 270$ nm (**4-1**) and $\lambda \approx 170$ nm (**4-2**).

The longer wavelength points to a lower energy transition (i.e. small optical band gap). The fact that **4-7** is by far the strongest acceptor in the series is reflected in these findings. Acceptor **4-9** gives an intense CT-band at short wave length with **4-2**. Surprisingly, the same compound fails to give any significant CT-transitions in combination with **4-1**. Using TCNQ (**4-6**) gives clear indications for charge-transfer for **4-1** (shoulder at $\lambda = 528$ nm) as well as **4-2** (broad CT-band around $\lambda = 728$ nm). Bromanil (**4-8**) and TCNE (**4-10**) fail to give evidence for significant CT for both donors. They were disregarded in further studies.

*Table IV-1: Optical parameters of CT-complexes with **4-1** and **4-2**.*

Complex	$\lambda_{max,CT}$ (nm)	$\varepsilon_{max,CT}$ (L*mol^{-1}*cm^{-1})
4-6 / 4-1	528 (sh), 865 (br)	43, 18
4-7 / 4-1	599, 1133 (br)	395, 181
4-8 / 4-1	677	5,6
4-8 / 4-1	504, 803	11, 17
4-10 / 4-1	502, 814	25, 44
4-6 / 4-2	716 (br)	1216
4-7 / 4-2	910	2174
4-8 / 4-2	619 (sh)	126
4-9 / 4-2	642	2220
4-10 / 4-2	739	337

When comparing the two donors it is noteworthy that the extinction coefficients of the CT-bands are roughly one order of magnitude larger for **4-2**. This suggests that the higher energy HOMO of **4-2** enables stronger charge-transfer interactions. To illustrate this, figure IV-3 shows the absorption spectra of **4-1**, **4-2** and **4-3** in combination with acceptor **4-7**.
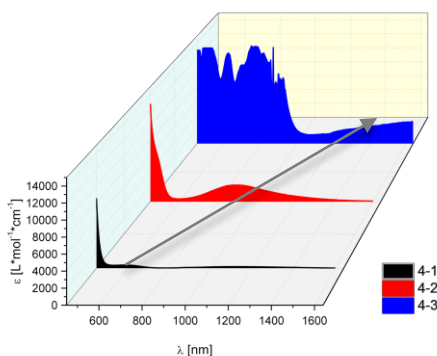
*IV-3: UV-vis absorption spectra of CT-complexes of acceptor **4-7** with donor **4-1** (black), **4-2** (red) and **4-3** (blue). (C = 1*10^{-3} mol/l, in CH$_2$Cl$_2$).*

As can be seen in the figure, the extinction coefficient increases for the stronger donor and the CT-band is shifted to larger wavelength. For **4-3** as donor the optical density of the

sample around $\lambda = 800$ nm at a concentration of $1*10^{-3}$ is too high (A > 3), thus resulting in the rugged spectrum. For further analysis the sample was diluted.

In order to quantify these qualitative findings the bonding model is determined by the continuous variation method.[330] For this, the sum of the donor concentration [D] and acceptor concentration [A] is kept at a constant value α. The donor concentration is varied from 0 to α in the course of the experiment. From the resulting series of UV-vis spectra the extinction coefficients of the respective CT-band is extracted and plotted versus the molar fraction χ (JOB plot).[331] In the JOB plot the location of the maximum gives information on the stoichiometry of the formed CT-complex (e.g. if the maximum is located at $\chi_D = 0.5$ a 1:1 complexation occurs[19]). The binding constant can be derived from the curvature of the plot.[330]

Due to the strong charge-transfer band of complexes formed with acceptors **4-6** and **4-7** these were chosen for this study. The resulting spectra and JOB plots are collected in figure IV-4.

Donor: **4-2**   Acceptor: **4-6**

Donor: **4-3**   Acceptor: **4-6**

---
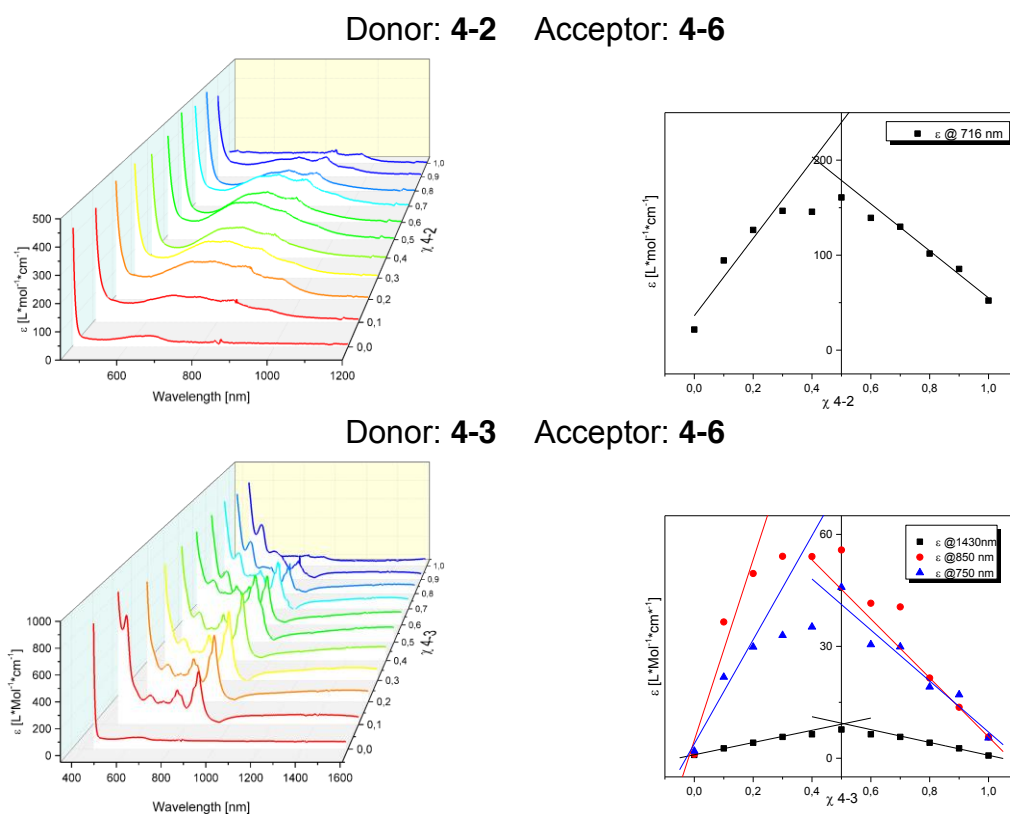
[19] From the JOB plot differentiation of a 1:1 and a 2:2 (or higher) binding arrangement is not possible.

Donor: **4-1**   Acceptor: **4-7**
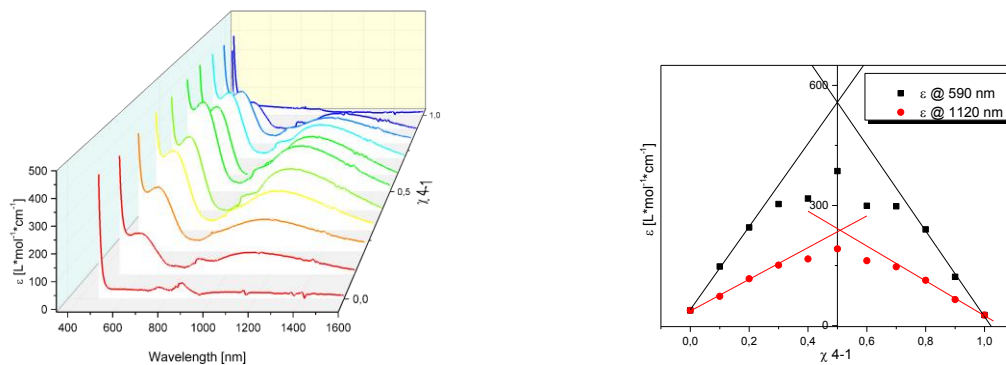
Donor: **4-2**   Acceptor: **4-7**
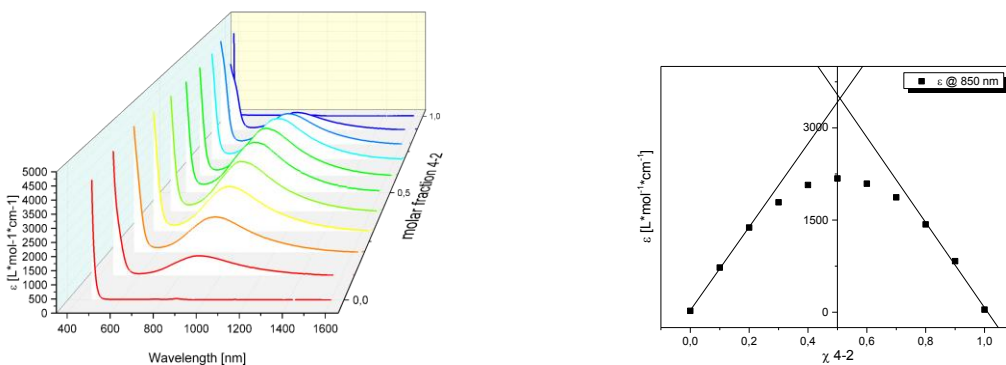
Donor: **4-3**   Acceptor: **4-7**
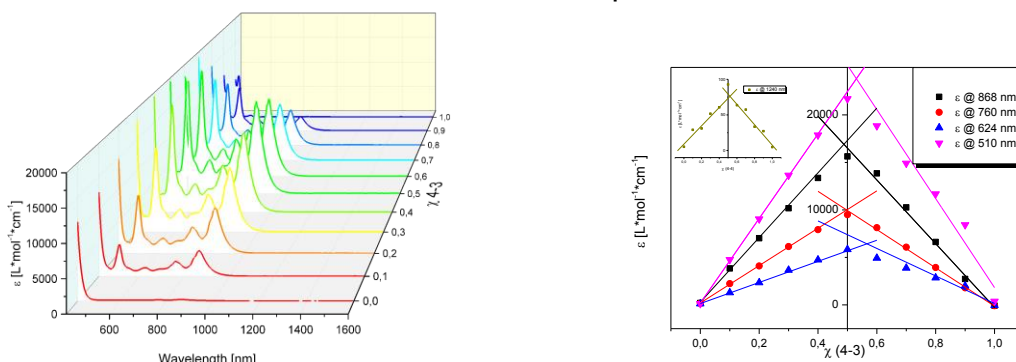
Donor: **4-4**   Acceptor: **4-7**
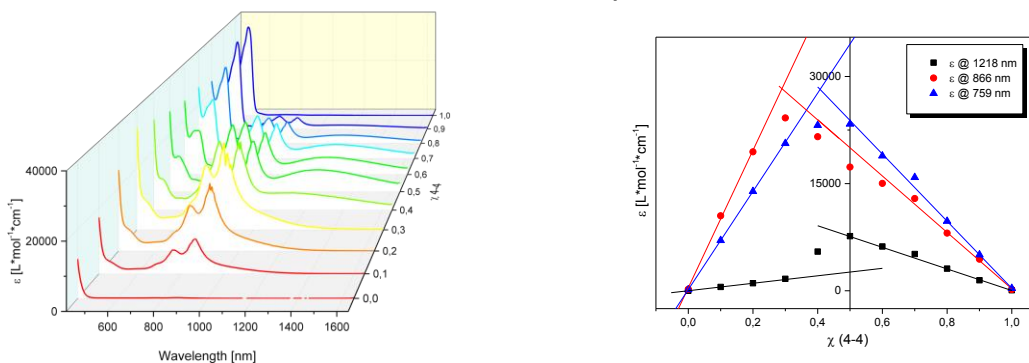
*IV-4: UV-vis absorption spectra resulting from continuous concentration method (left) and corresponding JOB plots (right). Spectra recorded in CH$_2$Cl$_2$ at c = 3*10^{-3} mol/l except **4-3**/**4-7** and **4-4**/**4-7** (c = 3*10^{-5} mol/l).*

For TCNQ (**4-6**) in combination with **4-2** a relatively smooth evolution of the plotted CT-band is observed. In the interval χ_{4-2} = 0 to $\chi_{4-2} \approx 0.4$ the broad band gains in intensity and declines from χ_{4-2} = 0.6 to $\chi_{4-2} \approx 0.8$. In the JOB plot on the right the evolution of ε at

λ_{max} is plotted. The absorption maximum is reached at $\chi_{4\text{-}2} \approx 0.5$ which indicates a 1:1 complexation model. The broad shape of the JOB curve is characteristic for a weak complex. The initial tangents intersect at $\chi_{4\text{-}2} \approx 0.4$ which can indicate a deviation from the 1:1 binding model but most likely this can be attributed to a low signal to noise ratio ($A_{UV\text{-}vis} < 0.01$) in the experiments. The 1:1 binding model is consistent with the 1:1 complex in the solid state as identified in single crystal X-ray diffraction crystallography (see section *IV.2.3.3*). In the case of donor **4-3** not only a smooth and broad charge-transfer band is observed ($\lambda_{max,CT} = 1430$ nm) but also features that can be attributed to the $[TCNQ]^{\bullet}$ radical anion ($\lambda = 750$ nm and $\lambda = 866$ nm).[332] As these signals have also been utilized in the characterization of CT-complexes, they are included in the JOB plot.[333] Whereas the CT-band evolves smoothly and reaches its maximum at $\chi_{4\text{-}3} \approx 0.5$, i.e. indicating a 1:1 complexation, the results for the radical anion are more scattered. The lopsided curve reaches a maximum at around $\chi_{4\text{-}3} \approx 0.3$. This is supported by the initial tangents intersecting at $\chi_{4\text{-}3} \approx 0.3$. For these results a 1:2 complexation of donor and acceptor is indicated. Apparently, two parallel reactions are taking place during complex formation. Unfortunately, the solid state structure is not available for comparison.

The combination of F_4-TCNQ (**4-7**) and **4-1** gives a strong, featureless CT-band. In the JOB plot, the maximum absorption is reached at $\chi_{4\text{-}1} = 0.5$, i.e. a 1:1 binding model is operational. The initial tangents intersect at $\chi_{4\text{-}1} = 0.55$ which can be attributed to experimental errors. The round curvature suggests a weak binding. 1:1 binding is also identified in the solid state (section *IV.2.3.2*). In the case of donors **4-3** and **4-4** in combination with acceptor **4-7** the concentration of the sample was reduced to $c = 5*10^{-5}$ mol/l. This gives clear spectra of the $[F_4\text{-}TCNQ]^{\bullet}$ radical species as well as additional CT-features for **4-4**. For donor **4-3** a 1:1 binding model is confirmed in the JOB plot for all investigated wavelengths. The low curvature in the plot suggests a strong binding of donor and acceptor. The inset gives the results for the very weak CT-band (two orders of magnitude) at $\lambda = 1240$ nm. Again a 1:1 binding is found in the JOB plot. For **4-4** the picture is more complicated. At $\lambda = 759$ nm a maximum in the JOB plot is observed at $\chi_{4\text{-}4} = 0.4$. For $\lambda = 866$ nm the maximum is recorded for $\chi_{4\text{-}4} = 0.3$. In addition to this, a broad, featureless absorption ($\lambda_{max} = 1280$ nm) arises sharply at $\chi_{4\text{-}4} = 0.4$ and falls off again at $\chi_{4\text{-}4} > 0.6$. It can be speculated that the significant decline of the signal at $\lambda = 866$ nm at $\chi_{4\text{-}4} > 0.3$ and the rising of the new band at $\lambda_{max} = 1280$ nm have a common cause. Yet, more sophisticated spectroscopic studies would be necessary to fully elucidate these findings.

IV.2.2   IR-Spectroscopy on TCNQ and F₄-TCNQ CT-complexes

The landmark publication by CHAPPELL *et al.* correlates the CN stretching mode ($\omega_{CN} = 2227$ cm^{-1}) to the degree of electron transfer in charge-transfer complexes

containing TCNQ (**4-6**). [334] IR-spectroscopy has thus become a popular method in the analysis of these compounds. The CN stretching mode is well suited to probe the degree of electron transfer, as it is very sensitive to the population of TCNQ's LUMO. Furthermore, it is seldom obscured by other modes.

The degree of charge-transfer Z is derived according to the empirically determined relationship (IV-1):

$$Z = \left| \frac{\left(\omega_{CN,TCNQ} - \omega_{CN,complex} \right)}{-44 (cm^{-1})} \right| \qquad (IV-1)$$

Eq. (IV-1): $\omega_{CN,TCNQ}$ is the frequency of the CN stretching mode of free TCNQ and $\omega_{CN,complex}$ the experimentally determined stretching mode in the investigated CT-complex. -44 cm^{-1} is an experimentally derived constant.

A series of TCNQ (**4-6**) and F$_4$-TCNQ (**4-7**) based CT-complexes was investigated. For clarity and consistency the signals were fitted with a GAUSS function to determine the maximum ω_{CN}. The results as well as the calculated degrees of charge-transfer Z are given in table IV-2.

Table IV-2: Results IR/ESR spectroscopy.

Complex	$\omega_{CN,complex}$ (cm^{-1})	Z	ESR activity[a]
4-6	2225.8	---	---
4-1 / 4-6	2218.5	0.17	Silent
4-1 / 4-6 (1:2 ratio)	2218.8	0.16	---
4-1 / 4-6 (2:1 ratio)	2218.1	0.18	---
4-1 / 4-7	2212.2	0.36	Silent
4-2 / 4-6	2216.6	0.21	Silent
4-2 / 4-6 (1:2 ratio)	2218.1	0.18	---
4-2 / 4-6 (2:1 ratio)	2216.3	0.22	---
4-3 / 4-6	2207.1; 2177.8	0.43; 1	Active
4-4 / 4-6	2182.2; 2156.8	0.99; 1	Active
4-5 / 4-7	2191.7; 2161.9	0.78; 1	---
	[a] determined using crystalline samples		

As expected the nature of the donor has significant impact on the degree of electron transfer in TCNQ complexes. Whereas **4-1** and **4-2** form non-ionic, neutral complexes with Z = 0.17 and Z = 0.21 the combination of **4-6** with **4-3** or **4-4** leads to fully ionic (Z ≥ 1) compounds.[168] Only the combination **4-3** / **4-6** has a significant component in the neutral-ionic region (0.5 > Z > 0.3) at (Z = 0.43). These results are mirrored by electron spin resonance (ESR) experiments performed with these compounds. The complexes containing **4-1** and **4-2** are ESR silent. Using **4-3** or **4-4** as donor, a clear ESR signal is observed.

In the context of the SFB/TR 49 framework not only complexes formed from a 1:1 ratio solution were investigated, but also from 2:1 and 1:2 mixtures. In figure IV-4 the UV-vis absorption spectra of these mixtures are included ($\chi = 0.3$ and $\chi = 0.7$ respectively). A shift of λ_{max} of the CT-band is not observed, thus no significant variation of the charge-transfer interaction is to be expected.[166] In the IR experiments only a minuscule change in the degree of electron transfer is observed. Counterintuitively, lower donor content leads to a larger Z. This observation agrees with results from the Near Edge X-ray Absorption Fine Structure (NEXAFS) spectroscopy study presented in section *IV.3.3.4*.

IV.2.3   Crystal structures

*IV-5: Optical microscopy of a batch of **4-1**/TCNQ cocrystals used for NEXAFS and HAXPES measurements (adapted from [335]). Millimeter sized cocrystals used for single-crystal conductivity measurements (pictures courtesy of Huth group).*

For cocrystallization experiments a $6*10^{-3}$ mol/l solution of donor and acceptor in 5 mL dichloromethane or THF was prepared. Crystals were grown by slow vapor diffusion of hexanes. [77] In addition to equimolar mixtures of donor (D) and acceptor (A) also 2:1 D/A and 1:2 D/A ratios of **4-1** and **4-2**/**4-6** were investigated. Cocrystals usually range in size from 10 μm to 100 μm but also crystals up to several millimeters in size have been prepared (IV-5, right panel). Equimolar mixtures afforded cocrystals suitable for X-ray diffraction structure elucidation. This was not the case for other D/A ratios. For further experiments cocrystals were separated from components by use of a micromanipulator assisted optical microscope. The difference in color (**4-1** and **4-2** colorless, TCNQ green, cocrystal black) allowed for this procedure.

IV.2.3.1   Crystal structure 4-1/TCNQ cocrystal

The solid state structure of a 1:1 cocrystal of **4-1**/TCNQ was determined by single crystal X-ray diffraction crystallography. A mixed stack of donor and acceptor is found in the crystal (figure IV-6). The unit cell encompasses 12 molecules in total, six units of TCNQ and six units of **4-1**. This large unit cell (a = 14.2441 Å, b = 14.6744 Å, c = 13.2556 Å, V = 2493 Å^3) is due to large positional variation of the subunits. It has a C2/c space group.
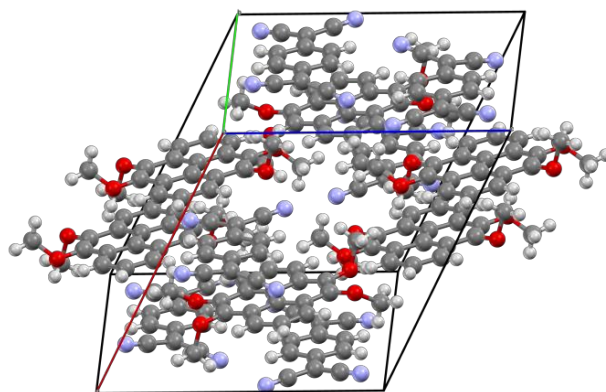
*IV-6: Unit cell of the **4-1**/TCNQ cocrystal.*

In general, a stratified geometry is found. A stratum of donor is placed between two strata of acceptor molecules and *vice versa* (figure IV-7). With respect to a plane defined by a TCNQ layer, each **4-1** subunit is twisted by 18°. TCNQ subunits are internally warped by 5° and centered alternatingly under the $2\text{-}3_a^1$ or $5_a^1\text{-}7$ carbon atoms of **4-1**. The short $\pi-\pi$ contacts between donor and acceptor are between 3.5 Å and 3.6 Å.
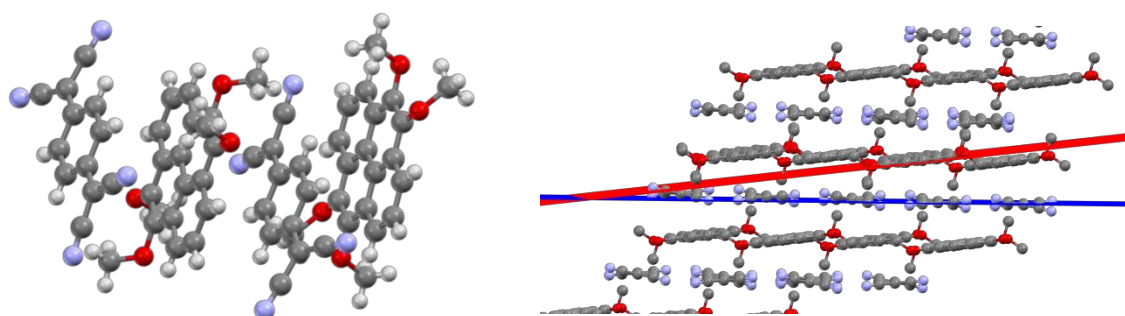
*IV-7: Packing motive in the **4-1**/TCNQ cocrystal. Left: A mixed stack of donor and acceptor is found. Right: **4-1** units are twisted by 18° with respect to the TCNQ strata (protons are omitted for clarity).*

IV.2.3.2   Crystal structure 4-1/F$_4$-TCNQ cocrystal

A **4-1**/F$_4$-TCNQ cocrystal suitable for X-ray diffraction crystallography was grown by slow evaporation of dichloromethane.
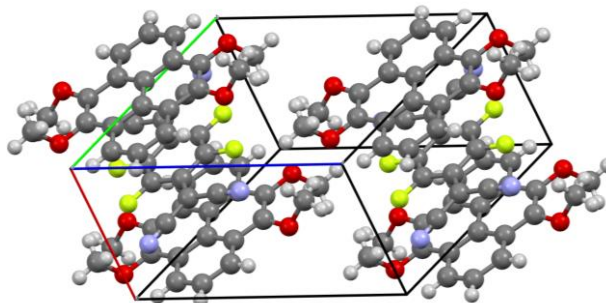
*IV-8: Unit cell of the **4-1**/F$_4$-TCNQ cocrystal.*

The complex adopts mixed stack arrangement. Compared to other CT-complexes in this chapter, the unit cell is small (a = 6.7723 Å,   b = 10.6602 Å,   c = 10.8483 Å, V = 653.354 Å^3) and adopts a P$_1$ space group.

As in **4-2**/TCNQ distinct columns of alternating donors and acceptors are formed. Furthermore, the F$_4$-TCNQ units are also centered under the 3_a^1 and 5_a^1 carbons of **4-1**. In contrast to the TCNQ cocrystals **4-2**/F$_4$-TCNQ possesses an alternating arrangement of donor and acceptor in the *a*-plane (figure IV-9, left). The π–π distances are short, ranging from 3.5 to 3.6 Å. Short contacts are identified between (methoxy) C-H···N (2.8 – 2.9 Å) and C-H···F (2.6 – 2.7 Å) indicating that weak hydrogen bonding can occur in this crystal (figure IV-9, right).

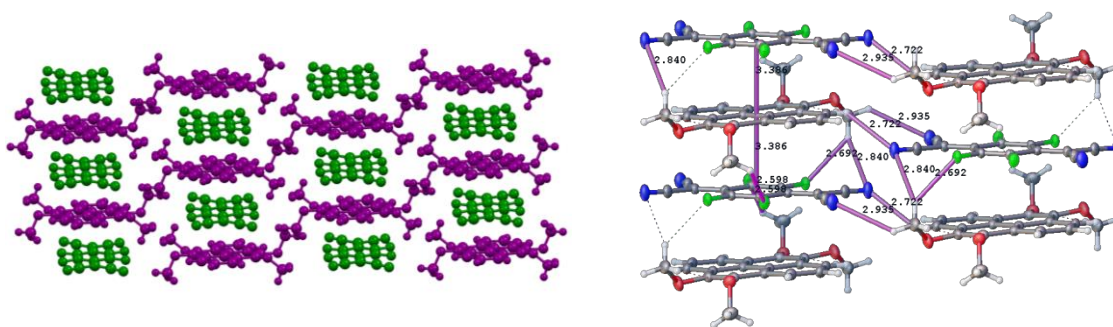*IV-9: Packing motive in **4-1**/F$_4$-TCNQ. Left: Alternating stacks (F$_4$-TCNQ in green, **4-1** in purple); alternation within the a-plane. Right: Short contacts and π–π interactions in the crystal (purple).*

IV.2.3.3   Crystal structure 4-2/TCNQ cocrystal

A cocrystal of **4-2** and TCNQ was initially grown by vapor diffusion of hexanes in a dichloromethane solution of both components. A twined crystal was obtained, that was recrystallized from DMSO. The structure was resolved as a DMSO solvate crystal. It was not possible to grow cocrystals suitable for X-ray diffraction crystallography without inclusions of the solvent.
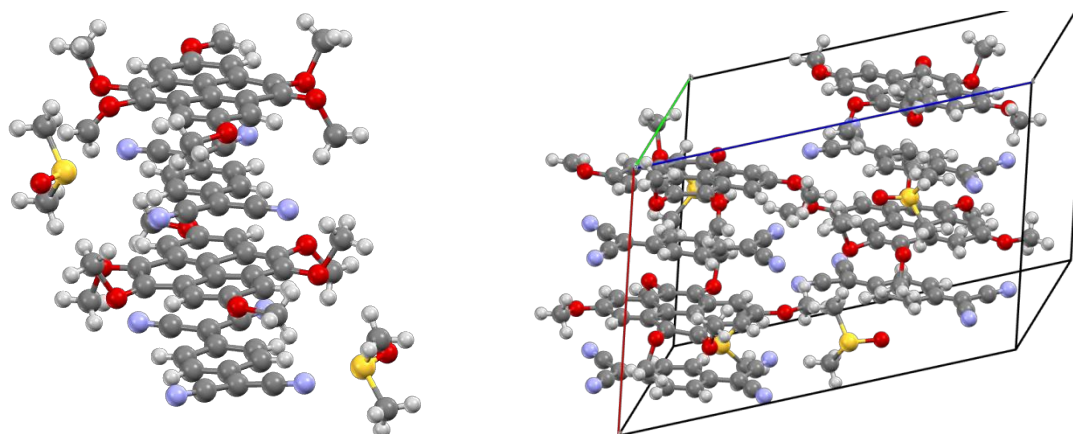
*IV-10: Structure of the **4-2**/TCNQ DMSO solvate cocrystal. Left: Mixed stack packing. Right: The unit cell DMSO is intercalated in the TCNQ layer.*

For the unit cell the following dimensions are observed: a = 13.1830 Å, b = 12.9270 Å and c = 19.6250 Å with a volume of V = 3150.96 Å^3 and a P$_n$ space group. Low symmetry and large size are a consequence of solvent intercalation.
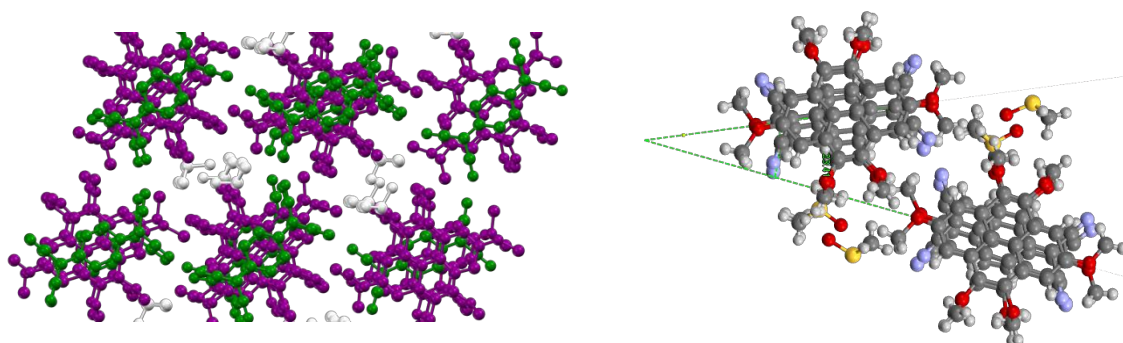
*IV-11: Columnar structure in the **4-2**/TCNQ cocrystal. Left: Stacks viewed along the a-axis (**4-2** in violet, TCNQ in green and DMSO in grey). Right: Stacks are arranged with 23° angle in respect to each other.*

The CT-complex crystallizes in mixed stack geometry with distinct columns of alternating donor and acceptor units. TCNQ is centered under the $3_a{}^1$ and $5_a{}^1$ carbons of **4-2**. The size mismatch between TCNQ and the donor provides large voids within the structure that are occupied by intercalated DMSO molecules. Closest intermolecular contacts are determined to 3.5 Å up to 3.8 Å paralleling the observations for **4-1**/TCNQ. In figure IV-11 the columnar structure is visualized. Within a layer (viewed along a-axis) an alternation of donor and acceptor is also observed. Stacks are arranged in an 8° angle in respect to each other (figure IV-11, right).

IV.2.3.4   Crystal structure 4-2/4-9 cocrystal
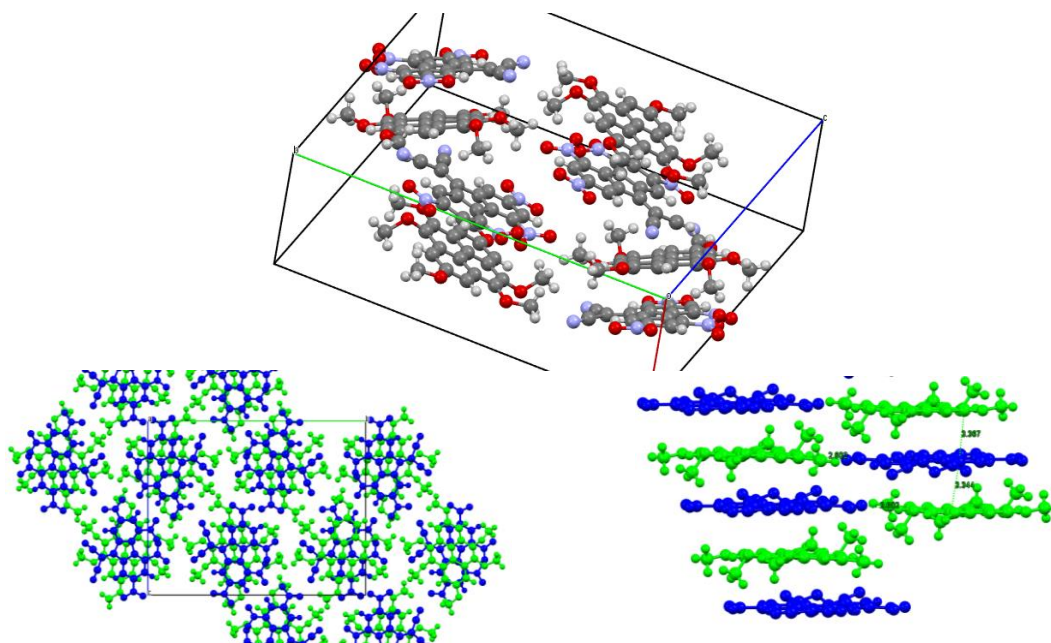
*IV-12: X-ray diffraction structure of the **4-2**/**4-9** cocrystal. Top: Unit cell. Bottom-left: Packing viewed along a-axis. Bottom-right: Packing perpendicular to growth axis (green: **4-2**, blue: **4-9**).*

The crystal grows in a mixed stack arrangement. Its unit cell incorporates 8 molecules (a = 7.3136 Å, b = 23.5579 Å, c = 18.9555 Å, V = 3229 Å³) with a P2₁/c space group. Significant twist between two stacks (38.6°) is evident in the unit cell (figure IV-12, top). A very short contact of 3.18 Å is found between the fluorenon-*9*- and the pyrene-*4*-carbon,

suggesting a strong interaction. The mean $\pi-\pi$ distance is expanded to 3.24 Å. The short $\pi-\pi$ distances indicate good geometrical matching as well as strong charge-transfer interactions.

IV.2.3.5   Crystal structure 4-2/TCNE cocrystal
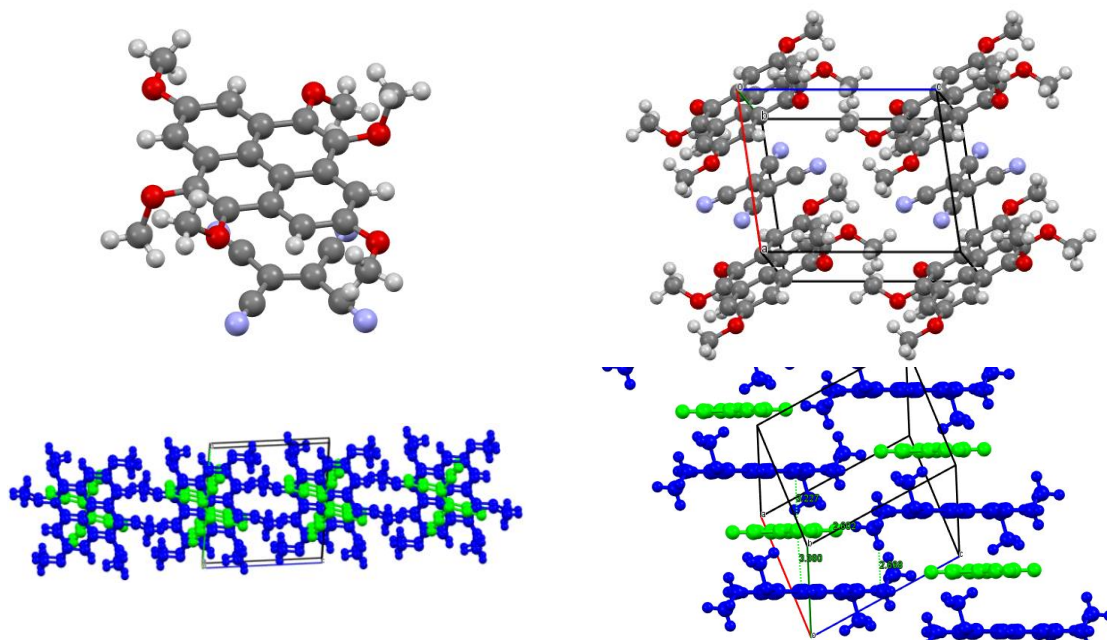
*IV-13: Solid state structure of the **4-2**/**4-10** cocrystal. Top-left: Single molecules arrangement. Top-right: Unit cell. Bottom-left: Packing viewed along a-axis. Bottom-right: Packing viewed perpendicular to growth axis (green: **4-10**, blue: **4-2**).*

The small tetracyanoethylene (**4-10**) is able to fit well between **4-2** layers to form an alternating stack arrangement. In the triclinic unit cell (P1, a = 7.4720 Å, b = 8.9918 Å, c = 9.0713 Å, V = 591.4 Å^3) six molecules are contained. The mean-plane $\pi-\pi$ distance is as low as 3.26 Å. The central C-C axis of TCNE is rotated by 61° in respect to the pyrene long axis. This arrangement ensures a close contact between the electron deficient nitrile nitrogen atoms of TCNE and the electron rich C-O bonds in 2 and 4 position of **4-2**.

IV.2.4   Overview CT-complexes

Table IV-3 gives an overview of the studied CT-complexes. The nature of both, donor and acceptor have significant impact on the degree of electron transfer, the CT-band but also the solid state arrangement.

Table IV-3: CT-complex comparison.

CT-complex	λ_{abs} (nm) / ΔE_{opt} (eV)[a]	Z[b]	Unit cell / space group[c]	Cell dimensions (Å)[c]	$\pi-\pi$ distance: short / mean plane (Å) [c]
4-1 / 4-6	528, 865 (br)	0.17	Monoclinic / C2/c	a = 14.2441 b = 14.6744 c = 13.2556 V = 2493 Å^3	3.43 / 3.84
4-1 / 4-7	599, 1133 (br)	0.36	Triclinic / P1	a = 6.7723 b = 10.6602 c = 10.8483 V = 653 Å^3	3.28 (C-F) / 3.39
4-2 / 4-6	716	0.21	Monoclinic / Pn	a = 13.1830 b = 12.9270 c = 19.6250 V = 3150 Å^3	3.24 / 3.24
4-2 / 4-9	642	0.18	Monoclinic / P2$_1$/c	a = 7.3136 b = 23.5579 c = 18.9555 V = 3229 Å^3	3.18 / 3.24
4-2 / 4-10	739	0.20	Triclinic / P1	a = 7.4720 b = 8.9918 c = 9.0713 V = 591.4 Å^3	3.24 / 3.42

[a] determined in CH_2Cl_2, [b] determined by IR spectroscopy, [c] derived from crystal structure

IV.3   CT-complexes studied in the context of the SFB/TR 49

IV.3.1   Introduction

| 4-1 (TMP) | 4-5 (TCNQ) | 4-2 (HMP) | 4-5 (TCNQ) | 4-1(TMP) | 4-6 (F$_4$-TCNQ) |
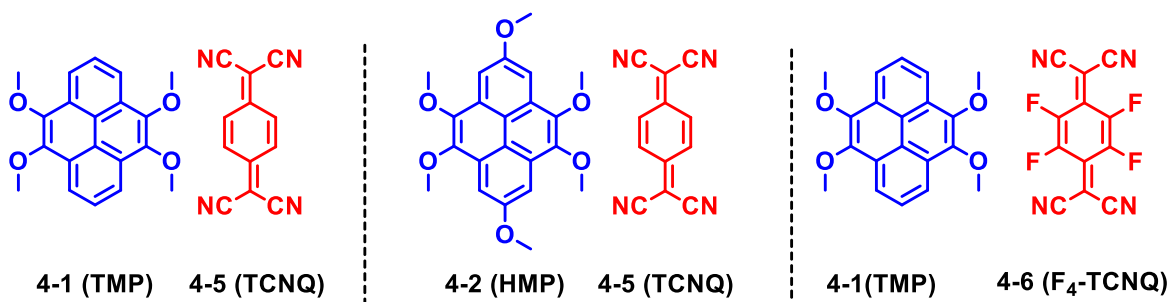
IV-14: Charge-transfer complexes studied in the SFB/TR 49 context.

Within the framework of the SFB/TR 49 charge-transfer complexes of 4,5,9,10-tetramethoxypyrene (**4-1**) and 2,4,5,7,9,10-hexamethoxypyrene (**4-2**) with TCNQ (**4-5**) were studied. In collaboration with the SCHÖNHENSE group thin films of these compounds were prepared and studied by ultraviolet photoelectron spectroscopy (UPS) and scanning tunneling spectroscopy (STS). Furthermore, properties of macroscopic crystals **4-1** / **4-2** and TCNQ (**4-6**) were investigated by near edge X-ray absorption fine structure (NEXAFS [20]) spectroscopy and hard X-ray photoelectron spectroscopy (HAXPES). In the HUTH group electronic properties of macroscopic cocrystals were studied. The **4-1**/F$_4$-TCNQ cocrystal was prepared at a later stage. The HUTH group mostly worked on this complex.

The following discussion stems from the tight collaboration within the SFB/TR 49 framework. Material preparation, cocrystallization and solution characterization were performed by the author of this manuscript. Structure elucidation by X-ray diffraction crystallography was done by ENKELMANN. Further studies in *status solidi* were performed by aforementioned collaborators.

In the following, results of solid state studies will necessarily be given in abridged form. A full account of these works is available in the following publications:

- Film characterization and UPS of **4-1**/TCNQ.[336, 337]
- NEXAFS study of **4-1**/TCNQ and **4-2**/TCNQ.[338]
- NEXAFS study of **4-1**/TCNQ and **4-2**/TCNQ under variation of cocrystal composition.[339]
- HAXPES study of **4-1**/TCNQ and **4-2**/TCNQ.[335]

---

[20] Also known as *X-ray absorption near edge structure* (XANES), the terms NEXAFS and XANES are used interchangeably in literature.

- Conductivity measurements [340]

IV.3.2   Basic CT-complex characterization
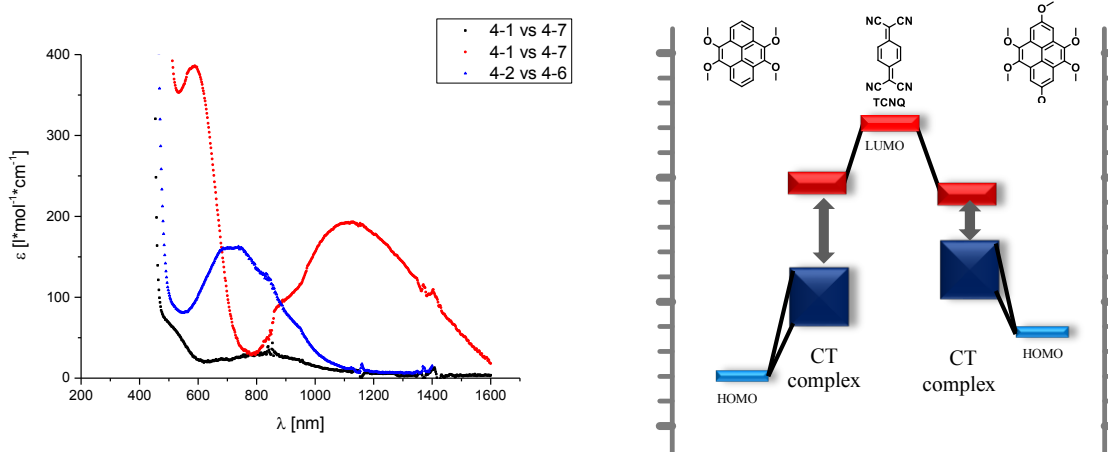
*IV-15: Left: UV-vis absorption spectra of **4-1**/TCNQ (black), **4-1**/F$_4$-TCNQ (red) and **4-2**/TCNQ (blue) in dichloromethane (c = 3*10^{-3} mol/l). Right: Schematic energy diagram of CT-complexes.*

UV-vis absorption spectra of the three CT-complexes are compared in figure IV-15. **4-1**/TCNQ has a shoulder at λ = 530 nm which is attributed to a weak charge-transfer from **4-1** to TCNQ. In contrast, for **4-2**/TCNQ a broad, discrete CT-band at λ_{max} = 710 nm is resolved. The bathochromic shift can be understood in terms of frontier orbital energy matching. The HOMO of **4-1** was established to $E_{HOMO,\mathbf{4\text{-}1}}$ = -5.3 eV (by CV) while the HOMO of **4-2** is located 0.15 eV higher in energy ($E_{HOMO,\mathbf{4\text{-}2}}$ = -5.1 eV). The LUMO of TCNQ is located at $E_{LUMO,TCNQ}$ = -4.3 eV.[341] Thus, complex formation is enhanced due to a smaller energy difference. In figure IV-15 (right) an energy scheme illustrates the CT-complex formation.[21] The higher energy HOMO of **4-2** provides a higher energy CT-complex state, i.e. a smaller energy gap which results in a bathochromic shift of the CT-band. For **4-1**/F$_4$-TCNQ the UV-vis absorption spectrum shows two significantly red shifted absorption bands ($\lambda_{max,1}$ = 590 nm and $\lambda_{max,2} \approx$ 1120 nm). The low energy LUMO ($E_{LUMO,F4\text{-}TCNQ}$ = -5.4 eV) explains this transition.

IV.3.3   Characterization in solid state

IV.3.3.1   Film formation

Thin films of CT-complexes were grown by UHV deposition (3*10^{-10} mbar) of the respective components on a gold surface. Evaporating donor and acceptor simultaneously from just one crucible (at 120 °C) onto clean gold surfaces produced thin films of CT-crystals despite the difference in vapor pressure of both components.

---

[21] Simple *linear combination of molecular orbitals* approximation.

In a film grown from **4-1**/TCNQ, X-ray diffraction shows a new crystallographic phase (figure IV-16). Reflections are observed at $2\theta = 10°$ and $2\theta = 13°$, this is equivalent to a lattice plane spacing of $d_1 = 8.94$ Å and $d_2 = 6.77$ Å. In this figure diffraction patterns of pure **4-1** and TCNQ on gold are included for reference. For the deposited CT-complex films the reflexes of the components are absent.
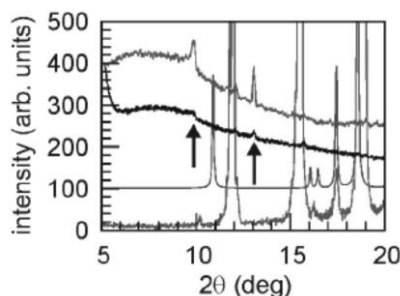
*IV-16: X-ray diffraction patterns of **4-1**/TCNQ on gold (purple), **4-1**/TCNQ on silica (black), TCNQ (blue) and **4-1** (red). New reflections arising from CT-complex are marked by arrows [figure adapted from MEDJANIK et al.[337]].*

IV.3.3.2   Ultraviolet photoelectron spectroscopy (UPS)

IV.3.3.2.1   Photoelectron spectroscopy (PES) basics

In photoelectron spectroscopy (PES) techniques photoelectrons generated by ionizing electromagnetic radiation is used to probe the electronic distribution in molecules (UPS) or atoms (X-ray photoelectron spectroscopy, XPS). In the experiments the kinetic energy of the photoelectrons (E_{kin}) is measured. The sample is irradiated with electromagnetic radiation h*ν. UPS (hard UV, usually $h\nu = 21$ eV), XPS (soft X-rays, $h\nu = 0.1 – 5$ keV) and HAXPES (hard X-rays, $h\nu > 40$ keV) are discerned by the photon energy used.[342]

The photoelectric effect is described by EINSTEIN's law:

$$h \times \nu = E^f(k) - E^i + E_{kin} \qquad\qquad (IV\text{-}2)$$

Eq. (IV-2): hν gives the photon energy, $E^f(k)$ gives the final energy of the molecule / atom after the electron was released for a state k, E^i gives the initial energy of the molecule / atom.[343]*

Figure IV-17 shows the relation between the energy level diagram of the sample and the energy distribution of emitted photoelectrons. The solid has core energy levels at $E = E_B$. At the top of the valance band ($E_B = 0$) the FERMI level (E_F) is located. The work function ϕ gives the energy difference from E_F to the vacuum level E_{vac}. A photon can ionize a molecule (i.e. release an electron from a molecule / atom) if its energy is larger than the electron binding energy E_B. Energy provided by the photon exceeding the binding energy will be carried by the ejected electron in the form of kinetic energy E_{kin}.[344]
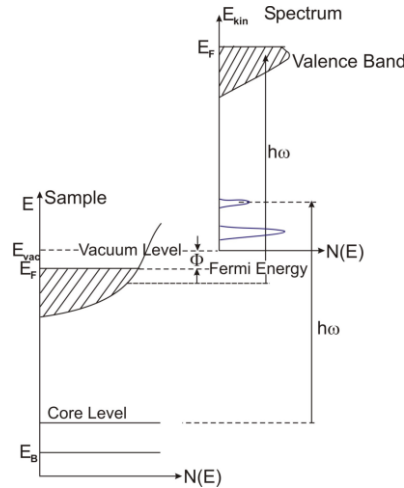
IV-17 : Relation between the energy level diagram of the sample (left) and the energy distribution of emitted photoelectrons (right). E_B = binding energy, E_F = Fermi energy, E_{vac} = vacuum level, ϕ = work function [figure adapted from HÜFNER [344]].

$$E_{kin} = h \times \nu - \phi - |E_B| \qquad\qquad\qquad \text{(IV-3)}$$

Eq. (IV-3): E_{kin} = kinetic energy of the photoelectron, ϕ = work function of the sample, E_B = binding energy.

On the right side of figure IV-17 the kinetic energy distribution of emitted photoelectrons is plotted. It mirrors the electron-energy distribution of the sample. Accordingly PES gives an insight into the electronic structure of a sample.
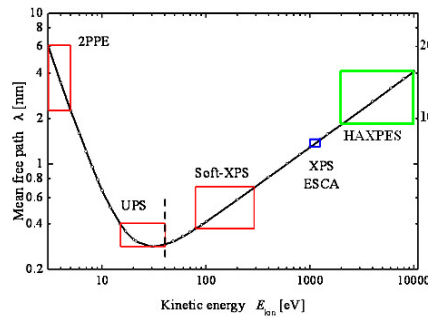
IV-18: Photoelectron mean free path λ as a function of photoelectron energy [figure adapted from SEAH et al.[345]].

UPS is a surface sensitive method only. The photoelectron mean free path λ_{pe} reaches a minimum at the UPS energy range. Therefore, only surfaces near photoelectrons are able the leave the sample and may be detected. Due to the high surface sensitivity UPS measurements are performed in UHV conditions preferably on samples prepared *in situ*.[345]

IV.3.3.2.2   Results UPS experiments on 4-1/TCNQ
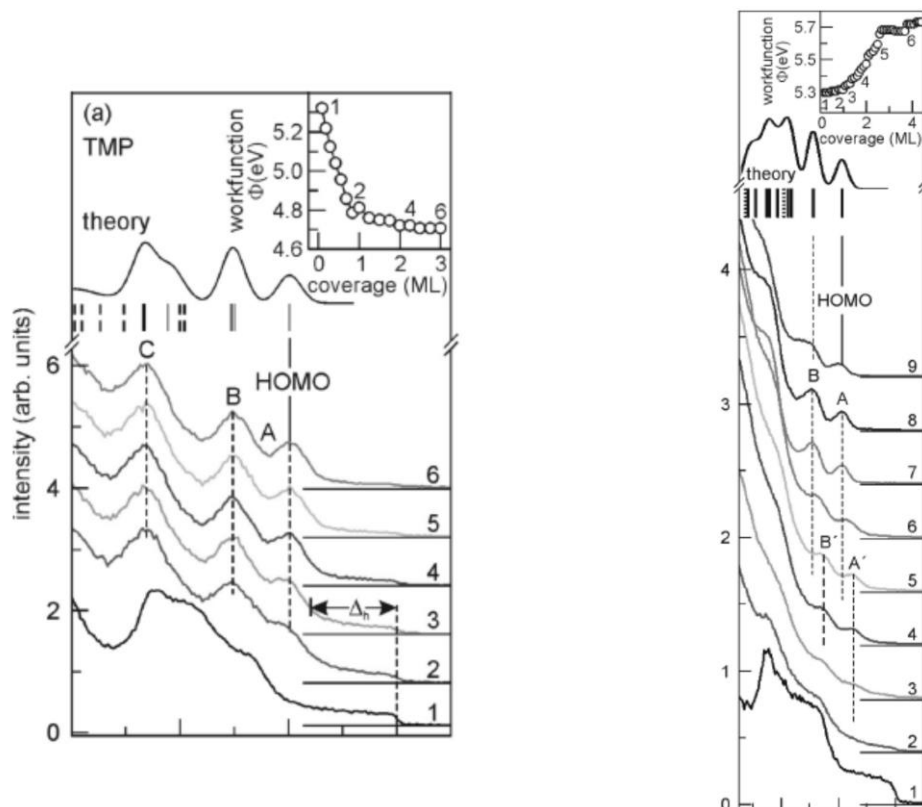
*IV-19 : UPS spectra of **4-1** (left) and **4-1**/TCNQ (right) thin-films on gold in dependence of multilayer thickness (from 1 – 6 resp. 1 – 9 layers). Insets: ϕ in dependence of multilayer thickness. Δh indicates the hole injection barrier [figure adapted from MEDJANIK et al. [337]].*

In the case of pure **4-1** on gold a significant drop of work function ϕ from 5.2 eV to 4.8 eV is observed as the first multilayer is grown (*1* to *2*). For the second multilayer (*3* to *4*) ϕ drops further to 4.75 eV, the characteristic features *A* (2.0, 3.0 and 4.6 eV below E_F), *B* and *C* emerge in the UPS spectrum. The predicted electronic structure of **4-1** is in good agreement with the experimental finds. For the third multilayer (*5* to *6*) the change in ϕ is negligible and remains at a value of 4.7 eV. The spectral features are fully formed. **4-1** behaves as a typical polycyclic aromatic hydrocarbon on a gold surface, the work function drop is attributed to the *push back effect*.[346] Spill-out charges from the gold surface experience PAULI repulsion from the first **4-1** monolayer, whereby the gold surface dipole is reduced and ϕ of the metal surface drops. It is possible to determine the hole injection barrier Δ_h, i.e. the energy gap between the FERMI edge of the metal and the onset of the organic material's HOMO (see fig. IV-19 left). From this the ionization energy of the organic material E_i can be estimated as follows:

$$E_i = \Delta_h + \phi = 1.6 + 5.7 = 6.3 eV \qquad (IV-4)$$

Eq. (IV-4): E_i denotes the ionization energy of the organic sample, Δ_h, the hole injection barrier of the system and ϕ the work function of the metal.

For **4-1** multilayers on gold the ionization energy is established to 6.3 eV. Theoretically, the binding energy E_B of electrons in the molecular orbitals of **4-1** was determined in delta self-consistent field (ΔSCF) using the B3LYP/6-31G(d) correlation functional.[347] From this it follows that $E_{B,\textbf{4-1}} = 6.18$ eV or 1.48 eV in respect to the FERMI energy. The ΔSCF results are in good agreement with the experimental findings (a shift of 0.5 eV aligns the theoretical spectrum to the experiment) and allow an assignment of the spectroscopic features. Feature *A* in figure IV-19 (left) stems from the HOMO level, feature *B* results from energetically close HOMO-1 and HOMO-2 while *C* encompasses signals from HOMO-3 down to HOMO-7. The mismatch in absolute energy between theory and experiment can be attributed to the single molecule nature of ΔSCF calculation.

In figure IV-19 (right) a series of photoelectron spectra for **4-1**/TCNQ CT-complexes in the range from sub-monolayer (spectrum 1-5) to multilayer coverage (7-9) is reproduced. The work function / coverage curve is shown as an inset. For low substrate coverage the growth of signals *A´* and *B´* at 1.5 and 2.5 eV below E_F as well as an increase of ϕ by 0.4 eV are characteristic. The organic-metal interface is polarized as charge-transfer from gold to the organic material occurs. Signals *A´* and *B´* reach their maximum intensity in *5*, the hole injection barrier is $D_h = 1.0$ eV. With spectrum *6* signals *A´* and *B´* as well as *A* and *B* are observed indicating the emergence of a second structure. The rise of ϕ stops from *5* to *6*. Further coverage (spectra *7* to *9*) results only in a weak increase of ϕ to 5.75 eV. Signal *A* (1.8 eV below E_F) and *B* (2.9 eV below E_F) grow while signals *A´* and *B´* are no longer observed. The energy level shift between spectra *1* to *5* and spectra *7* to *9* is attributed to a change in the film morphology. In figure IV-20 AFM images at different surface covering are reproduced. Section (i) corresponds to a surface covering for spectrum *6*. Smooth multilayer surfaces as well as 3D crystallites are observed. At higher coverage (ii), corresponding to spectrum *8*, a rough surface is observed.
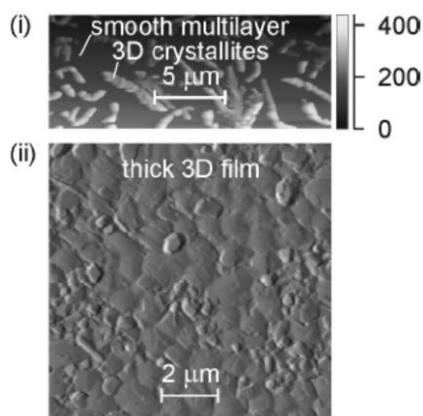
IV-20: AFM images of **4-1**/*TCNQ thin films. (i) shows the coexistence of a smooth layer covered with 3D crystallites (corresponding to spectrum 6). (ii) shows a rough film with micrometer sized crystallites at higher coverage (corresponding to spectrum 8) [figure adapted from MEDJANIK et al.[337]].*

From this, signals *A* and *B* are assigned to **4-1**/TCNQ CT-complex crystallites while *A'* and *B'* are assigned to a smooth layer of the complex. This suggests a STRANSKI-KRASTANOV or `layer-plus-island`-type epitaxial growth of **4-1**/TCNQ on gold.[348] Initially, molecules lie flat on the gold substrate (forming the smooth layers) while additional layers grow in crystallites (islands). This growth mechanism has also been observed for HBC.[349]

*IV-21: Left: SEM image of a low coverage **4-1**/TCNQ film on SiO$_2$. Right: SEM image of **4-1**/TCNQ film (dark) on gold (bright). Island growth is observed on both substrates (pictures courtesy of HUTH).*

SEM images of films grown on SiO$_2$ (figure IV-21, left) show a strong island formation tendency. It is not clear which growth mechanism is causing this film morphology.[350]

IV.3.3.3   Scanning tunneling spectroscopy (STS)
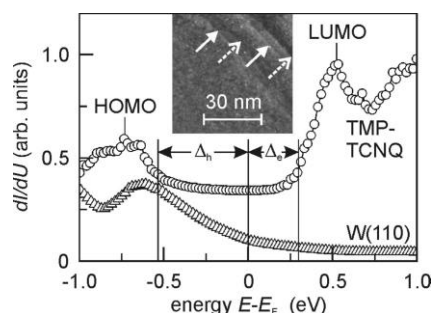
*IV-22: Scanning tunneling spectroscopy (STS). Differential conductivity (dI/dU) spectrum on an island of **4-1**/TCNQ on W(110) (circles) and the clean W(110) substrate (triangles). The sample voltage modulation was 50 mV and the tip was stabilized at U = 0.7 V and I = 0.35 nA. Δ_h and Δ_e denote the hole- and electron injection barriers. The inset gives a topographical STM image [figure adapted from MEDJANIK et al. [337]].*

By STS the local density of states (DOS) of a sample can be studied at the position of the STM tip.[351] By applying a positive (negative) bias to a sample the unoccupied (occupied) states i.e. LUMO (HOMO) energies in the thin film can be probed.[352] The inset of figure IV-22 shows a processed topographical STM image of the region where the spectra were measured. Arrows signpost substrate steps indicating an initial step flow growth mode.

For STS studies a thin-film of **4-1**/TCNQ was prepared on tungsten (110) by vacuum deposition. The spectrum shows a sharp signal at +0.5 eV (E-E$_F$), corresponding to the LUMO and a broader signal at -0.75 eV corresponding to the HOMO of the CT-complex. Thus, the bandgap of the material is identified as 1.25 eV. In contrast to the UPS results the hole injection barrier determined by STS is significantly smaller ($\Delta_{h,UPS} = 1$eV, $\Delta_{h,STS} = 0.5$ eV). The electron injection barrier is $\Delta_e = 0.3$ eV.

IV.3.3.4   NEXAFS spectroscopy

NEXAFS is an X-ray absorption spectroscopy technique.[353] In the following, only the basic principle can be outlined, a full discussion is beyond the scope of this work. The interested reader is referred to textbooks by STÖHR[354] or BUNKER[355].
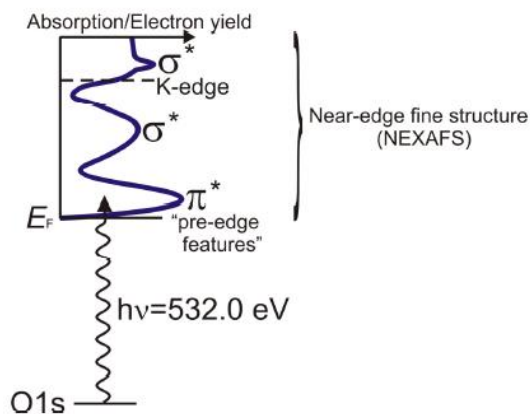
IV-23: X-ray absorption spectroscopy. Shell electrons are excited by monochromatic X-rays. NEXAFS probes electronic states around the absorption edge (K-edge of oxygen in this example, dashed line) of the element [figure adapted from MEDJANIK [356]].

In NEXAFS a sample is exposed to monochromatic X-rays. At wavelengths specific for each element, an excitation of the shell electrons (in figure IV-23 the 1s electrons of oxygen) to an empty or partially occupied valence state occurs. A strong increase of the attenuation coefficient occurs at energies sufficient to excite electrons to the continuum; the so-called K-edge arises in the absorption spectrum. In close proximity to the K-edge spectral features can be found which are investigated in NEXAFS experiments.

Due to its atom specific nature NEXAFS has found a broad field of application from materials science to geology and environmental chemistry.[354] As monochromatic X-rays are needed in this experiment a synchrotron facility is required. For the following study the ANKA synchrotron at the Karlsruhe Institute of Technology (KIT) was used. For the measurement total electron yield mode was chosen, this results in an information depth of 5 nm (i.e. bulk measurement).[338]

Charge-transfer generates hole states which were probed by NEXAFS. In both CT-complexes (**4-1**/TCNQ and **4-2**/TCNQ) the element sensitivity of NEXAFS allows the selective study of the donor (oxygen 1s) and the acceptor (nitrogen 1s). At the time of publication a few NEXAFS studies on CT-complexes were reported in literature. All focused on TTF/TCNQ and neglected the possible change in the unoccupied density of states upon CT-complex formation.[357] [358] [359]
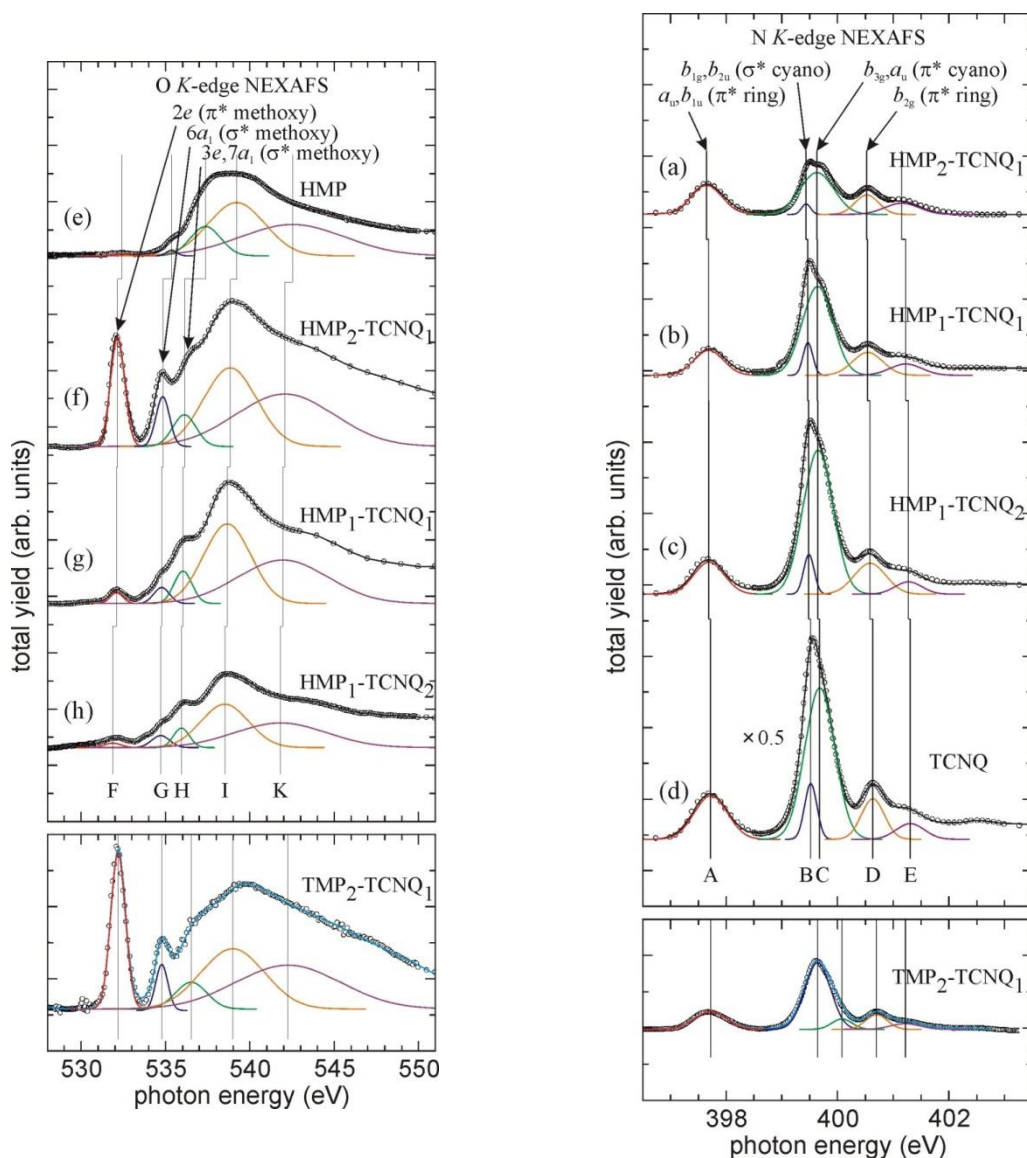
IV-24: NEXAFS study of CT-complexes with varying donor-acceptor composition. Left: Oxygen 1s edge. Right: Nitrogen 1s edge [figure adapted from MEDJANIK et al.[339]].

Firstly, the results for oxygen specific NEXAFS will be discussed, followed by the finds for nitrogen. As oxygen is only contained in **4-1/4-2**, it can act as a fingerprint for donors. Nitrogen is used as fingerprint for the acceptor. The resulting spectra are reproduced in figure IV-24. The **4-2** content decreases from spectrum *e* (pure donor) to *h*. Signals *F* to *K* were identified in the NEXAFS spectra. The assignment is analogous to methanol chemisorbed on Cu.[360] Signal *F* is located at 532.2 eV, in good agreement with the position of the lowest-lying peak in methanol (531.7 eV). *F* derives from the HOMO 2e of the methoxy anion. This HOMO is doubly degenerate and largely oxygen 2p-like (lone pair) with some hybridization with the antibonding π*-orbital of the C-O group. Transition *F* is denoted as ***O1s→2e [π*(C-O)]***. This transition is only observed for CT-complexes. In spectrum *e* (pure **4-2**) the 2e derived orbitals are filled, a transition is only very weak. Signal *G* also reaches its maximum intensity in spectrum *f* and is not observed for pure **4-1**.

G is assigned to the ***O1s→6a₁ [σ*(C-O)]*** transition. Signals *H*, *I* and *K* are corresponding to transitions into σ*- and π*-orbitals of the pyrene scaffold.

The NEXAFS spectrum of TCNQ was investigated by FRAXEDAS *et al.*[357] It follows for figure IV-24 (right) that transitions *A* and *D* are essentially delocalized on the benzene ring. Transitions *B* and *C* originate from the σ*- and π*-orbitals of the cyano-group. The weak feature *E* is due to delocalized σ-type orbitals containing σ*(C-C), σ*(C-H) and σ*(C≡N) contributions.

When the donor content is increased, i.e. the CT-complexes are studied (sequence spectra *d*, *c*, *b*, *a*), the intensity of signals *B* and *C* drop substantially. For 4-2₂/TCNQ₁ (spectrum a) signals *B* and *C* appear as a double peak with a separation of about 190 meV. This intensity drop is taken as an indication of charge being transferred into unoccupied orbitals of the acceptor molecule. Furthermore, the resonance position shifts towards lower energy as **4-2** content is increased (as visualized by vertical lines).

From this, signal *F* (oxygen NEXAFS) emerges as the ideal probe to study the intensity of charge-transfer. It is measurement for the cationic character of the methoxy subunit. The higher this signal is in intensity the more charge was transferred from the methoxy unit (and thus from the donor). A problem of this interpretation already emerges at a qualitative glance at the results in IV-24 (left). Signal *F* has the highest intensity for the **4-2₂**/TCNQ₁ mixture (spectrum *f*). At higher TCNQ content, the signal intensity decreases significantly. This behaviour was also quantified in the publication by MEDJANIK *et al.*[335] From this it would appear that the strongest charge-transfer was actually taking place when less acceptor is present in the cocrystal. Unfortunately, the solid state structure of the **4-2₂**/TCNQ₁ or **4-2₁**/TCNQ₂ cocrystals could not be resolved. Thus, the donor-acceptor arrangement is not clear. From the NEXAFS results a dramatic structural change from **4-2₂**/TCNQ₁ to **4-2₁**/TCNQ₁ can be expected. It was speculated that the higher donor content in the crystal might reduce the D-A distance by chemical pressure, thus facilitating a stronger charge-transfer. An intense ***O1s→2e [π*(C-O)]*** transition was also observed in **4-1₂**/TCNQ₁.
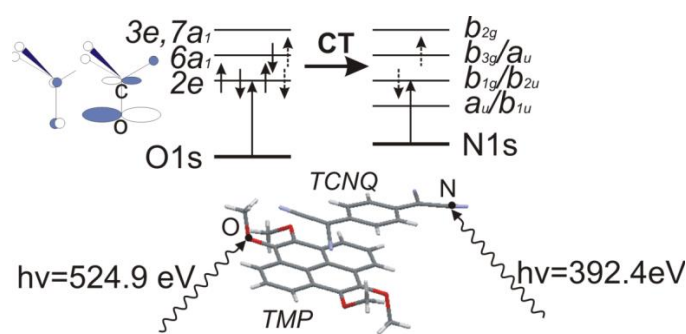
IV-25: *Charge-transfer transition scheme for **4-1** / **4-2** and TCNQ cocrystals. NEXAFS spectra reveal 2e and 6a₁ of the methoxy-group as donating and b₁g and b₂u of the cyano-group of TCNQ as the accepting orbitals [figure adapted from MEDJANIK et al.*[335]*].*

Figure IV-25 summarizes the results in terms of a charge-transfer transitions scheme. Surprisingly, the states $6a_1$ as well as b_{3g} and a_u contribute to the CT-process although they are expected to be completely empty. This might be caused by the fact that NEXAFS does not probe the pure ground state properties. During the excitation all states are shifted to lower energies as a result of the core-hole attraction and therefore appear partially occupied.

IV.3.3.5   Hard X-ray photoelectron spectroscopy (HAXPES)
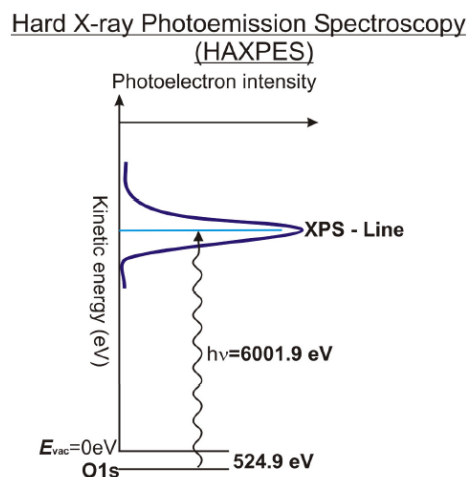
*IV-26: Schematic transition diagram for **O 1s** HAXPES experiments [figure adapted from MEDJANIK [356]]*.

Unlike UPS, X-ray photoelectron spectroscopy (XPES) techniques are element specific as they probe one element and its electronic environment.[361] UPS and STS are only surface sensitive methods (as discussed in IV.3.3.2.1) whereas HAXPES can give bulk information (figure IV-18). In the conducted experiments the information depth was 15 nm. Recent advances in HAXPES have been reviewed by KOBAYASHI.[362]

This study was one of the first to be conducted on the, at that time, new PETRA III instrument at *Deutsches Elektronen-Synchrotron* (DESY) in Hamburg. In combination with the appropriate experimental set up it allows retaining the chemical specificity of XPS in a HAXPES experiment.[363] The following results are described in full detail in the publication by MEDJANIK *et al*. mentioned in the introduction to this chapter.*[335]* For the sake of brevity, only results for **4-1**$_X$/TCNQ$_Y$ cocrystals will be discussed here. Rather surprisingly, **4-2**$_X$/TCNQ$_Y$ cocrystals gave very similar results.

As in NEXAFS the element specificity of HAXPES allows a direct "look" at the donor (oxygen containing) and the acceptor (nitrogen containing) prior to and after complexation.
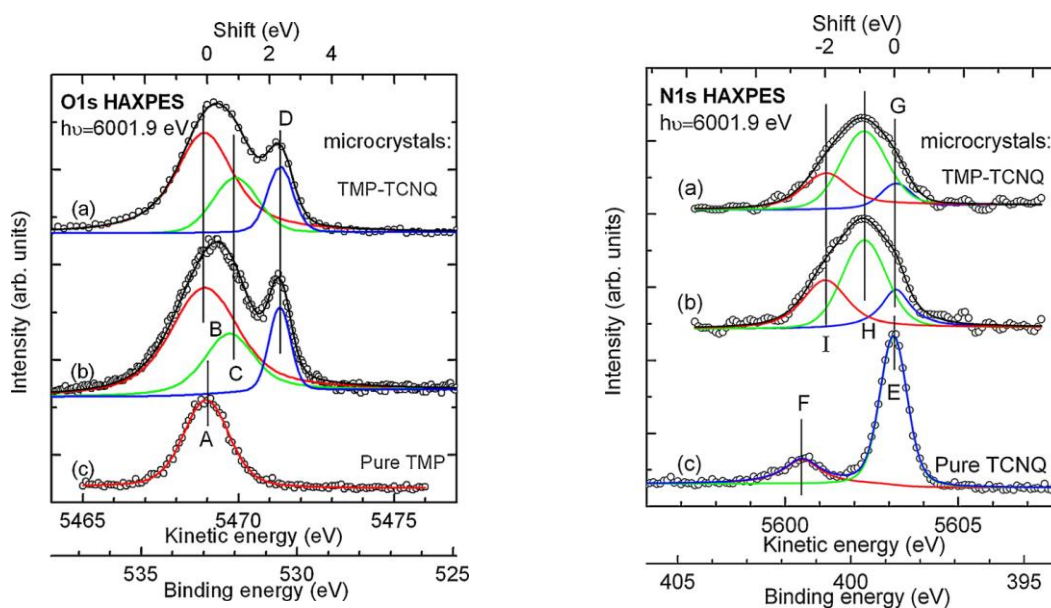
IV-27: Left: O 1s HAXPES spectra of 4-1$_X$/TCNQ$_Y$ cocrystals. a: 4-1$_1$/TCNQ$_2$, b: 4-1$_2$/TCNQ$_1$, c: pure 4-1 as reference. Right: N 1s HAXPES spectra of 4-1$_X$/TCNQ$_Y$ cocrystals. a: 4-1$_1$/TCNQ$_2$, b: 4-1$_2$/TCNQ$_1$, c: pure TCNQ as reference [figure adapted from MEDJANIK et al. [335]].

For the donor (O 1s HAXPES, E_{bind} = 525 - 540 eV) four signals were identified by curve fitting (*A, B, C* and *D*). Signal *A* is the free donor reference. Signal *B* is interpreted as residues of not complexed 4-1 in the crystalline sample. This indicates that the mechanical isolation of CT-complexes from 4-1 was not complete.[22] Thus, the CT-complex is characterized by signal *C* (shifted by 0.9 eV to lower E_{bind}) and signal *D* (shifted by 2.3 eV to lower E_{bind}) compared to pure 4-1 (signal *A*). In case of the acceptor TCNQ the N 1s HAXPES spectrum (E_{bind} = 395 - 405 eV) (spectrum *c*) is in good agreement with literature reported results. For the 4-1$_X$/TCNQ$_Y$ complexes three signals (*G, H* and *I*) are identified. *G* is assigned to pure TCNQ. The CT-complex is again characterized by two signals (*H* and *I*). In contrast to the donor, *H* and *I* are shifted towards higher binding energies E_{bind}. Signals *C, D* (donor) and *H, I* are separated by $\Delta E \approx 1.1$ eV.

For the assignment of *C, D, H* and *I* the effect of the number of valance electrons on the COULOMB attraction of the atom nucleus (*core-level screening*) has to be considered. Valance electrons counteract the COULOMB attraction of the nucleus. Thus, an increased number of valance electrons reduces the binding energy E_{bind} of the 1S electrons to the atom. In the N 1S HAXPES spectra, the cyano-group of TCNQ is scrutinized. In the case of the charged TCNQ$^-$ the additional electron will increase the core-level screening and is thus associated with the low E_{bind} signal *I* in figure IV-27 (right). From this follows that signal *H* stems from complexed yet not charged TCNQ^0. For 4-1 the argument is inversed. By abstracting an electron in the case of 4-1$^+$ the core-level screening is reduced and the species is identified at high binding energies (i.e. signal *D*). Signal *C* stems from

---

[22] Surprisingly, signal *B* was also observed in vapor deposited films of 4-1/TCNQ CT-complexes (not shown). This can be explained by 4-1 island growth on the substrate due to stronger substrate interactions compared to TCNQ.

complexed, yet neutral $4\text{-}1^0$ moieties. The $\Delta E_{TCNQ(-) - TCNQ0} \approx 1.1$ eV is in good agreement with the literature value for TCNQ/TMTSF CT-complexes.[364] For TCNQ/TTF a slightly larger splitting of 1.5 eV is reported.[365]

In preliminary IR absorption experiments a partial charge-transfer was established and is reconfirmed by these HAXPES results.[336] As in the works of GROBMAN *et al.* these results suggest that a partial charge-transfer should be interpreted similarly to a mixed valence state but here some moieties are in the ionic state and some are neutral.[366] The ratio of the signal intensities suggests 65 % in the neutral and 35 % in the ionic state. Within the error margin of the experiments neither the sample's stoichiometric composition (2:1 vs. 1:2) nor the nature of the donor (**4-1** vs **4-2**) had an effect on the degree of charge-transfer. This is in contrast to the solution UV-vis and powder IR absorption studies. In both the nature of the donor has a clear impact on the degree of charge-transfer ($Z_{4\text{-}1/TCNQ} = 0.17$ compared to $Z_{4\text{-}2/TCNQ} = 0.22$, table IV-3).

IV.3.4 Electrical conductivity measurements on 4-1/TCNQ and 4-1/F$_4$-TCNQ cocrystals

As stated in the introduction N/I transitions are only observed in segregated stack CT-crystals. In the SFB/TR 49 context the rare temperature induced neutral/ionic transitions (TINIT) are especially sought after. The HUTH group performed temperature dependent conductivity measurements on **4-1**/TCNQ and **4-1**/F$_4$-TCNQ.[340] This measurement is commonly used to establish TINIT behavior.[167]

4-1/TCNQ was studied as thin-films as well as a single crystal. In both cases the material behaves as an insulator with negligible temperature dependence of the resistivity. For thin-films a resistivity of $\rho = 1.76*10^8$ Ωcm ($\sigma = 5.68*10^{-10}$ S/cm) was found. For a contacted single crystal the resistivity was even higher ($\rho = 1.49*10^{11}$ Ωcm). This behavior is typically detected for organic insulating materials.[131]
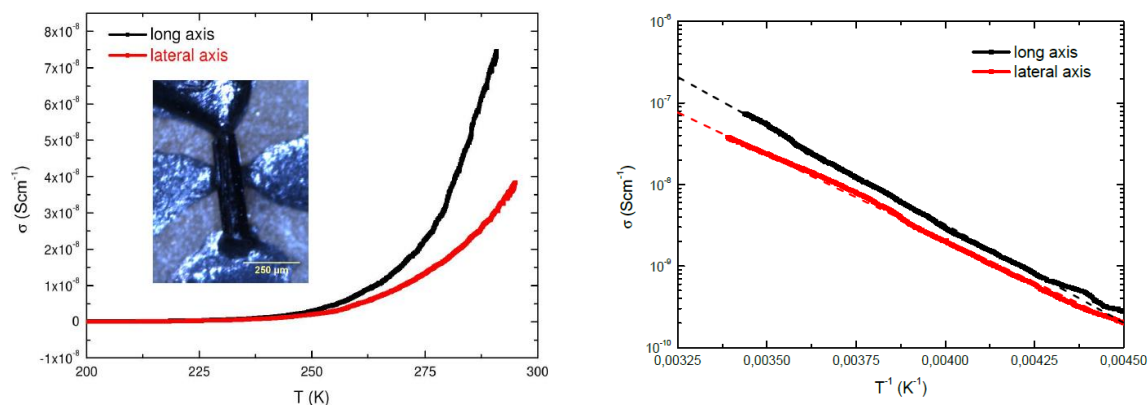
IV-28: Left: Anisotropic temperature dependent conductivity of a **4-1**/F$_4$-TCNQ cocrystal in the range 200 - 300 K. Inset: Micrograph of contacted cocrystal. Right: ARRHENIUS plot of σ(T) measurements (figure courtesy of HUTH).

In stark contrast to this, a contacted **4-1**/F$_4$-TCNQ cocrystal has much higher conductivity. The conductivity displays a semiconductor like temperature dependency, i.e. it increases with rising temperature.[367] For **4-1**/F$_4$-TCNQ this behavior is visible at temperatures of T = 220 K and above. At lower temperatures resistivity grew too large for reliable measurements. In contrast to ordinary semiconductors the conductivity is highly anisotropic.[368] When measured along the crystal's long axis (corresponding with the crystallographic a-axis) the conductivity reaches up to $\sigma_{\parallel,T=290\,K} = 7.5*10^{-8}$ S/cm while the measurement along the lateral axis (i.e. perpendicular to the crystallographic a-axis) only reached up to $\sigma_{\perp,T=290\,K} = 3.5*10^{-8}$ S/cm. An ARRHENIUS plot of the results clearly shows that both transport mechanisms are thermally activated but have different activation energies. Based on this plot, the collaborators determined the activation energy for the transport parallel to the a-axis to $E_{a,\parallel} = 0.98$ eV and perpendicular $E_{a,\perp} = 0.84$ eV. TINIT materials usually have activation energies $E_a \leq 0.15$ eV.[369]

Despite considerable effort it was not possible to induce an N/I-transition by a thermal stimulus in any studied CT-complex. Whereas a dramatic change in conductivity is reported for the transition point, no such feature is observed for the tested materials. Nevertheless, it is very interesting to see how the variation of the acceptor moiety in CT-complexes can fundamentally change the behavior of the assembly. The transition in crystal structure from a tilted (figure IV-7) to a coplanar arrangement (figure IV-9) leads to a change from insulator to semimetal with anisotropic conductivity. Additional calculations predict that the degree of charge-transfer Z is dependent on pressure along the a-axis for **4-1**/TCNQ. This is not predicted for **4-1**/F$_4$-TCNQ.

IV.4   Summary

A series of new charge-transfer complexes was prepared and characterized. For this, novel pyrene based donors reported in chapters *II* and *III* were combined with strong acceptors. In the series of UV-vis absorption spectra, the strongest acceptor (F4-TCNQ, **4-7**) gave by far the strongest response, i.e. the most intense and pronounced bathochromically shifted CT-band. While the latter is to be expected, due to the smallest $HOMO_{donor}/LUMO_{acceptor}$ gap in this series, the former was not anticipated. The strong CT-interaction that arises when **4-7** is used probably gives rise to a strongly bound state and as a consequence an intense transition.[252] The increase of the donor strength along a series (e.g. **4-1** -> **4-3**) sees the change from a neutral CT-state to an ionic system. The degree of charge-transfer, as established by IR spectroscopy, shows that **4-3** ($Z = 1$) is much more prone to charge-transfer as is the case for **4-2** ($Z = 0.22$). In the search for a CT-complex that will give a neutral-ionic transition upon external influences this means that **4-3** can be combined with much weaker acceptors to reach the $Z = 0.45 - 0.5$ regime. The solid state structure of a series of CT-complexes with **4-2** as donor was elucidated by single crystal X-ray diffraction crystallography. In all cases a mixed stack arrangement was found. The molecular arrangement varies significantly (twist angles, bend angles, $\pi-\pi$ distances etc.). The crystallization of an analogous series using **4-3** as donor did not provide single crystals suitable for X-ray diffraction, but only thin, intensely colored fibers.

In the context of SFB/TR 49 the possibility of a neutral-ionic transition for the **4-1/4-7** CT-complex was studied in cooperation with the HUHT group. For this system an N/I-transition was not observed in conductivity measurements. Other sulfur containing complexes are currently under investigation.

In the collaboration with the SCHÖNHENSE group the work-function shift by applying a thin layer of **4-1** and **4-2** (as well as TCNQ CT-complexes thereof) on a gold surface was studied by ultraviolet photoelectron spectroscopy (UPS). Using this as a starting point, NEXAFS study on a charge-transfer complex was conducted. This study was able to provide insight into the CT-process on an atomistic level. It pinpoints the transferred electron to stem from the oxygen *2e* and *$6a_1$* symmetric orbitals and to be directed to the nitrogen b_{1g} and b_{2u} symmetric orbitals. Single crystals required for this were provided by the author.

Hard X-ray photoelectron spectroscopy (HAXPES) was used to investigate the effect of a 2:1 stoichiometry on the **4-1**/TCNQ system. While solution UV-vis and IR spectroscopy show only little consequence, a significant change in ionicity was identified in the HAXPES experiment.

V.   Emitters for thermally delayed fluorescence in OLEDs

V.1   Introduction

With its International Research Training Groups (IRTG) the German Research Council (*Deutsche Forschungsgemeinschaft*, DFG) provides a framework for the international exchange of young scientists. The University of Mainz joined with Seoul National University and Hannam University (South Korea) to form IRTG 1404 "Self-organized Materials for Optoelectronics". Researchers may obtain a scholarship to carry out part of their work in the partner country and to subsequently obtain a joint degree from two participating universities. Within this framework a collaboration with Professor JANG JOO KIM on thermally delayed fluorescence (TADF) in organic light emitting devices (OLEDs) was initiated. This work encompassed the design of new emitters, their synthesis, the characterization in solution and in solid state and finally the fabrication of a working OLED device. The mechanism of TADF in OLEDs is discussed in detail in chapter *I.3.4*.

V.2   Molecular design

TADF emitters for blue OLEDs have the following prerequisites in common: [182]

- The molecule has a blue fluorescence in the solid state;
- Materials should have good fluorescence quantum yield;
- The singlet -> triplet energy gap should be small ($\Delta E_{S1\text{->}T1} < 0.5$ eV).

While the first two points may apply to all OLED chromophores, prerequisite three is necessary for efficient TADF.

Based on these guidelines two emitter molecule designs were developed: The oxadiazole based *OD series* and the pyrene based *Py series*.

V.2.1   Oxadiazole based emitters - The *OD series*

For the first series of molecules a linear *donor–π-spacer–acceptor* strategy was employed (illustrated in figure V-1).


D - donor
A - acceptor
X - spacer
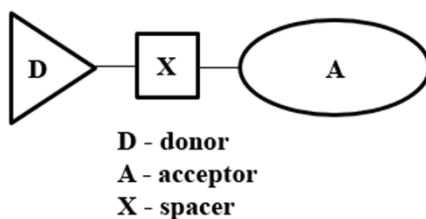
V-1: OD series design. The donor (D) is tied to the acceptor (A) by the π-spacer unit (X).

Fulfilling the first prerequisite, i.e. blue fluorescence, restricted the choice of donor and acceptor units to some degree. In collaboration with the IVANOVA group an extensive theoretical study was carried out to screen for promising donor and acceptor combinations. The results of this study are presented in abridged form. A comprehensive discussion can be found in the publication by VALCHANOV *et al*.[370] Donors and acceptors for this study were selected according to the following criteria:

(i)   All main structural fragments are stable π-conjugated chemical species;

(ii)   The donors have high-lying HOMOs and the acceptors low-lying LUMOs;

(iii)   The electron-donating / -withdrawing capacity of donors / acceptors is varied smoothly by extension of the π-conjugated system and / or by addition of functional groups to the main structural unit.

It became apparent that in order to achieve sufficient orbital partitioning an extension of the spacer-unit "X" from m-phenylene to m-biphenylene was necessary.

Oxadiazole (**5-7**) emerged as the most promising candidate from the series of studied acceptors. Keeping the acceptor moiety constant the donor residue was varied. Due to efficient orbital partitioning, the variation of the donor was found to have little effect on the LUMO energy.
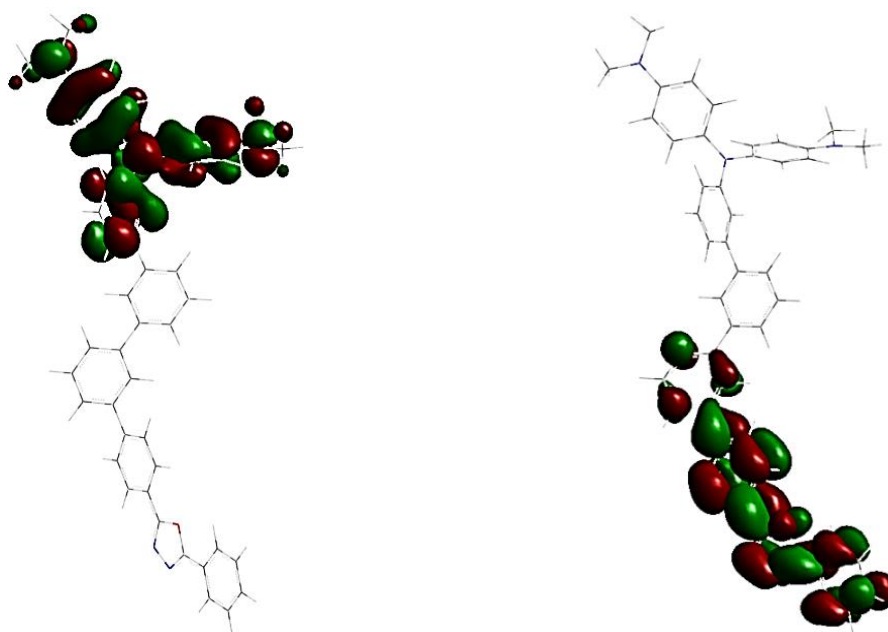
Donors

Acceptors
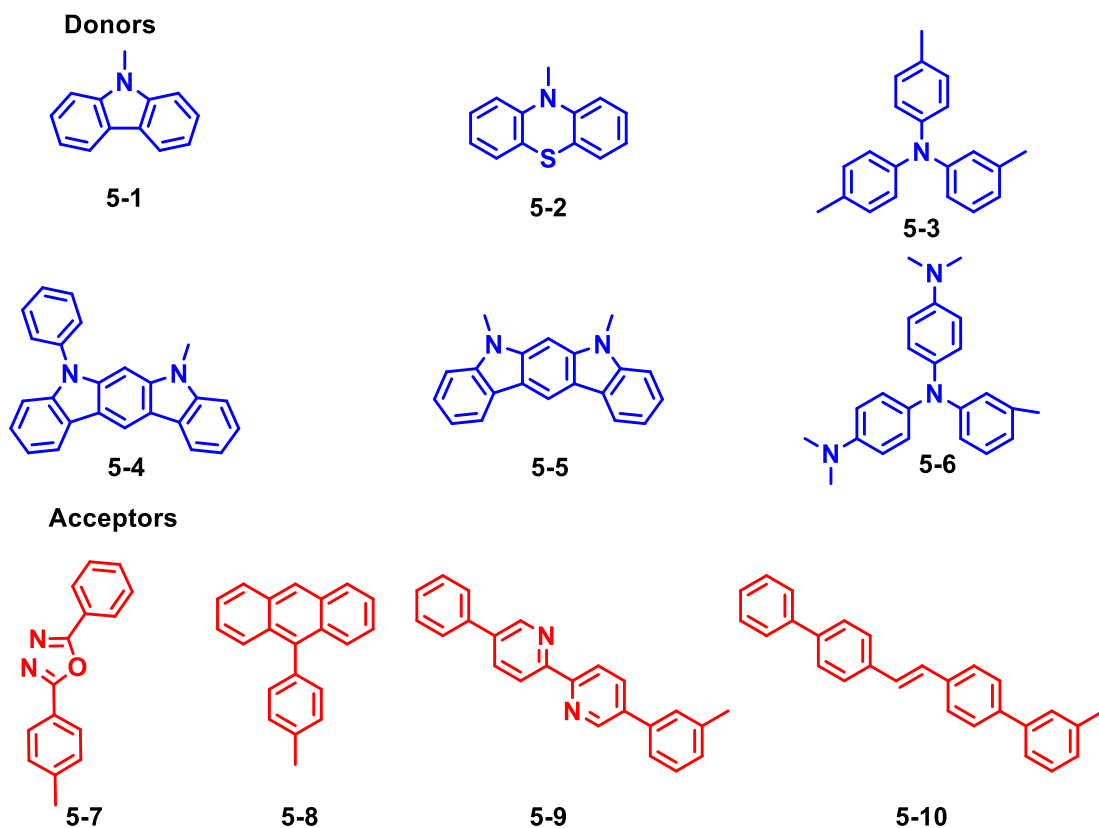
V-2: Building blocks used in the molecular modelling driven emitter design study.

The following structures were deemed most promising according to the calculation results. Henceforth, they will be collectively designated as *OD series* (figure V-3):
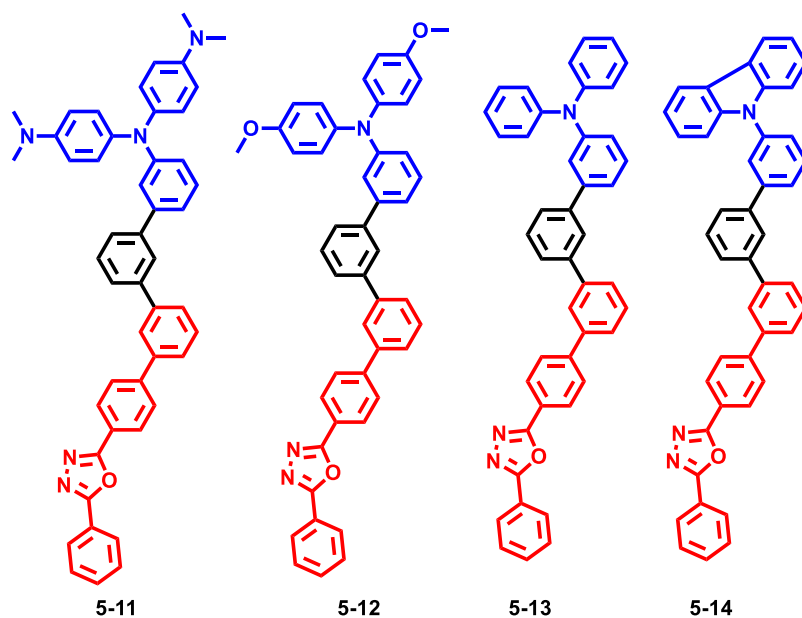
V-3: The OD series materials. A homologus series was prepared by variation of the donor moiety.

The calculated distribution of frontier orbitals in **5-11** is shown in figure V-4:

*V-4: Calculated frontier orbitals of **5-11**. The HOMO (left) is localized exclusively on the amine-donor. The LUMO (right) is located on the oxadiazole-acceptor moiety. Overlap of HOMO and LUMO is not observed (calculations courtesy of VALCHANOV et al.[370]).*

The orbital partitioning in **5-11** is significant. The HOMO is located on the amine-donor while the LUMO is found on the oxadiazole acceptor moiety. Due to the weak conjugation along the *m*-biphenylene bridge the respective frontier orbital is efficiently localized. For the central phenyl unit no electron density in the FMOs is predicted.

The following singlet – triplet energy gaps ($\Delta E_{S1 \to T1,calc}$) have been computed:

	5-11	**5-12**	**5-13**	**5-14**
$\Delta E_{S1 \to T1,calc}$ (eV)[a]	0.1	0.26	0.28	0.60
[a] calculations courtesy of VALCHANOV et al.[370]				

This series illustrates the effect of the donor variation on $\Delta E_{S1 \to T1,calc}$. A stronger donor apparently reduced the energy gap. Carbazole (**5-14**) significantly widens the gap compared to diphenylamine (**5-13**). **5-11** is the most promising candidate according to this computational study.

V.2.2   Pyrene based emitters – The *Py series*
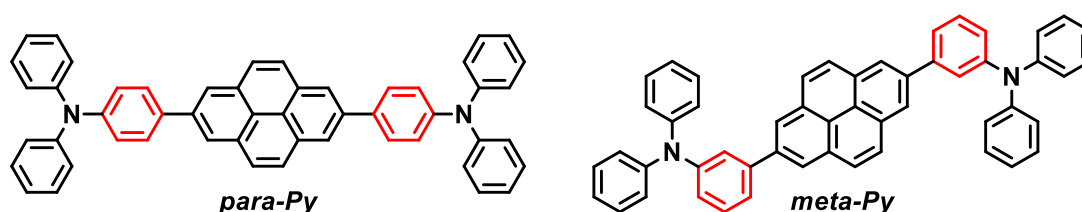
V-5: Py series designs for DFT study.

At the outset of the study, information on TADF emitter design was scarce. Thus, a second loosely related series of blue emitters was developed. Drawing on the design principles developed for the *OD series* the author of this manuscript chose pyrene as central building block. It is an efficient fluorescent emitter and has successfully been employed in OLED devices with a deep blue emission color.[28] As discussed in section *I.1* pyrene possesses a nodal plane in positions 2 and 7. Therefore, conjugation to substituents in these positions is weak. This is used as basis for extensive orbital partitioning. Parallel to the *OD series* diphenylamines were utilized as electron rich moiety. Compared to the *OD series* the donor-acceptor interactions are significantly reduced. Nevertheless, an efficient orbital partitioning is possible according to DFT calculations (*vide infra*) if in combination with the nodal plane, the appropriate phenylene spacer is selected.

HOMO

LUMO
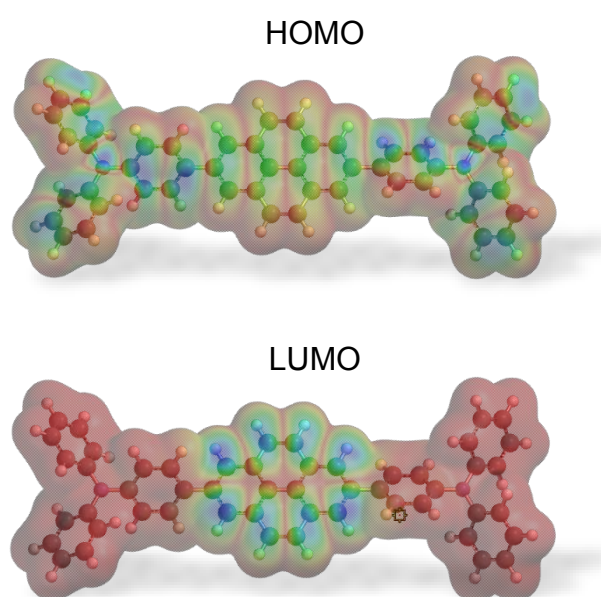
V-6: Fortier orbital densities of para-Py (cool colors indicate high orbital density).

As indicated, the connectivity of the phenylene linker plays a pivotal role in orbital partitioning as can be seen when figures V-6 and V-7 are compared. In the case of *para-Py* (figure V-6), the degenerated HOMO is mostly located on the triphenyl amine moiety. However, there is also a significant participation of the pyrene scaffold predicted (green and yellow color in the density plot).

HOMO-1   HOMO

LUMO
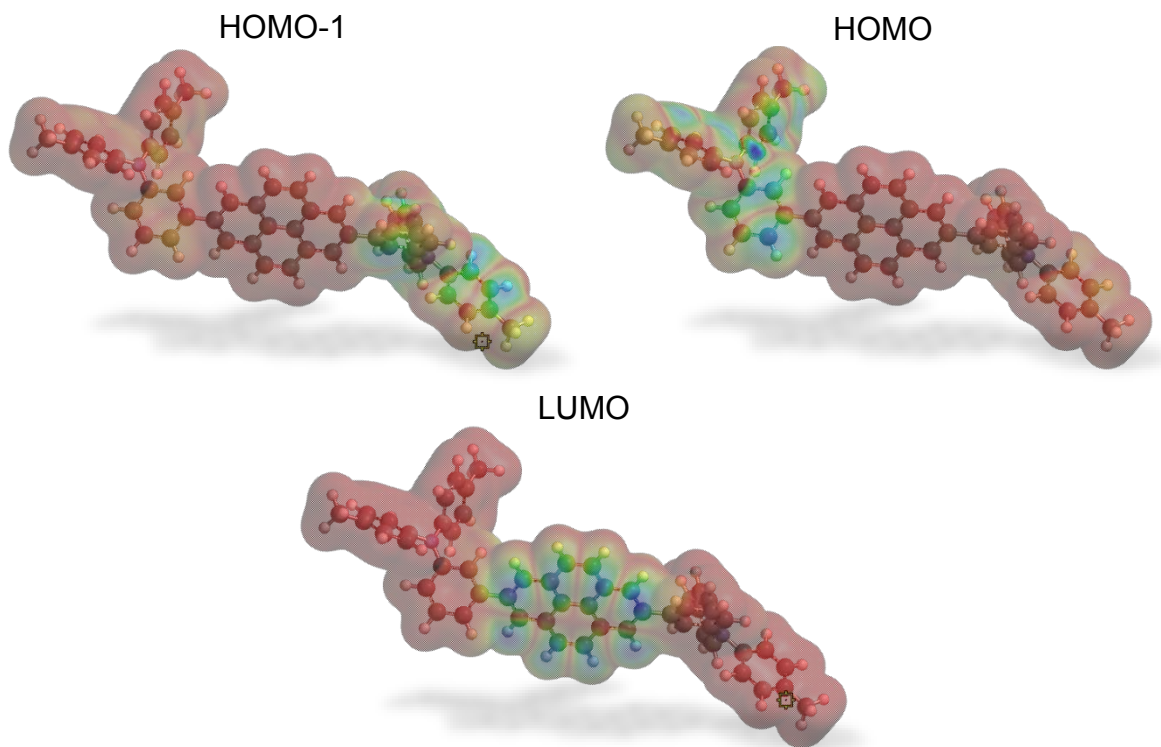
V-7: Frontier orbital densities of meta-Py materials (cool colors indicate high density).

In contrast, for *meta-Py* no participation of the pyrene-core in the HOMOs is observed. By employing a meta-linker design the frontier orbitals will be spatially separated and the triplet state destabilized. Furthermore, *H-H* repulsion between pyrene and the substituent will impose a twisted structure on the molecule thus further enhancing the orbital partitioning. In analogy to the *OD series* the amine moieties were varied to build up the *Py series*.
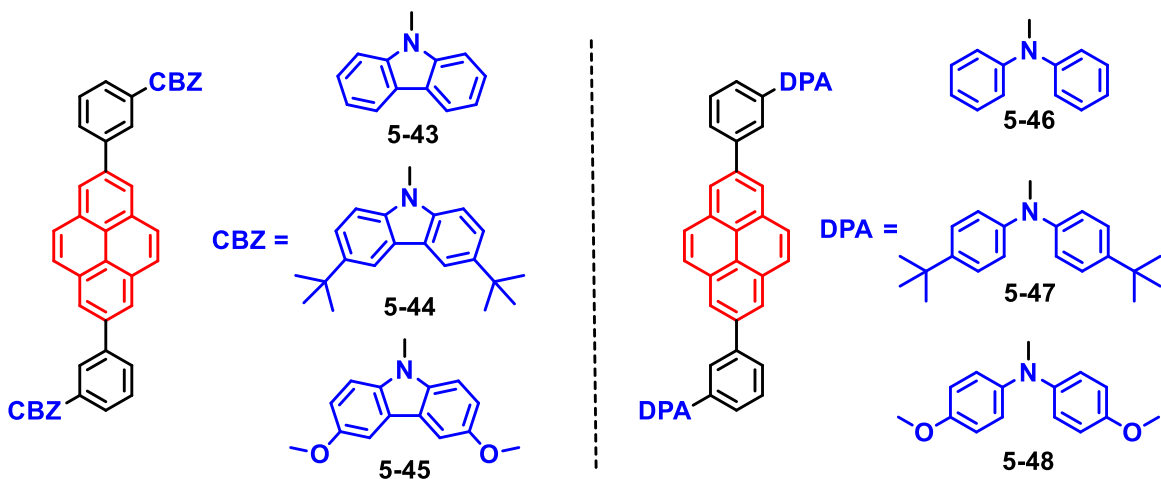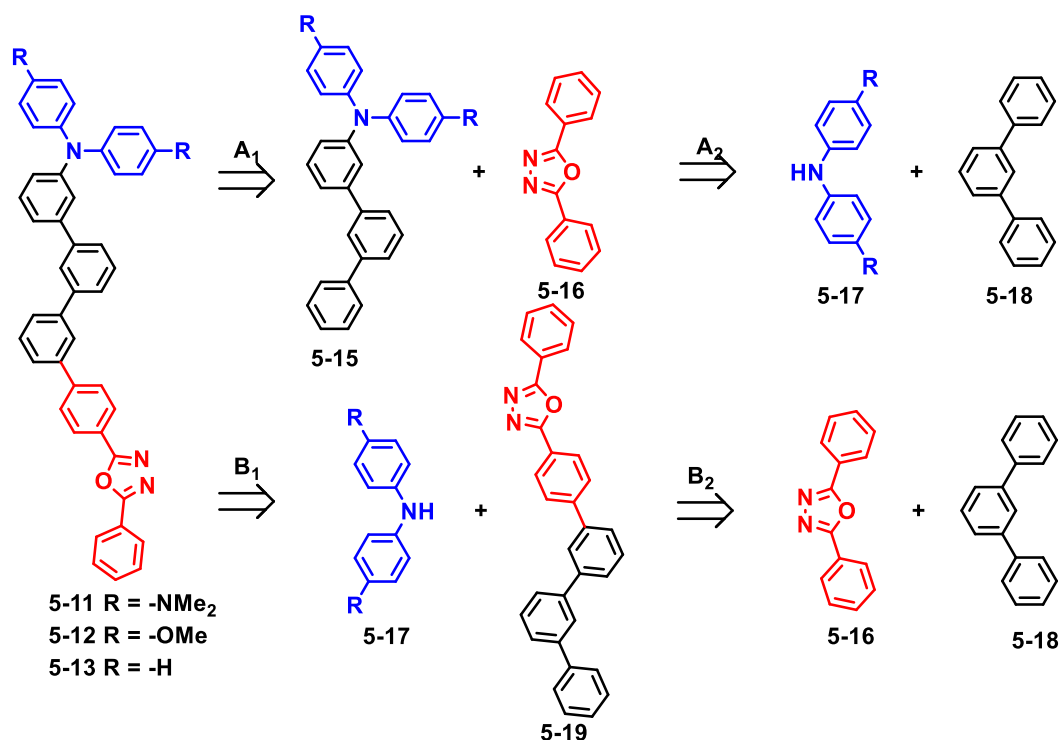

V-8: Py series materials.

In calculations an acceptor (-F, -CN) substitution of the pyrene core (4 position) resulted in the loss of wide bandgap behavior.[86] Therefore, no such derivatives were prepared.

V.3   Synthesis

V.3.1   The OD series

V-9: Retrosynthetic analysis of OD series materials.

A retrosynthetic deconstruction of the *OD series* was carried out to devise an efficient synthetic route.[371] The two represented disconnections *A* and *B* were deemed most useful. In *A* initially (*A₁*) diphenyloxadiazole (**5-16**) is split off followed by severing of the triphenyl amine bond yielding the symmetric diphenyl amine (**5-17**) and *m*-terphenyl (**5-18**). In *B* the diphenyl amine (**5-17**) is disconnected in the first step and in *B₂* the diphenyloxadiazole (**5-16**) is detached from the central terphenyl (**5-18**). Both disconnections provide simple, literature known building blocks.

Based on the disconnections the following synthetic route for the *OD series* materials was established (figure V-10):
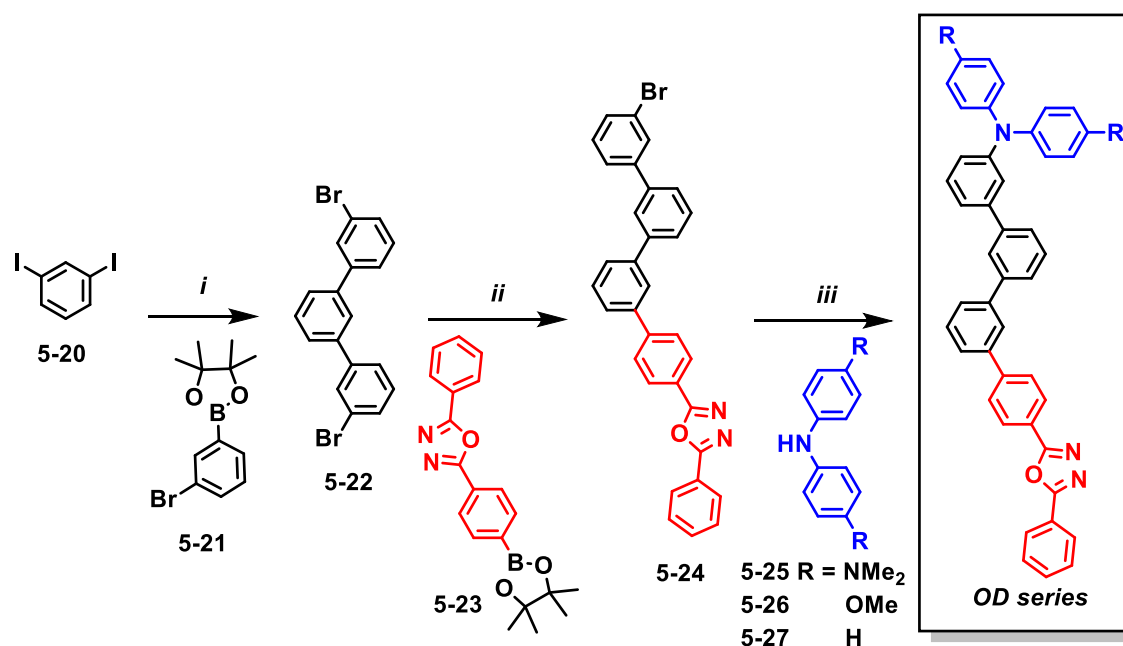
V-10: OD series synthetic scheme. i: Pd(PPh₃)₄, Na₂CO₃, Tol, 50 °C, 4 d, 50 %. ii: Pd(PPh₃)₄, Na₂CO₃, Tol, 100 °C, 16 h, 65 %. iii: QPhos, Pd(DBA)₂, NaOtBu, Tol, 100 °C, 16 h, 77 – 90 %.

In the first step a SUZUKI-MIYAURA cross coupling reaction of *m*-diiodobenzene (**5-20**) and 1-bromophenylboronic ester (**5-21**) provided the central bifunctional *m*-terphenyl unit (**5-22**).[372] Chemoselectivity was achieved by low reaction temperature (50°C) and repeated addition of small amounts of **5-21** as the reaction progressed. Long reaction times (4 days) were required for adequate conversion of **5-20**. The product was obtained in modest yields as the iodo-versus-bromo-selectivity this is type of palladium catalysed reactions is not very high. Increasing the reaction temperature resulted in a homo-oligomerization of the boronic ester component.

For the second step the bisphenyloxadiazole-boronic ester (**5-23**) had to be prepared by MIYAURA-borylation from the commercially available bromo-precursor.[231] Ester **5-23** reacted with the *m*-terphenyl **5-22** in another SUZUKI-MIYAURA step. The reaction yielded the product in 65 %. Debromination was the main side reaction. The coupling product **5-24** was the common precursor for the final synthesis step.
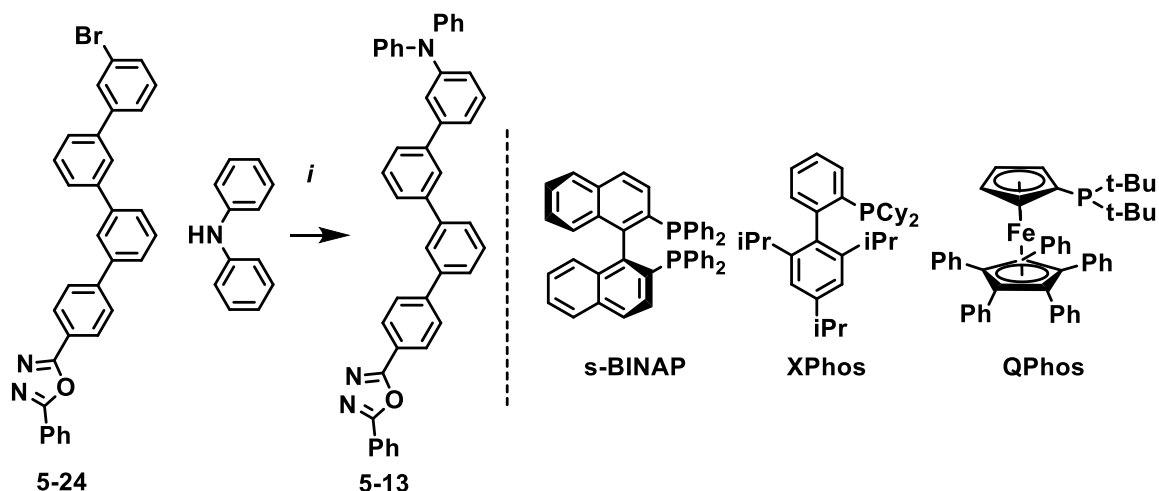
V-11: Ligand screening OD series. I: Ligand, Pd(DBA)₂, KOtBu, Tol, 100 °C, 16 h.

The desired target compounds were prepared either by BUCHWALD-HARTWIG-(**5-11** - **5-13**) or ULLMANN-type amination (**5-14**). All diphenylamine derivatives were prepared using the QPhos ligand system.[373] It emerged from a short ligand screening to provide superior results over XPhos or BINAP (table V-1).

Table V-1: Outcome ligand screening.

	Qphos[a]	XPhos[b]	Binap[c]
Yield (%)	> 90	76	30

[a] 1,2,3,4,5-pentaphenyl-1′-(di-*tert*-butylphosphino)ferrocene, [b] 2-dicyclohexylphosphino-2′,4′,6′-triisopropylbiphenyl, [c] (1,1′-binaphthalene-2,2′-diyl)bis(diphenylphosphine)

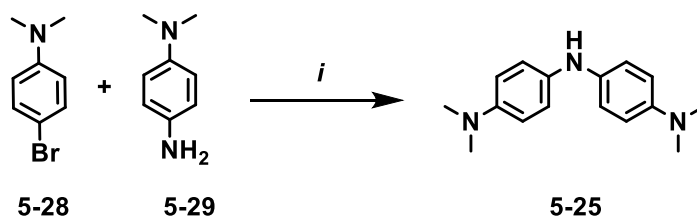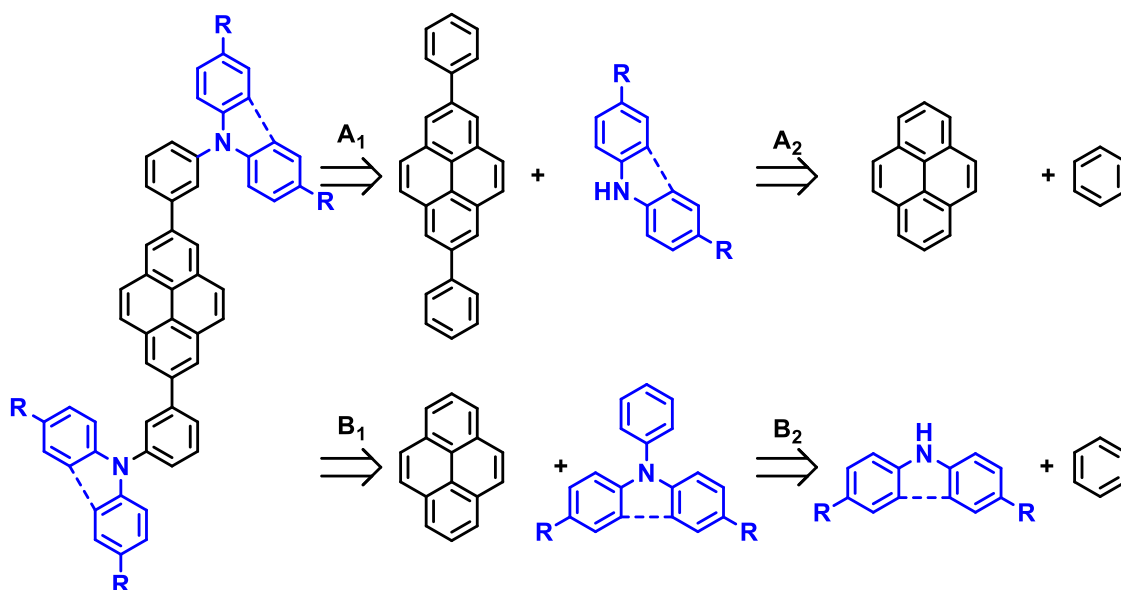Bis(*p*-dimethylaminophenyl)amine **5-25** was prepared using the same catalyst system.

*Figure V-12: Synthesis **5-25**. Qphos, Pd(DBA)₂, NaOtBu, Tol, 100 °C, 16 h.*

Surprisingly, the QPhos system failed in the conversion of carbazole. **5-14** was prepared by traditional ULLMANN-type reaction using copper iodide in DMF at 160°C.[374]

V.3.2   The Py series

DPA   **CBZ**
5-43 R = -H   **5-46 R = -H**
5-44 R = -tBu **5-47 R = -tBu**
5-45 R = -OMe **5-48 R = -OMe**

V-13: Retrosynthetic analysis of Py series.

The retrosynthetic analysis of the *Py series* design offers two disconnection approaches (*A* and *B*). In the first disconnection (*A₁*) a 2,7-bisphenylpyrene and the diphenylamine synthon are identified. In the second step (*A₂*) a 2,7-functionalized pyrene and phenyl are established. The second disconnection approach generates the 2,7-functionalized pyrene synthon in *B₁* and in a second step the diphenylamine synthon (*B₂*).

For the synthesis of *Py series* materials the second disconnection was chosen as biphenyl pyrenes have poor solubility which might hamper the synthetic effort. The 2,7-functionalized pyrene synthon is prepared in the form of **5-36** by regioselective C-H activation / borylation procedure reported by COVENTRY *et al.*[375] An alternative 2,7-dibromopyrene would have required a multi-step synthesis via tetrahydro pyrene.[55] The triphenylamines **5-33 – 5-35** were prepared by BUCHWALD-HARTWIG cross coupling whereas in the case of N-phenylcarbazole derivatives **5-40 – 5-42** ULLMANN-type reactions were used. The respective target compounds **5-43 – 5-48** were prepared by subsequent SUZUKI-MIYAURA reaction.
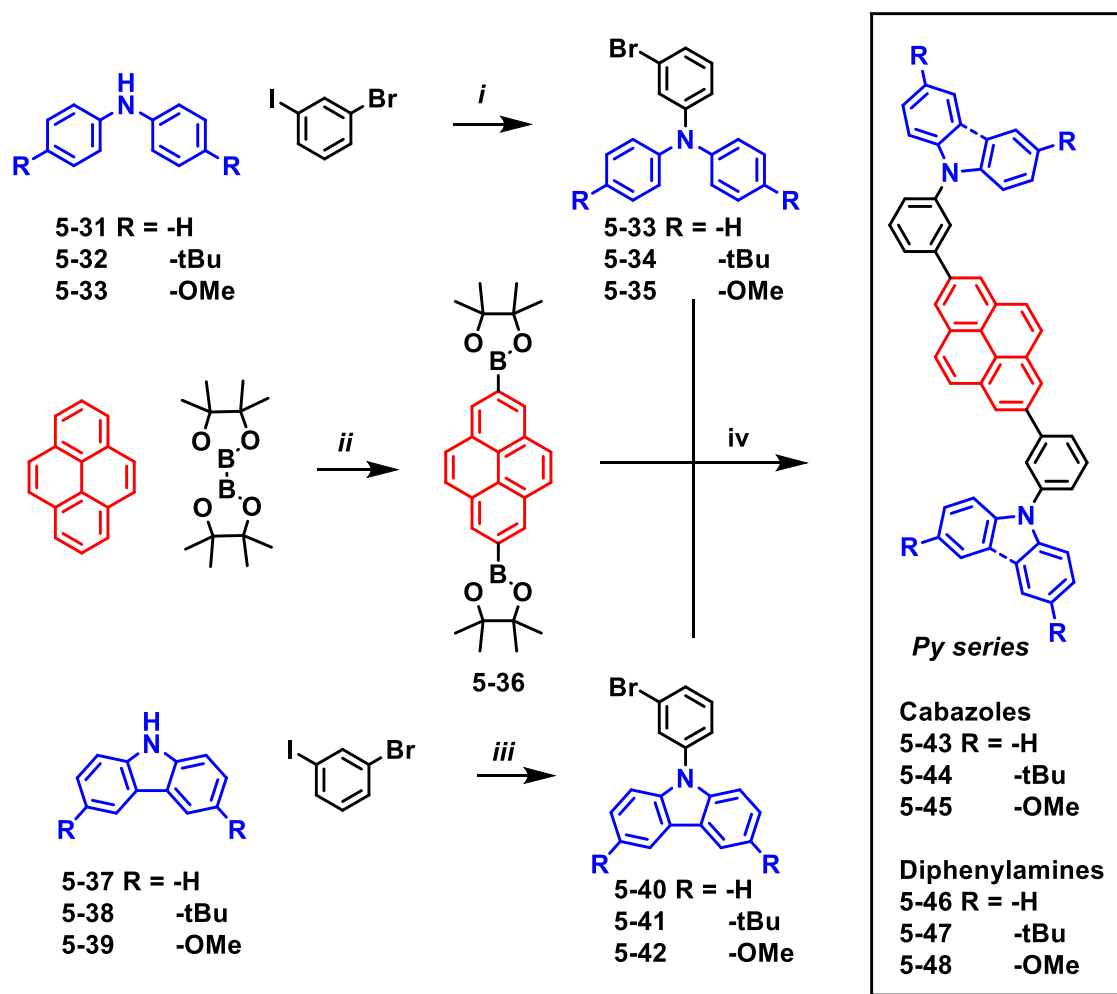
V-14: Synthetic scheme Py series. i: Qphos, Pd(DBA)₂, NaOtBu, Tol, 100 °C, 16 h 76 – 84 %. ii: [Ir(μ-OMe)(COD)]₂, tBuBipyr, Hex. 60 °C, 24 h 73 %. iii: CuI, K₂CO₃, DMF, 160 °C, 16 h. iv: Pd(PPh₃)₄, Na₂CO₃, Tol, 50 °C, 16 h, 50 %.

Molecules **5-43 – 5-48** were slightly soluble; purification by column chromatography was not applicable. Repeated recrystallization afforded the materials in high purity. The chromophores were prepared in > 500 mg scale. For vapor-deposition OLED-fabrication large amounts of the material were required.

V.4   Characterization

V.4.1   OD series

V.4.1.1   Structure determination

All materials were identified by FD-MS and elemental analysis.

The low symmetry of *OD series* molecules leads to complex ^{1}H-NMR spectra. As structural variation within the series is limited, the assignment will be discussed using the example of **5-13**.
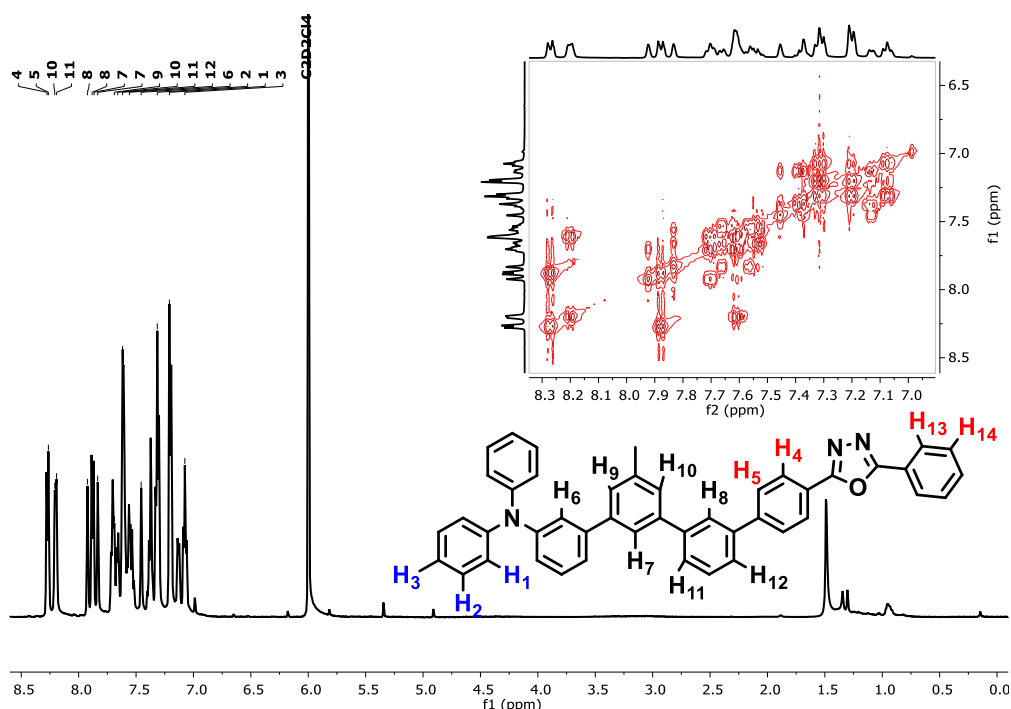
*V-15: ^{1}H- and H-H-COSY NMR spectra of **5-13** recorded in CD$_2$Cl$_2$ at 293 K.*

In collaboration with WAGNER the NMR signals were assigned to the positions in **5-13**. Signals *1*, *2* and *3* stem from the diphenylamine moiety. Signals *4*, *5* as well as *13* and *14* are assigned to the diphenyloxadiazole. The remaining signals (*6* through *12*) are generated by the *m*-triphenylene linker. For **5-11** and **5-12** additional methyl-group signals are identified at $\delta_{Me,\textbf{5-11}} = 2.4$ ppm and $\delta_{Me,\textbf{5-12}} = 3.2$ ppm respectively.

V.4.1.2   Optoelectronic properties

V.4.1.2.1   Cyclic voltammetry

To design efficient OLED devices it is essential to determine the frontier orbital energies of the chromophore in the emissive layer (EML). From this, hole- (HTL) and electron transport materials (ETL) can be chosen for efficient charge carrier transfer to the EML.[376]

In CV experiments only the oxidation signal was resolved under the employed conditions. As *OD series* materials can be considered donor-acceptor materials resolving the reduction signal might be expected as well.[87] When the calculated frontier orbital energies are taken into consideration (table V-2) it becomes clear that the oxadiazole LUMO is still very high in energy (i.e. its electron affinity is rather low). Thus, it is difficult to resolve the reduction signal. The low solubility of *OD series* materials in acetonitrile[23] prevented its use as a solvent.[286]
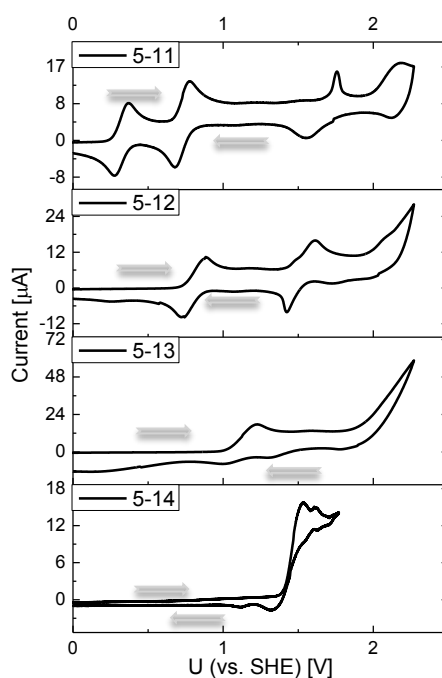
V-16: Cylic voltammograms of OD series recorded in dichloromethane at a scan rate of 100 mV/s using Bu₄NPF₆ as electrolyte. The voltammograms are referenced to the normal hydrogen electrode.[377]

For **5-11** three oxidation waves are observed. This can be interpreted as the stepwise oxidation of all three nitrogen centers. In contrast, **5-12** only shows two clear waves at higher potential. Methoxy-units are donating less electron density to the diphenylamine moiety rendering the oxidation harder. **5-13** only exhibits one clear oxidation wave for the first CV cycle (shown here). All three compounds behave similar to a series of substituted triphenylamines reported in literature.[378] The oxidation signal can be assigned to the triphenyl moieties in the materials. The N-phenylcarbazole derivative **5-14** gives a less clear oxidation wave suggesting reduced redox-activity.[379] Oxidation is observed at significantly higher potentials. From the onset of the oxidation wave the HOMO is derived by the following relation:

$$E_{HOMO} = -\left(U_{onset,Ox}\right) - U_{NHE} \rightarrow -\left(U_{onset,Ox}\right) - 4.6eV \qquad (V-1)$$

Eq. (V-1): U_{NHE} = -4.6 eV gives the standard electrode potential of the normal hydrogen electrode (NHE) on the zero vacuum level scale.[377]

---

[23] A solvent commonly used in CV for its superior electrochemical stability.

The computational results reliably predict the HOMO energy trend while the numerical values diverge from the experimental results. This disparity can be attributed to the fact that the DFT calculations are run in the gas-phase only, thus omitting intermolecular interactions. The results are collected in table V-2:

Table V-2: Frontier orbital energies of OD series materials.

	$U_{(onset)}$ (V)	$E_{HOMO,Ex}$ (eV)[a]	$E_{LUMO,Ex}$ (eV)[b]	$E_{HOMO,Calc.}$ (eV)[c]	$E_{LUMO,Calc.}$ (eV)[c]
5-11	0.2	-4.8	-1.7	-4.3	-1.7
5-12	0.7	-5.4	-1.8	-4.8	-1.7
5-13	1.0	-5.6	-2.0	-5.6	-1.7
5-14	1.4	-6.0	-2.4	-5.3	-1.7

[a] Determined using E_{NHE} = -4.6 eV. [b] derived in conjunction with the ΔE_{OPT} (Table V-3) [c]DFT.

V.4.1.2.2   UV-vis absorption and photoluminescence spectroscopy

In order to study the *OD series'* optical properties in the solid state, chromophores were spun-cast from dichloromethane solution on a fused silica waver. UV-vis absorption and PL spectra of the *OD series* in thin molecular films are collected in figure V-17.
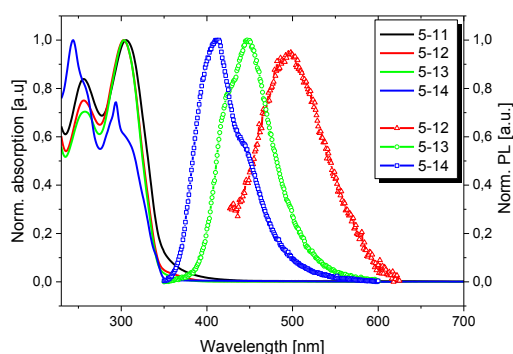
*V-17: Normalized film UV-vis absorption (solid line) and PL spectra (symbols) of the OD series materials. The PL intensity of **5-11** was too low to resolve its PL spectrum.*

The UV-vis spectra of the triphenylamine derivatives **5-11**, **5-12** and **5-13** show very similar absorption bands. The absorption maximum is observed at around $\lambda \approx 303$ nm and can be attributed to the triphenylamine moieties.[380] In **5-11** this band is slightly red shifted and shows a significant tail (down to $\lambda \approx 415$ nm) in contrast to **5-12** and **5-13**. The secondary band ($\lambda = 265$ nm) varies in intensity. **5-14** exhibits a different absorption behavior due to its carbazole moiety. Two sharp absorption peaks ($\lambda = 295$ nm $\lambda = 244$ nm) are observed and can be attributed to a phenylcarbazole moiety.[380] The optical bandgap is determined from the onset of the absorption spectrum. As expected, the band gap is reduced in donor substituted derivatives (table V-3).

The PL spectra of the *OD series* thin films are also included in figure V-17. A significant hypsochromic shift is observed in the series from **5-12** to **5-14**. The PL band of **5-12** is broad (FWHM = 90 nm) and featureless. Its maximum is found at $\lambda_{PLmax,\textbf{5-12}}$ = 498 nm (green emission color). The PL quantum yields were determined by integrating sphere method. It was found to be as low as Φ_{PL} = 5.3 %. For **5-13** the PL spectrum has its maximum at $\lambda_{PLmax,\textbf{5-13}}$ = 446 nm and a shoulder at 422 nm. The spectrum is sharper (FWHM = 70 nm) and has a higher quantum yield Φ_{PL} = 15.3 %. **5-14** has a deep-blue fluorescence in the thin film with $\lambda_{PLmax,\textbf{5-14}}$ = 410 nm with a weak shoulder at λ_{PL} = 442 nm. Within the *OD series* **5-14** has the sharpest emission peak (FWHM = 60 nm) as well as a superior fluorescence quantum yield of Φ_{PL} = 25.1 %. For **5-11** the PL intensity was insufficient to record a full PL spectrum.

Table V-3: Collected thin-film photophysical properties OD series.

	$\lambda_{Abs,max}$ (nm)	ΔE_{Opt} (eV)	$\lambda_{PL,max}$ (nm)	PL quantum yield (%)[a]	S -> T gap$_{calc.}$ (eV)[b]	S -> T gap$_{exp.}$ (eV)
5-11	306	2.91	≈ 570[c]	< 1	0.1	Not determined. [c]
5-12	302	3.24	498	5.3	0.26	Not determined. [c]
5-13	301	3.40	446	15.3	0.28	0.40
5-14	243	3.50	410	25.1	0.60	0.61

[a] determined by integrating sphere method. [b] calculations courtesy of VALCHANOV et al.[370]. [c] low PL intensity hampers determination.

The energy of the T_1 triplet level was determined by recording time resolved PL spectra at low temperatures. Long delay times make it possible to observe the weak organic phosphorescence signal generated by the slow T_1 -> S_0 transition. Low temperatures help in these experiments to suppress the non-radiative decay of the triplet state.[381] This method finds broad application in the study of organic triplet states.[382, 383]
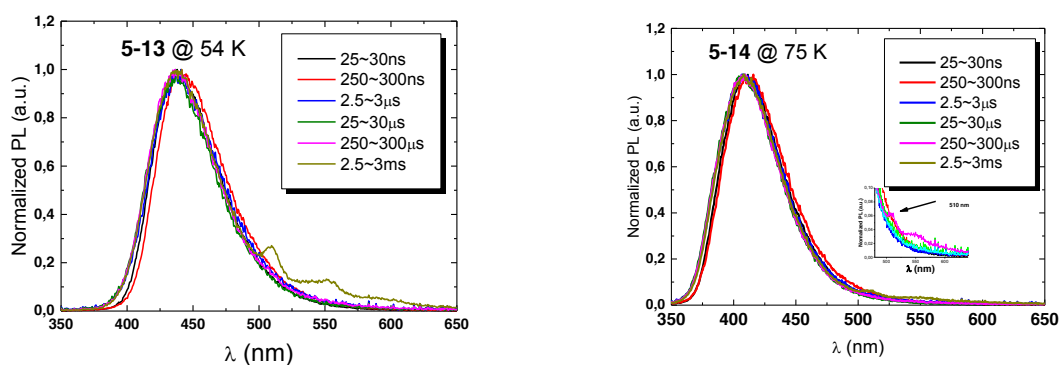

V-18: Time resolved low temperature PL spectra of **5-13** (left, at T = 54 K) and **5-14** (right, at T = 75 K). The inset (right) shows an expansion of the weak phosphorescence signal.

A series of time resolved PL spectra was recorded for **5-13** and **5-14** at 54 K and 75 K respectively. The delay time[24] was varied from 25 ns to 2.5 ms. Up to a delay time of 300 μs no significant change in the PL spectra is observed. Only at 2.5 ms delay new features arise at $\lambda = 510$ nm for **5-13** and at $\lambda = 506$ nm for **5-14**. These features are attributed to the respective $T_1 \rightarrow S_0$ transition. The energy difference between the phosphorescence and the fluorescence maximum gives the experimental $\Delta E_{S1\text{-}T1}$ energy gap collected in table V-3. For **5-11** and **5-12** the PL intensity was insufficient to observe delayed luminescence. As a consequence, the triplet energy could not be determined.

As mentioned in chapter *V.2.1* an extensive molecular modelling study accompanied the *OD series* design. The IVANOVA group calculated the $\Delta E_{S1\text{-}T1}$ gap by time dependent DFT calculations. For **5-14** the predicted value $\Delta E_{S1\text{-}T1,\text{calc.}} = 0.6$ eV and the experimental value $\Delta E_{S1\text{-}T1,\text{exp}} = 0.61$ eV are in good agreement. In the case of **5-13** the theoretical approach underestimated the gap by approximately 0.1 eV. Considering that TD-DFT methods often overestimate the triplet energy by 0.25 to 0.4 eV (depending on the used functional) the calculations are in excellent agreement with the experimental results.[384]

In order to gauge the film forming properties of the *OD series* materials, the prepared thin films were studied by optical microscopy. The dark field images are collected in figure V-19.
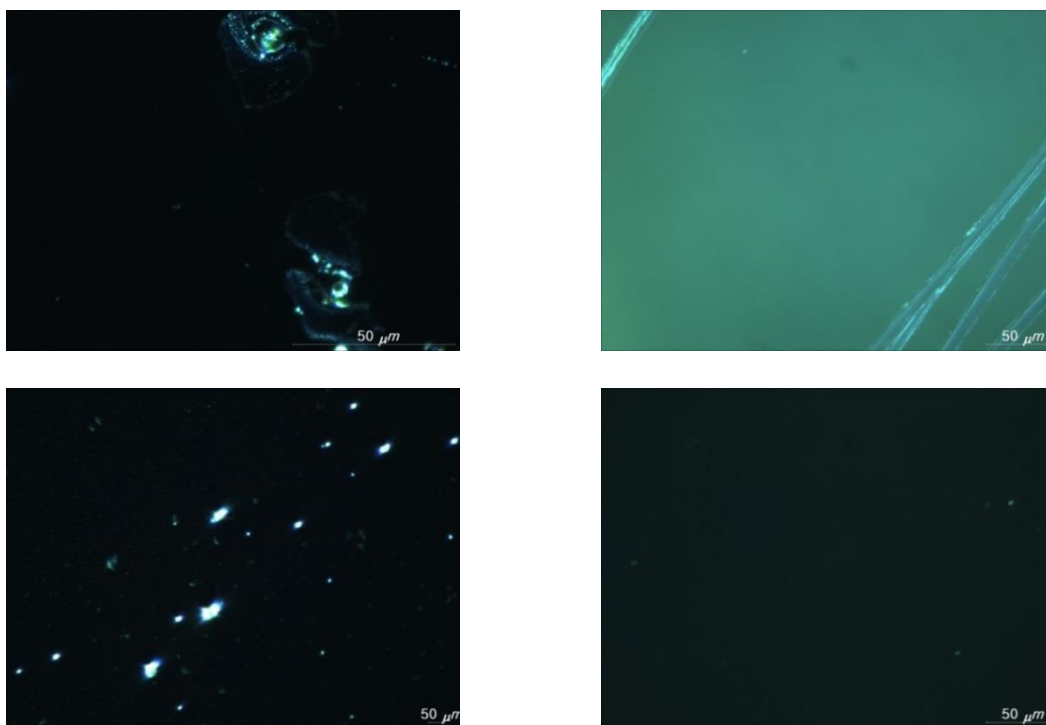
*V-19: Optical dark field micrographs of OD series films. **5-11** (top left) and **5-13** (bottom left) show bubbles wereas **5-12** (top right) and **5-14** (bottom right) form smooth films. Scratch marks (top right) result from stylus profilometry.*

---

[24] I.e. the delay between photo excitation and the recording of the PL spectrum.

All four materials form smooth films without grain boundaries. Grain bounderies in the organic film reduce the charge carrier mobilities and thus may reduce the efficiency of the device.[137] For **5-11** and **5-13** several bubbles are observed. This can be attributed to the non-optimized fabrication process. As the films were also subjected to stylus profilometry, the film of **5-12** shows some scrach marks but is otherwise smooth. Films were between 60 nm (**5-14**) to 110 nm (**5-13**) thick.

V.4.1.3 Conclusion

The *OD series* consists of four new molecules (**5-11** to **5-14**). The materials were designed as blue emitters for TADF based OLED devices. From the prerequisites suggested by ADACHI a molecular modeling study was conducted to minimize the ΔE_{S1-T1} energy gap.[181] From this, especially **5-11** emerged as a promising candidate.[370] A multistep synthesis was planned. It was aimed to allow simple donor moiety variation, while keeping the acceptor (oxadiazole) constant. Based on this strategy, materials **5-11** − **5-14** were prepared. The optoelectronic properties were studied as part of the IRTG 1404 program at Seoul National University in Korea during a three month research visit in the group of Prof. J. J. KIM. After the determination of the HOMO energies by CV the material was processed by spin-casting into thin-films. The optical properties of these films were investigated by UV-vis absorption and PL spectroscopy. The characterization of the triplet level energy was hampered by the disappointingly low PL efficiencies of **5-11** and **5-12**. It was possible to determine ΔE_{S1-T1} for **5-13** (0.40 eV) and **5-14** (0.60 eV), which is close to the $\Delta E_{S1-T1} < 0.5$ eV suggested by ADACHI. The determined photoluminescence quantum yields of all *OD series* materials were below $\Phi_{PL} < 30$ %. In order to fabricate efficient OLED devices it should be $\Phi_{PL} \geq 50$ %.[170] The *OD series* materials were not studied in OLED devices as a consequence.

The low fluorescence quantum yields of **5-11** and **5-12** can be explained in parts by CT-interactions taking place in the molecule. While CT-fluorophores are commonly used (e.g. coumarine dyes in bio imaging) they are impaired by low fluorescent quantum yields.[385] Furthermore, the diphenylamine-moieties of **5-12** and especially **5-11** are not stable in air. 4,4′-bis(dimethylamino)diphenylamine is used as redox indicator in analytical chemistry (BINDSCHEDLER's green).[386] ITO *et al.* identified a series of radical species.[290] The fluorescence of **5-12** and **5-11** is probably quenched by the formation of analogous oxidation products. The fact that fluorescence remained weak even after treating the film with a reducing agent suggests that also CT-quenching is operational. As recently discussed by LEE *et al.*, small ΔE_{S1-T1} often leads to poor PL efficiencies.[387] For **5-13** and **5-14** the PL quantum yield is improved to a level often found in oxadiazole containing fluorophores, but still far inferior to current fluorescent materials.[388, 389]

V.4.2   The Py series

Parallel to the *OD series* the pyrene based *Py series* (**5-43** to **5-48**, see figure V-8) was investigated.

V.4.2.1   Structure determination

All materials were identified by FD-MS and elemental analysis.

The structure of all materials was confirmed by ^{1}H- and ^{13}C-NMR spectroscopy. The assignment of NMR signals for triphenylamine derivatives is discussed on the basis of **5-46**.
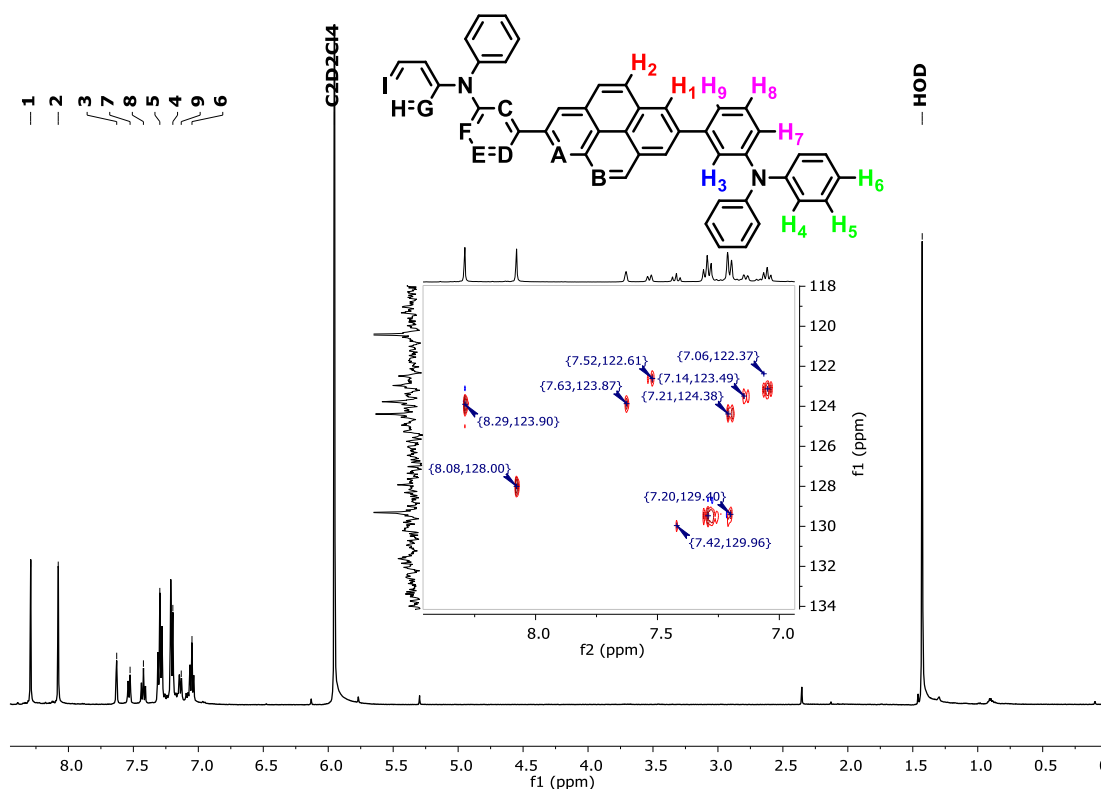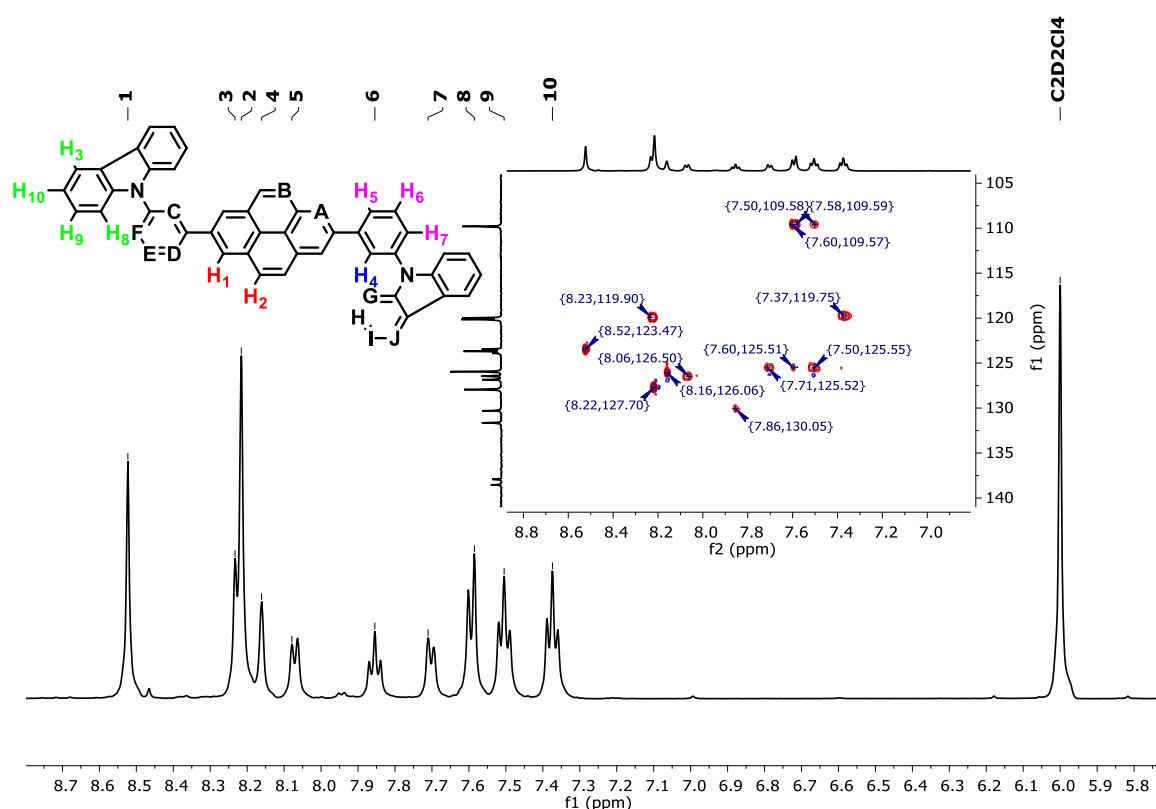

*V-20:^{1}H- (panel) and ^{1}H-^{13}C HSQC (inset) NMR spectra of **5-46** recorded in $C_2D_2Cl_4$ at 374 K.*

From the ^{1}H-NMR it follows that **5-46** has nine non-equivalent protons at elevated temperatures. At lower temperatures rotamers complicate the structure elucidation.The solubility of **5-46** is insufficient for ^{13}C-NMR spectroscopy. Two singlets *1* and *2* at $\delta = 8.29$ ppm (4 H) and $\delta = 8.08$ ppm (4 H) are assigned to the pyrene core at H_1 and H_2 respectively. The singlet *3* ($\delta = 7.63$ ppm, 2 H) can be identified as part of the m-phenylene linker (H_3). By considering the integration and splitting of signals *4* ($\delta = 7.19$ ppm, d, J = 7.25 Hz, 8H), *5* ($\delta = 7.30$ ppm, t, J = 7.25 Hz, 8H) and *6* ($\delta = 7.30$ ppm, t, J = 7.25 Hz, 4H) they can be assigned to the diphenylamine units. The remaining signals *7* ($\delta = 7.53$ ppm, d, J = 7.48 Hz, 2H), *8* ($\delta = 7.45$ ppm, t, J = 7.48 Hz, 2H) and *9* ($\delta = 7.53$ ppm, d, J = 7.14 Hz, 2H) are allocated to the *m*-phenylene linker.

Using a ^{1}H-^{13}C correlation spectrum signals *A* (δ = 123.9 ppm) and *B* (δ = 128.0 ppm) can be assigned to the pyrene scaffold. The *m*-phenylene linker generates signals *C* (δ = 123.9 ppm), *D* (δ = 123.5 ppm), *E* (δ = 130.0 ppm) and *F* (δ = 122.6 ppm). The diphenylamine moiety finally gives rise to signals *G* (δ = 124.4 ppm), *H* (δ = 129.5 ppm) and *I* (δ = 123.1 ppm). Quaternary carbon signals could not be resolved due to the low solubility of **5-46**.

5-43 is chosen as an example to discuss the NMR signal assignment for the carbazole substituted pyrene derivatives (**5-43** – **5-45**).

*V-21: ^{1}H- (panel) and ^{1}H-^{13}C HSQC spectra of **5-43** recorded in C$_2$D$_2$Cl$_4$ at 373 K.*

As in the case of **5-46** the pyrene scaffold can be identified by two singlets (*1* and *2*). In this case they are shifted slightly down field to δ = 8.52 ppm (H$_1$) and δ = 8.22 ppm (H$_2$). At 500 MHz NMR field strength signal *3* (δ = 8.23 ppm) is not fully resolved from singlet *2*. From a ^{1}H-^{1}H COSY experiment (not shown) it can be identified as belonging to the carbazole unit due to its strong coupling with signal *10* (δ = 7.37 ppm, t, J = 7.27 Hz, 4H). By an area-under-the-curve argument signals *9* (δ = 7.50 ppm, dd, J$_1$ = 7.27 Hz, J$_2$ = 8.20 Hz, 4H) and *8* (δ = 7.59 ppm, d, J = 8.20 Hz, 4H) can also be assigned to the carbazole moieties. The remaining signals *4* (δ = 8.07 ppm, d, J = 7.8 Hz, 2H), *5* (δ = 7.85 ppm, t, J = 7.8 Hz, 2H) and *6* (δ = 7.70 ppm, d, J = 7.8 Hz, 2H) stem from the *m*-phenylene linker.

From the HSQC spectrum the following assignment of the carbon atoms is possible. Signal *A* (δ = 123.5 ppm) and *B* (δ = 127.7 ppm) stem from the pyrene scaffold. The *m*-phenylene linker generates signals *C* (δ = 126.1 ppm), *D* (δ = 126.5 ppm), *E* (δ = 130.1 ppm) and *F* (δ = 125.5 ppm). Finally, signals *G* (δ = 109.6 ppm), *H* (δ = 125.6 ppm), *I* (δ = 119.8 ppm) and *J* (δ = 120.0 ppm) are assigned to the carbazole unit.

V.4.2.2 Optoelectronic properties

V.4.2.2.1 Cyclic voltammetry

As for the *OD series*, frontier orbital energies were determined by cyclic voltammetry. Only the oxidation waves were observed in the experiments. Accordingly, only HOMO energies were determined electrochemically. The LUMO energies were again derived in conjunction with the optical band gap ΔE_{OP}.

CV experiments were conducted in THF and tetrabutylammonium hexafluorophosphate as supporting electrolyte. For **5-43**, **5-44** and **5-46** NPB, while for **5-45**, **5-47** and **5-48** ferrocene was used as internal standard. In figure V-22 the voltammograms are referenced versus the NHE electrode.
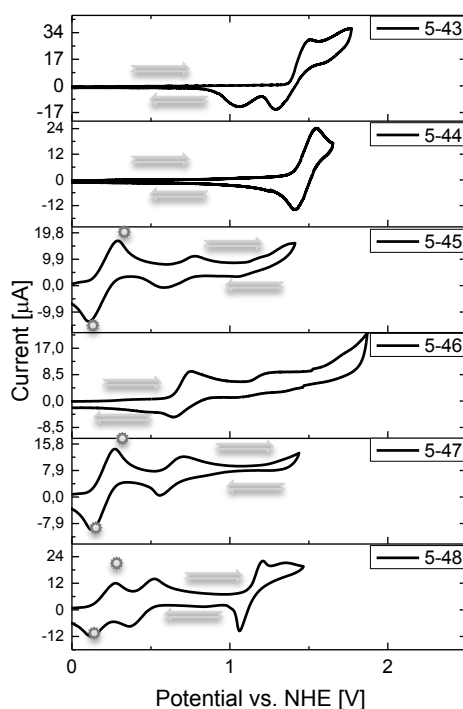
V-22: Cylic voltammograms of Py series recorded in THF at a scan rate of 100 mV/s using Bu₄NPF₆ as electrolyte. The voltammograms are referenced to the normal hydrogen electrode. When applicable, Fc/Fc⁺ wave is labeled with an asterisk (*) symbol.

The carbazole derivatives **5-43** – **5-45** show limited electrochemical activity. The oxidation waves of **5-43** and **5-44** have very similar onset values ($U_{Ox,\textbf{5-43}}$ = 1.37 V, $U_{Ox,\textbf{5-44}}$ = 1.41 V). As expected, alkylation only has a small effect on the HOMO energy

(table V-4). For **5-43** an irreversible reduction is observed at U = 1.2 V which is not detected for **5-44**. This reduction band might be an experimental artefact. The solubility of **5-43** is poor, thus the mass transport equilibrium at the working electrode may not be able to fully establish itself leading to an additional signal.[390] In the case of **5-45** the methoxy units clearly elevate the HOMO in terms of energy. The oxidation wave is recorded at $U_{OX,\mathbf{5\text{-}45}}$ = 0.6 V equivalent to a HOMO energy of -5.3 eV.

Table V-4: Frontier orbital energies of Py series materials.

	U (onset) (V)	$E_{HOMO,Ex}$ (eV)[a]	$E_{LUMO,Ex}$ (eV)[b]	$E_{HOMO,Calc.}$ (eV)[c]	$E_{LUMO,Calc.}$ (eV)[c]
5-43	1.37	-6.0	-2.4	-5.37	-1.73
5-44	1.41	-6.0	-2.6	-5.42	-1.98
5-45	0.68	-5.3	-2.1	-4.87	-1.69
5-46	0.71	-5.4	-2.2	-4.98	-1.52
5-47	0.60	-5.2	-2,0	-4.82	-1.47
5-48	0.39	-5.0	-1.9	-4.62	-1.39

[a] determined according to eq. (V-1) using E_{NHE} = -4.6 eV. [b] derived in conjunction with the ΔE_{OPT} (table V-3Table V-3). [c] DFT.

For the triphenylamine derivatives **5-46** – **5-48** a stronger electrochemical activity is registered. The first oxidation wave is consistently recorded at lower potentials ($U_{OX,\mathbf{5\text{-}46}}$ = 0.7 V, $U_{OX,\mathbf{5\text{-}47}}$ = 0.6 V and $U_{OX,\mathbf{5\text{-}48}}$ = 0.4 V) when compared to the carbazole congeners. For **5-46** and **5-48** a second oxidation signal (corresponding to the second triphenylamine substituent) is resolved at higher potential ($U_{OX2,\mathbf{5\text{-}46}}$ = 1.2 V, $U_{OX,\mathbf{5\text{-}47}}$ = 1.1 V). In the triphenylamine derivatives alkyl-substitution (**5-47**) raises the HOMO energy by 0.2 eV. As for the *OD series*, the DFT calculations are well predicting the trend of the frontier orbital energies and optical band gap of the *Py series*, yet the numerical values are too high.

LUMO energies were derived from the optical bandgap ΔE_{OP} (table V-5). All compounds have a significant bandgap ΔE_{OP} of 3.2 - 3.6 eV. As a consequence, the LUMO energy is relatively high especially for the triphenyl derivatives. This is problematic for the design of suitable OLED device structures (*vide infra*). At the time of writing, only **5-44** was studied in working OLED devices.

V.4.2.2.2   **Optical spectroscopy**

In figure V-23 UV-vis and PL spectra of *Py series* molecules in THF solution are collected. The corresponding absorption and emission maxima as well as the STOKES shift of each compound are reported in table V-5.

At first glance the UV-vis spectra of all materials of the series look similar. All have a strong absorption maximum ($\varepsilon \approx 4.8*10^5 - 5.7*10^5$ mol*L^{-1}*cm^{-1}) in the region between $\lambda_{Abs,max} = 289$ nm and 298 nm, a clear second band around $\lambda_{Abs} = 339$ nm and 344 nm as well as a weaker feature around $\lambda_{Abs} = 322$ nm and 327 nm. For clarity, the region between 310 and 400 nm is expanded in an inset in figure V-23. The vibrational splitting is not resolved for the main absorption band, as has been observed for other 2,7-functionalized pyrenes.[11, 77]
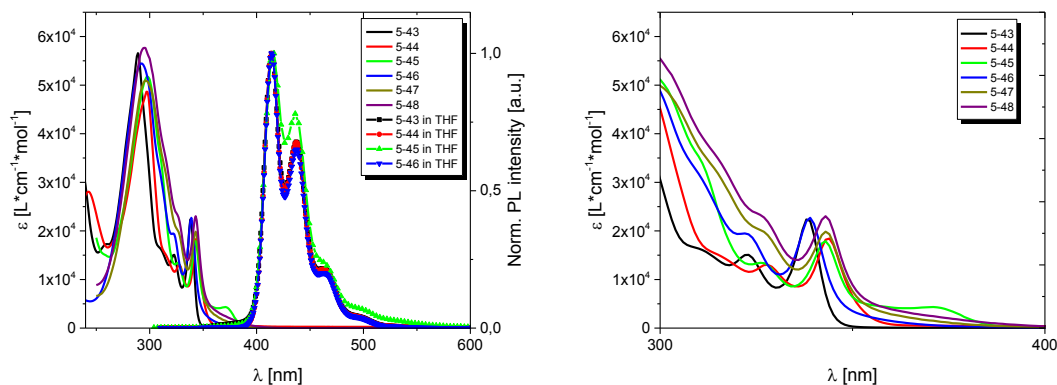
V-23: Left:UV-vis absorption (solid line) and PL spectra (symbols) of Py series materials in THF solution. Right: Expansion of the UV-vis absorption spectrum around the band gap.

The PL spectra look almost identical. All have a strong PL maximum at $\lambda_{PL,max} = 414$ nm, a second maximum at $\lambda_{PL} = 437$ nm and a third feature at $\lambda_{PL} = 466$ nm. The relative intensities of the spectral features are identical except for the methoxy substituted derivatives (**5-45** and **5-48**). In these materials the weaker spectral features show an increased intensity. All materials have a significant STOKES shift between 70 and 75 nm in common.

Table V-5: Collected photophysical properties Py series materials in THF solution.

Compound	$\lambda_{Abs,max}$ (nm) [ε] [($*10^5$ L*cm^{-1}*mol^{-1})] [a]	ΔE_{Opt} (eV) [b]	$\lambda_{PL,max}$ (nm) [a]	Stokes shift (nm) [a]
5-43	289 [5.7] 339 [2.2]	3.57	414, 437, 466	75
5-44	297 [4.9] 344 [1.8]	3.47	414, 437, 466	70
5-45	298 [5.1] 343 [1.8]	3.21	416, 436, 465	71
5-46	293 [5.4] 339 [2.3]	3.31	414, 437, 466	75
5-47	296 [5.1] 343 [2.0]	3.25	414, 437, 466	71
5-48	295 [5.8] 343 [2.3]	3.14	416, 436, 465	72
[a] recorded in THF, [b] onset of absorption				

KAAFARANI *et al*. reported a study on 2,7-bis(carbazol-9-yl)pyrenes.[71] They observed similar two-transition UV-vis absorption spectra. In their discussion they utilize the weaker, long wave absorption as absorption maximum ($\lambda_{Abs,max}$ = 341 nm) and disregard the stronger, high energy absorption ($\lambda_{Abs,max}$ < 330 nm). They report PL maxima at $\lambda_{PL,max}$ = 429 nm for **5-50** and $\lambda_{PL,max}$ = 450 nm for **5-51**. As discussed in the introductory chapter, the $S_0 \rightarrow S_1$ transition is usually rather weak whereas higher transitions $S_0 \rightarrow S_{(1+n)}$ can be very strong, especially in 2,7-substituted pyrenes.[11]
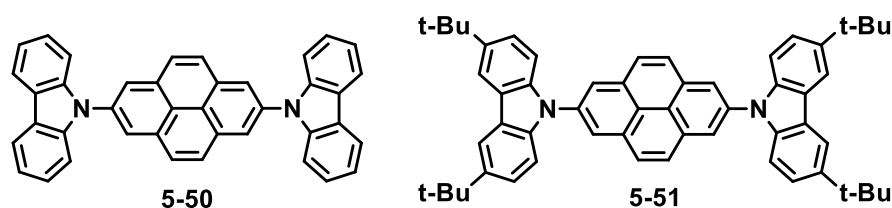
V-24: 2,7-bis(carbazol-9-yl)pyrenes reported by KAAFARANI *et al.*[71]

KAAFARANI *et al*. calculated $S_0 \rightarrow S_5$ and $S_0 \rightarrow S_7$ to be the first transitions having considerable transition dipole moments in **5-51** and attributed them to the low energy absorption maximum. In their discussion they use this to explain the large STOKES shift of 86 nm observed for **5-50** and even 109 nm for **5-51**. Their argument runs as follows: While excitation is occurring only in an $S_0 \rightarrow S_{(1+n)}$ transition, emission occurs in an $S_1 \rightarrow S_0$ transition. Between excitation and re-emission, energy is dissipated by internal conversion to the S1 state. This hypothesis was supported by relatively long fluorescent lifetimes.

Generally, STOKES shifts reflect the reorganization energy between the ground and excited state.[391, 392] Large STOKES shifts are often observed for donor-bridge-acceptor molecules where electron energy transfer (EET)[393] or intramolecular energy transfer (IMET)[394] cascades are often possible.

For the *Py series* materials it can be supposed that a similar mechanism as reported by KAAFARANI *et al*. is triggering the large STOKES shifts. Fluorescence lifetimes are also large in these molecules (V.4.2.2.5). In order to get a deeper understanding of the excitation and emission mechanism of the series solvatochromism experiments were conducted. It was to be tested whether the ground state was polarized in contrast to the excited state. This can be expected from the molecular modelling predicting high electron density on the pendent carbazole units (HOMO) whereas the LUMO is localized on the pyrene core (see figure V-7).

V.4.2.2.3   Solvatochromism

The dependency of spectroscopic properties (e.g. position or intensity of absorption / emission maxima) on the solvent in which the analyte is dissolved is called *solvatochromic*

effect or for short *solvatochromism*.[20, 392] The solvatochromic effect is caused by differential solvation of the ground and the excited state.[395] If, for example, the excited state is polar (i.e. has a dipole moment) while the ground state is not, interactions in polar solvents will differ. The polar excited state will be stabilized (i.e. lower in energy). In D-π-A dyes a significant solvatochromic effect is often observed.[396] As solvatochromism is usually more pronounced in the emission than in the excitation spectrum, the PL spectra of **5-43**, **5-44**, **5-45** and **5-46** in five different solvents were recorded and are reproduced in figure V-25. The following solvents were used(in the order of increasing polarity): hexane < toluene < chloroform < THF < DMSO.. The four molecules were chosen to be able to investigate the effect of changing the substituent on carbazole and the effect of TPA compared to carbazole.
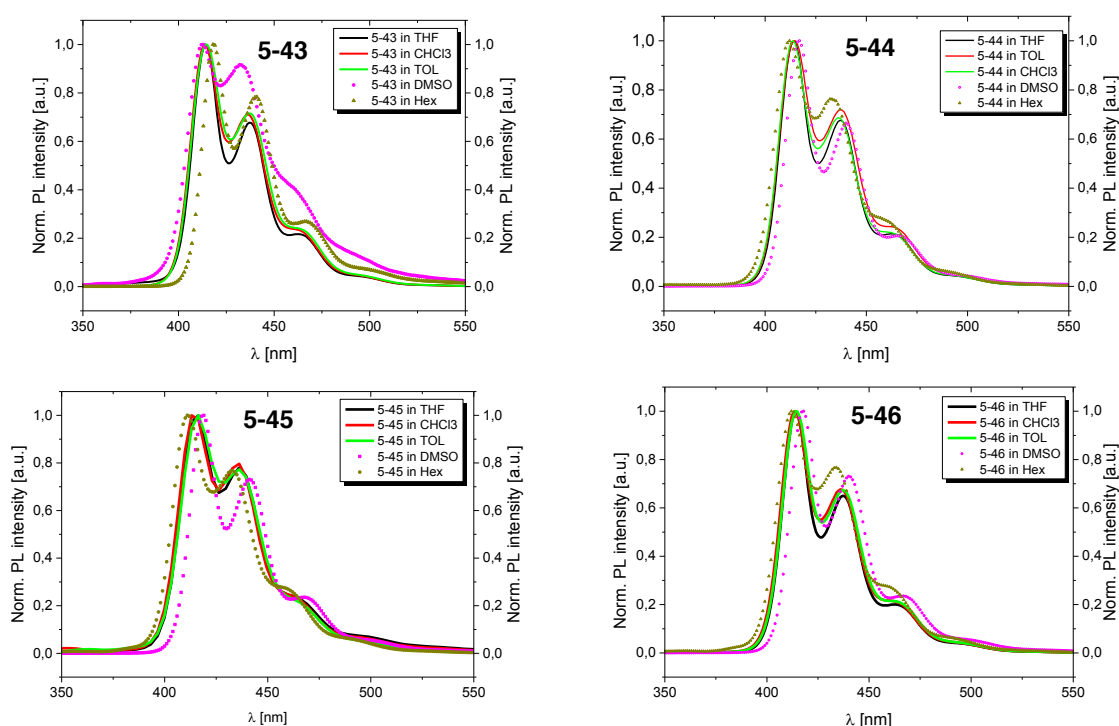
*V-25: Solvatochromism of **5-43** (top left), **5-44** (top right), **5-45** (bottom left) and **5-46** (bottom right). Clear solutions are shown as solid lines (c = 1*10⁻⁶ mol/l), symbols signify turbidity in the sample.*

The poor solubility of the studied materials allowed only for THF, chloroform and toluene to prepare visually clear solutions (c = 1*10⁻⁶ mol/l). These solutions are plotted as solid lines in figure V-25. For the remaining solvents the material was not fully soluble. The solid was allowed to settle for 1 h after sample preparation and decanted.

Small solvatochromic shifts in the position of the PL maxima are found and collected in table V-6. Between hexane and DMSO a shift between 5 – 9 nm is registered. The solvents have a significant influence on the relative band intensity ($\lambda_{PL,max}$ vs. $\lambda_{PL,2nd.max}$).[17] Yet, this influence is not consistent. For **5-43** the second PL maximum reaches 92 % intensity in DMSO and drops to 78 % in hexane. In contrast, for **5-44** the second PL maximum is as

low as 66 % in DMSO and only rises to 75 % in hexanes. For the intermediate polarity solvents the solvatochromic effect is even smaller. The maxima are shifted by about 1 nm in toluene. These solvents also show little effect on the relative band intensities.

Materials with strong solvatochromism experience a shift of around $\Delta\lambda = 80 - 100$ nm between both extreme ends of the solvent polarity spectrum.[395] ZÖPHEL *et al*. for example have reported push-pull substituted pyrene derivatives with a solvatochromic shift of $\Delta\lambda = 92$ nm between hexane and THF.[87] Compared to this **5-43**, **5-44**, **5-45** and **5-46** exhibit practically no solvatochromic effect.

*Table V-6: PL maxima of **5-43**, **5-44**, **5-45**, and **5-46** in fife different solvents.*

Compound	$\lambda_{PL,max}$ (nm) Hexane	$\lambda_{PL,max}$ (nm) Toluene	$\lambda_{PL,max}$ (nm) CHCl$_3$	$\lambda_{PL,max}$ (nm) THF	$\lambda_{PL,max}$ (nm) DMSO	$\Delta\lambda$ Hex -> DMSO (nm)
	413	415	414	414	418	5
5-43	432	437	436	437	441	9
	457	462	461	462	459	2
	412	416	414	414	417	6
5-44	432	437	436	437	440	8
	456	462	461	462	464	8
	411	416	414	416	418	7
5-45	431	436	436	436	441	10
	455	465	465	465	465	10
	412	415	414	414	418	6
5-46	434	437	436	437	440	6
	457	462	461	462	466	9

From this we can conclude that the states involved in the observable transitions (excited or ground) have no significant variation of their dipole moments.[395] Therefore, an asymmetric excitation (from the pyrene HOMO) to one of the triphenyl-amine termini (LUMO) does not take place. Rather, in the C_2 symmetric molecule both termini are equivalent and a symmetric excitation takes place.

V.4.2.2.4   Film study

Thin-film and OLED studies were conducted in the Organic Photonics Lab at Seoul National University during a research visit as part of the IRTG program. In order to gauge the emission properties of *Py series* molecules in an OLED device, thin films of **5-43**, **5-44** and **5-46** were prepared by thermal evaporation onto a SiO$_2$ substrate and their PL spectra recorded. In figure V-26 the solution and thin film emissions are compared. In the solid state PL spectra are usually broadened and often lack vibrational fine splitting observed in solution.[381] Molecules with an extended aromatic core may also form dimers by π-π interactions. This, in turn, can lead to the formation of excimers. As mentioned before,

in pyrene the fluorescence maximum is shifted to $\lambda \approx 470$ nm when excimers are established.[397] Excimer fluorescence can be the exclusive EL mechanism of pyrene based OLEDs, yet this sky blue emission color is not very desirable (e.g. for a full color display).[170, 398]
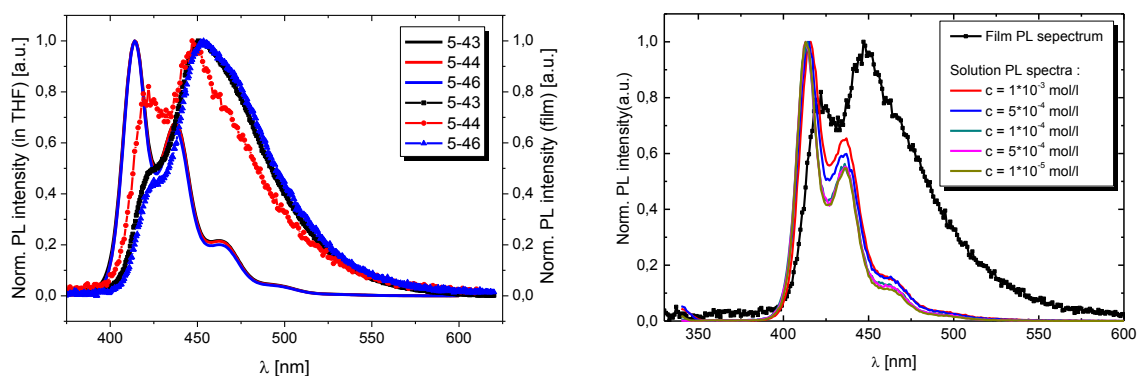
*V-26: Left: Solution (line) and film (symbols) PL spectra of **5-43** (black), **5-44** (red) and **5-46** (blue). Right: Solution spectra of **5-44** at different concentrations (line, red: 1*10⁻³ mol/l; blue: 5*10⁻⁴ mol/l; green: 1*10⁻⁴ mol/l; violet: 5*10⁻⁵ mol/l; yellow: 1*10⁻⁵ mol/l in CHCl₃) compared to the film PL spectrum (black).*

When the PL spectra in solution and in the solid state are compared, a significant bathochromic shift of $\lambda \approx 37$ nm ($\lambda_{max,solution}$ to $\lambda_{max,film}$) becomes apparent. In table V-7 details are presented. Only two PL bands can be identified in the solid state ($\lambda_{Shoulder} = 424$ nm, $\lambda_{max,film} \approx 450$ nm). In terms of intensity, it is noteworthy that the highest energy transition is not the strongest (for **5-46** the intensity in only 43 % and for **5-44** it is 76 % of the absorption maximum). The film spectra are significantly broadened (e.g. FWHM**5-44**,solution = 47 nm to FWHM**5-44**,film = 73 nm). The PL efficiencies in the films have been determined by the integrating sphere method and are quite high. In figure V-26 (right) it can be seen that excimer formation is well suppressed in **5-44**. Even at concentrations as high as c = 1*10⁻³ mol/l (i.e. close to saturation) an excimer emission (i.e. $\lambda > 470$ nm) is not observed. In the studied concentration range, emission is practically independent of the concentration.

*Table V-7: Solution and film PL spectra of **5-43**, **5-44** and **5-46** compared.*

	$\lambda_{PL,max}$ (nm) in THF (intensity in %)	$\lambda_{PL,max}$ (nm) Film	Shift of PL_{max} (nm)	Shift of PL bands (nm)	PL efficiency (film) (%)[a]
5-43	414 (100) 437 (67)	424 (49) 450 (100)	36	10 13	57
5-44	414 (100) 437 (67)	424 (76) 451 (100)	37	10 14	47
5-46	414 (100) 437 (63)	424 (43) 452 (100)	38	10 15	62
		[a] integrating sphere method			

The significant shift from solution to the film spectrum is not fully understood and currently under investigation by the KIM group. Three lines of explanation seem reasonable:

- Dimer formation;
- A new decay channel open in the solid state;
- Or type C excimer formation.

Formation of dimers is often found in PAHs in the solid state. Dimerization will shift the absorption and emission spectra of a molecule to lower energies. The work of KAAFARANI *et al.* discusses possible electronic transitions in **5-50** and **5-51**.[399] Not all transitions possible in the molecule, have high transition dipole moments. Due to symmetry constraints some transitions are very weak in solution. A change in geometry from solution to the solid state may open new decay channels and thus give rise to new emission features. In order to test this hypothesis it would be necessary to calculate the transition dipole moments of different geometries by TD-DFT. A collaborator for such a time consuming study is still needed. Alternatively, the formation of a C-type excimer might cause the significant change in the emission spectrum. NANDY *et al.* studied the formation of a static intramolecular pyrene excimer.[400] In their work they suggest three possible pyrene arrangements in the excimer:
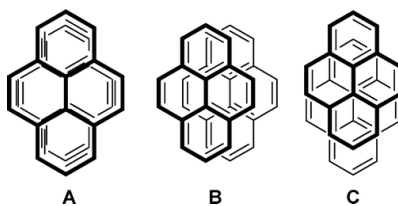
V-27: Three modes of pyrene – pyrene dimer formation. A: Superimposed. B: Displaced along the molecule short axis. C: Displaced along the molecule long axis (figure adapted from NANDY et al.[400]).

When *Py series* geometry is considered, type A excimer formation (figure V-27) is very unlikely due to the bulky pendant substituents. Type B and especially type C seem more plausible. For the type C excimer NANDY *et al.* report a blue shift of the excimer fluorescence to λ_{max} = 460 nm (in DCM).[400] A bathochromic shift (λ_{max} = 512 nm) in the solid state is attributed to additional intermolecular excimer formation. As was shown in the solvatochromism (figure V-25) and concentration study (figure V-26) excimer formation was not observed in solutions of *Py series* molecules, even in poor solvents. While this suggests that the substituents suffice to suppress the excimer formation in solution they might be insufficient to suppress type C excimers in the solid state.

All three hypotheses are able to explain why in **5-44** the single molecule emission maximum retains its relatively high intensity. The bulky tertiary-butyl groups hinder the molecular approach in the solid state. The intermolecular interactions are therefore suppressed.

V.4.2.2.5   Time resolved photoluminescence spectroscopy

By recording the prompt and delayed PL spectra of a material at cryogenic and room temperature it is possible to delineate the fluorescence, delayed fluorescence and phosphorescence components of a bulk materials' PL spectrum. By isolating the phosphorescence component it is possible to assess the energy of the triplet state T_1 and therefore the $\Delta E_{S1->T1}$ energy gap.[401] As stated in the introduction to this chapter the $\Delta E_{S1->T1}$ energy gap should be smaller than 0.5 eV to for efficient TADF in an OLED.[182]

Figure V-28 shows a series of PL film spectra of **5-43**, **5-44** and **5-46**. In the room temperature PL spectra (right column) only a small variation between the prompt and the delayed spectra is observed. At long delay times (up to 100 µs) noise creeps into the spectra due to low PL intensities.
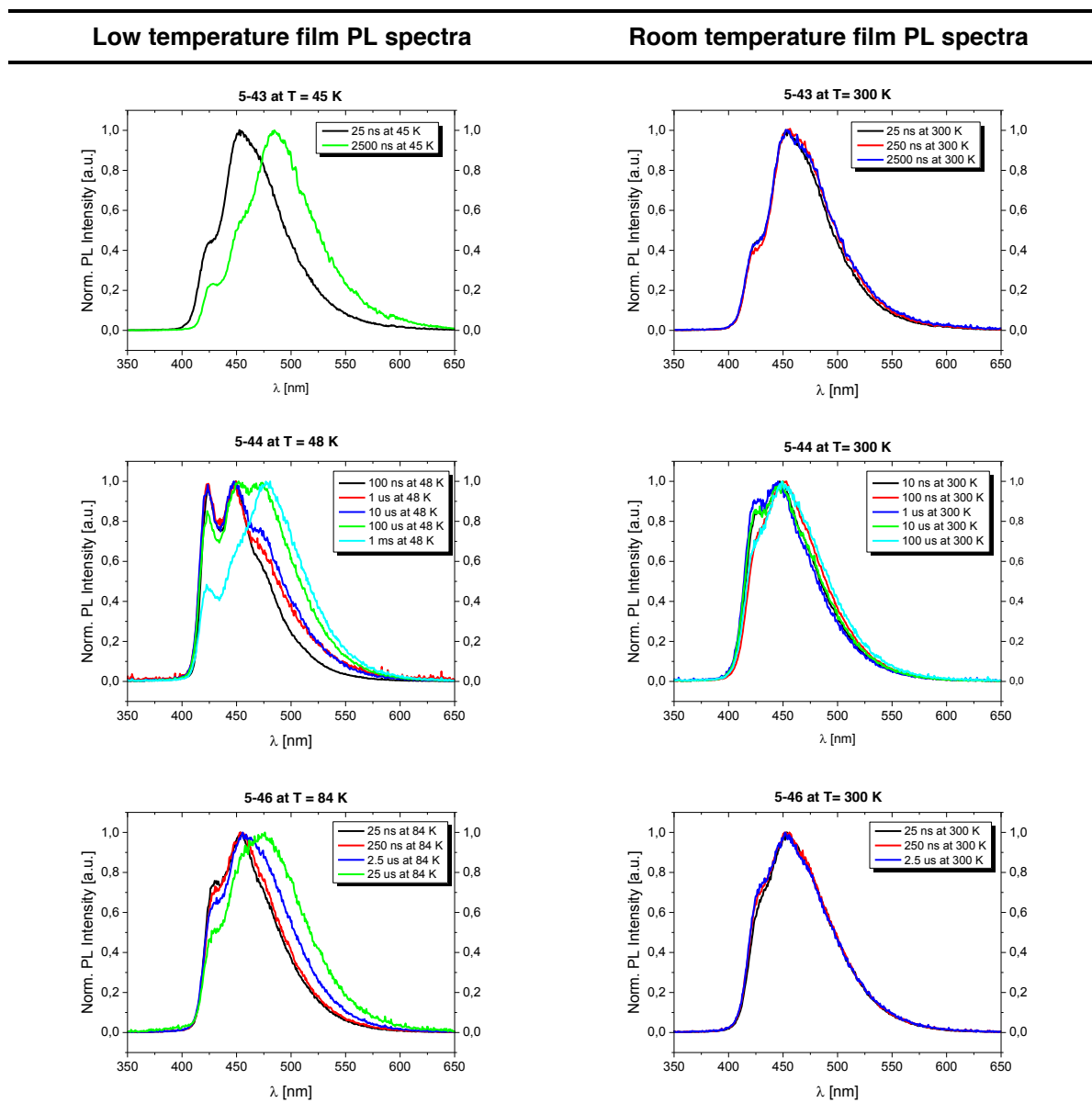
*V-28: Time resolved PL spectra of **5-43** (top), **5-44** (middle) and **5-46** (bottom) at cryogenic (left) and room temperature (right). The delay time is varied from 10 ns up to 1 ms.*

At lower temperatures a significant shift in the emission spectra can be observed between the prompt and the delayed acquisition (details are presented in table V-8). At short delay times the emission resembles the room temperature emission. At long delays an additional component is added. This is attributed to phosphorescence from the triplet state of the respective molecule.

Table V-8: PL maxima at different temperatures and delay times.

	$\lambda_{PL,max}$ (nm) t_{dealy} = 25 ns T = 45 K [a]	$\lambda_{PL,max}$ (nm) t_{dealy} = 25 μs [b] T = 45 K	$\lambda_{PL,max}$ (nm) t_{dealy} = 25 ns T = 300 K	$\lambda_{PL,max}$ (nm) t_{dealy} = 25 μs [b] T = 300 K	$\Delta E_{S1->T1,exp.}$ (eV) [c]
5-43	454	484	454	454	0.18
5-44	423, 448	451-471 (br)	426, 448	426, 450	0.36
5-46	432, 453	432, 473	454	454	0.13

[a] in the case of **5-46** T = 54 K, [b] in the case of **5-44** t_{dealy} = 100 μs [c] assuming the evolving band is not a p-type delayed fluorescence.

The triplet energies derived by this method are exceptionally small for pyrene based molecules (0.13 – 0.36 eV). MISTELBERGER and PORT report the triplet emission of a pyrene crystal at $\lambda = 592$ nm by a similar method which translates to $\Delta E_{S1->T1,pyrene} = 1.1$ eV.[402] This experimental gap agrees well with the TD-DFT calculated gap $\Delta E_{S1->T1,calc,\textbf{5-44}} = 1.2$ eV for **5-44**.[25]
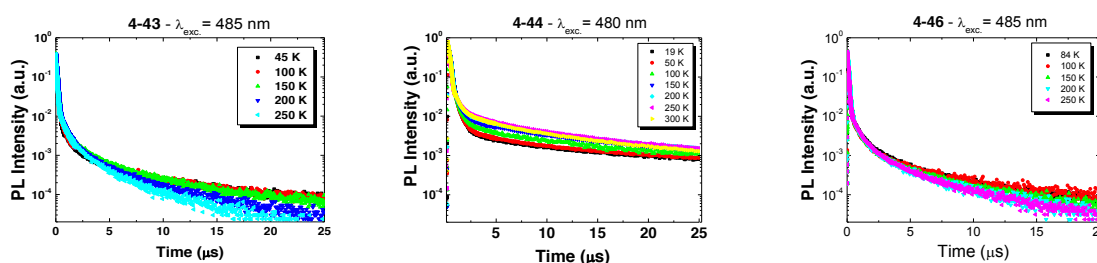
*V-29: Transient PL spectra of **5-43** (left), **5-44** (center) and **5-46** (right). The material is excited at a constant excitation wavelength (**5-43** = 485 nm, **5-44** = 480 nm, **5-46** = 475 nm) at an incremental change for temperature.*

In the transient PL experiment the PL intensity of only one emission wavelength is observed in the time domain. This gives information on the temporal evolution of the delayed emission. In figure V-29 a series of transient PL spectra of **5-43**, **5-44** and **5-46** at different temperatures is depicted. Often, an emission mechanism can be deduced by establishing a rate law for the decay of the PL intensity. At first glance at the figure it is obvious that delayed fluorescence is observed for all three materials. In **5-44** the decay rate is much lower than in **5-43** or **5-46**. Delayed luminescence lifetimes are extremely sensitive to impurities.[26] **5-44**'s improved solubility may have allowed reaching superior purity. For OLED device fabrication **5-44** was purified by zone refining.

---

[25] Calculations courtesy of IVANOVA group.

At the time of writing, it has not been possible to determine the rate constants and rate laws for the delayed fluorescence of the studied molecules. No linear relationship between temperature and decay rate can be established. Probably more than one decay mechanism is operational, as no single rate constant was able to describe the decay appropriately. Investigations continue in the KIM group. For TADF the decay rate will increase with temperature.[180, 186] At higher temperatures more energy (k*T) is available to the system and surmounting the activation barrier for reverse-ISC becomes more facile.[182] The current working hypothesis is that triplet-triplet annihilation may also be operational in the *Py series* emitters.[191]

V.4.2.3   OLED fabrication

To begin the investigations of the *Py series* performance in OLED devices **5-44** was chosen. It has a superior film PL spectrum (higher short wave length component, *vide supra*) as well as significantly extended delayed fluorescence lifetimes. However, **5-44** also has a significantly low energy component in its film PL. In the planned OLED devices **5-44** was not only to be used as a neat film but also doped into the mCPPO1 matrix material (host:guest system).[403]
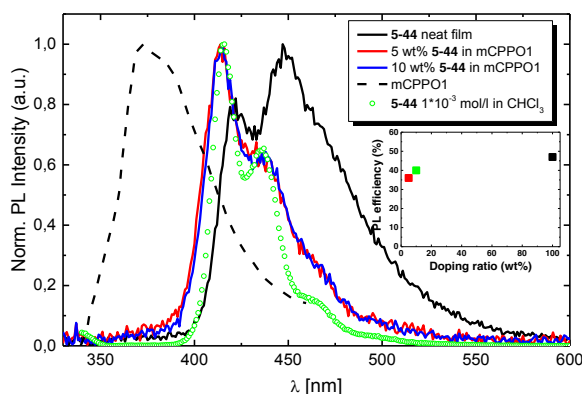

*V-30: Panel: Film PL spectra of **5-44** in a neat film (black), 10 % doped in mCPPO1 (blue) and 5 % doped in mCPPO1 (red). The dashed line gives the film PL spectrum of mCPPO1. For comparison a solution PL spectrum of **5-44** is given (yellow symbols). Inset: PL efficiency at different doping concentrations.*

Utilizing the host:guest system leads to a dramatic hypsochromic shift of the PL spectrum compared to the neat film of **5-44**. Irrespective of solid state broadening, the host:guest system's PL spectrum is identical to the solution emission in chloroform (c = 1*10^{-3} mol/l) (figure V-30). The fact that the emission maximum in the doped films reverts to λ_{max} = 414 nm makes this material very attractive for the use in OLED devices. One disadvantage is that the luminescence quantum yield drops from 47 % to 40 % (10 wt% of **5-44**) and even as low as 37 % (10 wt% of **5-44**). This occurs probably due to incomplete energy transfer from the host to the guest. Due to the large band-gap behavior of **5-44** the choice of matrix materials is limited. Especially the energetically high lying LUMO ($E_{LUMO,\textbf{5-44}}$ = -2.64 eV) restricts the choice of suitable ETL materials. It was found that

mCPPO1 ($E_{LUMO, mCPPO1}$ = -2.60 eV) provides a close match in terms of energy. Furthermore, mCPPO1 found broad applications for efficient exciplex co-host OLED devices in the KIM group.[404] For future studies a screening of alternative matrices (e.g. PO-T2T, E_{LUMO} = -2.82 eV) is planned.[405]

Four different OLED device layouts (A – D, figure V-31) were screened. Prior to device fabrication optical simulations were performed to minimize optical losses.[406]
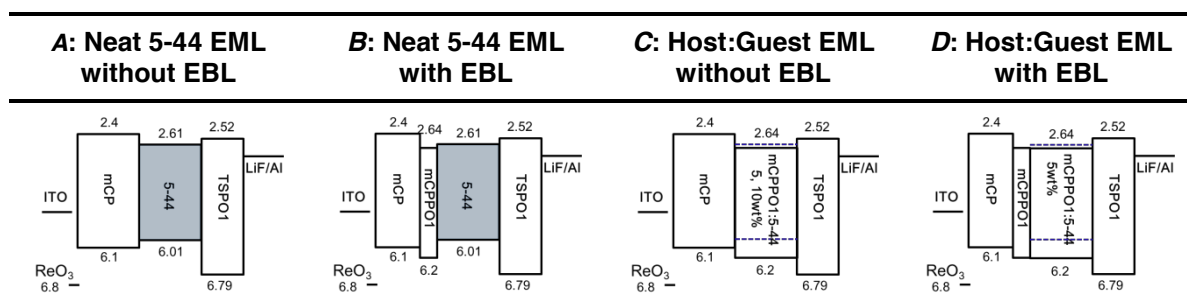
V-31: Device layouts tested in the optimization study.

All devices were prepared by stepwise thermal evaporation onto an ITO functionalized glass substrate (used as anode). Rhenium tetroxide was employed as hole injection layer, followed by mCP as hole transport layer.[407] In the cases of B and D mCPPO1 was introduced as electron blocking layer in cases A and C it was omitted. In designs A and B a layer of pure **5-44** was used as emitting layer (EML) whereas C and D made use of the mCPPO1:**5-44** host:guest system introduced in figure V-30. The thickness of the electron transport layer, comprising of TSPO1, was varied from 25 to 40 nm to empirically optimize the charge balance of the device.[403] Lithium fluoride was applied as electron injection layer and the stack covered with an aluminum cathode. A cover glass was glued on the final device before exposing it to air.

Results of the device optimization study are compiled in figure V-32. EL spectra, the current density vs. voltage as well as luminance vs. voltage curve and finally the external quantum yield vs. current density relation are displayed (columns from left to right). Key characterization data for the optimal ETL thicknesses (i.e. highest EQE) are collected in table V-9 for the respective device structures.

Table V-9: Results OLED fabrication / optimization study.

Device structure	Optimal ELT thickness (nm) [a]	EL maximum (nm)	FWHM EL spectrum (nm)	Turn on voltage (V)	Max. luminance (cd/m²)	Max EQE (%)
A	35	423	51	5.5	150 (11 V)	1.6
B	40	423	53	6.3	93 (13 V)	1.8
C	35	410	41	3.6	31 (6 V)	2.9
D	40	410	40	3.3	33 (6 V)	3.1

When the EL spectra of devices *A* and *B* are compared to the film PL data an unexpected hypsochromic shift is evident. A new emission maximum is found at $\lambda_{EL,max} = 423$ nm alongside a shoulder at $\lambda = 444$ nm. The intensity of this shoulder is dependent on the ETL thickness; therefore it may be caused by diffraction within the OLEDs (microcavity effect).[408] The absence of the PL maximum at $\lambda = 450$ nm in the EL spectrum suggest that this band is not generated by pyrene excimers. BISBERG *et al.* describe solely pyrene excimer EL in a polymer with strong excimer PL at around $\lambda = 470$ nm.[398] For devices *C* and *D* again a (smaller) hypsochromic shift of the fluorescence maximum to $\lambda_{EL,max} = 410$ nm is observed. The clear shoulder at $\lambda_{PL} = 435$ nm is less developed in the EL spectrum. Again the intensity of this feature depends on the ETL thickness. Additionally, the spectral purity of the emission is enhanced in the host:guest system. Full width at half maximum is decreased by approximately 10 nm.

Change of the EML structure not only has as significant effect on the EL spectrum but also on the electrical properties (e.g. turn-on voltage) of the devices. Devices *A* and *B* with their neat-film EML need much higher driving voltage to give off light ($U_{on,A} = 5.5$ V and $U_{on,B} = 6.3$ V) than their host:guest counterparts *C* ($U_{on,C} = 6.6$ V) and *D* ($U_{on,D} = 3.3$V). Lowering the driving voltages is important as this decreases the energy consumption of the device. Furthermore, the current density per cm^2 is also reduced. This usually helps to enhance the longtime stability of the device.[376]

The luminance values are very low. Yet, the external quantum yields are reasonably good. *A* and *B* show much higher luminance values (3 to 5 times higher), yet a lower EQE. It must be recalled that luminance is a photometric unit, i.e. the photon flux is modulated to the brightness *perceived* by the human eye.[409] The standard luminosity function is very low for wavelength $\lambda < 450$ nm.[410] Thus, the narrow deep-blue electroluminescence emitted by devices *C* and *D* give low luminance values. For devices *A* and *B* the EL spectrum is much broader and has a tail reaching $\lambda \approx 550$ nm, a region of high sensitivity of the human eye. The external quantum yield is not a photometric measurement. Thus, despite of low luminance values devices *C* and *D* give high EQEs. In the last column of figure V-32 EQE versus current density behavior of the devices is reported. For devices *A* and *B* the EQE increases rapidly and reaches its maximum at 1 mA/cm^2. Increasing current density leads to a rapid efficiency roll-off (the decrease of efficiency with increasing current density).[411] In contrast, devices *C* and *D* exhibit very high EQEs around the turn-on voltage, efficiency roll-off is starting to affect the devices at current densities exceeding 2 mA/cm^2.

Device	EL spectra	Luminance vs. voltage	EQE vs. current density
A			
B			
C			
D			
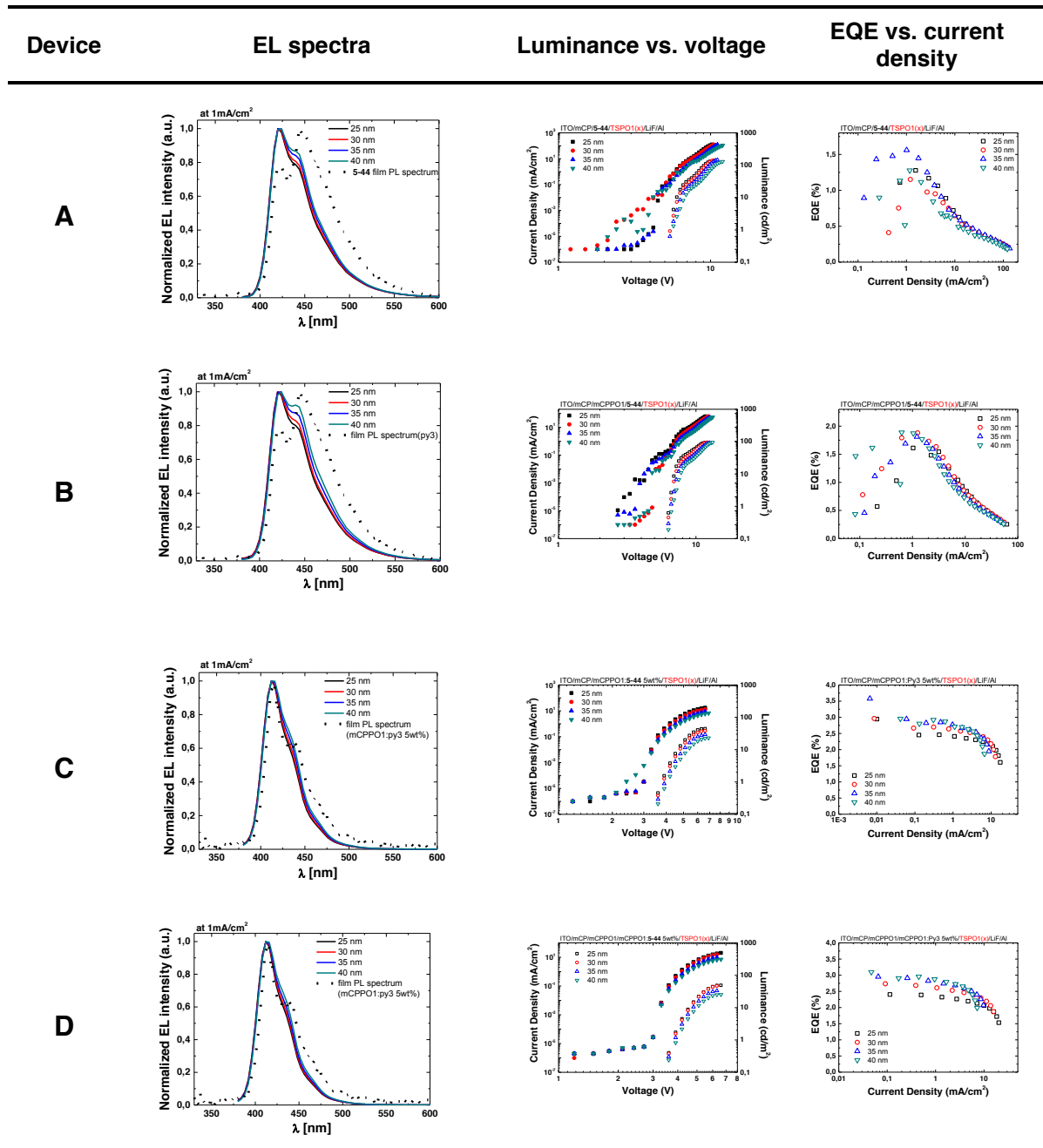
V-32: Results device optimization study.

The optimized device has a maximum EQE of 3.1 % and a turn on voltage of 3.3 V. The EL maximum is located at $\lambda_{max,EL} = 414$ nm around a narrow FWHM of 40 nm. The resulting CIE coordinates are x = 0.16 and y = 0.024. HU *et al.* recently reported a series of bisanthracene based chromophores of deep-blue OLEDs with CIE color coordinates of x = 0.16 and y = 0.06.[412] The international telecommunication union (ITU) parameter values for HDTV standard ITU-R BT.709 states for blue the CIE coordinates x = 0.15 and y = 0.06. The pyrene-based chromophores can be very well suited for wide color gamut display applications.

To put the EQE of 3.1 % for an OLED prepared from **5-44** in perspective it is useful to reconsider equation (1-7) from chapter *I.3.2*.

$$\eta_{EQE} = \gamma \times \chi \times \phi_{PL} \times \xi \qquad\qquad (\text{V-2})$$

Eq. (V-2): γ denotes the charge balance factor, χ the exciton spin factor, ϕ_{PL} the PL quantum yield, ξ the out-coupling efficiency.

Entering the known values for a fluorescence only device ($\chi = 0.25$, $\phi_{PL,\textbf{5-44}:5\text{ in mCPPO1}} = 0.36$ and $\xi = 20$ %) into this equation the maximum external quantum yield for an electronically balanced device ($\gamma = 1$) is given as:

$$\eta_{EQE} = 1 \times 0.25 \times 0.36 \times 0.2 \rightarrow \eta_{EQE,max} = 1.8\,\% \qquad (\text{V-3})$$

For an emitter with a relatively low ϕ_{PL} as **5-44**, $\eta_{eqe} = 3.1$ % is suggesting that $\chi > 0.25$, i.e. triplet states are most probably harvested in the device. As mentioned in section *V.4.2.2.5* the mechanism of triplet harvesting (TADF or/and TTA) is currently under investigation.

V.5   Summary

Thermally activated delayed fluorescence (TADF) is a very promising mechanism for triplet harvesting in transition metal free OLEDs. Although it has only recently been described in literature it already has attracted considerable academic attention. Dispensing with the need of transition metal complexes will be especially useful for the fabrication of blue electroluminescent devices.

In this study the efficacy of two different molecular structures was investigated. Both structures aimed at minimizing the singlet - triplet energy gap ΔE_{S1-T1} by destabilizing the triplet state as a consequence of frontier orbital partitioning. In the case of oxadiazole based materials (**5-11 – 5-14**) a push-pull arrangement with amine donors was chosen. For the pyrene based molecules orbital partitioning was given by virtue of the electronic structure of pyrene (nodal plane in positions 2 and 7). In both cases *m*-phenylene linkers enhance the effect.

The oxadiazole based chromophores (*OD series*) offered disappointingly low photoluminescent quantum yields and were not deemed useful for highly efficient OLEDs. Furthermore, emitters **5-11** and **5-12** failed to provide blue luminescence probably due to electron transfer from the strong donors.

Pyrene based materials **5-43 – 5-48** all provide blue luminescence in solution as well as in the molecular film. The PL quantum yields in thin films are ϕ_{PL} around 50 %.

In the KIM group photophysical properties were determined and OLED devices fabricated.

5-44 was used as emitter for a series of working devices. In all cases the carbazole groups suppressed the formation of excimers, a pure, deep-blue electroluminescence ($\lambda_{max} = 416$ nm) was observed in optimized devices.

The external quantum yield of $\eta_{eqe} = 3.1$ % observed in the best OLED prepared strongly suggests harvesting of triplet states for electro luminescence in that device. At the time of writing it was not clear which mechanism of triplet harvesting is operational in the system. In the KIM group this issue is currently being addressed.

For the near future the main focus should lie on finalizing the photophysical characterization and OLED fabrication of the additional pyrene derivatives prepared. The search for alternative matrices may lead to a more efficient energy transfer from the matrix to the emitter in the doped film. This will improve the $\phi_{PL,film}$ which in turn, will result in a higher external quantum efficiency.

Based on these results further structural modifications (e.g. dendronized phenyl carbazoles[413] or additional phenyl carbazoles in the 4 position of pyrene[86]) might become attractive structural variations.

Considering the later work of the ADACHI group, the reduction of flexibility in the molecule appears to be an essential concept to improve ϕ$_{PL}$. Furthermore, the twist between the termini and the pyrene core plays an essential role. In order to improve the rigidity of the molecule and to force a larger twist on the resulting molecule the introduction of a bulky substituent (R and R') on the *m*-phenylene bridge should prove helpful.
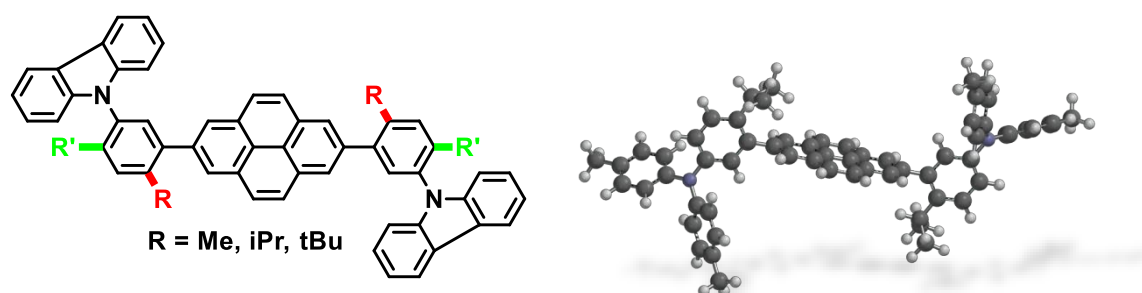
V-33: Modified Py series emitter design. Left: Lewis structure. Right: Calculated gas phase structure (R = iPr, R' = H).

R and R' will limit the freedom of rotation due to steric interactions, non-radiative decay will be hindered. In addition, the termini will be forced further out of the molecular plane of the pyrene core. Orbital partitioning will be enhanced in turn. Care has to be taken that the twist between the termini and the pyrene core will not reach 90° and, therefore, cancel the transition probability between both units. Theoretic simulations may assist in the search for a suitable combination of substituents R and R'.

VI. Functionalization of pyrene in the positions 4,9 and 10

ZÖPHEL *et al.* reported a selective K-region bromination of pyrene-4,5-dione (**6-2**) and used this to prepare de-symmetrized pyrene derivatives with strong push-pull character.[87]
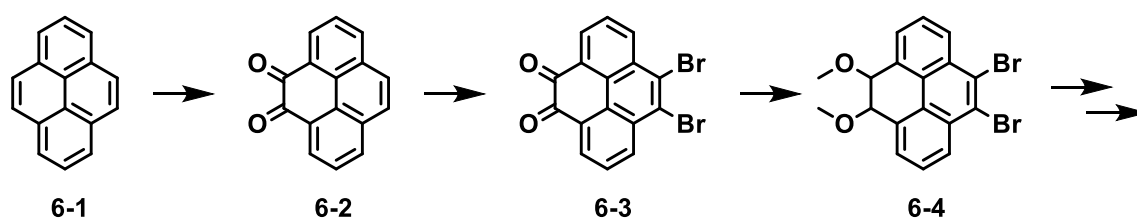
VI-1: Route to asymmetrically substituted pyrenes as described by ZÖPHEL et al.[87]

In the course of their work the mono-brominated derivative 9-bromopyrene-4,5-dione (**6-5**) was not relevant.
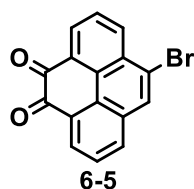
*VI-2: Structure of 9-bromopyrene-4,5-dione (**6-5**).*

This chapter will discuss two applications of **6-5** as building block for organic synthesis. The first use is the synthesis of a three dimensional acceptor molecule. Also, **6-5** serves as coupling partner in a SCHOLL-type oxidative cyclodehydrogenation reaction in the synthesis of donor substituted rylene-derivatives.

VI.1 [4,4'-Bipyrene]-9,9',10,10'-tetraone (6-6)

By 9,9'-carbon-carbon bond formation between two units of **6-5** [4,4'-bipyrene]-9,9',10,10'-tetraone can be attained. Steric repulsion forces the molecule to adopt a non-planar conformation. Figure VI-3 gives a molecular modelling (DFT) representation of **6-6**.
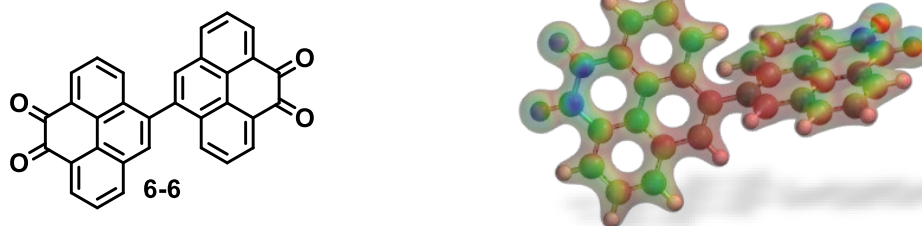
*VI-3: Left: LEWIS-formula of **6-6**. Right: Balls and sticks representation with LUMO distribution over-laid (cool colors signify high LUMO densities). The calculated dihedral angle between two pyrene units is 74°.*

According to these calculations the two pyrene units will adopt a bond angle of 74° in respect to each other. In this conformation the acceptor is no longer purely two dimensional. Yet, if the LUMO distribution is considered it becomes clear that it is strongly localized at the α-diketone functions. The ketone functions are situated along the molecule's long axis. Thus, an element of anisotropy is retained (in contrast to C_{60}). It was expected that the twisted geometry of **6-6** would improve its solubility compared to other pyrene-tetraketone derivatives. The LUMO energy is computed to $E_{LUMO,DFT} = -3.2$ eV, a value very similar to the one computed for **6-2** ($E_{LUMO,DFT} = -3.1$ eV). While not being a very strong acceptor it still falls into an interesting energy region, close to copper phthalocyanine CuPC ($E_{LUMO} = -3.5$ eV)[414] and PCBM ($E_{LUMO} = -3.7$ eV).[415]

VI.1.1 Synthesis

As discussed for pyrene-4,5,9,10-tetraone, **6-5** does not tolerate organometallic complex mediated cross coupling reaction conditions either. Thus, a reductive alkylation method was chosen for the synthesis. As established in chapter *II* for pyrene-4,5,9,10-tetraones, **6-7** was prepared by reductive alkylation as common precursor for further synthetic steps. The chemical stability of **6-7** enables purification by column chromatography to remove side products like **6-4**. Initially, the synthesis of **6-9** was attempted by YAMAMOTO-type nickel(0) mediated dimerization.[416, 417] Yields were surprisingly low (< 15 %), possibly due to steric effects. **6-8**, which was prepared for the synthesis of rylene-type molecules, enabled the synthesis of **6-9** by palladium catalyzed cross coupling reaction (SUZUKI-MIYAURA reaction). To counteract the steric hindrance of this dimerization reaction the *SPhos* ligand was employed. This system is reported to catalyze

SUZUKI-MIYAURA type reactions in sterically encumbered systems.[372, 418] Using this system **6-9** was prepared in 66% yield after column chromatography.
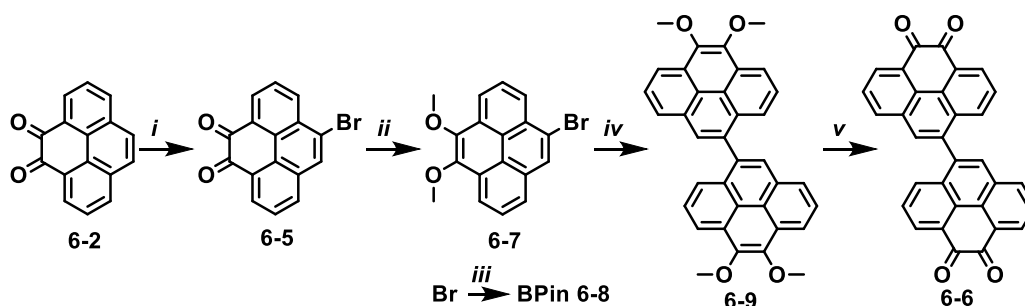

*VI-4: Synthesis of **6-6**. i: 1.1 eq. NBS, H₂SO₄, 2 h, RT, 62 %. ii: Me₂SO₄ Na₂SO₃, NaOH, THF, H₂O, 16 h, RT, 76 %. iii: B₂Pin₂, PdDPPF, NaOAc, DMF, 80 °C, 72 %. iv: SPhos, Pd₂DBA₃, Na₂CO₃, Tol, H₂O, 100 °C, 66 %. v: BBr₃, CH₂Cl₂, 2 d; THF, air, RT 1 d.*

A single crystal suitable for X-ray diffraction crystallography was grown by slow evaporation of dichloromethane. Deprotection of **6-9** by boron tribromide was performed in dichloromethane. The boron-complex precipitated from solution as a colorless solid. After two days the reaction was stopped by the addition of water. After removal of the volatiles the solid was re-dissolved in THF and stirred in air for one day. The crude product precipitated and was collected by filtration. It was washed with water and dichloromethane and subsequently recrystallized from THF. **6-6** was isolated as a red, poorly soluble solid in 23 % yield.

VI.1.2   Characterization

Compound **6-9** was identified by FD-MS (m/z) and NMR-spectroscopy.
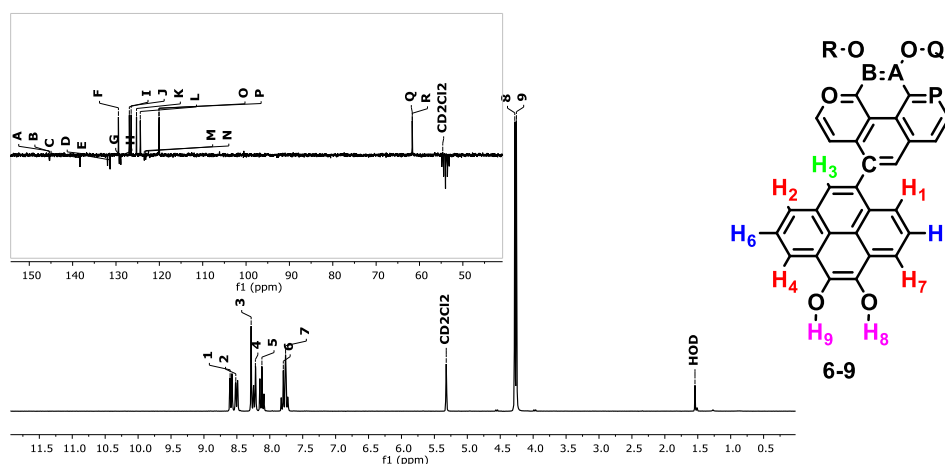
*VI-5: ¹H- (250 MHz, panel) and ¹³C-APT NMR (75 MHz, inset) spectra of **6-9** recorded in CD₂Cl₂ at 298 K.*

For the C_2 symmetric **6-9** nine signals in the proton NMR spectrum are observed. Signals *1* ($\delta = 8.59$ ppm, $J_1 = 7.7$, $J_2 = 1.2$ Hz), *2* ($\delta = 8.50$ ppm, $J_1 = 7.2$, $J_2 = 1.8$ Hz), *4* ($\delta = 8.32$ ppm, $J_1 = 7.8$ Hz, $J_2 = 1.2$ Hz) and *7* ($\delta = 7.74$ ppm, $J_1 = 7.8$, $J_2 = 1.8$ Hz) are doublets of doublets, generated by the protons in position 1,3,6 and 8 of pyrene. Signal *3*

(δ = 8.28 ppm, *s*) is assigned to the proton in 10 position. Triplets *5* (δ = 8.12, J_1 = 7.7 Hz) and *6* (δ = 7.8 ppm, J_1 = 7.8 Hz are caused by the protons in 2 and 7 position. Finally, the methoxy groups are identified by singlets *8* (δ = 4.28 ppm) and *9* (δ = 4.25 ppm).

From the ^{13}C-APT spectrum seven primary, two tertiary and nine quaternary carbon signals can be identified. The two tertiary signals *Q* (δ = 61.7 ppm) and *R* (δ = 61.6 ppm) can be assigned to the methoxy groups just as signals *A* (δ = 145.4 ppm) and *B* (δ = 145.3 ppm). Signal *C* is associated with the pyrene – pyrene bond. Other signals have not been assigned unequivocally.
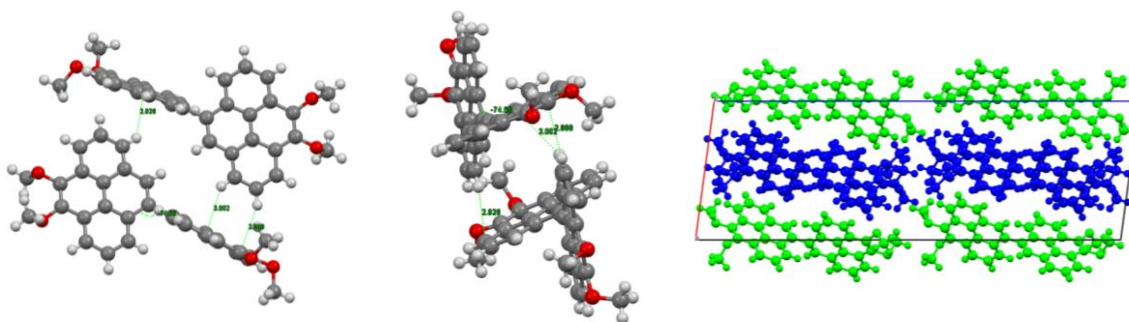
*VI-6: Solid state structure of **6-9** (single crystal X-ray diffraction crystallography). Left: Molecule viewed along a-axis. Center: Molecule viewed along c-axis. Right: Packing viewed along b-axis (colors give symmetry equivalents).*

In the solid state, **6-9** adopts a monoclinic unit cell of P 2_1/C symmetry. The large unit cell (a = 11.403 Å, b = 12.962 Å, c = 34.867 Å, V = 5107 Å^3) encompasses eight molecules. The molecules form dimers by CH-π stacking. Short contacts are found between 2.88 Å and 3.01 Å suggesting strong interactions. The two pyrene units of one molecule adopt a staggered conformation with a twist-angle of 74.5°. This is in very good agreement with the computed twist-angle in **6-6** (74°).

Low solubility allowed the characterization of **6-6** solely by MALDI-TOF mass spectroscopy. The resulting mass spectrum is shown in figure VI-7:
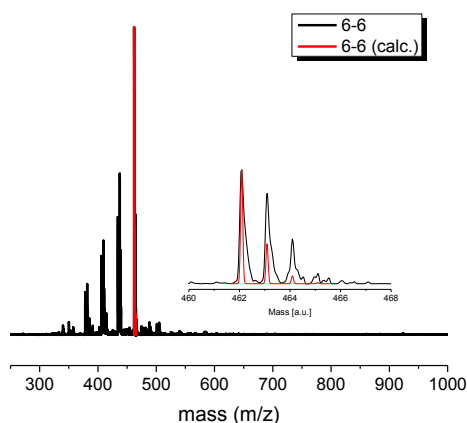

*VI-7: MALDI-TOF mass spectrum of **6-6** (black) compare to a calculated isotopic pattern of **6-6** (in red).*

The experimental mass spectrum is in very good agreement with the calculated isotopic pattern (as shown in the inset of figure VI-7). The main signals are observed at m/z = 462.086, 463.095 and 464.099 (calc. m/z = 462.089, 463.093 and 464.096). Signals are observed at m/z < 464. They are spaced by 28 Da. corresponding to the loss of carbonyl (C=O) from the molecule. This fragmentation is probably caused by high energy photons used in the MALDI process. A characterization by cyclic voltammetry was not possible due the low solubility of the product

VI.2   New rylene-type molecules

LORBACH *et al*. have shown in their study on SCHOLL-type reactions of pyrene derivatives that cyclodehydrogenation in the K-region is problematic.[99] In contrast, positions 1,3,6 and 8 show high activity in these oxidation reactions. The high orbital coefficients (HOMO) in these positions (chapter *I.2*) can be used to explain this behavior. The opposing positions (1 and 8) are activated by alkoxy-substitution in the K-region (4,5). VENKATARAMANA *et al*. utilized this for a selective bromination in these positions.[91] So far, this activation has only seldomly been exploited in SCHOLL-type reactions. LORBACH *et al*. report in their publication the cyclodehydrogenation of **6-9** to the corresponding perylene derivative **6-10**.[26] The improved solubility of **6-10** allowed an unequivocal proof by NMR spectroscopy that exclusively six-membered rings were formed. A temporarily discussed five-membered ring product (**6-11**) was thus ruled out.

6-9   **6-10**   **6-11**
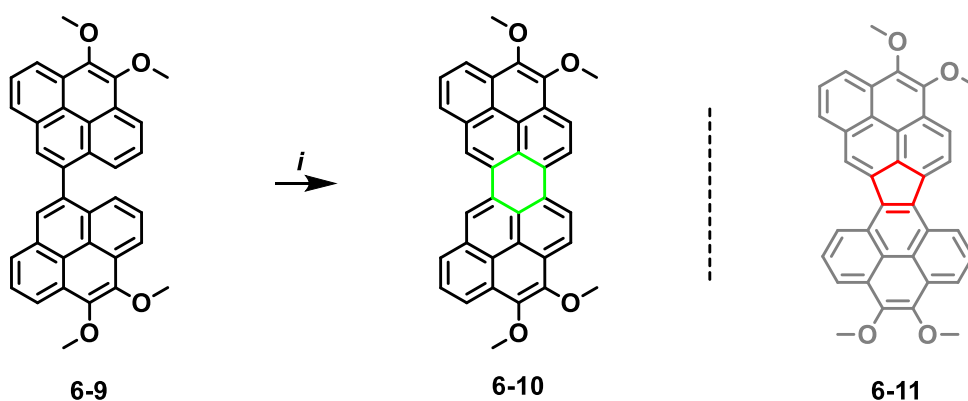
*VI-8: Cyclodehydrogenation of **6-9** reported by LORBACH. i: FeCl₃, CH₂Cl₂, MeNO₂, 30 min, RT.*

SCHOLL-type reactions have been used in the synthesis of higher rylene-type molecules.[419] To further investigate the usefulness of compound **6-8** as building block for subsequent SCHOLL-type reactions **6-13** was prepared by SUZUKI-MIYAURA-reaction. This reaction provided **6-13** as a yellow solid in good yields (78 %).

[26] **6-9** was provided by the author of this manuscript.
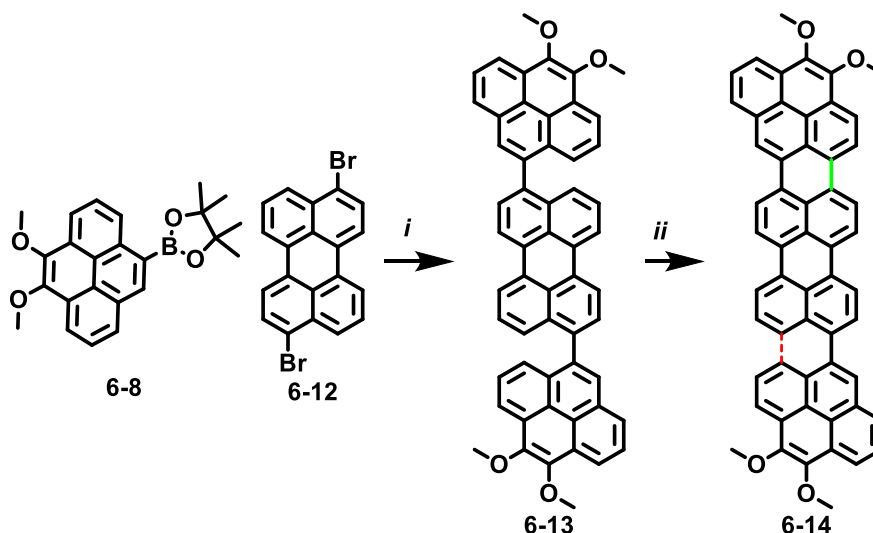
VI-9: Attempted cyclodehydrogenation of 6-13. Only one bond was formed in the reaction (indicated in green). i: Pd(PPh₃)₄, Na₂CO₃, Tol, H₂O, 100 °C, 78 %. ii: FeCl₃, CH₂Cl₂, CH₃NO₂, RT, 4 h.

In the cyclodehydrogenation reaction a color change was observed immediately after addition of the oxidant (ferrous chloride). Within minutes an insoluble solid precipitated out of the reaction mixture. It was found by MALDI-TOF mass spectroscopy that only one bond was closed in the precipitate (**6-14**). Extending the reaction time did not lead to the desired formation of the second bond (indicated in red in figure VI-9). This was attributed to the insufficient solubility of **6-14**.
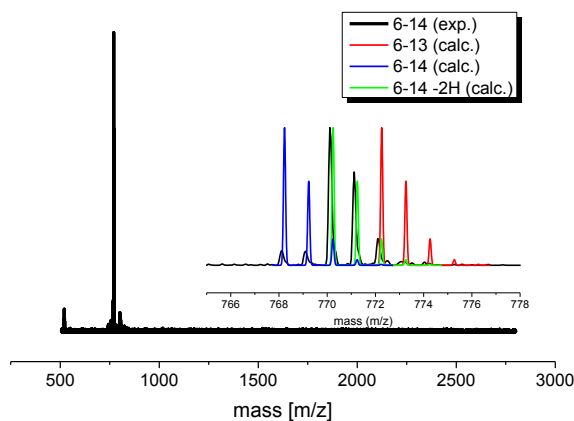
VI-10: MALDI-TOF mass spectrum of 6-14 (black). Inset: Cut-out compared to calculated isotopic patterns of 6-13 (red), 6-14 (blue) and the fully cyclodehydrogenated target compound 6-14[-2H] (green).

As can be seen in the MALDI-TOF spectrum of **6-14** (black curve in figure VI-10) the mass signal very closely matches the isotopic pattern of the suggested structure (i.e. only one C-C bond was formed, green pattern). The starting compound **6-13** is fully consumed. The spectrum overview shows that the chlorination side-reaction is precluded.
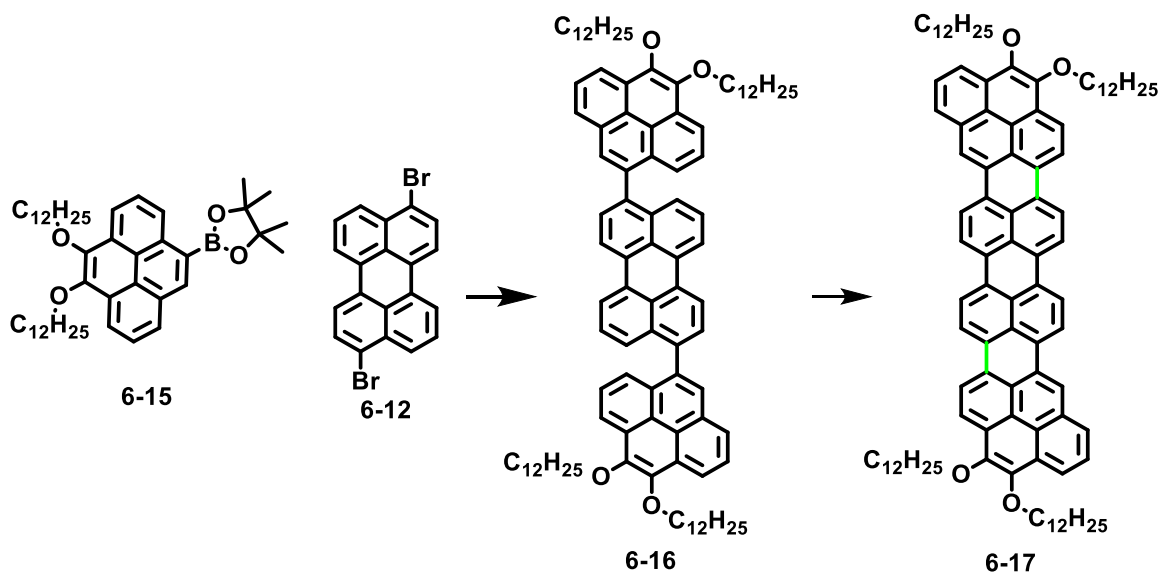
*VI-11: Pyrene-perylene-pyrene triade (**6-16**) with improved solubility. This allows full cyclodehydrogenation to **6-17**.*

To improve the solubility during the cyclodehydrogenation reaction, **6-15** was prepared and used as building block for **6-16**. It was assumed that **6-16** would act as a suitable substrate for FeCl₃ mediated SCHOLL-reaction to afford **6-17**. It was found that indeed **6-17** is formed and can be isolated from side products by size exclusion chromatography.
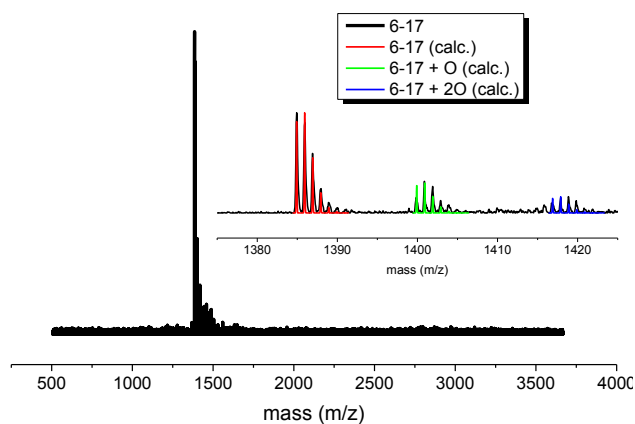
*VI-12: MALDI-TOF mass spectrum of **6-17** (black). Inset: Cut-out compared to calculated isotopic patterns of **6-17**(red), **6-17+O** (green) and **6-17+2O** (blue).*

Figure VI-12 gives the MALDI-TOF mass spectrum of **6-17** after purification. The calculated isotopic pattern for **6-17** (depicted in red) is in very good agreement with the main signal in the mass spectrum (m/z = 1384.849). Two additional signals at m/z = 1400.858 and m/z = 1416.882 are corresponding to the addition of 16 Da and 32 Da. This is consistent with the addition of one and two atoms of oxygen. The frontier orbital distribution of **6-17** according to DFT calculations is given in figure VI-13.
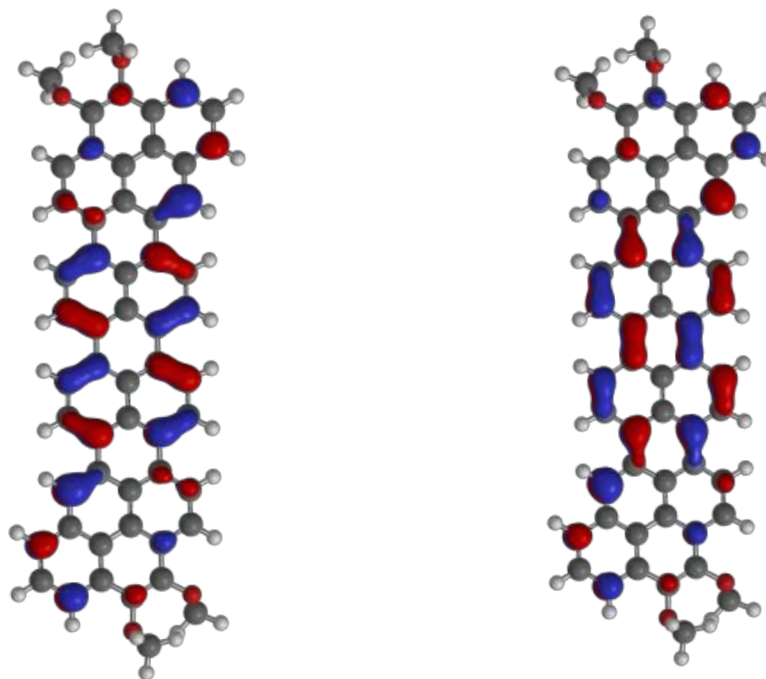
*VI-13: Frontier orbitals of **6-17** (alkyl chains have been approximated as methyl groups). Left, HOMO.*
Right: LUMO

In figure VI-13 the HOMO has a high orbital coefficient in the former pyrene-K-region
(left). The same is true for the LUMO. The calculations give a HOMO energy of
E_{HOMO} = -4.27 eV (E_{LUMO} = -2.60 eV), which is well above the -4.5 eV given by ZHAN
et al. for air tolerant OFET materials.[321]

When this is considered together with the findings from MALDI-TOF mass spectroscopy
an oxidation of **6-17** under ambient conditions is a plausible explanation for the two
additional signals in the mass spectrum. The high orbital coefficients in the
DFT calculations suggest two positions of high reactivity.

6-13 and **6-16** were fully characterized by NMR spectroscopy. The molecules give sharp
signals in the proton as well as in the carbon spectrum. In contrast to this, it was not
possible to resolve the NMR spectrum of **6-17**. Even in low concentrations
(c = 5*10^{-5} mol/l) and at elevated temperatures (393 K) only few sharp signals were
recorded. Broad, unstructured signals are observed at d = 8.2 ppm and d = 7.1 ppm. The
addition of an excess of reducing agent (hydrazine) did not help to resolve a sharp
spectrum. This suggests that molecular stacking may contribute to the signal broadening.
In the field of rylene-diimide chemistry bulky solubilizing groups
(e.g. 2,6-diisopropylphenyl) are often required to suppress molecular stacking.[420]
Introducing such sterically demanding groups into **6-5** may be problematic. Attempts to
use *tert*-butyl chloride for reductive alkylations failed for **6-5** as well as for **6-3**. The failure
is attributed in both cases to steric hindrance. For future work the use of branched alkyl-
chains may be helpful.
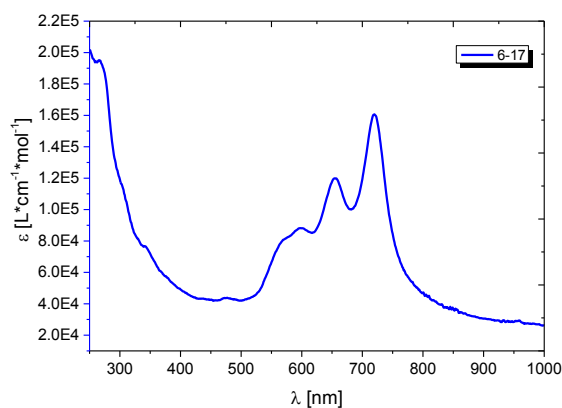
*VI-14: UV-vis absorption spectrum of **6-17** in THF.*

The UV-vis absorption spectrum of **6-17** recorded in THF is given in figure VI-14. It shows a structured absorption band with three peaks. The absorption maximum is located at λ_{max} = 720 nm. The S_0->S_2 absorption is located at 655 nm and the S_0->S_3 at 598 nm. The optical bandgap is determined to 1.63 eV and in good agreement with the theoretically predicted bandgap of $\Delta E_{calc.}$ = 1.67 eV. This spectrum resembles the absorption spectrum of quaterrylene diimide, yet its absorption maximum is located at $\lambda_{max,QDI}$ = 762 nm and the bandgap is as low as 1.40 eV.[421] The newly arisen rylene-type absorption features give further confirmation that **6-17** was prepared in the SCHOLL-type reaction.

VI.3 Summary and outlook

It has been shown in this chapter that the bromination in 4 position of pyrene-9,10-dione (**6-5**) can open new pathways of pyrene functionalization. This method complements the works of ZÖPHEL (**6-3**) as well as LORBACH on 4,10-functionalized pyrenes. In contrast to their work the approach presented here uses a monofunctional building block. This allows the targeted synthesis of dimers, e.g. **6-6**.

Compared to the approach by WALKER *et al.*[98] as implemented by LORBACH, this route gives more flexibility regarding the solubilizing group. **6-15** thus prepared was essential for the synthesis of the new quaterrylene derivative **6-17**. It is well dispersible in common organic solvents, yet the molecules have a strong tendency to form non-covalently bound aggregates in solution.

The versatility of this building block was not fully exploited. Future works in the field of rylene-type materials can easily be envisioned. Recently, the application of quaterrylene in an OFET device with thermo cleavable alkyl substituents was reported.[422]
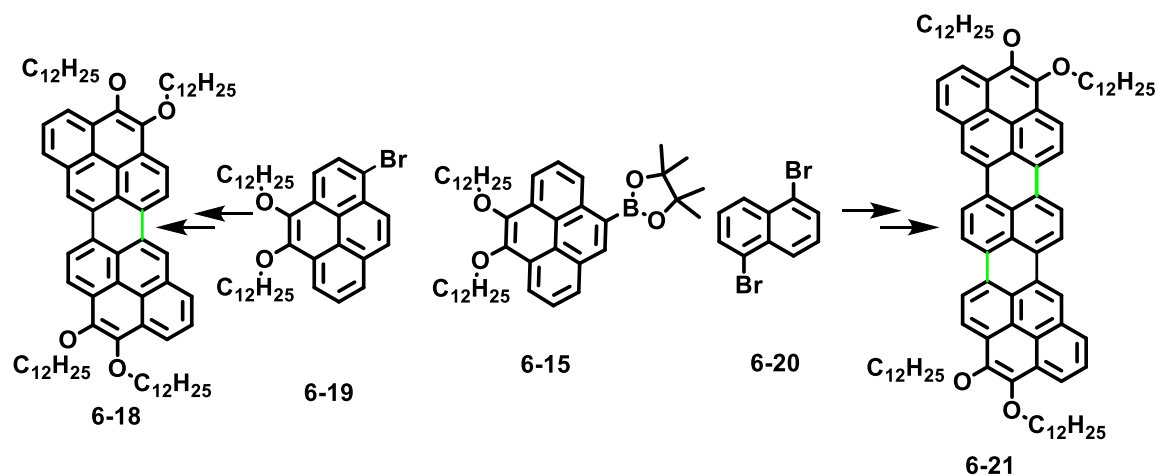
VI-15: Two possible extensions of the rylene-type molecule synthesis discussed in chapter VI.2.

Selective bromination of 4,5-dialkoxypyrenes in the 1 position provides access to **6-19**.[91] The SUZUKI coupling with **6-15** followed by a SCHOLL-type reaction can provide the dinapthto[8,8'1,1'2,2'-bcd-kml]perylene derivative **6-18**, i.e. the perylene analogue to **6-17**. Preliminary experiments indicate that the cyclodehydrogenation reaction can provide the desired product (identified in MALDI-TOF). Apparently, the reactivity of the 4 position is increased by the alkoxy substituents. **6-21** will give the corresponding terrylene derivative. By reducing the lateral extension of the molecule, the bandgap will increase.[423] Thus, **6-21** or **6-18** may be used in air-stable OFET devices.
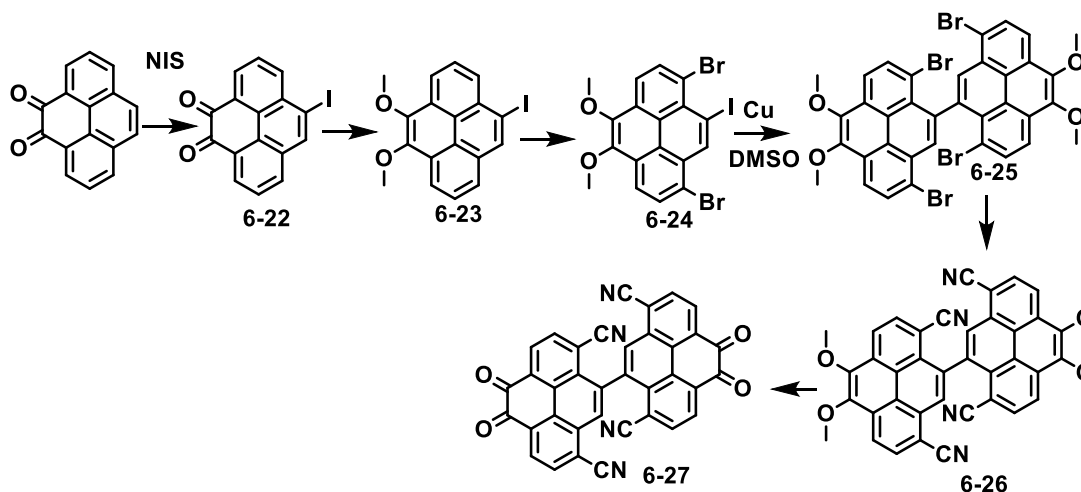
VI-16: Possible extension of 4,4'-bipyrene-9,9,10,10-tetraketone acceptor.

The acceptor strength of **6-6** might be improved by introducing additional electron withdrawing substituents. Selective bromination of 4,5-dialkoxypyrene (**6-23**) will provide access to **6-24**. The iodine substituent allows chemoselective C-C bond formation by ULLMANN-reaction to afford **6-25**. The bromine substituents can be used to introduce additional electron withdrawing groups (in this example nitrile). In a final step, the diketone is formed in a deprotection/oxidation step. The nitriles in this example not only lower the LUMO energy of **6-27** but will also enlarge the twist-angle between the two

pyrene units due to steric demand. In contrast to the failed synthesis of the 1,3,6,8-tetracyanopyrene-4,5,9,10-tetraone (chapter *III*) the deprotection/oxidation step should not be problematic as **6-27** is a weaker acceptor. Thus, the deprotection as well as the oxidation should proceed as in the case of 2,7-dicyanopyrene-4,5,9,10-tetraone.

It was shown that the simple 4,9,10-functionalization of pyrene can give rise to new molecular structures, thus far unattainable. Therefore this, so far overlooked, approach merits further investigation.

VII.   Conclusion

Almost 200 years have passed since its first description but still pyrene enjoys unbroken interest by chemists around the world. For 2014 alone more than 1500 publications are registered in the scientific search engine *Thomson Reuters* "Web of Science™". To a large extend this can be attributed to its interesting photophysical properties which can be exploited in biochemistry or material science.[424-428] [429-432]

The focus of this work was the synthesis of pyrene based acceptors and donors. In chapter *II* the 2,4,5,7,9,10-substitution pattern was investigated as a possible access to very strong acceptors with quinoid pyrene scaffold. It was not possible to isolate a stable quinoid pyrene derivative. A tendency for oligomerization as well as low solubility resulted in the failure of this endeavor. With **2-34** a new non-quinoidal pyrene-4,5,9,10-tetraone acceptor pigment was synthesized. Exploiting the good availability and high stability of 2,7-diiodo-4,5,9,10-tetramethoxypyrene a series of laterally extended electron rich molecules have been derived.

The synthetic approaches to a non-quinoidal, strong pyrene-4,5,9,10-tetraone based acceptor (1,3,6,8-tetracyanopyrene-4,5,9,10-tetraone, **3-29**) have been discussed in chapter *III*. In the course of this work, it emerged that the deprotection/reoxidation reaction procedure failed on electron deficient pyrene derivatives such as **3-16** and also on the less electron deficient **3-34**. Only **3-18** was successfully converted to the corresponding tetraketone **3-32**. Its experimental LUMO energy (E_{LUMO} = -4.2 eV) identifies **3-32** only as an intermediate acceptor. Therefore, it can be concluded that the chosen synthetic approach of reductive protection which was later followed by deprotection/reoxidation step is not suitable to prepare strong acceptors. The variation of the protection scheme was not compatible with the desired pyrene-4,5,9,10-tetraone substitution pattern.

In contrast, novel 1,3,6,8-substitued donors based on 4,5,9,10-tetramethoxypyrene have been presented in chapter *III*. 1,3,4,5,7,8,9,10-Octamethoxypyrene (**3-13**) as well as **3-14** have been characterized and later studied in CT-complexes in combination with TCNQ-type acceptors, as reported in section *IV*. Therein also the successes of the SFB/TR 49 collaboration were discussed. For the first time the electronic excitation in a non-TTF CT-complex was studied by HAXPES and NEXAFS.

Pyrene and its selective functionalization remain a fascinating challenge for synthetic chemists as well. A series of new protocols have been developed recently. Still, to this day, not all positions of pyrene can be addressed specifically.[28]

1,3,4,5,6,8,9,10-octa functionalization
Chaper III

4,9,10-tri functionalization
Chaper VI
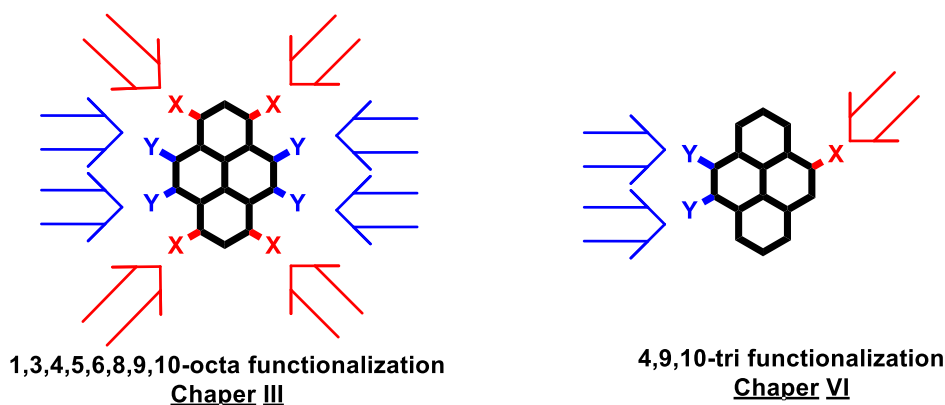
VII-1: New pyrene substitution patterns discussed in this work.

In this work, two new patterns of pyrene substitution have been developed. The synthesis of eightfold functionalized pyrenes was established and utilized in chapter *III*. It was shown that under suitable conditions a fourfold bromination of 4,5,9,10-tetramethoxypyrene is possible and a series of 1,3,4,5,6,8,9,10-substituted pyrene derivatives was achieved. By modifying the conditions reported by ZöPHEL *et al*. it was possible to obtain an asymmetric 4,9,10-substituted pyrene derivative. This has been utilized in chapter *VI* to prepare a non-planar acceptor molecule, [4,4'-bipyrene]-9,9',10,10'-tetraone (**6-6**). The asymmetric functionalization also allowed the synthesis of rylene-type molecules (**6-14** and **6-17**) by SCHOLL-type cyclodehydrogenation reactions. The flexible alkoxy-protection scheme allowed the introduction of solubilizing groups. This proved essential for the synthesis of **6-17**.

OD series   *Py series*
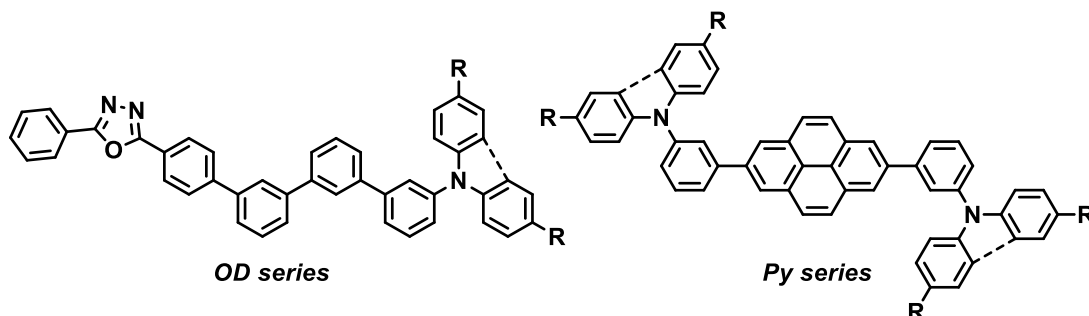
VII-2: Molecules designed as OLED emitters, as investigated in the IRTG 1404 collaboration.

Finally, two separate series of molecules intended as emitters for OLEDs were presented in chapter *V*. The molecules were designed to have a minimal singlet triplet energy gap ($\Delta E_{S1 \to T1}$) while retaining a high fluorescence quantum yield ϕ_{PL} and a deep blue emission spectrum. Thermally activated delayed fluorescence (TADF) in OLEDs attracted significant academic interest since it was first reported in 2011. TADF is considered a promising apporach to improve the efficiency of fluorescent OLEDs by harvesting triplet states as fluorescent emission quanta. A small $\Delta E_{S1 \to T1}$ is a prerequisite for TADF.

The *OD series* has a small $\Delta E_{S1 \to T1}$ (as established for **5-11**) yet, failed to provide a sufficient ϕ_{PL} for the use in OLEDs. The *Py series* emitters, in contrast, combine both desired properties and were successfully implemented in efficient OLED devices. Strong evidences for the harvesting of triplet-states are found. The mechanism thereof is yet under investigation.

VIII. Experimental Section

VIII.1 General methods

VIII.1.1 Chemicals and solvents

Chemicals and solvents used in this work were obtained from the companies *ABCR*, *Acros Organics*, *Alfa-Aesar*, *Bio-Rad Laboratories*, *Fluka*, *Merck KGaA*, *Sigma-Aldrich*, *Strem Chemicals* and *TCI Europe*. Unless otherwise mentioned, they were used as received without further purification.

VIII.1.2 Chromatography

Preparative column chromatography was performed using silica gel purchased from *Macherey-Nagel GmbH & Co. KG* and *Merck KGaA* with a grain size of 40−63 µm (flash silica gel) or 63−200 µm (silica gel). For analytical thin layer chromatography (TLC), silica gel "60 F$_{254}$" pre-coated on aluminium substrates procured from *Merck KGaA* were used. Compounds were detected by fluorescence quenching at 254 nm or UV-B (366 nm) self-fluorescence. Gel permeation chromatography was done using *BioBeads X10* GPC material provided by *Bio-Rad Laboratories*. Analytically pure solvents (p.a. or technical grade) were used as eluents.

VIII.1.3 Microwave-assisted synthesis

Microwave-assisted reactions were performed in a microwave reactor type *Discover (CEM GmbH)*. Reactions were typically run under temperature control regime (300 W heating power, air jet cooling of the glass reaction vessel). Internal pressures up to 14 bars were measured in the sealed reaction vessels.

VIII.1.4   Inert atmosphere

Oxygen- or moisture-sensitive reactions were carried out under argon atmosphere (*Westfalen AG,* grade 4.8). Unless stated otherwise, reactions were degassed by purging the reaction mixture with a stream of argon.

VIII.2   Analytical methods

VIII.2.1   Electron spin resonance spectroscopy (ESR)

ESR spectra were recorded using an X-band spectrometer *ESP300 E* (*Bruker GmbH*), equipped with an NMR gaussmeter *ER035* (*Bruker GmbH*), a frequency counter *ER041XK* (*Bruker GmbH*) and a variable temperature control continuous flow N_2 cryostat *B-VT 2000* (*Bruker GmbH*). Samples were either degassed solutions at a concentration of ~10^{-6} M or small crystallites. The g-factor corrections were obtained using the DPPH (g = 2.0037) as a standard.

VIII.2.2   Elemental analysis

Elemental analysis of solid samples was carried out on a *Vario EL* machine (*Foss Heraeus GmbH*) as a service measurement at the Institute for Organic Chemistry, Johannes-Gutenberg-Universität, Mainz. All samples were dried under vacuum in order to remove possible residues of solvent molecules and humidity. Values for some samples show higher variance than 0.40% from calculated values. The entrapment of solvent molecules and atmospheric gases such as CO_2 is a common phenomenon in the analysis of aromatic hydrocarbons.

VIII.2.3   Emission spectroscopy

Solution emission spectra were recorded at room temperature on a *TIDAS* spectrofluorometer (*J&M GmbH*). Analytical grade solvents were employed. Cuvettes made from *QS grade* Quartz (*Hellma GmbH & Co. KG*) were used for the experiments.

Film experiments were performed using the integrating sphere method in combination with an in-house built spectrofluorometer set-up in the organic photonics laboratory (OPL) at Seoul National University, Rep. of Korea.

VIII.2.4   Mass spectrometry

Field-desorption (FD) mass spectrometry was performed on a *ZAB 2 SE-FPD* spectrometer *(VG Instruments, Inc.)*.

MALDI-TOF mass spectrometry was conducted using a *Reflex II-TOF* spectrometer (*Bruker Daltonics GmbH*). The machine utilizes a 337 nm nitrogen laser. If not stated otherwise 1,8-dihydroxyanthracen-9(10H)-one (*dithranol*) or tetracyanoquinodimethane (TCNQ) was used as the matrix substance.

High resolution (HR) mass spectrometry was performed on a *maXis ESI-Q-TOF* system (*Bruker Daltonics GmbH*). The instrument was operated in wide pass quadrupole mode, for MS experiments, with the TOF data being collected between m/z 100–5000 with low-collision energy of 10-15 eV.

VIII.2.5   Melting point

Melting points were determined using a *Melting Point B-545 (Büchi Labortechnik AG)* apparatus under ambient atmosphere. Values reported are uncorrected.

VIII.2.6   Nuclear magnetic resonance spectroscopy

^{1}H-NMR, ^{13}C-NMR, H,H-COSY and C,H-COSY spectra were measured on *DPX 250, AMX 300, DRX 500* or *DRX 700* spectrometer (*Bruker GmbH*) in various deuterated solvents and at temperatures. The respective conditions are stated. Spectra were referenced as follows from the deuterated solvents: for $CHDCl_2$ $\delta(^1H) = 5.32$ ppm and CD_2Cl_2 $\delta(^{13}C) = 54.00$ ppm; for $CHCl_3$ $\delta(^1H) = 7.26$ ppm and $\delta(^{13}C) = 77.16$ ppm; for THF-d7H $\delta(^1H$, low field signal$) = 3.58$ ppm and THF-d8 $\delta(^{13}C$, low field signal$) = 67.57$ ppm; for C_2HDCl_4 $\delta(^1H) = 6.0$ ppm and $C_2D_2Cl_4$ $\delta(^{13}C) = 73.78$ ppm; for DMSO-d5H $\delta(^1H) = 2.50$ ppm and DMSO-d6 $\delta(^{13}C) = 39.52$ ppm. The temperature dependent experiments were performed between 298 and 393 K and regulated by a standard ^{1}H-methanol (low temperature) and glycol (high temperature) NMR sample.

VIII.2.7   UV-vis spectroscopy

A *Lambda 900* UV/Vis/NIR spectrometer (*Perkin-Elmer, Inc.*) was used for recording the spectra. Unless stated otherwise, a sample concentration of $1*10^{-5}$ mol$*$L^{-1} was used. The molar extinction ε is given in the unit L$*$mol$^{-1}*$cm^{-1}. Solvents of spectroscopic grade were used. Baseline correction was performed by subtracting the absorption measured for the cuvette filled with the neat solvent. Cuvettes made from *QS grade* quartz (*Hellma GmbH & Co. KG*) were used for the experiments.

VIII.2.8   Single crystal X-ray diffraction crystallography

Single crystal X-ray diffraction measurements were carried out by PD. Dr. V. ENKELMANN (Max Planck Institute for Polymer Research, Mainz) at 120 K with Mo Kα radiation (λ = 0.71073 Å) on a *KappaCCD* diffractometer (*Bruker Nonius B. V.*). The structure was solved by direct methods and refined on F by full-matrix least-squares cycles.

VIII.2.9   Voltammetry

Cyclic voltammetry was measured on a *Parstat 2273* instrument (*Princeton Applied Research, Inc*.) in anhydrous solvent under argon atmosphere in a total volume of 2 mL. Recrystallized and dried tetrabutylammonium hexafluorophosphate (Bu_4NPF_6) was used as conductive salt at 0.1 M concentration. To a 1 mM solution of the sample compound ferrocene was added as internal standard (0.5 mM). A platinum or glassy carbon working electrode (0.5 mm diameter), a platinum wire as counter electrode and a silver wire as quasireference electrode were applied. Scan rates are reported for the respective measurement. The voltammograms were calibrated according to the half-wave potential of ferrocene. $U_{onset}Fc/Fc^+$ = 0.63 V vs. normal hydrogen electrode (NHE) and E^0_{NHE} = -4.6 eV vs. vacuum.[377] The onset potentials were determined for the evaluation of the frontier orbital energy.

VIII.3   Synthesis

VIII.3.1   2,7-functionalized pyrene derivatives

VIII.3.1.1   Pyrene-4,5,9,10-tetraone (2-2)
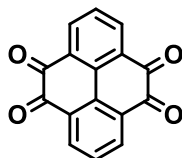
2-2

Pyrene-4,5,9,10-tetraone was prepared according to a modified procedure reported by HU *et al.* [59, 377]

MS (FD, 8KV):m/z 262.1 (100 %, M$^+$), calculated 262.02 g/mol.
^{1}H-NMR (250 MHz, DMSO-d$_6$): δ 8.34 (d, J = 7.7, 4H), 7.75 (t, J = 7.7, 2H).

VIII.3.1.2   2,7-Dibromopyrene-4,5,9,10-tetraone (2-3)
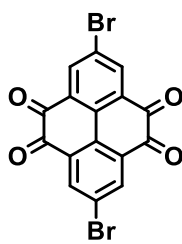
2-3

In a 25 mL Schlenk-flask pyrene-4,5,9,10-tetraone (**2-2**) (0.20 g, 0.76 mmol) was dissolved in H$_2$SO$_4$ (3 mL). N-Bromosuccinimide (0.30 g, 1.7 mmol) was added and the resulting mixture stirred at 40 °C for 4 h. The reaction mixture was poured onto water (100 mL), the precipitate was collected by filtration. The crude product was washed (water, ethanol, DCM and THF) and dried under high vacuum yielding the title compound a yellow solid (0.25 g, 78 %.).

Mp: 260 °C, (decomp.)
FD-MS (8 KV): m/z 420.1 (100 %, M$^+$), calculated 420.0.
^{1}H-NMR (C$_2$D$_2$Cl$_4$, 500 MHz, 140 °C): δ = 8.61 (s, 4H).
^{13}C-NMR (THF-d$_8$, 175 MHz): δ = 125.9, 133.4, 134.8, 137.6, 176.3.
Elemental analysis (%) found C, 46.04; H, 1.39; calculated C16H4Br2O4 C, 45.75; H, 0.96.

VIII.3.1.3   2,7-Diiodopyrene-4,5,9,10-tetraone (2-4)

2-4
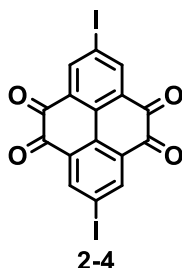
In a 25 mL Schlenk-flask, pyrene-4,5,9,10-tetraone (**2-2**) (0.20 g, 0.76 mmol) was dissolved in H_2SO_4 (3 mL). N-Iodosuccinimide (0.67 g, 3 mmol) was added and the resulting mixture stirred at 40 °C for 3 h. The reaction mixture was poured onto water (100 mL) and the precipitate was collected by filtration. The crude product was washed (water, ethanol, DCM and THF) than dried under high vacuum yielding the title compound as an orange solid (280 mg, 72 %).

Mp: 246 °C, (decomp.)
FD-MS (8 KV): m/z 513,4 (100 %, M$^+$), calculated 513.8.
^{1}H-NMR (THF-d$_8$, 300 MHz):δ = 8.5 (s, 4H).
^{13}C-NMR (THF-d$_8$, 75 MHz): δ = 125.6, 133.1, 134.6, 137.0, 175.9.
Elemental analysis (%) found C, 38.82; H, 0.77 calculated C16H4I2O4 C, 37.39; H, 0.78.

VIII.3.1.4   2,7-Diiodo-4,5,9,10-tetramethoxypyrene (2-5)

2-5
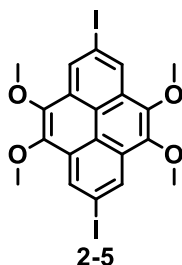
A mixture of 2,7-diiodopyrene-4,5,9,10-tetraone (**2-4**) (0.35 g, 0.68 mmol), *n*-Bu₄NBr (0.18 g, 0.50 mmol), Na₂S₂O₄ (0.82 g, 4.7 mmol), THF (5 mL) and water (3 mL) was stirred at 25 °C for 5 min. Dimethyl sulfate (0.78 g, 6.8 mmol) and a aqueous sodium hydroxide solution (2 mL, 18 mmol) were added and the mixture stirred at 40 °C for 4 h. Toluene and water were added and the resulting mixture extracted with toluene (50 mL × 3). The combined organic phases were washed with sat. NaCl solution (50 mL × 3), dried with MgSO₄ filtered and concentrated *in vacuo*. The residue was subjected to column chromatography (silica, 4:1 Hex/DCM). The product was dried under high vacuum yielding the title compound as a colorless solid (160 mg, 41 %).
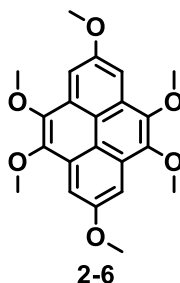
Mp: 240-243 °C
FD-MS (8 KV): m/z 573.3 (100 %, M$^+$), calculated 573.9.
^{1}H-NMR (CD₂Cl₂, 300 MHz): δ = 4.16 (s, 12H), 8.74 (s, 4H).
^{13}C-NMR (CD₂Cl₂, 75 MHz): δ = 61.8, 93.4, 119.8, 128.3, 130.4, 144.7

Elemental analysis (%) found C, 41.78; H, 2.84 calculated C20H16I2O4 C, 41.84; H, 2.81

VIII.3.1.5   2,4,5,7,9,10-Hexamethoxypyrene (2-6)

2-6

In a 100 mL flame-dried Schlenk-flask 2,7-diodo-4,5,9,10-tetramethoxypyrene (**2-5**) (1 g, 1.74 mmol) was dissolved in 40 mL anhydrous DMF and 15 mL anhydrous toluene at elevated temperatures ($\approx$ 65 ºC). Copper iodide (0.1 g, 0.52 mmol) and subsequently 2 mL anhydrous sodium methylate solution in methanol (30 vol.%) were added. The mixture was stirred 6 h at 100 ºC. After cooling, the reaction crude was poured onto ice water and extracted with CH_2Cl_2 (100 mL×3). The combined organic phases were washed with water (150 mL×3), sat. NaCl solution (150 mL) dried over Na_2SO_4 and filtered. The solvent was removed *in vacuo*. The residue subjected to column chromatography (toluene) and dried under high vacuum yielding the title compound as a colorless solid (220 mg, 33 %).

Mp: 190.5 °C
FD-MS (8 KV): m/z 382.5 (100 %, M$^+$), calculated 382.1
^{1}**H-NMR** (CD_2Cl_2, 250 MHz): δ = 7.91 (s, 4H), 4.16 (s, 12H), 4.10 (s, 6H)
^{13}**C-NMR** (CD_2Cl_2, 75 MHz): δ = 158.56, 145.4, 129.4, 116.7, 105.2, 61.6
Elemental analysis (%) found C, 68.52; H, 6.13 calculated C22H22O6 C, 69.1; H, 5.89
UV-vis [λ / nm, (ε / l*mol^{-1}*cm $^{-1}$)]: 323 (3,7*10^3), 338 (8,3*10^3), 354 (1,2*10^4), 378 (1,4*10^3), 399 (2,2*10^3).
Crystallographic data (CCDC deposition number): CCDC 857535
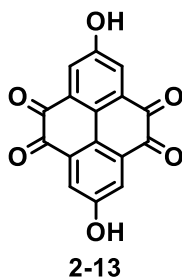
VIII.3.1.6   2,4,5,7,9,10-Hexahydroxypyrene (2-12)
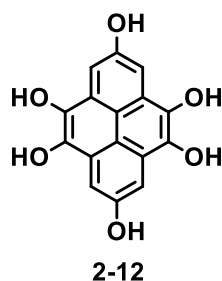
2-12

In a 100 mL flame-dried Schlenk-flask 2,4,5,7,9,10-hexamethoxypyrene (**2-6**) (100 mg, 0.26 mmol) was dissolved in 10 mL anhydrous CH_2Cl_2. At 0 °C (ice bath) borontribromide (3.14 mL 1 M solution in CH_2Cl_2, 3.14 mmol) was added. The mixture was allowed to warm to room temperature and stirred for 24 h. The reaction was quenched by the addition of water (50 mL) and extracted with CH_2Cl_2 (15 mL×3). The combined organic phases

were washed with sat. NaCl solution and the solvent removed *in vacuo*. The residue was subjected to size exclusion chromatography (BioBeads S-X1; THF) yielding the title compound as a colorless solid (12 mg, 15 %). It was not longtime stabile in air (< 1h).

FD-MS (8 KV): m/z 298.0 (100 %, M$^+$), calculated 298.1
MALDI-TOF: m/z = 297.84 (100 %), 298.84 (36 %) calculated 298.05, 299.05 (17 %)

VIII.3.1.7   2,7-Dihydroxypyrene-4,5,9,10-pyrenetetraone (2-13)

2-13

In a 100 mL flame-dried Schlenk-flask 2,4,5,7,9,10-hexamethoxypyrene (**2-6**) (100 mg, 0.26 mmol) was dissolved in 10 mL anhydrous CH_2Cl_2. At 0 °C (ice bath) borontribromide (3.14 mL, 1 M solution in CH_2Cl_2, 3.14 mmol) was added. The mixture was allowed to warm to room temperature and stirred for 24 h. The reaction was quenched by the addition of water (50 mL) and extracted with CH_2Cl_2 (15 mL×3). The combined organic phases were washed with sat. NaCl solution, dried with $MgSO_4$ and filtered. The solvent was evaporated *in vacuo*. The residue was picked up in 25 mL THF and stirred in air for 48 h, the solvent was evaporated *in vacuo*. The crude product was subjected to repeated to size exclusion chromatography (BioBeads S-X1; THF) yielding the title compound as a red solid (7 mg, 9 %).
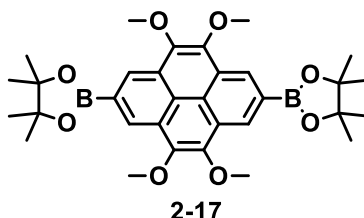
FD-MS (8 KV): m/z 293.8 (100 %, M$^+$), calculated 294.0
MALDI-TOF: m/z = 294.78 (100 %), 295.78 (10 %) calculated 294.04, 295.04 (17 %)
^{1}H-NMR (300 MHz, DMSO-d$_6$): δ 7.55 (s, 4H), 10.62 (s, 2H).
^{13}C-NMR (75 MHz, DMSO-d$_6$): δ 120.5, 126.6, 132.0, 157.7, 177.3.

VIII.3.1.8   2,2'-(4,5,9,10-Tetramethoxypyrene-2,7-diyl)bis(4,4,5,5-tetramethyl-1,3,2-dioxaborolane) (2-17)

2-17

In a 50 mL flame-dried Schlenk-flask 2,7-diodo-4,5,9,10-tetramethoxypyrene (**2-5**) (250 mg, 0.43 mmol), bis(pinacolato)diboron (442.3 mg, 1,7 mmol), potassium acetate (188 mg, 1.9 mmol) and [1,1′-bis(diphenylphosphino)ferrocene]dichloropalladium(II) (21.5 umol) were dissolved in anhydrous dioxane (20 mL) and stirred 16 h at 90 °C. After

cooling the mixture was poured onto sat. NaCl solution (200 mL) and extracted with CH$_2$Cl$_2$ (50 mL×3). The combined organic phases were washed with sat. NaCl solution (50 mL) dried with MgSO$_4$ and filtered. The solvent was removed *in vacuo*. The residue was subjected to column chromatography (silica/ CH$_2$Cl$_2$) yielding the title compound as a colorless solid (191 mg, 76 %).
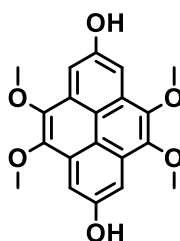
Mp: 167 °C (decomp.)
FD-MS (8 KV): m/z 574.3 (100 %, M$^+$), calculated 574.3
^{1}H-NMR (300 MHz, CD$_2$Cl$_2$): δ 1.36 (s, 24H), 4.12 (s, 12H), 8.71 (s, 4H).
^{13}C-NMR (75 MHz, CD$_2$Cl$_2$): δ 25.4, 61.6, 84.7, 122.8, 125.3, 128.5, 145.3.
Elemental analysis (%) found C, 69.34; H, 4.68 calculated C32H40B2O8 C, 66.93; H, 7.02.

VIII.3.1.9   4,5,9,10-Tetramethoxypyrene-2,7-diol (2-18)

2-18

In a 50 mL flame-dried Schlenk-flask 2,2'-(4,5,9,10-tetramethoxypyrene-2,7-diyl)bis(4,4,5,5-tetramethyl-1,3,2-dioxaborolane) (**2-17**) was dissolved in 35 mL THF. Finely ground sodium hydroxide (0.1 g) and hydrogen peroxide solution (30%; 10 mL) were added. The mixture was stirred for 3 h at room temperature. The mixture was poured on sat. NaCl solution (50 mL) and acidified with HCl to pH = 2 and extracted with THF (50 mL×3). The combined organic phases were dried with MgSO$_4$ and filtered. The solvent was removed *in vacuo*. The crude product was subjected to column chromatography (silica; Hex/EE 2:1) yielding the title compound as a colorless solid (32 mg, 42 %).

FD-MS (8 KV): m/z 354.1 (100 %, M$^+$), calculated 354.1
^{1}H-NMR (250 MHz, DMSO-d$_6$): δ 4.06 (s, 12H), 7.70 (s, 4H), 10.03 (s, 2H).
^{13}C-NMR (63 MHz, DMSO-d$_6$): δ 60.8, 105.9, 114.8, 127.9, 144.0, 155.4.

VIII.3.1.10   N2,N7-bis(4-hexylphenyl)-4,5,9,10-tetramethoxypyrene-2,7-diamine (2-20)
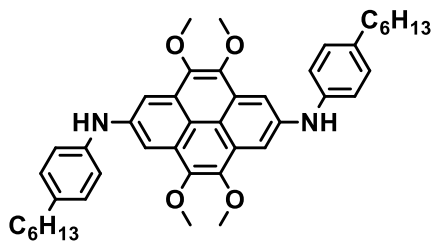
2-20

In a 25 mL flame-dried Schlenk-flask 2,7-diodo-4,5,9,10-tetramethoxypyrene **2-5** (40 mg, 66.9 μmol), 4-hexylaniline (142.3 mg, 0.8 mmol), potassium *tert*-butoxide (112.6 mg, 1 mmol), bis(2-diphenylphosphinophenyl)ether (*DPEphos*) (3.6 mg, 6.7 μmol) and palladium (II) acetate (0,75 mg, 3.3 μmol) were dissolved in 5 mL anhydrous toluene and stirred at 100°C for 16 h. The cooled mixture was poured on 100 mL water and extracted with CH_2Cl_2 (15 mL×3). The combined organic phases were washed with sat. NaCl solution, dried with $MgSO_4$ and filtered. The solvent was removed *in vacuo,* the residue subjected to column chromatography (silica, Hex/EE 10:1 to 3:1) yielding the title compound as a yellow crystalline solid (41 mg, 89 %). Crystals suitable for X-ray analysis were grown by slow evaporation of CH_2Cl_2.

Mp: 164-168 °C
FD-MS (8 KV): m/z 672.1 (100 %, M$^+$), calculated 672.4
^{1}H-NMR (300 MHz, CD_2Cl_2): δ 7.57 (s, 4H), 7.18 (dd, *J* = 9.4, 3.2 Hz, 1H), 6.17 (s, 2H), 2.59 (s, 1H), 1.87 (s, 13H), 1.65 (s, 3H), 1.32 (s, 1H), 0.89 (s, 1H).
^{13}C-NMR (75 MHz, CD_2Cl_2): δ 142.56 , 140.85 , 138.41 , 137.65 , 129.91 , 121.83 , 120.07 , 119.92 , 113.67 , 104.33 , 35.90 , 32.37 , 32.30 , 26.40 , 23.24 , 14.46 .
Crystallographic data (CCDC deposition number): CCDC 1025659

VIII.3.1.11   2-(7-Iodo-4,5,9,10-tetramethoxypyren-2-yl)malononitrile (2-21)
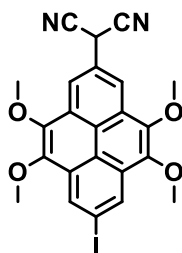
2-21

In a 50 mL flame-dried Schlenk-flask malononitrile (73 mg, 1.1 mmol) was dissolved in anhydrous toluene and sodium hydride (60% dispersion in mineral oil; 104 mg, 2.6 mmol) carefully added. The mixture was stirred at room temperature until the gas evolution abated. 2,7-Diodo-4,5,9,10-tetramethoxypyrene **(2-5)** (300 mg, 0.52 mmol) and bis(triphenylphosphine)palladium(II) dichloride (36.7 mg, 52.2 μmol) were added in argon counter-flow. The resulting mixture was stirred at 55 °C for 48 h. After cooling to room

temperature the suspension was poured onto 400 mL 5% HCl solution and extracted with CH_2Cl_2 (100 mL×3). 400 mL sat. NaCl solution was added to the aqueous phase and extracted with THF (150 mL×3). The organic phases were combined, washed with sat. NaCl solution (200 mL×2) and dried with $MgSO_4$. The solvent was evaporated, the residue was subjected to column chromatography (silica; Hex/EE 1:0 to 1:1) yielding the title compound as a colorless solid (144 mg, 54 %).
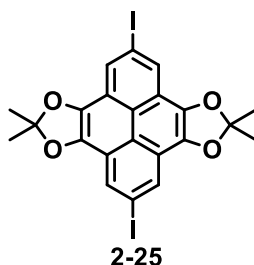
Mp: 134 °C, (decomp.)
FD-MS (8 KV): m/z 512.6 (100 %, M^+), calculated 512.3
^{1}H-NMR (300 MHz, CD_2Cl_2): δ 4.19 (s, 6H), 4.21 (s, 6H), 5.61 (s, 1H), 8.53 (s, 2H), 8.81 (s, 2H).
^{13}C-NMR (75 MHz, CD_2Cl_2): δ 29.7, 61.8, 118.0, 118.0, 128.8, 130.3, 130.7, 131.6.

VIII.3.1.12   2,8-Diiodo-5,5,11,11-tetramethylpyreno[4,5-d:9,10-d']bis([1,3]dioxole) (2-25)

2-25

In a 1000 mL Schlenk-flask 2,7-diiodopyrene-4,5,9,10-tetraone (**2-4**) (3.2 g, 6.2 mmol) was suspended in a mixture of H_2O (250 mL), acetonitrile (250 mL) and THF (250 mL). After degassing (freeze-pump-thaw cycling ×3) 2-nitropropane (4.4 g, 49.8 mmol) and sodium carbonate were added in rapid succession. The mixture was stirred at 60 °C for 16h. After cooling organic solvents were removed *in vacuo*. The residue was diluted with 250 mL sat. NaCl solution and extracted with CH_2Cl_2 (250 mL×3). The combined organic phases were washed with sat. NaCl solution, dried with $MgSO_4$ and filtered. The solvent was removed *in vacuo*, the residue subjected to column chromatography (silica; PE / DCM 5:1) yielding the title compound as a yellow solid (1.3 g, 35 %).
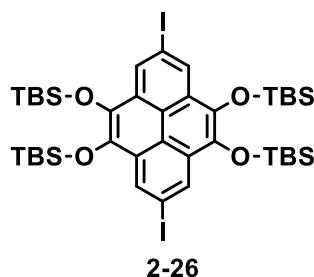
Mp: 244 °C, (decomp.)
FD-MS (8 KV): m/z 598.1 (100 %, M^+), calculated 597.9
^{1}H-NMR (500 MHz, THF-d_8): δ 1.90 (d, *J* = 2.7 Hz, 12H), 7.91 – 8.48 (m, 4H).
^{13}C-NMR (126 MHz, THF-d_8): δ 25.4, 26.1, 92.7, 116.5, 119.4, 121.8, 123.2, 125.5, 138.8.
Elemental analysis (%) found C, 44.22; H, 2.91; C22H16I2O4 C, 44.17; H, 2.70

VIII.3.1.13   ((2,7-Diiodopyrene-4,5,9,10-tetrayl)tetrakis(oxy))tetrakis(*tert*-butyldimethylsilane) (2-26)

2-26

In a 250 mL flame-dried Schlenk-flask 2,7-diiodopyrene-4,5,9,10-tetraone (**2-4**) (0.60 g, 1.2 mmol) and zinc powder (2.3 g, 35 mmol) were suspended in anhydrous 100 mL CH_2Cl_2 and stirred for 20 min. at room temperature. *Tert*-butylchlorodimethylsilane (1.76 g, 11.7 mmol) and N,N,N′,N′-tetramethylethylenediamine (2.1 mL, 14.0 mmol) were added and the mixture stirred under reflux 20 h. The cooled mixture was filtered through a folding filter. The solvent was evaporated *in vacuo*, the residue subjected to column chromatography (silica; PE/ CH_2Cl_2 8:1) yielding the title compound as a colorless solid (810 mg, 71 %). The product contained small amounts ($\approx$ 7 % according to ^{1}H-NMR) of the 2-bromo7-iodo-derivative that could not be removed.

Mp: 170-172 °C
**FD-MS** (8 KV): m/z 974.3 (100 %, M$^+$), calculated 974.2
^{1}H-NMR (300 MHz, CD_2Cl_2): δ 0.13 (s, 24H), 1.20 (s, 36H), 8.68 (s, 4H).
^{13}C-NMR (75 MHz, CD_2Cl_2): δ -3.0, 19.3, 26.8, 54.2, 91.6, 100.6, 118.2, 128.3, 131.3, 138.4.
Elemental analysis (%) found C, 49.79; H, 6.73 calculated C40H64I2O4Si4 C, 49.27; H, 6.62

Crystallographic data (CCDC deposition number): CCDC 1025657

VIII.3.1.14   N2,N8-Bis(4-hexylphenyl)-5,5,11,11-tetramethylpyreno[4,5-d:9,10-d']bis([1,3]dioxole)-2,8-diamine (2-28)

2-28
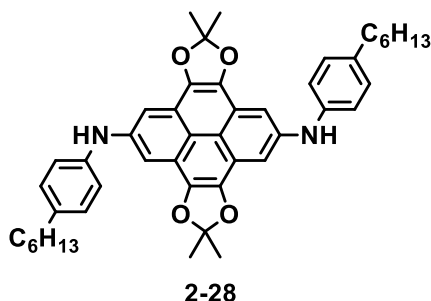
In a 25 mL flame-dried Schlenk-flask 2,8-diiodo-5,5,11,11-tetramethylpyreno[4,5-d:9,10-d']bis([1,3]dioxole) (**2-25**) (40 mg, 66.9 µmol) 4-hexylaniline (142.3 mg, 0.8 mmol), potassium *tert*-butoxide (112.6 mg, 1 mmol), palladium (II) acetate (0,75 mg, 3.3 µmol) and bis(2-diphenylphosphinophenyl)ether (*DPEphos*) (3.6 mg, 6.7 µmol) were dissolved in 5 mL anhydrous toluene and stirred at 100°C for 16 h. The cooled mixture was poured on

100 mL water and extracted with CH_2Cl_2 (15 mL×3). The combined organic phases were washed with sat. NaCl solution, dried with $MgSO_4$ and filtered. The solvent was removed *in vacuo*, the residue subjected to column chromatography (silica, Hex/EE 10:1 to 3:1) yielding the title compound as a green crystalline solid (41 mg, 89 %). Crystals suitable for X-ray analysis were grown by slow evaporation of CH_2Cl_2.

**Mp**: 191-192 °C
FD-MS (8 KV): m/z 696.6 (100 %, M$^+$), calculated 696.4
^{1}H-NMR (300 MHz, CD_2Cl_2): δ 0.91 (td, J = 5.5, 4.1, 2.3 Hz, 6H), 1.30 – 1.43 (m, 12H), 1.58 – 1.71 (m, 4H), 1.95 (d, J = 2.3 Hz, 12H), 2.56 – 2.68 (m, 4H), 6.17 (s, 2H), 7.15 – 7.30 (m, 8H), 7.57 (s, 4H).
^{13}C-NMR (75 MHz, CD_2Cl_2): δ 14.5, 23.2, 26.4, 29.6, 32.3, 32.4, 35.9, 104.3, 113.7, 119.9, 120.1, 121.8, 129.9, 137.7, 138.4, 140.9, 142.6.
Elemental analysis (%) found 79.31; H, 7.58; N, 4.00 calculated C46H52N2O4 C, 79.28; H, 7.52; N, 4.02
Crystallographic data (CCDC deposition number): CCDC 1025660

VIII.3.1.15   4,4'-(4,5,9,10-Tetramethoxypyrene-2,7-diyl)dibenzonitrile (2-30)
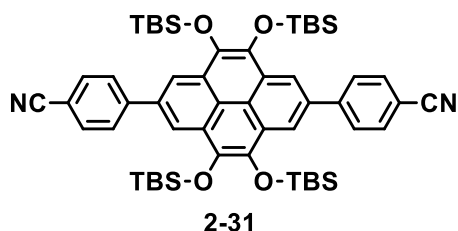

2-30
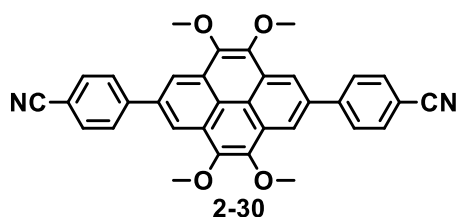
In a 50 mL flame-dried Schlenk-flask 2,7-diodo-4,5,9,10-tetramethoxypyrene (**2-5**) (1 g, 1.78 mmol)   and   4-(4,4,5,5-tetramethyl-1,3,2-dioxaborolan-2-yl)benzonitrile   (1 g, 4.35 mmol) were dissolved in a mixture of 20 mL toluene, 10 mL Na_2CO_3 solution (2 Mol/l*)* and 0.05 mL Aliquat 336 and degassed (freeze-pump-thaw cycling ×3). Tetrakis(triphenylphosphine)palladium (0.1 g, 0.87 mmol) was added and the mixture stirred at 100 °C for 16 h. The cooled solution was filtered through a sinter filer. The solid was washed with water (400 mL), methanol (400 mL), hexane (300 mL) and CH_2Cl_2 (50 mL). Recrystallization from THF yielded the title compound as a yellow solid (730 mg, 80 %).

Mp: 232 – 233 °C
FD-MS (8 KV): m/z 524.2 (100 %, M$^+$), calculated 524.2
^{1}H-NMR (300 MHz, THF-d$_8$): δ 4.24 (s, 12H), 7.89 – 7.98 (m, 4H), 8.12 – 8.19 (m, 4H), 8.74 (s, 4H).

VIII.3.1.16   4,4'-(4,5,9,10-Tetrakis((*tert*-butyldimethylsilyl)oxy)pyrene-2,7-diyl)dibenzonitrile (2-31)

In a 50 mL flame-dried Schlenk-flask ((2,7-diiodopyrene-4,5,9,10-tetrayl)tetrakis(oxy))tetrakis(*tert*-butyldimethylsilane) (**2-26**) (1.1 g, 1.13 mmol) and 4-(4,4,5,5-tetramethyl-1,3,2-dioxaborolan-2-yl)benzonitrile (0.59 g, 2.59 mmol) were dissolved in a mixture of 20 mL toluene, aq. Na_2CO_3 solution (2 mol/L, 10 mL) and 0.05 mL Aliquat 336 and degassed (freeze-pump-thaw cycling ×3). Tetrakis(triphenylphosphine)palladium (65.2 mg, 0.06 mmol) was added and the mixture was stirred at 100 °C for 16 h. The cooled solution was poured onto 100 mL water and extracted with CH_2Cl_2 (150 mL×3). The combined organic phases were washed with sat. NaCl solution (100 mL) and dried with $MgSO_4$. The solvent was removed, the residue subjected to column chromatography (silica; PE/DCM 2:1) and dried under high vacuum yielding the title compound as a yellow solid (840 mg, 82 %).

Mp: 194- 196 °C
FD-MS (8 KV): m/z 924.6 (100 %, M^+), calculated 924.5
^{1}H-NMR 300 MHz, CD_2Cl_2): δ 0.17 (s, 24H), 1.22 (s, 36H), 7.86 (d, *J* = 8.3 Hz, 4H), 8.00 (d, *J* = 8.3 Hz, 4H), 8.64 (s, 4H).
^{13}C-NMR (75 MHz, CD_2Cl_2): δ -2.9, 19.4, 26.9, 30.3, 111.6, 118.5, 128.9, 130.8, 133.4, 136.5, 139.5, 147.1.
Elemental analysis (%) found C, 70.03; H, 7.86; N, 3.05 calculated C54H72N2O4Si4 C, 70.08; H, 7.84; N, 3.03.

VIII.3.1.17   4,4'-((4,5,9,10-Tetramethoxypyrene-2,7-diyl)bis(ethyne-2,1-diyl))bis(N,N-dimethylaniline) (2-35)
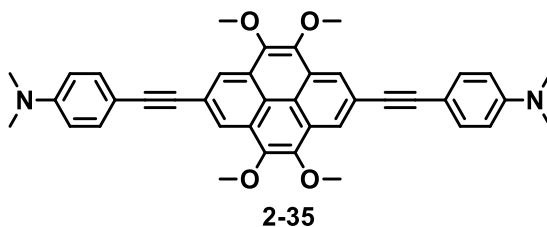
In a 25 mL flame-dried Schlenk-flask, 2,7-diodo-4,5,9,10-tetramethoxypyrene (120 mg, 0.21 mmol), 4-ethynyl-N,N-dimethylaniline (75 mg, 0.52 mmol), triphenylphosphine (5.5 mg, 21 μmol), copper iodide (8.0 mg, 42 μmol) and bis(triphenylphosphine)palladium(II) dichloride (13.4 mg, 21 μmol) were dissolved in 9 mL anhydrous toluene and 3 mL anhydrous triethylamine. The resulting mixture was stirred 16 h at 85°C. After cooling to room temperature the mixture was poured onto

100 mL water and extracted with CH_2Cl_2 (50 mL×3). The combined organic phases were washed with sat. NaCl solution (75 mL), dried with $MgSO_4$ and filtered. The solvent was removed *in vacuo*, the residue subjected to column chromatography (silica; hex / EE 3:1) yielding the title compound as a yellow solid (93 mg, 73 %).

Mp: 214-217 °C
FD-MS (8 KV): m/z 608.2 (100 %, M$^+$), calculated 608.3
^{1}H-NMR (300 MHz, CD_2Cl_2): δ 3.02 (s, 12H), 4.21 (s, 12H), 6.73 (d, *J* = 8.9 Hz, 4H), 7.44 – 7.58 (m, 4H), 8.50 (s, 4H).
^{13}C-NMR (75 MHz, CD_2Cl_2): δ 40.6, 61.7, 89.0, 91.9, 110.1, 112.4, 120.2, 122.1, 122.7, 129.1, 133.3, 145.2, 151.0.
Elemental analysis (%) found C, 78.79; H, 6.12; N, 4.59 calculated $C_{40}H_{36}N_2O_4$ C, 78.92; H, 5.96; N, 4.60

VIII.3.1.18   3,3'-(4,5,9,10-Tetramethoxypyrene-2,7-diyl)bis(2-(4-(dimethylamino)phenyl)buta-1,3-diene-1,1,4,4-tetracarbonitrile) (2-36)

2-36
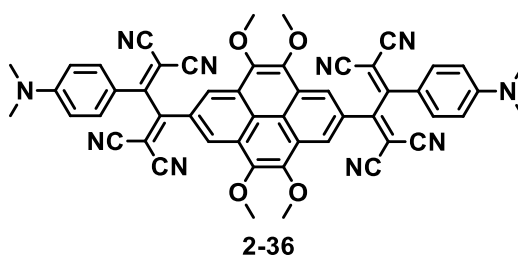
In a 25 mL flame-dried Schlenk-flask 4,4'-((4,5,9,10-tetramethoxypyrene-2,7-diyl)bis(ethyne-2,1-diyl))bis(N,N-dimethylaniline) (**2-35**) (55 mg, 85 μmol) was dissolved in anhydrous CH_2Cl_2. Tetracyanoethylene (23.2 mg, 180.1 μmol) was added, the mixture stirred for 2 h at room temperature. The solvent was removed *in vacuo*, the residue subjected to column chromatography (silica, Hex/EE 3:1 to 1:1) yielding the title compound as a red solid (98 mg, 85 %).
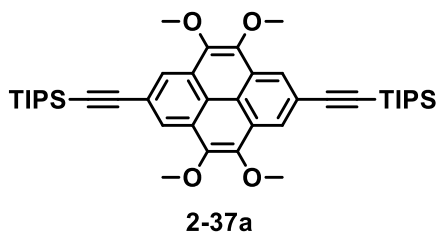
Mp: 186-189 °C, (decomp.)
FD-MS (8 KV): m/z 864.5 (100 %, M$^+$), calculated 864.3
^{1}H-NMR (300 MHz, CD_2Cl_2): δ 3.16 (s, 12H), 4.18 (d, *J* = 1.6 Hz, 12H), 6.72 – 6.87 (m, 4H), 7.84 – 8.00 (m, 4H), 8.74 (s, 4H).
^{13}C-NMR (75 MHz, CD_2Cl_2): δ 40.6, 53.3, 53.6, 54.4, 54.7, 62.4, 112.1, 112.8, 113.1, 114.3, 115.1, 118.5, 120.5, 122.4, 130.8, 131.4, 133.2, 146.1, 155.2, 163.7, 170.4.

VIII.3.1.19   ((4,5,9,10-Tetramethoxypyrene-2,7-diyl)bis(ethyne-2,1-diyl))bis(trimethylsilane) (2-37a)

2-37a

In a 50 mL flame-dried Schlenk-flask, 2,7-diodo-4,5,9,10-tetramethoxypyrene (100 mg, 0.70 mmol), ethynyltriisopropylsilane (79.4 mg, 0.44 mmol), triphenylphosphine (4.6 mg, 17.4 µmol), copper iodide (6.6 mg, 32.8 µmol) and bis(triphenylphosphine)palladium(II) dichloride (11.2 mg, 17.4 µmol) were dissolved in 12 mL anhydrous toluene and 6 mL anhydrous triethylamine. The resulting mixture was stirred 16 h at 85°C. After cooling to room temperature the mixture was poured onto 100 mL water and extracted with CH_2Cl_2 (100 mL×3). The combined organic phases were washed with sat. NaCl solution (100 mL), dried with $MgSO_4$ and filtered. The solvent was removed *in vacuo* and the crude product subjected to column chromatography (silica; PE/CH_2Cl_2 1:1) yielding the title compound as a colorless crystalline solid (107 mg, 90 %). Crystals suitable for X-ray analysis were grown by slow evaporation of CH_2Cl_2.
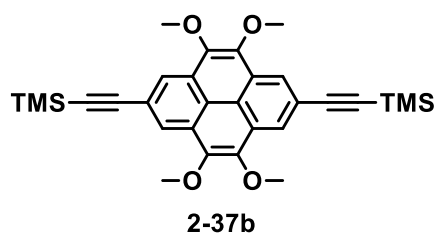
Mp: 173 – 176 °C, (decomp)
FD-MS (8 KV): m/z 682.8 (100 %, M^+), calculated 682.4
^{1}H-NMR. (300 MHz, CD_2Cl_2): δ 0.92 (s, 36H), 1.43 (h, 6H) 4.10 (s, 12H), 8.39 (s, 4H).
^{13}C-NMR (75 MHz, CD_2Cl_2): δ 18.9, 21.4, 61.7, 95.4, 106.1, 122.1, 122.9, 129.5, 145.2.

VIII.3.1.20   ((4,5,9,10-Tetramethoxypyrene-2,7-diyl)bis(ethyne-2,1-diyl))bis(trimethylsilane) (2-37b)

2-37b

In a 50 mL flame-dried Schlenk-flask, 2,7-diodo-4,5,9,10-tetramethoxypyrene (**2-5**) (100 mg, 0.17 mmol), ethynyltrimethylsilane (42.8 mg, 0.44 mmol), triphenylphosphine (4.6 mg, 17.4 µmol), copper iodide (6.6 mg, 32.8 µmol) and bis(triphenylphosphine)palladium(II) dichloride (11.2 mg, 17.4 µmol) were dissolved in 12 mL anhydrous toluene and 6 mL anhydrous triethylamine. The resulting mixture was stirred 16 h at 85°C. After cooling to room temperature the mixture was poured onto 100 mL water and extracted with CH_2Cl_2 (100 mL×3). The combined organic phases were washed with sat. NaCl solution (100 mL), dried with $MgSO_4$ and filtered. The solvent was removed *in vacuo*, the crude product subjected to column chromatography (silica;

PE/CH$_2$Cl$_2$ 1:1) yielding the title compound as a colorless crystalline solid (77 mg, 86 %).
Crystals suitable for X-ray analysis were grown by slow evaporation of CH$_2$Cl$_2$.
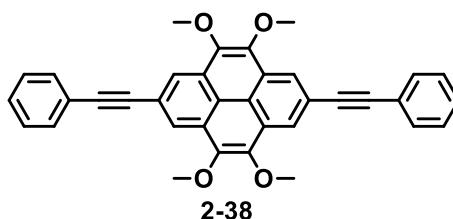
Mp: 162 °C, (decomp)
FD-MS (8 KV): m/z 514.2 (100 %, M$^+$), calculated 514.2
^{1}H-NMR (300 MHz, CD$_2$Cl$_2$): δ 0.26 (s, 18H), 4.10 (s, 12H), 8.39 (s, 4H).
^{13}C-NMR (75 MHz, CD$_2$Cl$_2$): δ 0.3, , 61.7, 95.5, 106.4, 121.8, 122.8, 129.2, 145.2.
Elemental analysis (%) found C, 70.02; H, 6.69 calculated C30H34O4Si2 C, 70.00; H, 6.66;

VIII.3.1.21   4,5,9,10-Tetramethoxy-2,7-bis(phenylethynyl)pyrene (2-38)

2-38

In a 100 mL flame-dried Schlenk-flask, 2,7-diodo-4,5,9,10-tetramethoxypyrene (**2-5**) (400 mg, 0.70 mmol), ethynylbenzene (234 mg, 2.3 mmol), triphenylphosphine (54.8 mg, 0.21 mmol), copper iodide (39.8 mg, 0.21 mmol) and bis(triphenylphosphine)palladium(II) dichloride (73.4 mg, 0.1 mmol) were dissolved in 30 mL anhydrous toluene and 15 mL anhydrous triethylamine. The resulting mixture was stirred 16 h at 85°C. After cooling to room temperature the mixture was poured onto 100 mL water and extracted with CH$_2$Cl$_2$ (150 mL×3). The combined organic phases were washed with sat. NaCl solution (200 mL), dried with MgSO$_4$ and filtered. The solvent was removed *in vacuo*, the crude product subjected to column chromatography (silica; CH$_2$Cl$_2$) yielding the title compound as a yellow solid (316 mg, 87 %).
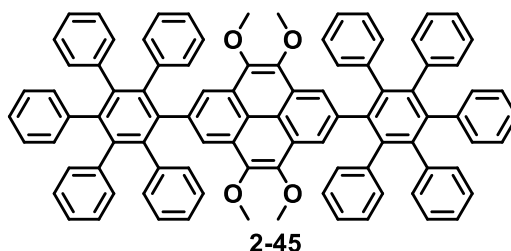
Mp: 259 – 262 °C
FD-MS (8 KV): m/z 522.3 (100 %, M$^+$), calculated 522.2
^{1}H-NMR (300 MHz, CD$_2$Cl$_2$): δ 4.22 (s, 12H), 7.43 (dd, J = 4.9, 2.3 Hz, 6H), 7.64 – 7.73 (m, 4H), 8.58 (s, 4H).
^{13}C-NMR (75 MHz, CD$_2$Cl$_2$): δ 90.3, 90.7, 100.4, 121.7, 122.3, 123.6, 128.9, 129.1, 132.1, 133.6, 145.1.
Elemental analysis (%) found C, 83.01; H, 5.09 calculated C36H26O4 C, 82.74; H, 5.01.

VIII.3.1.22   4,5,9,10-Tetramethoxy-2,7-bis(4',5',6'-triphenyl-[1,1':2',1''-terphenyl]-3'-yl)pyrene (2-45)

2-45

In a 10 mL microwave vial 4,5,9,10-tetramethoxy-2,7-bis(phenylethynyl)pyrene (**2-44**) (200 mg, 0.38 mmol) and 2,3,4,5-tetraphenylcyclopenta-2,4-dien-1-one (323.7 mg, 0.84 mmol) were suspended in a mixture of 3.3 mL diphenylether and 0.1 mL propylene carbonate and heated in a microwave reactor at 220 °C for 8 h. After cooling the mixture was poured on 500 mL hexane and filtered through a silica plug. The solvent was removed *in vacuo*, the crude product was subjected to column chromatography (silica/ PE / CH$_2$Cl$_2$ 3:1 to CH$_2$Cl$_2$) yielding the title compound as a colorless solid (320 mg, 67 %).

Mp: 257 °C
FD-MS (8 KV): m/z 1234.2 (100 %, M$^+$), calculated 1234.5
^{1}H-NMR (500 MHz, THF-d$_8$, 323K): δ 3.63 (s, 12H), 6.53 – 6.61 (m, 4H), 6.65 (dd, J = 8.4, 6.8 Hz, 8H), 6.70 – 6.82 (m, 18H), 6.86 (dddd, J = 10.3, 7.5, 3.5, 1.9 Hz, 20H), 7.86 (s, 4H).
^{13}C-NMR (126 MHz, THF-d$_8$, 323K): δ 61.3, 119.8, 123.7, 126.0, 126.0, 127.5, 127.7, 127.9, 132.5, 132.6, 132.8, 139.2, 141.6, 142.0, 142.0, 142.1, 142.1, 142.2, 145.7.
Elemental analysis (%) found C, 89.39; H, 5.49 calculated C92H66O4 C, 89.44; H, 5.38.

VIII.3.1.23   Cyclodehydration product (2-46)
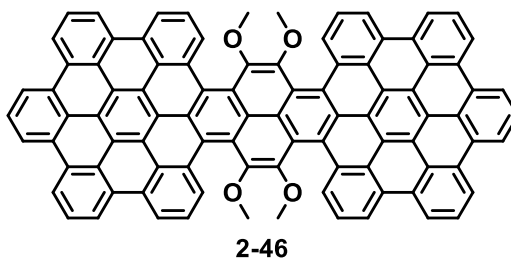

2-46

In a 25 mL flame-dried Schlenk-flask 4,5,9,10-tetramethoxy-2,7-bis(4',5',6'-triphenyl-[1,1':2',1''-terphenyl]-3'-yl)pyrene (**2-45**) was dissolved in degassed, stabilizer free CH$_2$Cl$_2$. The solution was purged by a CH$_2$Cl$_2$ saturated argon stream. Iron (III) chloride (72 eq) suspended in Nitromethane was added and was stirred for 7 d at room temperature. The mixture was poured on 100 mL ethanol to precipitate the product. The product was isolated by filtration through a glass frit.

MALDI-TOF (8 KV): m/z m/z: 1210.35 (100.0%), 1211.35 (99.5%), 1212.36 (42.8%), 1213.36 (11.7%) (100%), calculated: 1210.31 (100.0%), 1211.31 (99.5%), 1212.32 (42.8%), 1213.32 (11.7%)

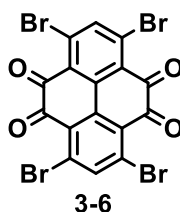## VIII.3.2 1,3,6,8-Functionalized pyrene derivatives

VIII.3.2.1 4,5,9,10-Tetramethoxypyrene (3-8)

3-8
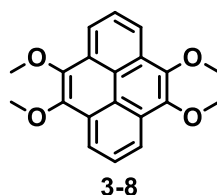
The compound was prepared according to the procedure reported by ZÖPHEL *et al.* [87]

Crystallographic data (CCDC deposition number): CCDC 1025939

### VIII.3.2.2 1,3,6,8-Tetrabromopyrene-4,5,9,10-tetraone (3-6)

3-6

In a 25 mL flame-dried Schlenk-flask 4,5,9,10-tetramethoxypyrene (**3-8**) (300 mg, 930 μmol) was dissolved in 15 mL anhydrous $PhNO_2$. Bromine (2.32 mL, 45.53 mmol) was added and the mixture heated to 160 °C for 16 h. After cooling methanol was added and the crude product isolated by filtration (glass frit), washed with water, methanol, CH_2Cl_2 and small amounts of THF and dried *in vacuo* yielding the title compound as an orange solid (12 mg, 2 %).

Mp: 241 °C, (decomp.)
FD-MS (8 KV): m/z 578.1 (100 %, M$^+$), calculated 577.66
^{1}H-NMR (500 MHz, 373K, $C_2D_2Cl_4$): δ 6.95 (s, 2H).

VIII.3.2.3 1,3,6,8-Tetrabromo-4,5,9,10-tetramethoxypyrene (3-10)

3-10
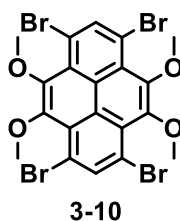
In a 100 mL flame-dried Schlenk-flask 4,5,9,10-tetramethoxypyrene (300 mg, 0.93 mmol) was dissolved in anhydrous carbon tetrachloride (20 mL) and warmed to 55°C. Freshly distilled bromine (1.19 g, 7.5 mmol) was added rapidly (CAUTION vigorous reaction!) and the mixture was stirred for additional 4 h. After cooling 15 mL $Na_2S_2O_3$ solution (2 Mol/L) were added, the mixture diluted by adding 100 mL water and extracted with CH_2Cl_2 (100 mL×3). The combined organic phases were washed with sat. NaCl solution

dried with MgSO$_4$ and filtered. The solvent was removed *in vacuo*, the crude product was subjected to column chromatography (silica; PE/CH$_2$Cl$_2$ 7:1) yielding the title compound as a yellow solid (256 mg, 43 %).

Mp: 267-272 °C
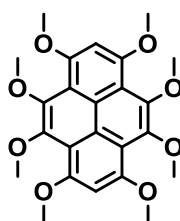**FD-MS** (8 KV): m/z 637.4 (100 %, M$^+$), calculated 637.7
^{1}H-NMR (500 MHz, 373K, C$_2$D$_2$Cl$_4$): δ 4.11 (s, 12H), 8.66 (s, 2H).
^{13}C-NMR (75 MHz, THF): δ 60.2, 100.0, 123.5, 125.6, 141.1, 147.1.
Elemental analysis (%) found C, 37.61; H, 2.24 calculated C20H14Br4O4 C, 37.66; H, 2.21
Crystallographic data (CCDC deposition number): CCDC 1025662

VIII.3.2.4   1,3,4,5,6,8,9,10-Octamethoxypyrene (3-13)

3-13

In a 25 mL flame-dried Schlenk-flask 1,3,6,8-tetrabromo-4,5,9,10-tetramethoxypyrene (**3-10**) (200 mg, 0.31 mmol) and copper iodide (280 mg, 1.47 mmol) were suspended in anhydrous DMF (10 mL). Water free sodium methoxide solution (30 %, 3.14 mL, 3.14 mmol) was added and the mixture stirred at 120 °C for 16 h. After cooling the mixture was poured onto aq. ammonia solution (10 %, 300 mL) and extracted with CH$_2$Cl$_2$ (100 mL×3). The combined organic phases were washed with ammonia solution (10%, 100 mL) and sat. NaCl solution, dried with MgSO$_4$ and filtered. The solvent was removed in vacuo, the crude product was subjected to column chromatography (silica; CH$_2$Cl$_2$) yielding the title compound as an orange crystalline solid (83 mg, 59 %). Crystals suitable for X-ray diffraction analysis were grown by slow vapor diffusion of PE into a dichloromethane solution of **3-13**.

Mp: 184-188 °C
FD-MS (8 KV): m/z 442.4 (100 %, M$^+$), calculated 442.2
^{1}H-NMR (300 MHz, CD$_2$Cl$_2$): δ 3.89 (s, 12H), 4.08 (s, 12H), 7.20 (s, 2H).
^{13}C-NMR (75 MHz, CD$_2$Cl$_2$): δ 57.9, 61.7, 99.7, 113.4, 126.7, 145.5, 153.7.
Elemental analysis (%) found C, 65.21; H, 5.31 calculated C24H26O8 C, 65.15; H, 5.92.
Crystallographic data (CCDC deposition number): CCDC 1025640

VIII.3.2.5   4,5,9,10-Tetramethoxy-N1,N1,N3,N3,N6,N6,N8,N8-octakis(4-methoxyphenyl)-3a,3a1-dihydropyrene-1,3,6,8-tetraamine (3-14)

3-14
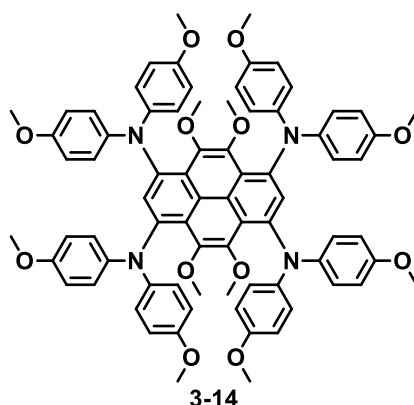
In a 50 mL flame-dried Schlenk-flask 1,3,6,8-tetrabromo-4,5,9,10-tetramethoxypyrene (**3-10**) (140 mg, 0.22 mmol), bis(4-methoxyphenyl)amine (211.3 mg, 0.92 mmol), bis(dibenzylideneacetone)palladium(0) (3.79 mg, 6.58 μmol), 1,2,3,4,5-pentaphenyl-1′-(di-*tert*-butylphosphino)ferrocene (*QPhos*) (9.4 mg, 13.2 μmol) and sodium *tert*-butoxide (158.2 mg, 1.65 mmol) were suspended in 15 mL anhydrous toluene and stirred 16 h at 105°C. The cooled solution was poured onto water (100 mL) and extracted with CH_2Cl_2 (50 mL×3). The combined organic phases were washed with 100 mL sat. NaCl solution, dried with $MgSO_4$ and filtered. The solvent was removed *in vacuo*, the crude product was subjected to column chromatography (silica, Hex/EE 10:1 to 3:1) yielding the title compound as a red solid (195 mg, 72 %).

Mp: 225-227 °C
**FD-MS** (8 KV): m/z 1232.0 (100 %, M$^+$), calculated 1232.5
^{1}H-NMR (300 MHz, CD_2Cl_2): δ 3.42 (s, 12H), 3.72 (s, 24H), 6.58 – 6.73 (m, 16H), 6.77 – 6.94 (m, 16H), 7.30 (s, 2H).
^{13}C-NMR (75 MHz, CD_2Cl_2): δ 55.9, 61.4, 99.7, 114.5, 121.7, 123.3, 133.2, 140.7, 143.1, 143.2, 146.0, 154.9.
Elemental analysis (%) found C, 74.10; H, 5.78; N, 4.53. calculated C76H70N4O12 C, 74.01; H, 5.88; N, 4.54.
Crystallographic data (CCDC deposition number): CCDC 1025641

VIII.3.2.6   ((4,5,9,10-Tetramethoxypyrene-1,3,6,8-tetrayl)tetrakis(ethyne-2,1-diyl))tetrakis(triisopropylsilane) (3-15)

3-15
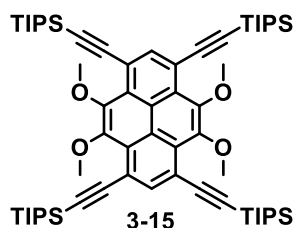
In a 50 mL flame-dried Schlenk-flask, 1,3,6,8-tetrabromo-4,5,9,10-tetramethoxypyrene (**3-10**) (200 mg, 0.31 mmol), ethynyltriisopropylsilane (343 mg, 1.88 mmol), triphenylphosphine (14.6 mg, 62.8 μmol), copper iodide (6 mg, 31.4 μmol) and

bis(triphenylphosphine)palladium(II) dichloride (22 mg, 31.4 μmol) were dissolved in 12 mL anhydrous toluene and 6 mL anhydrous triethylamine and stirred 16 h at 85°C. After cooling to room temperature the mixture was poured onto 100 mL water and extracted with CH_2Cl_2 (100 mL×3). The combined organic phases were washed with sat. NaCl solution (100 mL), dried with $MgSO_4$ and filtered. The solvent was removed in vacuo, the crude product subjected to column chromatography (silica; PE/CH_2Cl_2 4:1) yielding the title compound as an orange crystalline material (267 mg, 82 %). Crystals suitable for X-ray analysis were grown by slow evaporation of CH_2Cl_2.

Mp: 212-214 °C, (decomp.)
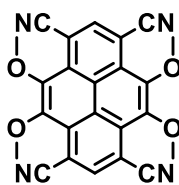**FD-MS** (8 KV): m/z 1043.0 (100 %, M$^+$), calculated 1042.7
^{1}H-NMR (300 MHz, CD_2Cl_2): δ 1.09 (s, 12H), 1.24 (s, 72H), 4.12 (s, 12H), 8.37 (s, 2H).
^{13}C-NMR (75 MHz, CD_2Cl_2): δ 12.3, 30.3, 54.2, 61.7, 97.0, 100.6, 108.9, 115.8, 129.2, 143.6, 148.3.
Crystallographic data (CCDC deposition number): CCDC 1025651

VIII.3.2.7   1,3,6,8-Tetracyano-4,5,9,10-tetramethoxypyrene (3-16)

3-16

In a 25 mL flame-dried Schlenk-flask 1,3,6,8-tetrabromo-4,5,9,10-tetramethoxypyrene (**3-10**) (200 mg, 0.31 mmol), sodium cyanide (92.2 mg, 1.88 mmol), copper iodide (35.8 mg, 0.19 mmol) and N^1,N^2-dimethylethane-1,2-diamine (110.6 mg, 1.25 mmol) were suspended in anhydrous toluene (7 mL) and stirred for 48 h at 105°C. The cooled suspension was poured on ammonia solution (30 %, 20 mL) and extracted with THF (100 mL×4). The combined organic phases were washed with sat. NaCl solution (200 mL) and dried with $MgSO_4$. The raw product was adsorbed onto silica and subjected to column chromatography (silica; EE/Hex 1:3 to EE) yielding the title compound as an orange solid (9 mg, 4 %).

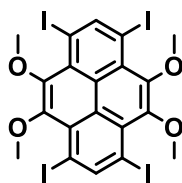**Mp**: 248-250 °C, (decomp.)
FD-MS (8 KV): m/z 422.1 (100 %, M$^+$), calculated 422.1
^{1}H-NMR (500 MHz, 373K, $C_2D_2Cl_4$): δ 4.21 (s, 12H), 8.72 (s, 2H).
^{13}C-NMR (125 MHz, THF-d_8): δ 60.2, 100.0, 117.4, 123.5, 125.6, 141.1, 147.1.

VIII.3.2.8   1,3,6,8-Tetraiodo-4,5,9,10-tetramethoxypyrene (3-17)

3-17

In a 50 mL flame-dried Schlenk-flask, 1,3,6,8-tetrabromo-4,5,9,10-tetramethoxypyrene (**3-10**) (128 mg, 0.2 mmol), sodium iodide (481.2 mg, 3.21 mmol), N^1,N^2-dimethylethane-1,2-diamine (4.83 mg, 0.16 mmol) and copper iodide (15.3 mg, 80,3 μmol) were suspended in anhydrous 1,4-dioxane and stirred for 48 h at 80 °C. The cooled solution was filtered through a plug of Celite which was washed with THF (300 mL). The organic solvents were evaporated, the crude product washed with water (200 mL), methanol (200 mL), hexane (200 mL) and CH_2Cl_2 (75 mL). The crude product was recrystallized from THF and dried under high vacuum yielding the title compound as a yellow solid (68 mg, 41 %).
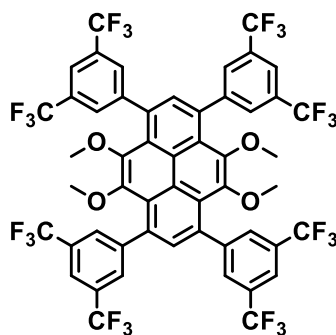
Mp: 231-234 °C, (decomp.)
FD-MS (8 KV): m/z 825.4 (100 %, M^+), calculated 825.7
^{1}H-NMR (500 MHz, 323 K, THF-d_8): δ 4.00 (s, 12H), 9.37 (s, 2H).
^{13}C-NMR (126 MHz, 323 K, THF-d_8): δ 61.1, 67.6, 83.9, 122.8, 129.1, 146.8, 156.7.
Elemental analysis (%) found 29.11; H, 1.78. calculated C20H14I4O4 C, 29.08; H, 1.71.

VIII.3.2.9   1,3,6,8-Tetrakis(3,5-bis(trifluoromethyl)phenyl)-4,5,9,10-tetramethoxypyrene (3-18)

3-18

In a 50 mL flame-dried Schlenk-flask 1,3,6,8-tetrabromo-4,5,9,10-tetramethoxypyrene (**3-10**) (75 mg, 0.12 mmol) and 2-(3,5-bis(trifluoromethyl)phenyl)-4,4,5,5-tetramethyl-1,3,2-dioxaborolane (139,9 mg, 0.71 mmol) were dissolved in a mixture of 4 mL toluene, Na_2CO_3 solution (2 mL, 2 mol/L) and 0.05 mL Aliquat 336 and degassed (freeze-pump-thaw cycling ×3). Tetrakis(triphenylphosphine)palladium (14.9 mg, 12.9 μmol) was added and the mixture was stirred at 100 °C for 16 h. The cooled mixture was poured on 50 mL of water and extracted with CH_2Cl_2 (50 mL×3). The combined organic phases were washed with sat. NaCl solution (100 mL), dried with $MgSO_4$ and filtered. Evaporation of

the solvents provided a crude product that was subjected to column chromatography (silica; PE/CH$_2$Cl$_2$ 2:1) yielding the title compound as a yellow solid (53 mg, 61 %).
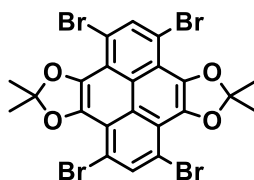
Mp: 277-279 °C
FD-MS (8 KV): m/z 1170.6 (100 %, M$^+$), calculated 1170.7
^{1}H-NMR (300 MHz, CD$_2$Cl$_2$): δ 3.33 (s, 12H), 7.73 (s, 2H), 7.96 (s (br), 4H), 8.01 (s (br), 8H).
^{13}C-NMR (75 MHz, CD$_2$Cl$_2$): δ 60.2, 120.8, 122.4, 126.0, 127.0, 129.5, 130.7, 131.1, 132.6, 134.2, 146.7.
Elemental analysis (%) found C, 40.67; H, 2.31. calculated C52H26F24O4 C, 53.35; H, 2.24.

VIII.3.2.10   3,7,9-Tetrabromo-5,5,11,11-tetramethylpyreno[4,5-d:9,10-d']bis([1,3]dioxole) (3-20)

3-20

In a 100 mL flame-dried Schlenk-flask 5,5,11,11-tetramethylpyreno[4,5-d:9,10-d']bis([1,3]dioxole) (200 mg, 0.58 mmol) was dissolved in anhydrous carbon tetrachloride (30 mL) and warmed to 55°C. Freshly distilled bromine (1.11 g, 6.93 mmol) was added rapidly (CAUTION vigorous reaction!) and the mixture stirred for 4 h at 55°C. The reaction was quenched by adding Na$_2$S$_2$O$_3$ solution (15 mL, 2 Mol/L), the phases were separated, the aqueous phase was diluted by adding 100 mL water and extracted with CH$_2$Cl$_2$ (100 mL×3). The combined organic phases were washed with sat. NaCl solution and dried with MgSO4. The solvent was evaporated, the crude product was subjected to column chromatography (silica; PE/CH$_2$Cl$_2$ 10:1) yielding the title compound as a yellow solid (187 mg, 46 %).
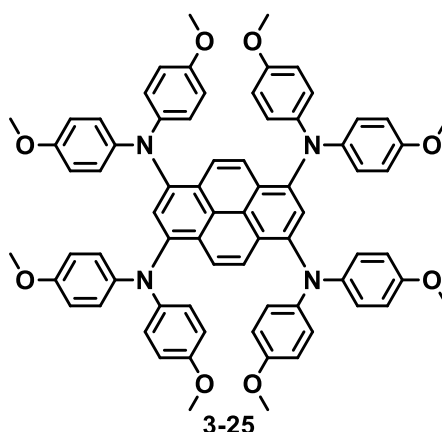
Mp: 282 °C, (decomp.)
FD-MS (8 KV): m/z 661.3 (100 %, M$^+$), calculated 661.8
^{1}H-NMR (300 MHz, THF-d$_8$): δ 1.91 (s, 12H), 8.47 (s, 2H).
Crystallographic data (CCDC deposition number): CCDC 1025642

VIII.3.2.11 N1,N1,N3,N3,N6,N6,N8,N8-Octakis(4-methoxyphenyl)-3a,3a1-dihydropyrene-1,3,6,8-tetraamine (3-25)

3-25

In a 50 mL flame-dried Schlenk-flask 1,3,6,8-tetrabromopyrene (**3-10**) (100 mg, 0.19 mmol), bis(4-methoxyphenyl)amine (265.7 mg, 1.16 mmol), bis(dibenzylideneacetone)palladium(0) (3.33 mg, 5.79 μmol), 1,2,3,4,5-pentaphenyl-1′-(di-*tert*-butylphosphino)ferrocene (*QPhos*) (8.26 mg, 11.59 μmol) and sodium *tert*-butoxide (139.2 mg, 1.45 mmol) were suspended in 30 mL anhydrous toluene and stirred 16 h at 105°C. The cooled solution was poured onto water (100 mL) and extracted with CH_2Cl_2 (50 mL×3). The combined organic phases were washed with 100 mL sat. NaCl solution, dried with $MgSO_4$ and filtered. The solvent was removed *in vacuo*, the crude product was subjected to column chromatography (silica, Hex/EE 10:1 to 3:1) yielding the title compound as an orange solid (195 mg, 72 %).

Mp: 213-215 °C
FD-MS (8 KV): m/z 1232.0 (100 %, M$^+$), calculated 1232.5
^{1}H-NMR (300 MHz, CD_2Cl_2): δ 3.72 (s, 24H), 6.67 − 6.76 (m, 16H), 6.84 − 6.91 (m, 16H), 7.46 (s, 2H), 7.90 (s, 4H).
^{13}C-NMR (75 MHz, CD_2Cl_2): δ 55.9, 115.0, 123.1, 123.8, 126.5, 129.2, 143.2, 155.4.
Crystallographic data (CCDC deposition number): CCDC 1025938

VIII.3.2.12 1,3,6,8-Tetrakis(3,5-bis(trifluoromethyl)phenyl)pyrene-4,5,9,10-tetraone (3-32)

3-32
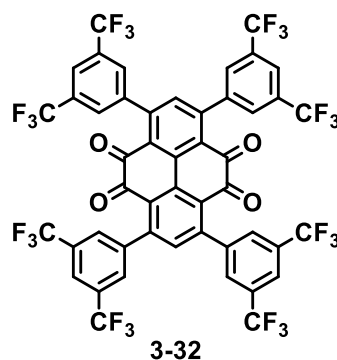
In a 25 mL flame-dried Schlenk-flask 1,3,6,8-tetrakis(3,5-bis(trifluoromethyl)phenyl)-4,5,9,10-tetramethoxypyrene (**3-18**) (40 mg, 34.2 μmol) was dissolved in 10 mL anhydrous

CH$_2$Cl$_2$. At 0 °C (ice bath) borontribromide (0.48 mL, 1 M solution in CH$_2$Cl$_2$, 0.48 mmol) was added. The mixture was allowed to warm to room temperature and stirred for 72 h. The reaction was quenched by the addition of nitric acid (65%, 50 mL) and stirred for an additional hour. The phases were separated, the aqueous phase was extracted with CH$_2$Cl$_2$ (15 mL×3). The combined organic phases were washed with sat. NaCl solution the solvent was removed *in vacuo*, the crude product was subjected to size exclusion chromatography (BioBeads S-X1; THF) yielding the title compound as a red solid.

Mp: 252- 259 °C, (decomp.)
FD-MS (8 KV): m/z 1110.3 (100 %, M$^+$), calculated 1110.1
^{1}H-NMR (300 MHz, CD$_2$Cl$_2$): δ 7.40 (s, 2H), 7.81 (s, 8H), 8.02 (s, 4H).
^{13}C-NMR (75 MHz, THF-d$_8$): δ 121.7, 125.3, 128.4, 130.2, 131.0, 131.4, 137.0, 143.1, 146.6, 178.3.
Elemental analysis (%) found C, 38.77; H, 1.14 calculated C48H14F24O4 C, 51.91; H, 1.27.

VIII.3.2.13   4,5,9,10-Tetramethoxy-1,3,6,8-tetrakis(trifluoromethyl)pyrene (3-34)

3-34
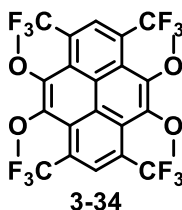
In a 25 mL flame-dried Schlenk-flask 1,3,6,8-tetraiodo-4,5,9,10-tetramethoxypyrene (**3-17**) (200 mg, 0.24 mmol) and (1,10-phenanthroline)(trifluoromethyl)copper(I) (326.8 mg, 1.05 mmol) were dissolved in anhydrous DMF and stirred at 60°C for 24 h. The mixture was poured onto water (300 mL) and extracted with CH$_2$Cl$_2$ (150 mL×3). The combined organic phases were washed with aq. ammonia solution (10 %, 100 mL×2), sat. NaCl solution (100 mL×2) dried with MgSO$_4$ and filtered. After removal of volatile solvents in vacuo, the crude product was subjected to column chromatography (silica; PE/CH$_2$Cl$_2$ 10:1 *v:v*) yielding the title compound as a yellow crystalline solid (113 mg, 78 %). Crystals suitable for X-ray analysis were grown by slow evaporation of CH$_2$Cl$_2$.
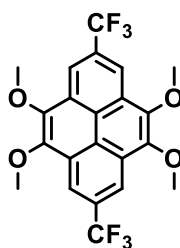
Mp: 245-247 °C
FD-MS (8 KV): m/z 594.1 (100 %, M$^+$), calculated 594.1
^{1}H-NMR (300 MHz, CD$_2$Cl$_2$): δ 4.08 (s, 12H), 8.92 (s, 2H).
^{13}C-NMR (75 MHz, CD$_2$Cl$_2$): δ 61.5, 122.5, 123.0, 123.2, 126.8, 127.0, 148.5.
Crystallographic data (CCDC deposition number): CCDC 1025646

VIII.3.2.14   4,5,9,10-Tetramethoxy-2,7-bis(trifluoromethyl)pyrene (3-36)

3-36

In a 25 mL flame-dried Schlenk-flask 2,7-diodo-4,5,9,10-tetramethoxypyrene (**2-5**) (200 mg, 0.35 mmol) and (1,10-phenanthroline)(trifluoromethyl)copper(I) (326.8 mg, 1.05 mmol) were dissolved in anhydrous DMF and stirred at 60°C for 24 h. The mixture was poured onto water (300 mL) and extracted with CH_2Cl_2 (150 mL×3). The combined organic phases were washed with aq. ammonia solution (10 %, 100 mL×2), sat. NaCl solution (100 mL×2) dried with $MgSO_4$ and filtered. After removal of volatile solvents in vacuo, the crude product was subjected to column chromatography (silica; PE/CH_2Cl_2 10:1 *v:v*) yielding the title compound as a colorless solid (167 mg, 83 %). Crystals suitable for X-ray analysis were grown by slow evaporation of CH_2Cl_2.

Mp: 244-246 °C
FD-MS (8 KV): 458.1 m/z (100 %, M$^+$), calculated 458.1
^{1}H-NMR (500 MHz, THF-d_8): δ 4.09 (s, 12H), 8.93 (s, 4H).
^{13}C-NMR (126 MHz, THF-d_8): δ 61.5, 67.6, 122.4, 123.0, 123.3, 123.5, 123.6, 123.8, 124.6, 126.7, 127.2, 128.9, 130.5, 149.2.
^{19}F NMR (471 MHz, THF-d_8): δ -57.9.
Elemental analysis (%) found C, 56.35; H, 3.09 calculated $C_{22}H_{16}F_6O_4$ C, 57.65; H, 3.52
Crystallographic data (CCDC deposition number): CCDC 1025644

VIII.3.2.15   2,7-Bis(trifluoromethyl)pyrene-4,5,9,10-tetraone (3-37)
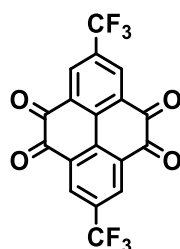
3-37

In a 100 mL flame-dried Schlenk-flask 4,5,9,10-tetramethoxy-2,7-bis(trifluoromethyl)pyrene (**3-36**) (50 mg, 0.11 mmol) was dissolved in 10 mL anhydrous CH_2Cl_2. At 0 °C (ice bath) borontribromide (1,75 mL 1 M solution in CH_2Cl_2, 1.75 mmol) was added. The resulting mixture was allowed to warm to room temperature and stirred for 24 h. The reaction was quenched by the addition of nitric acid (65%, 50 mL) and extracted with CH_2Cl_2 (15 mL×3). The combined organic phases were washed with sat. NaCl

solution. The solvent was removed *in vacuo*, the residue is re-dissolved in 25 mL THF and stirred in air for 48 h at room temperature. The solvent is removed, the residue subjected repeated to size exclusion chromatography (BioBeads S-X1; THF) yielding the title compound as an orange solid (13 mg, 29 %).

Mp: 226 °C, (decomp.)
FD-MS (8 KV): m/z 398.5 (100 %, M$^+$), calculated 398.5
^{1}H-NMR (300 MHz, CD$_2$Cl$_2$): δ 8.79 (s, 4H).

VIII.3.3   Materials for TADF OLEDs

VIII.3.3.1   N,N- Bis (4-(Dimethylamino)phenyl 4'''-(5-phenyl-1,3,4-oxadiazol-2-yl)-[1,1':3',1'':3'',1'''-quaterphenyl]-3-amine (5-11)
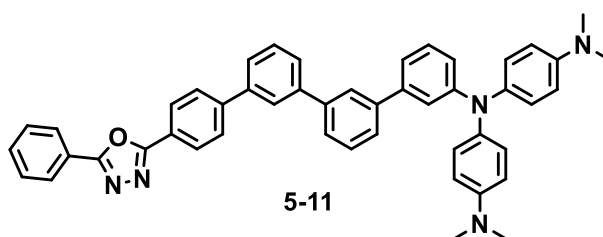
In a 25 mL flame-dried Schlenk-flask 2-(3'''-bromo-[1,1':3',1'':3'',1'''-quaterphenyl]-4-yl)-5-phenyl-1,3,4-oxadiazole (**5-24**) (0.1 g, 0.19 mmol), bis (4-(dimethylamino)phenyl)amine (96.4 mg, 0.38 mmol), bis(dibenzylideneacetone)palladium(0) (1.09 mg, 1.89 µmol), 1,2,3,4,5-pentaphenyl-1′-(di-*tert*-butylphosphino)ferrocene (*QPhos*) (2.7 mg, 3.8 µmol) and sodium *tert*-butoxide (45.4 mg, 0.48 mmol) were suspended in 15 mL anhydrous toluene and stirred 16 h at 105°C. The cooled solution was diluted with water, the phases were separated and the aqueous phase was extracted with CH$_2$Cl$_2$ (50 mL×3). The combined organic phases were washed with 100 mL sat. NaCl solution, dried with MgSO$_4$ and filtered. Evaporation of the solvent gave a crude product that was subjected to column chromatography (silica, CH$_2$Cl$_2$) and recycling GPC (chloroform) yielding the title compound as a colorless solid (110 mg, 82 %).

FD-MS (8 KV): m/z 703.3 (100 %, M$^+$), calculated 703.3
^{1}H- / ^{13}C-NMR: Due to diamagnetic interfernce NMR spectra were not resolved.

VIII.3.3.2   N,N-bis(4-Methoxyphenyl)-4'''-(5-phenyl-1,3,4-oxadiazol-2-yl)-[1,1':3',1":3",1'''-quaterphenyl]-3-amine (5-12)
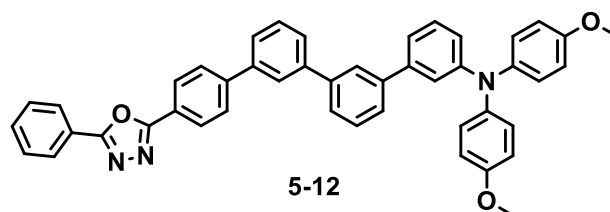
5-12

In a 25 mL flame-dried Schlenk-flask 2-(3'''-bromo-[1,1':3',1":3",1'''-quaterphenyl]-4-yl)-5-phenyl-1,3,4-oxadiazole (**5-24**) (0.1 g, 0.19 mmol), bis(4-methoxyphenyl)amine (65.0 mg, 0.28 mmol), bis(dibenzylideneacetone)palladium(0) (2.17 mg, 3.78 μmol), 1,2,3,4,5-pentaphenyl-1′-(di-*tert*-butylphosphino)ferrocene (*QPhos*) (5.4 mg, 7.6 μmol) and sodium *tert*-butoxide (45.4 mg, 0.48 mmol) were suspended in 15 mL anhydrous toluene and stirred 16 h at 105°C. The cooled solution was diluted with water, the phases were separated and the aqueous phase was extracted with CH_2Cl_2 (50 mL×3). The combined organic phases were washed with 100 mL sat. NaCl solution, dried with $MgSO_4$ and filtered. Evaporation of the solvent gave a crude product that was subjected to column chromatography (silica, CH_2Cl_2) and recycling GPC (chloroform) yielding the title compound as a colorless solid (102 mg, 80 %).

Mp: 209 – 211 °C
FD-MS (8 KV): m/z 677.4 (100 %, M$^+$), calculated 677.3
^{1}H-NMR (500 MHz, $C_2Cl_4D_2$): δ 3.79 (d, *J* = 2.1 Hz, 6H), 6.80 – 6.99 (m, 5H), 7.06 – 7.30 (m, 7H), 7.45 – 7.69 (m, 9H), 7.78 (d, *J* = 2.1 Hz, 1H), 7.83 (dd, *J* = 8.3, 2.1 Hz, 2H), 7.88 (t, *J* = 1.9 Hz, 1H), 8.15 (dq, *J* = 5.2, 2.6, 2.2 Hz, 2H), 8.23 (dd, *J* = 8.4, 2.1 Hz, 2H).
^{13}C-NMR (126 MHz, $C_2Cl_4D_2$): δ 55.7, 115.1, 120.4, 124.7, 126.0, 126.1, 126.2, 126.5, 127.0, 127.1, 127.5, 127.8, 129.1, 129.4, 147.4, 149.4, 149.8.
Elemental analysis (%) found C, 81.48; H, 5.29; N, 6.75 calculated C46H35N3O3 C, 81.51; H, 5.21; N, 6.20

VIII.3.3.3   N,N-Diphenyl-4'''-(5-phenyl-1,3,4-oxadiazol-2-yl)-[1,1':3',1":3",1'''-quaterphenyl]-3-amine (5-13)
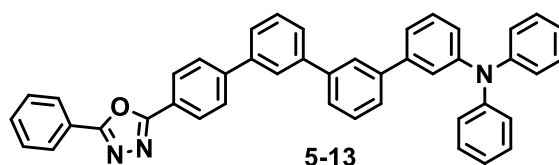
5-13

In a 25 mL flame-dried Schlenk-flask 2-(3'''-bromo-[1,1':3',1":3",1'''-quaterphenyl]-4-yl)-5-phenyl-1,3,4-oxadiazole (**5-24**) (0.1 g, 0.19 mmol), diphenylamine (63.9 mg, 0.38 mmol), bis(dibenzylideneacetone)palladium(0) (1.09 mg, 1.89 μmol), 1,2,3,4,5-pentaphenyl-1′-(di-*tert*-butylphosphino)ferrocene (*QPhos*) (2.7 mg, 3.8 μmol) and sodium *tert*-butoxide (45.4 mg, 0.48 mmol) were suspended in 15 mL anhydrous toluene and stirred 16 h at 105°C. The cooled solution was diluted with water, the phases were separated and the aqueous phase was extracted with CH_2Cl_2 (50 mL×3). The combined organic phases were

washed with 100 mL sat. NaCl solution, dried with MgSO$_4$ and filtered. Evaporation of the solvent gave a crude product that was subjected to column chromatography (silica, CH$_2$Cl$_2$) and recycling GPC (chloroform) yielding the title compound as a colorless solid (102 mg, 80 %).

Mp: 219 – 222 °C
FD-MS (8 KV): m/z 617.2 (100 %, M$^+$), calculated 617.3
^{1}H-NMR (500 MHz, 373 K , C$_2$Cl$_4$D$_2$): δ 7.02 – 7.10 (m, 2H), 7.11 – 7.42 (m, 12H), 7.45 (q, J = 2.1 Hz, 1H), 7.50 – 7.74 (m, 8H), 7.88 (ddd, J = 26.4, 18.0, 2.3 Hz, 4H), 8.20 (dt, J = 8.3, 2.3 Hz, 2H), 8.27 (dd, J = 8.5, 2.7 Hz, 2H).
^{13}C-NMR (126 MHz, 373 K, C$_2$Cl$_4$D$_2$): δ 120.2, 121.4, 122.7, 122.8, 122.9, 123.0, 124.2, 125.8, 125.9, 126.0, 126.1, 126.8, 126.9, 127.3, 127.7, 128.9, 129.0, 129.1, 129.2, 129.4, 131.5, 140.3, 147.7, 148.3.
Elemental analysis (%) found C, 85.59; H, 5.03; N, 6.84 calculated C44H31N3O C, 85.55; H, 5.06; N, 6.80.

VIII.3.3.4   2-(3'''-(9H-Carbazol-9-yl)-[1,1':3',1'':3'',1'''-quaterphenyl]-4-yl)-5-phenyl-1,3,4-oxadiazole (5-14)
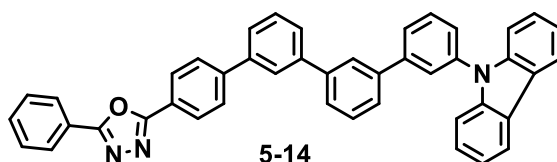
In a 25 mL flame-dried Schlenk-flask 2-(3'''-bromo-[1,1':3',1'':3'',1'''-quaterphenyl]-4-yl)-5-phenyl-1,3,4-oxadiazole (**5-24**) (0.1 g, 0.19 mmol), carbazole (63.2 mg, 0.38 mmol), bis(dibenzylideneacetone)palladium(0) (2.17 mg, 3.78 μmol), tri-*tert*-butylphosphane (2.3 mg, 11.3 μmol) and sodium *tert*-butoxide (45.4 mg, 0.48 mmol) were suspended in 15 mL anhydrous toluene and stirred 16 h at 105°C. The cooled solution was diluted with water, the phases were separated and the aqueous phase was extracted with CH$_2$Cl$_2$ (50 mL×3). The combined organic phases were washed with 100 mL sat. NaCl solution, dried with MgSO$_4$ and filtered. Evaporation of the solvent gave a crude product that was subjected to column chromatography (silica, CH$_2$Cl$_2$) and recycling GPC (chloroform) yielding the title compound as a colorless solid (83 mg, 64 %).

Mp: 143 °C, (decomp.)
FD-MS (8 KV): m/z 615.2 (100 %, M$^+$), calculated 615.2
^{1}H-NMR (500 MHz, 373 K, C$_2$Cl$_4$D$_2$): δ 7.31 – 7.38 (m, 2H), 7.47 (t, J = 7.6 Hz, 2H), 7.53 (d, J = 8.2 Hz, 2H), 7.57 – 7.66 (m, 6H), 7.71 (d, J = 7.6 Hz, 1H), 7.72 – 7.80 (m, 4H), 7.85 (d, J = 7.6 Hz, 1H), 7.87 – 7.91 (m, 2H), 7.92 – 8.01 (m, 3H), 8.13 – 8.23 (m, 4H), 8.26 (dd, J = 8.3, 1.8 Hz, 2H).
^{13}C-NMR (126 MHz, C$_2$Cl$_4$D$_2$): δ 109.9, 120.2, 120.3, 120.4, 123.6, 126.1, 126.4, 127.0, 127.1, 127.5, 127.9, 129.1, 129.5, 130.3, 131.7.
Elemental analysis (%) found 85.79; H, 4.78; N, 6.91. calculated C44H29N3O C, 85.83; H, 4.75; N, 6.82.

VIII.3.3.5   3,3''-Dibromo-1,1':3',1''-terphenyl (5-22)

5-22
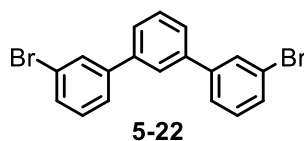
In a 500 mL flame-dried Schlenk-flask (3-bromophenyl)boronic acid (4.06 g, 20.22 mmol) and 1,3-diiodobenzene (3.33 g, 10.11 mmol) were dissolved in a mixture of 250 mL toluene, Na$_2$CO$_3$ solution (125 mL, 2 Mol/L) and 1.00 mL Aliquat 336 and (freeze-pump-thaw cycling ×3). Tetrakis(triphenylphosphine)palladium (0.58 g, 0.51 mmol) was added and the mixture was stirred at 70 °C for 48 h. The cooled mixture was poured on 250 mL of water and extracted with CH$_2$Cl$_2$ (250 mL×3). The organic phases were combined, washed with sat. NaCl solution (300 mL) and dried with MgSO$_4$. Evaporation of the solvents provided a crude product that was subjected to column chromatography (silica; PE) yielding the title compound as a colorless oil (840 mg, 24 %).

The analytical results agree with the reported data.[433]

VIII.3.3.6   2-Phenyl-5-(4-(4,4,5,5-tetramethyl-1,3,2-dioxaborolan-2-yl)phenyl)-1,3,4-oxadiazole (5-23)

5-23
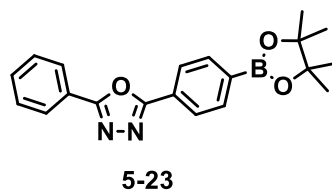
In a 50 mL flame-dried Schlenk-flask 2-(4-bromophenyl)-5-phenyl-1,3,4-oxadiazole (500 mg, 1.7 mmol), bis(pinacolato)diboron (632.4 mg, 2,5 mmol), [1,1'-bis(diphenylphosphino)ferrocene]dichloropalladium(II) (34.0 mg, 41.5 µmol) and potassium acetate (407 mg, 4.2 mmol) were dissolved in anhydrous dioxane (20 mL). The mixture was stirred 16 h at 90 °C. After cooling the mixture was poured onto sat. NaCl solution (200 mL), the suspension was extracted with CH$_2$Cl$_2$ (50 mL×3). The combined organic phases were washed with sat. NaCl solution (50 mL) and dried with MgSO$_4$. The solvent was removed; the residue was subjected to column chromatography (silica; CH$_2$Cl$_2$) yielding the title compound as a colorless solid (444 mg, 77 %).
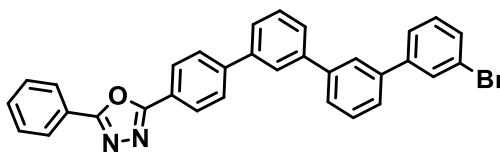
Mp: 172-174 °C, (decomp.)
FD-MS (8 KV): m/z 348.1 (100 %, M$^+$), calculated 348.2
^{1}H-NMR (300 MHz, CD$_2$Cl$_2$): δ 1.37 (d, J = 3.1 Hz, 12H), 7.50 − 7.66 (m, 3H), 7.87 − 8.04 (m, 2H), 8.05 − 8.30 (m, 4H).
^{13}C-NMR (75 MHz, CD$_2$Cl$_2$): δ 25.3, 84.8, 124.6, 126.4, 126.7, 127.4, 129.7, 132.3, 135.8, 165.1, 165.3.

### VIII.3.3.7 2-(3'''-Bromo-[1,1':3',1":3",1'''-quaterphenyl]-4-yl)-5-phenyl-1,3,4-oxadiazole (5-24)

5-24

In a 50 mL flame-dried Schlenk-flask 2-phenyl-5-(4-(4,4,5,5-tetramethyl-1,3,2-dioxaborolan-2-yl)phenyl)-1,3,4-oxadiazole (**5-23**) (0.28 mg, 0.81 mmol) and 3,3"-dibromo-1,1':3',1"-terphenyl (**5-22**) (0.63 g, 1.62 mmol) were dissolved in a mixture of 20 mL toluene, Na_2CO_3 solution (12 mL, 2 mol/L) and 0.1 mL Aliquat 336 and degassed (freeze-pump-thaw cycling ×3). Tetrakis(triphenylphosphine)palladium (28.1 mg, 24.4 μmol) was added and the mixture was stirred at 100 °C for 16 h. The cooled mixture was poured on 250 mL of water and extracted with CH_2Cl_2 (250 mL×3). The organic phases were combined, washed with sat. NaCl solution (300 mL) and dried with $MgSO_4$. Evaporation of the solvents provided a crude product that was subjected to column chromatography (silica; PE) yielding the title compound as a colorless solid (470 mg, 55 %).

Mp: 168 °C
FD-MS (8 KV): m/z 529.0 (100 %, M$^+$), calculated 528.1

VIII.3.3.8 Bis(4-(dimethylamino)phenyl)amine (5-25)
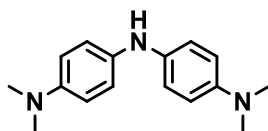
5-25

In a 100 mL flame-dried Schlenk-flask 4-bromo-N,N-dimethylaniline (5.0 g, 25.0 mmol), N^1,N^1-dimethylbenzene-1,4-diamine (3.4 g, 25.00 mmol), bis(dibenzylideneacetone)palladium(0) (143.7 mg, 0.25 mmol), 1,2,3,4,5-pentaphenyl-1'-(di-*tert*-butylphosphino)ferrocene (*QPhos*) (356.2 mg, 0.5 mmol) and sodium *tert*-butoxide (2.6 g, 27.5 mmol) were suspended in 15 mL anhydrous toluene and stirred 16 h at 105°C. The cooled solution was diluted with water, the phases were separated and the aqueous phase was extracted with CH_2Cl_2 (250 mL×3). The combined organic phases were washed with 100 mL sat. NaCl solution, dried with $MgSO_4$ and filtered. The solvent was removed *in vacuo*, the crude product was subjected to column chromatography (silica, CH_2Cl_2) yielding the title compound as a colorless solid (5.1 g, 80 %).

Mp: 121 °C, (decomp.)
FD-MS (8 KV): m/z 255.3 (100 %, M$^+$), calculated 255.2
The analytical results agree with the reported data.[290]

VIII.3.3.9   3-Bromo-N,N-diphenylaniline (5-33)
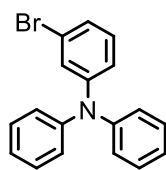
5-33

In a 50 mL flame-dried Schlenk-flask 1-bromo-3-iodobenzene (3.0 g, 10.75 mmol), diphenylamine (1.82 g, 10.75 mmol), copper iodide (40.9 mg, 0.21 mmol), cyclohexane-1,2-diamine (0,25 g, 2.15 mmol) and potassium *tert*-butoxide (1.81 g, 16.2 mmol) were suspended in 20 mL anhydrous dioxane and stirred at 100°C for 16 h. The cooled mixture was poured onto 400 mL ammonia solution (10 % in water) and extracted with CH$_2$Cl$_2$ (100 mL×3). The combined organic phases were washed with sat. NaCl solution dried with MgSO$_4$ and filtered. The solvent was removed *in vacuo*, the crude product was subjected to column chromatography (silica; PE/CH$_2$Cl$_2$ 5:1) yielding the title compound as a colorless solid (2.69 g, 77 %).

Mp: 194 °C
FD-MS (8 KV): m/z 325.0 (100 %, M$^+$), calculated 323.0
^{1}H-NMR (300 MHz, CD$_2$Cl$_2$): δ 6.93 – 7.01 (m, 1H), 7.02 – 7.14 (m, 8H), 7.15 – 7.20 (m, 1H), 7.24 – 7.34 (m, 4H).
^{13}C-NMR (75 MHz, CD$_2$Cl$_2$): δ 122.0, 123.2, 124.2, 125.3, 125.4, 126.0, 130.0, 131.0, 147.8, 150.1.

VIII.3.3.10   3-Bromo-N,N-bis(4-(*tert*-butyl)phenyl)aniline (5-34)

5-34

In a 50 mL flame-dried Schlenk-flask 1-bromo-3-iodobenzene (3.0 g, 10.75 mmol), bis(4-(*tert*-butyl)phenyl)amine (3.0 g, 10.75 mmol), copper iodide (40.9 mg, 0.21 mmol), cyclohexane-1,2-diamine (0,25 g, 2.15 mmol) and potassium *tert*-butoxide (1.81 g, 16.2 mmol) were suspended in 20 mL anhydrous dioxane and stirred at 100°C for 16 h. The cooled mixture was poured onto 400 mL ammonia solution (10 % in water) and extracted with CH$_2$Cl$_2$ (100 mL×3). The combined organic phases were washed with sat. NaCl solution and dried with MgSO$_4$ and filtered. The solvent was removed *in vacuo*, the crude product was subjected to column chromatography (silica; PE/CH$_2$Cl$_2$ 10:1) yielding the title compound as a colorless solid (3.51 g, 75 %).

Mp: 172-174 °C
FD-MS (8 KV): m/z 435.1 (100 %, M$^+$), calculated 435.2

¹H-NMR (300 MHz, CD₂Cl₂): δ 1.32 (s, 18H), 6.79 – 6.96 (m, 2H), 6.97 – 7.11 (m, 4H), 7.24 (dt, *J* = 6.8, 1.6 Hz, 1H), 7.27 – 7.34 (m, 4H), 7.35 (d, *J* = 1.9 Hz, 1H).
¹³C-NMR (75 MHz, CD₂Cl₂): δ 31.8, 34.8, 94.9, 121.9, 126.9, 130.7, 131.0, 145.1, 147.2, 150.3.

VIII.3.3.11   3-Bromo-N,N-bis(4-methoxyphenyl)aniline (5-35)
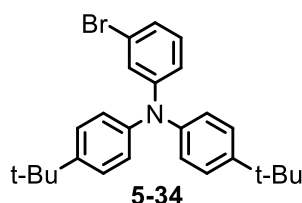

5-35
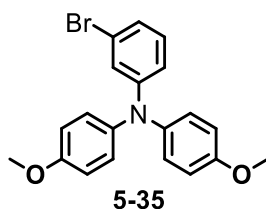
In a 50 mL flame-dried Schlenk-flask 1-bromo-3-iodobenzene (3.0 g, 10.75 mmol), bis(4-methoxyphenyl)amine (2.46 g, 10.75 mmol), copper iodide (40.9 mg, 0.21 mmol), cyclohexane-1,2-diamine (0,25 g, 2.15 mmol) and potassium *tert*-butoxide (1.81 g, 16.2 mmol) were suspended in 20 mL anhydrous dioxane and stirred at 100°C for 16 h. The cooled mixture was poured onto 400 mL ammonia solution (10 % in water) and extracted with CH₂Cl₂ (100 mL×3). The combined organic phases were washed with sat. NaCl solution and dried with MgSO₄ and filtered. The solvent was removed *in vacuo*, the crude product was subjected to column chromatography (silica; PE/CH₂Cl₂ 2:1) yielding the title compound as a colorless solid (2.69 g, 77 %).

Mp: 186-188 °C
FD-MS (8 KV): m/z 383.9 (100 %, M⁺), calculated 383.1
¹H-NMR (250 MHz, CD₂Cl₂): δ 3.79 (s, 6H), 6.73 – 6.91 (m, 6H), 6.98 – 7.11 (m, 4H), 7.14 (s, 1H), 7.20 (s, 1H).
¹³C-NMR (63 MHz, CD₂Cl₂): δ 56.0, 95.0, 115.3, 119.4, 127.5, 128.6, 129.2, 130.8, 140.6, 150.8, 157.0.

VIII.3.3.12   2,7-Bis(4,4,5,5-tetramethyl-1,3,2-dioxaborolan-2-yl)pyrene (5-36)
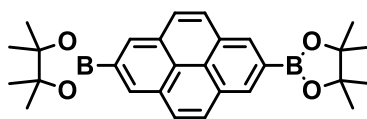
5-36

2,7-Bis(4,4,5,5-tetramethyl-1,3,2-dioxaborolan-2-yl)pyrene was prepared according to a modified procedure by COVENTRY *et al.*[375]

FD-MS (8 KV): m/z 454.3 (100 %, M⁺), calculated 454.25
¹H-NMR (250 MHz, CD₂Cl₂): δ 1.45 (s, 24H), 8.12 (s, 4H), 8.60 (s, 4H).
¹³C-NMR (63 MHz, CD₂Cl₂): δ 25.4, 84.7, 116.6, 126.7, 128.2, 131.4, 131.7.

VIII.3.3.13   3,6-Dimethoxy-9H-carbazole (5-39)
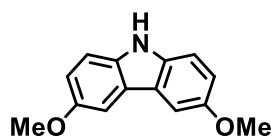
5-39

3,6-Dimethoxy-9H-carbazole (**5-39**) was prepared according to a procedure by ACKERMANN *et al.*[434]

FD-MS (8 KV): m/z 227.0 (100 %, M$^+$), calculated 227.1
^{1}H-NMR (250 MHz, CD$_2$Cl$_2$): δ 3.91 (s, 6H), 7.04 (dd, *J* = 8.8, 2.5 Hz, 2H), 7.33 (dd, *J* = 8.8, 0.6 Hz, 2H), 7.52 (d, *J* = 2.0 Hz, 2H), 7.93 (s, 1H).

VIII.3.3.14   9-(3-Bromophenyl)-9H-carbazole (5-40)
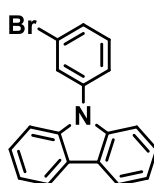
5-40

In a 100 mL flame-dried Schlenk-flask 1-bromo-3-iodobenzene (5.0 g, 17.7 mmol), carbazole (3.25 g, 19.44 mmol), copper iodide (841.3 mg, 4.42 mmol), 2,2'-bipyridine (689,9 mg, 4.42 mmol) and potassium carbonate (5.37 g, 38.9 mmol) were suspended in 40 mL anhydrous DMF and stirred at 120°C for 4 h. The cooled mixture was poured onto 400 mL ammonia solution (10 % in water) and extracted with CH$_2$Cl$_2$ (100 mL×3). The combined organic phases were washed with sat. NaCl solution and dried with MgSO$_4$ and filtered. The solvent was removed *in vacuo*, the crude product was subjected to column chromatography (silica; PE/CH$_2$Cl$_2$ 1:1) yielding the title compound as a colorless crystalline material (3.72 g, 65 %).

Mp: 188 °C
FD-MS (8 KV): m/z 321.3 (100 %, M$^+$), calculated 321.0
^{1}H-NMR (300 MHz, CD$_2$Cl$_2$): δ 7.20 (ddd, *J* = 8.0, 4.6, 3.6 Hz, 2H), 7.27 – 7.35 (m, 4H), 7.37 – 7.47 (m, 2H), 7.52 (dt, *J* = 7.5, 1.8 Hz, 1H), 7.65 (t, *J* = 1.9 Hz, 1H), 8.04 (dt, *J* = 7.7, 1.0 Hz, 2H).
^{13}C-NMR (75 MHz, CD$_2$Cl$_2$): δ 110.2, 120.9, 123.7, 124.0, 126.4, 126.7, 130.6, 131.1, 131.8, 139.7, 141.2.

VIII.3.3.15   9-(3-Bromophenyl)-3,6-di-*tert*-butyl-9H-carbazole (5-41)

5-41
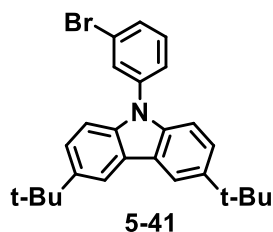
In a 50 mL flame-dried Schlenk-flask 1-bromo-3-iodobenzene (0.32 g, 1.14 mmol), 3,6-di-*tert*-butyl-9H-carbazole (0.35 g, 1.25 mmol), copper iodide (54.2 mg, 0.29 mmol), 2,2'-bipyridine (44,5 mg, 0.29 mmol) and potassium carbonate (0.35 g, 2.5 mmol) were suspended in 20 mL anhydrous DMF and stirred at 120°C for 4 h. The cooled mixture was poured onto 400 mL ammonia solution (10 % in water) and extracted with CH_2Cl_2 (100 mL×3). The combined organic phases were washed with sat. NaCl solution and dried with $MgSO_4$ and filtered. The solvent was removed *in vacuo*, the crude product was subjected to column chromatography (silica; PE/CH_2Cl_2 10:1) yielding the title compound as a colorless crystalline material (0.34 g, 68 %).

Mp: 172 °C
FD-MS (8 KV): m/z 433.3, 435.3 (100 %, M^+), calculated 433.15, 443.15
^{1}H-NMR (300 MHz, CD_2Cl_2): δ 1.48 (s, 18H), 7.28 – 7.43 (m, 2H), 7.46 – 7.63 (m, 4H), 7.67 – 7.85 (m, 1H), 7.88 – 8.22 (m, 2H).
^{13}C-NMR (75 MHz, CD_2Cl_2): δ 32.3, 35.2, 109.7, 116.9, 123.6, 124.1, 124.4, 125.9, 126.6, 130.2, 130.5, 131.7, 131.8, 136.1, 136.5, 139.5, 140.2, 144.0.

VIII.3.3.16   9-(3-Bromophenyl)-3,6-dimethoxy-9H-carbazole (5-42)

5-42
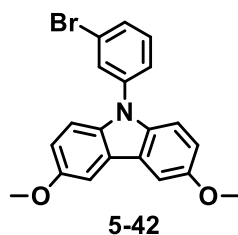
In a 50 mL flame-dried Schlenk-flask 1-bromo-3-iodobenzene (2.0 g, 7.0 mmol), 3,6-dimethoxy-9H-carbazole (**5-39**) (0.4 g, 1.76 mmol), copper iodide (76.2 mg, 0.4 mmol), 2,2'-bipyridine (62,5 mg, 0.4 mmol) and potassium carbonate (0.49 g, 3.5 mmol) were suspended in 20 mL anhydrous DMF and stirred at 120°C for 4 h. The cooled mixture was poured onto 400 mL ammonia solution (10 % in water) and extracted with CH_2Cl_2 (100 mL×3). The combined organic phases were washed with sat. NaCl solution and dried with $MgSO_4$ and filtered. The solvent was removed *in vacuo*, the crude product was subjected to column chromatography (silica; PE/CH_2Cl_2 1:2) yielding the title compound as a colorless crystalline material (0.53 g, 76 %).

Mp: 179 °C
FD-MS (8 KV): m/z 381.1, 383.1 (100 %, M^+%), calculated 381.0, 383.0

¹H-NMR (300 MHz, CD₂Cl₂): δ 3.94 (s, 6H), 7.04 (ddd, *J* = 9.0, 2.6, 0.8 Hz, 2H), 7.34 (dd, *J* = 8.9, 4.4 Hz, 2H), 7.40 – 7.56 (m, 2H), 7.58 (d, *J* = 2.5 Hz, 2H), 7.72 – 7.81 (m, 1H), 7.93 (t, *J* = 1.9 Hz, 1H).
¹³C-NMR (75 MHz, CD₂Cl₂): δ 56.5, 95.0, 103.5, 111.1, 115.7, 123.6, 124.5, 125.7, 126.4, 130.0, 130.4, 131.7, 131.8, 135.9, 136.4, 140.2, 155.0.

VIII.3.3.17   2,7-Bis(3-(9H-carbazol-9-yl)phenyl)pyrene (5-43)

5-43
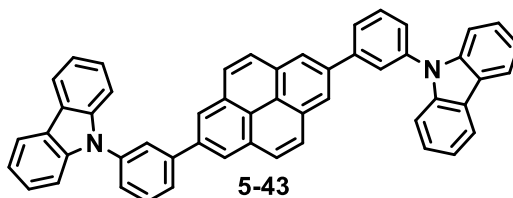
In a 50 mL flame-dried Schlenk-flask 2,7-bis(4,4,5,5-tetramethyl-1,3,2-dioxaborolan-2-yl)pyrene (0.75 g, 1.65 mmol) (**5-36**) and 9-(3-bromophenyl)-9H-carbazole (**5-40**) (1.12 g, 3.47 mmol) were dissolved in a mixture of 20 mL toluene, Na₂CO₃ solution (10 mL, 2 mol/L) and 0.05 mL Aliquat 336 and degassed (freeze-pump-thaw cycling ×3). Tetrakis(triphenylphosphine)palladium (95.4 mg, 82.6 μmol) was added and the mixture was stirred at 100 °C for 16 h. The cooled mixture was poured on 50 mL of water and filtered. The crude product was washed with water (300 mL), methanol (200 mL), hexane (200 mL) and cool CH₂Cl₂ (150 mL), recrystallized from toluene (×3) yielding the title compound as a colorless solid (593 mg, 52 %).

Mp: 257 °C
FD-MS (8 KV): m/z 684.2 (100 %, M⁺), calculated 684.3
¹H-NMR (500 MHz, 373 K, C₂Cl₄D₂): δ 7.37 (t, *J* = 7.5 Hz, 4H), 7.50 (t, *J* = 7.7 Hz, 4H), 7.59 (d, *J* = 8.2 Hz, 4H), 7.70 (d, *J* = 7.8 Hz, 2H), 7.85 (t, *J* = 7.8 Hz, 2H), 8.07 (d, *J* = 7.8 Hz, 2H), 8.16 (s, 2H), 8.22 (d, *J* = 8.5 Hz, 8H), 8.52 (s, 4H).
¹³C-NMR (126 MHz, 373 K, C₂Cl₄D₂): δ 109.8, 120.0, 120.1, 123.5, 123.7, 123.9, 125.9, 126.5, 126.8, 127.9, 130.3, 131.6, 137.9, 138.5, 141.1, 143.2.
Elemental analysis (%) found C, 91.24; H, 4.73; N, 4.03 calculated C52H32N2 C, 91.20; H, 4.71; N, 4.09

VIII.3.3.18   2,7-Bis(3-(3,6-di-*tert*-butyl-9H-carbazol-9-yl)phenyl)pyrene (5-44)
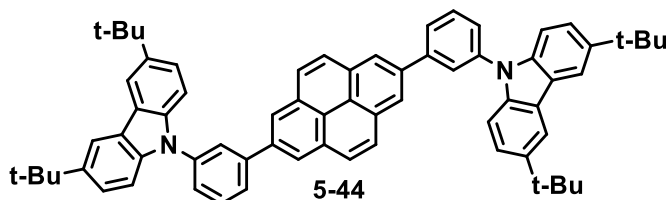
5-44

In a 50 mL flame-dried Schlenk-flask 2,7-bis(4,4,5,5-tetramethyl-1,3,2-dioxaborolan-2-yl)pyrene (**5-36**) (0.50 g, 1.1 mmol) and 9-(3-bromophenyl)-3,6-di-*tert*-butyl-9H-carbazole (**5-41**) (1.00 g, 2.31 mmol) were dissolved in a mixture of 20 mL toluene, Na₂CO₃ solution (10 mL, 2 mol/L) and 0.05 mL Aliquat 336 and degassed (freeze-pump-thaw cycling ×3). Tetrakis(triphenylphosphine)palladium (101.8 mg, 88.1 μmol) was added and the mixture

was stirred at 100 °C for 16 h. The cooled mixture was poured on 50 mL of water and filtered. The crude product was washed with water (300 mL), methanol (200 mL), hexane (200 mL) and cool CH_2Cl_2 (150 mL), filtered through a plug of silica (CH_2Cl_2), recrystallized from toluene (×3) yielding the title compound as a colorless solid (0.61 g, 61 %).

Mp: 225-226 °C
FD-MS (8 KV): m/z 909.3 (100 %, M$^+$), calculated 909.5
^{1}H-NMR (500 MHz, 373 K, $C_2Cl_4D_2$): δ 1.56 (s, 36H), 7.50 − 7.59 (m, 8H), 7.67 − 7.75 (m, 2H), 7.83 (t, J = 7.8 Hz, 2H), 8.02 (d, J = 8.1 Hz, 2H), 8.17 (t, J = 1.9 Hz, 2H), 8.22 (d, J = 2.4 Hz, 8H), 8.52 (d, J = 3.2 Hz, 4H).
^{13}C-NMR (126 MHz, 373 K, $C_2Cl_4D_2$): δ 31.9, 34.5, 73.8, 109.3, 116.1, 123.4, 123.6, 123.7, 123.9, 125.5, 126.0, 126.3, 127.9, 128.8, 130.1, 131.6, 138.1, 139.0, 139.4, 143.1.
Elemental analysis (%) found C, 89.77; H, 7.12; N, 3.11 calculated C68H64N2 C, 89.82; H, 7.09; N, 3.08.

VIII.3.3.19   2,7-Bis(3-(3,6-dimethoxy-9H-carbazol-9-yl)phenyl)pyrene (5-45)
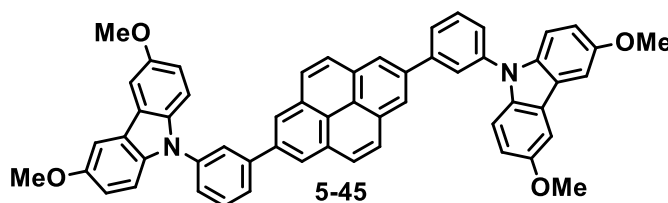
In a 50 mL flame-dried Schlenk-flask 2,7-bis(4,4,5,5-tetramethyl-1,3,2-dioxaborolan-2-yl)pyrene (**5-36**) (1.0 g, 2.2 mmol) and 9-(3-bromophenyl)-3,6-dimethoxy-9H-carbazole (**5-42**) (1.85 g, 4.84 mmol) were dissolved in a mixture of 20 mL toluene, Na_2CO_3 solution (10 mL, 2 mol/L) and 0.05 mL Aliquat 336 and degassed (freeze-pump-thaw cycling ×3). Tetrakis(triphenylphosphine)palladium (176.1 mg, 0.18 mmol) was added and the mixture was stirred at 100 °C for 16 h. The cooled mixture was poured on 50 mL of water and filtered. The crude product was washed with water (300 mL), methanol (200 mL), hexane (200 mL) and cool CH_2Cl_2 (150 mL), filtered through a plug of silica (CH_2Cl_2), recrystallized from toluene (×3) and yielding the title compound as a colorless solid (1.04 g, 59 %).

Mp: 239 °C, (decomp.)
FD-MS (8 KV): m/z 804.9 (100 %, M$^+$), calculated 805.0
^{1}H-NMR (500 MHz, 373 K $C_2Cl_4D_2$): δ 3.96 (s, 12H), 7.09 (dd, J = 8.9, 2.5 Hz, 4H), 7.45 (d, J = 8.9 Hz, 4H), 7.59 − 7.64 (m, 6H), 7.77 (t, J = 7.8 Hz, 2H), 7.97 (dt, J = 8.0, 1.2 Hz, 2H), 8.08 (t, J = 1.9 Hz, 2H), 8.17 (s, 4H), 8.46 (s, 4H).
^{13}C-NMR (126 MHz, 373 K, $C_2Cl_4D_2$): δ 56.5, 104.1, 110.8, 115.4, 120.4, 123.9, 124.0, 124.1, 125.7, 126.3, 126.6, 128.1, 130.4, 131.8, 136.9, 138.2, 139.2, 143.3, 154.5.
Elemental analysis (%) found C, 83.61; H, 5.05; N, 3.47. calculated C56H40N2O4 C, 83.56; H, 5.01; N, 3.48.

VIII.3.3.20   3,3'-(Pyrene-2,7-diyl)bis(N,N-diphenylaniline) (5-46)
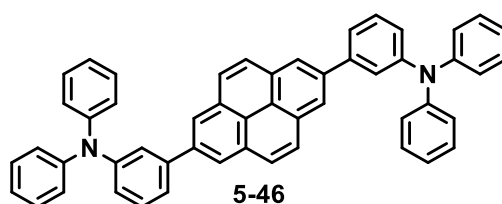
5-46

In a 50 mL flame-dried Schlenk-flask 2,7-bis(4,4,5,5-tetramethyl-1,3,2-dioxaborolan-2-yl)pyrene (**5-36**) (300.0 mg, 0.66 mmol) and 3-bromo-N,N-diphenylaniline (**5-33**) (535.4 mg, 1.65 mmol) were dissolved in a mixture of 10 mL toluene, Na_2CO_3 solution (5 mL, 2 mol/L) and 0.05 mL Aliquat 336 and (freeze-pump-thaw cycling ×3). Tetrakis(triphenylphosphine)palladium (38.2 mg, 33.0 µmol) was added and the mixture was stirred at 100 °C for 16 h. The cooled mixture was poured on 50 mL of water and filtered. The crude product was washed with water (300 mL), methanol (200 mL), hexane (200 mL) and cool CH_2Cl_2 (150 mL), recrystallized from toluene (×3) yielding the title compound as a colorless solid (347 mg, 76 %).

Mp: 246 °C
FD-MS (8 KV): m/z 688.3 (100 %, M$^+$), calculated 688.3
^{1}H-NMR (500 MHz, 373 K, $C_2Cl_4D_2$): δ 6.98 − 7.34 (m, 22H), 7.42 (t, J = 7.8 Hz, 2H), 7.53 (d, J = 7.6 Hz, 2H), 7.63 (t, J = 1.9 Hz, 2H), 8.08 (s, 4H), 8.29 (s, 4H).
^{13}C-NMR (126 MHz, 373 K, $C_2Cl_4D_2$): δ 120.4, 122.5, 123.0, 123.8, 124.4, 127.9, 129.3, 131.6.
Elemental analysis (%) found C, 90.62; H, 5.33; N, 4.05 calculated C52H36N2 C, 90.67; H, 5.27; N, 4.07.

VIII.3.3.21   3,3'-(Pyrene-2,7-diyl)bis(N,N-bis(4-(*tert*-butyl)phenyl)aniline) (5-44)
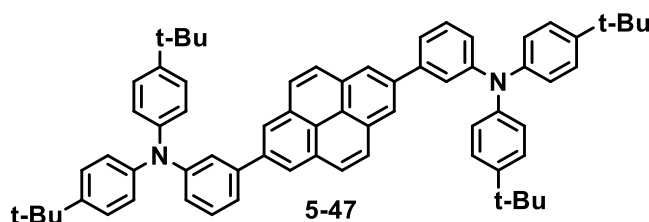
5-47

In a 50 mL flame-dried Schlenk-flask 2,7-bis(4,4,5,5-tetramethyl-1,3,2-dioxaborolan-2-yl)pyrene (**5-36**) (0.68 g, 1.5 mmol) and 3-bromo-N,N-bis(4-(*tert*-butyl)phenyl)aniline (**5-34**) (1.58 g, 3.27 mmol) were dissolved in a mixture of 20 mL toluene, Na_2CO_3 solution (10 mL, 2 mol/L) and 0.05 mL Aliquat 336 and (freeze-pump-thaw cycling ×3). Tetrakis(triphenylphosphine)palladium (137.4 mg, 0.12 mmol) was added and the mixture was stirred at 100 °C for 16 h. The cooled mixture was poured on 50 mL of water and filtered. The crude product was washed with water (300 mL), methanol (200 mL), hexane (200 mL) and cool CH_2Cl_2 (100 mL), filtered through a plug of silica (CH_2Cl_2), recrystallized from toluene (×3) yielding the title compound as a colorless solid (740 mg, 53 %).

Mp: 203-205 °C
FD-MS (8 KV): m/z 912.7 (100 %, M$^+$), calculated 912.5
^{1}H-NMR (500 MHz, 333 K, THF-d$_8$): δ 1.32 (s, 36H), 7.01 − 7.12 (m, 12H), 7.31 (d, J = 8.7 Hz, 8H), 7.37 (t, J = 7.9 Hz, 2H), 7.47 − 7.53 (m, 2H), 8.06 (s, 4H), 8.31 (s, 4H).
^{13}C-NMR (126 MHz, 333 K, THF-d$_8$): δ 32.0, 35.1, 122.9, 123.8, 124.1, 124.7, 124.9, 125.0, 127.0, 128.8, 130.6, 132.7, 140.1, 143.8, 146.7, 146.7, 150.2.
Elemental analysis (%) found C, 89.39; H, 7.53; N, 3.08 calculated C68H68N2 C, 89.43; H, 7.51; N, 3.07.

VIII.3.3.22   3,3'-(Pyrene-2,7-diyl)bis(N,N-bis(4-methoxyphenyl)aniline) (5-48)
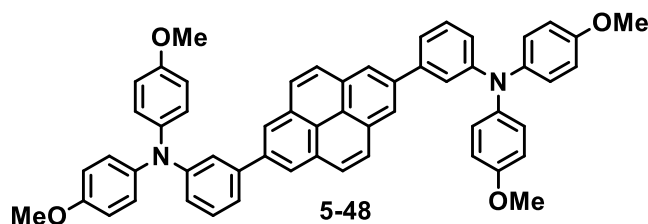
In a 50 mL flame-dried Schlenk-flask 2,7-bis(4,4,5,5-tetramethyl-1,3,2-dioxaborolan-2-yl)pyrene (**5-36**) (1.0 g, 2.2 mmol) and 3-bromo-N,N-bis(4-methoxyphenyl)aniline (**5-35**)(1.86 g, 4.84 mmol) were dissolved in a mixture of 20 mL toluene, Na$_2$CO$_3$ solution (10 mL, 2 mol/L) and 0.05 mL Aliquat 336 and degassed (freeze-pump-thaw cycling ×3). Tetrakis(triphenylphosphine)palladium (203.6 mg, 0.18 mmol) was added and the mixture was stirred at 100 °C for 16 h. The cooled mixture was poured on 50 mL of water and filtered. The crude product was washed with water (300 mL), methanol (200 mL), hexane (200 mL) and cool CH$_2$Cl$_2$ (150 mL), filtered through a plug of silica (CH$_2$Cl$_2$), recrystallized from toluene (×3) yielding the title compound as a colorless solid (760 mg, 42 %).

Mp: 229 °C, (decomp.)
FD-MS (8 KV): m/z 808.5 (100 %, M$^+$), calculated 808.3
^{1}H-NMR (500 MHz, 333 K, THF-d$_8$): δ 3.75 (s, 12H), 6.85 (d, J = 8.9 Hz, 8H), 6.93 (dd, J = 8.1, 2.3 Hz, 2H), 7.07 − 7.13 (d, J = 8.9 Hz, 8H), 7.30 (t, J = 7.9 Hz, 2H), 7.36 − 7.41 (m, 2H), 7.50 (d, J = 2.0 Hz, 2H), 8.07 (s 4H), 8.29 (s 4H).
^{13}C-NMR (126 MHz, 333 K, THF-d$_8$): δ 55.8, 67.6, 115.8, 121.3, 121.5, 121.6, 124.6, 124.9, 127.4, 128.8, 130.4, 132.7, 140.3, 142.5, 143.6, 150.9, 157.5.
Elemental analysis (%) found C, 83.20; H, 5.46; N, 3.51 calculated C56H44N2O4 C, 83.14; H, 5.48; N, 3.46.

VIII.3.4   4,9,10-Functionalized pyrenes

VIII.3.4.1   Pyrene-4,5-dione (6-2)

6-2
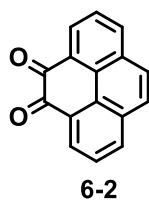
Pyrene-4,5-dione was prepared according to a procedure by HU *et al.*[59].

VIII.3.4.2   9-Bromopyrene-4,5-dione (6-5)

6-5
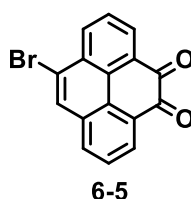
In a 25 mL flame-dried Schlenk-flask pyrene-4,5-dione (**6-2**) (1.0 g, 4.31 mmol) and N-bromosuccinimide (766.4 mg, 4.31 mmol) was dissolved in 10 mL concentrated sulfuric acid and stirred for 2 h at 40°C. The mixture was poured onto 300 mL ice water, the crude product was collected by filtration, washed with water, methanol, hexane and CH_2Cl_2 yielding the title compound as an orange solid (827 mg, 62 %).

Mp: 220-224 °C, (decomp.)
FD-MS (8 KV): m/z 309.8 (100 %, M$^+$), calculated 310.0

VIII.3.4.3   [4,4'-Bipyrene]-9,9',10,10'-tetraone (6-6)

6-6
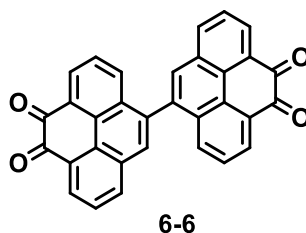
In a 25 mL flame-dried Schlenk-flask 9,9',10,10'-tetramethoxy-4,4'-bipyrene (**6-9**) was dissolved in 10 mL anhydrous CH_2Cl_2. At 0 °C (ice bath) borontribromide (0,48 mL 1 M solution in CH_2Cl_2, 0.48 mmol) was added. The mixture was allowed to warm to room temperature and stirred for 8 h. The reaction was quenched by the addition of nitric acid (65%, 50 mL) and stirred for an additional hour. The phases were separated, the aqueous phase was extracted with CH_2Cl_2 (15 mL×3). The combined organic phases were washed with sat. NaCl solution. The solvent was evaporated to give a crude product that is washed with hot THF and dried in high vacuum to provide the title compound as a red solid

Mp: 254 °C, (decomp.)
FD-MS (8 KV): m/z 462.1 (100 %, M⁺), calculated 462.1
MALDI-TOF: m/z = 462.086, 463.095 and 464.099 (calc. 462.089, 463.093 and 464.096)

VIII.3.4.4   9-Bromo-4,5-dimethoxypyrene (6-7)

6-7
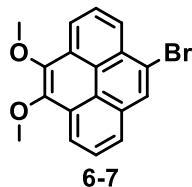
In a 100 mL flame-dried Schlenk-flask 9-bromopyrene-4,5-dione (**6-5**) (0.70 g, 2.25 mmol), Bu₄NBr (0.507 g, 1.57 mmol) and Na₂S₂O₄ (1.57 g, 9.0 mmol) were suspended in 10 mL THF and 5 mL water. Methyliodide (1.6 g, 11.3 mmol) was added followed by aqueous potassium hydroxide solution (7 mL 4.5 M). The reaction mixture was stirred at 40°C for 16 h. CH₂Cl₂ (40 mL) was added, the phases separated. The aqueous phase was extracted with CH₂Cl₂ (100 mL×3), the combined organic phases were dried with MgSO₄ and filtered. The solvent was removed *in vacuo*, the crude product was subjected to column chromatography (silica; PE/DCM 1:1) yielding the title compound as a colorless solid (430 mg, 56 %).

Mp: 171-173 °C
FD-MS (8 KV): m/z 340.2 (100 %, M⁺), calculated 340.0
¹H-NMR (300 MHz, CD₂Cl₂): δ 4.12 (d, *J* = 1.5 Hz, 6H), 7.86 − 8.20 (m, 3H), 8.37 (s, 1H), 8.42 − 8.80 (m, 3H).
¹³C-NMR (75 MHz, CD₂Cl₂): δ 61.7, 81.2, 98.0, 100.6, 101.2, 106.0, 112.9, 120.7, 121.2, 124.6, 124.9, 127.1, 127.2, 131.4.
Elemental analysis (%) found C, 63.41; H, 3.80 calculated C18H13BrO2 C, 63.36; H, 3.84.

VIII.3.4.5   2-(9,10-Dimethoxypyren-4-yl)-4,4,5,5-tetramethyl-1,3,2-dioxaborolane (6-8)

6-8
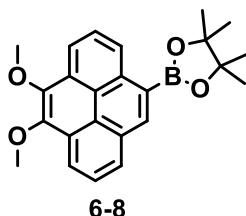
In a 25 mL flame-dried Schlenk-flask 9-bromo-4,5-dimethoxypyrene (**6-7**), (127 mg, 0.37 mmol) [1,1′-bis(diphenylphosphino)ferrocene]dichloropalladium(II) (5.44 mg, 7.5 μmol), bis(pinacolato)diboron (104.0 mg, 0.41 mmol) and potassium acetate (108 mg, 1.1 mmol) were dissolved in anhydrous DMF (10 mL). The mixture was stirred 16 h at 90 °C. After cooling the mixture was poured onto water (300 mL), the suspension was extracted with CH₂Cl₂ (50 mL×3). The combined organic phases were washed with sat. NaCl solution (50 mL), dried with MgSO₄ and filtered. The solvent was removed *in vacuo*,

the crude product was subjected to column chromatography (silica; CH_2Cl_2 yielding the title compound as a colorless solid (122 mg, 84 %).

FD-MS (8 KV): m/z 388.3 (100 %, M$^+$), calculated 388.2
^{1}H-NMR (250 MHz, CD_2Cl_2): δ 1.40 (s, 12H), 4.11 (d, J = 0.5 Hz, 6H), 7.96 (td, J = 7.8, 6.2 Hz, 2H), 8.11 (dd, J = 7.8, 1.2 Hz, 1H), 8.41 (ddd, J = 7.9, 5.9, 1.2 Hz, 2H), 8.60 (s, 1H), 8.96 (dd, J = 7.9, 1.1 Hz, 1H).
^{13}C-NMR (63 MHz, CD_2Cl_2): δ 25.4, 61.5, 61.6, 84.6, 119.7, 120.8, 123.2, 125.6, 126.1, 126.5, 126.6, 128.7, 129.0, 130.7, 133.2, 134.0, 138.8

VIII.3.4.6   9,9',10,10'-Tetramethoxy-4,4'-bipyrene (6-9)

6-9
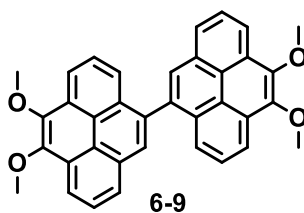
In a 25 mL flame-dried Schlenk-flask 9-bromo-4,5-dimethoxypyrene (180 mg, 0.52 mmol) and 2-(9,10-dimethoxypyren-4-yl)-4,4,5,5-tetramethyl-1,3,2-dioxaborolane (180 mg, 0.46 mmol) were dissolved in a mixture of 10 mL toluene, Na_2CO_3 solution (5 mL, 2 mol/L) and 0.05 mL Aliquat 336 and degassed (freeze-pump-thaw cycling ×3). Tetrakis(triphenylphosphine)palladium (42.9 mg, 37 μmol) was added and the mixture was stirred at 100 °C for 16 h. The cooled mixture was poured on 50 mL of water and extracted with CH_2Cl_2 (50 mL×3). The organic phases were combined, washed with sat. NaCl solution (100 mL), dried with $MgSO_4$ and filtered. The solvent was removed *in vacuo*, the crude product was subjected to column chromatography (silica; CH_2Cl_2) yielding the title compound as a colorless solid (207 mg, 85 %).

Mp: 227 - 229°C
FD-MS (8 KV): m/z 522.3 (100 %, M$^+$), calculated 522.2
^{1}H-NMR (250 MHz, CD_2Cl_2): δ 4.27 (d, J = 6.3 Hz, 12H), 7.71 – 7.84 (m, 4H), 8.12 (t, J = 7.7 Hz, 2H), 8.20 – 8.26 (m, 2H), 8.28 (s, 2H), 8.50 (dd, J = 7.2, 1.8 Hz, 2H), 8.59 (dd, J = 7.7, 1.2 Hz, 2H).
^{13}C-NMR (63 MHz, CD_2Cl_2): δ 61.6, 61.7, 100.5, 106.1, 120.0, 120.1, 122.5, 123.2, 123.5, 124.4, 125.3, 126.5, 126.9, 128.9, 129.2, 129.4, 131.4, 132.0, 138.3, 145.4, 209.7.
Elemental analysis (%) found C, 82.62; H, 5.07 calculated C36H26O4 C, 82.74; H, 5.01.

VIII.3.4.7   3,9-Bis(9,10-dimethoxypyren-4-yl)perylene (6-13)

6-13
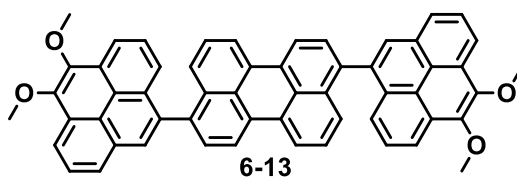
In a 50 mL flame-dried Schlenk-flask 3,9-dibromoperylene (39.9 mg, 97.4 μmol) and 2-(9,10-dimethoxypyren-4-yl)-4,4,5,5-tetramethyl-1,3,2-dioxaborolane (**6-8**) (84.0 mg,

0.22 mmol) were dissolved in a mixture of 4 mL toluene, Na$_2$CO$_3$ solution (10 mL, 2 mol/L) and 0.05 mL Aliquat 336 and degassed (freeze-pump-thaw cycling ×3). Tetrakis(triphenylphosphine)palladium (14.9 mg, 12.9 μmol) was added and the mixture was stirred at 100 °C for 16 h. The cooled mixture was poured on 50 mL of water and extracted with CH$_2$Cl$_2$ (50 mL×3). The organic phases were combined, washed with sat. NaCl solution (100 mL) dried with MgSO$_4$ and filtered. The solvent was removed *in vacuo*, the crude product was subjected to column chromatography (silica; CH$_2$Cl$_2$) yielding the title compound as a yellow solid (119 mg, 71 %).

Mp: 229-232 °C
FD-MS (8 KV): m/z 772.6 (100 %, M$^+$), calculated 772.3
^{1}H-NMR (500 MHz, 373 K, C$_2$D$_2$Cl$_4$): δ 4.29 (d, *J* = 6.1 Hz, 12H), 7.34 (dt, *J* = 12.3, 8.0 Hz, 2H), 7.46 – 7.55 (m, 2H), 7.74 (dd, *J* = 12.6, 7.6 Hz, 2H), 7.86 (q, *J* = 7.1, 5.8 Hz, 2H), 7.91 (td, *J* = 7.7, 1.9 Hz, 2H), 8.11 (t, *J* = 7.7 Hz, 2H), 8.15 – 8.25 (m, 4H), 8.27 (d, *J* = 7.4 Hz, 1H), 8.34 (d, *J* = 7.4 Hz, 1H), 8.43 (d, *J* = 7.6 Hz, 1H), 8.52 (dd, *J* = 15.0, 7.6 Hz, 3H), 8.58 (d, *J* = 7.9 Hz, 2H).
^{13}C-NMR (126 MHz, 373 K, C$_2$D$_2$Cl$_4$): δ 61.2, 119.7, 119.7, 120.2, 120.3, 120.4, 120.6, 120.7, 122.8, 123.2, 123.9, 124.7, 126.1, 126.3, 126.8, 126.9, 126.9, 128.5, 128.8, 128.8, 128.8, 129.0, 129.0, 130.9, 131.3, 131.4, 131.5, 131.6, 131.7, 134.5, 137.9, 138.5, 144.8, 145.0.
Elemental analysis (%) found C, 87.29; H, 4.30 calculated C56H36O4 C, 87.02; H, 4.70.

VIII.3.4.8   9-Bromo-4,5-bis(dodecyloxy)pyrene (6-15a)

6-15a
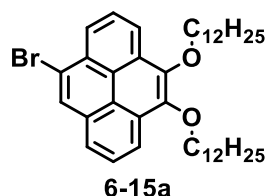
In a 100 mL flame-dried Schlenk-flask, 9-bromopyrene-4,5-dione (**6-5**) (0.70 g, 2.25 mmol), tetrabutylammonium bromide (0.57 g, 1.57 mmol) and sodium dithionite (1.57 g, 9.00 mmol) were suspended in a mixture of 35 mL THF and 20 mL water and stirred vigorously for five minutes at room temperature. 1-Bromodocecane (2.19 mL, 11.25 mmol) followed by aqueous potassium hydroxide solution (15 mL, 4 M) were added and the reaction was stirred at 40°C for 16 . CH$_2$Cl$_2$ (200 mL) was added and extracted with CH$_2$Cl$_2$ (100 mL×3). The combined organic phases were dried over MgSO$_4$ and filtered. The solvent was removed *in vacuo*, the crude product was subjected to column chromatography (silica; PE) yielding the title compound as a colorless oil (0.83 g, 56 %).

Mp: 178-179°C
FD-MS (8 KV): m/z 648.1 (100 %, M$^+$), calculated 648.4
^{1}H-NMR (300 MHz, CD$_2$Cl$_2$): δ 0.93 (t, *J* = 6.4 Hz, 6H), 1.10 – 1.55 (m, 32H), 1.64 (p, *J* = 7.0 Hz, 4H), 1.99 (p, *J* = 6.9 Hz, 4H), 4.33 (t, *J* = 6.8 Hz, 4H), 8.00 (d, *J* = 6.9 Hz, 2H), 8.09 (t, *J* = 8.0 Hz, 1H), 8.38 (s, 1H), 8.54 (dd, *J* = 16.8, 7.9 Hz, 3H).

^{13}C-NMR (75 MHz, CD$_2$Cl$_2$): δ 23.4, 27.0, 30.1, 30.3, 30.4, 30.4, 31.3, 32.6, 74.4, 120.8, 121.3, 122.4, 122.8, 124.0, 124.4, 124.8, 127.0, 127.1, 129.5, 129.8, 130.2, 131.4, 131.7, 144.5, 144.6.
Elemental analysis (%) found C, 72.01; H, 9.04 calculated C40H57BrO2 C, 73.94; H, 8.84.

VIII.3.4.9   2-(9,10-Bis(dodecyloxy)pyrene-4-yl)-4,4,5,5-tetramethyl-1,3,2-dioxaborolane (6-15)
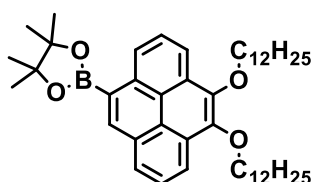
6-15

In a 25 mL flame-dried Schlenk-flask 9-bromo-4,5-bis(dodecyloxy)pyrene (**6-15a**) (1.60 g, 2.5 mmol), [1,1′-bis(diphenylphosphino)ferrocene]dichloropalladium(II) (36.0 mg, 49.3 μmol), bis(pinacolato)diboron (687.81 mg, 2.7 mmol) and potassium acetate (725 mg, 7.4 mmol) were dissolved in anhydrous DMF (10 mL) and stirred 16 h at 90 °C. After cooling the mixture was poured onto water (300 mL) and extracted with CH$_2$Cl$_2$ (100 mL×3). The combined organic phases were washed with sat. NaCl solution (50 mL) and dried with MgSO$_4$ and filtered. The solvent was removed *in vacuo*, the crude product was subjected to column chromatography (silica; PE/CH$_2$Cl$_2$ 2:1) yielding the title compound as a colourless oil (1.05 g, 61 %).

Mp: 168-171°C
FD-MS (8 KV): m/z 696.5 (100 %, M$^+$), calculated 696.5
^{1}H-NMR (250 MHz, CD$_2$Cl$_2$): δ 0.92 (q, *J* = 6.7, 4.7 Hz, 6H), 1.33 (q, *J* = 17.1, 13.5 Hz, 36H), 1.51 (s, 12H), 1.99 (d, *J* = 8.6 Hz, 4H), 4.35 (t, *J* = 6.6 Hz, 4H), 8.06 (dt, *J* = 8.8, 7.8 Hz, 2H), 8.16 – 8.28 (m, 1H), 8.54 (ddd, *J* = 7.8, 4.2, 1.2 Hz, 2H), 8.72 (s, 1H), 9.08 (dd, *J* = 7.9, 1.1 Hz, 1H).
^{13}C-NMR (63 MHz, CD$_2$Cl$_2$): δ 14.5, 23.3, 25.4, 26.9, 30.0, 30.2, 30.3, 30.3, 31.2, 32.6, 74.3, 84.6, 119.8, 121.0, 123.3, 124.4, 125.5, 126.0, 126.6, 129.3, 129.6, 130.7, 134.0, 138.9, 144.1, 144.8.

VIII.3.4.10   3,9-Bis(9,10-bis(dodecyloxy)pyrene-4-yl)perylene (6-16)
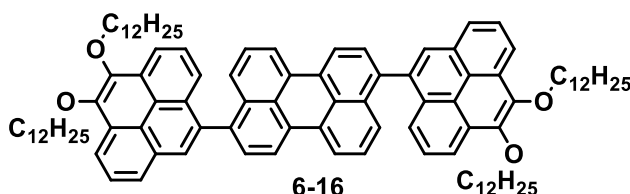
6-16

In a 50 mL flame-dried Schlenk-flask 3,9-dibromoperylene (79.5 mg, 0.19 mmol) and 2-(9,10-bis(dodecyloxy)pyrene-4-yl)-4,4,5,5-tetramethyl-1,3,2-dioxaborolane (**6-15**) (300.0 mg, 0.43 mmol) were dissolved in a mixture of 4 mL toluene Na$_2$CO$_3$ solution (10 mL, 2 mol/L) and 0.05 mL Aliquat 336 and degassed (freeze-pump-thaw cycling ×3).

Tetrakis(triphenylphosphine)palladium (29.9 mg, 25.8 μmol) was added and the mixture stirred at 100 °C for 16 h. The cooled mixture was poured on 50 mL of water and extracted with CH_2Cl_2 (50 mL×3). The organic phases were combined, washed with sat. NaCl solution (100 mL) dried with $MgSO_4$ and filtered. The solvent was removed *in vacuo*, the crude product was subjected to column chromatography (silica; CH_2Cl_2) yielding the title compound as a yellow solid (119 mg, 71 %).

Mp: 184-185°C
FD-MS (8 KV): m/z 1390.2 (100 %, M$^+$), calculated 1390.0
^{1}H-NMR (300 MHz, CD_2Cl_2): δ 0.93 (td, *J* = 6.8, 6.4, 4.0 Hz, 12H), 1.23 – 1.54 (m, 64H), 1.69 (dqd, *J* = 12.4, 7.1, 5.5, 3.4 Hz, 8H), 2.06 (ddd, *J* = 12.2, 6.1, 3.1 Hz, 8H), 4.43 (td, *J* = 6.6, 5.1 Hz, 8H), 7.27 – 7.49 (m, 4H), 7.75 (dd, *J* = 7.6, 4.9 Hz, 2H), 7.83 (dd, *J* = 7.9, 1.2 Hz, 2H), 7.93 (td, *J* = 7.8, 2.2 Hz, 2H), 8.14 (td, *J* = 7.7, 0.8 Hz, 2H), 8.19 – 8.28 (m, 4H), 8.31 (dd, *J* = 7.7, 1.2 Hz, 1H), 8.35 – 8.42 (m, 1H), 8.47 (d, *J* = 7.8 Hz, 1H), 8.53 (d, *J* = 7.8 Hz, 1H), 8.55 – 8.66 (m, 4H).
^{13}C-NMR (75 MHz, CD_2Cl_2): δ 14.5, 23.3, 27.0, 30.0, 30.2, 30.3, 31.2, 32.6, 74.4, 120.3, 120.8, 120.9, 121.1, 121.2, 123.1, 123.6, 124.2, 125.1, 126.6, 126.9, 127.3, 129.3, 129.4, 129.5, 129.5, 129.8, 131.4, 131.8, 132.1, 134.9, 138.3, 139.0, 144.8, 150.6
Elemental analysis (%) found C, 86.15; H, 8.95 calculated $C_{100}H_{124}O_4$ C, 86.40; H, 8.99

VIII.3.4.11   11,12,23,24-Tetrakis(dodecyloxy)benzo[vwx]naphtho[2,1,8,7-klmn]naphtho[2',1',8',7':6,7,8]tetrapheno[5,4,3-cde]hexaphene (6-17)
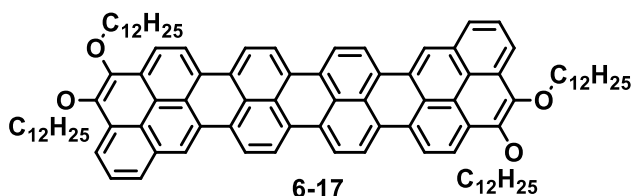
In a 25 mL flame-dried Schlenk-flask 9-bis(9,10-bis(dodecyloxy)pyrene-4-yl)perylene (**6-17**) (10 mg, 7.19 μmol) was dissolved in 10 mL stabilizer-free CH_2Cl_2 and purged by bubbling argon through the solution for 20 min. Iron(III)chloride (14 mg, 86.3 μmol) was dissolved in 2 mL nitromethane and added to the reaction mixture at room temperature. The mixture was stirred for 4 h at room temperature. The crude product was precipitated by the addition of methanol, collected by filtration, washed with water and methanol and subjected to size exclusion chromatography (CH_2Cl_2) yielding the title compound as a blue solid.

FD-MS (8 KV): m/z 1385.4 (100 %, M$^+$), calculated 1385.9
MALDI-TOF: m/z 1385.89 (100 %, M$^+$) calcd 1385.92

VIII.3.4.12   4,5,9',10'-Tetrakis(dodecyloxy)-1,4'-bipyrene (6-18a)
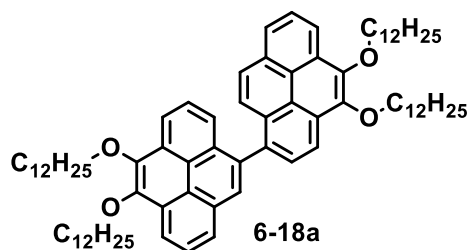
In a 25 mL flame-dried Schlenk-flask 1-bromo-4,5-bis(dodecyloxy)pyrene (**6-19**) (72.0 mg, 0.11 mmol) and 2-(9,10-bis(dodecyloxy)pyrene-4-yl)-4,4,5,5-tetramethyl-1,3,2-dioxaborolane (**6-15**) (77.2 mg, 0.11 mmol) were dissolved in a mixture of 4 mL toluene, Na_2CO_3 solution (10 mL, 2 mol/L) and 0.05 mL Aliquat 336 and (freeze-pump-thaw cycling ×3). Tetrakis(triphenylphosphine)palladium (6.4 mg, 5.5 μmol) was added and the mixture was stirred at 100 °C for 16 h. The cooled mixture was poured on 50 mL of water and extracted with CH_2Cl_2 (25 mL×3). The organic phases were combined, washed with sat. NaCl solution (100 mL) and dried with $MgSO_4$ and filtered. The solvent was removed *in vacuo*, the crude product was subjected to column chromatography (silica; CH_2Cl_2) yielding the title compound as a colorless solid (84 mg, 74 %).

Mp: 158°C
**FD-MS** (8 KV): m/z 1138.6 (100 %, M^+), calculated 1138.9
^{1}H-NMR (300 MHz, CD_2Cl_2): δ 0.82 – 0.98 (m, 12H), 1.30 (q, J = 6.5, 5.5 Hz, 63H), 1.67 (qd, J = 7.4, 3.4 Hz, 8H), 1.91 – 2.25 (m, 8H), 4.41 (p, J = 7.0 Hz, 8H), 7.61 (dd, J = 8.5, 4.1 Hz, 1H), 7.71 – 7.90 (m, 4H), 8.00 – 8.15 (m, 3H), 8.20 (q, J = 4.6, 4.0 Hz, 3H), 8.49 – 8.62 (m, 3H), 8.68 (d, J = 8.0 Hz, 1H).
^{13}C-NMR (75 MHz, CD_2Cl_2): δ 14.5, 14.5, 23.3, 23.3, 26.9, 27.0, 30.0, 30.0, 30.2, 30.3, 30.3, 31.2, 31.3, 32.5, 32.6, 74.4, 119.8, 120.2, 120.3, 123.1, 123.5, 123.5, 124.4, 124.9, 126.5, 126.7, 126.9, 127.9, 129.1, 129.5, 129.8, 129.9, 130.7, 131.3, 131.5, 132.2, 135.6, 138.7, 144.6, 144.7, 144.7.

VIII.3.4.13   1,2,9,10-tetrakis(dodecyloxy)dinaphtho[2,1,8,7-defg:2',1',8',7'-opqr]pentacene (6-18B)
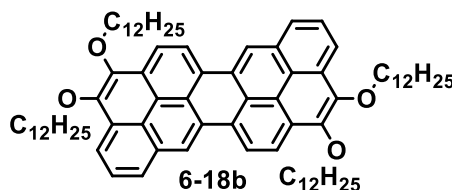
In a 25 mL flame-dried Schlenk-flask 4,5,9',10'-tetrakis(dodecyloxy)-1,4'-bipyrene (26 mg, 22.8 μmol) (**6-18**) was dissolved in 5 mL stabilizer-free CH_2Cl_2 and purged by bubbling argon through the solution for 20 min. Iron(III)chloride (14.8 mg, 91.3 μmol) was dissolved in 1 mL nitromethane and added to the reaction mixture at room temperature. The mixture was stirred for 4 h at room temperature. The crude product was precipitated by the addition of methanol, collected by filtration, washed with water and methanol and

subjected to size exclusion chromatography (CH_2Cl_2) yielding the title compound as a yellow solid.

FD-MS (8 KV): m/z 1137.2 (100 %, M$^+$), calculated 1136.9
^{1}H-NMR (250 MHz, CD_2Cl_2): δ 0.70 – 0.95 (m, 12H), 1.26 (s, 64H), 1.62 (d, J = 8.5 Hz, 8H), 1.99 (dd, J = 14.2, 7.6 Hz, 8H), 4.03 – 4.64 (m, 8H), 7.24 – 8.81 (m, 12H).

VIII.3.4.14   4,5-Bis(dodecyloxy)pyrene (6-19a)

6-19a
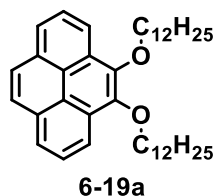
4,5-bis(dodecyloxy)pyrene was prepared according to a procedure published by VENKATARAMAN *et al.*[91]

VIII.3.4.15   1-Bromo-4,5-bis(dodecyloxy)pyrene (6-19)

6-19
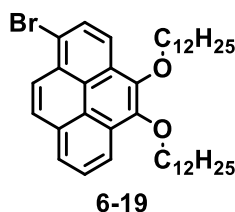
In a 25 mL flame-dried Schlenk-flask, 4,5-bis(dodecyloxy)pyrene (1.00 g, 1.75 mmol) was dissolved in 30 mL CH_2Cl_2. A bromine solution (1 M, in CH_2Cl_2, 1,93 mL, 1,93 mmol) was added slowly at room temperature and the resulting mixture was stirred for 2 h. $Na_2S_2O_3$ solution was added, the phases were separated, the aqueous phase was extracted with CH_2Cl_2 (100 mL×3). The combined organic phases were washed with sat. NaCl solution, dried with $MgSO_4$ and filtered. The solvent was removed *in vacuo*, the crude product was subjected to column chromatography (silica; PE/CH_2CL_2 5:1) yielding the title compound as a colorless solid (954 mg, 84 %).

Mp: 196-197 °C
FD-MS (8 KV): m/z 648.5 (100 %, M$^+$), calculated 648.4
^{1}H-NMR ^{1}H NMR (250 MHz, CD_2Cl_2): δ 0.79 – 1.01 (m, 6H), 1.31 (d, *J* = 7.5 Hz, 32H), 1.62 (dq, *J* = 10.5, 2.9 Hz, 4H), 1.96 (dqd, *J* = 10.3, 6.7, 3.7 Hz, 4H), 4.32 (td, *J* = 6.6, 4.1 Hz, 4H), 8.05 (t, *J* = 7.7 Hz, 1H), 8.11 – 8.27 (m, 3H), 8.37 (dd, *J* = 14.7, 8.8 Hz, 2H), 8.53 (dd, *J* = 7.8, 1.2 Hz, 1H).

VIII.3.4.16   1,5-Bis(9,10-bis(dodecyloxy)pyrene-4-yl)naphthalene (6-21a)

6-21a
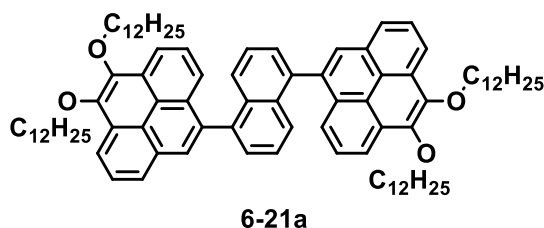
In a 50 mL flame-dried Schlenk-flask 1,5-dibromonaphthalene (70.0 mg, 0.24 mmol) and 2 (9,10-bis(dodecyloxy)pyrene-4-yl)-4,4,5,5-tetramethyl-1,3,2-dioxaborolane   (**6-15**) (358.0 mg, 0.51 mmol) were dissolved in a mixture of 4 mL toluene, Na_2CO_3 solution (10 mL, 2 mol/L) and 0.05 mL Aliquat 336 and degassed (freeze-pump-thaw cycling ×3). Tetrakis(triphenylphosphine)palladium (29.9 mg, 25.8 μmol) was added and the mixture was stirred at 100 °C for 16 h. The cooled mixture was poured onto water (50 mL) and extracted with CH_2Cl_2 (50 mL×3). The organic phases were combined, washed with sat. NaCl solution (100 mL) dried with $MgSO_4$ and filtered. The solvent was removed *in vacuo*, the crude product was subjected to column chromatography (silica; CH_2Cl_2) yielding the title compound as a colorless solid (127 mg, 41 %).

Mp: 198-201°C, (decomp.)
FD-MS (8 KV): m/z 1265.0 (100 %, M$^+$), calculated 1264.9
^{1}H-NMR (700 MHz, CD_2Cl_2): δ 0.89 (dt, J = 8.3, 7.0 Hz, 12H), 1.26 – 1.43 (m, 64H), 1.63 – 1.71 (m, 8H), 2.00 – 2.05 (m, 8H), 4.37 – 4.43 (m, 8H), 7.44 (ddd, J = 8.8, 6.7, 2.5 Hz, 2H), 7.64 – 7.70 (m, 4H), 7.72 (dd, J = 7.8, 1.0 Hz, 1H), 7.83 (dd, J = 7.7, 1.1 Hz, 1H), 7.90 (t, J = 7.7 Hz, 1H), 7.95 (t, J = 7.7 Hz, 1H), 8.12 (td, J = 7.6, 6.3 Hz, 2H), 8.18 (s, 1H), 8.21 – 8.27 (m, 3H), 8.55 (ddd, J = 14.5, 7.7, 1.1 Hz, 2H), 8.59 (ddd, J = 7.8, 2.1, 1.1 Hz, 2H).
^{13}C-NMR (176 MHz, CD_2Cl_2): δ 13.9, 22.7, 26.4, 29.4, 29.7, 30.6, 31.9, 73.8, 100.0, 114.0, 119.6, 125.9, 126.7, 128.0, 128.9, 130.7, 131.5, 133.2, 138.0, 143.4, 144.0, 144.2.

VIII.4   Crystallographic data

VIII.4.1   2,4,5,7,9,10-Hexamethoxypyrene (2-6)
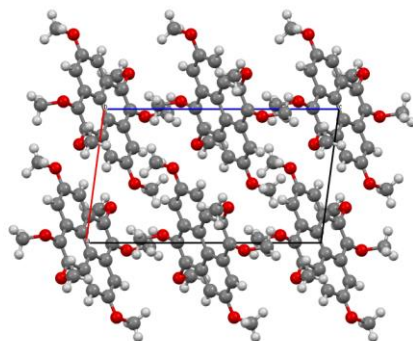
Crystal Data for $C_{22}H_{22}O_6$ (M =382.41): monoclinic, space group P2$_1$/c (no. 14), a = 8.1780(4) Å, b = 7.8530(2) Å, c = 14.2480(6) Å, β = 97.6840(15)°, V = 906.82(6) Å^3, Z = 2, T = 120.0 K, µ(Mo Kα) = 0.102 mm^{-1}, $Dcalc$ = 1.400 g/mm^3, 8692 reflections measured (7.226 ≤ 2Θ ≤ 61.944), 2875 unique (R_{int} = 0.042) which were used in all calculations. The final R_1 was 0.0414 (I>3.0σ(I)) and wR_2 was 0.0519 (all data).

Cambridge Crystallographic Data Centre (CCDC) deposition number: CCDC 857535

VIII.4.2   N2,N7-Bis(4-hexylphenyl)-4,5,9,10-tetramethoxypyrene-2,7-diamine (2-20)
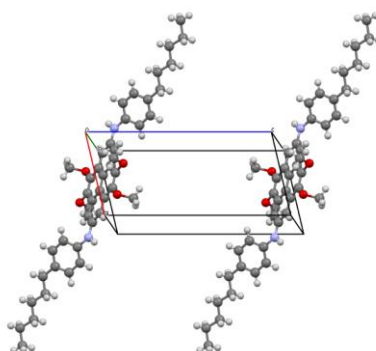
Crystal Data for $C_{22}H_{26}NO_2$ (M =336.45): triclinic, space group P-1 (no. 2), a = 7.3490(4) Å, b = 8.1540(6) Å, c = 15.9780(9) Å, α = 82.188(3)°, β = 76.849(4)°, γ = 77.044(4)°, V = 904.97(10) Å^3, Z = 2, T = 120.0 K, µ(Mo Kα) = 0.078 mm^{-1}, $Dcalc$ = 1.235 g/mm^3, 11743 reflections measured (5.146 ≤ 2Θ ≤ 60.094), 5201 unique (R_{int} = 0.050) which were used in all calculations. The final R_1 was 0.0794 (I>2.0σ(I)) and wR_2 was 0.0879 (all data).

Cambridge Crystallographic Data Centre (CCDC) deposition number: CCDC 1025659

VIII.4.3 (2,7-Diiodopyrene-4,5,9,10-tetrayl)tetrakis(oxy))tetrakis(*tert*-butyldimethylsilane) (2-26)
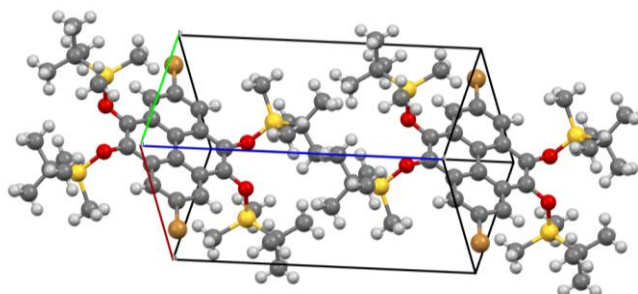
Crystal Data for $C_{40}H_{64}Br_2O_4S_4$ (M =897.02): triclinic, space group P-1 (no. 2), a = 7.5670(2) Å, b = 11.1324(4) Å, c = 14.4791(5) Å, α = 84.9791(16)°, β = 78.5154(19)°, γ = 74.8416(19)°, V = 1152.88(7) Å^3, Z = 1, T = 180.0 K, μ(Mo Kα) = 1.974 mm^{-1}, $Dcalc$ = 1.292 g/mm^3, 16764 reflections measured (5.746 ≤ 2Θ ≤ 61.884), 7278 unique (R_{int} = 0.079) which were used in all calculations. The final R_1 was 0.0489 (I>2.0σ(I)) and wR_2 was 0.0537 (all data).

Cambridge Crystallographic Data Centre (CCDC) deposition number: CCDC 1025657

VIII.4.4 N2,N8-Bis(4-hexylphenyl)-5,5,11,11-tetramethylpyreno[4,5-d:9,10-d']bis([1,3]dioxole)-2,8-diamine (2-28)
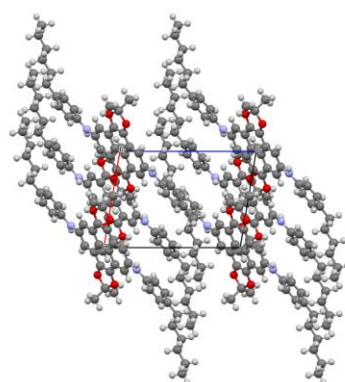
Crystal Data for $C_{46}H_{52}N_2O_4$ (M =696.93): monoclinic, space group P2$_1$/a (no. 14), a = 9.1357(7) Å, b = 16.1928(9) Å, c = 12.7618(9) Å, β = 99.423(3)°, V = 1862.4(2) Å^3, Z = 2, T = 120.0 K, μ(Mo Kα) = 0.078 mm^{-1}, $Dcalc$ = 1.243 g/mm^3, 12742 reflections measured (7.174 ≤ 2Θ ≤ 55.002), 4241 unique (R_{int} = 0.045) which were used in all calculations. The final R_1 was 0.0564 (I>2.0σ(I)) and wR_2 was 0.0575 (all data).

Cambridge Crystallographic Data Centre (CCDC) deposition number: CCDC 1025660

VIII.4.5   4,5,9,10-Tetramethoxypyrene (3-8)
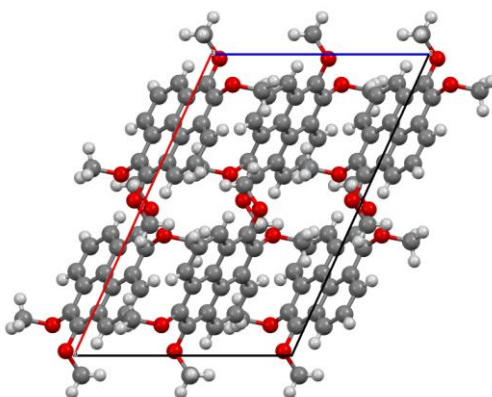
Crystal Data for $C_{10}H_9O_2$ (M =161.18): monoclinic, space group C2/c (no. 15), a = 15.5468(10) Å, b = 10.7779(10) Å, c = 10.2340(8) Å, β = 114.524(5)°, V = 1560.1(2) Å^3, Z = 8, T = 120.0 K, μ(Mo Kα) = 0.095 mm^{-1}, $Dcalc$ = 1.372 g/mm^3, 6636 reflections measured (4.752 ≤ 2Θ ≤ 61.008), 2336 unique (R_{int} = 0.051) which were used in all calculations. The final R_1 was 0.0429 (I>3.0σ(I)) and wR_2 was 0.0533 (all data).

Cambridge Crystallographic Data Centre (CCDC) deposition number: CCDC 1025939

VIII.4.6   1,3,6,8-Tetrabromo-4,5,9,10-tetramethoxypyrene (3-10)
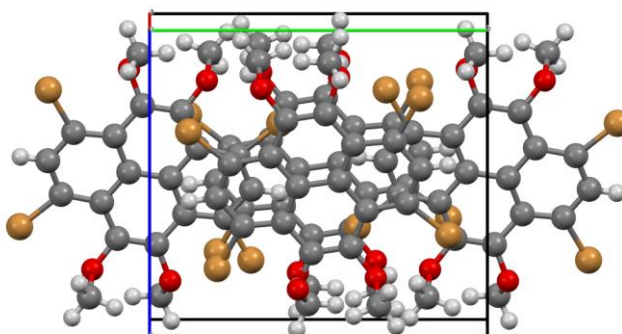
Crystal Data for $C_{20}H_{14}Br_4O_4$ (M =637.94): monoclinic, space group P2$_1$/a (no. 14), a = 8.1104(4) Å, b = 11.4863(6) Å, c = 10.3879(3) Å, β = 94.022(3)°, V = 965.34(7) Å^3, Z = 2, T = 120.0 K, μ(Mo Kα) = 8.364 mm^{-1}, $Dcalc$ = 2.195 g/mm^3, 9791 reflections measured (3.93 ≤ 2Θ ≤ 61.058), 2935 unique (R_{int} = 0.085) which were used in all calculations. The final R_1 was 0.0352 (I>3.0σ(I)) and wR_2 was 0.0425 (all data).

Cambridge Crystallographic Data Centre (CCDC) deposition number: 1025662

VIII.4.7 1,3,4,5,6,8,9,10-Octamethoxypyrene (3-13)

Crystal Data for $C_{24}H_{26}O_8$ (M =442.47): monoclinic, space group P2$_1$/n (no. 14), a = 11.9241(4) Å, b = 14.0125(6) Å, c = 13.6140(5) Å, β = 114.991(2)°, V = 2061.75(14) Å^3, Z = 4, T = 120.0 K, μ(Mo Kα) = 0.107 mm^{-1}, $Dcalc$ = 1.425 g/mm^3, 29966 reflections measured (6.604 ≤ 2Θ ≤ 60.078), 6002 unique (R_{int} = 0.062) which were used in all calculations. The final R_1 was 0.0679 (I>3.0σ(I)) and wR_2 was 0.0806 (all data).

Cambridge Crystallographic Data Centre (CCDC) deposition number: CCDC 1025640

VIII.4.8 4,5,9,10-Tetramethoxy-N1,N1,N3,N3,N6,N6,N8,N8-octakis(4-methoxyphenyl)-3a,3a1-dihydropyrene-1,3,6,8-tetraamine (3-14)
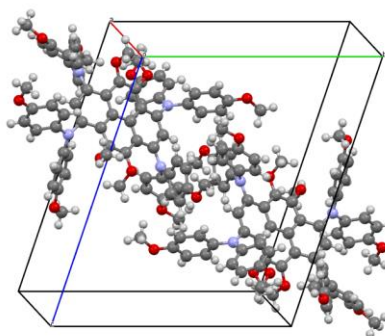
Crystal Data for $C_{76}H_{70}N_4O_{12}$ (M =1231.41): triclinic, space group P-1 (no. 2), a = 10.6026(2) Å, b = 16.5903(3) Å, c = 19.6502(5) Å, α = 108.7170(10)°, β = 98.4835(12)°, γ = 102.2777(12)°, V = 3110.66(12) Å^3, Z = 2, T = 120.0 K, μ(Mo Kα) = 0.089 mm^{-1}, $Dcalc$ = 1.315 g/mm^3, 35345 reflections measured (4.096 ≤ 2Θ ≤ 59.11), 17355 unique (R_{int} = 0.041) which were used in all calculations. The final R_1 was 0.0436 (I>3.0σ(I)) and wR_2 was 0.0535 (all data).

Cambridge Crystallographic Data Centre (CCDC) deposition number: CCDC 1025641

## VIII.4.9 ((4,5,9,10-Tetramethoxypyrene-1,3,6,8-tetrayl)tetrakis(ethyne-2,1-diyl))tetrakis(triisopropylsilane) (3-15)
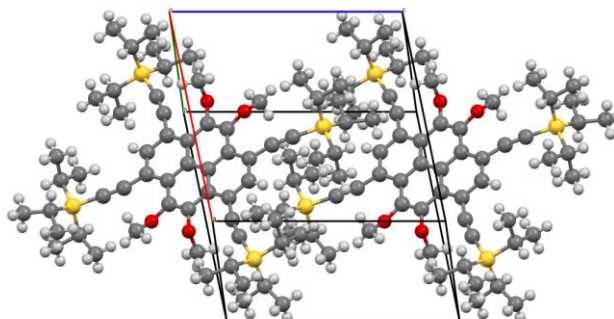
Crystal Data for $C_{32}H_{49}O_2S_2$ (M =529.87): triclinic, space group P-1 (no. 2), a = 11.4985(4) Å, b = 12.3173(4) Å, c = 12.5579(4) Å, α = 86.446(2)°, β = 78.3218(19)°, γ = 63.8690(14)°, V = 1562.99(9) Å^3, Z = 2, T = 120.0 K, μ(Mo Kα) = 0.195 mm^{-1}, $Dcalc$ = 1.126 g/mm^3, 22069 reflections measured (5.032 ≤ 2Θ ≤ 61.982), 9920 unique (R_{int} = 0.064) which were used in all calculations. The final R_1 was 0.0578 (I>2.0σ(I)) and wR_2 was 0.0605 (all data).

Cambridge Crystallographic Data Centre (CCDC) deposition number: 1025651

VIII.4.10 1,3,7,9-Tetrabromo-5,5,11,11-tetramethylpyreno[4,5-d:9,10-d']bis([1,3]dioxole) (3-20)
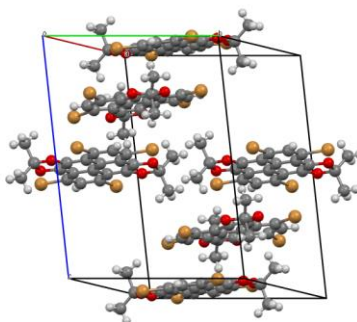
Crystal Data for $C_{44}H_{28}Br_8O_8$ (M =1323.93): triclinic, space group P-1 (no. 2), a = 11.7997(3) Å, b = 12.1281(3) Å, c = 16.8409(4) Å, α = 83.8786(14)°, β = 80.3786(14)°, γ = 61.2540(10)°, V = 2082.37(9) Å^3, Z = 2, T = 120.0 K, μ(Mo Kα) = 7.759 mm^{-1}, $Dcalc$ = 2.111 g/mm^3, 27626 reflections measured (2.454 ≤ 2Θ ≤ 63.052), 13841 unique (R_{int} = 0.078) which were used in all calculations. The final R_1 was 0.0484 (I>2.0σ(I)) and wR_2 was 0.0537 (all data).

Cambridge Crystallographic Data Centre (CCDC) deposition number: CCDC 1025642

VIII.4.11   N1,N3,N3,N6,N6,N8,N8-Octakis(4-methoxyphenyl)-3a,3a1-dihydropyrene-1,3,6,8-tetraamine (3-25)
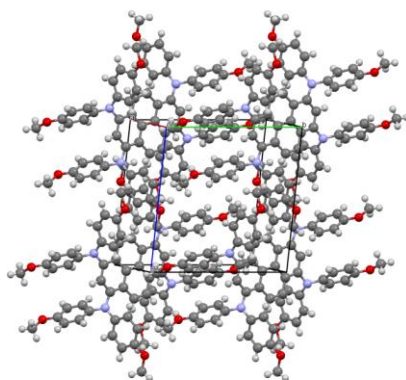
Crystal Data for $C_{36}H_{31}N_2O_4$ ($M = 555.65$): triclinic, space group P-1 (no. 2), $a = 10.4392(8)$ Å, $b = 11.5359(9)$ Å, $c = 12.3722(9)$ Å, $\alpha = 96.168(4)°$, $\beta = 91.560(4)°$, $\gamma = 107.034(4)°$, $V = 1413.61(19)$ Å^3, $Z = 2$, $T = 120.0$ K, μ(Mo Kα) = 0.085 mm^{-1}, $Dcalc = 1.305$ g/mm^3, 10117 reflections measured ($7.208 \leq 2\Theta \leq 55.016$), 6405 unique ($R_{int} = 0.055$) which were used in all calculations. The final R_1 was 0.0701 (I>2.0σ(I)) and wR_2 was 0.0612 (all data).

Cambridge Crystallographic Data Centre (CCDC) deposition number: CCDC 1025938

VIII.4.12   4,5,9,10-Tetramethoxy-1,3,6,8-tetrakis(trifluoromethyl)pyrene (3-34)
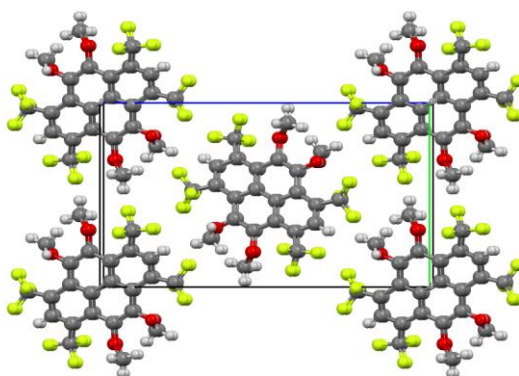
Crystal Data for $C_{12}H_7F_6O_2$ ($M = 297.17$): monoclinic, space group P2$_1$/c (no. 14), $a = 4.8990(2)$ Å, $b = 11.1511(6)$ Å, $c = 19.9813(9)$ Å, $\beta = 92.602(3)°$, $V = 1090.44(9)$ Å^3, $Z = 4$, $T = 120.0$ K, μ(Mo Kα) = 0.189 mm^{-1}, $Dcalc = 1.810$ g/mm^3, 10254 reflections measured ($7.132 \leq 2\Theta \leq 59.164$), 3046 unique ($R_{int} = 0.054$) which were used in all calculations. The final R_1 was 0.0447 (I>2.0σ(I)) and wR_2 was 0.0503 (all data).

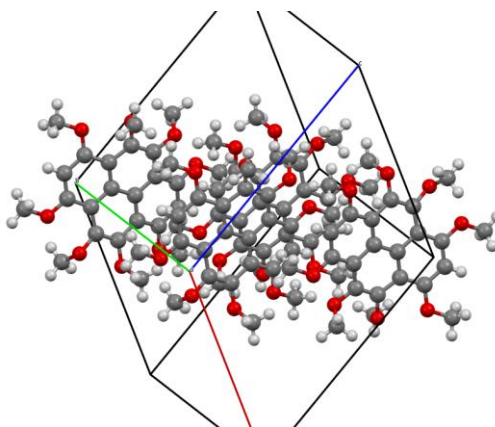Cambridge Crystallographic Data Centre (CCDC) deposition number: CCDC 1025646

VIII.4.13   4,5,9,10-Tetramethoxy-2,7-bis(trifluoromethyl)pyrene (3-36)
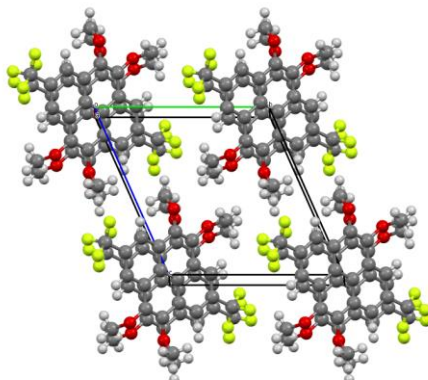
Crystal Data for $C_{11}H_8F_3O_2$ ($M =$229.18): triclinic, space group P-1 (no. 2), $a = 4.52450(10)$ Å, $b = 10.3279(5)$ Å, $c = 10.8332(6)$ Å, $\alpha = 65.981(2)°$, $\beta = 82.547(3)°$, $\gamma = 89.151(3)°$, $V = 458.08(4)$ Å^3, $Z = 2$, $T = 120.0$ K, μ(Mo Kα) = 0.153 mm^{-1}, $Dcalc = 1.661$ g/mm^3, 6375 reflections measured ($7.116 \leq 2\Theta \leq 61.972$), 2899 unique ($R_{int} = 0.073$) which were used in all calculations. The final R_1 was 0.0578 (I>2.0σ(I)) and wR_2 was 0.0672 (all data)

Cambridge Crystallographic Data Centre (CCDC) deposition number: CCDC 1025644

VIII.4.14   4,4',5,5',9,9',10,10'-Octamethoxy-3,3',6,6',8,8'-hexakis(trifluoromethyl)-1,1'-bipyrene (3-38)
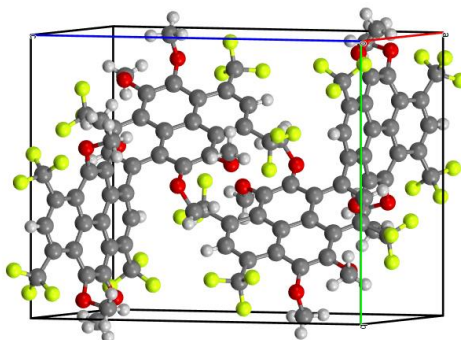
Crystal Data for $C_{23}H_{14}F_9O_4$ ($M =$525.34): triclinic, space group P-1 (no. 2), $a = 11.6508(2)$ Å, $b = 13.3556(3)$ Å, $c = 15.5913(3)$ Å, $\alpha = 91.0779(11)°$, $\beta = 109.4325(10)°$, $\gamma = 92.0461(10)°$, $V = 2285.19(8)$ Å^3, $Z = 4$, $T = 120.0$ K, μ(Mo Kα) = 0.152 mm^{-1}, $Dcalc = 1.527$ g/mm^3, 14547 reflections measured ($4.7 \leq 2\Theta \leq 62.016$), 14547 unique ($R_{int} = 0.062$) which were used in all calculations. The final R_1 was 0.0530 (I>2.0σ(I)) and wR_2 was 0.0594 (all data).

Cambridge Crystallographic Data Centre (CCDC) deposition number: 1025648

VIII.4.15   4-1/F4-TCNQ
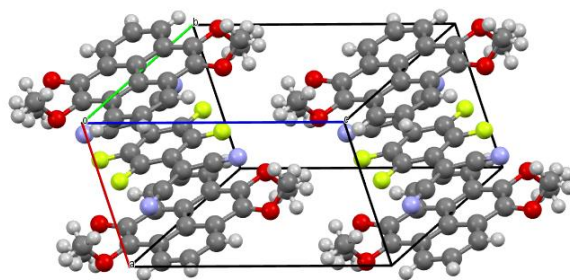
Crystal Data for $C_{16}H_9F_2N_2O_2$ (M =299.26): triclinic, space group P-1 (no. 2), a = 6.7723(3) Å, b = 10.6602(7) Å, c = 10.8483(6) Å, α = 61.385(2)°, β = 72.083(3)°, γ = 83.952(4)°, V = 653.35(7) Å^3, Z = 2, T = 120.0 K, μ(Mo Kα) = 0.121 mm^{-1}, $Dcalc$ = 1.521 g/mm^3, 8749 reflections measured (4.54 ≤ 2Θ ≤ 59.138), 3636 unique (R_{int} = 0.067) which were used in all calculations. The final R_1 was 0.0580 (I>2.0σ(I)) and wR_2 was 0.0652 (all data).

Cambridge Crystallographic Data Centre (CCDC) deposition number: CCDC 1025637

VIII.4.16   4-2/4-9
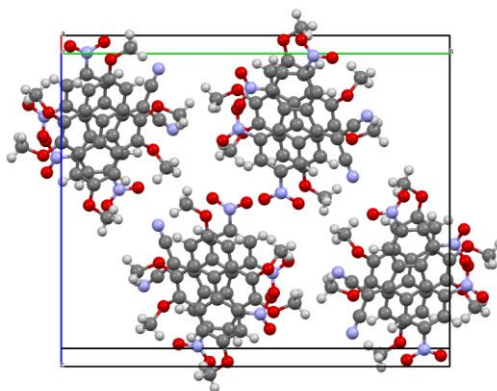
Crystal Data for $C_{38}H_{26}N_5O_{12}$ (M =744.65): monoclinic, space group P2$_1$/c (no. 14), a = 7.3136(2) Å, b = 23.5579(8) Å, c = 18.9555(6) Å, β = 98.6037(19)°, V = 3229.15(17) Å^3, Z = 4, T = 120.0 K, μ(Mo Kα) = 0.117 mm^{-1}, $Dcalc$ = 1.532 g/mm^3, 28814 reflections measured (2.776 ≤ 2Θ ≤ 60.124), 9371 unique (R_{int} = 0.054) which were used in all calculations. The final R_1 was 0.0381 (I>2.0σ(I)) and wR_2 was 0.0595 (all data).

Cambridge Crystallographic Data Centre (CCDC) deposition number: CCDC 1025940

VIII.4.17   4-2/4-10
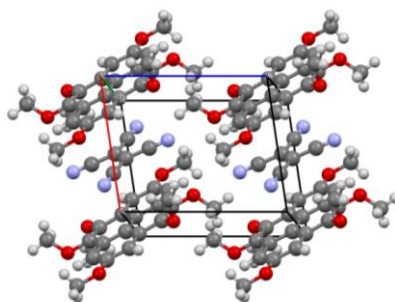
Crystal Data for $C_{28}H_{22}N_4O_6$ (M =510.51): triclinic, space group P-1 (no. 2), a = 7.4720(4) Å, b = 8.9918(5) Å, c = 9.0713(6) Å, α = 82.878(3)°, β = 81.549(4)°, γ = 80.473(3)°, V = 591.43(6) Å^3, Z = 1, T = 120.0 K, μ(Mo Kα) = 0.103 mm^{-1}, $Dcalc$ = 1.433 g/mm^3, 8700 reflections measured (4.564 ≤ 2Θ ≤ 58.36), 3187 unique (R_{int} = 0.077) which were used in all calculations. The final R_1 was 0.0782 (I>2.0σ(I)) and wR_2 was 0.0802 (all data).

Cambridge Crystallographic Data Centre (CCDC) deposition number: CCDC 1025638

## VIII.4.18   4-2/4-11
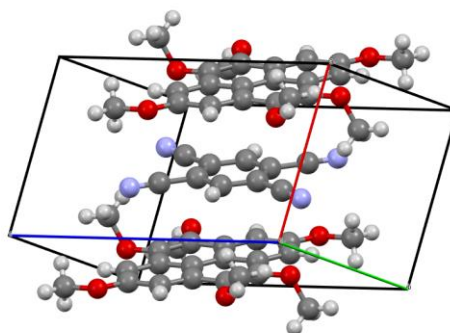
Crystal Data for $C_{16}H_{12}N_2O_3$ (M =280.28): triclinic, space group P-1 (no. 2), a = 7.2225(3) Å, b = 9.3797(5) Å, c = 10.9675(5) Å, α = 98.495(2)°, β = 109.029(3)°, γ = 105.728(2)°, V = 652.94(6) Å^3, Z = 2, T = 120.0 K, μ(Mo Kα) = 0.101 mm^{-1}, $Dcalc$ = 1.426 g/mm^3, 8917 reflections measured (5.34 ≤ 2Θ ≤ 60.132), 3817 unique (R_{int} = 0.079) which were used in all calculations. The final R_1 was 0.0697 (I>2.0σ(I)) and wR_2 was 0.0754 (all data).

Cambridge Crystallographic Data Centre (CCDC) deposition number: CCDC 1025639

VIII.4.19 4-2/TCNQ
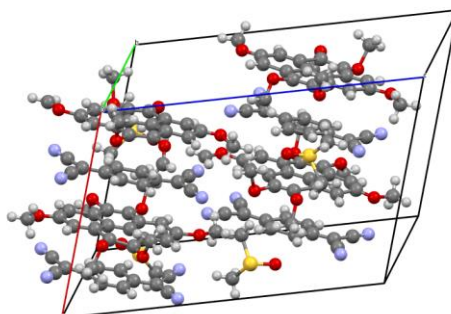
Crystal Data for $C_{36}H_{30.5}N_4O_7S$ (M =663.23): monoclinic, space group Pn (no. 7), a = 13.1830(7) Å, b = 12.9270(9) Å, c = 19.6250(9) Å, β = 109.584(4)°, V = 3151.0(3) Å^3, Z = 4, T = 293.0 K, μ(Mo Kα) = 0.161 mm^{-1}, $Dcalc$ = 1.398 g/mm^3, 23009 reflections measured (6.304 ≤ 2Θ ≤ 54.898), 7160 unique (R_{int} = 0.101) which were used in all calculations. The final R_1 was 0.2064 (I>3.0σ(I)) and wR_2 was 0.2212 (all data).

Cambridge Crystallographic Data Centre (CCDC) deposition number: CCDC 857537

VIII.4.20 4-1/TCNQ
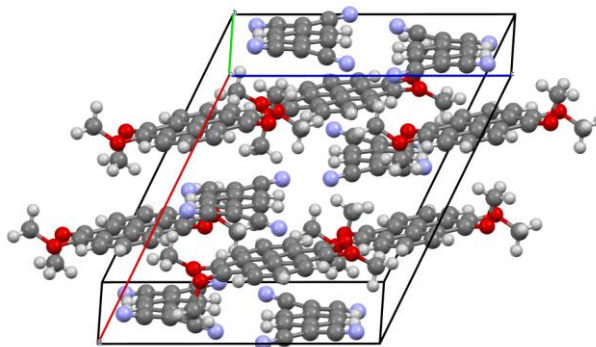
Crystal Data for $C_{32}H_{22}N_4O_4$ (M =526.55): monoclinic, space group C2/c (no. 15), a = 14.2441(5) Å, b = 14.6744(7) Å, c = 13.2556(4) Å, β = 115.853(2)°, V = 2493.44(17) Å^3, Z = 4, T = 120.0 K, μ(Mo Kα) = 0.095 mm^{-1}, $Dcalc$ = 1.403 g/mm^3, 11259 reflections measured (6.24 ≤ 2Θ ≤ 60.042), 3640 unique (R_{int} = 0.056) which were used in all calculations. The final R_1 was 0.0485 (I>3.0σ(I)) and wR_2 was 0.0591 (all data).

Cambridge Crystallographic Data Centre (CCDC) deposition number: CCDC 857536

VIII.4.21   2,7-Bis(4,4,5,5-tetramethyl-1,3,2-dioxaborolan-2-yl)pyrene (5-36)
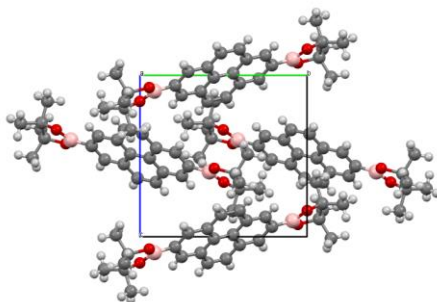
Crystal Data for $C_{14}H_{16}BO_2$ (M =227.09): monoclinic, space group P2$_1$/n (no. 14), a = 10.6936(3) Å, b =   11.0380(5) Å, c =   11.2861(5) Å, β =   109.120(2)°, V = 1258.68(9) Å^3, Z = 4, T = 120.0 K, μ(Mo Kα) = 0.077 mm^{-1}, $Dcalc$ = 1.198 g/mm^3, 13829 reflections measured (4.556 ≤ 2Θ ≤ 62.166), 4018 unique (R_{int} = 0.069) which were used in all calculations. The final R_1 was 0.0550 (I>2.0σ(I)) and wR_2 was 0.0596 (all data).

Cambridge Crystallographic Data Centre (CCDC) deposition number: CCDC 1025661

VIII.4.22   9,9',10,10'-Tetramethoxy-4,4'-bipyrene (6-9)
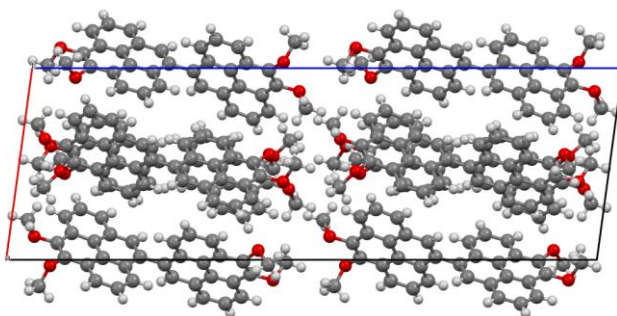
Crystal Data for $C_{36}H_{26}O_4$ (M =522.60): monoclinic, space group P2$_1$/c (no. 14), a = 11.4032(6) Å, b = 12.9621(5) Å, c = 34.8672(9) Å, β = 97.744(4)°, V = 5106.7(4) Å^3, Z = 8, T = 120.0 K, μ(Mo Kα) = 0.088 mm^{-1}, $Dcalc$ = 1.359 g/mm^3, 22011 reflections measured (4.732 ≤ 2Θ ≤ 54.828), 11645 unique (R_{int} = 0.055) which were used in all calculations. The final R_1 was 0.0411 (I>2.0σ(I)) and wR_2 was 0.0213 (all data).

Cambridge Crystallographic Data Centre (CCDC) deposition number: CCDC 1025645

## VIII.4.23   4,4,5,5,9,9,10,10-Octafluoro-4,5,9,10-tetrahydropyrene
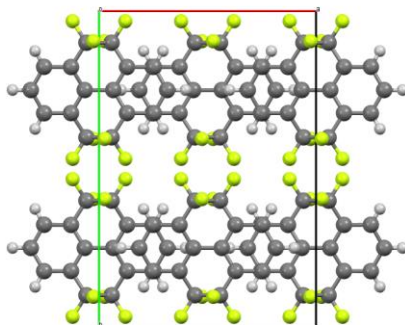
Crystal Data for $C_{16}H_6F_8$ (M =350.21): orthorhombic, space group Ccce (no. 68), a = 11.2305(4) Å, b = 16.3268(5) Å, c = 6.8922(2) Å, V = 1263.74(7) Å^3, Z = 4, T = 120.0 K, μ(Mo Kα) = 0.190 mm^{-1}, $Dcalc$ = 1.841 g/mm^3, 6904 reflections measured (4.99 ≤ 2Θ ≤ 61.994), 1008 unique (R_{int} = 0.048) which were used in all calculations. The final R_1 was 0.0358 (I>2.0σ(I)) and wR_2 was 0.0426 (all data).

Cambridge Crystallographic Data Centre (CCDC) deposition number: CCDC 1025643

IX.   Bibliography

1.   G. P. Moss, *Pure and Applied Chemistry*, 1998, **70**, 143-216.
2.   A. Laurent, *Ann. Chim. Phys.*, 1837, **66**, 136.
3.   R. D. Welham, *J. Soc. Dyers Color*, 1963, **79**, 98.
4.   A. E. Siegrist, C. Eckhardt, J. Kaschig and E. Schmidt, in *Ullmann's Encyclopedia of Industrial Chemistry*, Wiley-VCH Verlag GmbH & Co. KGaA, 2000.
5.   H. Tappe, W. Helmling, P. Mischke, K. Rebsamen, U. Reiher, W. Russ, L. Schläfer and P. Vermehren, in *Ullmann's Encyclopedia of Industrial Chemistry*, Wiley-VCH Verlag GmbH & Co. KGaA, 2000.
6.   R. Ismael, H. Schwander and P. Hendrix, in *Ullmann's Encyclopedia of Industrial Chemistry*, Wiley-VCH Verlag GmbH & Co. KGaA, 2000.
7.   L. Zou, X.-Y. Wang, K. Shi, J.-Y. Wang and J. Pei, *Org. Lett.*, 2013, **15**, 4378-4381.
8.   E. Clar, *Polycyclic hydrocarbons ; Vol. 1*, Acad. Press {[u.a.], New York, NY, 1964.
9.   E. Clar, *Spectrochim. Acta*, 1950, **4**, 116-121.
10.   T. Yoshinaga, H. Hiratsuka and Y. Tanizaki, *Bull. Chem. Soc. Jpn.*, 1977, **50**, 3096-3102.
11.   A. G. Crawford, A. D. Dwyer, Z. Liu, A. Steffen, A. Beeby, L.-O. Pålsson, D. J. Tozer and T. B. Marder, *J. Am. Chem. Soc.*, 2011, **133**, 13349-13362.
12.   M. Perry, C. Carra, M. N. Chrétien and J. C. Scaiano, *The Journal of Physical Chemistry A*, 2007, **111**, 4884-4889.
13.   A. Nakajima, *Bull. Chem. Soc. Jpn.*, 1971, **44**, 3272-3277.
14.   J. M. Dixon, M. Taniguchi and J. S. Lindsey, *Photochem. Photobiol.*, 2005, **81**, 212-213.
15.   C. A. Parker and C. G. Hatchard, *Transactions of the Faraday Society*, 1963, **59**, 284-295.
16.   M. Cooper and J. K. Thomas, *Radiat. Res.*, 1977, **70**, 312-324.
17.   D. C. Dong and M. A. Winnik, *Can. J. Chem.*, 1984, **62**, 2560-2565.
18.   J. B. Birks and L. G. Christophorou, *Spectrochim. Acta*, 1963, **19**, 401-410.
19.   T. Förster and K. Kasper, *Z. Elektrochem.*, 1955, **59**, 976.
20.   B. Valeur and M. N. Berberan-Santos, in *Molecular Fluorescence*, Wiley-VCH Verlag GmbH & Co. KGaA, 2012, pp. 75-107.
21.   F. M. Winnik, *Chem. Rev.*, 1993, **93**, 587.
22.   D. Kraskouskaya, M. Bancerz, H. S. Soor, J. E. Gardiner and P. T. Gunning, *J. Am. Chem. Soc.*, 2014.
23.   G. Drummen, *Molecules*, 2012, **17**, 14067-14090.
24.   A. K. Soutar, H. J. Pownall, A. S. Hu and L. C. Smith, *Biochemistry*, 1974, **13**, 2828-2836.
25.   P. Conlon, C. J. Yang, Y. Wu, Y. Chen, K. Martinez, Y. Kim, N. Stevens, A. A. Marti, S. Jockusch, N. J. Turro and W. Tan, *J. Am. Chem. Soc.*, 2007, **130**, 336-342.
26.   J. B. Birks, *The Journal of Physical Chemistry*, 1963, **67**, 2199-2200.
27.   K. K. Rohatgi-Mukherjee, *Fundamentals of Photochemistry*, Wiley, 1978.
28.   T. M. Figueira-Duarte and K. Müllen, *Chem. Rev.*, 2011, **111**, 7260-7314.
29.   R. Trattnig, T. M. Figueira-Duarte, D. Lorbach, W. Wiedemair, S. Sax, S. Winkler, A. Vollmer, N. Koch, M. Manca, M. A. Loi, M. Baumgarten, E. J. W. List and K. Müllen, *Opt. Express*, 2011, **19**, A1281-A1293.
30.   M. Freund and K. Fleischer, *Liebigs Ann.*, 1914, **402**, 77.
31.   M. Sola, *Front Chem*, 2013, **1**, 22.
32.   K. Fukui, T. Yonezawa and H. Shingu, *The Journal of Chemical Physics*, 1952, **20**, 722-725.
33.   I. Fleming, in *Molecular Orbitals and Organic Chemical Reactions*, John Wiley & Sons, Ltd, 2010, pp. 1-67.

34.   J. M. Casas-Solvas, J. D. Howgego and A. P. Davis, *Organic & Biomolecular Chemistry*, 2014, **12**, 212-232.
35.   C. Graebe, *Liebigs Ann.*, 1871, **158**, 285.
36.   M. Minabe, S. Takeshige, Y. Soeda, T. Kimura and M. Tsubota, *Bull. Chem. Soc. Jpn.*, 1994, **67**, 172-179.
37.   H. Vollmann, H. Becker, M. Corell and H. Streeck, *Liebigs Ann.*, 1937, **531**, 1.
38.   S. Qu, M. Li, L. Xie, X. Huang, J. Yang, N. Wang and S. Yang, *ACS Nano*, 2013, **7**, 4070-4081.
39.   Y.-L. Zhao and J. F. Stoddart, *Acc. Chem. Res.*, 2009, **42**, 1161-1171.
40.   H. Hofmeier and U. S. Schubert, *Chem. Soc. Rev.*, 2004, **33**, 373-399.
41.   R. M. Edkins, K. Fucke, M. J. G. Peach, A. G. Crawford, T. B. Marder and A. Beeby, *Inorg. Chem.*, 2013, **52**, 9842-9860.
42.   M. Kaur, P. Kaur, V. Dhuna, S. Singh and K. Singh, *Dalton Transactions*, 2014, **43**, 5707-5712.
43.   Y. Zhou, J. Won, J. Y. Lee and J. Yoon, *Chem. Commun.*, 2011, **47**, 1997-1999.
44.   J. You, G. Li and Z. Wang, *Polymer*, 2012, **53**, 5116-5123.
45.   M. Gingras, V. Placide, J.-M. Raimundo, G. Bergamini, P. Ceroni and V. Balzani, *Chem. Eur. J.*, 2008, **14**, 10357-10363.
46.   B. A. G. Hammer, M. Baumgarten and K. Müllen, *Chem. Commun.*, 2014, **50**, 2034-2036.
47.   D. Turp, T.-T.-T. Nguyen, M. Baumgarten and K. Müllen, *New J. Chem.*, 2012, **36**, 282-298.
48.   J. You, G. Li, R. Wang, Q. Nie, Z. Wang and J. Li, *PCCP*, 2011, **13**, 17825-17830.
49.   J. Grimshaw and J. Trocha-Grimshaw, *J. Chem. Soc. Perkin Trans. 1*, 1972, 1622.
50.   H. Sogawa, Y. Miyagi, M. Shiotsuki and F. Sanda, *Macromolecules*, 2013, **46**, 8896-8904.
51.   Y. J. Xing, X. J. Xu, P. Zhang, W. J. Tian, G. Yu, P. Lu, Y. Q. Liu and D. B. Zhu, *Chem. Phys. Let.*, 2005, **408**, 169.
52.   Y. Hashimoto and K. Shudo, *CHEMICAL & PHARMACEUTICAL BULLETIN*, 1984, **32**, 1992-1994.
53.   A. Berg, J. Lam and P. E. Hansen, *Acta Chem. Scand., Ser. B*, 1986, **B40**, 665-677.
54.   P. P. Fu, H. M. Lee and R. G. Harvey, *The Journal of Organic Chemistry*, 1980, **45**, 2797-2803.
55.   H. Lee and R. G. Harvey, *The Journal of Organic Chemistry*, 1986, **51**, 2847-2848.
56.   F. G. Oberender and J. A. Dixon, *The Journal of Organic Chemistry*, 1959, **24**, 1226-1229.
57.   C. J. R. Bataille and T. J. Donohoe, *Chem. Soc. Rev.*, 2011, **40**, 114-128.
58.   F. G. Oberender and J. A. Dixon, *J. Org. Chem.*, 1959, **24**, 1226.
59.   J. Hu, D. Zhang and F. W. Harris, *The Journal of Organic Chemistry*, 2004, **70**, 707.
60.   M. Z. Kassaee, M. Hattami and L. Moradi, *Acta Chim. Slov.*, 2004, **51**, 743-750.
61.   T. Yamato, M. Fujimoto, A. Miyazawa and K. Matsuo, *J. Chem. Soc., Perkin Trans. 1*, 1997, 1201-1208.
62.   D. Wasserfallen, M. Kastler, W. Pisula, W. A. Hofer, Y. Fogel, Z. Wang and K. Müllen, *J. Am. Chem. Soc.*, 2006, **128**, 1334-1339.
63.   A. Mateo-Alonso, *Chem. Soc. Rev.*, 2014.
64.   T. Yamato, A. Miyazawa and M. Tashiro, *Chem. Ber.*, 1993, **126**, 2505-2511.
65.   P. Boldt and D. Bruhnke, *Journal für Praktische Chemie/Chemiker-Zeitung*, 1994, **336**, 110-114.
66.   S.-i. Kawano, C. Yang, M. Ribas, S. Baluschev, M. Baumgarten and K. Müllen, *Macromolecules*, 2008, **41**, 7933-7937.
67.   D. Kamp and V. Boekelheide, *The Journal of Organic Chemistry*, 1978, **43**, 3470-3475.
68.   H. Dang, T. Maris, J.-H. Yi, F. Rosei, A. Nanci and J. D. Wuest, *Langmuir*, 2007, **23**, 11980-11985.
69.   D. Rausch and C. Lambert, *Org. Lett.*, 2006, **8**, 5037-5040.
70.   C. E. Godinez, G. Zepeda and M. A. Garcia-Garibay, *J. Am. Chem. Soc.*, 2002, **124**, 4701-4707.

71.   B. R. Kaafarani, A. a. O. El-Ballouli, R. Trattnig, A. Fonari, S. Sax, B. Wex, C. Risko, R. S. Khnayzer, S. Barlow, D. Patra, T. V. Timofeeva, E. J. W. List, J.-L. Bredas and S. R. Marder, *J. Mater. Chem. C*, 2013, **1**, 1638-1650.

72.   M. Inouye, M.-a. S. Itoh and H. Nakazumi, *The Journal of Organic Chemistry*, 1999, **64**, 9393-9398.

73.   K. Imai, T. Sasaki, J. Abe, A. Kimoto, Y. Tamai and N. Nemoto, *Polym. J*, 2009, **41**, 584-585.

74.   T. Iwamoto, E. Kayahara, N. Yasuda, T. Suzuki and S. Yamago, *Angew. Chem. Int. Ed.*, 2014, **53**, 6430-6434.

75.   A. Yagi, G. Venkataramana, Y. Segawa and K. Itami, *Chem. Commun.*, 2014, **50**, 957-959.

76.   H. Omachi, Y. Segawa and K. Itami, *Acc. Chem. Res.*, 2012, **45**, 1378-1389.

77.   S.-I. Kawano, M. Baumgarten, D. Chercka, V. Enkelmann and K. Müllen, *Chem. Commun.*, 2013, **49**, 5058-5060.

78.   T. Ishiyama, J. Takagi, K. Ishida, N. Miyaura, N. R. Anastasi and J. F. Hartwig, *J. Am. Chem. Soc.*, 2001, **124**, 390-391.

79.   D. N. Coventry, A. S. Batsanov, A. E. Goeta, J. A. K. Howard, T. B. Marder and R. N. Perutz, *Chem. Commun.*, 2005, 2172-2174.

80.   L. Gao, M. A. Peay, D. V. Partyka, J. B. Updegraff, T. S. Teets, A. J. Esswein, M. Zeller, A. D. Hunter and T. G. Gray, *Organometallics*, 2009, **28**, 5669-5681.

81.   D. S. Yang, K. H. Kim, M. J. Cho, J.-I. Jin and D. H. Choi, *J. Polym. Sci., Part A: Polym. Chem.*, 2013, **51**, 1457-1467.

82.   H. Chen, X. Hu and S.-C. Ng, *J. Polym. Sci., Part A: Polym. Chem.*, 2010, **48**, 5562-5569.

83.   Y. Kim, J. Hong, J. H. Oh and C. Yang, *Chem. Mater.*, 2013, **25**, 3251-3259.

84.   A. G. Crawford, Z. Liu, I. A. I. Mkhalid, M.-H. Thibault, N. Schwarz, G. Alcaraz, A. Steffen, J. C. Collings, A. S. Batsanov, J. A. K. Howard and T. B. Marder, *Chem. Eur. J.*, 2012, **18**, 5022-5035.

85.   Y. Chen, W.-t. Yu, Z.-q. Liu and P. Yu, *Acta Crystallographica Section E*, 2012, **68**, o771.

86.   Z. Liu, Y. Wang, Y. Chen, J. Liu, Q. Fang, C. Kleeberg and T. B. Marder, *The Journal of Organic Chemistry*, 2012, **77**, 7124-7128.

87.   L. Zöphel, V. Enkelmann and K. Müllen, *Org. Lett.*, 2013, **15**, 804-807.

88.   L. Zöphel, K. S. Mali, P. S. Reddy, M. Wagner, S. De Feyter, W. Pisula and K. Müllen, *Chem. Eur. J.*, 2012, **18**, 3264-3276.

89.   L. Zöphel, R. Berger, P. Gao, V. Enkelmann, M. Baumgarten, M. Wagner and K. Müllen, *Chem. Eur. J.*, 2013, **19**, 17821-17826.

90.   L. Zöphel, D. Beckmann, V. Enkelmann, D. Chercka, R. Rieger and K. Müllen, *Chem. Commun.*, 2011, **47**, 6960-6962.

91.   G. Venkataramana, P. Dongare, L. N. Dawe, D. W. Thompson, Y. Zhao and G. J. Bodwell, *Org. Lett.*, 2011, **13**, 2240-2243.

92.   X. Feng, J.-Y. Hu, L. Yi, N. Seto, Z. Tao, C. Redshaw, M. R. J. Elsegood and T. Yamato, *Chemistry – An Asian Journal*, 2012, **7**, 2854-2863.

93.   X. Feng, F. Iwanaga, J.-Y. Hu, H. Tomiyasu, M. Nakano, C. Redshaw, M. R. J. Elsegood and T. Yamato, *Org. Lett.*, 2013, **15**, 3594-3597.

94.   X. Feng, J.-Y. Hu, F. Iwanaga, N. Seto, C. Redshaw, M. R. J. Elsegood and T. Yamato, *Org. Lett.*, 2013, **15**, 1318-1321.

95.   T. M. Figueira-Duarte, S. C. Simon, M. Wagner, S. I. Druzhinin, K. A. Zachariasse and K. Müllen, *Angew. Chem. Int. Ed.*, 2008, **47**, 10175-10178.

96.   G. Cheng, T. Hasell, A. Trewin, D. J. Adams and A. I. Cooper, *Angew. Chem. Int. Ed.*, 2012, **51**, 12727-12731.

97.   B. L. Merner, L. N. Dawe and G. J. Bodwell, *Angew. Chem. Int. Ed.*, 2009, **48**, 5487-5491.

98.   D. B. Walker, J. Howgego and A. P. Davis, *Synthesis*, 2010, **2010**, 3686-3692.

99.   D. Lorbach, M. Wagner, M. Baumgarten and K. Müllen, *Chem. Commun.*, 2013, **49**, 10578-10580.

100.   Z.-Y. Gao, W.-S. Jiang, D. Sun, Y. Xie, Z.-L. Chen, L.-J. Yu, S.-Y. Xie, R.-B. Huang and L.-S. Zheng, *Talanta*, 2010, **81**, 48-54.

101. Y.-Z. Tan, B. Yang, K. Parvez, A. Narita, S. Osella, D. Beljonne, X. Feng and K. Müllen, *Nat Commun*, 2013, **4**.

102. D. Harrison, M. Stacey, R. Stephens and J. C. Tatlow, *Tetrahedron*, 1963, **19**, 1893-1901.

103. G. G. Yakobson, V. M. Vlasov and Vorozhts.Nn, *Doklady Akademii Nauk Sssr*, 1966, **169**, 855-&.

104. J. Koenigsberger and K. Schilling, *Annalen der Physik*, 1910, **337**, 179-230.

105. A. Bernanose, *British Journal of Applied Physics*, 1955, **6**, S54.

106. W. Helfrich and W. G. Schneider, *Phys. Rev. Lett.*, 1965, **14**, 229-231.

107. G. Inzelt, in *Conducting Polymers*, Springer Berlin Heidelberg, 2008, pp. 1-282.

108. H. Naarmann, in *Ullmann's Encyclopedia of Industrial Chemistry*, Wiley-VCH Verlag GmbH & Co. KGaA, 2000.

109. C. Veaceslav, G. Victor, A. d. S. F. Demetrio, L. Roberto, L. Philippe, C. Jérôme, B. Jean-Luc and B. David, in *Conjugated Polymers*, CRC Press, 2006.

110. G. Witte and C. Wöll, *J. Mater. Res.*, 2004, **19**, 1889-1916.

111. H. Sirringhaus, *Adv. Mater.*, 2014, **26**, 1319-1335.

112. H. Dong, X. Fu, J. Liu, Z. Wang and W. Hu, *Adv. Mater.*, 2013, **25**, 6158-6183.

113. S. Günes, H. Neugebauer and N. S. Sariciftci, *Chem. Rev.*, 2007, **107**, 1324-1338.

114. L. Dou, J. You, Z. Hong, Z. Xu, G. Li, R. A. Street and Y. Yang, *Adv. Mater.*, 2013, **25**, 6642-6671.

115. D. Koziej, A. Lauria and M. Niederberger, *Adv. Mater.*, 2014, **26**, 235-257.

116. J. Y. Kim, O. Voznyy, D. Zhitomirsky and E. H. Sargent, *Adv. Mater.*, 2013, **25**, 4986-5010.

117. B. O'Regan and M. Gratzel, *Nature*, 1991, **353**, 737-740.

118. L. M. Goncalves, V. de Zea Bermudez, H. A. Ribeiro and A. M. Mendes, *Energy & Environmental Science*, 2008, **1**, 655-667.

119. J.-H. Lee, C. Y. Koh, J. P. Singer, S.-J. Jeon, M. Maldovan, O. Stein and E. L. Thomas, *Adv. Mater.*, 2014, **26**, 532-569.

120. W.-G. Bae, H. N. Kim, D. Kim, S.-H. Park, H. E. Jeong and K.-Y. Suh, *Adv. Mater.*, 2014, **26**, 675-700.

121. Y. Olivier, D. Niedzialek, V. Lemaur, W. Pisula, K. Müllen, U. Koldemir, J. R. Reynolds, R. Lazzaroni, J. Cornil and D. Beljonne, *Adv. Mater.*, 2014, **26**, 2119-2136.

122. R. R. Søndergaard, M. Hösel and F. C. Krebs, *J. Polym. Sci., Part B: Polym. Phys.*, 2013, **51**, 16-34.

123. F. C. Krebs, N. Espinosa, M. Hösel, R. R. Søndergaard and M. Jørgensen, *Adv. Mater.*, 2014, **26**, 29-39.

124. Y. Zhao, Y. Guo and Y. Liu, *Adv. Mater.*, 2013, **25**, 5372-5391.

125. L. E. Germany, www.presse.lge.de, 2013.

126. K. S. Novoselov, A. K. Geim, S. V. Morozov, D. Jiang, M. I. Katsnelson, I. V. Grigorieva, S. V. Dubonos and A. A. Firsov, *Nature*, 2005, **438**, 197-200.

127. S. Pang, Y. Hernandez, X. Feng and K. Müllen, *Adv. Mater.*, 2011, **23**, 2779-2795.

128. J. Du, S. Pei, L. Ma and H.-M. Cheng, *Adv. Mater.*, 2014, **26**, 1958-1991.

129. U. N. Maiti, W. J. Lee, J. M. Lee, Y. Oh, J. Y. Kim, J. E. Kim, J. Shim, T. H. Han and S. O. Kim, *Adv. Mater.*, 2014, **26**, 40-67.

130. D. Jérome and H. J. Schulz, *Advances in Physics*, 2002, **51**, 293-479.

131. G. Saito and Y. Yoshida, *Bull. Chem. Soc. Jpn.*, 2007, **80**, 1-137.

132. D. Jérome and H. J. Schulz, *Advances in Physics*, 1982, **31**, 299-490.

133. B. Lüssem, M. Riede and K. Leo, *physica status solidi (a)*, 2013, **210**, 9-43.

134. H. Sasabe and J. Kido, *J. Mater. Chem. C*, 2013, **1**, 1699.

135. N. Thejo Kalyani and S. J. Dhoble, *Renew. Sust. Energ. Rev.*, 2012, **16**, 2696-2723.

136. B. Geffroy, P. Le Roy and C. Prat, *Polym. Int.*, 2006, **55**, 572.

137. T. Tsujimura, *OLED Display Fundamentals and Applications*, Wiley, 2012.

138. S. Braun, W. R. Salaneck and M. Fahlman, *Adv. Mater.*, 2009, **21**, 1450-1472.

139. C. W. Tang, *Appl. Phys. Lett.*, 1986, **48**, 183-185.

140. K. Cnops, B. P. Rand, D. Cheyns, B. Verreet, M. A. Empl and P. Heremans, *Nat Commun*, 2014, **5**.

141. B. P. Rand, J. Genoe, P. Heremans and J. Poortmans, *Progress in Photovoltaics: Research and Applications*, 2007, **15**, 659-676.

142.   C. Rovira, *Chem. Rev.*, 2004, **104**, 5289-5318.
143.   H. Usta, A. Facchetti and T. J. Marks, *Acc. Chem. Res.*, 2011, **44**, 501-510.
144.   H. Tatsuo and T. Jun, *Science and Technology of Advanced Materials*, 2009, **10**, 024314.
145.   S. S. Sun and L. R. Dalton, *Introduction to Organic Electronic and Optoelectronic Materials and Devices*, Taylor & Francis Group, 2008.
146.   T.-C. Tseng, C. Urban, Y. Wang, R. Otero, S. L. Tait, M. Alcamí, D. Écija, M. Trelka, J. M. Gallego, N. Lin, M. Konuma, U. Starke, A. Nefedov, A. Langner, C. Wöll, M. Á. Herranz, F. Martín, N. Martín, K. Kern and R. Miranda, *Nat Chem*, 2010, **2**, 374-379.
147.   T. Yanagimoto, K. Takimiya, T. Otsubo and F. Ogura, *J. Chem. Soc., Chem. Commun.*, 1993, 519-520.
148.   A. W. Addison, N. S. Dalal, Y. Hoyano, S. Huizinga and L. Weiler, *Can. J. Chem.*, 1977, **55**, 4191-4199.
149.   D. S. Acker and W. R. Hertler, *J. Am. Chem. Soc.*, 1962, **84**, 3370-3374.
150.   J. Diekmann, W. R. Hertler and R. E. Benson, *The Journal of Organic Chemistry*, 1963, **28**, 2719-2724.
151.   N. Martin, R. Behnisch and M. Hanack, *The Journal of Organic Chemistry*, 1989, **54**, 2563-2568.
152.   D. Canevet, M. Salle, G. Zhang, D. Zhang and D. Zhu, *Chem. Commun.*, 2009, 2245-2269.
153.   N. Martin, *Chem. Commun.*, 2013, **49**, 7025-7027.
154.   M. C. Etter, *Acc. Chem. Res.*, 1990, **23**, 120-126.
155.   A. D. McNaught and A. Wilkinson, *IUPAC. Compendium of Chemical Terminology, 2nd ed. (the "Gold Book")*, WileyBlackwell; 2nd Revised edition edition.
156.   A. Heckmann and C. Lambert, *Angew. Chem. Int. Ed.*, 2012, **51**, 326-392.
157.   A. Proń, G. Zhou, H. Norouzi-Arasi, M. Baumgarten and K. Müllen, *Org. Lett.*, 2009, **11**, 3550-3553.
158.   U. Bach, D. Lupo, P. Comte, J. E. Moser, F. Weissortel, J. Salbeck, H. Spreitzer and M. Gratzel, *Nature*, 1998, **395**, 583-585.
159.   T. W. Hamann, R. A. Jensen, A. B. F. Martinson, H. Van Ryswyk and J. T. Hupp, *Energy & Environmental Science*, 2008, **1**, 66-78.
160.   J. B. Nagy, O. B. Nagy and A. Bruylants, *The Journal of Physical Chemistry*, 1974, **78**, 980-983.
161.   J. Ferraris, D. O. Cowan, V. Walatka and J. H. Perlstein, *J. Am. Chem. Soc.*, 1973, **95**, 948-949.
162.   D. Jérome, *Chem. Rev.*, 2004, **104**, 5565-5592.
163.   T. Ishiguro, K. Yamaji and G. Saito, in *Organic Superconductors*, Springer Berlin Heidelberg, 1998, vol. 88, pp. 1-14.
164.   J. B. Torrance, J. J. Mayerle, V. Y. Lee and K. Bechgaard, *J. Am. Chem. Soc.*, 1979, **101**, 4747-4748.
165.   J. J. Mayerle, J. B. Torrance and J. I. Crowley, *Acta Crystallographica Section B*, 1979, **35**, 2988-2995.
166.   J. B. Torrance, J. E. Vazquez, J. J. Mayerle and V. Y. Lee, *Phys. Rev. Lett.*, 1981, **46**, 253-257.
167.   S. Horiuchi, R. Kumai, Y. Okimoto and Y. Tokura, *Chem. Phys.*, 2006, **325**, 78-91.
168.   G. Saito and T. Murata, *Philosophical Transactions of the Royal Society A: Mathematical, Physical and Engineering Sciences*, 2008, **366**, 139-150.
169.   J. B. Torrance, A. Girlando, J. J. Mayerle, J. I. Crowley, V. Y. Lee, P. Batail and S. J. LaPlaca, *Phys. Rev. Lett.*, 1981, **47**, 1747-1750.
170.   J. Kwon, R. Pode, H. Kim and H. Chung, in *Applications of Organic and Printed Electronics*, ed. E. Cantatore, Springer US, 2013, pp. 57-81.
171.   H. Sasabe and J. Kido, *Eur. J. Org. Chem.*, 2013, **2013**, 7653-7663.
172.   R. Coehoorn, V. van Elsbergen and C. Verschuren, in *Applications of Organic and Printed Electronics*, ed. E. Cantatore, Springer US, 2013, pp. 83-100.
173.   H. Yersin, in *Transition Metal and Rare Earth Compounds*, Springer Berlin Heidelberg, 2004, vol. 241, pp. 1-26.

174. H. Yersin, A. F. Rausch, R. Czerwieniec, T. Hofbeck and T. Fischer, *Coord. Chem. Rev.*, 2011, **255**, 2622-2652.
175. T. Tsutsui, E. Aminaka, C. P. Lin and D.-U. Kim, *Philosophical Transactions of the Royal Society of London. Series A: Mathematical, Physical and Engineering Sciences*, 1997, **355**, 801-814.
176. N. C. Greenham, R. H. Friend and D. D. C. Bradley, *Adv. Mater.*, 1994, **6**, 491-494.
177. R. Meerheim, B. Lussem and K. Leo, *Proceedings of the IEEE*, 2009, **97**, 1606-1626.
178. K. Yamae, H. Tsuji, V. Kittichungchit, N. Ide and T. Komoda, *SID Symposium Digest of Technical Papers*, 2013, **44**, 916-919.
179. M. N. Berberan-Santos and J. M. M. Garcia, *J. Am. Chem. Soc.*, 1996, **118**, 9391-9394.
180. C. Baleizão and M. N. Berberan-Santos, *Ann. N.Y. Acad. Sci.*, 2008, **1130**, 224-234.
181. A. Endo, K. Sato, K. Yoshimura, T. Kai, A. Kawada, H. Miyazaki and C. Adachi, *Appl. Phys. Lett.*, 2011, **98**, 083302.
182. H. Uoyama, K. Goushi, K. Shizu, H. Nomura and C. Adachi, *Nature*, 2012, **492**, 234-238.
183. L. H. Smith, J. A. E. Wasey and W. L. Barnes, *Appl. Phys. Lett.*, 2004, **84**, 2986-2988.
184. D. Tanaka, H. Sasabe, Y.-J. Li, S.-J. Su, T. Takeda and J. Kido, *Japanese Journal of Applied Physics*, 2007, **46**, L10-L12.
185. F. B. Dias, K. N. Bourdakos, V. Jankus, K. C. Moss, K. T. Kamtekar, V. Bhalla, J. Santos, M. R. Bryce and A. P. Monkman, *Adv. Mater.*, 2013, **25**, 3707-3714.
186. K. Goushi, K. Yoshida, K. Sato and C. Adachi, *Nat Photon*, 2012, **6**, 253-258.
187. D. Y. Kondakov, T. D. Pawlik, T. K. Hatwar and J. P. Spindler, *J. Appl. Phys.*, 2009, **106**, 124510-124510-124517.
188. D. Y. Kondakov, *J. Appl. Phys.*, 2007, **102**, -.
189. S. M. King, M. Cass, M. Pintani, C. Coward, F. B. Dias, A. P. Monkman and M. Roberts, *J. Appl. Phys.*, 2011, **109**, -.
190. Y. Luo and H. Aziz, *Adv. Funct. Mater.*, 2010, **20**, 1285-1293.
191. A. P. Monkman, *ISRN Materials Science*, 2013, **2013**, 19.
192. S. More, R. Bhosale, S. Choudhary and A. Mateo-Alonso, *Org. Lett.*, 2012, **14**, 4170-4173.
193. D. Wasserfallen, M. Kastler, W. Pisula, W. A. Hofer, Y. Fogel, Z. H. Wang and K. Müllen, *J. Am. Chem. Soc.*, 2006, **128**, 1334.
194. J. E. Anthony, A. Facchetti, M. Heeney, S. R. Marder and X. Zhan, *Adv. Mater.*, 2010, **22**, 3876-3892.
195. G. H. Gelinck, E. van Veenendaal, E. J. Meijer, E. Cantatore, H. E. A. Huitema, P. J. G. van Lieshout, F. J. Touwslager, A. W. Marsman and D. M. de Leeuw, in *Org. Electron.*, Wiley-VCH Verlag GmbH & Co. KGaA, 2006, pp. 323-343.
196. A. B. Sieval and J. C. Hummelen, in *Organic Photovoltaics*, Wiley-VCH Verlag GmbH & Co. KGaA, 2014, pp. 209-238.
197. D. Chercka, Technische Universität Braunschweig, 2010.
198. P. Phillips, *Annals of Physics*, 2006, **321**, 1634-1650.
199. K. Rajesh, M. Somasundaram, R. Saiganesh and K. K. Balasubramanian, *The Journal of Organic Chemistry*, 2007, **72**, 5867-5869.
200. G. K. S. Prakash, T. Mathew, D. Hoole, P. M. Esteves, Q. Wang, G. Rasul and G. A. Olah, *J. Am. Chem. Soc.*, 2004, **126**, 15770-15776.
201. , WO2010006852A1, 2010.
202. R. Rieger, M. Kastler, V. Enkelmann and K. Müllen, *Chem. Eur. J.*, 2008, **14**, 6322-6325.
203. K. Medjanik, D. Kutnyakhov, S. A. Nepijko, G. Schonhense, S. Naghavi, V. Alijani, C. Felser, N. Koch, R. Rieger, M. Baumgarten and K. Müllen, *PCCP*, 2010, **12**, 7184-7193.
204. M. Hesse, H. Meier and B. Zeeh, *Spektroskopische Methoden in der organischen Chemie*, Thieme, 2005.
205. M. E. Jung and M. A. Lyster, *The Journal of Organic Chemistry*, 1977, **42**, 3761-3764.

206.   L. E. Overman, D. J. Ricca and V. D. Tran, *J. Am. Chem. Soc.*, 1997, **119**, 12031-12040.
207.   B. N. Boden, K. J. Jardine, A. C. W. Leung and M. J. MacLachlan, *Org. Lett.*, 2006, **8**, 1855-1858.
208.   M. Node, K. Nishide, M. Sai, K. Ichikawa, K. Fuji and E. Fujita, *Chem. Lett.*, 1979, 97-98.
209.   P. G. Williard and C. B. Fryhle, *Tetrahedron Lett.*, 1980, **21**, 3731-3734.
210.   J. G. Cannon, A. N. Brubaker, J. P. Long, J. R. Flynn, T. Verimer, P. Harnirattisai, B. Costall, R. J. Naylor and V. Nohria, *J. Med. Chem.*, 1981, **24**, 149-153.
211.   G. Speier, *J. Mol. Catal.*, 1986, **37**, 259-267.
212.   L. Cohen, E. P. Go and G. Siuzdak, in *MALDI MS*, Wiley-VCH Verlag GmbH & Co. KGaA, 2007, pp. 299-337.
213.   R. G. Bryant, *J. Chem. Educ.*, 1983, **60**, 933.
214.   R. Willstätter and L. Kalb, *Berichte der deutschen chemischen Gesellschaft*, 1906, **39**, 3474-3482.
215.   B. R. Brown and A. R. Todd, *Journal of the Chemical Society (Resumed)*, 1954, 1280-1285.
216.   T. Takata, R. Tajima and W. Ando, *The Journal of Organic Chemistry*, 1983, **48**, 4764-4766.
217.   A. Pelter and S. Elgendy, *Tetrahedron Lett.*, 1988, **29**, 677-680.
218.   C. A. Mulrooney, B. J. Morgan, X. Li and M. C. Kozlowski, *The Journal of Organic Chemistry*, 2009, **75**, 16-29.
219.   C. Tepper and G. Haberhauer, *Chem. Eur. J.*, 2011, **17**, 8060-8065.
220.   Y. Tatewaki, T. Watanabe, K. Watanabe, K. Kikuchi and S. Okada, *Dalton Transactions*, 2013, **42**, 16121-16127.
221.   P. Boldt and D. Bruhnke, *Journal Fur Praktische Chemie-Chemiker-Zeitung*, 1994, **336**, 110-114.
222.   M. Maxfield, A. N. Bloch and D. O. Cowan, *J. Org. Chem.*, 1985, **50**, 1789-1796.
223.   M. Maxfield, S. M. Willi, D. O. Cowan, A. N. Bloch and T. O. Poehler, *J. Chem. Soc., Chem. Commun.*, 1980, 947-948.
224.   R. H. Mitchell, X. Jin, T. Otsubo and K. Takimiya, *Can. J. Chem.*, 1997, **75**, 611-615.
225.   P. Ravat, Y. Ito, E. Gorelik, V. Enkelmann and M. Baumgarten, *Org. Lett.*, 2013, **15**, 4280-4283.
226.   J. A. Letizia, S. Cronin, R. P. Ortiz, A. Facchetti, M. A. Ratner and T. J. Marks, *Chem. Eur. J.*, 2010, **16**, 1911-1928.
227.   S. Enthaler and A. Company, *Chem. Soc. Rev.*, 2011, **40**, 4912-4924.
228.   C. A. Parrish and S. L. Buchwald, *The Journal of Organic Chemistry*, 2001, **66**, 2498-2500.
229.   G. Bartoli, M. Bosco, A. Carlone, M. Locatelli, E. Marcantoni, P. Melchiorre and L. Sambri, *Adv. Synth. Catal.*, 2006, **348**, 905-910.
230.   G. A. Molander, S. L. J. Trice and S. D. Dreher, *J. Am. Chem. Soc.*, 2010, **132**, 17701-17703.
231.   T. Ishiyama, M. Murata and N. Miyaura, *The Journal of Organic Chemistry*, 1995, **60**, 7508-7510.
232.   J. M. Murphy, C. C. Tzschucke and J. F. Hartwig, *Org. Lett.*, 2007, **9**, 757-760.
233.   Y. Tsubata, T. Suzuki, T. Miyashi and Y. Yamashita, *The Journal of Organic Chemistry*, 1992, **57**, 6749-6755.
234.   E. M. Geniès, A. Boyle, M. Lapkowski and C. Tsintavis, *Synth. Met.*, 1990, **36**, 139-182.
235.   Z. Wei, T. Laitinen, B. Smarsly, O. Ikkala and C. F. J. Faul, *Angew. Chem.*, 2005, **117**, 761-766.
236.   J. P. Sadighi, M. C. Harris and S. L. Buchwald, *Tetrahedron Lett.*, 1998, **39**, 5327-5330.
237.   P. C. J. Kamer, P. W. N. M. van Leeuwen and J. N. H. Reek, *Acc. Chem. Res.*, 2001, **34**, 895-904.
238.   F. H. Allen, O. Kennard, D. G. Watson, L. Brammer, A. G. Orpen and R. Taylor, *Journal of the Chemical Society, Perkin Transactions 2*, 1987, S1-S19.
239.   P. J. Kocienski, *Protecting Groups*, Georg Thieme Verlag, 2005.

240. S. Itoh, K. Nii, M. Mure and Y. Ohshiro, *Tetrahedron Lett.*, 1987, **28**, 3975-3978.
241. L. Zhai, R. Shukla, S. H. Wadumethrige and R. Rathore, *The Journal of Organic Chemistry*, 2010, **75**, 4748-4760.
242. M. Lalonde and T. H. Chan, *Synthesis*, 1985, **1985**, 817-845.
243. P. G. M. Wuts and T. W. Greene, in *Greene's Protective Groups in Organic Synthesis*, John Wiley & Sons, Inc., 2006, pp. 367-430.
244. S. Hanessian, R. Margarita, A. Hall, S. Johnstone, M. Tremblay and L. Parlanti, *J. Am. Chem. Soc.*, 2002, **124**, 13342-13343.
245. J. Zhang, X. Wang, Q. Su, L. Zhi, A. Thomas, X. Feng, D. S. Su, R. Schlögl and K. Müllen, *J. Am. Chem. Soc.*, 2009, **131**, 11296-11297.
246. R. Chinchilla and C. Nájera, *Chem. Rev.*, 2007, **107**, 874-922.
247. H. Doucet and J.-C. Hierso, *Angew. Chem. Int. Ed.*, 2007, **46**, 834-871.
248. G. Saito, H. Hosoda, Y. Yoshida, J. Hagiwara, K. Nishimura, H. Yamochi, A. Otsuka, T. Hiramatsu, Y. Shimazaki, K. Kirakci, S. Cordier and C. Perrin, *J. Mater. Chem.*, 2012, **22**, 19774-19791.
249. T. Michinobu, C. Boudon, J.-P. Gisselbrecht, P. Seiler, B. Frank, N. N. P. Moonen, M. Gross and F. Diederich, *Chem. Eur. J.*, 2006, **12**, 1889-1905.
250. M. Kivala, C. Boudon, J.-P. Gisselbrecht, P. Seiler, M. Gross and F. Diederich, *Angew. Chem.*, 2007, **119**, 6473-6477.
251. Y. Li and T. Michinobu, *Polymer Chemistry*, 2010, **1**, 72-74.
252. M. Kivala, C. Boudon, J.-P. Gisselbrecht, B. Enko, P. Seiler, I. B. Müller, N. Langer, P. D. Jarowski, G. Gescheidt and F. Diederich, *Chem. Eur. J.*, 2009, **15**, 4111-4123.
253. T. Michinobu, J. C. May, J. H. Lim, C. Boudon, J.-P. Gisselbrecht, P. Seiler, M. Gross, I. Biaggio and F. Diederich, *Chem. Commun.*, 2005, 737-739.
254. M. D. Watson, A. Fechtenkötter and K. Müllen, *Chem. Rev.*, 2001, **101**, 1267-1300.
255. P. Herwig, C. W. Kayser, K. Müllen and H. W. Spiess, *Adv. Mater.*, 1996, **8**, 510-513.
256. W. Pisula, M. Zorn, J. Y. Chang, K. Müllen and R. Zentel, *Macromol. Rapid Commun.*, 2009, **30**, 1179-1202.
257. A. J. Berresheim, M. Müller and K. Müllen, *Chem. Rev.*, 1999, **99**, 1747-1786.
258. R. Scholl and J. Mansfeld, *Berichte der deutschen chemischen Gesellschaft*, 1910, **43**, 1734-1746.
259. M. Grzybowski, K. Skonieczny, H. Butenschön and D. T. Gryko, *Angew. Chem. Int. Ed.*, 2013, **52**, 9900-9930.
260. B. T. King, J. Kroulík, C. R. Robertson, P. Rempala, C. L. Hilton, J. D. Korinek and L. M. Gortari, *The Journal of Organic Chemistry*, 2007, **72**, 2279-2288.
261. S. J. Cyvin, R. Tosic, D. Masulovic, B. N. Cyvin and J. Brunvoll, *Acta Chem. Scand.*, 1993, **47**, 541-546.
262. J. Bart, *Acta Crystallographica Section B*, 1968, **24**, 1277-1287.
263. H. Kruse, L. Goerigk and S. Grimme, *The Journal of Organic Chemistry*, 2012, **77**, 10824-10834.
264. J. P. Ferraris and G. Saito, *J. Chem. Soc., Chem. Commun.*, 1978, 992-993.
265. T. Hasegawa, K. Inukai, S. Kagoshima, T. Sugawara, T. Mochida, S. Sugiura and Y. Iwasa, *Chem. Commun.*, 1997, 1377-1378.
266. N. Sato, K. Seki and H. Inokuchi, *Journal of the Chemical Society, Faraday Transactions 2: Molecular and Chemical Physics*, 1981, **77**, 1621-1633.
267. G. Saito and J. P. Ferraris, *Bull. Chem. Soc. Jpn.*, 1980, **53**, 2141-2145.
268. W. Gao and A. Kahn, *Appl. Phys. Lett.*, 2001, **79**, 4040-4042.
269. , FR761627, 1934.
270. A. Mateo-Alonso, N. Kulisic, G. Valenti, M. Marcaccio, F. Paolucci and M. Prato, *Chem. Asian J.*, 2010, **5**, 482.
271. N. Kulisic, S. More and A. Mateo-Alonso, *Chem. Commun.*, 2011, **47**, 514-516.
272. S. Kajigaeshi, M. Moriwaki, T. Tanaka, S. Fujisaki, T. Kakinami and T. Okamoto, *J. Chem. Soc., Perkin Trans. 1*, 1990, 897-899.
273. H. M. Gilow and D. E. Burton, *The Journal of Organic Chemistry*, 1981, **46**, 2221-2225.
274. R. H. Mitchell, Y.-H. Lai and R. V. Williams, *The Journal of Organic Chemistry*, 1979, **44**, 4733-4735.

275.   J. G. Cannon, A. N. Brubaker, J. P. Long, J. R. Flynn, T. Verimer, P. Harnirattisai, B. Costall, R. J. Naylor and V. Nohria, *J. Med. Chem.*, 1981, **24**, 149-153.
276.   M. B. Rubin, *J. Org. Chem.*, 1963, **28**, 1949-1952.
277.   K. Smith, P. He and A. Taylor, *Green Chemistry*, 1999, **1**, 35-38.
278.   P. G. M. Wuts and T. W. Greene, *Greene's Protective Groups in Organic Synthesis*, Wiley, 2012.
279.   Y. Shirai, A. J. Osgood, Y. Zhao, Y. Yao, L. Saudan, H. Yang, C. Yu-Hung, L. B. Alemany, T. Sasaki, J.-F. Morin, J. M. Guerrero, K. F. Kelly and J. M. Tour, *J. Am. Chem. Soc.*, 2006, **128**, 4854-4864.
280.   J. Almog, N. Stepanov and F. Dubnikova, *Tetrahedron Lett.*, 2008, **49**, 1870-1876.
281.   S. V. Ley, D. K. Baeschlin, D. J. Dixon, A. C. Foster, S. J. Ince, H. W. M. Priepke and D. J. Reynolds, *Chem. Rev.*, 2000, **101**, 53-80.
282.   H. E. Katz, Z. Bao and S. L. Gilat, *Acc. Chem. Res.*, 2001, **34**, 359-369.
283.   A. Lund, M. Shiotani and S. Shimada, in *Principles and Applications of ESR Spectroscopy*, Springer Netherlands, 2011, pp. 79-164.
284.   R. R. Gagne, C. A. Koval and G. C. Lisensky, *Inorg. Chem.*, 1980, **19**, 2854-2855.
285.   J. T. Hupp, *Inorg. Chem.*, 1990, **29**, 5010-5012.
286.   J. R. Aranzaes, M.-C. Daniel and D. Astruc, *Can. J. Chem.*, 2006, **84**, 288-299.
287.   I. Noviandri, K. N. Brown, D. S. Fleming, P. T. Gulyas, P. A. Lay, A. F. Masters and L. Phillips, *The Journal of Physical Chemistry B*, 1999, **103**, 6713-6722.
288.   G. Gritzner and J. Kuta, *Pure Appl. Chem.*, 1982, **54**.
289.   H. Günther, *NMR Spectroscopy: Basic Principles, Concepts and Applications in Chemistry*, Wiley, 2013.
290.   A. Ito, H. Ino, Y. Matsui, Y. Hirao, K. Tanaka, K. Kanemoto and T. Kato, *The Journal of Physical Chemistry A*, 2004, **108**, 5715-5720.
291.   N. J. Jeon, J. Lee, J. H. Noh, M. K. Nazeeruddin, M. Grätzel and S. I. Seok, *J. Am. Chem. Soc.*, 2013, **135**, 19087-19090.
292.   N. J. Jeon, H. G. Lee, Y. C. Kim, J. Seo, J. H. Noh, J. Lee and S. I. Seok, *J. Am. Chem. Soc.*, 2014, **136**, 7837-7840.
293.   W. Kaim and J. Fiedler, *Chem. Soc. Rev.*, 2009, **38**, 3373-3382.
294.   W. K. Hagmann, *J. Med. Chem.*, 2008, **51**, 4359-4369.
295.   E. C. Vauthier, A. Cossé-Barbi, M. Blain and S. Fliszár, *Journal of Molecular Structure: THEOCHEM*, 1999, **492**, 113-121.
296.   R. C. Larock, *Comprehensive Organic Transformations*, John Wiley & Sons Incorporated, 1999.
297.   P. Pollak, G. Romeder, F. Hagedorn and H.-P. Gelbke, in *Ullmann's Encyclopedia of Industrial Chemistry*, Wiley-VCH Verlag GmbH & Co. KGaA, 2000.
298.   J. Lindley, *Tetrahedron*, 1984, **40**, 1433-1456.
299.   P. Anbarasan, T. Schareina and M. Beller, *Chem. Soc. Rev.*, 2011, **40**, 5049-5067.
300.   D. F. McMillen and D. M. Golden, *Annu. Rev. Phys. Chem.*, 1982, **33**, 493-532.
301.   Q. Wen, J. Jin, L. Zhang, Y. Luo, P. Lu and Y. Wang, *Tetrahedron Lett.*, 2014, **55**, 1271-1280.
302.   M. R. Pitts, P. McCormack and J. Whittall, *Tetrahedron*, 2006, **62**, 4705-4708.
303.   M. T. Martin, B. Liu, B. E. Cooley Jr and J. F. Eaddy, *Tetrahedron Lett.*, 2007, **48**, 2555-2557.
304.   T. Schareina, A. Zapf and M. Beller, *Chem. Commun.*, 2004, 1388-1389.
305.   H. R. Chobanian, B. P. Fors and L. S. Lin, *Tetrahedron Lett.*, 2006, **47**, 3303-3305.
306.   J. Zanon, A. Klapars and S. L. Buchwald, *J. Am. Chem. Soc.*, 2003, **125**, 2890-2891.
307.   R. Polley and M. Hanack, *The Journal of Organic Chemistry*, 1995, **60**, 8278-8282.
308.   A. Klapars and S. L. Buchwald, *J. Am. Chem. Soc.*, 2002, **124**, 14844-14845.
309.   B. C. Ranu and S. Bhar, *Org. Prep. Proced. Int.*, 1996, **28**, 371-409.
310.   C. Sousa and P. J. Silva, *Eur. J. Org. Chem.*, 2013, **2013**, 5195-5199.
311.   J. F. W. McOmie, M. L. Watts and D. E. West, *Tetrahedron*, 1968, **24**, 2289-2292.
312.   R. L. Burwell, *Chem. Rev.*, 1954, **54**, 615-685.
313.   H. Veisi, *Synthesis*, 2010, **2010**, 2631-2635.
314.   S. Purser, P. R. Moore, S. Swallow and V. Gouverneur, *Chem. Soc. Rev.*, 2008, **37**, 320-330.
315.   M. Oishi, H. Kondo and H. Amii, *Chem. Commun.*, 2009, 1909-1911.

316. H. Morimoto, T. Tsubogo, N. D. Litvinas and J. F. Hartwig, *Angew. Chem. Int. Ed.*, 2011, **50**, 3793-3798.
317. W. F. Bailey and J. J. Patricia, *J. Organomet. Chem.*, 1988, **352**, 1-46.
318. D. Seyferth, *Organometallics*, 2005, **25**, 2-24.
319. S. Yagi and H. Nakazumi, in *Heterocyclic Polymethine Dyes*, ed. L. Strekowski, Springer Berlin Heidelberg, 2008, vol. 14, pp. 133-181.
320. Q. A. Acton, *Aromatic Polycyclic Hydrocarbons—Advances in Research and Application: 2013 Edition*, ScholarlyEditions, 2013.
321. X. Zhan, A. Facchetti, S. Barlow, T. J. Marks, M. A. Ratner, M. R. Wasielewski and S. R. Marder, *Adv. Mater.*, 2011, **23**, 268-284.
322. J. R. Levine, J. B. Cohen, Y. W. Chung and P. Georgopoulos, *J. Appl. Crystallogr.*, 1989, **22**, 528-532.
323. J. Youn, S. Kewalramani, J. D. Emery, Y. Shi, S. Zhang, H.-C. Chang, Y.-j. Liang, C.-M. Yeh, C.-Y. Feng, H. Huang, C. Stern, L.-H. Chen, J.-C. Ho, M.-C. Chen, M. J. Bedzyk, A. Facchetti and T. J. Marks, *Adv. Funct. Mater.*, 2013, **23**, 3850-3865.
324. D. H. Mathew, J. D. Peter, J. G. David, G. Alexander, S. Jonathan, M. Eric and E. T. Mark, *New Journal of Physics*, 2013, **15**, 105029.
325. P. Sullivan, A. Duraud, l. Hancox, N. Beaumont, G. Mirri, J. H. R. Tucker, R. A. Hatton, M. Shipman and T. S. Jones, *Advanced Energy Materials*, 2011, **1**, 352-355.
326. A. Facchetti, in *Organic Photovoltaics*, Wiley-VCH Verlag GmbH & Co. KGaA, 2014, pp. 239-300.
327. K. P. Goetz, D. Vermeulen, M. E. Payne, C. Kloc, L. E. McNeil and O. D. Jurchescu, *J. Mater. Chem. C*, 2014, **2**, 3065-3076.
328. H. A. Benesi and J. H. Hildebrand, *J. Am. Chem. Soc.*, 1949, **71**, 2703-2707.
329. G. G. Aloisi and S. Pignataro, *J. Chem. Soc., Faraday Trans. 1*, 1973, **69**, 534-539.
330. J. S. Renny, L. L. Tomasevich, E. H. Tallmadge and D. B. Collum, *Angew. Chem. Int. Ed.*, 2013, **52**, 11998-12013.
331. K. Hirose, *Journal of inclusion phenomena and macrocyclic chemistry*, 2001, **39**, 193-209.
332. N. Sakai, I. Shirotani and S. Minomura, *Bull. Chem. Soc. Jpn.*, 1970, **43**, 57-63.
333. I. A. Darwish, *Anal. Chim. Acta*, 2005, **549**, 212-220.
334. J. S. Chappell, A. N. Bloch, W. A. Bryden, M. Maxfield, T. O. Poehler and D. O. Cowan, *J. Am. Chem. Soc.*, 1981, **103**, 2442-2443.
335. K. Medjanik, A. Gloskovskii, D. Kutnyakhov, C. Felser, D. Chercka, M. Baumgarten, K. Müllen and G. Schoenhense, *J. Electron Spectrosc. Relat. Phenom.*, 2012, **185**, 77-84.
336. K. Medjanik, S. Perkert, S. Naghavi, M. Rudloff, V. Solovyeva, D. Chercka, M. Huth, S. A. Nepijko, T. Methfessel, C. Felser, M. Baumgarten, K. Müllen, H. J. Elmers and G. Schoenhense, *arXiv.org, e-Print Arch., Condens. Matter*, 2010, 1-20, arXiv:1008.4722v1001 [cond-mat.mtrl-sci].
337. K. Medjanik, S. Perkert, S. Naghavi, M. Rudloff, V. Solovyeva, D. Chercka, M. Huth, S. A. Nepijko, T. Methfessel, C. Felser, M. Baumgarten, K. Müllen, H. J. Elmers and G. Schonhense, *Phys. Rev. B: Condens. Matter Mater. Phys.*, 2010, **82**, 245419/245411-245419/245419.
338. K. Medjanik, D. Chercka, P. Nagel, M. Merz, S. Schuppler, M. Baumgarten, K. Müllen, S. A. Nepijko, H.-J. Elmers, G. Schoenhense, H. O. Jeschke and R. Valenti, *J. Am. Chem. Soc.*, 2012, **134**, 4694-4699.
339. K. Medjanik, S. A. Nepijko, H. J. Elmers, G. Schoenhense, P. Nagel, M. Merz, S. Schuppler, D. Chercka, M. Baumgarten and K. Müllen, *arXiv.org, e-Print Arch., Condens. Matter*, 2010, 1-13, arXiv:1012.3467v1011 [cond-mat.mtrl-sci].
340. M. Rudloff, K. Ackermann, M. Huth, H. O. Jeschke, M. Tomic, R. Valenti, B. Wolfram, M. Broering, M. Bolte, D. Chercka, M. Baumgarten and K. Muellen, *arXiv.org, e-Print Arch., Condens. Matter*, 2014, 1-10, arXiv:1410.5552v1411 [cond-mat.mtrl-sci].
341. A. M. Kini, D. O. Cowan, F. Gerson and R. Moeckel, *J. Am. Chem. Soc.*, 1985, **107**, 556-562.
342. P. Willmott, *An Introduction to Synchrotron Radiation: Techniques and Applications*, Wiley, 2011.

343. A. Marfunin, in *Spectroscopy, Luminescence and Radiation Centers in Minerals*, Springer Berlin Heidelberg, 1979, pp. 38-75.
344. S. Hüfner, in *Photoelectron Spectroscopy*, Springer Berlin Heidelberg, 2003, pp. 1-60.
345. M. P. Seah and W. A. Dench, *Surf. Interface Anal.*, 1979, **1**, 2-11.
346. H. Ishii, K. Sugiyama, E. Ito and K. Seki, *Adv. Mater.*, 1999, **11**, 605-625.
347. A. D. Becke, *The Journal of Chemical Physics*, 2014, **140**, -.
348. J. A. Venables, *Introduction to Surface and Thin Film Processes*, Cambridge University Press, 2000.
349. J. Fraxedas, *J. Phys. IV France*, 2004, **114**, 661-666.
350. S. A. Burke, J. M. Topple and P. Grütter, *J. Phys.: Condens. Matter*, 2009, **21**, 423101.
351. M. Morgenstern, D. Haude, V. Gudmundsson, C. Wittneven, R. Dombrowski, C. Steinebach and R. Wiesendanger, *J. Electron. Spectrosc. Relat. Phenom.*, 2000, **109**, 127-145.
352. H. J. W. Zandvliet and A. van Houselt, *Annual Review of Analytical Chemistry*, 2009, **2**, 37-55.
353. J. Haase, *Chem. unserer Zeit*, 1992, **26**, 219-231.
354. J. Stöhr, *NEXAFS Spectroscopy*, Springer, 1992.
355. G. Bunker, *Introduction to XAFS*, Cambridge University Press, 2010.
356. K. Medjanik, *Electron spectroscopy of novel charge transfer systems based on polycyclic aromatic hydrocarbons*, Mainz, Univ., Diss., 2011, 2011.
357. J. Fraxedas, Y. J. Lee, I. Jiménez, R. Gago, R. M. Nieminen, P. Ordejón and E. Canadell, *Physical Review B*, 2003, **68**, 195115.
358. M. Sing, J. Meyer, M. Hoinkis, S. Glawion, P. Blaha, G. Gavrila, C. S. Jacobsen and R. Claessen, *Physical Review B*, 2007, **76**, 245119.
359. R. Claessen, M. Sing, U. Schwingenschlögl, P. Blaha, M. Dressel and C. S. Jacobsen, *Phys. Rev. Lett.*, 2002, **88**, 096402.
360. K. Amemiya, Y. Kitajima, Y. Yonamoto, S. Terada, H. Tsukabayashi, T. Yokoyama and T. Ohta, *Physical Review B*, 1999, **59**, 2307-2312.
361. C. S. Fadley, *Nuclear Instruments and Methods in Physics Research Section A: Accelerators, Spectrometers, Detectors and Associated Equipment*, 2009, **601**, 8-31.
362. K. Kobayashi, *Nuclear Instruments and Methods in Physics Research Section A: Accelerators, Spectrometers, Detectors and Associated Equipment*, 2009, **601**, 32-47.
363. A. Gloskovskii, G. Stryganyuk, G. H. Fecher, C. Felser, S. Thiess, H. Schulz-Ritter, W. Drube, G. Berner, M. Sing, R. Claessen and M. Yamamoto, *J. Electron. Spectrosc. Relat. Phenom.*, 2012, **185**, 47-52.
364. I. Ikemoto, K. Kikuchi, K. Yakushi, H. Kuroda and K. Kobayashi, *Solid State Commun.*, 1982, **42**, 257-259.
365. I. Ikemoto, T. Sugano and H. Kuroda, *Chem. Phys. Lett.*, 1977, **49**, 45-48.
366. W. D. Grobman and B. D. Silverman, *Solid State Commun.*, 1976, **19**, 319-322.
367. D. Wolpert and P. Ampadu, in *Managing Temperature Effects in Nanoscale Adaptive Systems*, Springer New York, 2012, pp. 15-33.
368. J. D. Wright, *Molecular Crystals*, Cambridge University Press, 1995.
369. S. Horiuchi, T. Hasegawa and Y. Tokura, *Molecular Crystals and Liquid Crystals*, 2006, **455**, 295-304.
370. G. Valchanov, A. Ivanova, A. Tadjer, D. Chercka and M. Baumgarten, *Org. Electron.*, 2013, **14**, 2727-2736.
371. S. Warren, *Organic Synthesis, Workbook: The Disconnection Approach*, Wiley, 1982.
372. T. E. Barder, S. D. Walker, J. R. Martinelli and S. L. Buchwald, *J. Am. Chem. Soc.*, 2005, **127**, 4685-4696.
373. N. Kataoka, Q. Shelby, J. P. Stambuli and J. F. Hartwig, *The Journal of Organic Chemistry*, 2002, **67**, 5553-5566.
374. I. P. Beletskaya and A. V. Cheprakov, *Coord. Chem. Rev.*, 2004, **248**, 2337-2364.
375. D. N. Coventry, A. S. Batsanov, A. E. Goeta, J. A. K. Howard, T. B. Marder and R. N. Perutz, *Chem. Commun.*, 2005, **16**, 2172-2174.

376. H. Sasabe and J. Kido, *J. Mater. Chem. C*, 2013, **1**, 1699-1707.
377. J. Pommerehne, H. Vestweber, W. Guss, R. F. Mahrt, H. Bässler, M. Porsch and J. Daub, *Adv. Mater.*, 1995, **7**, 551-554.
378. K. Yuan Chiu, T. Xiang Su, J. Hong Li, T.-H. Lin, G.-S. Liou and S.-H. Cheng, *J. Electroanal. Chem.*, 2005, **575**, 95-101.
379. J. Qu, R. Kawasaki, M. Shiotsuki, F. Sanda and T. Masuda, *Polymer*, 2006, **47**, 6551-6559.
380. W. A. Schroeder, P. E. Wilcox, K. N. Trueblood and A. O. Dekker, *Anal. Chem.*, 1951, **23**, 1740-1747.
381. M. Sauer, J. Hofkens and J. Enderlein, in *Handbook of Fluorescence Spectroscopy and Imaging*, Wiley-VCH Verlag GmbH & Co. KGaA, 2011, pp. 1-30.
382. A. P. Monkman, H. D. Burrows, L. J. Hartwell, L. E. Horsburgh, I. Hamblett and S. Navaratnam, *Phys. Rev. Lett.*, 2001, **86**, 1358-1361.
383. A. Köhler and H. Bässler, *Materials Science and Engineering: R: Reports*, 2009, **66**, 71-109.
384. D. Jacquemin, E. A. Perpète, I. Ciofini and C. Adamo, *Journal of Chemical Theory and Computation*, 2010, **6**, 1532-1537.
385. U. Resch-Genger, M. Grabolle, S. Cavaliere-Jaricot, R. Nitschke and T. Nann, *Nat Meth*, 2008, **5**, 763-775.
386. S. Nakano, M. Sakai, M. Tanaka and T. Kawashima, *Chem. Lett.*, 1979, **8**, 473-476.
387. S. Y. Lee, T. Yasuda, Y. S. Yang, Q. Zhang and C. Adachi, *Angew. Chem.*, 2014, **126**, 6520-6524.
388. Y.-J. Pu, T. Kurata, M. Soma, J. Kido and H. Nishide, *Synth. Met.*, 2004, **143**, 207-214.
389. W. C. H. Choy, K. N. Hui, Y. J. Liang, K. L. Tong, S. K. So, L. M. Leung, N. J. Xiang and G. Menglian, 2005.
390. R. G. Compton, C. Batchelor-McAuley and E. J. F. Dickinson, in *Understanding Voltammetry*, World Scientific Publishing Co., 2012, pp. 57-66.
391. S. Rihn, P. Retailleau, A. De Nicola, G. Ulrich and R. Ziessel, *The Journal of Organic Chemistry*, 2012, **77**, 8851-8863.
392. J. Lakowicz, in *Principles of Fluorescence Spectroscopy*, ed. J. Lakowicz, Springer US, 2006, pp. 1-26.
393. R. Ziessel and A. Harriman, *Chem. Commun.*, 2011, **47**, 611-631.
394. N. Boens, V. Leen and W. Dehaen, *Chem. Soc. Rev.*, 2012, **41**, 1130-1172.
395. C. Reichardt, *Chem. Rev.*, 1994, **94**, 2319-2358.
396. A. Marini, A. Muñoz-Losa, A. Biancardi and B. Mennucci, *The Journal of Physical Chemistry B*, 2010, **114**, 17128-17135.
397. M. Banerjee, V. S. Vyas, S. V. Lindeman and R. Rathore, *Chem. Commun.*, 2008, 1889-1891.
398. J. Bisberg, W. J. Cumming, R. A. Gaudiana, K. D. Hutchinson, R. T. Ingwall, E. S. Kolb, P. G. Mehta, R. A. Minns and C. P. Petersen, *Macromolecules*, 1995, **28**, 386-389.
399. B. R. Kaafarani, L. A. Lucas, B. Wex and G. E. Jabbour, *Tetrahedron Lett.*, 2007, **48**, 5995.
400. R. Nandy, M. Subramoni, B. Varghese and S. Sankararaman, *The Journal of Organic Chemistry*, 2007, **72**, 938-944.
401. O. L. J. Gijzeman, J. Langelaar and J. D. W. Van Voorst, *Chem. Phys. Lett.*, 1970, **5**, 269-272.
402. K. Mistelberger and H. Port, *Molecular Crystals and Liquid Crystals*, 1980, **57**, 203-226.
403. S. O. Jeon, S. E. Jang, H. S. Son and J. Y. Lee, *Adv. Mater.*, 2011, **23**, 1436-1441.
404. H. Shin, S. Lee, K.-H. Kim, C.-K. Moon, S.-J. Yoo, J.-H. Lee and J.-J. Kim, *Adv. Mater.*, 2014, **26**, 4730-4734.
405. W.-Y. Hung, G.-C. Fang, S.-W. Lin, S.-H. Cheng, K.-T. Wong, T.-Y. Kuo and P.-T. Chou, *Sci. Rep.*, 2014, **4**.
406. C.-C. Lee, M.-Y. Chang, P.-T. Huang, Y. C. Chen, Y. Chang and S.-W. Liu, *J. Appl. Phys.*, 2007, **101**, -.
407. S.-J. Yoo, J.-H. Chang, J.-H. Lee, C.-K. Moon, C.-I. Wu and J.-J. Kim, *Sci. Rep.*, 2014, **4**, 03902.

408. K. J. Vahala, *Nature*, 2003, **424**, 839-846.
409. B. Valeur, in *Molecular Fluorescence*, Wiley-VCH Verlag GmbH, 2001, pp. 34-71.
410. L. T. Sharpe, A. Stockman, W. Jagla and H. Jägle, *Journal of Vision*, 2005, **5**.
411. J.-W. Kang, S.-H. Lee, H.-D. Park, W.-I. Jeong, K.-M. Yoo, Y.-S. Park and J.-J. Kim, *Appl. Phys. Lett.*, 2007, **90**, -.
412. J.-Y. Hu, Y.-J. Pu, F. Satoh, S. Kawata, H. Katagiri, H. Sasabe and J. Kido, *Adv. Funct. Mater.*, 2014, **24**, 2064-2071.
413. Q. Peng, J. Xu, M. Li and W. Zheng, *Macromolecules*, 2009, **42**, 5478-5485.
414. P. Peumans and S. R. Forrest, *Appl. Phys. Lett.*, 2001, **79**, 126-128.
415. C. J. Brabec, A. Cravino, D. Meissner, N. S. Sariciftci, M. T. Rispens, L. Sanchez, J. C. Hummelen and T. Fromherz, *Thin Solid Films*, 2002, **403–404**, 368-372.
416. M. F. Semmelhack, P. M. Helquist and L. D. Jones, *J. Am. Chem. Soc.*, 1971, **93**, 5908-5910.
417. B. M. Rosen, K. W. Quasdorf, D. A. Wilson, N. Zhang, A.-M. Resmerita, N. K. Garg and V. Percec, *Chem. Rev.*, 2010, **111**, 1346-1416.
418. R. A. Altman and S. L. Buchwald, *Nat. Protocols*, 2007, **2**, 3115-3121.
419. , 2008.
420. S. Sergeyev, W. Pisula and Y. H. Geerts, *Chem. Soc. Rev.*, 2007, **36**, 1902-1929.
421. S. K. Lee, Y. Zu, A. Herrmann, Y. Geerts, K. Müllen and A. J. Bard, *J. Am. Chem. Soc.*, 1999, **121**, 3513-3520.
422. J. H. Oh, W.-Y. Lee, T. Noe, W.-C. Chen, M. Könemann and Z. Bao, *J. Am. Chem. Soc.*, 2011, **133**, 4204-4207.
423. Z. Sun, Q. Ye, C. Chi and J. Wu, *Chem. Soc. Rev.*, 2012, **41**, 7857-7889.
424. P. Somerharju, *Chem. Phys. Lipids*, 2002, **116**, 57-74.
425. P. Bandyopadhyay and A. K. Ghosh, *Sensor Letters*, 2011, **9**, 1249-1264.
426. Y. Niko and G. Konishi, *Journal of Synthetic Organic Chemistry Japan*, 2012, **70**, 918-927.
427. M. Beija, M. T. Charreyre and J. M. G. Martinho, *Prog. Polym. Sci.*, 2011, **36**, 568-602.
428. A. C. Benniston, A. Harriman, I. Llarena and C. A. Sams, *Chem. Mater.*, 2007, **19**, 1931-1938.
429. X. Feng, J. Y. Hu, H. Tomiyasu, N. Seto, C. Redshaw, M. R. J. Elsegood and T. Yamato, *Organic & Biomolecular Chemistry*, 2013, **11**, 8366-8374.
430. A. O. El-Ballouli, R. S. Khnayzer, J. C. Khalife, A. Fonari, K. M. Hallal, T. V. Timofeeva, D. Patra, F. N. Castellano, B. Wex and B. R. Kaafarani, *Journal of Photochemistry and Photobiology a-Chemistry*, 2013, **272**, 49-57.
431. H. Jian-Yong, F. Xing, H. Tomiyasu, N. Seto, U. Rayhan, M. R. J. Elsegood, C. Redshaw and T. Yamato, *J. Mol. Struct.*, 2013, **1047**, 194-203.
432. Y. Zhang, T. W. Ng, F. Lu, Q. X. Tong, S. L. Lai, M. Y. Chan, H. L. Kwong and C. S. Lee, *Dyes and Pigments*, 2013, **98**, 190-194.
433. , JP2010155985A, 2010.
434. J. ACKERMANN and M. Wang, Google Patents, 2013.

X.   List of publications

1. D. Chercka, S.-J. Yoo, M. Baumgarten, J.-J. Kim and K. Müllen, *J. Mater. Chem. C*, 2014, **2**, 9083-9086.

2. M. Rudloff, K. Ackermann, M. Huth, H. O. Jeschke, M. Tomic, R. Valenti, B. Wolfram, M. Broering, M. Bolte, D. Chercka, M. Baumgarten and K. Müllen, *arXiv.org, e-Print Arch., Condens. Matter*, 2014, 1-10, arXiv:1410.5552v1411 [cond-mat.mtrl-sci].

3. G. Valchanov, A. Ivanova, A. Tadjer, D. Chercka and M. Baumgarten, *Org. Electron.*, 2013, **14**, 2727-2736.

4. S.-I. Kawano, M. Baumgarten, D. Chercka, V. Enkelmann and K. Müllen, *Chem. Commun.*, 2013, **49**, 5058-5060.

5. K. Medjanik, A. Gloskovskii, D. Kutnyakhov, C. Felser, D. Chercka, M. Baumgarten, K. Müllen and G. Schoenhense, *J. Electron Spectrosc. Relat. Phenom.*, 2012, **185**, 77-84.

6. K. Medjanik, D. Chercka, P. Nagel, M. Merz, S. Schuppler, M. Baumgarten, K. Müllen, S. A. Nepijko, H.-J. Elmers, G. Schoenhense, H. O. Jeschke and R. Valenti, *J. Am. Chem. Soc.*, 2012, **134**, 4694-4699.

7. L. Zoephel, D. Beckmann, V. Enkelmann, D. Chercka, R. Rieger and K. Müllen, *Chem. Commun. (Cambridge, U. K.)*, 2011, **47**, 6960-6962.

8. K. Medjanik, S. Perkert, S. Naghavi, M. Rudloff, V. Solovyeva, D. Chercka, M. Huth, S. A. Nepijko, T. Methfessel, C. Felser, M. Baumgarten, K. Müllen, H. J. Elmers and G. Schonhense, *Phys. Rev. B: Condens. Matter Mater. Phys.*, 2010, **82**, 245411-245419.

9. B. H. Northrop, D. Chercka and P. J. Stang, *Tetrahedron*, 2008, **64**, 11495-11503.

XII.   Curriculum vitae

Dennis Chercka
Wallaustraße 65
55118 Mainz
Born: 21 February 1982 in Wolfsburg

03/2010 – 01/2015	**PhD Thesis – Max Planck Institute for Polymer Research, Mainz**	
	July 2011 – 2015	PhD Student – Johannes Gutenberg University
	July 2011 – July 2014	Scholar of the International Research Training Group 1404 – *"Self-organized Materials for Optoelectronics"*
	02/2013 – 06/2013 and 02/2012 – 05/2012	Research at Seoul National University, South Korea under the supervision of Professor Jang Joo Kim
09/2002 – 02/2010	**Technische Universität Carolo-Wilhelmina zu Braunschweig** **Subject: Chemistry, Degree: Diplomchemiker** **Final grade: „Gut"; 02.02.2010**	
	05/2009 – 02/2010	Max Planck Institute for Polymer Research, Mainz Diploma-thesis, in the group of Professor K. Müllen, Grade: "Sehr gut"
	08/2007 – 05/2008	University of Utah, Salt Lake City, USA; ISEP scholar.
8/1992 - 6/2001	**Heinrich Nordhoff comprehensive School, Wolfsburg** **Degree: Allgemeine Hochschulreife, Grade: 2,5; 22.06.2001**	

국문초록

약 200 년 전에 파이렌이 최초로 발견되었고, 그 이후로 이 물질은 전 세계의 화학자들에게 끊임없는 관심을 받아왔다. 파이렌에 관한 수많은 화학 연구 분야 중, 선택적 기능화는 큰 조명을 받아온 분야 중 하나이다. 왜냐하면 분자의 다른 위치들에 특정한 기능화를 하는 것은 현재까지도 굉장히 어려운 주제이기 때문이다.

이번 논문에서는 파이렌 치환의 두가지 새로운 양식들을 개발하였다. 적절한 조건에서 4,5,9,10-tetramethoxypyrene 의 네 겹의 브롬화는 여덟 겹으로 기능화된 파이렌들의 생산을 가능하게 해준다. 위와 같은 분자들을 기반으로 1,3,4,5,6,7,9,10 위치가 치환된 새로운 파이렌 파생물들을 얻을 수 있다. Non-quinoidal 합성법은 전자 수용체의 중간체에 적절하게 적용될 수 있었지만, 전자가 거의 없는 파이렌 파생물을 얻는 데는 실패하였다. 또한, 전자 증여체로써의 4,5,9,10-tetramethoxypyrene 도 합성되었고, 위 물질들의 전하 이동 복합체로서의 역할에 관한 연구를 진행하였다. 고체 상태에서 SFB/RT 49 을 통해 위 복합체들을 분석하였고, non-TTF CT-complex 에서의 전하이동을 HAXPES 와 NEXAFS 를 통해 연구하였다.

Zöphel 외 두 명의 연구를 기반으로 비대칭의 4,9,10 위치가 치환된 파이렌 파생물을 얻을 수 있다. 이것은 판형이 아닌 전자 수용체 분자에 더하여 전자가 풍푸한 파이렌 타입의 분자들을 합성하기 위한 블록으로 사용되었다.

마지막으로 두가지 분리된 구조의 분자들이 유기발광소자의 발광체로 사용되었다. 유기발광소자 중 열활성화 지연형광은 형광 유기발광소자의 효율을 증진시킬 수 있는 획기적인 방법으로 학계의 큰 관심을 받고 있다. 이번 연구에서 합성한 물질들은 굉장히 깊은 청색 발광을 가지면서 동시에 높은 형광 발광 효율을

유지하면서 단일상태와 삼중상태의 에너지 차이가 최소가 되도록 설계되었다. 초기의 OD 시리즈들은 굉장히 작은 에너지 차이를 가졌지만 유기 발광소자에 사용하기에는 불충분한 절대 발광 효율을 가지고 있었다. 반대로 파이렌 시리즈들은 앞의 두 가지 특성들을 동시에 반족시킴으로써, 효율이 좋은 유기발광소자에 발광체로 효과적으로 적용되었다.